

A thesis submitted in total fulfilment of the requirements

for the degree of Doctor of Philosophy

Investigating the role of TANK-binding kinase 1 in autophagy and amyotrophic lateral sclerosis

Reka Petra Toth

(Master in Molecular Biology and Master of Research)

MACQUARIE UNIVERSITY

Faculty of Medicine and Health Sciences

Department of Biomedical Sciences

July 2019

Contents

Contents	i
Abstract	ii
Declaration	iv
Preface	v
Acknowledgements	vii
Table of contents	vii
List of tables	xvi
List of figures	xvii
Publications	xxi
Abbreviations	xxii
Units of magnitude	xxvii

Abstract

Amyotrophic lateral sclerosis (ALS) is a progressive fatal neurodegenerative disease leading to death 3 to 5 years from symptom onset. Protein inclusions containing Tar DNA binding protein of MW 43 (TDP-43) within dying motor neurons are the pathological hallmark of ALS. Mutations in *TANK-binding kinase 1* (*TBK1)* have been identified in ALS as well as in the related conditions, frontotemporal dementia (FTD), but the underlying mechanisms remain largely unknown. Autophagy is responsible for the degradation of damaged organelles and insoluble protein inclusions in mammalian cells. TBK1 is a ubiquitously expressed kinase with a central role in the control of autophagic elimination of mitochondria and bacteria as well as in innate immune response. However, the wider functions of TBK1 in autophagy remain to be elucidated. Therefore, this thesis questioned how TBK1 is involved in other types of autophagy; basal or non-selective autophagy; and aggrephagy, the elimination of protein aggregates. Furthermore, it was also examined whether ALS/FTD mutant TBK1 leads to dysfunctional autophagy. The role of TBK1 in the aggregation of TDP-43 and clearance of ubiquitin was also studied. Here it was shown that the kinase activity of TBK1 is involved in degradation of autophagosomes during the three types of autophagy examined, suggesting a fundamental role for TBK1 in a wide variety of autophagy subtypes. Furthermore, TBK1's kinase activity was required for the formation of autophagosomes during basal autophagy. These results imply that TBK1 is involved in different stages of autophagy and its functions are restricted to specific types of autophagy. Inhibition of the kinase activity of TBK1 led to the impaired formation of autophagosomes, which was linked to impaired binding of microtubule-associated proteins 1A/1B light chain 3B (LC3) and autophagy receptors mediated by TBK1. This implies that TBK1 may act as a platform protein to bring LC3 and autophagy receptors together. In contrast, complete knock-out of TBK1 did not alter autophagosome formation or degradation, suggesting that dysfunctional TBK1 may be more harmful than the lack of protein expression. The knock-out of TBK1 enhance the degradation of ubiquitin, while overexpression resulted in elevated ubiquitin levels, indicating that TBK1 may be involved ubiquitin degradation. Unexpectedly, ALS/FTD mutant TBK1 did not cause autophagy dysfunction, however it induced the aggregation of TDP-43.

In summary, it was shown here for the first time that TBK1 is central regulator of basal autophagy and starvation-induced autophagy. However, disease mechanisms linked to ALS/FTD mutant TBK1 do not involve dysfunctional autophagy, but instead, mutant TBK1 induces aggregation of TDP-43.

Declaration

I declare that the work presented in this thesis titled "Investigating the role of Tank-binding kinase 1 in autophagy and amyotrophic lateral sclerosis" has not previously been submitted for a degree or diploma in any university apart from where it was indicated. Appendix I describes the generation of ALS-TBK1-FLAG plasmids that were submitted to Macquarie University for Master of Research degree in 2015 by the author of this thesis, Reka P. Toth. Therefore, Appendix I represent a non-examinable part of this thesis. To the best of my knowledge and belief, this thesis contains no material previously published or written by another person except where due reference is made in the thesis itself. Unless otherwise acknowledged, this work was carried out by the author.

Reka P. Toth Date: 26/07/2019

Preface

The work described in this thesis was performed by the author, except where hereby stated. The author acknowledges the following people for assistance in performing the following experiments reported in this thesis:

Chapter 3

The primers for amplifying and sequencing TBK1 knock-out CRIPSR/Cas9 clones were designed by Jennifer Fifita, Macquarie University, Sydney.

Acknowledgements

I would like to thank everyone who has helped and accompanied me during my PhD journey.

Firstly, and foremost I would like to thank my supervisor, Professor Julie Atkin. Your encouragement and constant support have been essential during this three-year journey. I am very grateful for the opportunity to work with you and learn from you and I am so thankful that you always had the time to catch up especially in the last year. Your scientific expertise and insightful advices have helped me tremendously during my PhD and writing the thesis. It would not have been possible without your help and support. Special thanks to my co-supervisors Dr Angela Laird and Dr Adam Walker. I truly appreciate the time you took on providing suggestions for my experiments and thesis. Having you both as co-supervisors has truly enriched my PhD experience and I have learned a lot from you both.

I would also like to thank all the members from Julie Atkin's lab, actual and former: Cyril, Sina, Shafi, Audrey, Anna, Mariana, Emma, Sonam, Hamideh, Jess, and Eric. Thanks for always sharing a laugh in the lab, helping me out if I needed to use the microscope or ran out of gels. In particular, I would like to thank Marta, who has become a great friend. I am so happy that I had the chance to share this experience with you. You were a great support; someone I could always count on. Thank you.

Thanks to my friends, for helping me feel like I have never left and supported me from the long distance. Thanks to all my wonderful family for caring for me and for believing in me. I am so grateful to my mom who never stopped believing in me and always supported me. You thought me the values of being a good and honest person and this has helped me tremendously during this PhD journey.

And finally, a big thank you to my partner, Karl. I can't thank you enough for all the patience and support and encouragement you have given me. Your dedication and work ethic have taught me a to be better scientist.

Table of contents

1. General Introduction 1
1.1. Amyotrophic lateral sclerosis 2
1.1.1. Clinical presentation 2
1.1.2. Epidemiology of ALS 3
1.1.3. Genetics of ALS 3
1.1.3.1. TDP-43 4
1.1.3.2. C9orf72 5
1.1.3.3. FUS 7
1.1.3.4. SOD1 8
1.1.3.5. Genes mutated in rare cases of ALS 9
Optineurin 9
CHCHD10 9
MATR3 9
CCNF 10
VCP 10
VAPB 10
Angiogenin 11
Ubiquilin2 11
Dynactin 1 11
1.1.4. Therapeutics of ALS 12
1.1.5. The ALS/FTD spectrum and ALS variants 13
1.1.5.1. Primary laterals sclerosis 13
1.1.5.2. Progressive muscular atrophy 14
1.1.5.3. Frontotemporal dementia 14
1.1.6. Pathophysiology of ALS 15
1.1.6.1. Protein aggregation 15
1.1.6.2. RNA toxicity 16
1.1.6.3. Excitotoxicity 17
1.1.6.4. Non-cell autonomous mechanisms 17
1.1.6.5. Impairment of axonal transport 19
1.1.6.6. ER-stress 20

1.1.6.7. DNA damage 21
1.1.6.8. Oxidative stress 22
1.1.6.9. Mitochondria dysfunction 22
1.1.6.10. Autophagy dysfunction 23
1.2. Autophagy 26
1.2.1. Types of autophagy in mammalian cells 26
1.2.1.1. Chaperone mediated autophagy 26
1.2.1.2. Microautophagy 26
1.2.1.3. Macroautophagy 27
1.2.2. Autophagic machinery 28
1.2.3. LC3 and GABARAP subfamilies 32
1.2.4. Membrane sources for autophagosomes 32
1.2.5. Selective autophagy vs non-selective autophagy 33
1.2.5.1. Basal autophagy 34
1.2.5.2. Non-selective autophagy 35
1.2.6. Autophagy in neuronal cells and neurodegeneration 37
1.2.7. Autophagy dysfunction in the pathophysiology of ALS 38
1.2.7.1. SOD1 38
1.2.7.2. TDP-43 39
1.2.7.3. FUS 39
1.2.7.4. p62 39
1.2.7.5. VCP 40
1.2.7.6. VAPB 40
1.2.7.7. C9orf72 40
1.2.7.8. Optineurin 41
1.2.8. Experimental detection of autophagy 41
1.3. TANK-binding kinase 1 43
1.3.1. Protein structure of TBK1 43
1.3.2. Post-translational modifications and activation of TBK1 43
1.3.3. The role of TBK1 in autophagy 44
1.3.3.1. Mitophagy 44
1.3.3.2. Xenophagy 46
1.3.3.3. Other types of selective autophagy 47
1.3.4. The role of TBK1 in ALS 47

1.3.4.1. TBK1 mutations in ALS 47
1.3.4.2. Pathogenic mechanisms linked to TBK1 in ALS 50
Overall aims of this thesis 51
2. Materials and Methods 54
2.1. Molecular biology 55
2.1.1. Vectors used for protein expression 55
2.1.1.1. LC3-EGFP 55
2.1.1.2. LC3-EGFP-mCherry 55
2.1.1.3. TBK1-FLAG 56
2.1.1.4. DFCP1-EGFP 56
2.1.1.5. TDP-43WT/M337V-GFP 56
2.1.1.6. TDP-43-GFP-WT and TDP-43 dNLS GFP 57
2.1.1.7. p62-EGFP 57
2.1.1.8. Optineurin-EGFP 58
2.1.2. Preparation of Luria Bertanu (LB) broth and LB agar 58
2.1.3. Transformation of bacteria 59
2.1.4. Bacteria amplification for plasmid purification 59
2.1.5. Plasmid purification 59
2.1.6. Plasmid quantification by Nanodrop 60
2.1.7. Sequencing of plasmid DNA 60
2.2. Mammalian cell culture techniques 60
2.2.1. General maintenance 60
2.2.2. Long-term storage of frozen cells 61
2.2.3. Thawing of cells 61
2.2.4. Densities of cells 62
2.2.5. Counting of cells 62
2.2.6. Transfection of cells 62
2.3. Protein chemistry methods 63
2.3.1. Lysis of cells 63
2.3.2. BCA protein quantification 64
2.3.3. Immunoblotting 65
2.4. Microscopy techniques 66
2.4.1. Fixation of cells 66
2.4.2. Staining of cells 66

2.4.3. Microscopy analysis 66
2.4.3.1. Image acquisition 66
2.5. Flow cytometry techniques 67
2.5.1. Autophagy analysis using LC3-EGFP-mCherry overexpressing plasmid 67
2.6. Statistics 68
3. Investigating the role of TBK1 in basal and starvation-induced autophagy 69
3.1. Introduction 70
3.1.1. The role of TBK1 in basal autophagy 70
3.1.2. The role of TBK1 in starvation-induced autophagy 71
3.1.3. Monitoring autophagy experimentally 71
3.1.4. Use of LC3-I and LC3-II to monitor autophagy 72
3.1.5. Using bafilomycin to identify defect in autophagosome formation and degradation 72
3.1.6. Autophagy detection by confocal microscopy using fluorescently tagged autophagy markers 73
3.1.7. Use of dual-tagged LC3 construct to monitor autophagy 74
3.1.8. Autophagy detection via flow cytometry 74
3.1.9. Inhibitors of the kinase activity of TBK1 76
3.1.10. CRISPR/Cas9 genome editing 77
3.2. Objectives of this chapter 79
3.3. Materials and Methods 80
3.3.1. TBK1 inhibition 80
3.3.1.1. BX795 80
3.3.1.2. MRT67307 80
3.3.2. Autophagy induction 80
3.3.2.1. Basal autophagy 80
3.3.2.2. Non-selective autophagy 81
3.3.3. Microscopy techniques 82
3.3.3.1. Quantification of LC3-EGFP and DFCP1-EGFP vesicles 82
3.3.4. CRISPR cell generation 82
3.3.4.1. Generation of gRNA expression plasmid 82
3.3.4.2. Generation of TBK1 KO cells 83
3.3.4.2.1. Transfection with TBK1 KO CRISPR/Cas9 plasmid 83
3.3.4.2.2. Single cell selection 83

3.3.4.2.3. Sequencing of TBK1 KO clones 83
3.4. Results 85
3.4.1. Establishing novel methods using saponin and FC to specifically detect LC3-II 85
3.4.2. Optimising saponin conditions to specifically detect LC3-II 86
3.4.3. Establishing of methods to detect basal autophagy 89
3.4.4. Inhibition if TBK1 perturbs basal autophagy but does not affect omegasome formation 92
3.4.5. Generation of TBK1 knock-out cells via CRISPR/Cas9 editing 104
3.4.6. Short-tandem-repeat (STR) analyses of CRISPR/Cas9 clones 106
3.4.7. TBK1 knock-out does not affect basal autophagy 109
3.4.8. Summary of basal autophagy results obtained 112
3.4.9. Optimisation of conditions to induce non-selective autophagy in HEK293T cells 114
3.4.10. TBK1 inhibition leads to inhibited omegasome formation during starvation-induced autophagy 117
3.4.11. Summary of starvation-induced autophagy obtained 124
3.4.12. TBK1 knock-out does not affect non-selective autophagy 125
3.4.13. Summary 126
3.5. Discussion 128
3.5.1. Limitations of autophagy detection techniques 128
3.5.2. TBK1 kinase activity facilitates autophagosome lysosome fusion 130
3.5.3. Genome-editing “control” clone differs from HEK293T parental cells 132
3.5.4. TBK1 knock-out does not mimic TBK1 inhibition 134
3.5.5. TBK1 and omegasome formation 135
3.5.6. Moderate effects of TBK1 on starvation-induced autophagy 135
3.5.7. TBK1 autoregulation upon inhibition 136
3.5.8. Summary 137
4. Investigation the role of TBK1 in autophagy receptor regulation of ALS-linked mutations in basal and starvation-induced autophagy 140
4.1. Introduction 141
4.1.1. Autophagy receptors in selective, basal autophagy and starvation-induced autophagy 141
4.1.2. TBK1 phosphorylates autophagy receptors 142

4.1.3. The role of TBK1 in ALS 143
4.2. Objectives of this chapter 145
4.3. Materials and Methods 146
4.3.1. Mammalian cell culture techniques 146
4.3.1.1. Transfection efficiency of FLAG-TBK1 146
4.3.1.2. Analysis of TBK1 retention post-saponin treatment 146
4.3.1.3. Analysis of mean fluorescent intensity 147
4.3.1.4. Autophagy analysis of TBK1-FLAG overexpressing cells 147
4.3.2. Protein analysis 147
4.3.2.1. GFP-Trap immunoprecipitation 147
4.4. Results 149
4.4.1. Autophagy receptors do not degrade via autophagy in basal and starvation-induced autophagy 149
4.4.2. TBK1 inhibition increases autophagy receptor levels during basal autophagy 153
4.4.3. Inhibition of TBK1's kinase activity does not prevent LC3-autophagy receptor binding during basal autophagy 156
4.4.4. TBK1 knock-out prevents LC3-p62 binding during basal autophagy 159
4.4.5. TBK1 inhibition does not effect the levels of autophagy receptors during starvation-induced autophagy 161
4.4.6. TBK1 knock-out does not affect LC3 binding towards autophagy receptors during starvation-induced autophagy 163
4.4.7. ALS mutant TBK1 during basal autophagy and starvation-induced autophagy. 165
4.4.8. R357Q ALS-mutant TBK11 is a loss-of expression mutant 165
4.4.9. Examining the intracellular retention of TBK1-FLAG protein 167
4.4.10. TBK1-FLAG overexpression impairs autophagosome degradation during basal autophagy 168
4.4.11. Summary 177
4.4.12. Kinase deficient mutant TBK1 inhibits autophagosomes degradation during starvation-induced autophagy 178
4.4.13. Summary 185
4.5. Discussion 186

4.5.1. Autophagy receptors p62, NDP52 and optineurin are likely to be involved in basal and starvation-induced autophagy 186
4.5.2. TBK1 inhibition decreased the degradation of autophagy receptors during basal autophagy 188
4.5.3. Autophagy receptors are not affected by TBK1 inhibition during starvation-induced autophagy 189
4.5.4. TBK1's substrate binding domain facilitates LC3-autophagy binding 189
4.5.5. TBK1 in amyotrophic lateral sclerosis 191
4.5.6. ALS-TBK1 mutants impair autophagosome degradation similar to WT-TBK1 192
4.5.7. Summary 194
5. Investigation the role of TBK1 in aggrephagy and protein aggregation 195
5.1. Introduction 196
5.1.1. Protein degradation by autophagy and UPS 196
5.1.2. Induction of aggrephagy by UPS inhibition 197
5.1.3. Role of TBK1 in protein degradation 197
5.2. Objectives of this chapter 199
5.3. Materials and Methods 200
5.3.1. Induction of aggrephagy 200
5.3.2. Cell lysis for total ubiquitin detection 200
5.3.3. Fractionation of cell lysated into soluble and insoluble fractionation 200
5.3.4. Quantification of ubiquitin 200
5.3.5. Analysis of TDP-43 aggregation via immunoblotting 201
5.3.6. Analysis of TDP-43 aggregation via microscopy analysis 201
5.3.7. Ubiquitin quantification by fluorescence microscopy 202
5.4. Results 203
5.4.1. Optimisation of autophagy induction via inhibited ubiquitin proteasome system, to allow monitoring of aggrephagy 203
5.4.2. TBK1 inhibition by MRT67307 impedes autophagosome formation following MG132 treatment 209
5.4.3. TBK1 inhibition by MRT67307 impairs p62 degradation upon MG132 treatment 212

5.4.4. TBK1 inhibition by MRT67307 inhibits omegasome formation during MG132 induced autophagy 214
5.4.5. Summary 216
5.4.6. TBK1 knock-out does not affect autophagy upon UPS inhibition 217
5.4.7. Overexpression of TBK1 does not influence MG132 induced autophagy 219
5.4.8. Summary 228
5.4.9. TBK1 inhibition does not affect ubiquitin degradation 229
5.4.10. TBK1 knock-out elevates ubiquitin clearance 233
5.4.11. TBK1 expression does not affect ubiquitin levels 236
5.4.12. TBK1 inhibition leads to increased TDP-43 aggregation 242
5.4.13. TBK1 knock-out does not affect the insolubility of TDP-43 252
5.4.14. E696K ALS-mutant TBK1 induces the inclusion formation of TDP-43 253
5.4.15. Summary 258
5.5. Discussion 259
5.5.1. TBK1 may not regulate autophagosome formation and degradation during MG132 induced autophagy 260
5.5.2. TBK1 inhibits ubiquitin degradation 261
5.5.3. TDP-43 aggregation and clearance are linked to optineurin 262
6. Final Discussion 266
6.1. The difficulties involved in autophagy detection 267
6.2. The role of TBK1 in autophagosome formation and degradation 269
6.3. The role of TBK1 in omegasome formation 271
6.4. TBK1 knock-out does not affect autophagosome formation and degradation 271
6.5. TBK1 is involved in TDP-43 aggregation 272
6.6. Involvement of autophagy receptors in basal and starvation and MG132 induced autophagy 273
6.7. Major findings of this thesis 274
6.8. Limitations of the study 276
6.9. Future perspectives 277
7. Supplementary data 278
Appendix I 281
Appendix II 285
Appendix III 298

References 306

List of tables

Table 1.1. List of ALS associated genes. 11

Table 1.2. List of TBK1 variants identified in ALS and FTD and other neurodegenerative diseases. 48

Table 2.1. Dilution of transfection reactions for a single well. 63

Table 2.2. BCA standard curve. 64

Table 2.3. Antibodies used int this study. 65

Table 3.1. Summary of results obtained from TBK1 inhibition studies during basal autophagy. 104

Table 3.2. Summary of results obtained from TBK1 inhibition studies during starvation-induced autophagy. 124

List of figures

Figure 1.1. Underlying pathomechanisms in ALS. 24
Figure 1.2. In mammalian cells micro-, macro-, and chaperone mediated autophagy exists. 28
Figure 1.3. Macroautophagic machinery. 29
Figure 1.4. Domain structure of TBK1. 43
Figure 1.5. Major questions of this thesis. 52
Figure 2.1. Diagram of pEGFP-C1 vector. 55
Figure 2.2. Diagram of pBABE-puro vector. 55
Figure 2.3. Diagram of pcDNA3.1 vector. 56
Figure 2.4. Diagram of pEGFP-C2 vector. 56
Figure 2.5. Diagram of pCMV6-AC-GFP vector. 57
Figure 2.6. Diagram of pLenti-C-mGFP vector. 57
Figure 2.7. Diagram of pEGFP-N3 vector. 58
Figure 2.8. Diagram of EGFP-C3 vector. 58
Figure 3.1. Schematic representation of methods to detect autophagy. 75
Figure 3.2. Optimisation of methods to specifically detect LC3-II using saponin. 88
Figure 3.3. Establishing FC methods to measure basal autophagy in HEK29T cells. 91
Figure 3.4. TBK1 inhibition by MRT67307 inhibits autophagosome-lysosome fusion and autophagosome degradation during basal autophagy in HEK293T cells. 95
Figure 3.5. MRT67307 treatment leads to decreased LC3-II accumulation upon bafilomycin treatment. 98
Figure 3.6. TBK1 inhibition by BX795, but not MRT67307, inhibits autophagosome formation in HEK293T cells. 101
Figure 3.7. TBK1 inhibition does not affect omegasome formation in basal autophagy. 103
Figure 3.8. Generation of TBK1 KO HEK293T cells using CRISPR/Cas9 editing. 108
Figure 3.9. TBK1 knock-out does not affect basal autophagy. 111
Figure 3.10. Starvation induces degradation of autophagosomes in HEK293T cells. 116

Figure 3.11. Omegasome formation is inhibited in TBK1 inhibited HEK293T cells during starvation-induced autophagy. 118
Figure 3.12. TBK1 inhibition leads to impaired autophagosome maturation during starvation in HEK293T cells. 121
Figure 3.13. TBK1 inhibition by BX795, but not by MRT67307, inhibits autophagosome formation during starvation-induced autophagy detected by confocal microscopy. 123
Figure 3.14. TBK1 knock-out does not affect starvation-induced autophagy. 125
Figure 3.15. Summary of the results described in this chapter; proposed roles of TBK1 in basal and non-selective autophagy. 138
Figure 4.1 Optineurin levels decrease, but TBK1 and autophagy receptors levels do not change following bafilomycin treatment during basal autophagy. 150
Figure 4.2. Autophagy receptors do not change upon starvation-induced autophagy. 152
Figure 4.3. TBK1 inhibition using MRT67307 elevates p62 and NDP52 levels. 155
Figure 4.4. The kinase activity of TBK1 mediates the interaction between autophagy receptors p62, optineurin, and TBK1. 158
Figure 4.5. TBK1 mediates the interaction between p62 and LC3. 160
Figure 4.6. Autophagy receptors p62, optineurin and NDP52 are not affected by the kinase activity of TBK1 during non-selective autophagy. 162
Figure 4.7. TBK1 knock-out does not affect autophagy receptor levels and interaction with LC3 during non-selective autophagy. 164
Figure 4.8. R357Q ALS-mutant TBK1 is expressed at lower levels than WT-TBK1. 168
Figure 4.9. Overexpression of TBK1-FLAG proteins leads to more autophagosomes, implying impaired fusion between the autophagosome and lysosome during basal autophagy. 170
Figure 4.10. No differences in the numbers of autophagosomes in TBK1 expressing cells during basal autophagy. 173
Figure 4.11. Omegasome formation is not affected by TBK1-FLAG expression during basal autophagy. 176
Figure 4.12. The TBK1 mutants do not impair autophagosome degradation during starvation-induced autophagy. 179

Figure 4.13. Overexpression of TBK1-FLAG does not affect autophagosome formation during starvation-induced autophagy. 181
Figure 4.14. There are no differences in formation of the omegasome following overexpression of TBK1 proteins in starvation-induced autophagy. 184
Figure 5.1. MG132 induces the degradation of insoluble ubiquitin via autophagy and not the formation of autophagosomes. 208
Figure 5.2. MRT67307 inhibits autophagosome formation and maturation during MG132 induced autophagy. 211
Figure 5.3. p62 accumulates following MRT67307 treatment during MG132 induced autophagy. 213
Figure 5.4. MRT67307 inhibits omegasome formation during MG132 induced autophagy. 215
Figure 5.5. TBK1 knock-out does not affect MG132 induced autophagy. 218
Figure 5.6. TBK1-FLAG overexpression does not affect autophagosome lysosome fusion in MG132 induced autophagy. 222
Figure 5.7. TBK1-FLAG overexpression does not affect autophagosome formation during MG132 treatment. 224
Figure 5.8. Omegasome formation is not affected by WT or mutant TBK1-FLAG overexpression in MG132 treated cells. 227
Figure 5.9. TBK1 inhibition using BX795 does not impair autophagic elimination of ubiquitin. 232
Figure 5.10. Less ubiquitin is present in CRISPR/Cas9 knock-out clones. 234
Figure 5.11. TBK1 knock-out enhances ubiquitin degradation via autophagy. 235
Figure 5.12. Increased fluorescent intensity of ubiquitin in G159A TBK1-FLAG overexpressing cells. 238
Figure 5.13. Increased levels of insoluble TDP-43 ^{M337V} are present in BX795 treated cells. 243
Figure 5.14. BX795 treatment induces the aggregation of TDP-43 ^{dNLS}. 249
Figure 5.15. MRT67307 does not affect TDP-43 insolubility. 251
Figure 5.16. TBK1 knock-out does not affect WT and dNLS-TDP-43 insolubility. 252
Figure 5.17. The E696K ALS/FTD mutant TBK1 induces TDP-43^{WT} aggregation. 255

Figure 6.1. Schematic overview of results obtained in this thesis and proposed role of TBK1 in autophagy. 275

Publication originated during this candidature

Protein Quality Control and the Amyotrophic Lateral Sclerosis/ Frontotemporal Dementia Continuum

Hamideh Shahheydari, Audrey Ragagnin, Adam K. Walker, **Reka P. Toth,** Marta Vidal, Cyril J. Jagaraj, Emma R. Perri, Anna Konopka, Jessica M. Sultana, and Julie D. Atkin

Frontiers of Molecular Neuroscience 2017; 10: 119.

ERp57 is protective against mutant SOD1-induced cellular pathology in amyotrophic lateral sclerosis

Sonam Parakh, Cyril J Jagaraj, Marta Vidal, Audrey M G Ragagnin, Emma R Perri, Anna Konopka, **Reka P Toth,** Jasmin Galper, Ian P Blair, Colleen J Thomas, Adam K Walker, Shu Yang, Damian M Spencer, and Julie D Atkin

Human Molecular Genetics, Volume 27, Issue 8, 15 April 2018, Pages 1311–1331

Dysfunction of Optineurin in Amyotrophic Lateral Sclerosis and Glaucoma

Reka P. Toth and Julie D. Atkin

Frontiers in Immunology, 2018; 9: 1017.

Impaired NHEJ repair in Amyotrophic Lateral Sclerosis is associated with TDP-43 mutations

Anna Konopka, Donna R. Whelan, Md Shafi Jamali , Emma Perri, Hamideh Shahheydari, **Reka P. Toth**, Sonam Parakh, Tina Robinson, Alison Cheong, Prachi Mehta, Marta Vidal, Audrey MG Ragagnin , Ivan Khizhnyak , Cyril J. Jagaraj, Jasmin Galper, Natalie Grima, Sina Shadfar, Shu Yang, Suzanne Cutts, Zuzana Horejsi, Toby D. M. Bell, Adam Walker, Ian Blair, Julie D. Atkin

Accepted for publication at Molecular Neurodegeneration.

Abbreviations

aa	Amino acid
AD	Alzheimer’s disease
AKT	Protein kinase B
ALS	Amyotrophic lateral sclerosis
AMBRA1	Autophagy and beclin 1 regulator 1
AMPA	α-amino-3-hydroxy-5-methyl-4-isoxazolepropionic acid
AMPK	AMP-activated protein kinase
AMP	Adenosine monophosphate
APC	Allophycocyanin
Atg	Autophagy related protein
ATP	Adenosine triphosphate
BafA1	Bafilomycin A1
Bax	Bcl-2-associated_X_protein
BCA	Bicinchoninic acid
Bp	Base pair
BSA	Bovine serum albumin
bvFTD	Behavioural variant FTD
C9orf72	C9 open reading frame 72
Ca^{2+}	Calcium
CCD	Coil-coiled domain
CFTR	Cystic fibrosis transmembrane conductance regulator
CHMP2B	Charged multivesicular protein 2B
CNS	Central Nervous System
CMA	Chaperone mediated autophagy
CRISPR	Clustered regularly interspaced short palindrom repeat
DCTN1	Dynactin subunit 1
DENN	Differentially expressed in neoplastic versus normal cells
DEP	Dishevelled EGL-10 and pleckstrin domain
DEPTOR	DEP protein containing mTOR interacting protein
DFCP1	Zinc finger FYVE domain-containing protein 1
DMEM	Dulbecco's modified eagle medium
DMSO	Dimethyl sulfoxide

DNA	Deoxyribonucleic acid
DPRs	Dipeptide repeat proteins
DSBs	Double-strand breaks
E. coli	Escherichia coli
EAAT2	Excitatory amino acid transporter 2
EGF	Epidermal growth factor
EGFP	Enhanced green fluorescent protein
ER	Endoplasmic Reticulum
ERAD	Endoplasmic-reticulum-associated protein degradation
EV	Empty vector
fALS	Familial ALS
FbS	Fetal bovine serum
FC	Flow cytometry
FDA	Food and drug administration
FTD	Frontotemporal dementia
FTLD	Frontotemporal lobar degeneration
FUS	Fused in Sarcoma
GABARAP	Gamma-aminobutyric acid receptor-associated protein
GAPDH	Glyceraldehyde-3-Phosphate Dehydrogenase
GFP	Green Fluorescent Protein
HBSS	Hank's Balanced Salt Solution
HD	Huntington disease
HDAC	Histone deacetylases
HEK293T	Human embryonic kidneys 293T
hnRNP	Heterogeneous nuclear ribonucleoprotein
HSE	Herpes simplex encephalitis
Hsc70	Heat shock protein of 70 kDa
Htt	Huntingtin
IKK	IκB kinase
IP	Immmunoprecipitation
iPSCs	Induced pluripotent stem cells
IRF	Interferon regulatory factor
KD	Kinase domain
KRAS	Kirsten rat sarcoma

KO	Knock-out
LAMP-2A	Lysosome-associated membrane protein type 2A
LB	Luria Bertani
LC3	Microtubule-associated proteins 1A/1B light chain 3B
LE	Late endosome
LIR	LC3- interacting region
LMN	Lower motor neurons
LRRK2	Leucine-rich repeat kinase 2
Lys	Lysine
MAPT	Microtubule-associated protein tau
MFI	Mean fluorescent intensity
MICOS	Mitochondrial contact site and cristae organizing system
mLST8	Mammalian lethal Sec13 protein 8
mRNA	Messenger RNA
mTOR	Mammalian target of rapamycin
MTOC	Microtubule organizing center
MVB	Multivesicular bodies
MW	Molecular weight
N2A	Neuro-2a
NBR1	Neighbour of BRCA1 gene 1 protein
NDP52	Nuclear dot protein of 52kDA
NEFL	Neurofilament Light Protein
NEMO	NFκB essential modulator
NES	Nuclear export signal
NFκB	Nuclear factor kappa-light-chain-enhancer of activated B cells
NHEJ	Non-homologous end joining
NLS	Nuclear Localisation Signal
NMJ	Neuromuscular junction
NSCLC	Non-small cell lung cancer
NT	Non-transfected
NUFIP1	Nuclear fragile X retardation-interacting protein 1
PAGE	Polyacrylamide gel electrophoresis
PAM	Proto-spacer sequence
PAS	Phagophore assembly site

PBS	Phosphate buffer saline
PCR	Polymerase chain reaction
PD	Parkinson's disease
PDK1	3-phosphoinositide-dependent kinase 1
PE	Phosphatidylethanolamine
PFA	Paraformaldehyde
PI3K	Phosphatidylinositol 3-kinase
PINK1	PTEN-induced kinase 1
PLS	Primary lateral sclerosis
PMA	Progressive muscular sclerosis
PPA	Primary progressive aphasia
PRAS40	Proline-rich AKT substrate of 40kDa
PRGN	Progranulin
PTPIP51	Mitochondrial resident tyrosine phosphatase-interacting protein-51
RAN	Repeat-associated non ATG
Raptor	Regulator-associated protein of mammalian target of mTOR
RILP	Ran-interacting lysosomal protein
RIPK1	Receptor-interacting serine/threonine-protein kinase 1
RBP	RNA binding protein
RNA	Ribonucleic acid
RNS	Nitrogen species
ROS	Reactive oxygen species
RRM	RNA recognition motif
RT	Room temperature
sALS	Sporadic ALS
SDS	Sodium dodecyl sulfate
SDD	Scaffold dimerization domain
SEM	Standard error of the mean
Ser	Serine
S	Serine
siRNA	Silencing RNA
SNARE	Soluble *N*-ethylmaleimide-sensitive factor attachment protein receptors

SOD1	Superoxide dismutase 1
STR	Short tandem repeat
SUMO	Small ubiquitin like modifier
TANK	TRAF Family Member Associated NFKB Activator
TAXBP1	Tax1 binding protein 1
TBK1	TANK binding kinase 1
TBS	Tris-buffered saline
TBS-T	TBS tween-20
TDP-43	TAR DNA-binding protein 43
TLR	Toll like receptor
TNF	Tumour necrosis factor
TRAF	TNF receptor associated factor
TUBA4A	Tubulin Alpha 4a
Ub	Ubiquitin
UBQLN2	Ubiquilin 2
UBD	Ubiquitin binding domain
ULK1	Unc-51 like autophagy activating kinase 1
UMN	Upper motor neurons
UPR	Unfolded Protein Response
UPS	Ubiquitin-Proteasome System
USP30	Ubiquitin carboxyl-terminal hydrolase 30
UVRAG	UV Radiation Resistance-Associated Gene Protein
VAPB	Vesicle-associated membrane protein-associated protein B
VCP	Valosin-containing protein
WES	Whole exome sequencing
WGS	Whole-genome sequencing
WIPI	WD repeat domain phosphoinositide-interacting protein
WT	Wild-Type
ZnF	Zinc finger
ΔNLS-TDP-43	TDP-43 without a nuclear localization signal

Units of magnitude

°C	celsius
Da	dalton/s
g	gravitational acceleration at the Earth's surface
g	gram/s
hr	hour/s
l	litre/s
m	metre/s
m	milli
M	molar
min	minute/s
n	nano
N	number of units in a dataset
p	p-value
rpm	revolution/s per minute
s	second/s
V	volt/s
X	magnification
μ	micro

Chapter 1

General introduction

1.1 Amyotrophic Lateral Sclerosis

Motor neuron disease (MND) or amyotrophic lateral sclerosis (ALS) is a neurodegenerative disease that is characterised by the loss of upper and lower motor neurons in the cortex, brainstem and ventral horn of the spinal cord. ALS is a progressive, mostly adult-onset disease that affects 1 per 300 people on average, and males are affected more frequently than females [proi1]. ALS overlaps pathologically and clinically with frontotemporal dementia (FTD), and ALS and FTD are thought to represent two ends of the same disease spectrum [2].

1.1.1 Clinical presentation

ALS is characterised by progressive motor deficits that usually lead to death within 3-5 years from symptom onset. Classical or "typical" ALS is associated with the progressive loss of both upper and lower motor neurons [3]. Other motor neuron diseases are associated with the predominate denervation of one group of motor neurons only, either upper or lower, and these types of diseases include primary lateral sclerosis (PLS) and progressive muscular atrophy (PMA). These diseases have a longer survival rate than ALS [4, 5].

Lower motor neurons innervate skeletal muscles, respiratory muscles and muscles responsible for facial expression and swallowing, therefore voluntary movement, speech and breathing are affected during ALS. However, motor neurons in the oculomotor nuclei and Onuf's nucleus remain unaffected until disease end-stages, therefore eye movement and sphincter control stay intact during the disease course [6]. The clinical presentation of ALS is very heterogenous and symptoms usually appear in one particular muscle group first before spreading to contiguous regions [7, 8]. Spinal or limb onset ALS is the most common form. Symptoms first appear in the upper limbs, manifesting in asymmetrical distal weakness [9]. In the lower limbs, foot drop or frequent tripping may be an early symptom. However, in 20% of patients, symptoms start in the bulbar region, and patients may experience slurring of speech due to impaired tongue movement [10, 11]. The least common form of ALS involves respiratory onset, which manifests in shortness of breath, dyspnoea or orthopnoea [9]. Regardless of the site of onset, gradual and progressive paralysis occurs, until finally the breathing muscles become affected and death occurs

due to respiratory failure. No specific diagnostic test is currently available for ALS and diagnose is based on the progression of symptoms and the exclusion of other conditions. The El Escorial or Awaji diagnostic criteria are a set of guidelines used to diagnose patients with ALS [12-14].

1.1.2 Epidemiology of ALS

A global literature analysis [15] based on 37 previous studies concluded that the mean age of onset of ALS is 61.8 +/- 3.8 years. In addition, diagnosis of ALS takes 12.6 months on average. In Europe, the median prevalence of ALS is 5,4 individuals per 100.000 and the incidence rate is 2,08 per 100.000 [15]. In the USA, the prevalence and incidence rates of ALS are lower; the prevalence is 3,4/100.000 persons while incidence of ALS is 1,75/100.000 individuals [15]. The lowest prevalence and incidence rates of ALS have been detected in Asian populations; where the prevalence is 2,34/100.000 and incidence is 0,6/100.000 persons [15]. The prevalence of ALS in Australia was 8,7/100.000 persons in 2015 (MND Australia website https://m.mndaust.asn.au/Get-informed/What-is-MND/Facts-and-figures).

1.1.3 Genetics of ALS

The majority of ALS cases (90%) are thought to be sporadic events (sporadic ALS-sALS), meaning that only one affected individual is present in an extended family. However, in 10% of cases, more than one family member is affected by ALS (familial ALS-fALS). Genetic studies involving whole-genome sequencing (WGS) or whole-exome sequencing (WES) of fALS families have identified a wide variety of mutations in genes that are causative or associated with ALS. Recent advances in sequencing techniques have led to studies identifying mutations in some sALS cases also.

Mutations in several major causative genes (*SOD1, TARDBP, FUS, C9orf72*) account for 60-70% of fALS cases and 10% of sALS cases [16]. Much rarer variants have also been identified in the following genes amongst others; *TBK1 [17, 18], ANG [19], CHCD10 [20], VAPB [21], VCP [22], MATR3 [23], CCNF [24], OPTN [25], p62 [26], UBQLN2 [27], DCTN1* [28]. A complete list of ALS causative genes is provided in **Table 1.1**. The above listed genes will be individually introduced below.

1.1.3.1 TDP-43

Transactive response DNA binding protein 43kDa (TDP-43) is a 414-amino acid protein encoded by the *TARDBP* gene on chromosome 1p36.22. It is a RNA/DNA binding protein that belongs to heterogenous nuclear ribonucleoprotein (hnRNP), and it comprises an N-terminal region with a nuclear localisation signal (NLS), two RNA recognition motifs (RRM1, RRM2), a nuclear export signal (NES), and a C-terminal region that contains the prion-like glutamine/asparagine rich region [29-34]. Almost all cases of ALS possess pathological forms of TDP-43 in affected motor neurons [2], highlighting its importance in ALS.

TDP-43 is ubiquitously expressed and localised to the nucleus due to its nuclear localisation signal [35], however it can also shuttle to the cytoplasm due to its nuclear export sequence [36, 37]. It was first identified as a repressor protein associated with HIV-1 transcription [38], and it is also known to be involved in mRNA splicing of cystic fibrosis transmembrane conductance regulator (CFTR) exons [37]. TDP-43 is involved in several stages of RNA metabolism, including transcription, translation, mRNA transport, mRNA stabilization, long-coding and microRNA processing [2, 39, 40]. Genome-wide RNA immunoprecipitation studies have revealed that more than 6000 mRNAs are associated with TDP-43, which represents 30% of the entire transcriptome [40-42]. More recently, novel roles for TDP-43 in DNA repair have been demonstrated [43-45].

TDP-43 was found to be the major component of the ubiquitinated insoluble aggregates in ALS and FTD brains [46, 47] in 2006. This pathological, aggregated form of TDP-43 is characteristically hyper-phosphorylated, ubiquitinated and C-terminally truncated (18–26, 35 kDa) [48-50]. The C-terminal fragments and both the cleaved and full-length protein are hyperphosphorylated in the aggregates [47, 49, 51]. TDP-43 pathology is present in almost all (97%) ALS cases and 45% of FTD cases [2, 52]. In ALS, TDP-43 also mislocalises from the nucleus to the cytoplasm [35, 47]. Furthermore, mutations in *TARDBP* are causative of 3.3% of fALS and 0.5% of all sALS cases [53]. Most ALS-associated mutations are located in exon 6 of the *TARDBP* gene, encoding the C-terminal glycine-rich region of TDP43. These mutations enhance the intrinsic aggregation prone behaviour of TDP-43 [54], therefore leading to increased cytoplasmic

aggregation [55]. The pathogenicity of TDP-43 is debated, whether this involves the loss of its normal nuclear function or from gain of a new toxic function in the cytoplasm.

The nuclear and cytoplasmic distribution of TDP-43 is tightly autoregulated. Depletion of nuclear TDP-43 leads to a loss-of-function and reduces its levels available for RNA processing, while increased cytoplasmic concentrations leads to a gain-of toxic function in ALS and FTD [56, 57]. The C-terminal fragment of TDP-43 associated with TDP-43 pathology has also been implicated in toxicity [58]. TDP-43 was recently shown to also be associated with stress granules, which are accumulations of untranslating messenger ribonucleoproteins [59, 60]. Mutant TDP-43^{G348C} accumulates in stress granules more than WT-TDP-43, and also incorporates into stress granules earlier than TDP-43 ^{WT}[61, 62]. Stress granules are formed when translation initiation is inhibited pharmacologically or by cellular stress [63]. There are now several mouse models available based on TDP-43. One transgenic mouse model that expresses human TDP-43 lacking the NLS (dNLS) has been shown to accumulate insoluble, phosphorylated cytoplasmic TDP-43 in the brain and spinal cord. Motor neuron loss, leading to progressive motor impairments, was also present [64]. TDP-43^{Q331K} mice develop age-dependent motor neuron disease accompanied by lower motor neuron loss, and loss and gain of splicing functions of selected RNA targets [65]. Furthermore, knockout of TDP-43 in neuronal cells in mice, leads to progressive motor neuron degeneration with ALS-like pathology [66]. This provides further evidence for both loss of function and toxic gain of function in disease.

The involvement of TDP-43 in the autophagy and ALS will be further detailed in section 1.2.7. Autophagy dysfunction in the pathophysiology of ALS.

1.1.3.2 C9orf72

C9 open reading frame 72 (C9orf72) also has an important role and ALS and FTD. In 2011, a hexanucleotide repeat expansion, GGGGCC, in the *C9orf72* gene , located on chromosome 9, was found to be the most frequent genetic cause of ALS and FTD in Europe and North America [67, 68]. This mutation is responsible for 22.5% of all fALS cases and 3.1% of all sALS cases worldwide [53]. Healthy individuals have less than 11 GGGGCC repeats [69-71], and while there is no clearly defined pathological threshold

regarding repeat numbers it is generally accepted that longer than 30 repeats is pathogenic. In fact, affected individuals may have up to several thousand repeats [70-73].

The GGGGCC hexanucleotide repeat expansion is transcribed directionally into repetitive RNA that forms sense and antisense RNA foci [74-78] that can be found in the frontal cortex and spinal cord of C9-ALS/FTD patients [79]. Furthermore, these foci are mostly detected in the nucleus and not in the cytoplasm [74, 76, 77]. This repetitive RNA is also known to be translated via a non-canonical translational mechanism; 'repeat-associated non-ATG (RAN)' translation, into 5 different dipeptide repeat protein (DPR); poly-GA, poly-GP, poly-GR, poly-PA and poly-PR [77, 78, 80-82]. The pathological mechanisms associated with C9orf72 remain unclear, but the repeat expansion may contribute to ALS via 3 different mechanisms; (1) loss of function of the normal C9orf72 protein by hapfloinsufficiency, (2) toxic gain of function from the RNA foci and (3) toxic gain of function from the DPRs.

In terms of loss of function, decreased levels of C9orf72 protein was detected in frontal cortex of ALS patients [83]. Furthermore, decreased transcript levels were detected in the brain [84] or lymphoblast cells lines [67] of ALS and FTD patients. Increased toxicity and aggregation of ataxin 2, which is associated with increased risk for ALS [85], was also demonstrated upon C9orf72 knockdown. GGGGCC repeat RNA forms secondary structures, including hairpins and highly stable G-quadruplexes, which can sequester RNA binding proteins leading to RNA toxicity [86, 87], and are also implicated in inducing DNA damage [88]. Gain of toxic functions via the generation of RNA foci are associated with reduced survival in neuronal cells [89] and motor axonopathy in zebrafish [90]. Alternatively, the C9orf72 repeat expansion may induce toxicity by the DPRs. DRP aggregates, which are p62 positive [91], are most commonly found in the cerebellum or hippocampus, and are rarely detected in the brainstem or spinal cord [91]. Interestingly, DRP pathology does not overlap with TDP-43 pathology [80, 92, 93]. Overexpression of DPR leads to neurodegeneration of the eye in Drosophila [94, 95]. A recently published mouse model showed that depletion of C9orf72 results in motor deficits in a dose dependent manner of C9orf72 depletion [96]. Furthermore, similar to abnormal RNA, the C9orf72 DRPs are thought to induce DNA damage [97].

The involvement of C9orf72 in the autophagy and ALS will be further detailed in section 1.2.7. Autophagy dysfunction in the pathophysiology of ALS.

1.1.3.3 FUS

Fused in sarcoma (FUS) is a 526 amino acid DNA/RNA binding protein that contains a N-terminal glutamine-glycine-serine-tyrosine rich (QGSY-rich) transcriptional activation domain, three arginine-glycine-glycine repetitive regions, an RNA recognition motif, Cys2-Cys2 zing finger (ZnF) motif, nuclear export signal and a C-terminus non-classical NLS [98, 99]. FUS was originally identified as an oncogene on chromosome 16 in liposarcoma [100]. Similar to TDP-43, FUS is a member of the hnRNP family and it is involved in DNA repair, RNA transport, translation and processing of microRNAs [101]. Furthermore, it also binds to promoter regions [102, 103] and transcription factors [104-107] to modify the transcription of target genes. Mutations in *FUS* were identified in 2009 [108] and cause 3% of all fALS cases and 0.4% of all sALS cases [53]. Also, similar to TDP43, FUS is mainly localised in the nucleus but it normally shuttles to the cytoplasm, and the cytoplasmic mislocalisation of FUS is present in ALS. The ALS mutations also mainly localise to NLS region of FUS [109-111]. The disease mechanisms associated with FUS include loss-of function in the nucleus due to depletion, and gain-of-toxic functions in the cytoplasm, such as induction of tau splicing [112], DNA damage and RNA splicing defects [113].

Several rodent models based on FUS are also available. Rats overexpressing human R521C mutant FUS develop paralysis and have reduced survival [114] highlighting a gain of toxic function. Transgenic mice expressing FUS^{R521C} under Syrian hamster prion promoter lead to significant and progressive neuronal loss however, no cytoplasmic inclusions were noted [115]. In contrast, mice expressing truncated FUS (1-359) remained asymptomatic until the final stages of disease but did display formation of massive FUS-positive inclusions and activation of microglia [116] indicating loss of function as an underlying mechanism.

The involvement of FUS in the autophagy and ALS will be further detailed in section 1.2.7. Autophagy dysfunction in the pathophysiology of ALS.

1.1.3.4 SOD1

The gene encoding copper/zinc superoxide dismutase 1 [117] (SOD1) was the first to be linked to ALS in 1993 [117] and the protein is localised to nucleus peroxisomes and mitochondrial intermembrane of eukaryotes [118-120]. SOD1 is highly conserved and ubiquitously expressed [121, 122] and it is responsible for the clearance of ROS by converting superoxide into hydrogen peroxide and molecular oxygen. Mutations in *SOD1*, chromosome 21, account for 18.9% of fALS cases and 1.2% of sALS cases [53]. Mutations in *SOD1* are generally thought to be pathogenic via gain of a toxic function. In contrast, mutations such as a recently identified novel mutation; p.Ser108LeufsTer15, resulting in an early stop codon; were undetectable in the insoluble protein fraction, despite having normal mRNA expression, potentially indicating that pathogenicity of this particular mutant may be due to the loss of activity [123].

Transgenic mice overexpressing human mutant SOD1 proteins are still the most widely used animal model for therapeutics, despite their reported drawbacks [124]. The most commonly used SOD1 mouse model harbours a Gly93 → Ala substitution; $SOD1^{G93A}$. These animals display disease onset at 3 months of age, that leads to progressive paralysis in the hindlimbs due to MN loss from the spinal cord, and they die at 5 months of age [125]. This mouse model carries 25 ± 1.5 copies of the human SOD1 transgene, so it has been criticised for displaying very high levels of protein expression. An improved mouse model carrys 8 ± 1.5 copies of human $SOD1^{G93A}$ transgene and has a slower disease progression with paralysis beginning at 6-8.5 months of age [126, 127]. Other SOD1 mice models have been developed including mice expressing human $SOD1^{G37R}$ [128], human G85R [129], or mouse G86R [130], however at more physiological levels.

The involvement of SOD1 in the autophagy and ALS will be further detailed in section 1.2.7. Autophagy dysfunction in the pathophysiology of ALS.

1.1.3.5 Genes mutated in the rarer cases of ALS

Optineurin

Optineurin is 67-kDa protein consisting of 577 amino acids and *OPTN*, the gene encoding optineurin, is located on chromosome 10 [131]. Optineurin contains domains that bind to LC3 and ubiquitin, and it also possesses a NFκB essential modulator (NEMO)-like domain, multiple coil-coiled motifs and C-terminal zinc finger [132-136]. It is involved in a wide variety of cellular functions including vesicular trafficking, autophagy, Golgi maintenance, and control of the NFκB pathway [137]. In 2010, mutations in *OPTN* were first detected in ALS patients [25] and they account for account for 4% of fALS and 0.4% of sALS cases in Asian populations, whereas this frequency is much lower in European populations (1.5 and 0.3%, respectively) [138]. These mutations have been shown in cellular models to induce Golgi fragmentation and perturb autophagosome degradation [139], while depletion of optineurin induces $SOD1^{G93A}$ aggregation [140]. Optineurin interacts with another protein known to be mutated in ALS; TBK1 [132]. TBK1 is the main focus of this thesis, therefore TBK1's involvement in ALS and its connection with optineurin will be detailed in Section 1.3.

The involvement of optineurin in the autophagy and ALS will be further detailed in section 1.2.7. Autophagy dysfunction in the pathophysiology of ALS.

CHCHD10

CHCHD10 is part of the mitochondrial contact site and cristae organizing system (MICOS) with mitofilin, CHCHD3 and CHCHD6, which is involved in the formation and maintenance of mitochondrial cristae structure [141]. Mutations in CHCHD10, chromosome 22, were identified in ALS in 2014 [20] and they contributes to less than 2% of fALS and 1% of sALS [142] and they are associated with impaired mitochondrial genome maintenance [141].

MATR3

MATR3 is nuclear matrix protein that binds to DNA and RNA and was shown to stabilise messenger RNA species [143, 144] . It also interacts with FUS and TDP-43 and

was shown to induce nuclear export defects in TDP-43 and FUS RNA [145]. Mutations in MATR3, chromosome 5, are observed in less than 1% of all ALS patients [23, 142].

CCNF

Cyclin F is member of the cyclin protein family and it is encoded by the *CCNF* gene and located on chromosome 16. Unlike other cyclins, cyclin F does not bind to cyclin dependent kinases, but it controls genome stability by ubiquitin mediated proteolysis because it is a part of an E3 ubiquitin ligase complex [146]. Cyclin F therefore assists in catalyzing the transfer of ubiquitin to specific proteins, targeting them towards the ubiquitin proteasome system (UPS) for degradation [147]. Mutations in *CCNF* were first associated with ALS in 2016 [24]. The ALS-linked mutant Ser621Gly was subsequently shown to impair the UPS, leading to TDP-43 accumulation in neuronal cells [148].

VCP

Valosin containing protein (VCP) is an AAA+ATPase involved in protein clearance and other cellular processes, including DNA repair and regulation of the cell cycle [149]. Mutations in VCP were identified in ALS in 2010 [22] and they account for 1-2% of fALS [22]. Cells containing ALS-associated mutations in VCP have impaired stress responses upon oxidative and ER-stress [150].

The involvement of VCP in the autophagy and ALS will be further detailed in section 1.2.7. Autophagy dysfunction in the pathophysiology of ALS.

VAPB

Vesicle-associated membrane protein-associated protein B (VAPB) is an ER tail-anchored transmembrane protein involved in membrane trafficking, lipid transport and metabolism. VAPB is located on chromosome 20 and was found to be mutated in ALS in 2004 [21].

The involvement of VAPB in the autophagy and ALS will be further detailed in section 1.2.7. Autophagy dysfunction in the pathophysiology of ALS.

Angiogenin

Angiogenin is a pancreatic ribonuclease that inhibits protein translation and it is also involved in rRNA biogenesis and proliferation [151-153]. *ANG* is located on chromosome 14 and it was originally identified in ALS patients from Ireland and Scotland [151]. Mutations in *ANG* are thought to cause loss of ribonucleolytic activity [154].

Ubiquilin 2

Ubiquilin 2 (UBQLN2) is a member of the ubiquitin like protein family and it delivers ubiquitinated proteins to the UPS for degradation [155]. Mutations in *UBQLN2* impair protein degradation leading to an abnormal protein aggregation and neurodegeneration [155]. Mutations in *UBQLN2* are found in ALS patients [27] furthermore, ubiquilin 2 inclusions can be seen in the spinal cord in patients with *UBQLN2* mutations [27].

Dynactin 1

Dynactin 1 is a subunit of dynactin and it forms a complex with dynein-1, a microtubule motor protein. This binding is critical in axonal transport of vesicles and organelles [156]. Mutation in the p150 subunit of *DCTN1* gene, located on chromosome 2, have been found in ALS and FTDALS patients [28]. Therefore, *DCTN1* mutations are thought to cause neurodegeneration by impairing axonal transport in motor neurons.

Table 1.1. List of ALS associated genes.

Protein	***Gene***	***References***
Superoxide dismutase 1	*SOD1*	[117]
Angiogenin	*ANG*	[19]
Sequestosome 1/p62	*SQSTM1/p62*	[26]
Dynactin 1	*DCTN1*	[28]
Vesicle-associated membrane protein (VAMP)-associated protein B	*VAPB*	[21]
Valosin-containing protein	*VCP*	[22]
TAR DNA binding protein-43 (TDP-43)	*TARDBP*	[47]
Fused in sarcoma	*FUS*	[108]

Ataxin 2	*ATXN2*	[85]
Optineurin	*OPTN*	[25]
Chromosome 9 open reading frame 72	*C9orf72*	[67]
TATA-binding associated factor 15	*TAF15*	[157]
Ubiquilin 2	*UBQLN2*	[27]
Profilin-1	*PFN1*	[158]
Human heterogeneous nuclear ribonucleoprotein A1	*hnRNPA1*	[159]
Human heterogeneous nuclear ribonucleoprotein A2B1	*hnRNPA2B1*	[159]
Coiled-coil-helix-coiled-coil-helix domain containing 10	*CHCHD10*	[20]
Matrin 3	*MATR3*	[23]
TANK-binding kinase 1	*TBK1*	[17]
Tubulin alpha-4A chain	*TUBA4A*	[160]
Sec1 family domain containing 1	*SCFD1*	[161]
Myelin-Associated Oligodendrocyte Basic Protein	*MOBP*	[161]
Chromosome 21 open reading frame 2	*C21orf2*	[162]
Cyclin F	*CCNF*	[24]
Never in mitosis gene A (NIMA)-related kinase 1	*NEK1*	[17]
Neurofilament, heavy polypeptide 200kDa, heavy chain	*NEFH*	[163]

1.1.4 Therapeutics for ALS

There is currently no effective ‘cure’ available for ALS, however two drugs have been approved for administration to patients. Riluzole was approved in 1995 by the US Food and Drug Administration (FDA) and currently is available worldwide [164]. Edavarone was approved by the FDA in 2017, but it is currently approved only in the USA and Japan [164]. The effectivity of riluzole has been analysed in several randomised clinical trials involving thousands of patients [165-167], which demonstrated that it

increased survival by 3 months on average, and it was mostly beneficial in later stages of ALS [168]. However, riluzole is not particularly effective because it has only a small effect on survival and, overall, it does not reduce mortality. The mechanism of action of riluzole, a benzothiazole, involves blocking the excessive release of glutamate, because it is a glutamate antagonist. Given that glutamate in an excitatory neurotransmitter [169], overstimulation of post-synaptic neurons in ALS leads to high Ca^{2+} levels in both neurons and glial cells, resulting in excitotoxicity [170, 171]. This subsequently leads to damage of DNA, RNA and mitochondria and induction of oxidative stress [172]. Riluzole is thought to inhibit the release of glutamate at the presynaptic neuron, inactivating voltage gated Na^{+} channels or by slowing inactivation of K^{+} channels [164].

Edavarone is the second FDA approved drug for ALS, which has been shown to improve motor function in ALS patients and delay disease progression significantly in its early stages. However it is only suitable for a small subpopulation of patients [173]. The molecular targets of edavarone are currently unknown, however it was shown to reduce the levels of 3-nitrotyrosine that are implicated in inducing oxidative stress [174], and thus it is thought to act as a reactive oxygen species (ROS) scavenger [175]. Furthermore, it may be protective against oxidative stress by upregulating peroxiredoxin-2 and downregulating protein disulfide isomerase A3 [176]. Due to the lack of effective therapies for ALS there is currently an unmet and pressing need to identify common pathways and cellular mechanisms relevant to patients that allow the development of more effective drugs.

1.1.5 The ALS-FTD spectrum and ALS variants

PLS and PMA are motor neuron diseases where the upper or lower motor neurons undergo degeneration but not both.

1.1.5.1 Primary lateral sclerosis

PLS is part of the ALS spectrum and affects mainly upper motor neurons [177-179]. 1-3% of all ALS patients have PLS [179, 180]. Patients may represent with clumsiness or poor coordination [181] and during examination, upper motor neuron signs are present, including spasticity and spread of reflexes. Lower motor neuron findings such as fasciculations and muscle wasting are absent [181]. Average age of onset is 46.9+/- 9

years [182], which is lower than of ALS. The median survival may be up to 19 years, hence patients survive much longer than ALS [180].

1.1.5.2 Progressive muscular atrophy

For patients with PMA, affecting lower motor neurons, a significant proportion (22-35%) will develop ALS due to later involvement of upper motor neurons [183]. The incidence of PMA is 0.02/100.000 people and it is more common in men than in women, similar to other motor neuron diseases. The mean age of onset is higher than of ALS. The symptoms of PMA are characteristic of lower motor neurons, involving flaccid weakness, muscle atrophy, fasciculations, and hyporeflexia or areflexia [184].

1.1.5.3 Frontotemporal dementia

Frontotemporal dementia (FTD), involving frontotemporal lobar degeneration (FTLD), is a progressive neuronal atrophy affecting the frontal and temporal cortices. FTD may manifest as either behavioural changes, which is termed 'behavioural variant FTD (bvFTD)' [185] or in the impairment of language skills, which is called 'primary progressive aphasia (PPA)' [186]. FTD is the most common dementia affecting people under the age of 60 [187]. FTD has a strong genetic component; on average 30% of cases are familial, particularly bvFTD, (48%), although this true for only 12% of PPA cases [188]. Microtubule-associated protein tau (*MAPT*) [189] and progranulin (*PRGN*) [190, 191] were the first genes identified as causative in FTD, and the majority of familial cases are due to mutations in these genes and *C9orf72* [67, 68, 192]. Other genes are mutated less frequently in FTD include *TARDBP* [46, 47], *FUS [193], UBQLN2 [194], VCP [195], SQSTM1 [196], TBK1 [197, 198]* and *OPTN [197],* thus highlighting the strong link with ALS. Protein aggregation is also characteristic of FTD, similar to ALS, and TDP-43 is found in the ubiquitinated aggregates in motor neurons of 45% FTD patients (FTLD-TDP) [2]. Tau positive aggregates are found in a similar proportion of patients (FTLD-tau) [2], and FUS can also be present (9%, FTLD-FUS) [2]. Approximately 15% of FTD patients meet the criteria for ALS, and vice versa [2]. Therefore, ALS and FTD are clinically, pathologically and mechanistically linked. It is now accepted that ALS and FTD represent the two ends of the same disease spectrum [2].

1.1.6 Pathophysiology of ALS

The underlying disease mechanisms involved in ALS are not very well understood. A variety of cellular mechanisms have been proposed to explain pathophysiology, including the presence of protein aggregates, RNA toxicity, excitotoxicity, neuroinflammation, impaired axonal trafficking, ER stress, DNA damage, mitochondria dysfunction and dysfunctional autophagy (reviewed recently in [199]).

1.1.6.1 Protein aggregation

The presence of insoluble ubiquitinated protein aggregates in affected tissues are the characteristic pathological hallmark of ALS. Protein aggregates are insoluble, oligomeric complexes that form due to partial unfolding caused by mutation or RNA modification and can be of variable size. In contrast, inclusion bodies are intracellular sequestration of aggregated proteins that are usually visible with a light microscope [200]. In familial forms of disease the proteins that are mutated misfold and form inclusions, including SOD1 [201], FUS [202, 203], optineurin [204] and C9orf72 [67]. However, whilst the genes associated with ALS are mutated in only a small fraction of ALS patients, wildtype forms of several of the proteins encoded by these genes aggregate in a much wider range of patients. The typical example is TDP-43 which, as described above, is present in ubiquitinated aggregates in 97% of ALS cases [2]. In addition, inclusion bodies containing SOD1 are also common [205, 206], furthermore aggregates of misfolded SOD1 have prion-like capabilities and can be transmitted from cell to cell [207, 208]. The presence of protein aggregates is not restricted to ALS and it is a general characteristic of many neurodegenerative diseases such as FTD, Alzheimer's disease, Parkinson's disease and Huntington's disease [209].

In ALS, the misfolded protein inclusions are present in motor neurons and surrounding glial cells [201]. The majority of these aggregates are skein-like inclusions or Lewy body-like hyaline inclusions, which appear as randomly oriented filaments covered with fine granules that are ubiquitinated [49, 210, 211]. Bunina bodies can also be detected, which are small eosinophilic ubiquitin-negative inclusions that consist of amorphous electron-dense material, surrounded by tubular and vesicular structures [212]. Wildtype TDP-43 is present in the aggregates in spinal cord motor neurons, hippocampal and frontal cortex neurons and glial cells, in all sALS patients and in SOD1-negative

fALS patients. However, interestingly, TDP-43 aggregates are rarely found in SOD1-associated ALS [213, 214].

The underlying cause for the aggregation of misfolded proteins is debated, but the presence of low-complexity domains in TDP-43 and FUS renders them more prone to form inclusions and stress granules, leading to dysfunction in protein degradation pathways [215]. Misfolded or unfolded proteins can be degraded by either the UPS or via autophagy, and dysfunction in both processes are implicated in the pathophysiology of ALS. The UPS typically degrades soluble proteins, whereas insoluble protein aggregates are usually removed by autophagy [216].

1.1.6.2 RNA toxicity

Being RNA binding proteins (RBPs), TDP-43 and FUS function in the co-ordination of transcription, splicing regulation, miRNA biogenesis, stabilization of long introns and stress granule formation [2, 39, 40] [101-103] [104-107]. Hence, due to the importance of TDP-43 pathology in ALS and the presence of mutations in both proteins in ALS, the role of dysfunctional RNA metabolism is now implicated as an important disease mechanism in ALS. Both TDP-43 and FUS bind to a similar number of RNA targets in the brain; 6000 for TDP-43 and 5500 for FUS, representing 30% the transcriptome [101] [40, 41]. Therefore, depletion of TDP-43 and FUS from the nucleus in ALS is thought to dysregulate RNA metabolism. The C9orf72 mutation has also been implicated in RNA toxicity, due to the production of expanded RNA containing the repeat, forming intranuclear RNA foci that may trap RNA-binding proteins, therefore inhibiting their functions [67].

Other proteins, such TAF15 and angiogenin, are also linked to RNA dysfunction. TAF15 is mutated in ALS and it normally functions in DNA damage and repair, and RNA processing [217-220]. However, upon mutation in ALS TAF1 aggregates and causes neurodegeneration in Drosophila models.

1.1.6.3 Excitotoxicity

During glutamatergic neurotransmission, glutamate is released from the presynaptic membrane, which activates ionotropic glutamate receptors on the postsynaptic membrane. This opens Na^+ and Ca^{2+} channels leading to depolarization of the postsynaptic membrane and generation of the action potential. Excitotoxicity refers to neuronal cell death due to the overstimulation of glutamate receptors [221]. Excitatory amino acid transporter 2 (EAAT2) is the most important glutamate transporter expressed by astrocytes. EAAT2 function is perturbed in both fALS and sALS patients both in the cortex and spinal cord [222-224], possibly due to its downregulation [225, 226]. In the $SOD1^{G93A}$ mouse model of ALS, the loss of EAAT2 is an early event in disease course [227], and disease onset can be delayed by its overexpression [228]. Excitotoxicity may also result from increased release of glutamate. *In vitro* studies using synaptosomes from $SOD1^{G93A}$ mice showed increases in the basal glutamate flux compared to synaptosomes from $SOD1^{WT}$ mice, and they also displayed increased glutamate release upon depolarization [229]. Compelling evidence for glutamate excitotoxity as a pathogenic mechanism in ALS is that riluzole that prolongs survival, which is a glutamate antagonist [165-167]. The theory of excitotoxity as a potential underlying cause for ALS has been challenged by several studies [230, 231], therefore this needed to be carefully considered'

1.1.6.4 Non-cell autonomous mechanisms

Neuroinflammation is characterised by the activation of microglia (microgliosis) and astrocytes (astrogliosis), infiltration of T-cells and overproduction of inflammatory cytokines in the central nervous system (CNS). Astrogliosis and microgliosis are considered to be pathological hallmarks of ALS [232, 233]. Microglia are the primary innate immune cells of the CNS. They continuously survey the CNS and upon infection, cellular damage or due to the presence of protein aggregates, they become active, whereby they change their morphology from ramified to amoeboid and clear cellular debris by phagocytosis [233]. During this process they may also release proinflammatory cytokines or reactive oxygen species that can cause neuronal death. Microglia can acquire two different activation states, and M1 classically activated and M2 alternatively activated, are the most commonly described forms. M1 microglia are considered to be cytotoxic because they secrete proinflammatory cytokines and have impaired phagocytic activity.

In contrast, M2 microglia secrete autoinflammatory cytokines and therefore are considered to be cytoprotective [234].

Astrocytes have multiple homeostatic functions in the CNS; they maintain the blood brain barrier, provide neurotrophic support for MNs, and they regulate the plasticity of synapses and synthesis of neurotransmitters [235-237]. Astrocytes are also implicated in the progression of ALS. Lack of mutant $SOD1^{G93A}$ expression in astrocytes leads to slower decease progression but does not affect disease onset [238, 239]. In contrast, MN specific depletion mutant $SOD1^{G37R}$ however delays disease onset [240, 241]. Similar to microglia, two subset of astrocytes have been described in adult CNS, A1 and A2 with A1 reactive astrocytes associated with motor neuron and oligodendrocytes death [242-244].

Oligodendrocytes myelinate the axons in the CNS. TDP-43 pathology is present in oligodendrocytes during ALS [46, 213, 214]. Patient carrying mutant FUS^{R521C} or FUS^{P525L} have cytoplasmic FUS inclusions in the oligodendrocytes [245]. Oligodendrocyte loss is detected in $SOD1^{G93A}$ mice furthermore it proceeds MN loss and resulting in only partially myelinates MN axons [246, 247] .

While ALS is characterised by the selective death of motor neurons, several studies have shown that microglia, astrocytes and oligodendrocytes contribute to the development of ALS. SOD1 transgenic mouse models shed light on the role of non-neuronal cells in ALS. Mutant $SOD1^{G37R}$ expression only in neurons, driven by the neurofilament light chain promoter, in mice does not lead to neurodegeneration [248, 249], whereas in chimeric mouse models, an ALS phenotype was apparent only when glial cells express mutant SOD1 as well as motor neurons [250]. In mice expressing mutant $SOD1^{G85R}$ in motor neurons but not astrocytes or microglia, disease progression is significantly delayed and survival is prolonged [239, 241, 251]. Mutant SOD1 expressing astrocytes are toxic for motor neurons. However this toxicity is cell specific; neurons in the dorsal root ganglion or interneurons are not affected by toxic astrocytes. Furthermore, mutant SOD1 fibroblast or cortical neurons are not toxic to co-cultured MNs [252-255]. SOD1 microglia purified from mice is toxic for human derived MNs [256]. This indicates that SOD1 toxicity can originate from glial cells and that these cells have an important role in disease progression of ALS [241, 257]. Furthermore, the degree of

microgliosis in living ALS patients has also been shown to correlate with the severity of ALS [258].

1.1.6.5 Impairment of axonal transport

Intracellular trafficking is responsible for the distribution of organelles, protein, mRNA and membrane bound vesicles within the cells. Efficient cellular trafficking is particularly important for all neurones due to their specialised morphology. Motor neurons may be especially vulnerable to trafficking disturbances because their axons may stretch for up to a metre in length in an adult human. Most protein synthesis occurs in the cell body (although local translation of proteins in the neurities is increasingly recognised), therefore axonal trafficking is required for transport along the axon.

In neurons, microtubules and neurofilaments are the major cytoskeletal filaments. Microtubules are rigid hollow rods composed of alpha and beta tubulin and they are polarised, constantly growing at the positive end and decreasing at the negative end. Interestingly *TUB4A*, the gene encoding tubulin alpha 4a, is mutated in a proportion of ALS patients [160]. Microtubules are uniformly oriented in axons [259], with their negative end pointing towards the cell body [259]. Motor proteins are responsible for the movement of cargo along microtubules in a unidirectional manner; kinesins move cargo towards the plus end, whereas dynein transport cargo towards the negative end [260]. Therefore, kinesins mediate anterograde transport (away from the cell body) while dynein mediates retrograde transport (towards the cell body). In contrast it was shown that motor protein such as dynein's are structurally flexible and that allows a so called 'backstepping" when dynein can move cargo *in anterograde direction opposite to its normal transport direction* [261, 262]. Mutations in dynactin [28], a co-factor of dynein, and kinesin, a motor proteins that moves along the microtubules, are also present in ALS patients [263]. Neurofilaments are intermediate filaments of the neurons and *NEFH*, the gene encoding neurofilament heavy polypeptide, is mutated in a proportion of ALS patients [163]. Post-mortem analysis of ALS patient motor neurons revealed the presence of abnormally accumulated phosphorylated neurofilaments [264, 265], and mitochondria and lysosomes also accumulate at the proximal axon of large motor neurons. Transport of axonal cargo slows down or even pause while passing by stationary organelles such as mitochondria or endosomes [266]. Research indicated that bulky axonal structure can

significantly alter both retrograde and anterograde axonal transport and this may be linked to neurodegeneration [266].

Axonal transport defects are well documented in ALS. In the $SOD1^{G93A}$ mouse model of ALS, defective dynein mediated retrograde axonal transport is present [267, 268]. Furthermore, retrograde axonal transport defects in motor neurons are already present at embryonic stages in $SOD1^{G93A}$ mice [267]. Abnormal distribution of mitochondria was also detected in SOD1 mice [269, 270]. ALS mutant forms of $VAPB^{P56S}$ and $TDP\text{-}43^{A315T}$ expressed in mice also lead to abrogated mitochondria axonal transport [269, 271, 272]. Dynein is also responsible for the retrograde axonal transport of autophagosomes along the axon [273]. These studies together indicate that functional axonal transport is an important process for neurons and that dysfunctional axonal transport may have multiple harmful consequences for motor neurons.

There is also evidence that other forms of cellular trafficking are perturbed in ALS. The normal cellular function of C9orf72 involves cellular trafficking in conjunction with several Rab proteins [274]. Rabs belong to the small GTPases and they are master regulators of intracellular membrane trafficking [275]. Mutations in another ALS gene, *ALS2,* which encodes alsin, a Rab GEF for Rab5 disturb Rab5-GEF activity and impair endosome and α-amino-3-hydroxy-5-methyl-4-isoxazolepropionic acid (AMPA) receptor trafficking [276, 277]. ALS mutant TDP-43 was recently shown to impair endosomal trafficking [278] and ALS mutant optineurin inhibits trafficking from the Golgi to plasma membrane [139]. ER-Golgi trafficking is also known to be perturbed by ALS mutant forms of SOD1, TDP-43 and FUS [279]. Consistent with these studies, fragmentation of the Golgi apparatus is a well described feature in ALS patients, and animal and cellular models [280].

1.1.6.6 ER-stress and unfolded protein response

The endoplasmic reticulum (ER) is a dynamic intracellular organelle consisting of membranous tubular structures located in the cellular perinuclear region. It is responsible for protein synthesis, post-translational modifications, protein folding, Ca^{2+} storage and the synthesis of phospholipids. ER stress is induced when misfolded or unfolded proteins accumulate in the ER. The unfolded protein response (UPR) is a

cellular response that aims to restore ER homeostasis. During the UPR, ER-chaperones are upregulated to prevent protein aggregation and facilitate proper protein folding. Protein translation is temporarily inhibited and degradation of unfolded proteins is initiated via activating endoplasmic reticulum-associated protein degradation (ERAD). ER-stress is now widely described in ALS. Changes in ER morphology are present in ALS patients, such as fragmentation [281], dilated ER or wavy membranous structures lacking ribosomes extending from the ER [282]. ER stress and induction of the UPR are present in sporadic [283] and familial ALS patients. Mutations in ALS-linked proteins such as SOD1 [284], TDP-43 [59], FUS [285] and UBQLN2 impair[286] ER to Golgi transport *and this either initiates or* enhances ER-stress[279]. ER-stress can be induced *in vitro* by ALS mutant forms of FUS [285], TDP-43 [59], and C9orf72 [287]. Importantly, in SOD1 mouse models, ER stress is present early in disease and the most vulnerable motor neurons to degenerate develop ER stress [288]. These studies clearly show that ER stress is a widespread phenomenon in ALS.

1.1.6.7 DNA damage

Genomic integrity is essential for all cells, but particularly for neurons due to their high metabolic turnover and transcription-associated continuously open chromatin state, that renders them much more susceptible for DNA damage [88]. Furthermore, being post mitotic, neurons are not capable repairing damaged DNA via homologous recombination (HR) which is present only in dividing cells [289, 290]. Instead they perform the much more error prone mechanism of DNA repair; non-homologous end joining (NHEJ). Double stranded breaks (DSBs) are the most severe form of DNA damage, that can lead to chromosome rearrangements and cell death.

DNA damage is becoming increasingly implicated in ALS. ALS patients carrying C9orf72 expansions showed more DSBs and upregulation of DNA-damage repair (DDR) markers [97]. The accumulation of R-loops and DSBs, indicating genomic instability, are also associated with C9orf72 expansions [291]. FUS is involved in DSB repair by mediating HR and NNHEJ-related repair [292]. In fact, inactivation of FUS leads to an 80% decline in DNA repair mechanisms *in vitro* [293] and ALS patients carrying FUS mutations show increased DNA damage [293]. More recently, TDP-43 has also been linked to DNA damage, and loss of nuclear expression of TDP-43 is linked to impaired

DNA repair [45]. Oxidative DNA damage has also been implicated as a contributing factor to ALS. However, mutations in SOD1, a free radical scavenging enzyme, do not lead to DNA damage [294, 295]. Nevertheless, these data show that DNA damage may be an important underlying disease mechanism in ALS or potentially consequence of disease progression.

1.1.6.8 Oxidative stress

Oxidative stress is characterised by an increase of ROS or nitrogen species (RNS) within cells and it has been linked to ALS [296]. Several oxidation products, including malondialdehyde, hydroxynonenal, and oxidized proteins, DNA or membrane phospholipids, are elevated in ALS patients [297-301] and mouse models of ALS [125, 302-304]. Mutations in SOD1 increase neuronal vulnerability to oxidative stress [305].

1.1.6.9 Mitochondria dysfunction

Mitochondria are the powerhouses of the cell, with important functions in ATP production, phospholipid biogenesis [306], calcium homeostasis [307] and the induction of apoptosis [308]. Neurons have a high metabolic rate, and given that the brain consumes 20% of the body's resting ATP production [309], they therefore rely heavily on efficient mitochondrial function. Mitochondrial dysfunction has been long been associated with ALS. Aggregated, swollen and vacuolated mitochondria have been observed in motor neurons of ALS patients [310, 311]. The consequences of mitochondria damage in ALS are thought to be defective ATP production [312], oxidative stress [301, 313-315] or generation of pro-apoptotic signalling [316]. Mitochondrial dysfunction has also been recapitulated in animal models of ALS; WT and ALS mutant TDP-43 overexpression leads to aggregated, fragmented and vacuolated mitochondria *in vitro* and *in vivo* [317-319], whereas overexpression of mutant SOD1 leads to elongated, swollen and aggregated mitochondria [269, 320] and perturbation of axonal transport of mitochondria [321]. Furthermore, in mouse primary neuron isolated from mutant FUS expressing mice (R521G, R521H) showed shortened mitochondria [322]. Hence several mutant proteins cause mitochondria dysfunction in ALS.

1.1.6.10 Autophagy dysfunction

Autophagy is a lysosomal degradation system in which the cargo to be degraded is delivered to the lysosome via a chaperone-mediated mechanism, or via the formation of a double membrane vesicle, called an 'autophagosome'. Autophagy is the only degradation system thought to degrade insoluble protein aggregates [216]. Due to the accumulation of misfolded protein inclusions in ALS patients, autophagy dysfunction is strongly implicated in ALS pathology. Furthermore, several proteins that are involved in autophagy, including, optineurin, TBK1, p62, VCP, and ubiquilin2, are mutated in ALS and FTD patients, providing further evidence that autophagy is relevant in pathophysiology. In addition, mutant forms of other ALS-linked proteins, including SOD1, TDP-43 [323], FUS [324] and C9orf72 [325] lead to dysfunctional autophagy both *in vitro* and *in vivo* (discussed in detail in section 1.8), further suggesting that autophagy dysfunction is an important pathway in ALS. The role of autophagy in ALS is a major focus of the studies described in this thesis. Hence autophagy and its detailed mechanisms of action during ALS and it potential links to TBK1 will be further described in details in the following sections.

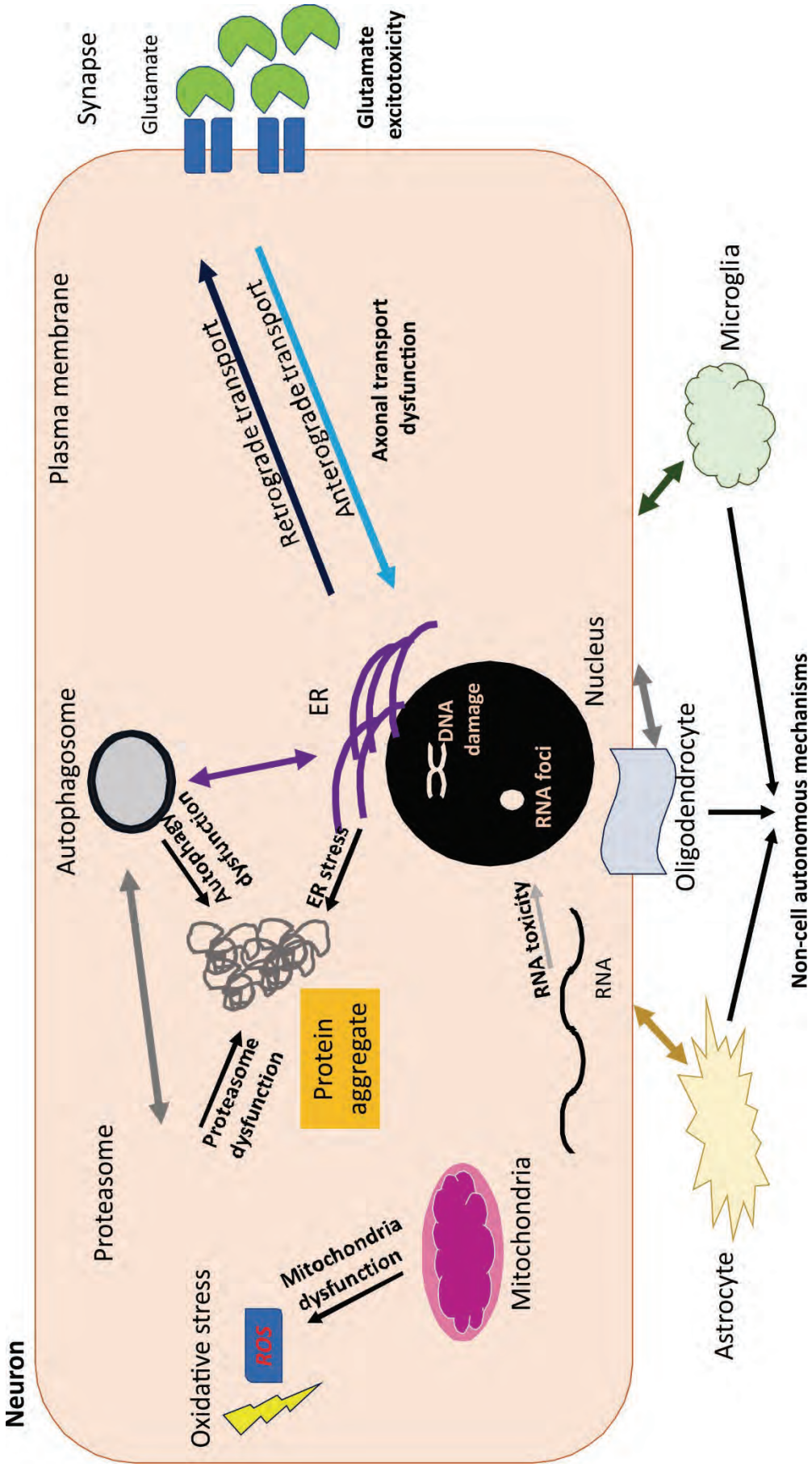

Synapse
Glutamate
Glutamate excitotoxicity
Plasma membrane
Retrograde transport
Anterograde transport
Axonal transport dysfunction
Microglia
Autophagosome
ER
DNA damage
RNA foci
Nucleus
Autophagy dysfunction
ER stress
Oligodendrocyte
RNA toxicity
RNA
Protein aggregate
Proteasome dysfunction
Proteasome
Non-cell autonomous mechanisms
Mitochondria
Mitochondria dysfunction
Astrocyte
Oxidative stress
ROS
Neuron

Figure 1.1. Underlying pathomechanisms in ALS. Protein aggregations are the hallmark of ALS, that arise due to ER-stress, autophagy dysfunction and/or impaired proteasome system. Impaired axonal transport, RNA toxicity, oxidate stress and mitochondria dysfunction are also potential underlying mechanism for ALS. Glia cells contribute to MN death via non-cell autonomous mechanism.

1.2 Autophagy

Autophagy is a bulk degradation system involving the degradation of proteins, organelles, portions of the cytoplasm, or even invading bacteria. Degradation is mediated by hydrolytic enzymes that are localised within lysosomes.

1.2.1 Types of autophagy in mammalian cells

In mammalian cells, three types of autophagy exist: chaperone mediated autophagy, microautophagy and macroautophagy.

1.2.1.1 Chaperone mediated autophagy (CMA)

CMA involves the degradation of target proteins recognised by a specific amino acid motif, the pentapeptide (KFERQ) [326] **(Figure 1.2)** . Heat shock protein 70-kDa (Hsc70) recognises this motif [327] and targets substrates to the lysosome, where Hsc70 interacts with lysosome-associated membrane protein type 2A (LAMP-2A) [328]. Substrates need to first unfold in order to cross the membrane of the lysosome [329], and this is followed by their degradation via hydrolytic enzymes. Approximately 40% of the mammalian proteome contain the KFERQ-like motif, which therefore can be degraded by CMA [326].

1.2.1.2 Microautophagy

Microautophagy is a process mostly so far described in yeast by which randomly selected portions of cytosol and intracellular organelles such as nucleus, peroxisomes and mitochondria are degraded by direct invagination of the lysosomal membrane [330-332] **(Figure 1.2)**. Microautophagy has been mostly researched in yeast, but the yeast genes involved in this process are not present in mammals. Hence, it is has been speculated that microautophagy takes place in late endosomes/multivesicular bodies (LE/MVB) instead of lysosomes in mammals, in a process termed ‘endosomal microautophagy’ [333]. Endosomal microautophagy overlaps with CMA somewhat because Hsc70 targets protein substrates containing the KFERQ-motif towards microautophagy [333-335]. Microautophagy is an integrated component of

starvation-induced autophagy [336] that occurs independently of mammalian target of Rapamycin (mTOR)-mediated autophagy and canonical macroautophagy.

1.2.1.3 Macroautophagy

The most well-known type of mammalian autophagy is macroautophagy, which involves the formation of a double membrane vesicle (the 'autophagosome') around the cargo for degradation, which may be damaged organelles, part of the cytosol or protein aggregates [337] **(Figure 1.2)**. The autophagosome then fuses with the lysosome and its contents are degraded [338]. It was long thought that macroautophagy, (termed simply 'autophagy' from here onwards) is a non-selective, bulk degradation system that allows the recycling of resources. However, it is now recognised that autophagy is a highly selective process that maintains intracellular homeostasis under basal and under cellular stress conditions [337].

Autophagy begins with the formation of the isolation membrane or 'phagophore', a small cup-shaped precursor of the autophagosome membrane formed upon induction of autophagy. It is now accepted that phagophores are formed *de novo* by nucleation of pre-existing membranes. In yeast, the phagophore forms at a specific 'phagophore assembly site' (PAS) [339]. In mammalian cells, however, a similar site has not been identified, thus phagophores are thought to form at multiple different cellular locations. The phagophore then elongates and encloses around the cargo, forming the autophagosome, which then fuses with endosome, forming amphisomes [338]. When the autophagosome is fully mature it fuses with the lysosome, forming an autolysosome [338]. The pH is acidic within the autolysosome, therefore the lysosomal enzymes degrade its cargo into macromolecules, which are then recycled. Ubiquitination of cargo is a signal for autophagic degradation, similar to the UPS [337].

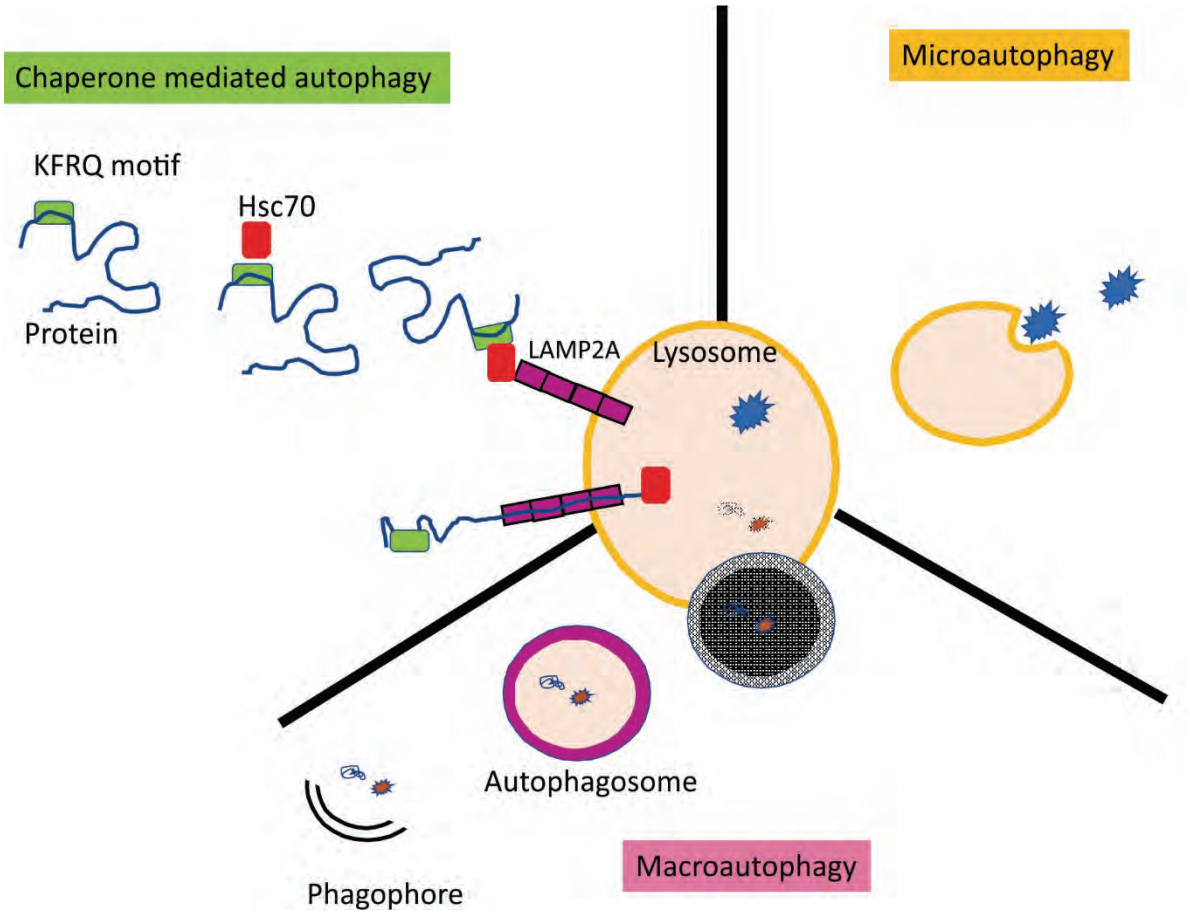


Figure 1.2. In mammalian cells micro-, macro-, and chaperone mediated autophagy exists. Microautophagy degrades proteins via direct invagination of lysosomal membrane. During chaperone mediated autophagy, Hsc70 carries the protein towards the lysosome for degradation. In macroautophagy, the autophagosome forms around the cargo that fuses with lysosome, leading to cargo degradation.

1.2.2 Autophagic machinery

The first description of autophagy and identification of autophagy related genes was in yeast, where in protease deficient yeast strains, autophagic bodies accumulated upon nitrogen, carbon and amino acid starvation [340]. Mutagenesis of these strains led to the discovery of the first autophagy related genes (atg); atg1 and atg2 [341]. The same study postulated that at least 15 more genes are involved in vacuole formation in yeast [341]. It is now recognised that atg1 is a serine-threonine protein kinase, which is a homologue of the Unc1 protein kinase in *C. elegans* [342]. In mammalian cells, atg1 is called Unc-51 Like autophagy activating kinase 1 (ULK1), which is a target of the mTOR

kinase [343]. ULK1 is the first complex involved in autophagy that initiates the formation of the phagophore.

Altogether, there are five protein complexes that are necessary for the formation of the autophagosome; (1) ULK1 protein complex kinase, (2) class III PI3K-kinases complex, (3) Atg9- WD-repeat protein interacting with phosphoinositides (WIPI) complex, (4) Atg12 conjugation system and (5) Atg8 (LC3) conjugation system **(Figure 1.3)**.

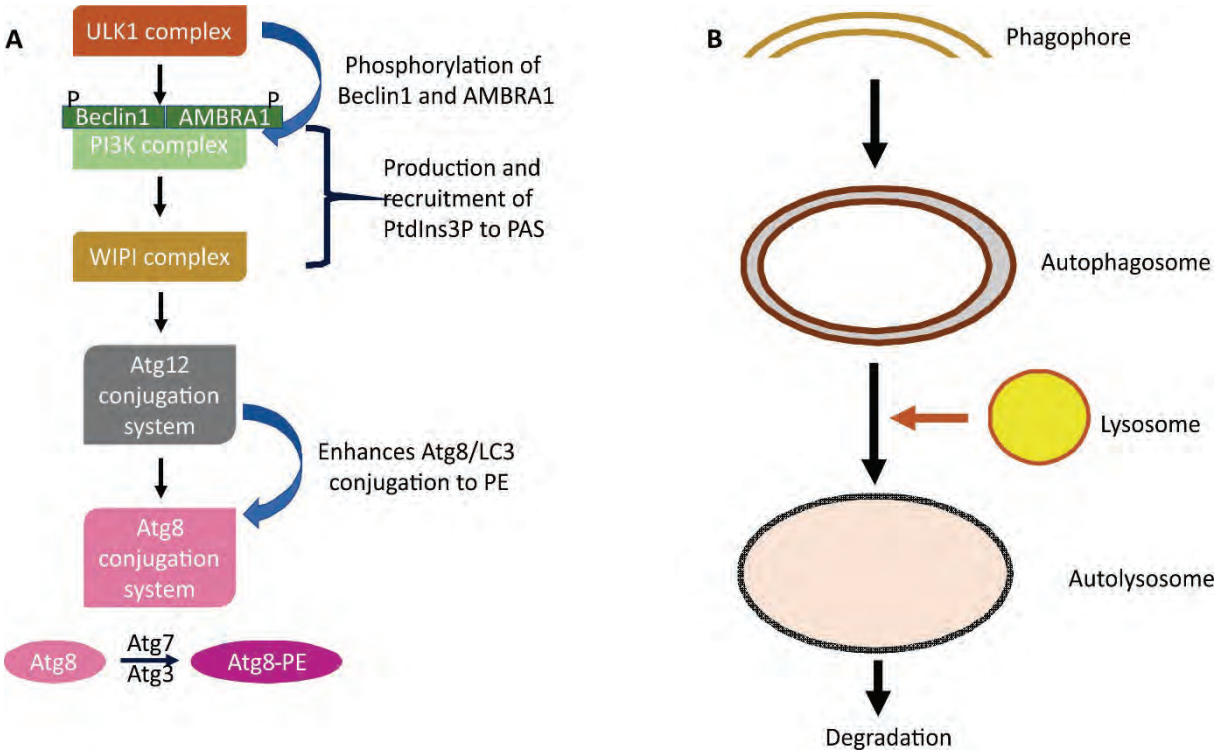


Figure 1.3. Macroautophagic machinery. (A) Five complexes take part in the initiation of autophagy. The ULK1 complex leads to the phosphorylation of Beclin1 and AMBRA1 in the PI3K complex, which contributes to the recruitment of PtdIns3P to the phagophore assembly site. The atg12 conjugation system enhances the lipidation of LC3/atg8 and it facilitates the elongation of phagophores. **(B)** Formation of phagophore is followed by engulfment of the double layered membrane, forming the autophagosome. The autophagosome then fuses with the lysosome and the degradation of cargo takes place in the autolysosomes.

The ULK1 protein complex consists of ULK1, atg13, focal adhesion kinase (FAK)-family interacting protein of 200 kDa (FIP200) and atg101. Mammalian target of

rapamycin complex 1 (mTORC1) directly phosphorylates atg13 and ULK1 [344], which normally prevents the induction of autophagy. However, upon mTORC1 inactivation, the inhibition of ULK1 complex is released, therefore ULK1 can now phosphorylate Beclin1 and its regulator autophagy and beclin 1 regulator 1 (AMBRA1) which is part of the class III phosphatidylinositol 3-kinase **(**PI3K) complex [345, 346].

Class III phosphatidylinositol 3-kinase (PI3K) complex is responsible for the production of phosphatidylinositol inositol 3-phosphate (PtdIns3P) and recruitment of the autophagic machinery to the PAS [347]. PtdIns3P is an inverted, cone-shaped membrane lipid that creates a platform for the binding of membrane active proteins [348]. Three different PI3K complexes exist in mammalian cells. atg14/PI3KR4/PIK3C3/Beclin1 is involved in the formation of autophagosomes, the UVRAG/PI3KR4/PIK3C3/Beclin1 complex mediates autophagosomes/lysosome fusion and endocytic trafficking, and the Rubicon/UVRAG/PI3KR4/PIK3C3/Beclin1 complex inhibits autophagosome maturation and endocytic trafficking [347]. PtdIns3p facilitates the recruitment of autophagy proteins such as the WIPIs to the membrane [349].

The Atg9 and WIPI complex provides a stage for vesicle nucleation and it recruits PtdnIs3P binding proteins to the PAS [350]. Atg9 is normally localised in the Golgi [351, 352], however upon starvation it relocates to the ER and is involved in delivering membranes to the expanding phagophore site. The last two steps of autophagosome formation involves two conjugation systems [353].

The Atg12/Atg5/Atg16L1 conjugations system is the first of these. Atg12 is activated by atg7, an E1-like enzyme, then atg12 is conjugated to atg5 via an E2-like enzyme, atg10 [354, 355]. This is followed by covalent interaction of Atg16L1 with atg12-conjugated atg5 but not unconjugated atg5. Atg16L1 then oligomerises which leads to cross-linking of atg5 with atg16L1 and the formation of a stable protein complex. Atg16L1 is not essential for atg12-atg5 conjugation, however the Atg12-Atg5 conjugate requires atg16L1 to accomplish its role in autophagy [356]. Furthermore, the formation of this complex and its activity in autophagy depends on the oligomerization state of Atg16L1 [357]. The atg12/atg5/atg16L1 complex is localised to the phagophore which strongly enhances the formation of atg8- phosphatidylethanolamine (atg8-PE) [358].

Atg8 (LC3) conjugation system involves Atg8 being covalently conjugated to PE by an ubiquitin-like system. Atg8 is an ubiquitin like protein that is activated by Atg7 [359, 360], an E1-like enzyme, which is transferred to atg3, an E2-like enzyme [361]. Atg7 then activates atg8 [362] and directs it towards atg3 [362]. The atg12-atg5 conjugate promotes the transfer of atg8 from atg3 to PE by enhancing the activity of atg3 [358]. Deconjugation of LC3-PE is mediated via atg4, which controls phagophore elongation and/or closure. Atg8-PE is membrane bound and enriched on the isolation membrane, where it forms large punctate structures during starvation [363].

Atg8 is required for autophagosome formation, membrane tethering and hemi-fusion [364] which is initiated by the conjugation of atg8 to PE. Hemi-fusion is an intermediate state during fusion, whereby the outer (contacting) leaflet of two opposed lipid bilayer merges, but the inner (distal) leaflets remain intact [365]. atg8 controls expansion of the phagophore and formation of the autophagosome [366]. The cellular cytoplasmic concentration of atg8 determines the size of the autophagosome, although the number of autophagosomes are unaffected. The cycle of autophagosome formation includes the trafficking and recruitment of atg8 to the site of the expanding autophagosome, followed by its release, which is essential for this process to occur. Atg8 forms an expanding structure which then dissociates from the site of vesicle formation [366]. Atg4 is important for the closure of the autophagosome [367] and only closed autophagosomes can fuse with the lysosome [368]. Autophagosomes are mature when all outside atg proteins are removed and they are then able to fuse with lysosome [368].

Autophagosomes can form anywhere in the cytoplasm, however late endosomes and lysosomes tend to accumulate at the perinuclear region of the cell [369]. Therefore, the closed autophagosomes need to be transported to this region prior to fusion. As the minus end of microtubules is located at the perinuclear region, therefore the dynein-dynactin motor complex is involved in the transfer of autophagosomes towards the perinuclear region [370]. When lysosomes are located in perinuclear region, the fusion of autophagosomes and lysosomes is enhanced, whereas localisation of lysosomes to the periphery inhibits the rate of fusion [371]. Rab7 links the late autophagosome to microtubules via Rab-interacting lysosomal protein (RILP), the cholesterol sensor ORP1L and dynein, thus facilitating movement towards the perinuclear region [372]. The exact mechanism of how autophagosomes and lysosomes fuse is not well understood.

However, it is most likely mediated via Rabs, including Rab7, and soluble NSF attachment proteins receptor (SNARE) proteins [373]. In some instances, LC3 and gamma-aminobutyric acid receptor-associated protein (GABARAP) are also involved in the fusion of the autophagosome and lysosome [374].

1.2.3 LC3 and GABARAP subfamilies

In humans, six genes encode the homologues of yeast atg8 genes, and the proteins encoded by these genes are well characterised in autophagy [375]. These proteins are grouped into two subfamilies; (1) the LC3 subfamily, including LC3A/LC3B/LC3C; and (2) the Gamma-aminobutyric acid receptor-associated protein (GABARAP) subfamily; containing GABARAP, GABARAPL1 and GABARAPL2. Both subfamilies undergo PE conjugation [376]. The LC3 family is essential for elongation of the isolation membrane when autophagy is initiated, whereas GABARAP is required for the later stages of autophagy, in the maturation of the autophagosome [377]. The members of these sub-families have different roles in autophagy. During induction of basal autophagy, LC3B and GABARAP are expressed, whereas LC3A and LC3C are absent. Depletion of LC3B and GABARAP alone is not enough to abrogate lysosomal degradation of long lived proteins, however simultaneous depletion of both can [378]. Furthermore, the two subfamilies have different binding affinities to autophagy receptors. LC3B has a greater affinity to the LC3-interacting region (LIR) of p62 compared to GABARAPs [377]. p62 colocalizes with LC3B puncta, and 50% of LC3 puncta are positive for p62, but there is little co-localisation between GABARAP and p62. Furthermore, LC3B is indispensable for the selective turnover of p62, but this is not true for the GAPARAP family [375].

1.2.4 Membrane source for autophagosomes

Several early studies concluded that the ER is the source of the autophagosome membrane because the ER and the growing phagophore were associated [367, 379, 380], and the cup-shaped phagophore was found to emerge from the PtdIns3P-rich subdomains of ER [381]. Other suggestions have been proposed for the source of the autophagosome membrane, including mitochondria [382], plasma membrane [383] and the Golgi apparatus [384]. It has also been suggested that the autophagosome may form at ER-mitochondria contact sites in mammalian cells [385]. Upon starvation, phagophores nucleate at an intricate membranous structure, termed the ‘omegasome’. These structures

were originally identified as ER-associated spots that could be labelled with PtdIns3P binding double FYVE-containing protein 1 (DFCP1) [381]. Furthermore, in neurons, the ER is the major membrane source for autophagosomes, which form from DFCP1-positive subdomains of the ER [386].

Recently it has been suggested that that the early expansion of the phagophore requires vesicles coated with a protein complex called Coat Protein Complex II (COPII) [387], which is involved in ER to Golgi transport. COPII is a vesicle coat protein complex, and COPII was shown to promote autophagosome biogenesis by stimulating LC3 lipidation in a nutrient dependent manner [388]. Sec23b, a component of COPII, is targeted towards lysosomal degradation in nutrient rich conditions, thus inhibiting autophagy flux [388]. In contrast, upon nutrient deprivation, ULK1 phosphorylates sec23b and inhibits its degradation [388]. This further confirms that the ER has a crucial part in autophagy. Interestingly, damaged ER also undergo autophagy degradation, ER-phagy mediated by a newly identified autophagy receptor, sec24, a COPII subunit [389]. This recent paper suggested that sec24 is required for ER-phagy suggesting that COPII cargo adaptors are involved in packaging of ER domains into membrane that are directed towards ER-phagy [389].

1.2.5 Selective autophagy vs non-selective autophagy

Based on target recognition, two broad types of autophagy can be distinguished; non-selective and selective autophagy. Non-selective autophagy is a cellular stress response to nutrient deprivation, whereas selective autophagy describes the selective degradation of intracellular organelles including mitochondria, ER, ribosomes or protein aggregates. The initiation of autophagy and the formation of the autophagosome is different between selective and non-selective autophagy. During non-selective autophagy, inhibition of mTORC1 leads to activation of the ULK1 complex and the phagophore then begins elongating, followed by part of the cytoplasm becoming engulfed. During selective autophagy, however, ubiquitination of the specific cargo to be degraded is the initiation signal that recruits autophagy receptors; LC3-binding proteins that recruit this ubiquitinated cargo via their ubiquitin binding domain [390]. The autophagy receptors then consequently recruit the autophagic machinery, resulting in the formation of the phagophore [390]. Therefore, during selective autophagy, cargo

selection precedes the formation of phagophore, while during non-selective autophagy, phagophore formation is the initiating step [390].

Multiple forms of selective autophagy have been described, depending on the cargo to be degraded, including; mitophagy (mitochondria), xenophagy (bacteria), ribophagy (ribosome), aggrephagy (protein aggregate), pexophagy (peroxisomes), reticulophagy (endoplasmic reticulum), nucleophagy (nucleus), lysophagy (lysosome), lipophagy (lipid droplets), ferritinophagy (ferritin), and glycophagy (glycogen) [reviewed in [391]] . The selectivity of autophagy is determined by the involvement of autophagy receptors, because they appear to be associated with different subtypes of autophagy. These autophagy receptors include, p62, NDP52, optineurin and NBR1. Autophagy proteins directly bind to LC3 via their LC3-interacting motif (LIR) which initiates the recruitment of autophagic machinery [132]. p62 is involved in mitophagy [392], xenophagy, aggrephagy, pexophagy and lysophagy, whereas NDP52 has been shown to be involved in xenophagy and mitophagy [391]. Optineurin is involved in mitophagy, xenophagy and aggrephagy, while NBR1 is involved in aggrephagy and pexophagy [391].

1.2.5.1 Basal autophagy

Basal autophagy, also referred to as ‘quality control autophagy’, is a subtype of autophagy that occurs when cells are subject to nutrient rich conditions, therefore it can be interpreted as a combination different subtypes of selective autophagy. Basal autophagy is responsible for recycling essential amino acids [393] and damaged organelles [392, 394], and it controls the turnover of long-lived proteins [395]. Furthermore, basal autophagy is implicated in broader functions, such as neurogenesis in humans and *Drosophila* [396, 397], the induction of apoptosis, vesicular trafficking, and inflammatory responses [398]. It also participates in the catabolism of certain oligosaccharides, including sialyloligosaccharides [399].

Autophagy is critical for cell survival, not just for the degradation of damaged organelles but also for maintaining intracellular homeostasis. Studies involving the depletion of autophagy genes *(atg5* and *atg7)* in mice have revealed the importance of basal, or constitutive, autophagy in survival and neurogenesis. In healthy mice, elevated levels of autophagy are apparent 3-6 hr after birth, whereas this is absent in mice lacking

either *atg5* [400] and *atg7* [393] and they die one day after birth [393, 400]. Furthermore, *atg5*$^{-/-}$ mice show decreased LC3-II levels and increased LC3-I levels compared to WT mice, suggesting dysfunctional autophagosome formation [400]. Similarly, upon depletion of *atg7*, increased LC3-I levels, and lower concentrations of amino acids are also detected [393]. Importantly, suppression of basal autophagy by depletion of *atg7* only in neurons in mice leads to neurodegeneration [401]. These mice develop progressive motor and behavioural deficits at 3 weeks of age, and in adults, large ubiquitin-positive cytoplasmic inclusions are present in several regions of the brain, indicating that loss of basal autophagy leads to the generation of inclusion bodies [401]. Together these findings indicate that functional basal autophagy is crucial for survival, neuronal health, and preventing neurodegeneration.

1.2.5.2 Non-selective autophagy

Starvation is a major stressor for the cell and cells facing nutrient deprivation increase their autophagic activity to cope with the demand for resources [402]. Hence, during non-selective autophagy (also called cargo independent autophagy), non-essential molecules, proteins and organelles are degraded to cope with the stress. Whilst the initiation of starvation-induced autophagy is different from selective autophagy, once the autophagosome is formed, both mechanisms proceed the same.

mTOR is a serine-threonine protein kinase, previously identified as an antifungal and immunosuppressant agent [403], that mediates multiple cellular pathways. As well as non-selective autophagy [404], this includes protein synthesis, mitochondrial biogenesis and metabolism, microtubule organisation, lipid biosynthesis and metabolism [405]. mTOR signalling is mediated via two complexes; mTORC1 and mTORC2, and autophagy is meditated by mTORC1. The mTORC1 complex consists of mTOR, mammalian lethal sec13 protein 8 (mLST8), Dishevelled, Egl-10 and Pleckstrin domain (DEP) protein containing mTOR interacting protein (DEPTOR), regulator-associated protein of the mammalian target of mTOR (Raptor), and proline-rich Akt substrate of 40kDA (PRAS40) [406]. mTORC1 activity and therefore non-selective autophagy is controlled via several pathways [404].

mTOR is activated by Ras homolog enriched in brain (Rheb), a small GTPase [407, 408]. Rheb activity can be suppressed by the tuberous sclerosis complex 1 and 2

(TSC1/2) [409, 410]. TSC is inhibited by several kinase cascades, including ERK, ribosomal S6 kinase (p90-RSK), AKT and glycogen synthase KINASE 3B (GSK-3B) via the Wnt-signalling pathway [411]. Inhibition of TSC2 leads to activated mTOR [411]. Furthermore, PTEN can inactivate PI3K, which suppresses signalling of mTOR. AMPK also regulates mTOR indirectly by phosphorylation and activation of TSC2 and by direct phosphorylation of Raptor in the mTORC1 complex [412].

Under serum-rich conditions, phosphorylated and activated mTOR inhibits autophagy by preventing autophagosome formation via ULK1 inhibition. Furthermore, in nutrient rich conditions, AKT inhibits TSC2 and AMPK, a cellular energy sensor that monitors the ratio of AMP/ATP. However, upon nutrient starvation, mTOR is inhibited, which consequently induces autophagy [413]. mTOR is activated via Rheb, leading to phosphorylation of ULK1 on P757, which disrupts the interaction between ULK1 and AMPK. Nutrient-deprivation induced autophagy is dependent on AMP. Upon AMPK activation, catabolic pathways are initiated in the cell, including gluconeogenesis, glycogen synthesis, glycolysis, lipolysis and fatty acid oxidation, along with induction of autophagy via inhibition of mTORC1. In fact, AMPK induces autophagy on multiple levels. It normally inhibits Raptor, hence blocking the mTOR pathway, but it also activates the previously blocked TSC2, which indirectly inhibits mTORC1 via inhibition of its activator, Rheb. Furthermore, inactive mTOR prevents the normal inhibitory effects on ULK1, thus allowing its interaction with AMPK, therefore inducing autophagy (reviewed in [414]).

mTOR appears to have important functions in neurons. It has a significant role in neurodevelopment, because mutations in mTOR lead to mice lacking the telencephalon [415]. However, overactivated mTOR can be detrimental; in the early stages of development this leads to microencephaly [416], while in post mitotic neurons, this leads to neurodegeneration and the formation of ubiquitin positive inclusion bodies [417]. Loss of the mTOR regulator TSC1/2 leads to prominent changes in neuronal architecture and differentiation [418]. Moreover, the formation of neuronal circuits [419] and synaptic plasticity are also regulated by mTOR [420]. Together these findings indicate that mTOR has fundamental roles in neurons in the development and function of the healthy brain.

1.2.6 Autophagy in neuronal cells and neurodegeneration

Given the importance of autophagy as a fundamental process that maintains intracellular homeostasis, it is not surprising that dysfunction to autophagy can lead to lethal consequences for the cell. Furthermore, dysfunctional autophagy is increasingly associated with disease, including neurodegenerative disorders[421]. Mechanistical and genetical aspects of dysfunctional autophagy in ALS are described in the following section (1.2.7 'Autophagy dysfunction in the pathophysiology of autophagy'). Being highly specialised post-mitotic cells, neurons lack the ability to divide and dilute the burden of damaged proteins and organelles via cell division, as in other cell types. Furthermore, due to their unique morphology and high metabolic rate they therefore rely heavily on functional autophagy for viability [422, 423]. Therefore, autophagy must be strictly regulated in neurons.

The initiation of autophagy in neurons and the formation of the autophagosome is mostly restricted to the distal part of the axon [273] [386]. Less frequently, autophagosomes can form in the soma [424]. Autophagosomes display spatial maturation as they move along the axon, fusing with endosomes/lysosomes at its distal end [273]. However, in this location, the majority of autophagosomes are not acidic and only undergo acidification when being transported along the axon. However, more proximal to the cell body, most (almost 70%) autophagosomes are fully acidified [273]. Furthermore, autophagosome formation follows a spatially regulated pathway in neurons [386].

Autophagy is a robust process in neurons. Compared to other cell types, there appears to be high rates of ongoing basal autophagy in neurons [424]. However, it is controversial whether starvation induce autophagy of these cells or not; autophagosomes accumulate in the soma following bafilomycin treatment, but not after starvation [424]. In contrast starvation-induced autophagy of isolated primary neurons *in vitro* [425, 426]. Interestingly, neurons do not elevate their autophagic rate even if misfolded proteins aggregates are present, such as when mutant $SOD1^{G93A}$ aggregates accumulate in the axon [273]. This finding indicates that neurons rely heavily on functional basal autophagy to prevent the formation of aggregates.

1.2.7 Autophagy dysfunction in the pathophysiology of ALS

The very presence of protein aggregates in ALS and other neurodegenerative diseases implies that protein degradation pathways are dysfunctional. As described above, several genes mutated in fALS encode proteins that normally function in autophagy, but furthermore, several ALS-associated proteins are known to cause autophagy dysfunction in cellular and animal models, as detailed below. Examination of ALS patient post-mortem tissue suggests that autophagy impairment exists in ALS. Lumbar spinal cords of sALS patients showed degenerating motor neurons that were positive for both p62 and LC3-II inclusions [427]. Furthermore, inclusions were associated with autophagosomes and/or autolysosomes, indicating autophagic activity [427]. In iPSC-derived neurons from patients carrying the C9orf72 expansion enrichment of p62-positive inclusions was detected [428]. Similarly, reduced autophagy was observed in iPSC neurons derived from ALS/FTD patients with C9orf72 haploinsufficiency [429].

1.2.7.1 SOD1

ALS-mutant $SOD1^{G93A}$ enhances LC3 turnover *in vitro* [430] and increases LC3-II levels *in vivo* in symptomatic SOD1 mice [431], suggesting that it increases autophagic activity. In contrast, mSOD1 inhibits autophagosome transport in the axon in mice, possibly by binding dynein and thus overloading retrograde axonal transport [432]. This dynein-mutant $SOD1^{G93A}$ interaction occurs early in disease course in these animals, prior to symptom onset [432]. Autophagosomes mature along the axon and accumulate in the soma of neurons [273, 386], implying that mSOD1 inhibits the degradation of autophagosomes. Hence it remains unclear how SOD1 mutations contribute to autophagy dysfunction in ALS. Furthermore, conflicting findings have been obtained in studies examining the effects of modulating autophagy on ALS. In transgenic mutant SOD1 mice (G93A, G86R), autophagy enhancers , including lithium, valproate, trehalose, cystatin c and resveratrol, were found to delay symptom onset, disease progression, prolong lifespan, and diminish MN loss [433-438]. However, in another study, autophagy induction led to worsened neuropathology, accelerated MN degeneration and shortened lifespan of $SOD1^{G93A}$ mice [439, 440].

A recent study used rilmenidine, an imidazoline-1 receptor antagonist, to induce autophagy $SOD1^{G93A}$ transgenic mice and showed upregulated autophagy and mitophagy in spinal cord and increased the abundance of autophagosomes. Regardless of autophagy induction detected *in vivo* rilmenidine worsened motor neuron degeneration and symptom progression and increased the accumulation of $SOD1^{G93A}$ aggregates [441]. Hence it remains unclear whether enhancing autophagy is harmful or beneficial in SOD1-associated ALS.

1.2.7.2 TDP-43

Several studies have shown that TDP-43 (WT and mutant) can influence autophagy. Overexpression of cytoplasmic TDP-43 (both WT and mutant; M337V, Q331K, G348C, A382T) was shown to induce autophagy via loosening ER-mitochondria contacts [442, 443]. TDP-43 depletion *in vitro* was shown to downregulate atg7, which is an enzyme required for LC3 lipidation [444]. Furthermore, autophagosome-lysosome fusion was inhibited by the loss of TDP-43 thorough dynactin downregulation [323].

TDP-43 has been also shown to enhance autophagy. TDP-43 controls the level of RAPTOR, that maintain the activity of mTOR. TDP-43 was also required for autophagosome-lysosome fusion via stabilising the mRNA of dynactin1. TDP-43 downregulation decreased dynactin 1 levels and impaired autophagosome lysosome fusion [323].

1.2.7.3 FUS

FUS has been shown to perturb autophagy. Mutant FUS (P525L, R522G) expressing neuronal cells showed accumulation of ubiquitinated proteins. Furthermore, p62 levels increased, indicating impaired autophagy. The formation of omegasomes and autophagosome was also inhibited upon ALS-mutant FUS expression. Similarly, in motor neurons from the spinal cord of an ALS patient carrying a FUS^{R521C} mutation, more LC3-positive vesicles were detected, confirming impaired autophagosome degradation [324].

1.2.7.4 p62

Sequestosome-1 (SQSTM1)/p62 is an autophagy receptor that tethers cargo to autophagosomes. p62 was the first described autophagy receptor in mammals [445]. p62

has been examined in mutant SOD1^{G93A} mice models and mSOD1 was showed to be recognised by p62 and initiating its degradation via autophagy [446]. Interestingly, p62 is mutated in a small proportion of ALS and FTD patients [26, 196].

1.2.7.5 VCP

VCP is involved in autophagosome-autolysosome fusion specifically during basal autophagy, but not in starvation-induced autophagy [447, 448]. VCP was also shown to repress negative regulators of autophagy, calpain2 as well as mTOR, following insulin withdrawal-induced autophagy, while also upregulating GSK-3beta, an inducer of autophagy [449].

1.2.7.6 VAPB

VAPB interacts with a mitochondrial protein, PTPIP52 that acts as a scaffold to tether the two organelle. Overexpression of these proteins tightens the ER-mitochondria interactions, whilst simultaneously impairing autophagosome formation [443]. In contrast, depletion of both proteins leads to loosened ER-mitochondrial interaction, and induction of autophagosome formation [443]. Furthermore VAPB-PTPIP52 complex, which appears to be involved in synaptic activity, is disturbed in FTD and ALS [450]. VAPB has also been shown to be recruited to sites of autophagosome formation on the ER following autophagy induction [451] and VAPB interacts with FIP200 and ULK1 to stabilise these complexes at autophagosome formation sites. The ALS-associated P56S mutant VAPB reduces ULK1-FIP200 interaction and impairs autophagy *in vitro* in 293T and COS7 cells [451].

1.2.7.7 C9orf72

Based on an initial bioinformatics structural analysis, C9orf72 was thought to act as a guanine exchange factor (GEF) for Rab proteins [452, 453], and indeed subsequent studies have shown that it interacts with Rabs involved in autophagy, including Rab1, Rab5, Rab7 and Rab11 [454, 455]. Depletion of C9orf72 inhibits autophagy initiation mediated via ULK1 potentially via Rab1a, implying that C9orf72 interacts with the ULK1/FIP200/atg13/atg101 complex [429].

1.2.7.8 Optineurin

Optineurin is an autophagy receptor which is also mutated in a small proportion of fALS and FTD patients. Optineurin is normally phosphorylated by TBK1, which induces its binding to LC3 [132] and it is known to be involved in the selective degradation of mitochondria (mitophagy) [394, 456] and protein aggregates (aggrephagy) [140]. ALS-associated mutation E478G inhibits the fusion of the autophagosome with the lysosome, thus inhibiting autophagy, due to lack of binding to myosin VI [139]. The role of TBK1 in autophagy will be discussed in detail in the next section.

1.2.8 Experimental detection of autophagy

Whilst autophagy is an important cellular process, there are significant problems associated with detecting autophagy experimentally. Countless papers have listed the major limitations and difficulties in the interpretation and analysis of autophagy [457-463]. Therefore, internationally agreed guidelines to create standards for the experimental examination of autophagy, led by Daniel Kliosnky (3rd edition published in 2016) and featuring several thousands authors, were established [464].

These guidelines are extensive (200 pages), but the major points are summarised here. Firstly, it is impossible to draw conclusions from autophagy experiments by relying on one single technique. A combination of multiple techniques is required to confirm any experimental findings. Secondly, LC3 is a marker of the phagophores/autophagosome not of autophagy itself. However, detection of one single marker, such as LC3 alone, is not enough. Autophagy receptors or other markers also need to be evaluated. Thirdly, the use of pharmacological agents that inhibit specific stages of autophagy, such as either bafilomycin, chloroquine or wortmannin, are important controls that are required to identify where dysfunction in autophagy arises. Therefore conclusive, well described observations only can be made if multiple techniques and markers are used with the combination of the appropriate controls, such as bafilomycin. Furthermore, differences in autophagy need to be detectable with multiple techniques [464]. It is interesting to note that these guidelines are not always mentioned in autophagy studies and often a single marker, such as LC3-II, is used to monitor autophagy.

Hence, in summary, the involvement of a wide variety of ALS-linked proteins in autophagy, and the consequent induction of autophagy dysfunction in cellular or animal models based on these proteins, indicates that autophagy is an important disease mechanism in ALS. Hence obtaining a precise understanding of the role of autophagy in ALS is crucial in examining pathophysiology.

A major protein in the control of autophagy, TBK1, was lately linked genetically to ALS [17]. It remains to be elucidated how TBK1 contributes to ALS and whether its harmful effects are mediated by impaired autophagy remains to be elucidated. Therefore, this thesis aimed to examine the connection between dysfunctional TBK1 and autophagy.

1.3 TANK-binding kinase-1 (TBK1)

1.3.1 Protein structure of TBK1

Tumor necrosis factor (TNF) receptor-associated factor NF-kB activator (TANK)-binding kinase 1 (TBK1) is a kinase that was discovered as a binding partner for TANK from a yeast two hybrid screen, and it was consequently named 'TANK-binding kinase 1' [465]. The mammalian form is 729 aa long with a molecular weight of 84kDa. TBK1 contains a kinase domain (KD) (9-299aa), an ubiquitin-like domain (305-383aa), and two coil-coiled domains (603-650aa, 679-712aa) for substrate binding, as detailed on **Figure 1.4** [466]. The coil-coiled domain 1 (CCD1) is also referred to as the 'scaffold dimerization domain (SDD)' [466, 467]. TBK1 belongs to the IKK-related kinase family, which also includes IKKε. TBK1 and IKKε directly phosphorylate interferon (IFN) regulatory factor 3 and 7 (IRF3, IRF7), leading to their translocation to the nucleus and induction of type 1 IFNs [468].



Figure 1.4. Domain structure of TBK1. TBK1 consist of a kinase domain, ubiquitin-like domain and coil-coiled domain.

1.3.2 Post-translational modification and activation of TBK1

TBK1 undergoes several post-translational modifications that affect its activity, including sumoylation, ubiquitination and phosphorylation [469-472]. Sumolyation is the covalent addition of small ubiquitin like modifiers (SUMOs) [473], and the kinase activity of TBK1 is required for the attachment of SUMO 1 or 2 at K694. TANK binding is prevented by sumoylation of this residue, therefore sumoylation inhibits protein-protein interactions with its substrate, TANK [469]. TBK1 also undergoes another post-translational modification; K48-linked polyubiquitinated at Lys670 - mediated by Dtx4, an E3 ubiquitin ligase that is recruited by NLRP4 -induces TBK1 degradation. In the absence of TBK1 degradation due to the lack of NLRP4, enhanced phosphorylation of TBK1 were detected, consequently activating downstream effectors including type I interferon pathway [470].

TBK1 also undergoes phosphorylation at Ser172 in order to become enzymatically active. TBK1 activation may occur via trans-autophosphorylation [471] or via other, so far unknown, kinases [472]. In order for TBK1 to undergo autophosphorylation it needs to form a dimer, either a homodimer, or a heterodimer with IKK-ε. During homodimer formation, two TBK1 subunits form an elongated dimer, with a central stalk formed by the two SDD (407-657aa) [474]. The KD is comprised of N-terminal and C-terminal lobes, and the TBK1 active sites are located between these two lobes [466, 471]. The activation loop is located in the KD at positions Leu164-Gly199, which thus includes Ser172. The KD,ULD and SDD interact with each other to form a globular head at the end of the stalk, formed by the SDD [474]. In an inactive form, KD projects away from the C-lobe of the other TBK1 subunit comprising the dimer [466, 471]. Autophosphorylation occurs through the interaction of the KDs and the activation loop [466, 471]. The dimer is stabilised by contacts between the ULD and KD, and with the SDD of the contralateral subunit [474]. Phosphorylation of Ser172 leads to a conformation change in the activation loop, allowing an interaction with its own KD, thus allowing substrate binding to occur [466, 471].

K63-linked polyubiquitination of TBK1 at Lys 30 and Lys401 is required for its activation [474]. Ubiquitination of at least one of these two sites, plus dimer formation, are required for phosphorylation of Ser172 in the kinase activation loop [474]. ULD is also important for the kinase activity, because its depletion abrogates the enzymatic activity [475].

1.3.3 The role of TBK1 in autophagy

TBK1 interacts with autophagy receptors that mediate the selective autophagic degradation of organelles including mitochondria and invading bacteria. TBK1 has been extensively studied in the selective autophagy of bacteria and mitochondria, but not in other forms of autophagy.

1.3.3.1 Mitophagy

Mitophagy refers to the selective degradation of mitochondria via autophagy. Upon depolarization, the mitochondria that are ready to be degraded, undergo

ubiquitination and then they are targeted toward the autophagosome. PTEN-induced kinase 1 (PINK1), a mitochondrial serine threonine kinase, detects mitochondrial damage and activates Parkin, an E3 ubiquitin ligase, by phosphorylating Parkin and ubiquitin [476]. Phosphorylated Parkin then adds ubiquitin chains to damaged mitochondria. Ubiquitination is a signal to recruit autophagy receptors, which bind to ubiquitinated mitochondria via their ubiquitin binding domains [476]. Ubiquitin carboxyl-terminal hydrolase 30 (USP30), a deubiquitinase, acts as a brake for mitophagy by opposing Parkin-mediated ubiquitination [476]. Interestingly, mutations in both PINK1 and Parkin are associated with Parkinson's disease highlighting the role of mitophagy in neurogenerative diseases [477].

TBK1 influences mitophagy via its interaction with autophagy receptors NDP52, p62 and optineurin, via its phosphorylation at several serine and threonine residues [478]. TBK1 facilitates the interaction of NDP52 with the FIP200/ULKI complex on ubiquitinated mitochondria. The presence of NDP52 on mitochondria induces their autophagic engulfment by recruiting and activating the ULK1 complex [479]. Phosphorylation of NDP52 in response to mitochondria depolarisation is dependent of TBK1, as well as on PINK1 and Parkin [480]. PINK1 may also recruit NDP52 to mitochondria in a Parkin independent manner [481]. While TBK1 phosphorylates NDP52, the activation of TBK1 by mitochondria depolarisation requires NDP52 [480], indicating that a positive feedback loop exists. In contrast, another study showed that NDP52 was not the main TBK1 binding receptor for mitophagy [456].

TBK1 phosphorylates optineurin at Ser177 upon mitochondria damage when TBK1 and optineurin are co-recruited to depolarized mitochondria [456], and TBK1's recruitment to mitochondria is mediated via optineurin [478]. Inhibition or depletion of TBK1 blocks efficient autophagosome formation during mitophagy [456]. Similar to NDP52, the recruitment of optineurin to mitochondria also requires TBK1 [480]. Furthermore, TBK1 activation during mitochondrial damage also requires binding of optineurin to polyubiquitin chains [480].

TBK1 is thought to also phosphorylate p62 at Ser403, however this occurs only transiently during mitophagy, and p62 phosphorylation is required for the efficient autophagic engulfment of mitochondria [392]. When the TBK1 activity is inhibited, p62

interacts with Parkin-recruited mitochondria, however mitochondria were not engulfed by the autophagosome, implying that the kinase activity of TBK1 is required for this process [392].

TBK1 also has been linked to Rab proteins during mitophagy. TBK1 phosphorylates Rab7A (S72) during PINK1/Parkin dependent mitophagy. Non-phosphorylated Rab7a fails to recruite atg9a-positive vesicles to mitochondria [482]. Another Rab, Rab35, regulates the recruitment of NDP52 to damaged mitochondria, and the NDP52 and Rab35 interaction is facilitated by TBK1 [483].

Together, these data therefore provide compelling evidence to indicate that TBK1 is involved in mitophagy, and that this involvement is mediated by autophagy receptors; p62, NDP52 and optineurin.

1.3.3.2 Xenophagy

Xenophagy is an evolutionary conserved mechanism that aims to remove pathogens after host invasion [484]. Enzymatically active TBK1 is required to eliminate bacteria via autophagy. The recruitment of WIPI1 and WIPI2 to Salmonella is essential for xenophagy and mediated by TBK1 [485]. WIPIs are essential PtdIns3P effectors that are rapidly recruited to endomembranes upon autophagy induction, and they incorporate into the phagophore and autophagosome membranes [349]. The signals required to recruit TBK1 to bacteria are the presence of NDP52 on bacteria or K48-, K63-linked ubiquitination of the bacteria [485]. Each signal alone is sufficient to recruit TBK1 and restrict bacteria growth [485, 486] .

Similar to mitophagy, TBK1 interacts with other autophagy adaptors during xenophagy, including optineurin, and several Rabs. TBK1 phosphorylates optineurin, which enhances the binding of LC3 to bacteria, leading to their autophagosomal degradation [132]. Rab8b is known to be involved in the xenophagy of *Mycobacteria tuberculosis* [487] by interacting with TBK1, because TBK1 depletion prevented their autophagic destruction due to inhibited autophagosome maturation [487]. TBK1 also mediates the interaction between Rab35 and NDP52 during xenophagy [483] and Rab35 recruits NDP52 to bacteria. Both NDP52 and Rab35 were able to recruit and activate

TBK1 to bacteria [483]. NDP52 facilitates autophagosome maturation during xenophagy [488] mediated via Rab35 and TBK1 [483].

These studies together clearly indicate that TBK1 has a major involvement in xenophagy, thus providing evidence that TBK1 is required for several diverse types of selective autophagy.

1.3.3.3 Other types of selective autophagy

The role of TBK1 in the selective degradation of paternal organelles by autophagy, termed 'allophagy', has also been examined in *Caenorhabditis elegans*. The *C. elegans* homologue of TBK1, IKKE-1, phosphorylates ALLO-1, an autophagy receptor that initiates autophagosome formation around paternal organelles [489]. This study therefore implies that TBK1 has an evolutionary conserved role in autophagy.

1.3.4 The role of TBK1 in ALS

1.3.4.1 TBK1 mutations in ALS

TBK1 was identified as an ALS causative gene in 2015 via whole exome sequencing [17, 18]. 18 TBK1 mutations were first identified in this study, and these mutations showed deficient kinase activity or inhibited its binding towards optineurin, suggesting that pathogenicity may be linked to dysfunctional autophagy [18]. Since then, almost 100 variants have been identified in TBK1 **(Table1.2, Figure 1.6)**. Furthermore, TBK1 mutations are also present in Alzheimer's disease and FTD, suggesting a wider involvement in neurodegenerative diseases than previously realised [18, 490]. Overall mutation frequency for confirmed *TBK1* loss-of-function mutations in the European cohort was 0.7%. Mutation frequency was less in FTD subgroup; 0.4%, while higher in ALS; 1.3% or in FTD-ALS; 3.6% [491]. Loss of function mutations that were identified in *TBK1* gene such as p.Ala417X or p.Ile450LysfsX15 **(Table 1.2)** co-segregated with ALS/FTD [18] indicating pathogenicity. 8 loss of function mutations identified in the same study were heterozygous and resulted in loss of expression, indicating that haploinsufficiency may be implicated in the pathogenicity of TBK1 [18]. In contrast, not all variants are pathogenic suggesting that some mutations in *TBK1* may be only risk factors for ALS [17].

In some instances, more than one ALS gene carries mutations. Pathogenic mutations in both *TBK1* and *OPTN* gene were identified in FTD patients [197]. Interestingly, *TBK1/OPTN* double mutant patients presented only FTD symptoms. Post-mortem examination confirmed no neuron loss in the motor cortex or brainstem [197], indicating that *TBK1/OPTN* double mutant may be a feature of FTD and not ALS.

Table 1.2. List of TBK1 variants identified in ALS and FTD and other neurodegenerative diseases and their localisation to functional domains.

KD: kinase domain, UBD: ubiquitin binding domain, CCD: coil-coiled domain.

Variant	Protein change	Disease	References	Domain localisation of mutation
c.958_958delA	p.Thr320GlnfsX40	fALS	[18]	UBD
c.1343_1346delAATT	p.Ile450LysfsX15	fALS	[18]	-
c.1433_1435delTG	p.Val479GlufsX4	fALS	[18]	-
c.555T>A	p.Tyr185X	fALS	[18, 492]	KD
c.358+2T>C	p.Thr77TrpfsX4	fALS	[18, 492]	KD
c.1340+1G>A	p.Ala417X	fALS, sALS, FTD	[18, 491]	-
c.2138+2T>C	p.690-713del	fALS	[18]	CCD2
c.1318C>T	p.Arg440X	fALS	[18, 198]	-
c.1928_1930delAAG	p.Glu643del	progressive cerebral ataxia, dementia, FTD, FTD-ALS, ALS	[18] [491-495]	CCD1
c.140G>A	p.Arg47His	fALS	[18, 492]	KD
c.314A>G	p.Tyr105Cys	sALS	[18]	KD
c.914T>C	p.Ile305Thr	sALS	[18]	UBD
c.923G>A	p.Arg308Gln	sALS	[18]	UBD
c.1070G>A	p.Arg357Gln	fALS	[18, 494, 496, 497]	-
c.1676T>G	p.Met559Arg	fALS	[18]	-
c.1712C>T	p.Ala571Val	sALS	[18]	-
c.1792A>G	p.Met598Val	sALS	[18]	-
c.2086G>A	p.Glu696Lys	fALS, sALS	[18]	CCD2
c.1197delC	p.L399fs	fALS	[498]	-
c.467_468delCA	p.Thr156ArgfsX6	FTD-ALS	[198, 499]	KD
c.1446T>G	p.Tyr482X	FTD-ALS	[198, 499]	-
c.1960-2A>G	-	FTD-ALS	[198, 499]	CCD1
c.1963C>T	p.Gln655X	FTD-ALS	[198, 499]	CCD2

c.10A>G	p.Thr4Ala	FTD	[198]	-
c.1985T>C	p.Met662Thr	FTD-ALS	[198]	-
c.77G>A	p.Gly26Glu	ALS	[198]	KD
c.427C>T	p.Arg143Cys	ALS	[198]	KD
c.959C>T	p.Thr320Ile	ALS	[198]	UBD
-	p.Gln2X	FTD	[493, 494]	-
-	p.Asp167del	ALS	[491, 493]	KD
-	p.Gly272_Thr331del	FTD	[491, 493]	KD/UBD
-	p.Ser398ProfsX11	ALS	[491, 493]	-
-	p.Ser518LeufsX32	ALS	[491, 493]	-
-	p.Arg271Leu	FTD	[493]	KD
-	p.Ala535Thr	FTD	[493]	-
-	p.Lys291Glu	FTD, ALS	[493, 496]	KD
-	p.His322Tyr	ALS	[493]	UBD
-	p.Ile515Thr	ALS	[493]	-
c.1150C>T	p.Arg384Trp	sALS	[500]	-
c.1424T>C	p.Ile475Thr	sALS	[500]	-
c.1426G>A	p.Glu476Lys	sALS	[500]	-
c.1414delA	p.Ile472SerfsX8	sALS	[500]	-
c.86delA	p.Lys29ArgfsX15	FTD	[491]	KD
c.288delT	p.Val97PhefsX2	FTD-ALS	[491]	KD
c.349C>T	p.Arg117X	FTD-ALS	[491]	KD
c.379C>T	p.Arg127X	ALS	[491]	KD
c.1335G>A	p.Trp445X	FTD	[491]	-
c.1385_1388delCAGA	p.Thr462LysfsX3	FTD-ALS	[491]	-
c.235_237delACA	p.Thr79del	FTD-ALS	[490, 491, 494]	KD
c.228+1G>A	p.Lys30_Glu76del	ALS	[491]	KD
c.1001C>T	I334T	ALS	[501]	UBD
c.184T>C	L62P	ALS	[501]	KD
c.127A>G	p.I43V	ALS	[502]	KD
c.881G>A	p.G294D	ALS	[502]	KD
c.1330C>T	p.R444X	ALS	[502]	-
c.1331G>A	p.Arg444Gln	ALS/ALS-FTD	[503]	-
c.2070delG	p.Met690fs	ALS/ ALS-FTD	[503]	CCD2
c.1150C>T	p.Arg384Thr	ALS/ALS-FTD	[503]	-
c.176dupT	p.Leu59PhefsX16	ALS	[496]	KD
c.358+5G>A	-	ALS	[496]	-
c.352G>A	p.Asp118Asn	ALS	[496, 504]	KD
c.1190T>C	p.Ile397Thr	ALS	[490, 496]	-

c.1644-5_1644-2delAATA	-	ALS	[496]	-
c.1959_1960insGT	p.E653fs	FTD-ALS	[505]	CCD2
c.2063_2064delTT	p.L688RfsX14	FTD-ALS	[505]	CCD2
c.2099_2100del	p.Val700GlyfsX2	ALS	[506]	CCD2
-	p.His307Asp	Alzheimer	[490]	UBD
-	p.Arg405His	Alzheimer	[490]	-
-	p.Ile418Val	Alzheimer	[490]	-
-	p.Asp639His	Alzheimer	[490]	CCD1
-	p.Met673Leu	Alzheimer	[490]	-
-	p.Val726Ile	Alzheimer	[490]	-
-	p.Val23Ile	sALS	[504]	KD
-	p.Ile207Thr	sALS	[504]	KD
-	p.His322Arg	sALS	[504]	UBD
-	p.Arg358Cys	sALS	[504]	UBD
-	p.Thr478Ile	sALS	[504]	-
-	p.Tyr609His	sALS	[504]	CCD1
-	p.Arg357term	sALS	[17, 494, 504]	UBD
-	p.Pro378_Ile379del	sALS	[504]	UBD
-	p.Thr419_Gly420del	sALS	[504]	-
c.1869_1875del	p.Met623IlefsdX9	ALS	[494]	CCD1
c.1887_1890del	p.Gln629HisfsX4	ALS	[494]	CCD1
c.92A>G	p.Thr31Ala	ALS	[494]	KD
c.1073G>A	p.Arg358His	ALS	[494, 497]	UBD
c.64A>C	p.Asn22His	ALS	[17, 494]	KD
c.385A>G	p.Asn129Asp	ALS	[17, 494]	KD
c.649G>A	p.Gly217Arg	ALS	[17, 494]	KD
c.1180T>G	p.Tyr394Asp	ALS	[17, 494]	-
c.1412G>A	p.Cys471Tyr	ALS	[17, 494]	-
c.1694A>C	p.Gln565Pro	ALS	[17, 494]	-
c.1270T>G	p.Tyr424Asp	ALS	[507]	-
c.1852_1854delGAA	p.E618del	sALS	[497]	-
c.2040dupT	p.N681X	sALS	[497]	CCD1/CCD2
c.1445_1446delAT	p.Y482X	sALS	[497]	CCD1/CCD2
c.2170C>T	p.R724C	sALS	[497]	-
c.684dupT	p.R229X	sALS	[497]	KD

1.3.4.2 Pathogenic mechanisms linked to TBK1 in ALS

How TBK1 contributes to ALS is unknown, but haploinsufficiency has been suggested as a major underlying mechanism [18]. Several lines of evidence now imply

that haploinsufficiency is involved in TBK1 pathogenicity. Loss of TBK1 expression leads to decreased survival of iPSC-derived motor neurons from TBK1 mutant ALS patients [508]. Decreased TBK1 levels also inhibit the AKT-mTOR pathway and reduce the survival of iPSC derived motor neuron cells during long term culturing [508]. Furthermore, increased aggresome formation was detected in these cells, which was not targeted towards autophagic degradation [508]. TBK1's loss of binding towards its substrate, optineurin, due to ALS/FTD mutation [18] blocks efficient autophagosome formation during mitophagy [456], due to abrogated the formation of optineurin TBK1 complex [478].

Depletion of TBK1 increased SOD1 aggregate formation detected by microscopy, and lead to decreased LC3-II [140]. Furthermore, overexpression of TBK1 reduced the accumulation of $SOD1^{G93C}$ aggregates [140], suggesting the involvement of TBK1 in the clearance of $SOD1^{G93C}$ aggregates via autophagy. In contrast, in neuronal like cells, overexpression of TBK1 did not induce autophagy. Furthermore, the overall levels of $SOD1^{G93A}$ did not change [509]. However, $SOD1^{G93A}$ aggregates did decrease upon TBK1 overexpression, but due to more mutant SOD1 becoming soluble [509]. Overexpression of WT-TBK1 in $SOD1^{G93A}$ mice did not delay disease onset, but it extended lifespan and improved impaired motor function [509]. This indicates that TBK1 may not affect SOD1 toxicity via control of autophagy. Furthermore, TBK1 was shown to modulate microglia activation in SOD1 mice [510].

TBK1 knock-out is lethal in mice, which die between embryonic day 13.5 and 14.5, and no live births are produced [511]. However, heterozygous depletion of TBK1 in mice does not lead to a motor phenotype [510]. TBK1 depletion in primary motor neurons results in increased LC3-II, p62 and optineurin expression, while the expression levels of SOD1, TDP-43 are unchanged. *In vivo*, increased p62 and GABARAPL1 accumulation/aggregates are detected at early time points in $TBK1^{+/-}$ mice overexpressing $SOD1^{G93A}$, indicating that autophagy is dysfunctional [510]. Furthermore, homozygous depletion of TBK1 in $SOD1^{G93A}$ mice proceeds both the clinical onset and muscular denervation of $SOD1^{G93A}$ mice [510]. Depletion of TBK1 alone in mice, however, does not induce p62 or GABARAP aggregates at any time point. In contrast, at later timepoints, a lack of TBK1 expression reduces the load of p62 aggregates in $SOD1^{G93A}$ mice, and

diminishes microglial neuroinflammation, decelerates disease progression, and extends survival [510].

Taken together, these studies indicate that TBK1 may be involved in other types of autophagy besides mitophagy and xenophagy, and that this may be related to pathophysiology in ALS. Therefore, it remains to be elucidated how and if TBK1 leads to abrogated autophagy in ALS. Similarly, it remains unclear if TBK1 affects accumulation of the most abundant aggregate component in ALS motor neurons, TDP-43 by impairment of autophagy

Overall aims of the thesis

In this thesis it was hypothesised that TBK1 is involved in basal, starvation-induced autophagy and aggrephagy and ALS/FTD mutant TBK1 leads to dysfunctional autophagy resulting in protein aggregation.

There is considerable evidence suggesting that autophagy, and more precisely basal autophagy and aggrephagy, are involved in the development or progression of ALS. TBK1 is mutated in familial and sporadic ALS/FTD patients. However, there has been few extensive analyses to understand how these mutations lead to ALS.

Therefore, in this thesis I intended to describe the involvement of TBK1 in autophagy dysfunction in ALS.

In this thesis I aimed to **(Figure 1.5)**

- Examine how TBK1 affects autophagosome formation and maturation during basal starvation-induced autophagy and aggrephagy
- Determine whether the knock-out of TBK1 carries same consequences as the inhibition of TBK1's kinase activity
- Describe the involvement of autophagy receptors including, p62, optineurin and NDP52 in basal, starvation-induced autophagy and aggrephagy
- Determine whether mutations associated with ALS influences the function of TBK1 in basal, starvation-induced autophagy and aggrephagy
- Analyse the effect of TBK1 inhibitors, knockout of TBK1 or the presence of ALS-TBK1 on soluble and insoluble ubiquitin accumulation
- Examine the relationship between TDP-43 and TBK1, and to evaluate the consequences of TBK1 dysfunction in the aggregation of TDP-43.

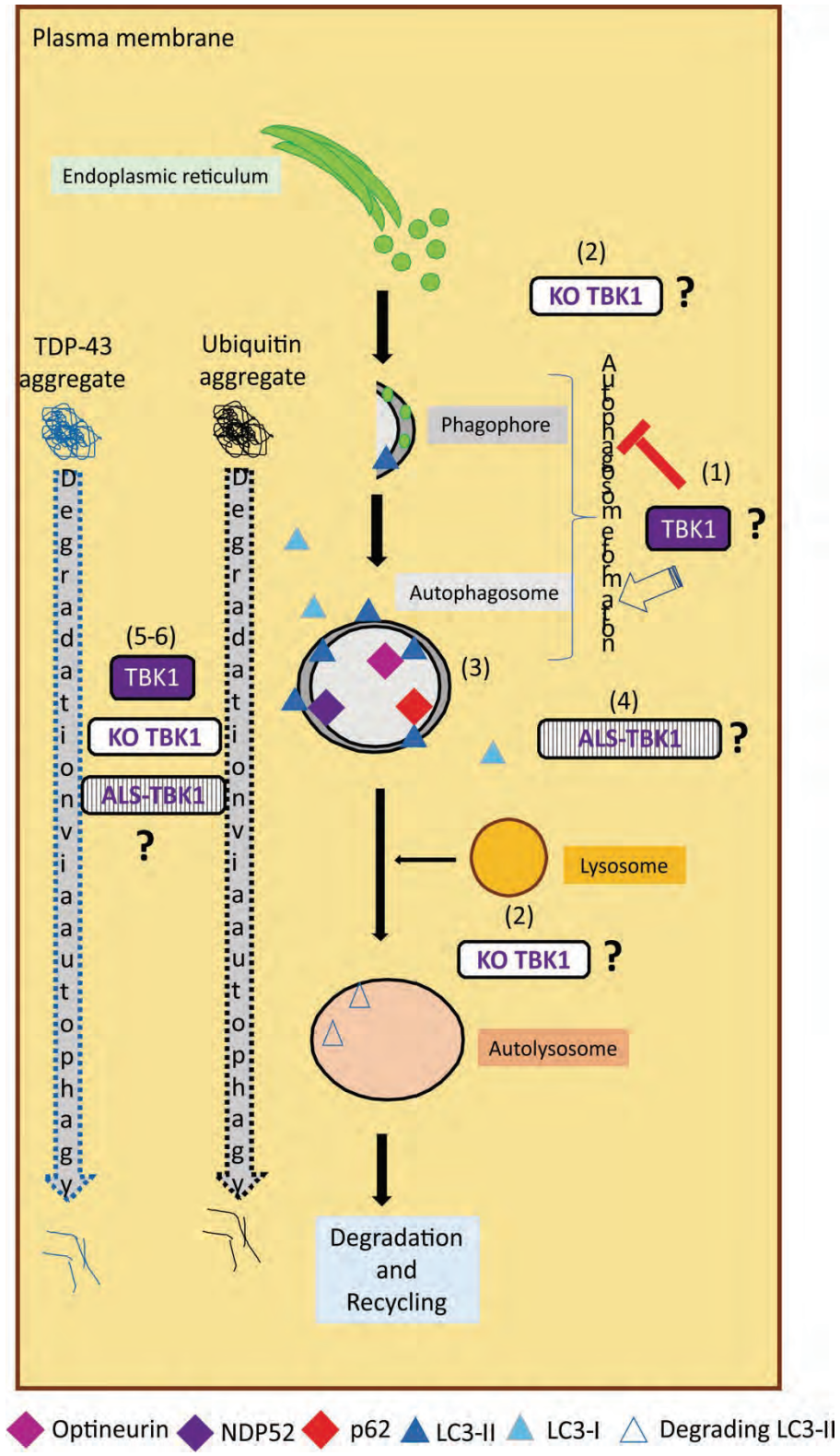


Figure 1.5. Major questions of the thesis. The role of TBK1 in autophagosome formation (1) and maturation (2) was examined by knocking out TBK1 (4) or overexpressing ALS mutant TBK1 (5) in HEK293T cells. How TBK1 influences autophagy receptors during autophagy was also examined (3). The pathological hallmark of ALS is the presence of insoluble ubiquitin and TDP-43. Therefore, the

degradation of ubiquitin and TDP-43 was analysed following TBK1 knock-out and in the presence of ALS-TBK1 (5-6).

Chapter 2

Materials and Methods

2.1 Molecular biology

2.1.1 Vectors used for protein expression

The following vectors were used in this thesis;

2.1.1.1 LC3-EGFP

The LC3-EGFP overexpressing construct, with the pEGFPC1 backbone, was a kind gift of Rogan Tinsley from Monash University (**Figure 2.1**).

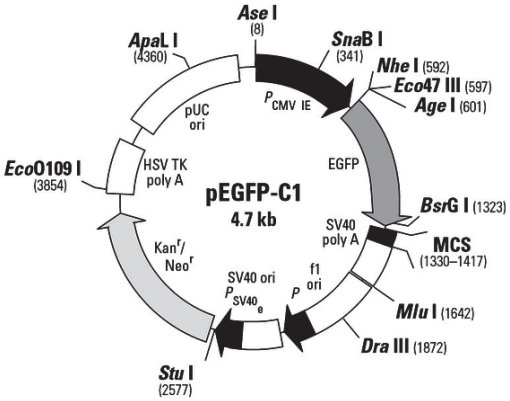


Figure 2.1. Diagram of pEGFP-C1 vector. Source of image: addgene.com.

2.1.1.2 LC3-EGFP-mCherry

The LC3B-EGFP-mCherry overexpressing plasmid, in the pBABE-puro background, was obtained from Addgene (#22418), deposited by Dr Jayanta Debnath [512] (**Figure 2.2**).

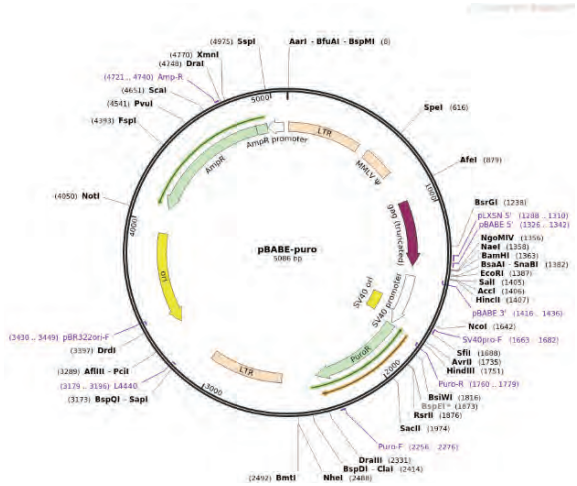


Figure 2.2. Diagram of pBABE-puro vector. Source of image addgene.com.

2.1.1.3 TBK1-FLAG

The WT-TBK1-FLAG, G159A-TBK1-FLAG and empty vector (pcDNA3.1) overexpressing plasmids, in a pcDNA3.1 + backbone, was a kind gift of Jean-Laurent Casanova, Rockefeller University [513] (**Figure 2.3**). Generation of the ALS-associated mutations used in this thesis is described in the Appendix.



Figure 2.3. Diagram of pcDNA3.1 vector. Source of image addgene.com.

2.1.1.4 DFCP1-EGFP

The DFCP1-EGFP overexpressing plasmid, in a pEGFP-C2 backbone, was a kind gift of Dr Nicholas Ktistakis, Babraham Institute, United Kingdom (**Figure 2.4**).

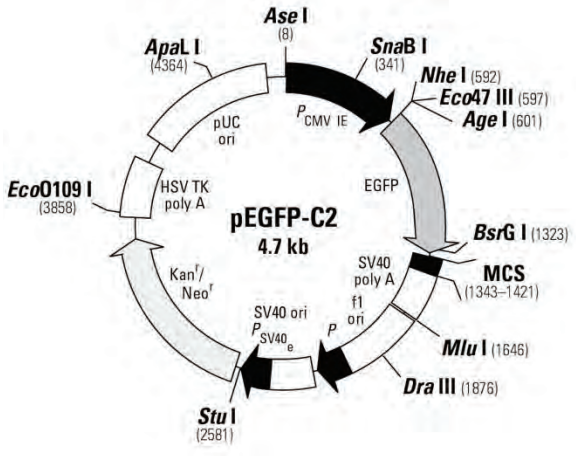


Figure 2.4. Diagram of pEGFP-C2 vector. Source of image: addgene.com.

2.1.1.5 TDP-43-GFP $^{WT/M337V}$

The TDP-43-GFP overexpressing plasmid, in the in pCMV6-AC-GFP backbone, was obtained from Origene (USA) (**Figure 2.5**).

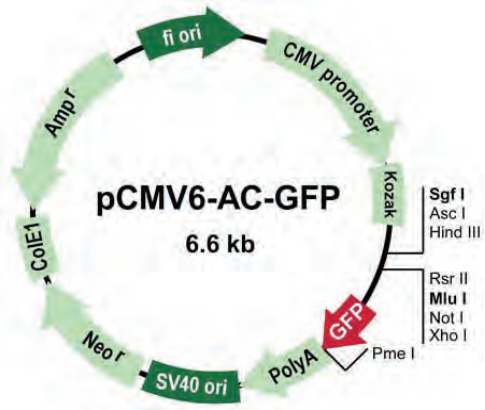


Figure 2.5. Diagram of pCMV6-AC-GFP vector. Source of image: origene.

2.1.1.6 TDP-43-GFP^{WT} and TDP-43-GFP^{dNLS}

The TDP-43-GFP^{WT} overexpressing plasmid, in the in pLenti-C-mGFP backbone, was a kind gift of A/Prof Anna King (Wicking Dementia Research and Education Centre, Tasmania, Australia) and the TDP-43^{dNLS} was a kind gift from Dr Adam Walker (Queensland Brain Institute, Brisbane, Australia) (**Figure 2.5**)..

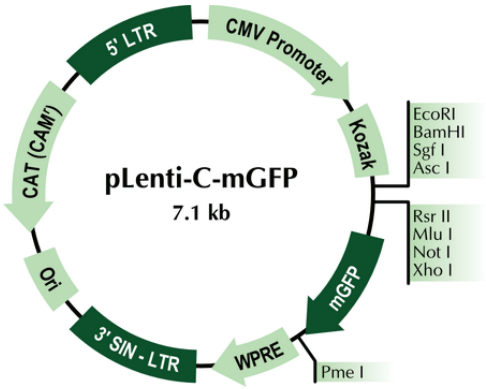


Figure 2.6. Diagram of pLenti-C-mGFP vector. Source of image: Origene.

2.1.1.7 p62-EGFP

The p62-EGFP overexpressing plasmid, in the pEGFP-N3 backbone, was a kind gift of Professor Guanghui Wang, Soochow University College of Pharmaceutical Sciences, Suzhou [514] (**Figure 2.6**).

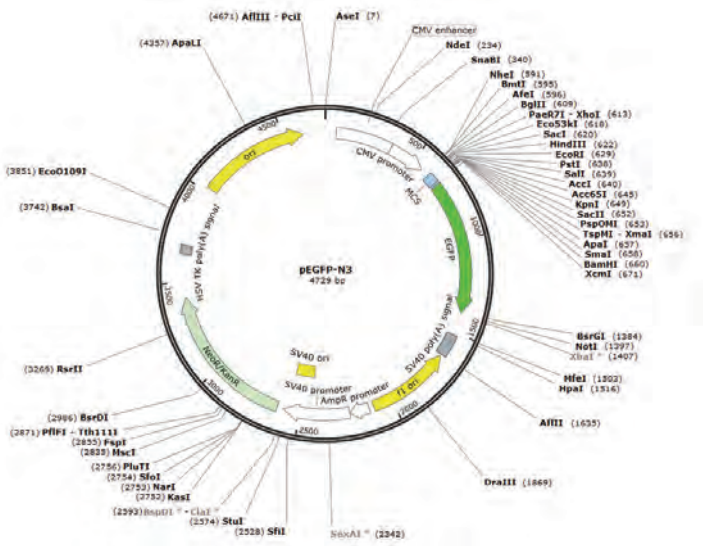


Figure 2.7. Diagram of pEGFP-N3 vector. Source of image snappgene.com.

2.1.1.8 Optineurin-EGFP

The Optineurin-EGFP overexpressing plasmid, in the in pEGFP-C3 backbone, was a kind gift of Dr Ghanshyam Swarup, Centre for Cellular and Molecular Biology, Hyderabad, India [515] (**Figure 2.7**).

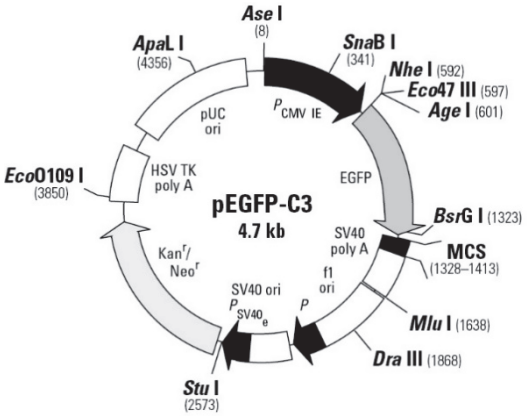


Figure 2.8. Diagram of EGFP-C3 vector. Source of image addgene.com.

2.1.2 Preparation of Luria Bertani (LB) medium and LB agar

For the preparation of LB broth, 20 g LB powder (Bacto Laboratories) was dissolved in 1 l of MiliQ water, the pH was set to 7, then the broth was autoclaved and stored at RT. For the preparation of LB agar, 20 g LB powder (Bacto Laboratories) and 10 g agar (Sigma) were dissolved in 1 l of miliQ water and pH was set to 7. Then the LB agar solution was autoclaved and cooled to 40°C, followed by the addition of the

appropriate antibiotic (Ampicillin: 100 μg/ml [Sigma], Kanamycin: 50 μg/ml [Sigma], Chloramphenicol: 25 μg/ml [Sigma] and 15ml of LB agar was spread on sterile petri dishes. Agar plates were stored at 4°C up to two weeks.

2.1.3 Transformation of bacteria

Competent cells were purchased from Bioline (Alpha Select Gold, BIO-85027) and stored at -80°C. Prior to transformation, they were thawed on ice, then the appropriate volume of DNA (1-2 μl) was added to 50 μl of cells, and gently swirled to mix. The cells were then incubated on ice for 30 min, and heat-shocked at 42°C for 30 seconds. Cells were immediately placed on ice for 5 min, then 250 μl warm Super Optimal broth with Catabolite repression (SOC) medium (Invitrogen) was added to each tube. Tubes were shaken horizontally at ~250 rpm, 37°C for 1 hr. Aliquots of 50 μl and 200 μl of each reaction were spread onto pre-warmed LB plates containing the appropriate antibiotic, which was allowed to absorb before being incubated at 37°C overnight (12-16 hr).

2.1.4 Bacteria amplification for plasmid purification

For plasmid purification, a single bacteria colony was selected from the LB agar plate and placed in a 50 ml falcon tube containing 35 ml of LB media containing the appropriate antibiotic/s. Alternatively, a sample was taken from glycerol stocks stored at -80 °C. Falcon tubes were incubated by shaking at ~250 rpm, 37°C overnight. The next day, the cell suspension was centrifuged at 6000 g for 15 min at 4°C and cell pellets were processed for plasmid purification or stored at -80°C.

2.1.5 Plasmid purification

Plasmid DNA was purified using QIAGEN® PLASMID PLUS Midi Kit according to manufacturer's protocol. Briefly, an overnight bacteria culture was centrifuged at 6000 g for 15 min at 4°C and the cell pellet was resuspended in 4 ml of resuspension buffer (P1). Then 4 ml of lysis buffer (P2) was added, inverted for 4-6 times and left to stand for 3 min. Next, 4 ml of neutralisation buffer (S3) was added and mixed. The suspension was loaded onto a QIAfilter Cartridge and incubated at RT for 10 min. Then the cell lysates were filtered using a plunger and the clear supernatant was mixed

with 2 ml of buffer BB. QIAQEN Plasmid Plus spin columns were placed into a QIAvac 24 Plus. The lysates were then transferred to QIAQEN Plasmid Plus spin columns on the QIAvac24. A 300 mbar vacuum was applied until the liquid was drawn through each column, which were then washed with 0.7 ml Buffer ETR and 0.7 ml Buffer PE using vacuum suction. Columns were then placed into an Eppendorf tube and centrifuged at 10.000 g for 1 min to remove excess washing buffer, and the DNA was eluted by adding 200 μl Buffer EB. Columns were incubated for 1 min and then centrifuged for 1 min. The DNA concentration and purity was than quantified by Nanodrop.

2.1.6 Plasmid quantification by Nanodrop

DNA quantification and purification quality were evaluated by Nanodrop2000, using Nanodrop 2000 software. The Nanodrop apparatus was blanked using EB buffer from Qiagen (vehicle solution) and each sample was measured individually. The resulting plasmid DNA was suitable for use if the absorbance ratios for 260nm:230nm were in the range of 2.0-2.2 and the 260nm:280nm ratio was approximately 1.8. Plasmid samples were aliquoted and stored at -20°C.

2.1.7 Sequencing of plasmid DNA

Plasmid DNA and DNA fragments were sequenced at the Garvan Institute. Primers (Sigma) for sequencing were dissolved at a stock concentration of 100 μM (100 pmol/μl) and a working concentration of 1 μM. 30 ng of plasmid was mixed with 3.2 pmol of primer for each reaction. Sequencing results were analysed with ApE and FinchTV software.

2.2 Mammalian cell culture techniques

2.2.1 General maintenance

HEK293T [516] cells were cultured in DMEM (Gibco) supplemented with 10% heat activated FBS (Gibco) at 37°C with 5% CO_2. Authentication of cells via STR analysis was carried out by the Garvan Institute of Medical Research, Sydney (Appendix). Cells were regularly passaged at 80-90% confluency and were discarded after 15 passages

in culture. For regular passaging, the old media was removed, and the cells attached to the plate were rinsed with sterile PBS (Life Technologies). Then the cells were rinsed with pre-warmed trypsin-EDTA (Sigma) and placed in the incubator for 2 min. Detachment of the cells was followed by a light-microscope. Trypsinization was neutralized by the addition of fresh serum-supplemented media (4 ml-T75flask, 2 ml-T25flask). Cells were placed in a new flask at a dilution ratio of 1:4 - 1:8.

Cells were regularly tested for mycoplasma contamination (using a kit from LONZA, MycoAlert™ Mycoplasma Detection Kit). Briefly, 2 ml of media from cells in culture for 48 hr was collected and centrifuged at 120 g for 5 min. 100 μl of the supernatant was added to a 96-well plate, then 100 μl of "Substrate 1" was added. The luminescence was immediately measured with a Benchmark spectrometer (PHERstar FS) (Reading A). Then 100 μl of "Substrate B" was added to each well and incubated for 15 min at RT. Luminescence was measured using the same settings (Reading B). The ratio between the two measurements was calculated (Reading B/Reading A). Cultures with a ratio above 1.2 were discarded whereas those with a ratio of lower than 0.9 were considered suitable for use. Positive and negative controls supplied by the manufacturer were included at every testing.

2.2.2 Long-term storage of frozen cells

Cells were trypsinsed at 80-90% confluence, washed with PBS, then rinsed with trypsin and the flasks incubated for 2 min. Cells were collected in media containing 10% FBS and centrifuged 120 g, 5 min at 37 °C. The cell pellet was resuspended in 95% FBS, containing 5% DMSO (DMSO: Sigma). Cells from a T75 flask were resuspended in 5 ml of FBS/DMSO mixture and aliquoted into 5 cryovials, and stored overnight in CoolCell containers (Corning) at -80°C. The next day, the frozen cells then were transferred to liquid nitrogen for long term storage.

2.2.3 Thawing of cells

Cryovials were collected from liquid nitrogen and placed on ice. Each vial was incubated in a 37 °C water bath for 30 sec, then resuspended in warm DMEM containing 10% FBS. Thawed cells were placed in the incubator overnight. The next day the media

was replaced with fresh DMEM/10% FBS. Cells were passaged at least once before using in experiments.

2.2.4 Densities of cells

Experiments were carried out in 6, 12 or 24-well plates and cells were plated in 2, 1 and 0.5 ml of media respectively. For experiments lasting for 72 hr the following densities were used; for immunoprecipitation and immunoblotting cells were plated in 6-well plates and 12-well plates respectively, at 52.000/cm^2 density. For microscopy analysis, cells were plated in 24-well plates on coverslips at 50.000/cm^2 density. Cells were incubated overnight and transfected or treated the following day. For experiments lasting for 48 hr cells were plated at 62.500/cm^2 density.

2.2.5 Counting of cells

Cells at 80-90% confluency were rinsed with PBS and trypsinized as above. The number of cells present was quantified using Scepter™ 2.0 Handheld Automated Cell Counter from Milipore or Countess II FL from Life Technologies. For the Scepter™ 2.0, the cell suspension was diluted in 1:10 in DMEM containing 10% FBS to a final volume of 150 µl. For Countess II FL, cell suspensions, cells was mixed with mixed with Tryphan Blue (Sigma) in 1:1 ratio and loaded into Countess cell counting chamber slides.

2.2.6 Transfection of cells

Cells were examined prior to transfection and transfection was only carried out if cells were 70-80% confluent. Transfection was performed in 1 ml of media in 6-well plates or in 0.5 ml of media in 24-well plates. Opti-MEM (Thermoscientific) was warmed at 37 °C in a water bath and solutions containing DNA and Opti-MEM, and Lipofectamine and Opti-MEM, were prepared according to *Table 2.*1. Then both tubes were incubated for 5 min at RT before being mixed gently, followed by incubation for 20 min, and then added to the cells drop by drop. Cells were incubated overnight and the next day the media was changed.

Table 2.1. Dilution of transfection reactions for a single well.

	Tube 1	Tube 2
0.5ml media (24-well-plate)	• 1 µg DNA • 50 µl Opti-MEM	• 2 µg Lipofectamine 2000 • 50 µl Opti-MEM
1ml media (6-well plate)	• 2 µg DNA • 100 µl Opti-MEM	• 4 µg Lipofectamine 2000 • 100 µl Opti-MEM

2.3 Protein chemistry methods

2.3.1 Lysis of cells

For immunoprecipitation and immunoblotting experiments, cells were rinsed with PBS and lysed in TN buffer (50 mM Tris, 150 mM NaCl, 0.1% NP40, 0.1% SDS, pH7.6, with protease inhibitors (Roche, 1 tablet/10 ml) and phosphatase inhibitor (Roche, 1tablet/10 ml) by incubation on ice for 15 min then transferred to Eppendorf tubes and stored at -20° C at least overnight. Lysates were then thawed on ice and centrifuged at 15.000 rpm for 15 min at room temperature. The viscous pellet containing DNA and insoluble proteins were removed and the supernatants containing cell lysates were subjected to BCA protein quantification.

2.3.2 BCA protein quantification

Protein concentration was determined using Pierce BCA Protein Assay Kit (Thermosfisher). BCA standard cure was prepared as described in **Table 2.4**.

Table 2.2. BCA standard curve.

Vial	Volume of lysis buffer (µl)	Volume of 2mg/ml BSA (µl)	Final BSA conc. (µg/ml)
A	0	300 of stock	2000
B	125	375 of stock	1500
C	325	325 of stock	1000
D	175	175 of vial B	750
E	325	325 of vial C	500
F	325	325 of vial E	250
G	325	325 of vial F	125
H	400	100 of vial G	25
I	400	0	blank

10 μl of standard curve was loaded into 96-well plates in duplicates. Then 10 μl of samples were diluted 1:5 and loaded in duplicates onto 96-well plate. Next, reagent A and reagent B was mixed in 50:1 ratio in adequate quantities required to fill all wells containing sample or standard curve. Then 100 μl of the reagent A/B mix was added to each well and incubated at 60 °C for 15 min. Protein concentration was then detected via a Benchmark spectrometer (PHERstar FS) with absorbance wavelength of 560 nM.

2.3.3 Immunoblotting

10-30 μg of protein was mixed with 10X NuPage reducing agent (ThermoFisher) and in 4x Lamelli buffer (BioRad) to a final concentration of 1X. The volume was adjusted to 30 µl with TN buffer. Samples were then denaturated at 95°C for 10 min using a Thermocycler (POCD Scientific) and loaded onto pre-prepared BioRad 4-15% gradient SDS-polyacrylamide gels. As a reference ladder for molecular weight assessment, Precision Plus Protein^{TM} Dual Color Standards (BioRad) were used.

Electrophoresis was carried out at 150 V in BioRad tanks using SDS-glycine electrophoresis buffer supplied by BioRad. Separated proteins were transferred to nitrocellulose membrane using BioRad Trans-Turbo system. Settings for transfer were 20 min, 2.5 A, 25 V. Nitrocellulose membrane then was processed for immunoblotting.

Membranes were blocked in 5% skim milk or 5% BSA (Sigma) in TBS-T (50 mM Tris, 150 mM NaCl, pH7.6, 0.1%Tween) for 1 hr at RT, then incubated with primary antibody overnight at 4^{o}C in blocking media (**Table 2.5**). Membranes were washed 3x 5 min in TBS-T and incubated with HRP-conjugated secondary antibody at 1/2000-1/5000 concentration in blocking media. Then membrane was washed 3x 5 min in TBS-T and revealed using ECL chemiluminescence reagent (Bio-rad) and Chemidoc XRS (Bio-rad). Multiple images were taken of each membrane prior to signal saturation. Membranes were stripped using Reblot Plus solution (Chemicon) according to the manufacturer's protocol and re-probed for other proteins of interest or a loading control protein. Densitometry analysis was carried out using ImageJ software (v. 1.47. National Institutes of Health).

Table 2.3. Antibodies used int this study.

Antibody	Species	Manufacturer	Dilution for IB	Dilution for ICC
TBK1	rabbit	Abcam Ab40676	1/1000	1/400
LC3B	rabbit	Novus Biologicals NB100-2220	1/1000	-
p62	mouse	Cell signaling 88588	1/1000	-
NDP52	rabbit	Cell signaling 607325	1/1000	-
Optineurin	rabbit	Cayman Chemicals 100002-100 μl	1/500	-
GAPHD	mouse	Proteintech 60004-I-Ig	1/5000	-
Actin	mouse	Sigma A2228	1/5000	-
TDP-43	rabbit	Cosmo Bio co TIP-TD-P09	1/1000	-
EGFP	mouse	Sigma G1546-100 μl	1/1000	-
Ubiquitin	mouse	Abcam ab122	1/10000	-

2.4 Microscopy techniques

2.4.1 Fixation of cells

For microscope analysis, cells were plated onto coverslips (Thermofisher Scientific) in 24-well plates. Following transfection and/or treatment cells were rinsed in PBS and fixed in 4% (v/v) PFA-PBS (PFA: ProSciTech) for 10 min. The cells were then washed with PBS three times and processed for staining or stored at 4°C for up to 1 week prior to processing.

2.4.2 Staining of cells

Prior to staining, cells were permeabilised in 0.1% Triton-PBS (Sigma) for 2 min and washed with PBS three times, then blocked in 3% BSA-PBS for 60 min. Cells were incubated with the specific antibody overnight at 4 °C in 1% BSA-PBS. The following day, cells were washed three times with PBS and incubated with fluorescently-labelled secondary antibody (Life Technologies) at 1/200 concentration for 1 hr with gentle agitation at RT. Then nuclei were then stained with Hoechst 33342 (Sigma) (3/10.000, 3 min) and coverslips were mounted in Dako fluorescent mounting media (Dako). Coverslips were then left to dry at RT for overnight and stored at 4°C in dark.

2.4.3 Microscopy analysis

2.4.3.1 Image acquisition

Images were taken with a Zeiss LSM 880 inverted confocal laser-scanning microscope equipped with LSM-TPMT camera (Zeiss) with 63x/na=1.4 or 100x/na=1.46 objectives. In the case of multichannel imaging, photomultiplier sensitivities and offsets were set to a level at which bleed through effects from one channel to another were negligible. Alternatively, pictures were taken with Zeiss epifluorescent microscope at 40x magnification. Images were analysed using Zen software (Zeiss) blue or black edition.

2.5 Flow cytometry techniques

For flow cytometry analysis, cells were treated with saponin, fixed and analysed via BD LSR Fortessa X-20 and FACS Diva software. The media was first removed and the cells were washed once with PBS. Then, saponin-PBS (Sigma) solution at the appropriate concentration was gently added to the cells and incubated for 5 min at RT. Saponin solution was then gently removed and the cells were detached in cold PBS and centrifuged for 5 min at 1000 RPM. Supernatants were removed and cells were immediately fixed (section 6.2). Control cells that were not treated with saponin were subject to the same procedure in the presence of PBS alone.

Cells pellets were resuspended in 500 μl of 4% (v/v) PFA-PBS and incubated for 10 min at RT. After 10 min, the samples were centrifuged at 120 g for 5 min, PFA was removed and the pellets were washed three times with PBS. Cells were processed for staining, alternatively, if staining was not required, cells were processed by FC.

TBK1-FLAG overexpressing cells were stained with FLAG-APC fluorescently labelled primary antibody for 30 min at RT, then centrifuged, resuspended in PBS and processed immediately using the BD LSR Fortessa X-20. Alternatively, cells were processed without additional staining for FC analysis. No overlay was detected between the channels, therefore no compensation was needed for multiple channel analysis. The appropriate fluorescence cut-off was determined based on non-transfected/non-stained cells. Analysis was carried out using FACS diva software.

2.5.1 Autophagy analysis using LC3-EGFP-mCherry overexpressing plasmid

LC3-EGFP analysis

Threshold for fluorescent intensity was determined based on non-transfected cells. The EGFP positive subpopulation of cells were gated. The percentage of $EGFP^+$ cells was calculated as follows:

($EGFP^+$ cells/ total analysed cell number) x 100.

Averaged data based on at least 3 biological replicates are shown in each figure. In each biological replicate, at least 10.000 $EGFP^+$ events were recorded.

Autophagosome/ autolysosome ratio

Threshold for fluorescent intensity was determined based on non-transfected cells. For analysis $mCherry^+$ cells were gated then the subpopulation of EGFP+ cells was calculated as follows in $mCherry^+$ cells:

$$(EGFP^+ \text{ cells}/mCherry^+ \text{ cells}) \times 100$$

Averaged data based on at least 3 biological replicates are shown in each figure. In each biological replicate, at least 10.000 $mCherry^+$ events were recorded.

2.6 Statistics

One-way ANOVA with Tukey or Dunnett post-hoc and un-paired student t-test were performed as indicated. Significance was established when a p value of 0.05 or less was obtained.

Chapter 3

Investigating the role of TBK1 in basal and starvation-induced autophagy

3.1. Introduction

Defective autophagy is one of the proposed mechanisms associated with motor neuron degeneration, as discussed in Chapter 1. Hence, defining the precise role of TBK1 in autophagy is important in understanding disease mechanisms in ALS. The overall aim of the studies described in this chapter was to systematically determine whether TBK1 is required for basal autophagy and starvation-induced autophagy, and to analyse how TBK1 functions in these pathways.

3.1.1. The role of TBK1 in basal autophagy

Basal autophagy is involved in cellular quality control that aims to maintain intracellular homeostasis. During normal cellular processes, intracellular organelles may become damaged or, due to changes in the rates of metabolism, may become unnecessary [517] and need to be degraded.

Very few studies have analysed the role of TBK1 during basal autophagy in normal cells. In fact, most previous studies have focussed on the role of autophagy in enhancing the survival and growth of cancer cells. Basal autophagy is upregulated and essential in hypoxic tumour conditions [518]. Cancer cells harbouring oncogenic mutations in *Kirsten rat sarcoma (KRAS)* require highly efficient autophagy to maintain oxidative metabolism, glycolysis and consequently their growth and survival [519-522]. These mutations are most common in aggressive cancers with poor outcomes, including pancreatic, colon and lung cancers [523]. RNA interference studies have identified TBK1 as an essential element for survival in KRAS mutant cells [524]. TBK1 drives basal autophagy in KRAS-dependent lung cancer cells via the sequestration of NDP52 and consequent induction of non-canonical NFκB signalling [525]. Interestingly inhibition of autophagy prolongs TBK1 activation and TBK1 induced inflammation in pancreatic cancer cells [526], indicating that the role of TBK1 in autophagy is linked to its role in inflammation. In contrast, the contribution of TBK1 to basal autophagy in non-cancer cells remains to be elucidated. Neurons rely heavily on basal autophagy, similar to cancer cells, for their survival [393, 400]. Hence, it is feasible that TBK1 normally functions in basal autophagy, and this possibility was therefore examined in this chapter.

3.1.2. The role of TBK1 in starvation-induced autophagy

TBK1's involvement in starvation-induced autophagy has not been widely studied either. Inhibition of the kinase activity of TBK1 or knock-out of TBK1 inhibited the starvation-induced autophagic engulfment of bacteria (*M. tuberculosis*) in macrophages [487]. This may be mediated by p62, NDP52, LC3, UVRAG and Rab8b, because these proteins were shown to co-fractionate with TBK1 [487]. Interestingly, UVRAG is the component of the Beclin 1- hVPS34 complex II that controls autophagosome maturation into lytic compartments [527]. Furthermore, UVRAG colocalises with TBK1 [487]. This raises the possibility that TBK1 may take part in the fusion of autophagosome and lysosomes during starvation-induced autophagy. Interestingly, the levels of phosphorylated TBK1 decrease upon starvation [526], while depletion of *atg3* or *atg7* prolongs the phosphorylation of TBK1 [526], therefore suggesting that whilst TBK1 induces autophagy, a negative feedback mechanism exist to inhibit TBK1 [526]. However, the exact role of TBK1 in starvation-induced autophagy remains to be elucidated.

It is controversial whether starvation-induced autophagy exists in neurons. Brain tissues generally have a very high ratio of LC3-I:LC3-II [1]. Furthermore, it was shown that autophagy is not activated in neurons upon starvation *in-vivo*, [402] and LC3-I remains largely diffuse [528]. In contrast, other studies have shown that starvation induces autophagy in primary cortical neuron cultures *in vitro* [425, 426]. Hence, it remains inconclusive how neurons respond to starvation.

3.1.3. Monitoring autophagy experimentally

Autophagy is a complex, multistep process, and according to an the internationally accepted guidelines of Klionsky et. al, [464, 529, 530], strict rules apply for reliable autophagy examination. Accurate detection of autophagy induction, autophagy flux and autophagosome-lysosome fusion, requires the combination of multiple techniques [464, 529, 530]. Therefore, a combination of several methods was used throughout this chapter (and the rest of the thesis) to analyse autophagosome formation and degradation under conditions of both basal, non-selective autophagy (this chapter) and aggrephagy (Chapter 5).

3.1.4. Use of LC3-I and LC3-II to monitor autophagy

Lipidated LC3 (LC3-II) is present on the autophagosome and it associates with the nascent phagophore [358]. The most commonly used method to detect the levels of LC3-II is immunoblotting, because LC3-I and LC3-II are easily differentiated on SDS-PAGE. Whilst LC3-II has a larger molecular weight than LC3-I due to the covalent addition of the phospholipid PE, LC3-II migrates faster due to its greater hydrophobicity [531]. Analysis of LC3-II levels via immunoblotting reflects the total amount of autophagosomes in the population and thus can be used to monitor autophagy. It must be noted that LC3-II is also located to phagophores, therefore LC3-II levels represent both phagophores and autophagosome [390], however it is generally accepted that LC3-II detect autophagosomes rather than autophagy [464]. Furthermore, quantification of LC3-II levels in combination with bafilomycin treatment can be used to monitor both autophagosome formation and degradation [457]. However, autophagy is cell type dependent and in some cells autophagy induction may manifest in decreased levels of LC3-I rather than increased LC3-II [464]. Therefore, for accurate detection of autophagy, both LC3-I and LC3-II levels should be evaluated [464].

3.1.5. Using bafilomycin to identify defects in autophagosome formation and degradation

Bafilomycin is an inhibitor of the vacuolar H^+-ATPase, which prevents the fusion of autophagosomes to lysosomes, as well as the acidification of lysosomes [532]. Bafilomycin is used in autophagy studies to provide insights into the mechanisms underlying autophagy dysregulation. For example, elevated LC3-II levels detected experimentally indicate that autophagosomes have accumulated. However, this observation alone cannot allow us to determine whether this has arisen from increased autophagosome formation, or from inhibition of fusion between autophagosomes and lysosomes, so that the degradation of the autophagosome is abrogated. Therefore, the use of bafilomycin to artificially inhibit the fusion between autophagosomes and lysosomes, and thus effectively eliminate this part of the autophagy pathway, allows us to distinguish between these two possibilities. To illustrate, several possible scenarios are shown in **Figure 3.1**. An experimental treatment 'A' **(Figure 3.1A)** leads to increased LC3-II levels in the absence of bafilomycin. To determine whether more autophagosomes are formed or less autophagosomes fuse with lysosomes, cells are treated with bafilomycin. If

autophagosome-lysosome fusion is prevented by treatment A (Scenario A), similar levels of LC3-II accumulate when cells are treated with bafilomycin as in untreated conditions. This occurs because the production of LC3-II does not change upon treatment A, and autophagosome degradation cannot take place due to the presence of bafilomycin. Therefore, similar levels of autophagosomes (LC3-II) accumulate in bafilomycin treated and untreated conditions (Scenario A, **Figure 3.1A**). However, alternatively, if treatment A results in the production of more autophagosomes, then upon bafilomycin treatment, even more LC3-II will accumulate, because bafilomycin inhibits their fusion with lysosomes (Scenario B, **Figure 3.1A**). In contrast, if an experimental treatment 'B' leads to lower LC3-II levels, this indicates that either autophagy flux is increased or fewer autophagosomes are formed. Hence, upon induction of autophagy, in the presence of bafilomycin, increased levels of LC3-II accumulate if autophagy flux is increased (Scenario C, **Figure 3.1A**), but in the absence of bafilomycin, due to more autophagosome degradation the levels of LC3-II do not increase. However, alternatively, if fewer autophagosomes are formed by treatment B, less LC3-II would accumulate in the presence of bafilomycin (Scenario D, **Figure 3.1A**). Therefore, the formation and degradation of autophagosomes needs to be analysed by parallel experiments in which cells are treated with bafilomycin, or other lysosomal inhibitors.

3.1.6. Autophagy detection by confocal microscopy using fluorescently tagged autophagy markers

As well as immunoblotting for LC3-II, another commonly used technique to monitor autophagy is fluorescent confocal microscopy of cells expressing constructs encoding LC3 **(Figure 3.1B)** or DFCP1 **(Figure 3.1C)**, to visualise either autophagosomes or omegasomes (the precursor of the autophagosomes) respectively. Overexpression of fluorescently tagged-LC3 allows the detection of both LC3-I (displaying diffuse cytoplasmic localisation), and LC3-II (expressed as vesicular structures) [464]. To quantitate the formation of autophagosomes, the total number of cells containing one or more autophagosomes, or the total number of autophagosomes produced per cell, can be determined. Similarly, the formation of omegasomes can be quantitated by quantification of DFCP1-positive puncta in cells [324]. While in most cells the autophagosome membrane can originate from either the ER, mitochondria or Golgi, in neurons the main source of the autophagosome membrane is the ER [386]. Hence, in

this study, the most physiologically relevant marker to examine alongside LC3 was DFCP1 to monitor the formation of the omegasome.

3.1.7. Use of dual-tagged LC3 construct to monitor autophagy

As well as using constructs encoding LC3 with a single tag, dual tagged constructs have also been developed specifically for monitoring autophagy [447]. Overexpression of LC3 conjugated to both EGFP and mCherry (LC3-EGFP-mCherry) allows the detection of both autophagosomes and autolysosomes simultaneously. This technique is based on the pH sensitivity of EGFP, which is quenched in acidic pH [533-535]. As the interior of the autophagosome is relatively neutral (pH 6.2-5.8 [535]), both EGFP and mCherry are excitable, and thus autophagosomes appear yellow in fluorescent conditions due to expression of both fluorophores ($EGFP^+/mCherry^+$) **(Figure 3.1D)**. However, in contrast, due to more acidic environment of autolysosomes (pH 5.4-5) [535], the EGFP signal becomes quenched and only mCherry is excitable. Hence autolysosomes appear red under fluorescent conditions ($EGFP^-/mCherry^+$) **(Figure 3.1D)**.

3.1.8. Autophagy detection via flow cytometry

Whilst immunoblotting and microscopy analysis of LC3 are widely used to monitor autophagy, these approaches can also be problematic and labour-intensive [464]. During immunoblotting, individual cells cannot be analysed, and the whole population is sampled. Therefore, it can sometimes be difficult to detect differences in LC3-II by this method, particularly for studies in which there is a low transfection efficiency. In contrast, using microscopy analysis, single cells can be analysed individually. However, the disadvantage to this method is that this is much more labour intensive and much fewer cells can be examined in comparison. Other limitations of microscopy may include subjectiveness of how cells are imaged and counted. Furthermore, usually not the whole cell is sampled but only one focal section of cell is analysed, therefore microscopy analysis can be inaccurate. In contrast, a small number of reports have used flow cytometry (FC) to monitor autophagy under various conditions, which has the advantage of being a quick, robust, high throughput single cell analysis method [534, 536-541]. However, this method is still not widely used.

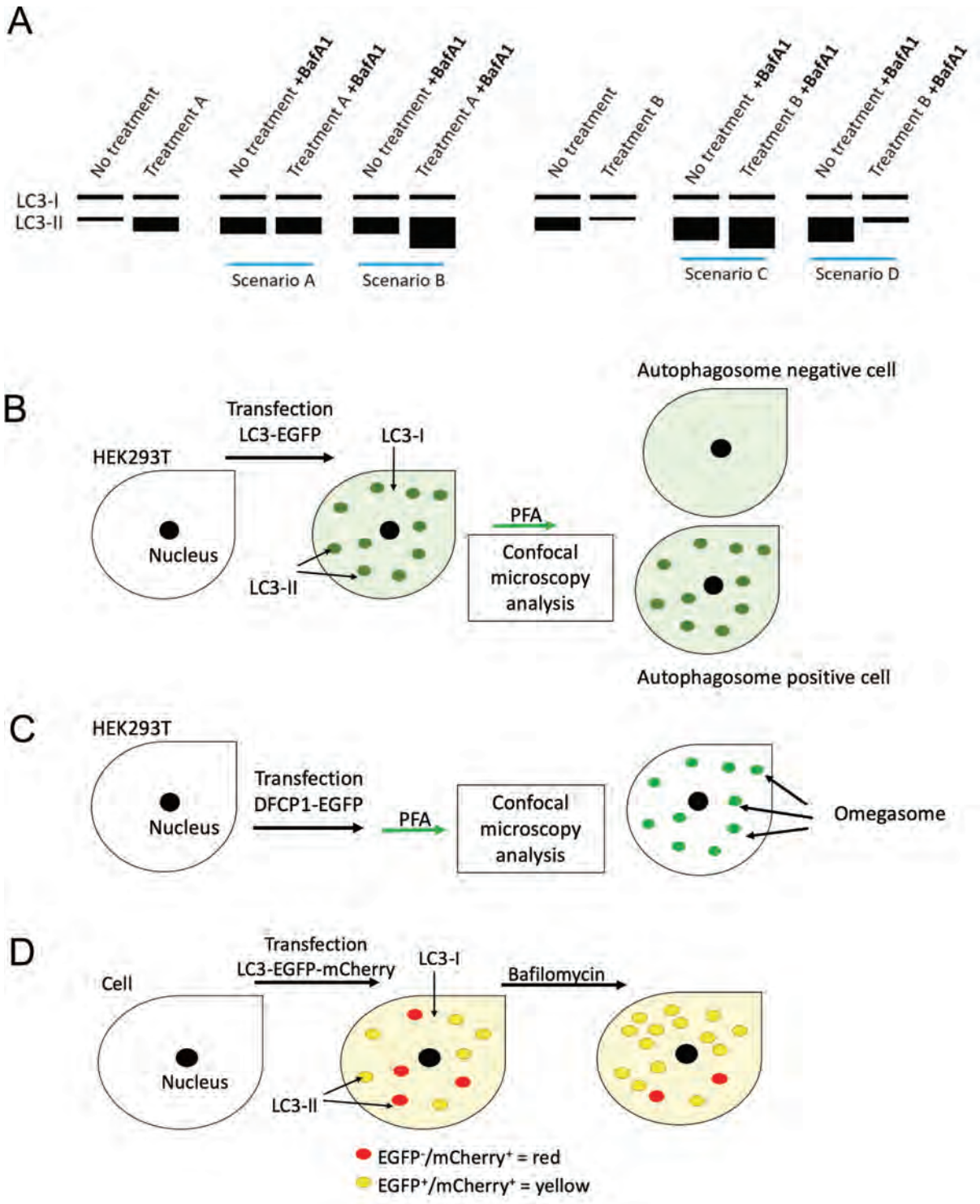


Figure 3.1. Schematic representation of methods to detect autophagy. (A) *The use of bafilomycin and its effect on autophagosome degradation.* Bafilomycin inhibits the fusion of the autophagosome to the lysosome, therefore inhibiting the degradation of the autophagosome. Treatment with 'A' inhibits autophagosome-lysosome fusion, which manifests as increased LC3-II levels and similar levels in the presence of bafilomycin, indicating that 'A' prevents autophagosome degradation (Scenario A). However, when

more autophagosomes are formed by treatment with 'A', increased LC3-II levels are present in cells treated with bafilomycin (Scenario B). Decreased LC3-II levels upon treatment B may be due to induced autophagosome degradation resulting in elevated LC3-II accumulation upon lysosomal inhibition (Scenario C). In contrast, in the case of decreased autophagosome formation, lower LC3-II levels accumulate upon bafilomycin treatment (Scenario D). **(B)** *Schematic representation of microscopy analysis to examine autophagosome formation.* HEK293T cells are transfected with LC3-EGFP. Autophagosome vesicles are apparent under the microscope, and cells containing LC3-EGFP vesicles are categorised as autophagosome positive cells. **(C)** *Schematic representation of microscopy analysis to examine omegasome formation.* HEK293T cells are transfected with DFCP1-EGFP. Omegasomes are counted in each transfected cell. **(D)** *Schematic representation of flow cytometry analysis to examine autophagy.* Cells are transfected with dual tagged LC3. Cells positive for both EGFP and mCherry are autophagosomal cells, while cells positive for only mCherry are autolysosome positive cells.

3.1.9. Inhibitors of the kinase activity of TBK1

TBK1 belongs to the IKK-related kinase family with IKKε [542], and its role in innate immunity has been well characterised using several inhibitors [543-545]. Upon activation, TBK1 undergoes auto-phosphorylation on serine residue 172 [471, 546], which is mediated by ATP binding to a cleft between the N- and C-lobes [466]. Two previously developed inhibitors of the kinase activity (BX795, MRT67307) were selected [547] to use in this thesis, which compete with ATP [466, 472] and inhibit the auto-phosphorylation of TBK1.

BX795 was originally developed as 3-phoshphoinositide-dependent kinase 1 (PDK1) inhibitor [548] but was later found to also be a potent inhibitor of TBK1 and IKKε. Furthermore, it was subsequently found to be a more potent inhibitor of TBK1 than of PDK1 [549]. BX795 was previously shown to block TBK1 and IKKε mediated activation of IRF3 and production of IFN-β, independently of PDK1 [472]. While BX795 inhibits TBK1 autophosphorylation upon overexpression, surprisingly BX795 did not inhibit phosphorylation of endogenous TBK1 [472], nonetheless BX795 still supressed

the phosphorylation of interferon regulatory factor 3 (IRF3) by TBK1 in response to lipopolysaccharide (LPS) [472] proving TBK1 inhibition.

Several derivatives of BX795 were later developed to be more effective inhibitors of TBK1 [550] including MRT67307, which also inhibits TBK1 meditated phosphorylation of IRF3 [550]. Furthermore, MRT67307 inhibited the phosphorylation of endogenous TBK1 [550]. Several off-target effectors of MRT67307 are known, including ULK1 and ULK2, which are involved in autophagy [551]. Therefore, the concentrations of MRT67307 used through this thesis were below the concentrations known to affect ULK1/2.

3.1.10. CRISPR/Cas9 genome editing

CRISPR/CAS9 is a genome editing tool that can be used to create knockout (KO) cell lines. Prokaryotes contain short DNA repeats known as 'clustered regularly interspaced short palindrome repeats' (CRISPR), that are recognized by regular spacing between the recurring units [552, 553]. These elements are derived from pre-existing foreign genetic sequences, such as bacteriophages or conjugative plasmids, and represent an underlying immunity mechanism of prokaryotes [554, 555] that uses antisense RNAs as memory signatures of past infections [556].

In prokaryotes, CRISPR repeat space arrays are transcribed and processed into short CRISPR RNAs (crRNA), containing conserved repeat fragments and guide RNA sequences complementary to the invading nucleic acid strand [557-559]. During attack on a prokaryote, the invading DNA or in the case of laboratory genome editing, the (human) genome is recognised by a proto-spacer sequence (PAM) [560] [554], which is a short motif adjacent to crRNA-targeted sequences on the invading DNA/human genome. crRNA (or during genome editing this is named 'guide RNA' (gRNA)), combines with Cas proteins that recognise the genome by pairing to the complementary strand, inducing sequence specific cleavage [559, 561]. Cas9 is a type II endonuclease that can be directed [562] [552] to induce double stranded breaks (DSB) in the target DNA and has been previously used in human cells [563]. DSB introduced by Cas enzymes need to be repaired, and in mammalian cells, this is facilitated by non-homologous end joining (NHEJ) or homology directed repair (HDR) [564]. However, in neurons, only NHEJ is present [565, 566]. In genome editing studies, NHEJ is generally

used to knockout genes, whereas HDR is utilised to introduce specific mutations to the genome [567]. Hence, using this technique, expression of specific genes can be knocked out by introducing a DSB close to the initiator ATG sequence. Cells where gene expression is depleted due to faulty DNA repair are then selected.

3.2 Objectives of this chapter

Dysfunction of macroautophagy is now widely reported in ALS. However, whilst TBK1 has been extensively studied in the context of mitophagy [132, 392, 394, 456, 478, 479, 482, 485-487, 568]and xenophagy, few studies have examined the role of TBK1 in basal and starvation-induced macroautophagy. In both mitophagy and xenophagy, TBK1 is known to phosphorylate several autophagy adaptors, including optineurin [132], p62 [392] and NDP52 [478], thus facilitating the autophagic degradation of cargo. TBK1 also promotes the survival of cancer cells via basal autophagy [525, 569-571]. However, the normal functions of TBK1 in basal autophagy and whether this is dysfunctional in ALS are undefined. Hence, the studies described in this chapter aim to characterise the role of TBK1 in both basal and starvation-induced macroautophagy. This analysis therefore forms the basis of future studies examining the role of TBK1 in autophagy in ALS, as described in chapters 4 and 5.

- The involvement of TBK1 in basal and starvation-induced autophagy was systematically analysed using several methods approved by the Klionksy guidelines [464] including flow cytometry, microscopy analysis and immunoblotting. Basal and starvation-induced autophagy was followed by addition of fresh media or HBSS, respectively.
- Specific TBK1 inhibitors, BX795, MRT67307, were used to examine the role of the kinase activity in autophagosome formation and degradation using flow cytometry and immunoblotting.
- CRISPR/Cas9 editing was then used to create HEK293T TBK1 KO cells. Basal and starvation-induced autophagy was analysed in these genome edited cells.

3.3 Materials and Methods

3.3.1 TBK1 inhibition

TBK1 inhibition of transfected or transfected cells were carried out as described below.

3.3.1.1 BX795 treatment

BX795 (Cayman Chemicals) was dissolved at 10 mM final concentration in sterile DMSO, aliquoted and stored at -20°C. Prior to treatment, an aliquot was thawed and diluted in DMEM/10% FBS to a final concentration of 1 μM. Cells were treated with BX795 for total of 24 hr with additional treatment as described elsewhere (Autophagy Induction).

3.3.1.2 MRT67307 treatment

MRT67307 (Sigma) was dissolved at 25 μM concentration in sterile miliQ H_2O and stored at 4 °C. Prior to treatment it was diluted in DMEM/10% FBS for final concentration of 25 nM. Cells were treated with MRT67307 for total of 24 hr with additional treatment as described elsewhere (Autophagy Induction).

3.3.2 Autophagy induction

3.3.2.1 Basal autophagy

Basal autophagy was followed in the presence of 100 nM bafilomycin A1 (Sigma) dissolved in DMSO (Sigma) for 4 hr.

- In TBK1 inhibited cells; cells were incubated overnight, then cells were pre-treated with BX795 and MRT67307 for 20 hr and then media was replaced with medium containing TBK1 inhibitors, bafilomycin A and/or vehicle control and incubated for additional 4 hr (DMSO/DMSO, DMSO/BafA1, BX795/DMSO, BX795/BafA1 or H_2O/DMSO, H_2O/BafA1, MRT67307/DMSO, MRT67307/BafA1).

- CRIPSR/Cas9 edited cells were cultured for 2 days prior to induction of basal autophagy by changing the serum rich media in the presence of 100 nM bafilomycin A or DMSO and incubated for 4 hr.

- Plasmid expressing cells (LC3-EGFP, LC3-EGFP-mChrery, DFCP1-EGFP) were transfected and cultured for 44 hr post-transfection. Basal autophagy was induced by addition of fresh serum rich media in the presence of 100 nM bafilomycin A or DMSO and incubated for a further 4 hr. Alternatively, cells were treated with TBK1 inhibitors at 24 hr post-transfection for 20 hr then media was replaced with medium containing TBK1 inhibitors, bafilomycin A and/or vehicle control, and incubated for additional 4 hr.

3.3.2.2 Non-selective autophagy

Non-selective autophagy was induced by Hank's basal salt solution (HBSS) (Gibco) for 4 hr in the presence or absence of 100 nM bafilomycin A1.

- In TBK1 inhibited cells; cells were incubated overnight, then pre-treated with BX795 and MRT67307 for 20 hr. Then HBSS was administered, containing TBK1 inhibitors, bafilomycin A and/or vehicle control (DMSO/DMSO, DMSO/BafA1, BX795/DMSO, BX795/BafA1 or H_2O/DMSO, H_2O/BafA1, MRT67307/DMSO, MRT67307/BafA1).

- CRIPSR/Cas9 edited cells were cultured for 2 days prior to induction of non-selective autophagy by changing the media to HBSS in the presence of 100 nM bafilomycin A1 or DMSO, followed by incubation for 4 hr.

- Plasmid expressing cells (LC3-EGFP, LC3-EGFP-mCheery, DFCP1-EGFP) were transfected) and cultured for 44 hr post-transfection and non-selective autophagy was induced by changing the media to HBSS in the presence of 100 nM bafilomycin A1 or DMSO and incubated for a further 4 hr. Alternatively, cells were treated with TBK1 inhibitors at 24 hr post-transfection for 20 hr then media

was changed to HBSS containing TBK1 inhibitors, bafilomycin A1 and/or vehicle control and incubated for additional 4 hr.

3.3.3 Microscopy techniques

3.3.3.1 Quantification of LC3-EGFP and DFCP1-EGFP vesicles

Images were taken with 63x/na=1.4 or 100x/na=1.46 objectives on a Zeiss LSM 880 inverted confocal laser-scanning microscope, equipped with a LSM-TPMT camera (Zeiss) and analyzed by Zen software (Zeiss, blue edition). Coverslip sections to image were selected blindly, based on Hoechst staining alone, therefore no preference was introduced into imaging cells with autophagosomes or omegasome. Cell counting was performed blindly. Due to the low average number of LC3-vesciles in cells and high number of cells not presenting with LC3-EGFP vesicles, the ratio of cell undergoing autophagy was counted. Cells undergoing autophagosomes were counted if EGFP positive round vesicles were present outside of the nucleus. Not all LC3-EGFP positive cell contained autophagosome therefore a ratio of autophagosome positive cells were calculated, by dividing the number of autophagosome positive cells with the number of LC3-EGFP transfected cells. Omegasome formation was analyzed by the presence of cytoplasmic DFCP1-EGFP vesicles. Not all DFCP1-EGFP positive cell contained omegasome therefore, the average number of omegasomes was calculated, by dividing the total number of omegasomes with the number of DFCP1-EGFP transfected cells. In each condition at least 50 transfected cells were analysed.

3.3.4 CRISPR cell generation

3.3.4.1 Generation of gRNA expression plasmid

TBK1 KO HEK293T cells were generated using CRIPSR/Cas9 system (GeneArt® CRISPR Nuclease Vector with OFP Reporter Kit, Thermofisher, A21174). Double stranded DNA complementary to TBK1 specific guide RNA sequence was inserted into the expression plasmid. Previously described forward and reverse strand oligonucleotides [480], to form the double stranded DNA, were synthesised by Sigma. Ligation was performed according to the manufacturer's protocol. Briefly, to generate double stranded oligos the following were mixed at RT; 5 μl of forward strand

oligonucleotide (200 μM), 5 μl of reverse strand oligonucleotide (200 μM), 2 μl of 10X oligonucleotide annealing buffer and 8 µl DNase/RNase-free water. The oligonucleotides were heated at 95 °C for 4 min and cooled to 25 °C for 10 min. Oligonucleotides stock (50 μM) was diluted 100 fold in DNAse/RNAse-free water and another 100 fold in DNase/RNase-free water/annealing buffer mixture, for a final concentration of 5 nM. Next, double stranded oligonucleotide was ligated into the vector. The ligation mix was prepared as follows 4 μl 5X Ligation buffer, 2 μl ds oligonucleotide (5 nM), 2 μl Linearized GeneArt CRISPR nuclease vector, 11 μl DNase/RNase-free water and 1 μl T4 DNA ligase and incubated at RT for 10 min. 3 μl of the ligation mix then was used to transform 50 μl competent cells. The transformed bacteria were amplified in LB media and the plasmid was purified. The success of ligation reaction was confirmed by sequencing (Garvan Institute).

3.3.4.2 Generation of TBK1 KO cells

3.3.4.2.1 Transfection with TBK1 KO CRISPR/Cas9 plasmid

Cells were plated in a 6-well-plate and transfected with TBK1 gRNA containing CRISPR/Cas9 vector. 48 hr post-transfection cells were trypsinsed and plated in 96-well plates following by a serial dilution to achieve the presence of single cell in each well.

3.3.4.2.2 Single cell selection

Growth of the cell population was followed by daily examination of the plates with a light microscope. Wells that initially contained more than 1 cell per colony were instantly discarded. Dot-blotting of the remaining cell colonies was used to screen for TBK1 KO cell lines. Western blotting was performed on cell lysates to confirm TBK1 knock-out. Single cell sub-selection was carried out as described above to ensure that the all populations bore the same mutation. In selected clones the genomic region was amplified via MyTaq™ Extract-PCR Kit (Bioline) and sequenced. Two rounds of single clone sub-selection were performed.

3.3.4.2.3 Sequencing of TBK1 KO clones

MyTaq™ Extract-PCR Kit (Bioline) was used to extract genomic DNA and amplify genomic DNA adjacent to the region of gRNA binding of the selected clones for

sequencing. 100, 000 cells were placed in an Eppendorf tube and centrifuged for 5 min at 120 g, then the supernatant (media) was removed. The cell pellet was lysed in 20 μl buffer A, 10 μl buffer B and 70 μl of miliQ water. Lysates were incubated for 5 min at 75°C while occasionally vortexing. Then lysis was inhibited by heating the samples to 95°C for 10 min followed by centrifugation at 27670 g for 1 min. Supernatant containing DNA was transferred then into a clean 1.5 ml Eppendorf tube. Supernatant was then diluted ten-fold in water and 1 μl was used for PCR. Following PCR mix was set up; 1 μl template, 2x 0.5 μl primers(20 μM each), 12.5 μl MyTaq HS Red Mix 2x and water 10.5 μl. PCR was performed in Eppendorf Mastercycler pro S machine with the following details; initial denaturation- 95 °C-3min-1 cycle, denaturation 95 °C-15 sec, annealing 53.7 °C-15 sec, extension 72 °C-20 sec for 35 cycle.

The PCR product was sent to Garvan Institute (Sydney) for sequencing. Sequencing primers (Forward: 5'ttgtttcttagctgtgttactccc3', Reverse: 5'tcaaaatcaccaagtcacacac3') were designed by Dr. Jennifer Fifita (Macquarie University, Sydney) and synthesised by Sigma.

3.4 Results

It is well established that examining autophagy can be problematic because there are no specific standards that are applicable to every experimental situation [464]. Indeed, the internationally agreed guidelines emphasise the importance of optimising assays to detect autophagy in the specific experimental systems used. Hence, to accurately investigate the role of TBK1 in macroautophagy, it was decided to first optimise the methods to detect autophagy in our laboratory. Prior to use in experiments to characterise TBK1 function, optimisation of each of these paradigms was carried out, as outlined below. A new approach was established using flow cytometry to follow autophagosome formation and autophagosome-lysosome fusion via overexpression of fluorescently tagged LC3. More conventional methods were also used; immunoblotting to detect endogenous LC3-I and LC3-II, and immunocytochemistry analysis combined with confocal microscopy to detect LC3 vesicles (autophagosome) and DFCP1 vesicles (omegasome).

3.4.1 Establishing novel methods using saponin and FC to specifically detect LC3-II

A new approach to detect autophagy using FC and saponin was first established. Previous studies used either fluorescently tagged LC3 [534, 537, 538] or immunolabelled endogenous LC3 using antibodies [539, 541] to follow autophagy by FC. Here, fluorescently tagged-LC3 (EGFP/mCherry) was used to avoid prior labelling with antibodies. Therefore, using FC analysis, cells that contain both EGFP and mCherry signals were categorised as autophagosome-positive cells, whereas cells containing the mCherry signal alone were autolysosome-positive cells.

All previously published autophagy studies using FC and LC3-EGFP-mCherry [534] examined the levels of total LC3. Hence, the fluorescent signals detected represent total LC3, comprising both LC3-I and LC3-II. Unlike immunoblotting and microscopy analyses, detection of total LC3 via FC cannot differentiate between LC3-I and LC3-II. However, the use of saponin has been used to deplete LC3-I from cells, thus allowing the specific detection of LC3-II via both FC [572] and microscopy analysis [573]. Saponin is a plant glycoside that interacts with and removes cholesterol in the plasma membrane,

leaving 10 nM 'holes' behind [574, 575]. Treatment of cells with saponin therefore results in the diffusion of soluble proteins, including LC3-I and GAPDH, from the cell, whereas insoluble and organelle/membrane-bound proteins, such as LC3-II, remain **(Figure 3.2A)**. To date no previously published study combined the use of saponin and LC3 tagged with both EGFP and mCherry to simultaneously analyse autophagosomes and autolysosomes, on single cells using FC. Therefore, a new FC method, combining overexpression of double-tagged LC3 [534] and elimination of LC3-I via saponin [572], was investigated to detect autophagosomes and their fusion with lysosomes, without interference of the LC3-I signal.

3.4.2 Optimising saponin conditions to specifically detect LC3-II

Overexpression of fluorescently-labelled LC3 usually results in relatively higher levels of LC3-I compared to LC3-II [464]. Hence, to optimise the conditions for saponin treatment, endogenous LC3 levels were first examined, due to the relatively higher levels of endogenous LC3-II compared to overexpressed LC3. Before proceeding to FC analysis, immunoblotting of cell lysates was performed because this allows the precise detection of LC3-I and LC3-II separately and this method is well established. First, the duration of saponin treatment was examined. HEK293T cells were incubated overnight and the following day, cells were treated with 100 nM bafilomycin (4 hr) to inhibit autophagosome degradation and accumulate LC3-II for easier detection. Then cells were incubated with 0.03% saponin-PBS for different times and LC3-I depletion was analysed via immunoblotting. The protein concentration of saponin-treated cells could not be quantified due to depletion of all soluble proteins from the cell, therefore bafilomycin treated cells were used to quantify protein expression instead. The absence of GAPDH after 5 min or longer saponin treatment indicated that the soluble proteins had diffused from the cell **(Figure 3.2B)**. Similarly, LC3-I was undetectable after 5 min of saponin treatment, even after extended exposure (**Figure 3.1C**, oversaturated blot/right hand side). Hence, this finding indicated that as little as 5 min saponin treatment was sufficient to completely deplete cytosolic LC3-I. LC3-II, however, remained detectable even after 30 min of saponin treatment (although less was detected over time), indicating that LC3-II was retained in the cell via membrane association as expected.

Next, the concentration of saponin was optimised. HEK293T cells were cultured as above, then treated for 5 min with the following concentrations of saponin-PBS: 0.03%, 0.01%, 0.003% and 0.001%. Immunoblotting for GAPDH demonstrated that concentrations of 0.003% and 0.001% did not deplete GAPDH or LC3-I, suggesting that these saponin concentrations were too low to efficiently permeabilise the cells (**Figure 3.1C**). In contrast, concentrations of 0.03% and 0.01% saponin both depleted LC3-I and GAPDH. However, some residual LC3-I levels were present in 0.01% saponin-PBS treated cells. Hence, for all further experiments, to ensure complete depletion of LC3-I, optimised conditions of 0.03% saponin-PBS treatment for 5 min were used. These conditions were therefore specifically used to examine LC3-II levels in cells via flow cytometry.

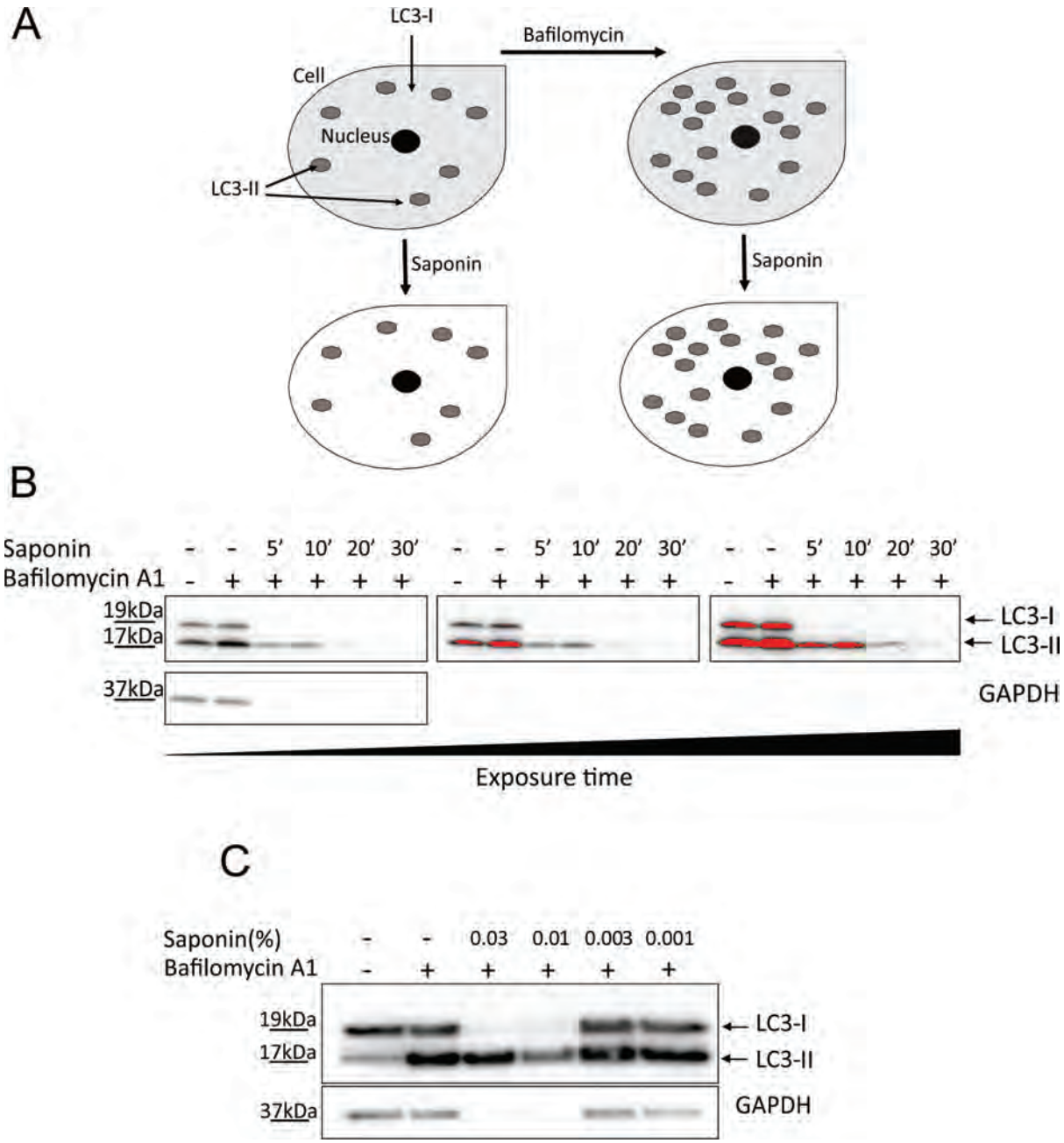


Figure 3.2. Optimisation of methods to specifically detect LC3-II using saponin. (A) *Schematic representation of the effects of bafilomycin and saponin treatment.* LC3-I is normally diffuse in the cytoplasm (grey) whereas LC-II is localised to autophagosomes (black). Bafilomycin inhibits autophagosome degradation, leading to increased numbers of autophagosomes per cell. Saponin treatment eliminates cytoplasmic LC3-I, allowing selective detection of LC3-II. **(B)** *Time-dependent extraction of LC3-I upon saponin treatment.* Cells were treated with 0.03% saponin for the indicated time, lysed and separated by SDS-PAGE. Immunoblotting for LC3 and GAPDH was then performed. Saponin extraction for 5 min was sufficient to eliminate both LC3-I and GAPDH from cell lysates. **(C)** *Dose-dependent extraction of LC3-I upon saponin treatment.* Cells were

treated with 0.01-0.001% saponin for 5 min and immunoblotting for LC3 and GAPDH was performed. A concentration of 0.03% saponin was found to be optimal, whereby both LC3-I and GAPDH, but not LC3-II, were depleted.

3.4.3 Establishing of methods to detect basal autophagy

Conditions for monitoring of basal autophagy in HEK293T cells, using saponin treatment both via FC and immunoblotting, were then established. Administration of fresh media containing serum upregulates basal autophagy for up to 4 hr [464]. Furthermore, bafilomycin is the only autophagy inhibitor that can be used to monitor basal autophagy because, unlike other drugs such as chloroquine and vinblastine that affect mTOR phosphorylation and direct autophagy towards non-selective autophagy [576], bafilomycin does not affect mTOR pathways. Hence, basal autophagy was examined 4 hr after the addition of fresh media containing 10% FBS in the presence or absence of 100 nM bafilomycin.

For FC analysis, cells were transfected with dual-tagged LC3-EGFP-mCherry [512] (**Figure 3.3A**). First, EGFP positive cells were analysed without saponin treatment to detect both cytosolic and autophagosome-linked LC3 (LC3-I and LC3-II). EGFP was detected in 44.3% of the cells using FC, which was taken to be the transfection efficiency of LC3-EGFP-mCherry vector in HEK293T cells. This proportion was not significantly different when treated with bafilomycin, as expected **(Figure 3.3B)**, confirming that in the absence of saponin, the total LC3 levels examined by FC are not sensitive enough to detect autophagosome formation. Therefore, LC3-I depletion was performed by saponin treatment using the optimised conditions. Here, only 4.6% of cells displayed an EGFP signal, due to elimination of soluble LC3-I. Bafilomycin treatment significantly increased ($p=0.02$) this proportion, to 7.5%, consistent with inhibition of autophagosome degradation **(Figure 3.3B)**. Hence these results demonstrate that basal autophagy in HEK293T cells can be monitored with saponin 4 hr after the addition of serum. They therefore confirm the validity of the novel saponin-FC method to monitor basal autophagy.

Next, FC was used to examine the fusion of the autophagosome to the lysosome, by determining the percentage of $EGFP^+$ cells present within the $mCherry^+$ subpopulation

only. Hence non-transfected cells were excluded from this analysis. In the absence of saponin treatment, on average 89.2% of mCherry positive cells also displayed an EGFP signal ($EGFP^+/mCherry^+$), which increased, however not significantly, to 92.9% when bafilomycin was added **(Figure 3.3C/D)**. However, after saponin treatment, the proportion of $EGFP^+/mCherry^+$ cells dramatically decreased to 49.4%, representing loss of cytosolic LC3-I that is not recruited into autophagosomes. Bafilomycin treatment significantly increased the proportion of $EGFP^+/mCherry^+$ cells to 70% ($p=0.0002$), due to inhibition of autophagosome-lysosome fusion. Hence this finding shows that basal autophagy can only be detected using FC if cells are treated with saponin. To confirm that FC accurately detected basal autophagy of HEK293T cells using these conditions, immunoblotting of endogenous LC3 was performed in non-transfected cells. Bafilomycin significantly increased the levels of endogenous LC3-II **(Figure 3.3E)**, consistent with the FC results. Therefore, these results show that the combination of FC with saponin treatment more precisely monitors autophagy than the existing methods. These findings therefore establish a new approach to detect autophagosome formation, fusion to the lysosome, and consequently autophagosome degradation, via FC.

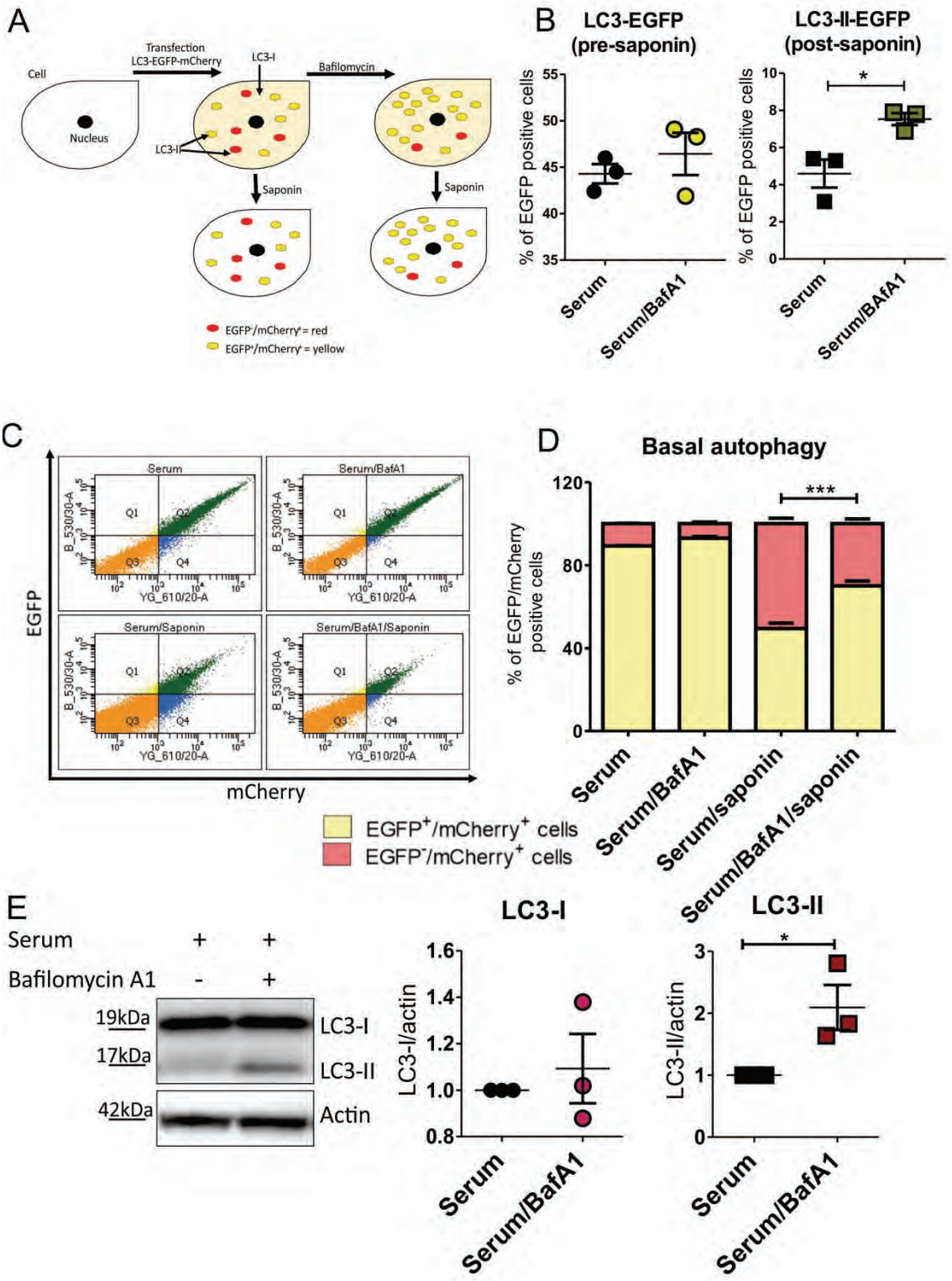


Figure 3.3. Establishing FC methods to measure basal autophagy in HEK29T cells. **(A)** *Schematic representation of LC3 detection via FC*. HEK293T cells were transfected with dual tagged LC3-EGFP-mCherry plasmid. Autophagosomes possess both excitable EGFP and mCherry and are therefore represented as yellow. In contrast, EGFP is quenched in autolysosomes, therefore only mCherry is detectable. Saponin treatment eliminates LC3-I. **(B)** *Assessment of % autophagosome-positive HEK293T cells under*

basal autophagy conditions. HEK293T cells were transfected with dual tagged LC3-EGFP-mCherry and basal autophagy was induced for 4 hr in the presence of 100 nM bafilomycin. The percentage of EGFP positive cells, analysed before and after saponin treatment, significantly increased upon bafilomycin treatment, illustrating ongoing autophagosome formation. N=3 +/- SEM, unpaired t-test, *>0.05. **(C/D)** *Assessment of the autophagosome/autolysosome ratio in HEK293T cell under basal autophagy conditions*. HEK293T cells were transfected with dual tagged LC3-EGFP-mCherry and basal autophagy was induced for 4 hr in the presence of 100 nM bafilomycin. Cells were treated with saponin and analysed by FC. (**C)** Representative images of FC analysis. Increasing EGFP signals along the y axis and increasing mCherry signals along the x axis were detected. Q1: $EGFP^{+}/mCherry^{-}$, Q2: $EGFP^{+}/mCherry^{+}$, Q3: $EGFP^{-}/mCherry^{-}$, Q4: $EGFP^{-}/mCherry^{+}$. (**D)** Significantly more autophagosome positive cells were detected upon bafilomycin treatment. N=3 +/- SEM, one-way ANOVA with Tukey post-hoc test, ***>0.0005. **(E)** *LC3 immunoblotting of HEK293T cells confirms induction of basal autophagy using these conditions.* Cells were treated with 100 nM bafilomycin for 4 hr, then lysed and LC3 immunoblotting was performed (left panel). Bafilomycin treatment led to accumulation of LC3-II (right panel), whereas LC3-I levels were unaffected (centre panel). Band intensity was quantified using ImageJ and normalised to loading control, actin. N=3 +/- SEM, unpaired t-test, *>0.05.

3.4.4 Inhibition of TBK1 perturbs basal autophagy, but does not affect omegasome formation

Now that experimental techniques to detect autophagy in HEK293T cells were optimised in line with the Klionsky guidelines [464], the normal role of TBK1 in autophagy (this chapter) and of mutant TBK1 associated with ALS (chapter 4 and chapter 5) could be examined using FC. ALS mutant TBK1 has been postulated to be pathogenic via haploinsufficiency [18], hence inhibition of TBK1 kinase activity, and/or depletion of TBK1, may mimic the scenario in ALS patients. Therefore, first, the effect of two highly specific and potent TBK1 inhibitors, BX795 and MRT67307, was tested on basal autophagy of HEK293T cells [472]. The IC^{50} for BX795 was previously reported to be 1 μM [577] in cell culture of HEK293T-stably expressing TLR3-FLAG [472], which was used for all experiments in this thesis. MRT67307 is a derivative of BX795 that shows higher specificity and lower IC^{50} towards TBK1 [550] than BX795. IC^{50} of MRT67307

in cell culture was determined to be 19 nM [577]. In this thesis the conditions for MRT67307 were first optimised and 25 nM was used throughout (data not shown). BX795 was dissolved in DMSO, therefore in all BX795 experiments DMSO was used as vehicle control. In contrast, MRT67307 was dissolved in H_2O, therefore H_2O was used as the vehicle control.

First, autophagosome formation was examined by FC. HEK293T cells were transfected with dual tagged LC3-EGFP-mCherry and treated with BX795 or MRT67307 **(Figure 3.4A)**. After saponin treatment, the relative proportion of $EGFP^+$ cells showed a trend towards a small increase when treated with BX795 **(Figure 3.4D)** but this was not statistically significant. Bafilomycin treatment of control DMSO treated cells led to an increase in the proportion of $EGFP^+$ cells ($p=0.03$) as expected, confirming ongoing autophagosome formation (as in **Figure 3.2B**). Overall no difference was detected in $EGFP^+$ cells accumulating following BX795 and bafilomycin co-treatment, compared to DMSO and bafilomycin treated conditions. Therefore, these data suggest BX795 does not affect autophagosome fusion with the lysosome in basal autophagy. In contrast, treating cells with MRT67307 after saponin extraction significantly increased the proportion of $EGFP^+$ cells compared to vehicle treated conditions ($p=0.004$) **(Figure 3.4E)**. Upon bafilomycin treatment, control cells without MRT67307 displayed elevated $EGFP^+$ as expected ($p=0.03$). No difference was detected in $EGFP^+$ cells when treated with MRT67307 and bafilomycin. These results therefore imply that MRT67307 treatment leads to abrogated autophagosome-lysosome fusion, unlike BX795.

To further analyse the effect of the TBK1 inhibitors on autophagosome-lysosome fusion, the proportion of $EGFP^+/mCherry^+$, and $EGFP^-/mCherry^+$ cells were examined by FC. Only saponin treated cells were analysed as previous data showed **(Figure 3.3 D)** that in the absence of saponin no difference could be detected by FC. After saponin treatment, 50.4% of DMSO control cells were positive for both mCherry and EGFP **(Figure 3.4F)**. However, BX795 administration significantly increased this proportion to 60.8% ($p=0.04$), indicating either induction of autophagy or inhibition of degradation of autophagosomes in these cells (purple square on **Figure 3.3F**). Bafilomycin treatment then led to significantly more $EGFP^+/mCherry^+$ cells in both DMSO control treated ($p<0.0001$) and BX795 treated cells ($p=0.002$) (1^{st} vs. 3^{rd} and 2^{nd} vs. 4^{th} column, **Figure 3.4F**). However, the proportion of $EGFP^+/mCherry^+$ cells following BX795 treatment did

not significantly differ from the proportion of $EGFP^+/mCherry^+$ cells with DMSO treatment with bafilomycin (**Figure 3.4F**, green square). Hence these data indicate that the observed significant increase in $EGFP^+/mCherry^+$ cells upon BX795 treatment (purple square) is due to abrogated autophagosome lysosome fusion, leading to more accumulation of autophagosomes. Similar analyses using MRT67307 treatment were also performed. After saponin treatment, 49.1% of $mCherry^+$ cells possessed a detectable EGFP signal and this proportion increased significantly ($p<0.0001$) (from 49.1% to 80.8%) by MRT67307 treatment (**Figure 3.4G**, purple square). Bafilomycin treatment resulted in a significant increase in $EGFP^+/mCherry^+$ cells compared to vehicle treatment ($p<0.0001$) (from 49.1% to 74.92%) but TBK1 inhibition with MRT67307 prevented this increase (1^{st} vs. 3^{rd} and 2^{nd} vs. 4^{th} column, **Figure 3.4G**). These results imply that there is no ongoing autophagosome degradation in that 4 hr period in MRT67307 treated cells as lysosomal inhibition did not contribute to the accumulation of autophagosomes. Hence these findings indicate that the increased proportion of $EGFP^+/mCherry^+$ cells with MRT67307 treatment alone was due to abrogated autophagosome degradation.

These data together indicate that TBK1 inhibition leads to abrogated autophagosome degradation, however to a different degree between the two inhibitors. BX795 treatment leads to a partial block in autophagosome degradation because bafilomycin was still able to block this degradation and accumulate more autophagosomes. In contrast, MRT67307 lead to a complete block in autophagosome degradation as bafilomycin treatment did not result in the accumulation of more autophagosomes, consistent with it being a more potent and more specific inhibitor of TBK1.

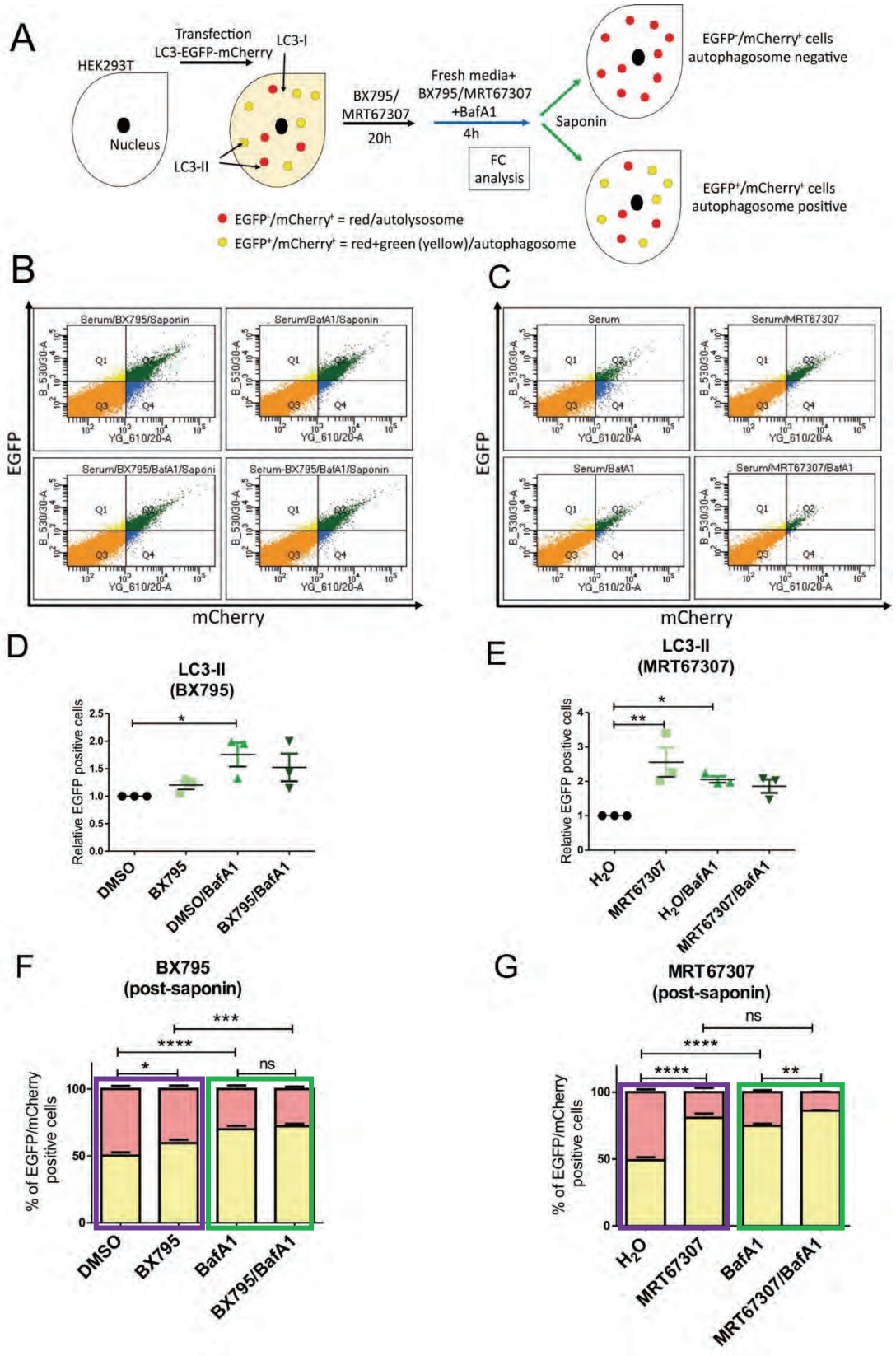


Figure 3.4. TBK1 inhibition by MRT67307 inhibits autophagosome-lysosome fusion and autophagosome degradation during basal autophagy in HEK293T cells. (A) *Schematic representation of the detection of autophagosome lysosome fusion via FC upon TBK1 inhibition*. HEK293T cells were transfected with dual tagged LC3-EGFP-mCherry

and basal autophagy was induced for 4 hr by the addition of fresh media in BX795 and MRT67307 pre-treated cells. Following saponin treatment, cells were analysed via FC. Cells positive for both EGFP and mCherry ($EGFP^+/mCherry^+$) were categorised as representing autophagosomes only, whereas cells positive for only mCherry ($EGFP^-/mCherry^+$) were categorised as autolysosomal cells. (**B/C)** *Representative images of FC analysis of TBK1 inhibited HEK293T cells under basal autophagy.* Increasing EGFP signals along the y axis and increasing mCherry signals along the x axis is shown. Q1: $EGFP^+/mCherry^-$, Q2: $EGFP^+/mCherry^+$, Q3: $EGFP^-/mCherry^-$, Q4: $EGFP^-/mCherry^+$. (**D/E**) *Percentage of autophagosome positive HEK293T cells during basal autophagy.* The percentage of EGFP positive cells was analysed before and after saponin treatment. MRT67307 treatment leads to abrogated autophagosome lysosome fusion. N=3 +/- SEM, one-way ANOVA with Dunnett post-hoc test, *>0.05, **>0.005. **(F/G)** *Autophagosome/autolysosome ratio in HEK293T cell under basal autophagy conditions*. BX795 treatment causes partial a block of autophagosome-lysosome fusion, whereas MRT67307 completely blocks the fusion between autophagosome and lysosomes. N=3 +/- SEM, one-way ANOVA with Tukey post-hoc test, *<0.05, **<0.005, ***<0.0005, ****<0.00005.

To confirm these results, immunoblotting of BX795 and MRT67307 treated HEK293T cell lysates for endogenous LC3-I and LC3-II was performed. LC3-I levels were not significantly affected by either BX795 or MRT67307 treatment **(Figure 3.5A/B/E/F)**. BX795 treatment did not significantly increase the levels of LC3-II, whereas bafilomycin did increase LC3-II levels in control DMSO cells as expected (p=0.03, **Figure 3.5C**). Furthermore, upon bafilomycin treatment, similar levels of LC3-II accumulated in both DMSO control and BX795 treated cells. These results are therefore in agreement with the FC results, where no significant difference was detected following BX795 treatment. In contrast, TBK1 inhibition using MRT67307 showed a trend towards increased LC3-II levels in the absence of bafilomycin treatment compared to vehicle treated cells, however, was not significant (p=0.07, **Figure 3.5G**). In addition, significantly less LC3-II accumulated upon bafilomycin treatment in MRT67307 treated cells compared to H_2O control treated cells, indicating that MRT67307 treated inhibited the formation of the autophagosome during basal autophagy.

Bafilomycin treatment displayed a decreasing trend of LC3-II levels with BX795 treated cells compared to vehicle treated conditions **(Figure 3.5C)**, however this did not reach significance as stated above. In contrast, following bafilomycin treatment, relative comparison between cells treated with TBK1 inhibitors (BX795/BafA1) or vehicle control (DMSO/BafA1) indicated significantly less LC3-II accumulation was detected upon TBK1 inhibition (data not shown). The lack of significance in **Figure 3.5C** may be due to the variable LC3 levels detected between replicates. Therefore, to further analyse whether inhibition of TBK1 indeed lead to inhibited autophagosome formation, confocal microscopy analyses was carried out to follow autophagosomes via LC3-EGFP overexpression.

The TBK1 levels were also evaluated to analyse the effect of the inhibitors. A trend was apparent showing that bafilomycin may increase and therefore potentially stabilise TBK1 as shown in **Figure 3.5A/D**. However due to variability between the biological replicates this increase was not statistically significant **(Figure 3.5D)**. Furthermore, these data implied that MRT67307 inhibitor may lead to decreased TBK1 levels as shown in **Figure 3.5E**, however this trend did not reach statistical significance either **(Figure 3.5 H)**. Overall, these data indicates that TBK1 levels do not change upon TBK1 inhibition indicating that changes detected in LC3-II levels are not due to lower TBK1 protein levels.

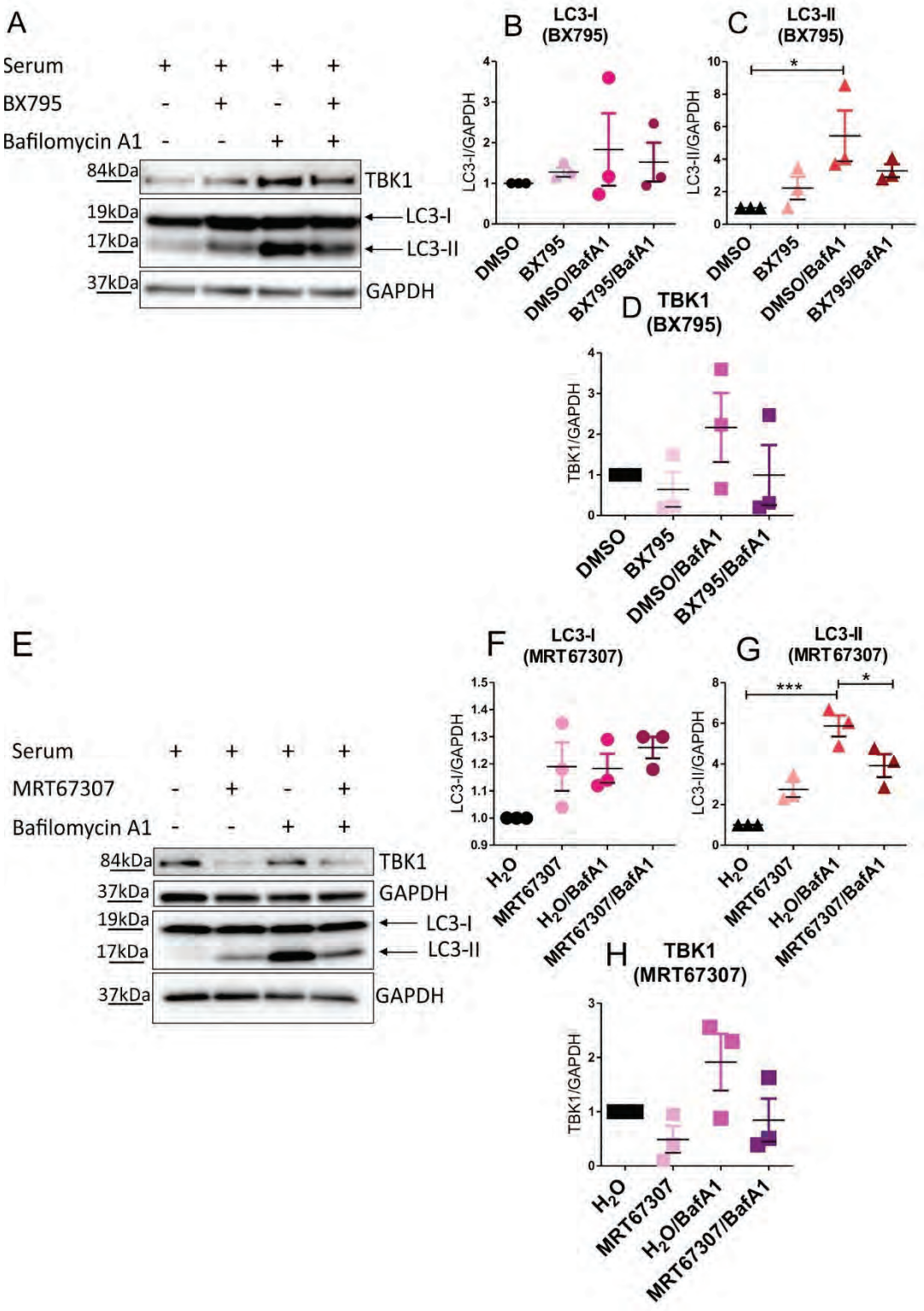
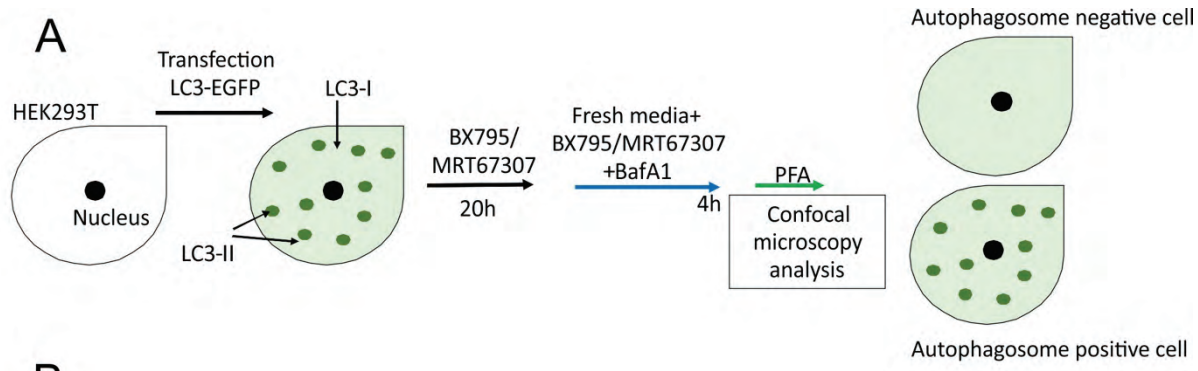
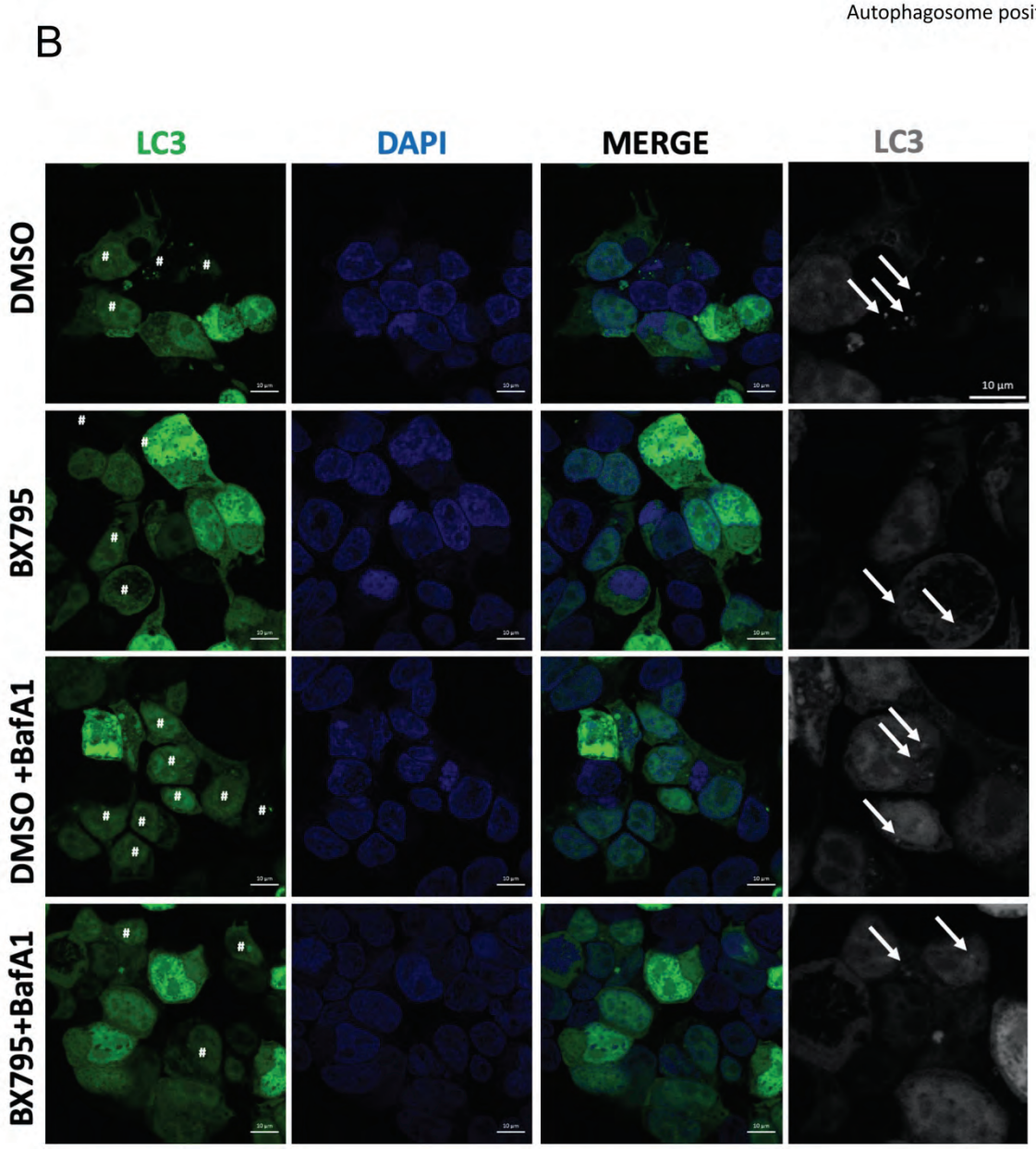


Figure 3.5. MRT67307 treatment leads to decreased LC3-II accumulation upon bafilomycin treatment. HEK293T cells were treated with BX795 (1 μM) **(A-D)** or MRT67307 (25 nM) **(E-H)** for 20 hr, then treated with bafilomycin to follow basal autophagy. Lysates were separated on SDS-polyacrylamide gels and immunoblotted for LC3 and GAPDH as a loading control. Representative immunoblots are shown **(A/E)**.

Band intensity was quantified using ImageJ and normalised to internal loading control, GAPDH. Relative expression levels are shown by quantification; LC3-I **(B/F)**, LC3-II **(C/G)** and TBK1 **(D/H)**. MRT67307 leads to inhibited autophagosome formation. N=3 +/- SEM, one-way ANOVA with Tukey post-hoc test, *<0.05, ***<0.0005.

To further examine the role of TBK1 in autophagosome formation, confocal microscopy analyses of HEK293T cells expressing LC3-EGFP treated with BX795 or MRT67307 were performed **(Figure 3.6A)**. Here the single tagged construct was used so that LC3-EGFP and hence autophagosomes only were analysed. Overexpression of an exogenous LC3 construct does not induce autophagy, therefore high free LC3-I levels (diffuse cytoplasmic LC3) were present in cells **(Figure 3.6B/C)** [464]. Hence, few LC3-EGFP transfected cells showed LC3 puncta. Therefore, the overall ratio of cells positive for EGFP puncta were quantitated. However, BX795 **(Figure 3.6B/D)** and MRT67307 **(Figure 3.6C/E)** treatment did not affect the proportion of cells with LC3-EGFP puncta, representing autophagosomes. In vehicle treated cells, the proportion of autophagosome-positive cells increased slightly upon bafilomycin treatment as expected, but this did not reach statistical significance. Hence these data suggest that quantification of cells with $EGFP^+$ vesicles using confocal microscopy is not as precise as FC analysis, given that autophagosome-positive cells should increase significantly following bafilomycin treatment. Nevertheless, significantly fewer cells contained autophagosomes in BX795 treated cells, compared to DMSO only (p=0.02), showing decreased autophagosome formation, unlike in MRT67307 treated cells.


A
Transfection
LC3-EGFP
LC3-I
HEK293T
Nucleus
LC3-II
BX795/
MRT67307
20h
Fresh media+
BX795/MRT67307
+BafA1
4h
PFA
Confocal
microscopy
analysis
Autophagosome negative cell
Autophagosome positive cell


B
LC3
DAPI
MERGE
LC3
DMSO
BX795
DMSO +BafA1
BX795+BafA1
10 µm

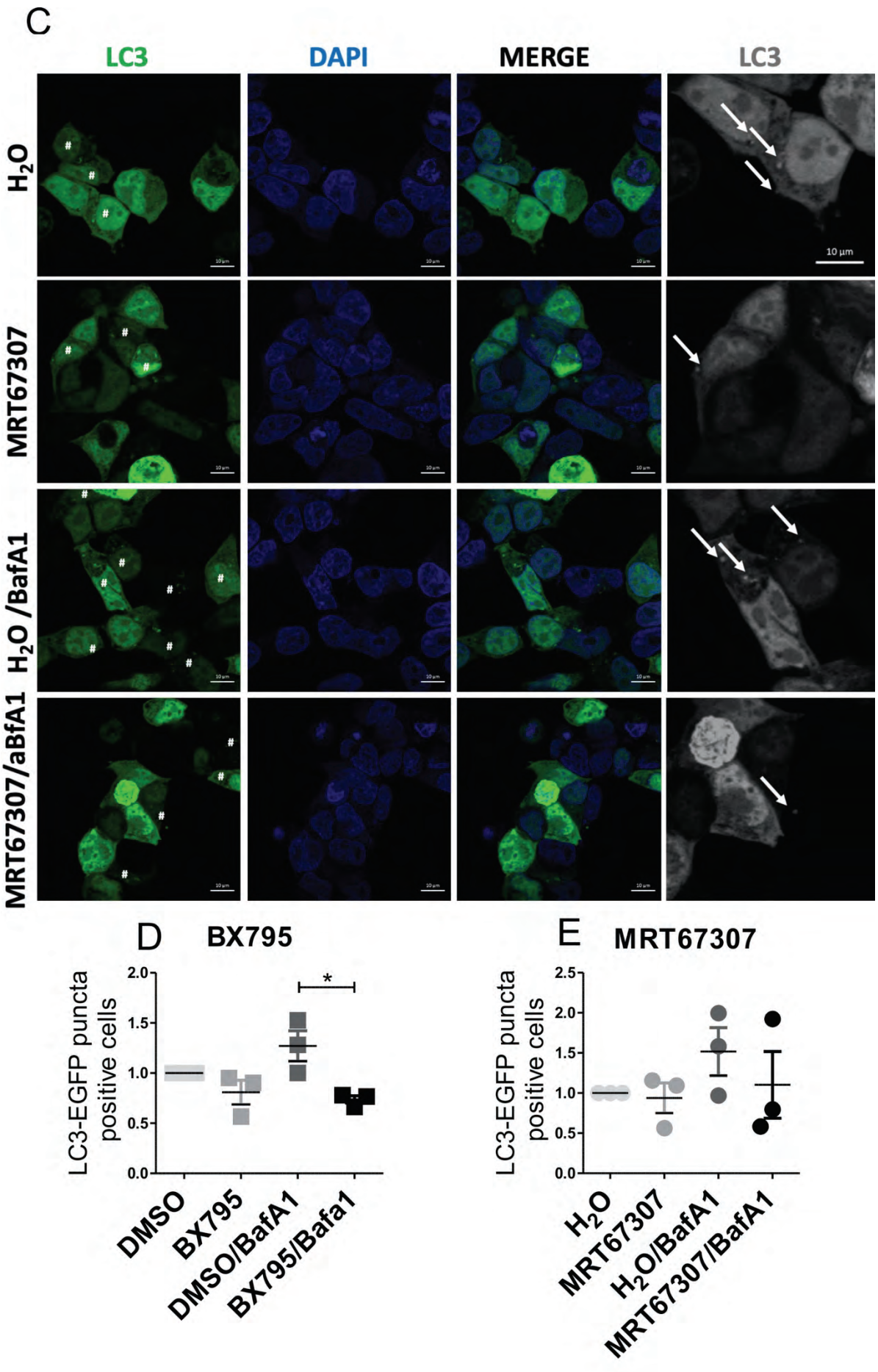
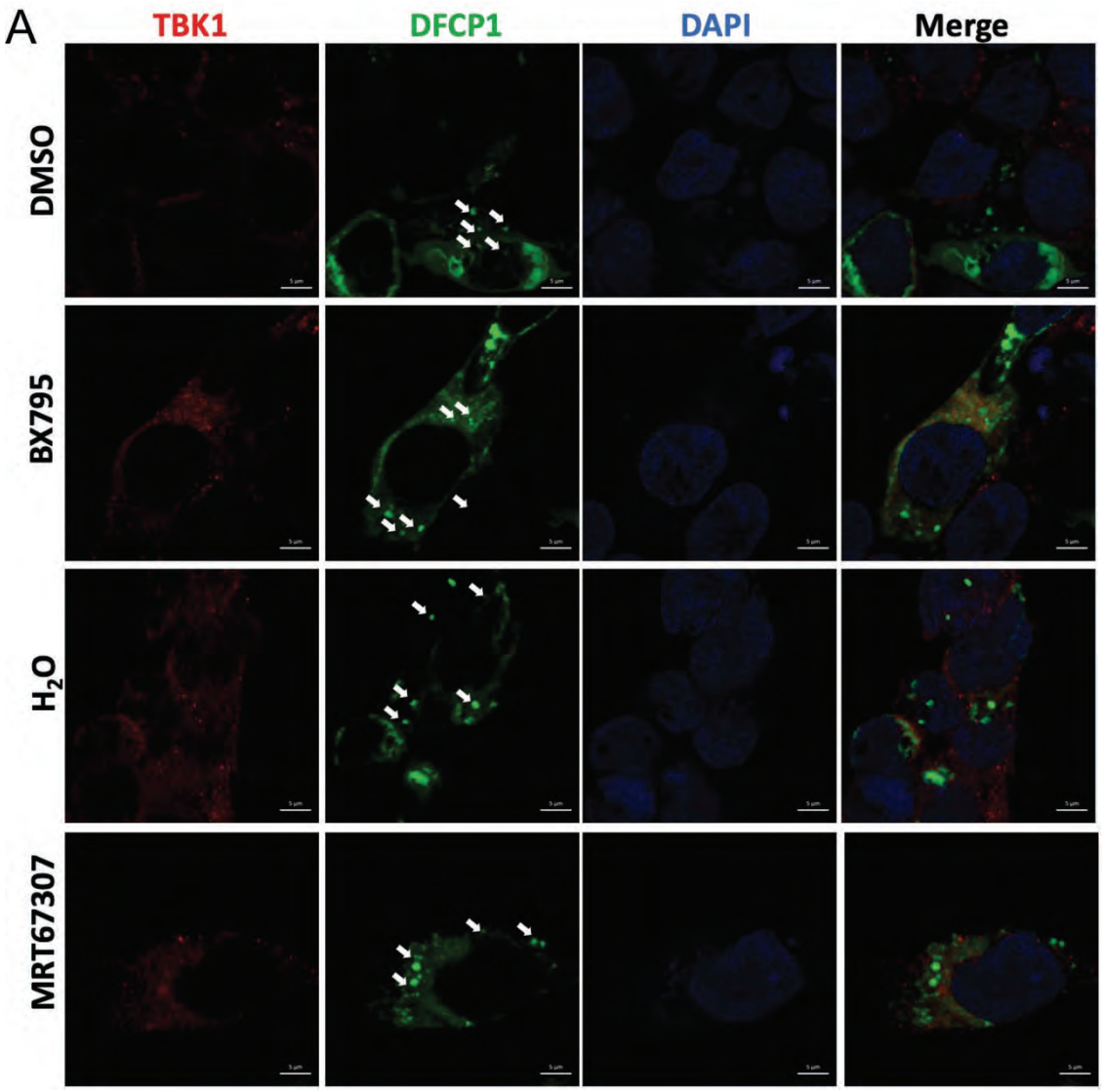
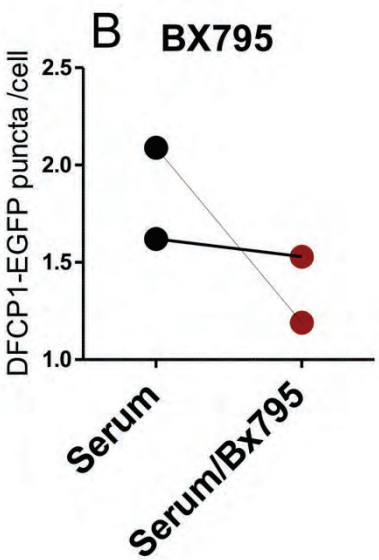

C
LC3
DAPI
MERGE
LC3
H2O
MRT67307
H2O /BafA1
MRT67307/aBfA1
10 µm
D
BX795
LC3-EGFP puncta positive cells
2.0
1.5
1.0
0.5
0.0
*
DMSO
BX795
DMSO/BafA1
BX795/Bafa1
E
MRT67307
LC3-EGFP puncta positive cells
2.5
2.0
1.5
1.0
0.5
0.0
H2O
MRT67307
H2O/BafA1
MRT67307/BafA1

Figure 3.6. TBK1 inhibition by BX795, but not MRT67307, inhibits autophagosome formation in HEK293T cells. (A) *Schematic representation of autophagy detection via confocal microscopy.* Cells were transfected with LC3-EGFP then basal autophagy was followed for 4 hr in 1 μM BX795 (B/D) and 25 nM MRT67307 (C/E) pre-treated cells, in the presence or absence of 100 nM bafilomycin. Cells with EGFP-positive vesicles were counted. *BX795 treatment leads to fewer numbers of autophagosomes in HEK293 cells.* LC3-EGFP vesicles positive cells were counted in 50+ cells per coverslip. Representative images **(B/C)** and relative differences **(D/E)** are shown based on 3 replicates. N=3 +/- SEM, one-way ANOVA with Tukey post-hoc test, *<0.05. Scale: 10 μm. Cells labelled with # are autophagosome positive cells. White arrow shows individual LC3 vesicles.

These data imply that TBK1 may both inhibit autolysosome-autophagosome fusion **(Figure 3.4)** and autophagosome formation **(Figure 3.5)**. This possibility was further examined by investigating whether TBK1 is involved in formation of the omegasome, the precursor of the autophagosome [386]. For this purpose, the omegasome marker DFCP1-EGFP was overexpressed in HEK293T cells and cells were treated with TBK1 inhibitors as above. DFCP1 is localised to mitochondria, ER and Golgi, however upon autophagy induction, DFCP1 positive puncta appear dispersed in the cytoplasm [578]. As DFCP1 is localised to the membranes of intracellular organelles other than autophagosomes, it was not possible to quantitate DFCP1 vesicles using FC. The formation of the omegasome was analysed by quantitating the number of DFCP1-EGFP puncta in transfected cells [324]. However, there was no difference in DFCP1-EGFP puncta formed per cell in BX795 and MRT67307 treated cells, compared to the respective vehicle control cells **(Figure 3.7)**. Co-localisation between endogenous TBK1 and DFCP1-EGFP also revealed that TBK1 was not recruited to DFCP1-EGFP vesicles, indicated by the absence of TBK1 staining in DFCP1 vesicles, either in the presence or in the absence of TBK1 inhibitors. Further experiment needed (N=2) to confirm but these results suggest that the kinase activity of TBK1 is not involved in the formation of the omegasome, and consistent with this, TBK1 was not localised to omegasomes. These findings therefore suggest that TBK1 is not involved in the omegasome forming from the ER. Furthermore, this data cannot confirm that TBK1 is involved in autophagosome formation during basal autophagy.


A
TBK1
DFCP1
DAPI
Merge
DMSO
BX795
H2O
MRT67307


B
BX795
DFCP1-EGFP puncta /cell
2.5
2.0
1.5
1.0
Serum
Serum/Bx795

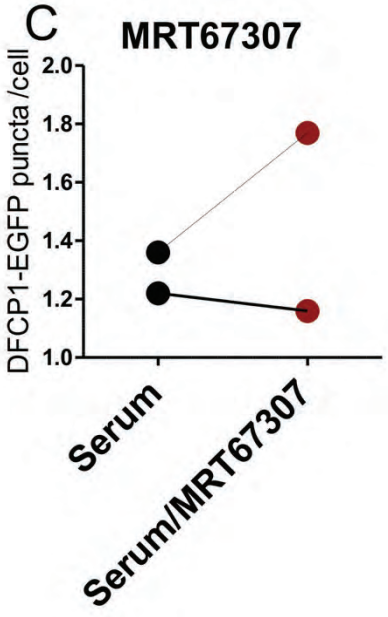

C
MRT67307
DFCP1-EGFP puncta /cell
2.0
1.8
1.6
1.4
1.2
1.0
Serum
Serum/MRT67307

Figure 3.7. TBK1 inhibition does not affect omegasome formation in basal autophagy. Representative images **(A)** and quantification **(B/C)** of DFCP1-EGFP puncta in TBK1 inhibited cells. HEK293T cells were transfected with DFCP1-EGFP overexpressing vector and basal autophagy was induced for 4 hr in BX795 (1 μM) or MRT67307 (25 nM) pre-treated cells. DFCP1 EGFP puncta was counted. Scale: 5 μm. Arrows show the presence of omegasomes.

These data overall suggest that TBK1 may be involved in basal autophagy, by facilitating autophagosome degradation via its kinase activity and potentially autophagosome formation **(Table 3.1)**. However, this does remain somewhat inconclusive because the two TBK1 inhibitors gave differing results. Furthermore, major differences were detected using the different methods; FC, immunoblotting and confocal microscopy.

Table 3.1. Summary of results obtained from TBK1 inhibition studies during basal autophagy.

Basal autophagy	BX795		MRT67307	
	Autophagosome formation	Autophagosome maturation	Autophagosome formation	Autophagosome maturation
FC: $EGFP^+$ cells	-	-	-	Inhibited
FC: $EGFP^+$-$mCherry^+$ cells	-	Inhibited	-	Inhibited
Immunoblotting-LC3-I/LC3-II	-	-	Inhibited	-
LC3-EGFP microscopy	Inhibited	-	-	-
Omegasome formation	-		-	

3.4.5 Generation of TBK1 knock-out cells via CRISPR/Cas9 editing

The inhibition of TBK1's kinase activity can reveal how TBK1 mediated phosphorylation affects autophagy. However, TBK1 contains a substrate binding domain located in the C-terminus. Upon inhibited kinase activity, TBK1 can still interact with its substrate binding partners due to its intact substrate binding domain, however due to the lack of kinase activity it cannot function properly or modulate autophagy. Therefore, if

TBK1 is knocked out and both its kinase activity and substrate binding capability is absent, TBK1 substrates may interact with different kinases instead. Therefore, a feasible hypothesis is that the lack of binding between TBK1 and its interacting partner may contribute differently to autophagy, then when TBK1 enzymatic activity is inhibited. Therefore, knock-out of TBK1 via CRISPR/Cas9 editing was also performed.

For this purpose, stable HEK293T cells in which TBK1 was knocked out were created using CRISPR/Cas9 genome editing. First, a previously described gRNA specifically targeting TBK1 was synthesised [480] **(Figure 3.8A)** and ligated into a Cas9 overexpressing vector (GeneArt CRISPR Nuclease Vector with OFP reporter kit-Thermofisher). The ligation products were then used to transfect HEK293T cells and the resulting cells were cloned twice by limiting dilution to ensure that the clones produced were monoclonal. During the first round of selection, the resulting clones were examined for TBK1 expression using dot blotting **(Figure 3.8B)**. Clones that retained TBK1 expression were discarded, and only clones that displayed no detectable expression of TBK1 **(Figure 3.8B)** underwent a second round of cloning by limiting dilution. From this first round of selection, 14 clones were selected for the second round of cloning. At the end of the second round, 7 TBK1 knock-out (KO) cell lines were generated. Knock-out of TBK1 was confirmed in each clone via immunoblotting (**Figure 3.8C**).

Of these clones, four (clone #52.2, #118.2, #4.2, #29.2) displayed complete loss of TBK1 expression as expected **(Figure 3.8C)**. However, two clones still expressed TBK1 (clone #122.2, #81.2) to a similar degree as the parental cell HEK293T line, and one clone (clone #50.2) showed decreased TBK1 expression compared to the parental line (**Figure 3.8B**, full blot **Figure S1.**). These three TBK1 expressing clones had been produced from what was assumed to be a TBK1 KO clone. Hence, the presence of TBK1 in second round clones indicates that the first round TBK1 KO clone contained a mixed population of cells originally, from which TBK1 expressing cells were positively selected for in the population. The genomic region surrounding the binding site of the guide RNA was then sequenced in all seven of the clones (Appendix III). Not surprisingly, clones #122.2 and #81.2 were found to contain the wildtype TBK1 sequence, thus explaining the observed expression of TBK1 in these cell lines **(Figure 3.8D)**. In contrast, mutations were present in clones #52.2 and #118.2, thus explaining the loss of TBK1 expression in these clones **(Figure 3.8A)**. In clone #52.2 a deletion of 5 nucleotides at position 8863-8867

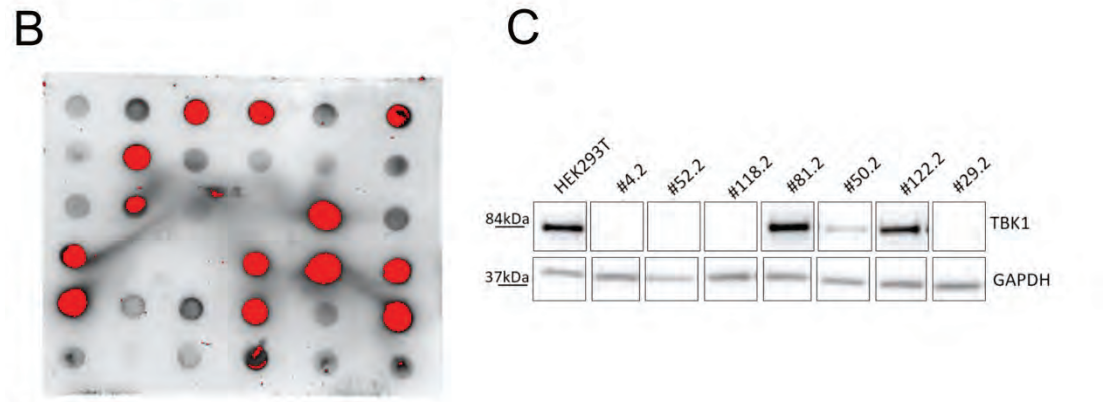
(NG_046906.1) was present, resulting in a frameshift mutation and consequently the introduction of an early stop codon **(Figure 3.8A)**. Similarly, clone #118.2 contained an insertion of adenine at position 8867 (NG_046906.1), leading to another frameshift mutation and insertion of a stop codon downstream **(Figure 3.8A)**. Due to the complete loss of TBK1 expression in clone #52.2 and #118.2 and the sequencing results we assumed that both TBK1 alleles were affected. Clones #52.2 and #118.2 were therefore selected for further analysis. Identification of the exact mutations was not feasible in clones #4.2, #29.2 and #50.2, because the sequence could not be resolved correctly.

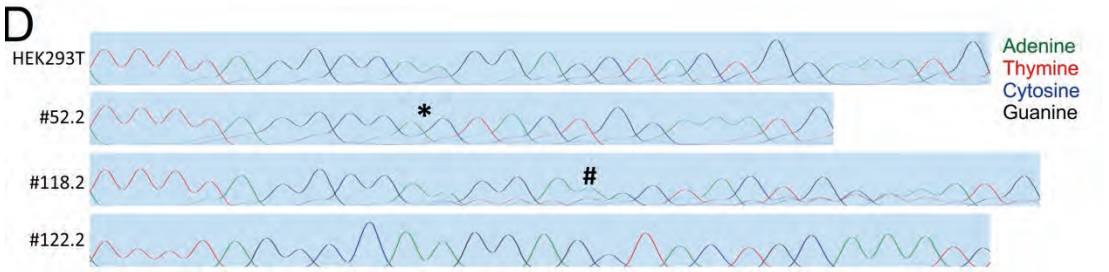
3.4.6 Short-tandem-repeat (STR) analyses of CRISPR/Cas9 clones

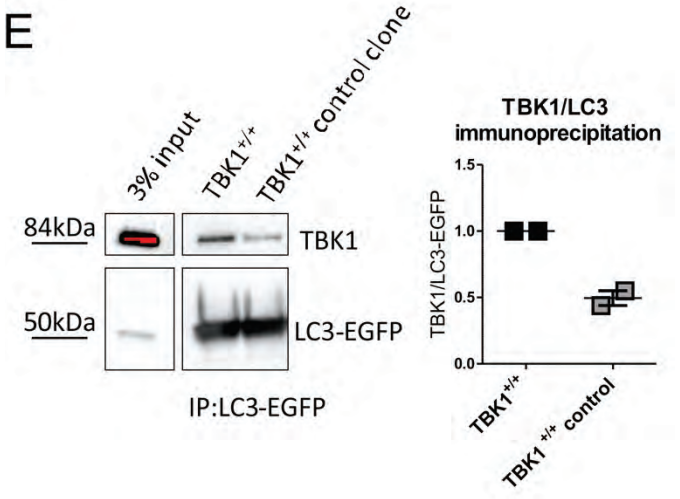
During genome editing, off target effects are known to occur [579]. Hence, short-tandem-repeat (STR) analyses of the CRISPR/Cas9 cell lines was performed (Garvan Institute, Garvan Molecular Genetics, Sydney, NSW) to confirm they were still indeed HEK293T cells following genome editing. TBK1 expressing clones (#122.2, #81.2) were initially thought to be good candidates to use to as 'negative control' cell lines, to determine if non-specific binding effects of gRNA were present. Therefore, clone #122.2 was selected at random and included in the initial the experiments examining the effect of TBK1 on autophagy. Hence, all 3 clones (#122.2, #81.2 and the TBK1 KO clones #52.2 and #118.2) and HEK293T parental cells underwent STR analyses (Proof of identification is presented in **Appendix II**). While some differences in repeat number were detected between the parental HEK293T cell line and the all the 3 clones, however comparison to the HEK293T STR profile showed that the #122.2 clone resembled HEK293T cells the least (81%), while the TBK1 KO clones #52.2 and 118.2 clones showed more similarities to HEK293T cells (84% and 87% respectively; greater than 80% similarity between two cell lines means they are still considered to be related (Garvan Certificate, **Appendix II**). Therefore, #122.2 clone was still considered to be HEK293T, however, it underwent more genomic changes than #52.2 or #118.2. However, unexpectedly, the TBK1 expressing clone #122.2 showed decreased growth compared TBK1 knock-out and the parental HEK293T cells (data not shown), and in some instances significantly altered interaction was detected between TBK1 expressed by the #122.2 clone and LC3, unlike the parental HEK293T cells **(Figure 3.8E.)**. Therefore the #122.2 clone was considered to be not a true negative control cell line, and it was subsequently excluded from all further analysis. Hence, some blots presented in this thesis were

cropped as indicated in the text, due to exclusion of this clone. From here onwards, #52.2 clone was referred to as ‘clone #1’ and #118.2 was termed ‘clone #2’.


A
HEK293T
5'AGACATTTGCAGTAGCTCC(TGG)'3 antisense DNA
8860
8882
Target sequence
5061
TBK1 protein
55055
8813- ATG start codon
#52.2
8860
8882
Target sequence
5061
-AGGAG
8863-8868
15aa
10aa
STOP
8813
#118.2
8860
8882
Target sequence
5061
+A
8867
17aa
12aa
STOP
8813


B
C
HEK293T
#4.2
#52.2
#118.2
#81.2
#50.2
#122.2
#29.2
84kDa
TBK1
37kDa
GAPDH


D
HEK293T
#52.2
#118.2
#122.2
*
#
Adenine
Thymine
Cytosine
Guanine


E
3% input
TBK1+/+
TBK1+/+ control clone
84kDa
TBK1
50kDa
LC3-EGFP
IP:LC3-EGFP

TBK1/LC3
immunoprecipitation
TBK1/LC3-EGFP
1.5
1.0
0.5
0.0
TBK1+/+
TBK1 +/+ control

Figure 3.8. Generation of TBK1 KO HEK293T cells using CRISPR/Cas9 editing. **(A)** *Schematic representation of the gRNA binding site and the location of the mutations detected in the TBK1 gene.* Knock-out of TBK1 in genome edited HEK293T cells was confirmed via dot blotting **(B)** and immunoblotting **(C)** using anti-TBK1 antibodies. **(D)** Successful knockout of TBK1 and the presence of the mutations were identified by sequencing of genomic DNA adjacent to the gRNA binding site. Clone #52.2 displayed a deletion of 5 nucleotides (indicated by *), leading to a frameshift mutation at stop codon, after 25 amino acid, whereas in clone #118.2 clone one nucleotide was inserted (indicated by #), which resulting in a frameshift mutation resulting in a stop codon after 27 amino acid. **(E)** *Less precipitation of TBK1 with LC3 in the 'control' CRISPR/Cas9 clone upon MG132 treatment.* HEK293T ($TBK1^{+/+}$ /$TBK1^{+/+\ control}$) cells were transfected with LC3-EGFP and treated with 1 μM MG132 for 24 hr. Cell lysates were prepared and precipitated using GFP-trap, then immunoblotting was performed. Representative blots are and quantification are shown. N=2+/-SEM.

3.4.7 TBK1 knock-out does not affect basal autophagy

Autophagosome formation was analysed first in the TBK1 knock-out clones, following transfection with the dual-tagged LC3-EGFP-mCherry construct together with saponin treatment. Flow cytometry analysis however indicated that there was no significant difference in the proportion of $EGFP^+$ cells in the TBK1 KO cells compared to control HEK293T cells **(Figure 3.9A/B)**. Furthermore, upon bafilomycin treatment, the proportion of $EGFP^+$ cells in the two TBK1 knock out populations (#1, #2) was very variable compared to control HEK293T cells expressing TBK1. Hence these data indicate that, knock-out of TBK1 does not affect autophagosome formation and degradation in basal autophagy of HEK293T cells.

To further analyse the effects of TBK1 knock-out on basal autophagy, next autophagosome and autolysosome fusion was analysed by gating the mCherry population and evaluating only the $EGFP^+$ subpopulation. TBK1 knock-out did not alter the proportion of $EGFP^+/mCherry^+$ cells, either in the absence or in the presence of bafilomycin due to the variability of replicates **(Figure 3.9C)**. Hence, immunoblotting for LC3-I and LC3-II was then performed. The LC3-I levels did not change upon TBK1 knock-out. No statistically significant difference was detected in the levels of LC3-II in

the TBK1$^{-/-}$ clones (#1 and #2) **(Figure 3.9F)**. Similarly, in the presence of bafilomycin no difference was detected in LC3-II levels between TBK$^{+/+}$ and TBK1$^{-/-}$ clones. These data together therefore suggest that TBK1 knock-out using CRISPR/Cas9 editing does not have the same effect on basal autophagy as inhibition of its kinase activity.

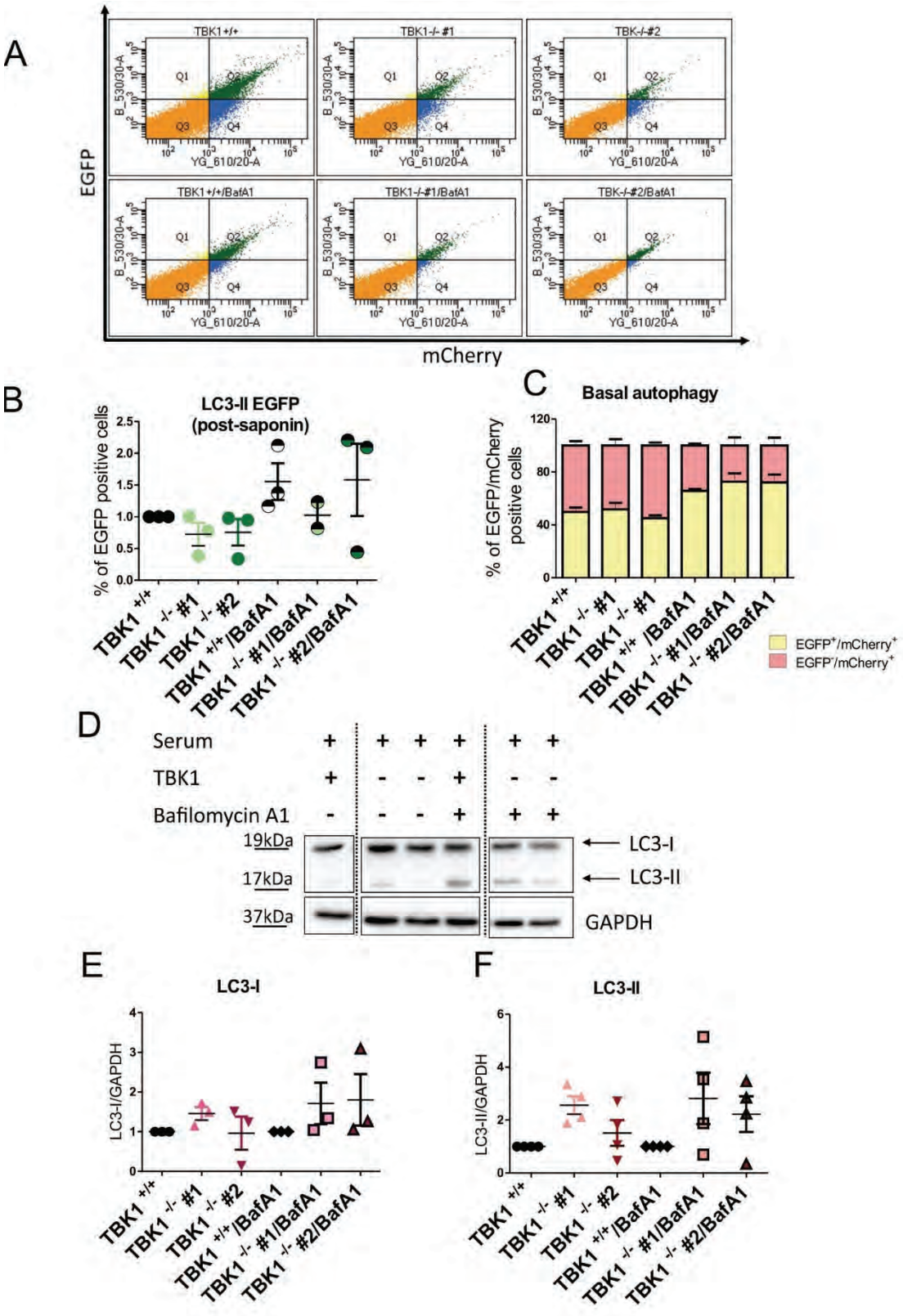


Figure 3.9. TBK1 knock-out does not affect basal autophagy. (A-C) TBK1 knock-out HEK293T cells were transfected with LC3-EGFP-mCherry and basal autophagy was monitored for 4 hr in the presence or absence of 100 nM bafilomycin. **(A)** *Representative images of FC analysis of TBK1 knock-out HEK293T cells under basal autophagy.*

Increasing EGFP signal along the y axis and increasing mCherry signal along the x axis. Q1: $EGFP^{+}/mCherry^{-}$, Q2: $EGFP^{+}/mCherry^{+}$, Q3: $EGFP^{-}/mCherry^{-}$, Q4: $EGFP^{-}/mCherry^{+}$. **(B)** *Percentage of autophagosome positive TBK1 knock-out HEK293T cells under basal autophagy.* The percentage of EGFP positive cells did not change upon TBK1 knock-out. N=3 +/- SEM. One-way ANOVA with Tukey post-hoc test. **(C)** *Autophagosome/autolysosome ratio in TBK1 knock-out HEK293T cell under basal autophagy conditions*. TBK1 knock-out did not influence autophagosome lysosome fusion. N=3 +/- SEM. One-way ANOVA with Tukey post-hoc test **(D-F)** *LC3 expression in TBK1 knock-out HEK293 cells during basal autophagy.* TBK1 knock-out HEK293T cells were treated with 100 nM bafilomycin or DMSO for 4 hr to follow basal autophagy. Lysates were separated on SDS-polyacrylamide gels and immunoblotted for LC3, and GAPDH as a loading control. Representative blots are shown **(D)**. The band intensity was quantified using ImageJ and normalised to the internal control, GAPDH. Relative expression levels are shown in quantification. More LC3-II was detected in one TBK1 knock-out clone (#1), but otherwise no differences were detected in LC3-I **(E)** and LC3-II **(F)**. N>3 +/- SEM, one-way ANOVA with Tukey post-hoc test. Dashed line indicates the cropping of 'control' clone.

In contrast to expectations and the results obtained with the TBK1 inhibitors, knock-out of TBK1 via genome editing did not significantly affect basal autophagy. However, the generation of CRISPR/Cas9 KO clones requires their culturing over a long period. Given that autophagy is a vital cellular function, it is possible that this extended growth in culture may allow cells to develop compensatory mechanisms.

3.4.8 Summary of basal autophagy results obtained

Taken together, the data presented so far were somewhat conflicting depending on which techniques were used to monitor autophagy. The results obtained using BX795 and MRT67307 suggested that the kinase activity of TBK1 may be involved in autophagosome-lysosome fusion, but this could not be fully confirmed because using some assays, no significant results were obtained. Furthermore, TBK1 knockout CRISPR/Cas9 genome edited cells showed no significant differences in basal autophagy. This data indicates that lack of TBK1 expression and inhibiting TBK1 kinase activity may be influence basal autophagy differently.

TBK1 has been previously shown to associate with mTOR [569, 577, 580], and deactivation of mTOR upon starvation leads to induction of autophagy [404]. However, it has not been previously investigated whether TBK1 plays a role in non-selective autophagy. Hence, the role of TBK1 in non-selective autophagy was then investigated.

3.4.9 Optimisation of conditions to induce non-selective autophagy in HEK293 cells

As autophagy is cell-type dependent, the conditions to induce non-selective autophagy by starvation in HEK293T cells, by replacing serum rich media with HBSS, were first optimised. The response of HEK293T cells to starvation for different times was first analysed via immunoblotting for LC3. While overall no significant differences were detected using immunoblotting, some clear trends were obvious. The levels of LC3-I increased 1 hr after the removal of serum, and a trend towards increased LC3-II levels was observed **(Figure 3.10A/B)**. In the absence of bafilomycin, the levels of LC3-I decreased following another hour in serum free conditions, and then a continuous trend of a decrease was observed. In contrast, the levels of LC3-II showed a decrease both after 2 and 4 hr of HBSS treatment. These changes may therefore represent either increased autophagy flux or inhibition of autophagosome formation. However, in the presence of bafilomycin to block autophagosome-autolysosome fusion, increased LC3-II levels, representing the formation of more autophagosomes are expected. Significantly, more LC3-II accumulated at 2 hr, 4 hr or 6 hr after starvation comparing to 1 hr starvation, indicating that more LC3-II was conjugated, as expected. The levels of LC3-I in the presence of bafilomycin remained relatively constant with a slight decrease by 6 hr of HBSS conditions compared to 1 hr.

An important marker of starvation-induced autophagy is the increased formation of omegasomes [381]. Consistent with the immunoblotting results, starvation increased the numbers of DFCP1-EGFP puncta, representing omegasomes, as expected (**Figure 3.10C)**, indicating that autophagy was induced upon starvation. Flow cytometry was then used to compare starvation-induced autophagy to basal autophagy, this time using only 4 hr HBSS treatment because at this timepoint LC3-II showed a clear decrease upon starvation compared to one 1hr while showed an increased accumulation of LC3-II in the presence of bafilomycin A1. Surprisingly, significantly less $EGFP^+$ cells accumulated 4 hr after starvation following bafilomycin treatment compared to nutrient rich conditions, both before and after saponin treatment (representing total LC3 and LC3-II), although no differences were found in cells not treated with bafilomycin **(Figure 3.10E)**. Analysis of the ration of autophagosomes/autolysosomes also confirmed that overall less EGFP-positive cells accumulated under HBSS treatment compared to complete media **(Figure**

3.10F). However, this may represent induction of endosomal microautophagy, as previously shown [581]. Starvation induces endosomal microautophagy which can decrease the levels of LC3-II by 50% [581]. Nonetheless, lysosomal inhibition by bafilomycin elevated the percentage of autophagosome positive cells confirming ongoing autophagosome formation under starvation conditions. Taken together, these data suggest that autophagy flux is elevated in HEK293T cells under starvation conditions, although this could only be detected when bafilomycin was present. These conditions therefore established the baseline for starvation-induced autophagy in HEK293T cells. Hence these approaches were used in subsequent experiments.

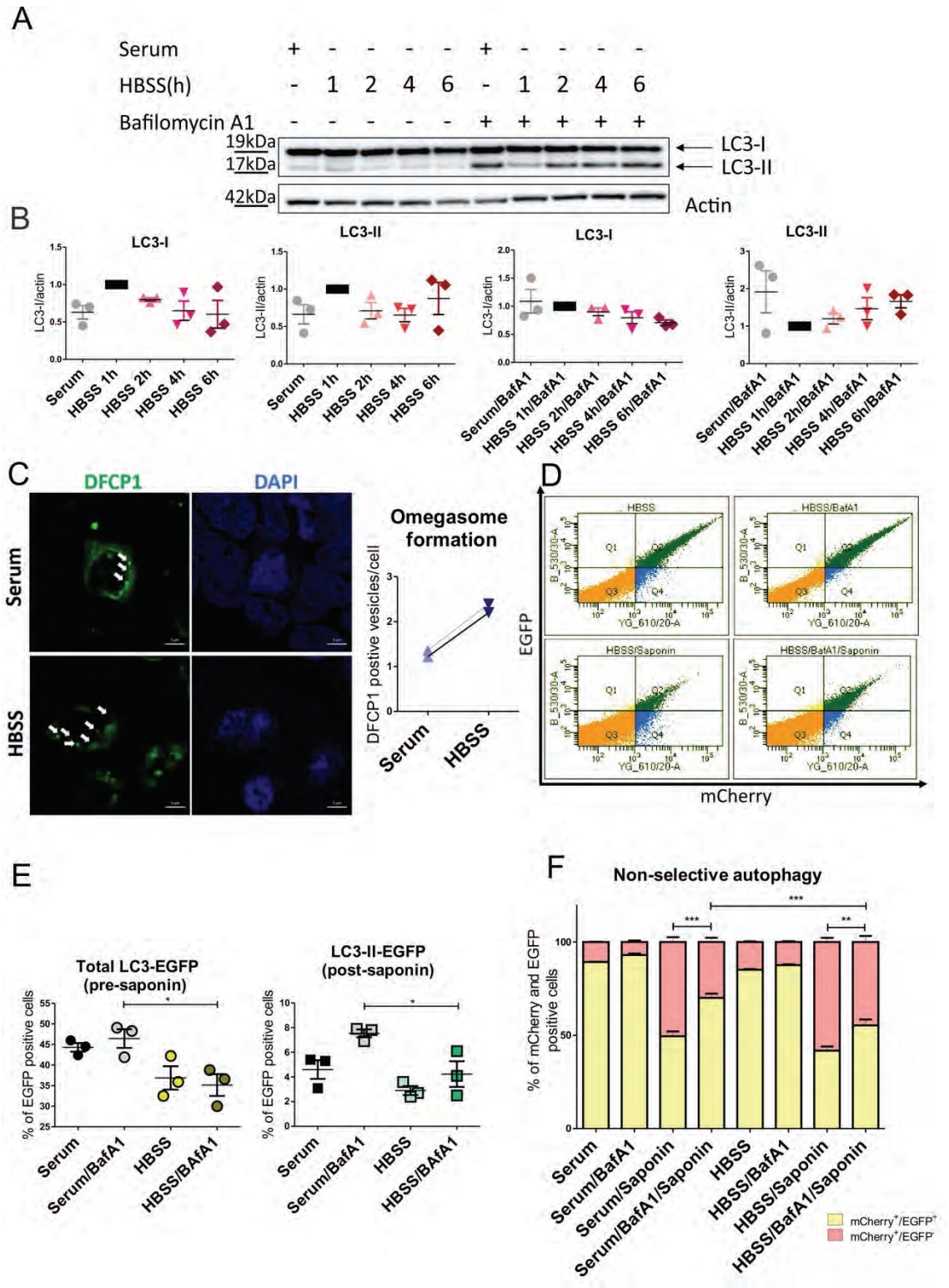


Figure 3.10. Starvation induces degradation of autophagosomes in HEK293T cells. **(A/B)** *Starvation induces autophagosome degradation*. HEK293T cells for starved in HBSS for 1 hr, 2 hr, 4 hr or 6 hr, then lysed and separated on SDS-polyacrylamide gel. LC3 and GAPDH immunoblotting was performed. Representative blots are shown. Band intensity was quantified using ImageJ and normalised to internal control, GAPDH. Relative expression levels are shown in quantification. N=3+/-SEM, one-way ANOVA

with Tukey post-hoc test. **(C)** *Starvation induces omegasome formation.* HEK293T cells were grown on coverslips and transfected with DFCP1-EGFP plasmid and starved for 4 hr in HBSS or cultured in serum rich media. DFCP1-EGFP puncta was counted in 50+cells per replicate. Representative pictures and quantification are shown. Scale: 5μm. **(D-F)** HEK293T cells were transfected with LC3-EGFP-mCherry overexpressing vector and starved for 4 hr in HBSS, then processed for FC analysis. **(D)** *Representative images of FC analysis of TBK1* knock-out *HEK293T cells under basal autophagy.* Increasing EGFP signal along the y axis and increasing mCherry signal along the x axis. Q1: $EGFP^{+}/mCherry^{-}$, Q2: $EGFP^{+}/mCherry^{+}$, Q3: $EGFP^{-}/mCherry^{-}$, Q4: $EGFP^{-}/mCherry^{+}$. (**E)** *Percentage of autophagosome positive HEK293T cells under starvation-induced autophagy.* EGFP positive cells significantly decreased upon starvation compared to serum rich condition both with and without saponin treatment. N=3 +/- SEM, one-way ANOVA with Tukey post-hoc test, *>0.05. (**F)** *Autophagosome/autolysosome ratio in HEK293T cell under starvation.* Autophagosome positive cells decrease during starvation. N=3 +/- SEM, one-way ANOVA with Tukey post-hoc test, **>0.005, ***>0.0005.

3.4.10 TBK1 inhibition leads to inhibited omegasome formation during starvation-induced autophagy

Next, the consequence of inhibiting TBK1 using BX795 and MRT67307 on starvation-induced autophagy was examined. The formation of the omegasome is known to be increased as a key response to starvation [381]. Hence, the formation of the omegasome was first analysed during non-selective autophagy. Starvation was induced in HBSS for 4 hr, in BX795 or MRT67307, or vehicle (water or DMSO as appropriate) pre-treated cells. Replacement of serum with HBBS (containing vehicle solution) led to significantly more DFCP1-EGFP puncta as expected, indicating that more omegasomes were formed, and hence that non-selective autophagy was induced in both vehicle control treated cells (p=0.04, p=0.005). However, significantly fewer DFCP1-EGFP puncta were detected in both BX795 (p=0.01) and MRT63607 (p=0.007) treated cells, compared to the respective vehicle only conditions **(Figure 3.11B/C)**. Furthermore, there was no significant difference in the proportion of cells with DFCP1-EGFP puncta between cells in the presence of serum and cells treated with BX795 or MRT67307, demonstrating that starvation did not induce omegasome formation in cell treated with the TBK1 inhibitors

as it did in vehicle treated cells. This result suggests that TBK1 is involved in omegasome formation during non-selective autophagy.

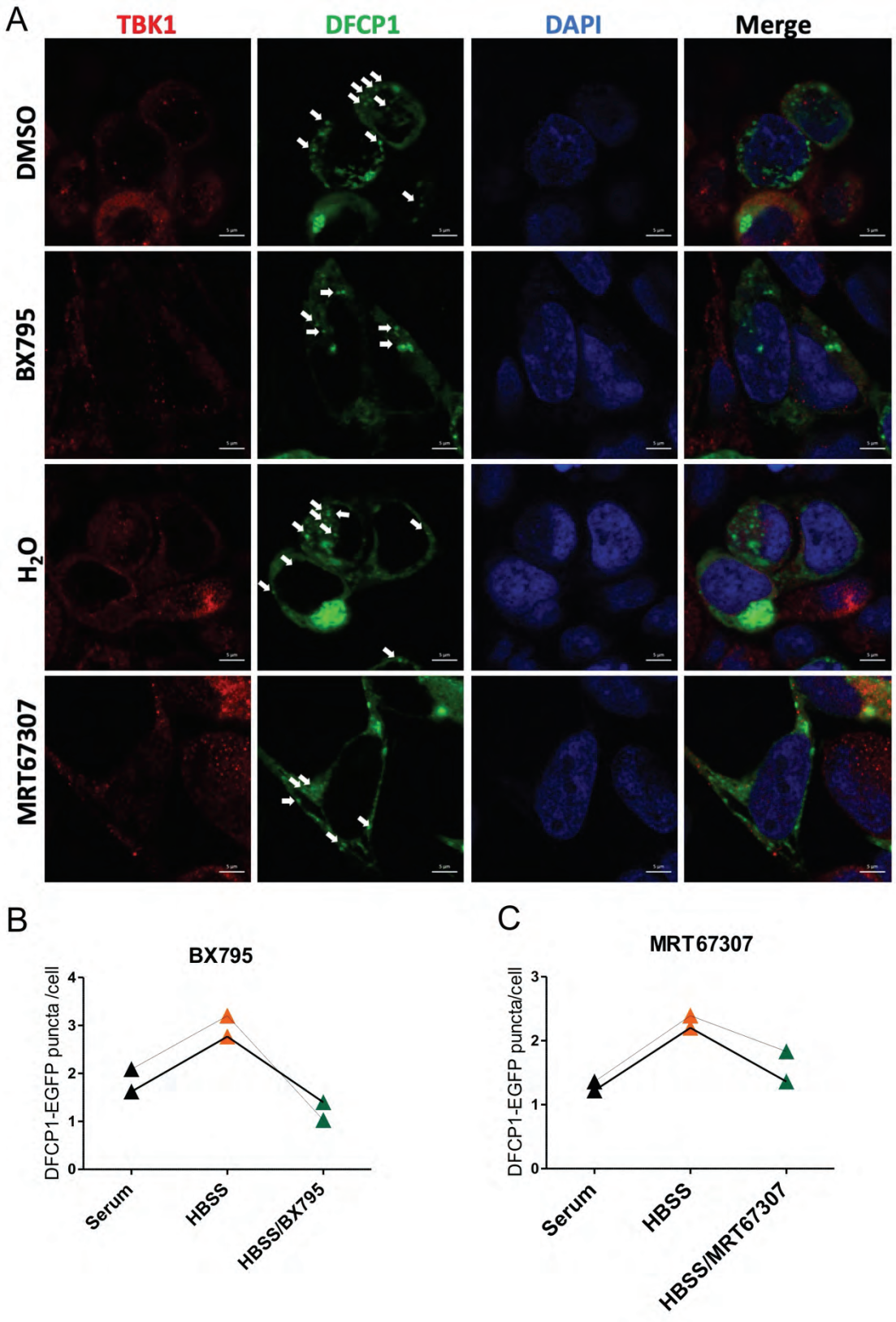


Figure 3.11. Omegasome formation is inhibited in TBK1 inhibited HEK293T cells during starvation-induced autophagy. HEK293T cells were transfected with DFCP1-EGFP overexpressing vector and BX795 (1 μM) or MRT67307 (25 nM) inhibited cells were starved in HBSS for 4 hr. DFCP1-EGFP puncta were quantitated. Cells were fixed and stained with anti-TBK1 antibody. DFCP1-EGFP puncta was counted in 50+ cells per replicate. **(A)** Representative images from confocal microscopy analysis of cells undergoing starvation. **(B/C)** Relative comparison of DFCP1-EGFP puncta. Scale: 5 μm. Arrows show omegasomes.

Autophagosome formation in cells overexpressing dual tagged LC3-EGFP-mCherry was next examined by FC. Non-selective autophagy was induced by starvation of TBK1 inhibited cells in HBSS for 4 hr. As **Figure 3.10E** showed that by examining only EGFP positivity of the cell, significant increase upon bafilomycin treatment could not be detected (HBSS vs HBSS/BafA1) as was expected, these analyses were not carried out here or onwards. In contrast, bafilomycin significantly increased ($p<0.0001$) the ratio of $EGFP^+/mCherry^+$ cells in vehicle treated conditions **(Figure 3.10F)** therefore conclusions were made from this analysis. BX795 treatment lead to a significant, increase of $EGFP^+/mCherry^+$ cells compared to vehicle conditions ($p=0.006$, **Figure 3.12A/C**, purple square). However, upon accumulation of autophagosomes by bafilomycin, no differences were observed in $EGFP^+/mCherry^+$ positive cells compared to DMSO treated cells (**Figure 3.12C**, green square). These data indicate that BX795 leads to inhibited autophagosome lysosome fusion similar to basal autophagy. Upon MRT67307 treatment, the proportion of $EGFP^+/mCherry^+$ cells significantly increased compared to H_2O treated conditions **(Figure 3.12B/D)**, both in the absence and presence of bafilomycin (**Figure 13D**, purple square, green square). This result suggests that MRT67307 abrogates autophagosome degradation, implying that TBK1 mediates the fusion between autophagosomes and lysosomes. These data suggest that, both BX795 and MRT67307 decreased autophagosome lysosome fusion.

Next, to detect LC3-I and LC3-II individually, immunoblotting of LC3 was performed on HBSS starved HEK293T cells treated with the TBK1 inhibitors. In contrast to expectation, the treatment of cells with either inhibitor did not significantly effect LC3-I or LC3-II levels, both with and without bafilomycin **(Figure 3.12E-L)**. In contrast to

the results obtained during basal autophagy, significantly lower levels of TBK1 were present following TBK1 inhibition both with BX795 and MRT67307 (**Figure 3.12H/L**, p=0.02, p=0.01). This finding suggests the presence of a possible autoregulatory loop, whereby the expression level of TBK1 is mediated by its kinase activity during starvation-induced autophagy. Furthermore, upon MRT67307, but not BX795, treatment, significantly lower (p=0.03) TBK1 levels were detected in bafilomycin treated cells compared to vehicle control, indicating that degradation of TBK1 was not via autophagy. Decreased TBK1 levels upon starvation may therefore explain the lack of effect of starvation-induced autophagy by the two TBK1 inhibitors examined here.

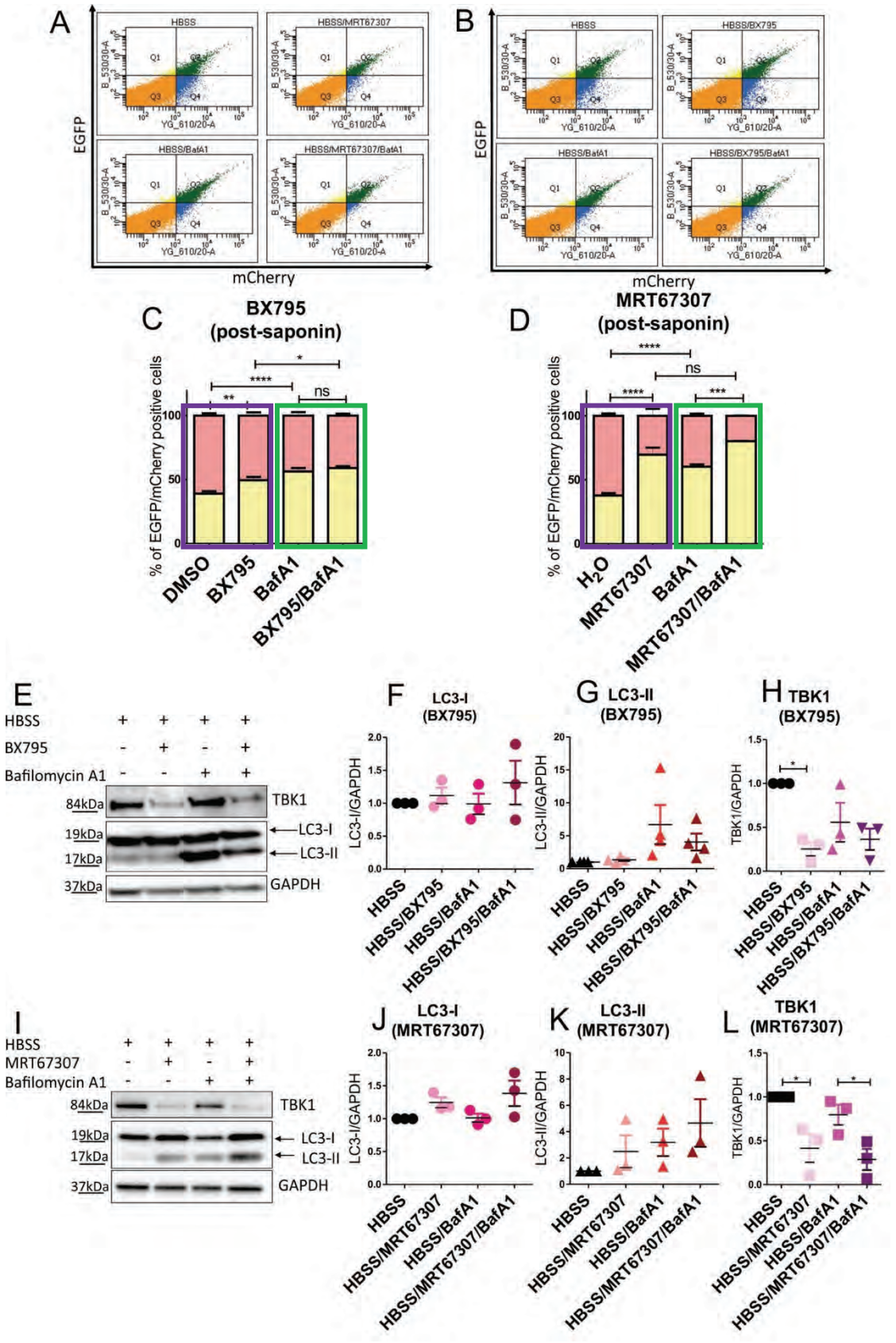


Figure 3.12. TBK1 inhibition leads to impaired autophagosome maturation during starvation in HEK293T cells. (A-D) *TBK1 inhibition decreases autophagosome-lysosome fusion.* HEK293T cells were transfected with dual tagged LC3-EGFP-mCherry

and autophagy was induced by starvation in HBSS for 4 hr of 1 μM BX795 and 25 nM MRT67307 treated cells in the presence or absence of 100 nM bafilomycin. (**A/B)** Representative images of FC analysis are shown. Increasing EGFP signal along the y axis and increasing mCherry signal along the x axis. Q1: $EGFP^+/mCherry^-$, Q2: $EGFP^+/mCherry^+$, Q3: $EGFP^-/mCherry^-$, Q4: $EGFP^-/mCherry^+$. **(C/D)** *Autophagosome/autolysosome ratio in TBK1 inhibited HEK293T cell under starvation.* TBK1 inhibition did not affect the ratio of autophagosome and autolysosome ratio. N=3 +/- SEM. One-way ANOVA with Tukey post-hoc test, *<0.05, ***<0.0005, ****<0.00005. **(E-L)** *TBK1 inhibition does not affect LC3-II levels, while TBK1 levels decrease upon inhibition.* HEK293T cells were plated and treated with BX795 (1 μM) and MRT67307 (25 nM) for 20 hr and then starved for 4 hr with or without bafilomycin (100 nM). Cell lysates were separated on SDS-polyacrylamide gels and immunoblotted for LC3, TBK1 and GAPDH as a loading control. Representative blots and quantifications are shown. Band intensity was quantified using ImageJ and normalised to internal control, GAPDH. Relative expression levels are shown in quantification. N=3 +/- SEM, one-way ANOVA with Dunnett post-hoc test, *<0.05.

To further examine the role of TBK1 in non-selective autophagy, LC3-EGFP vesicles were also quantitated after BX795 or MRT67307 treatment followed by 4 hr starvation in HBSS, using confocal microscopy. In contrast to the FC and immunoblotting analyses, inhibition of TBK1 by BX795 led to fewer LC3-EGFP puncta positive cells upon bafilomycin treatment compared to the DMSO control **(Figure 3.13C)**, indicating that TBK1 may mediate autophagosome formation. In contrast, MRT67307 treatment did not lead to any statistically significant differences **(Figure 3.13D)**, however there was considerable variability in the experimental replicates. Therefore, these data provide conflicting results as to whether TBK1 is involved in autophagosome formation during starvation-induced autophagy.

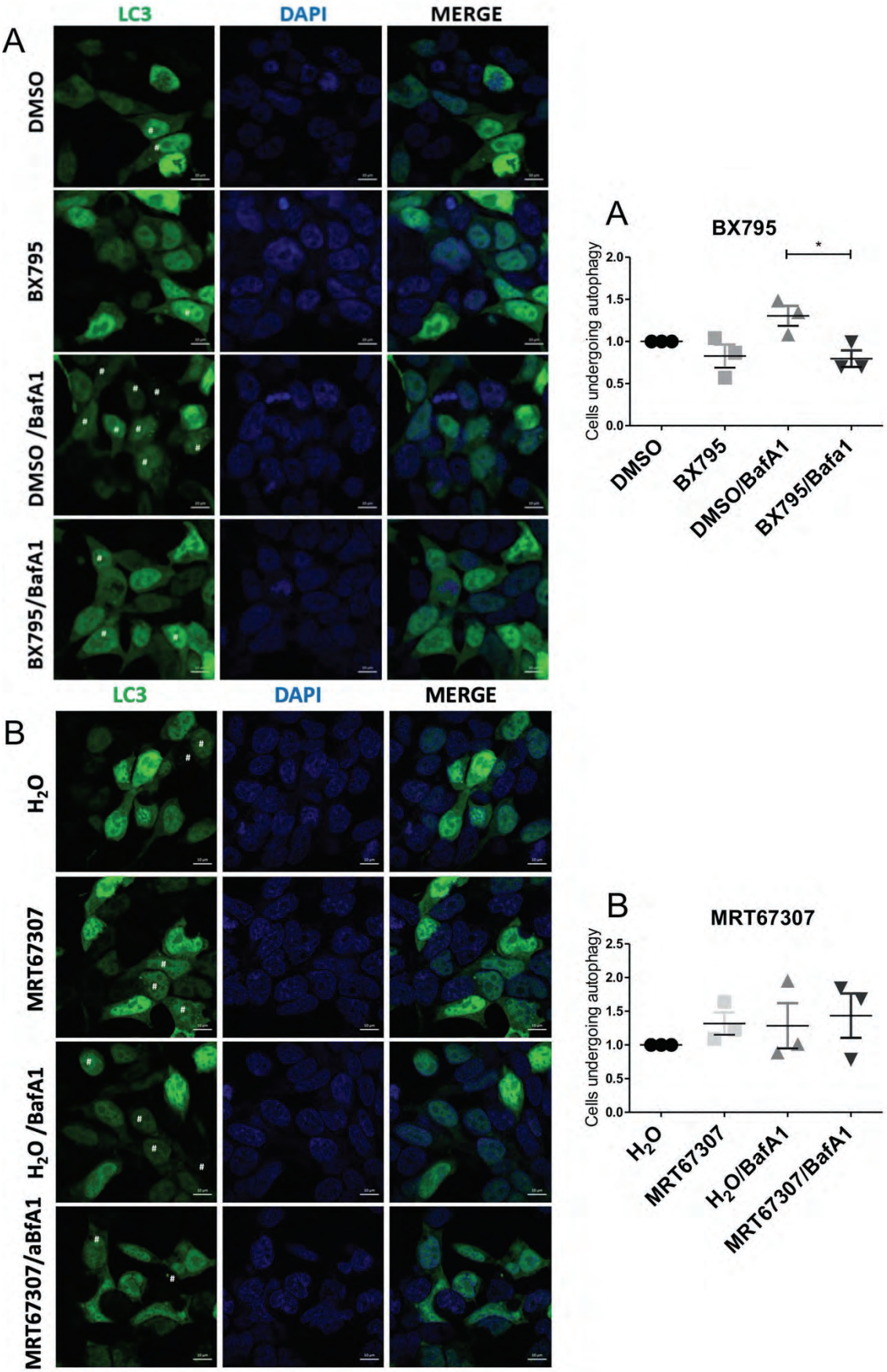

A
LC3
DAPI
MERGE
DMSO
BX795
DMSO /BafA1
BX795/BafA1
B
LC3
DAPI
MERGE
H2O
MRT67307
H2O /BafA1
MRT67307/aBfA1
A
BX795
Cells undergoing autophagy
2.0
1.5
1.0
0.5
0.0
*
DMSO
BX795
DMSO/BafA1
BX795/Bafa1
B
MRT67307
Cells undergoing autophagy
2.5
2.0
1.5
1.0
0.5
0.0
H2O
MRT67307
H2O/BafA1
MRT67307/BafA1

Figure 3.13. TBK1 inhibition by BX795, but not by MRT67307, inhibits autophagosome formation during starvation-induced autophagy detected by confocal microscopy. HEK293T cells were grown on coverslips and transfected with LC3-EGFP overexpressing vector and BX795 (1 μM) or MRT67307 (25 nM) inhibited cells were starved in HBSS for 4 hr. LC3-EGFP vesicle positive cells were counted. **(A/C)** Representative images of confocal microscopy analysis. **(B/D)** Relative comparison of cells undergoing autophagy. At least 50 cells were analysed in each biological replicate. N=3 +/- SEM, one way-ANOVA with Tukey post-hoc test, *<0.05. Scale: 10 μm.

3.4.11 Summary of starvation-induced autophagy results obtained

These data together reveal that the kinase activity of TBK1 mediates the formation of the omegasome, but not the autophagosome, during starvation-induced autophagy. Furthermore, these data suggested that the kinase activity of TBK1 mediates the fusion between autophagosomes and lysosomes upon starvation of HEK293T cells. However, this finding could not be confirmed by immunoblotting. In fact, using confocal microscopy, conflicting results were obtained between the two inhibitors, which may reflect the differing specificity of these inhibitors for TBK1, and the differing sensitivity between the different techniques used to detect autophagy.

Table 3.2. Summary of results obtained from TBK1 inhibition studies during starvation-induced autophagy.

Non-selective autophagy	BX795		MRT67307	
	Autophagosome formation	Autophagosome maturation	Autophagosome formation	Autophagosome maturation
FC: $EGFP^+$ cells	-	-	-	-
FC: $EGFP^+$-$mCherry^+$ cells	-	Inhibited	-	Inhibited
Immunoblotting-LC3-I/LC3-II	-	-	-	-
LC3 –EGFP microscopy	Inhibited	-	-	-
Omegasome formation	Inhibited		Inhibited	

3.4.12 TBK1 knock-out does not affect starvation-induced autophagy

Knock-out of TBK1 and inhibition of the kinase activity of TBK1 previously demonstrated different effects on basal autophagy. It is therefore possible that knock-out of TBK1 may produce different effects to TBK1 inhibition, on starvation-induced autophagy. Hence, it was next analysed whether knock-out of TBK1 affects non-selective autophagy by examining the CRISPR/Cas9 TBK1 KO clones.

Non-selective autophagy was induced by replacing serum with HBBS for 4 hr. The fusion of autophagosomes and lysosomes was next analysed in genome edited TBK1$^{-/-}$ (#1, #2) clones. However, no significant differences were obtained in the ratio of EGFP$^{+/}$mCherry^{+} and EGFP$^{-/}$mCherry^{+} cells between the clones when starved **(Figure 3.14C)**. Immunoblotting of LC3-I and LC3-II was next performed on TBK1 knock-out cells under starvation. However, the CRISPR/Cas9 edited TBK1 KO cells showed no significant differences in the expression of either LC3-I or LC3-II **(Figure 15D/E)**. Therefore, these data suggest that TBK1 knock-out does not influence starvation-induced autophagy in HEK293T cells.

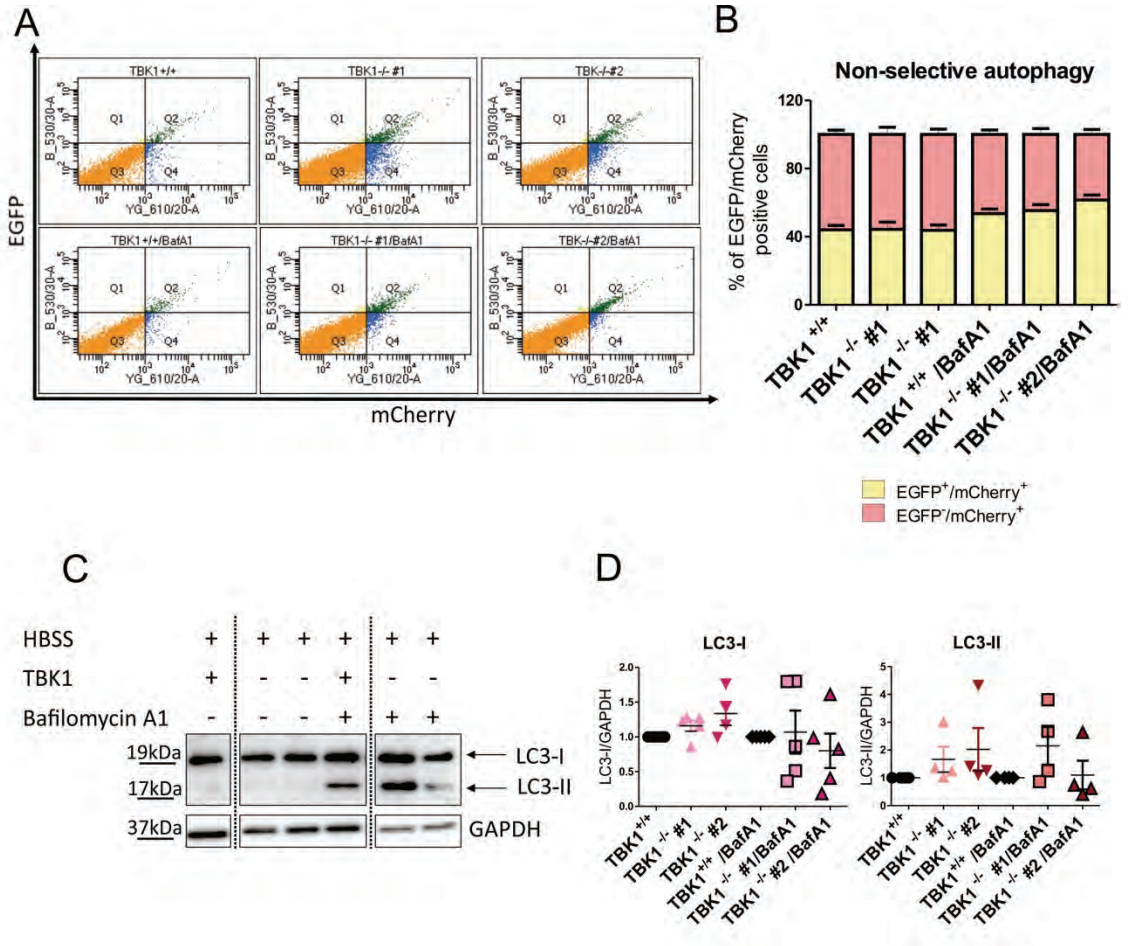


Figure 3.14. TBK1 knock-out **does not affect starvation-induced autophagy. (A/B)** *TBK1* knock-out *may induce autophagosome degradation.* TBK1$^{+/+}$ and TBK1 $^{-/-}$ #1/#2 HEK293T cells were transfected with dual tagged LC3-EGFP-mCherry and autophagy was induced by starvation in HBSS for 4 hr in the presence or absence of 100 nM bafilomycin. **(A)** Representative images of FC analysis are shown. Increasing EGFP signal along the y axis and increasing mCherry signal along the x axis. Q1: EGFP^{+}/mCherry^{-}, Q2: EGFP^{+}/mCherry^{+}, Q3: EGFP^{-}/mCherry^{-}, Q4: EGFP^{-}/mCherry^{+}. (**B)** *TBK1* knock-out *did not affect the ratio of autophagosome and autolysosome ratio.* N=3 +/- SEM. **(C/D)** *TBK1* knock-out *does not change LC3-I and LC3-II levels in starved cells*. TBK1$^{+/+}$ and TBK1 $^{-/-}$ #1/#2 HEK293T cells were starved for 4h in HBSS then lysed and separated on SDS polyacrylamide gels followed by immunoblotting for LC3 and GAPDH as a loading control. Representative blots **(C)** and quantifications **(D)** are shown. Band intensity was quantified using ImageJ and normalised to internal control, GAPDH. Relative expression levels are shown in quantification. N=3 +/- SEM, one-way ANOVA with Tukey post-hoc test. Dashed line indicates the cropping of 'control' clone.

3.4.13 Summary

These data together suggest that TBK1 is involved in basal autophagy, and possibly also in starvation-induced autophagy. The kinase activity of TBK1 contributes to autophagosome formation and degradation in basal autophagy, and during starvation-induced autophagy. Interestingly, knock-out of TBK1 via genome editing did not affect basal autophagy or starvation-induced autophagy. However, the results demonstrate that TBK1 clearly mediates the formation of the omegasome during starvation-induced autophagy while it is not involved in basal autophagy. Due to the difference results detected by the FC and immunoblotting the role of TBK1 in non-selective autophagy may although remains somewhat inconclusive however suggest that TBK1 may also be involved in autophagosome lysosome fusion during starvation-induced autophagy.

It was interesting that inhibition of the kinase activity of TBK1 and its knock-out have opposing consequences on both basal and non-selective autophagy. Hence it was hypothesised that this might reflect the two functional domains of TBK1; the kinase and substrate binding domains. This was explored further by evaluating autophagy receptors during basal and non-selective autophagy under TBK1 inhibited and knock-out

conditions. Autophagy receptors and their binding to LC3 were therefore analysed in Chapter 4 to examine how TBK1 may exert these effects.

3.5 Discussion

3.5.1 Limitations of autophagy detection techniques

Autophagy is a multistep, and complex cellular process that involves several phases: including phagophore formation and elongation, autophagosome formation and closure, and finally fusion of the autophagosome with lysosome and degradation. To ensure the uniform detection of autophagy, the specific detailed guidelines established by Klionsky et al. [464, 529, 530]. Hence, in this chapter, a combination of flow cytometry, confocal imaging and immunoblotting was used to follow autophagy, and an extensive panel of assays was developed to monitor autophagy in HEK293T cells. However, all these techniques have their limitations, and the results were found to variable between the techniques.

The levels of LC3-II detected by immunoblotting are reflective of the amount of autophagosomes present in the cellular population. However, immunoblotting itself is not the most accurate way to quantitate protein levels [464]. It samples the whole population, which is therefore dependent on transfection efficiency. Hence small differences in the levels of LC3-II may not be detectable using immunoblotting. LC3-II should be always compared to a housekeeping protein, such as actin or GAPDH, and not to LC3-I [464] as LC3-I degrades faster in cellular lysates than LC3-II. Therefore, biological replicates of LC3-II detected by immunoblotting may be very variable, which was observed in this chapter.

Confocal microscopy analysis of autophagosomes allows the quantification of single cells, and thus is not dependent on transfection efficiency. However, it will depend on expression level. Furthermore, autophagosome vesicles can be examined individually, therefore this may arguably provide a more precise description of autophagy compared to immunoblotting. In addition, using the dual tagged LC3 construct, both autophagosome and autolysosome-fusion can be examined at the same time. However, microscopy analysis can be very time consuming and only a limited number of cells in the whole population can be analysed without high throughput microscopy systems, as in this study. Automated quantification tools are however available, that could be assessed in the future.

Furthermore, the high background of LC3-I upon overexpression can make the detection of LC3-II vesicles difficult by microscopy [464], and only one vertical section of the cell is analysed. Therefore, even though each cell is individually analysed, the whole volume of the cell is not examined, just a fraction of it, which also provides limitations in monitoring autophagy.

The use of flow cytometry to detect autophagy combines the advantages of immunoblotting and microscopy analysis. It allows the detection of single cells in a more high-throughput manner than microscopy, and using the dual tagged LC3 construct, both autophagosome and autolysosome-fusion can be examined, similar to microscopy analysis. The biggest limitations of flow cytometry analysis however are that signals are collected from the entire cell, and individual vesicles cannot be examined as they can using microscopy. Therefore, the autophagic status of the whole cell is determined, rather than the ratio of autophagosome and autolysosomes in each cell. In this study, the autophagic state of each cell was determined using quadrant gating to group cells into a category of interest; cells with autophagosome or cells without autophagosomes.

Due to limitations of all techniques described, the combination of these techniques was used on this thesis to more accurately determine the autophagy status.

LC3 is the most widely used marker to detect autophagy. However, the Klionsky guidelines state that other autophagy related proteins need to also be evaluated alongside LC3 [464]. On accordance with these guidelines, the omegasome marker, DFCP1 was chosen here. Furthermore, in Chapter 4, autophagy receptors p62 and NDP52 - that tether the cargo towards the forming autophagosome – were examined. Another mechanism to examine autophagy is to follow the degradation of cargo, such as ubiquitin. This strategy was used in the studies described Chapter 5.

The results obtained in this chapter were variable depending on which technique to detect autophagy was used. They therefore highlight the need for strict guidelines to monitor autophagy. All experiments in this chapter however were performed in strict accordance with Klionsky guidelines [464].

3.5.2 TBK1 kinase activity facilitates autophagosome lysosome fusion

BX795 and MRT67307 have been previously characterised as highly specific inhibitors of the kinase activity of TBK1. Here, in some instances, similarities were observed between their effects on autophagy in including the inhibition of autophagosome-lysosome fusion detected by multiple technique and autophagosome formation during basal autophagy showed by both inhibitors. These results indicate that TBK1's kinase activity is involved in the fusion and degradation of autophagosomes in basal autophagy and potentially in the formation of autophagosomes.

In contrast, some important differences were also noted between the two inhibitors. An interesting question is what outcome may result if both inhibitors were used together. This should be further analysed in the future. Inhibition of TBK1 by BX795 led to inhibited autophagosome formation, as detected by confocal microscopy. In contrast, BX795 treatment did not lead to significant changes when $EGFP^+$ cells were analysed with FC, potentially due to differences in transfection efficiency. Furthermore, abrogated autophagosome lysosome fusion was detected by FC analysis of $EGFP^+/mCherry^+$ cells. In contrast, inhibition of TBK1 using MRT67307 - analysed by FC - led to abrogated autophagosome degradation, as detected by an increase in the proportion of $EGFP^+$ and $EGFP^+/mCherry^+$ cells. However, this could not be confirmed by immunoblotting. Furthermore, less autophagosome formation was also detected by immunoblotting, but not by the other techniques. Hence, overall these results indicate that while both inhibitors prevented autophagosome formation and fusion in at least some of the assays used here, differences in these findings were detected.

BX795 was previously shown to inhibit autophagosome lysosome fusion in mouse embryonic fibroblasts during xenophagy [39], whereas the inhibition of autophagosome maturation by MRT67307 has not yet been described in the literature. However, MRT67307 is a derivative of BX795 that was previously shown to have a higher specificity for TBK1 [550], so the results obtained here are consistent with these previous studies. BX795 treatment only partially inhibited autophagosome-lysosome fusion, as bafilomycin treatment still led to increased $EGFP^+/mCherry^+$ cells, whereas MRT67307 inhibited fusion completely, as shown by the lack of increase in $EGFP^+/mCherry^+$ cells

upon lysosomal inhibition with bafilomycin treatment, implying that MRT67307 is a more potent inhibitor of TBK1 than BX795. TBK1 was also previously shown to facilitate delivery of the lysosomal hydrolase cathepsin D to autolysosomes [582] by an unknown mechanism. This is a possible explanation for how inhibition of TBK1 by MRT67307 and BX795 led to decreased autophagosome maturation in HEK293T cells in this study, by inhibiting cathepsin D delivery to autolysosomes.

It must be noted that MRT67307 did not inhibit autophagosome formation more than BX795, which would have been expected based on its increased potency. The reasons for these discrepancies are unclear. MRT67307 has been shown to inhibit other kinases in addition to TBK1 [548], including ULK1 and ULK2 [551]. However, this known off-target effect of MRT67307 cannot explain the discrepancies seen here. If MRT67307 inhibited ULK1 and ULK2 as well as TBK1, more pronounced results would be expected on autophagy. Whilst MRT67307 has been shown to inhibit autophagosome formation by inhibiting ULK1 in mouse embryonic fibroblasts (MEFs), that was at a much higher IC^{50} than is required than to inhibit TBK1 (19 nM vs 45 nM and 38 nM respectively) [551]. In this particular study a 400 times higher concentration of MRT67307 (10 μM, for 1hr) was used than in this thesis [551]. In microglia, a MRT67307 concentration of 10 μM and 8 hr treatment inhibited ULK1, which diminished both LC3-I and LC3-II levels, and led to microglial activation [583]. MRT67307 previously also inhibited the formation of autophagosomes in pancreatic cancer cells at a concentration 200 times higher than used in this thesis [526]. Furthermore, ULK1 activity can be measured by phosphorylation of *atg*13 [584], and inhibition with MRT67307 decreases *atg*13 phosphorylation only during starvation-induced autophagy, and not during basal autophagy [584]. Hence these data indicate that ULK1 does not regulate basal autophagy [551]. This indicates that in this thesis when MRT67307 treatment decreased autophagosome formation during basal autophagy, this was not likely due to ULK1 inhibition, but more probably due to TBK1 inhibition. It must be noted however that TBK1 inhibition was not evaluated upon MRT67307 treatment in these previous studies [583] [526] [584], therefore it is possible that TBK1 inhibition contributed to the effects realised in these studies, especially since TBK1 inhibition upon MRT67307 most certainly occurred at such high concentrations. Hence, the phosphorylation status of

ULK1 could be evaluated following MRT67307 treatment in the future, to ensure that its effects were strictly due to TBK1 inhibition, and not ULK1 inhibition.

3.5.3 Genome editing "control" clone differs from HEK293T parental cells

TBK1 KO HEK293T cell lines were generated using CRISPR/Cas9 editing to examine the consequence of loss of expression of TBK1 on autophagy. These cells underwent two rounds of limiting dilution to select individual clones to ensure that a homogenous cell population was achieved, whereby all cells possess the same mutation in the *TBK1* gene. Two TBK1 knock-out clones were selected for analysis rather than studying only one clone. This was to ensure that any phenotype detected was due to knock-out of TBK1 specifically, hence only results that were consistent between the clones were considered. By using a previously published gRNA sequence [480] to generate the clones in this study, I also aimed to minimise off-target effects. The results using the TBK1 KO clones however gave unexpected results, as discussed further below.

To ensure further stringency in the results, a 'control' clone was also selected randomly from the analysis, with the aim of excluding off-target effects due to genome editing. This control line had undergone CRISPR/Cas9 editing and survived two rounds of cloning by limiting dilution, but it was found to still retain expression of TBK1 (#122.2). Furthermore, sequencing, covering 300 base pair region around gRNA binding site confirmed that no mutations were present in this clone at the. Interestingly, previous studies describing genome editing are not consistent in the use of controls. Many studies do not use the type of control cell line used in this study – the control cell lines used are usually the parental cell line. Furthermore, many CRISPR/Cas9 studies use only one knock-out clone only [585]. In this study, we aimed to use a more thorough approach than usually described in the literature, using the 'control' cell lines and the use of two TBK1 knock-out clones. Surprisingly however, the control cell line exhibited decreased cell growth and unexpectedly, TBK1 showed decreased interaction with LC3 **(Figure 5.8E)**. Furthermore, STR analysis showed that this 'control' clone resembled HEK293T cells the least of all the cell lines tested. In contrast, the TBK1 knock-out cells showed no

change in growth and were more similar to HEK293T cells. Hence, the ‘control’ clone was not included in the analysis, and its suitability as ‘control’ was therefore questioned.

Genome editing is a very promising technique; however, it is still a relatively new field and is developing very fast. Off-target effects are a concern with any method involving genetic modification. They can be detected by genome-wide, unbiased identification of DSBs enabled by sequencing (GUIDE-seq) [586], which detects genome-wide profiling of off-target cleavage by CRISPR-Cas nucleases. Since generation of the TBK1 KO cell lines in this study was completed, various strategies to limit off-target effects have been proposed [587]. One example is modification of the sgRNA sequence by truncating the region complementary to the target site at the 5′ end of the sgRNA by 3 nucleotides [588]. Another potential solution to limit off-targets effects is trialling lower concentrations of the Cas9/gRNA construct, although this may also inhibit on-target cleavage [589-593]. Alternatively, wild-type Cas9 can be replaced by a mutant ‘nickase’ version of the nuclease and paired with two sgRNAs that each cleave only one strand. This technique can reduce off-target activity by 50–1,500-fold [589-593]. However, it is important to note that off-target effects can still lead to major alterations in the cell, including chromosomal truncations [594].

Sequencing of the resulting KO clones following CRISPR/Cas9 editing is rarely reported in the literature; if expression of the targeted protein is knocked-out, then it is assumed that editing has been successful and that the target sequence does indeed contain a stop codon. Here, again in aiming to be stringent in this study, sequencing of the resulting KO clones was performed, although this was restricted to the binding site of the gRNA. Therefore, in the future, sequencing of the entire TBK1 gene would be worthwhile in the KO clones, to determine if another mutation was present in the ‘control’ cell lines, which could explain its unexpected properties. Another strategy that could be employed in the future is generation of a new control cell line using empty vectors lacking the gRNA, rather than producing lines from cells transfected with the TBK1 gRNA, as previously reported [395].

3.5.4 TBK1 knock-out does not mimic TBK1 inhibition

The aim of the TBK1 KO studies was to investigate how basal and starvation-induced autophagy were altered when TBK1 was knocked-out. Based on data obtained using BX795 and MRT67307 treatment, and published studies in the literature on xenophagy/mitophagy [140, 456, 487], lower autophagic activity was expected in the TBK1 KO cells during basal autophagy. However, contrary to expectations, knock-out of TBK1 resulted in no change in LC3-II levels, as detected by immunoblotting and flow cytometry analysis, therefore suggesting that knock-out of TBK1 did not affect basal autophagy. The observed differences obtained between TBK1 knock-out and TBK1 inhibition may be due to various reasons.

Firstly, upon TBK1 inhibition, the substrate binding activity of TBK1 to its substrates was still intact. Hence, there is the possibility that, due to the loss of binding activity when the expression of TBK1 is knocked-out, substrates that normally bind to TBK1, such as p62 and NDP52, may bind to alternative kinases, such as AMPK [595] or ULK1 [596]. A second possible explanation for the differences observed in this study between TBK1 knock-out and TBK1 inhibition, is that the KO cells may have adapted to the knock-out of TBK1. Moreover, ULK1 is a good candidate to compensate for TBK1's function; whilst ULK1 phosphorylates p62 on a different serine residue to TBK1, it increases the p62-mediated clearance of protein aggregates [596], therefore enhancing autophagy. Thirdly, loss of TBK1 may indirectly affect the expression of autophagy genes. Loss of expression of RIPK1, a serine threonine kinase similar to TBK1, leads to a significant increase in the expression of autophagy genes [597]. RIPK1 regulates TFEB, a transcription factor that essentially regulates the expression of autophagy and lysosomal proteins. Interestingly, TBK1 is an endogenous inhibitor of RIPK1 [598] that directly phosphorylates residues T190/T189, and this blocks trans-activation of RIPK1 [598]. It is therefore possible that knock-out of TBK1 in the CRISPR/Cas9 clones in this study over-activates RIPK1, which consequently induces autophagy, therefore opposing the expected inhibition of autophagy caused by the knock-out of TBK1, resulting in no obvious change. Detection of RIPK1 and ULK1 and their phosphorylation status should therefore be examined in future in the KO cells, to determine whether this possibility

could explain the observed differences between TBK1 knock-out and TBK1 inhibition in this study.

3.5.5 TBK1 and omegasome formation

The formation of the omegasome has not been directly linked to TBK1 before. In this chapter, however, treatment of cells with BX795 or MRT67307 showed decreased omegasome formation during starvation, although there was no effect on omegasome formation during basal autophagy. Further analysis is required to confirm these results that could be combined with analysing the size of omegasome affected by TBK1 inhibitors. Omegasomes, unlike autophagosomes, cannot be accumulated via bafilomycin treatment [576], therefore the dynamics of omegasome formation is difficult to follow during basal autophagy. Starvation-induced autophagy, however, is strongly dependent on the production of the omegasome for formation of the autophagosome [381]. Hence, it is possible that TBK1 is required for omegasome formation during starvation-induced autophagy only. WD repeat domain phosphoinositide-interacting protein 2 (WIPI2), also called atg18, regulates the formation and maturation of omegasomes [599]. WIPI2 accumulates at the phagophore, recruits Atg16L1 to the phagophore and facilitates LC3 lipidation [600]. Interestingly, TBK1 interacts with WIPI2 and induces WIPI2-dependent autophagy of Salmonella by a mechanism involving its kinase activity and C-terminus [485]. TBK1 may therefore regulate omegasome formation by a mechanism involving WIPI2. Hence, in future studies, microscopy analysis of WIPI2 and its colocalization with LC3, DFCP1 and TBK1, could be evaluated in cells treated with TBK1 inhibitors, to establish whether the effect of TBK1 inhibition on omegasome formation is mediated by WIPI2.

3.5.6 Moderate effects of TBK1 on starvation-induced autophagy

In this study, inhibition of TBK1 kinase activity prevented basal autophagy, whereas it had little effects on starvation-induced autophagy. As a kinase, TBK1 phosphorylates autophagy receptors that selectively recognise the cargo for degradation, such as mitochondria, protein aggregates or invading bacteria, and recruit the autophagic machinery around the cargo. Non-selective autophagy - as suggested by the name - lacks the selectivity component of some types of autophagy. This cellular stress response is

mediated by mTORC1 inhibition, and consequent activation of the ULK1 complex, and TBK1 regulates mTOR both via its activation and inhibition. TBK1 directly interacts and phosphorylates mTORC1 at S2159, in an EGF stimulus-dependent manner [601]. TBK1 also supports AKT/mTORC1 activation during the cellular transition from starvation to serum rich conditions via activation of targets, both upstream and downstream from mTORC1 [569]. In prostate cancer cells, knock-out of TBK1 leads to increased phosphorylation of mTOR, while overexpression of TBK1 blocks the phosphorylation of mTORC1 at S7056 [580]. These effects are mediated by the kinase domain of TBK1 and are dependent on an intact mTOR signalling motif [580]. Hence, activation of mTORC1 would be expected to inhibit autophagy, and chronic activation of TBK1 should inhibit mTORC1 activity and therefore activate autophagy [577]. Based on these previous findings, it was expected that TBK1 inhibition would have a significant effect on starvation-induced autophagy in this study. However, due to the limited response following TBK1 inhibition, it is most likely that TBK1's role in non-selective autophagy is most likely mediated by autophagy receptors, and not by regulating mTORC1 activity.

It should be mentioned that TBK1 inhibition leads to inhibited autophagosome-lysosome fusion, both during basal and starvation-induced autophagy at least in some of the assays used here. Autophagy receptors are not required for autophagosome-lysosome fusion, suggesting that TBK1 may have a role in autophagy independently of these interacting partners. This further explains why the kinase activity of TBK1 affected fusion, even under starvation conditions. To what extent autophagy receptors are involved in non-selective autophagy remains to be elucidated.

3.5.7 TBK1 autoregulation upon inhibition

While inhibition of autophagosome-lysosome fusion was detected after treatment with both TBK1 inhibitors via FC following starvation, this result could not be confirmed via immunoblotting or microscopy analysis. However, this result may be explained by the decreased levels of TBK1 upon inhibition following starvation. Interestingly, upon inhibition by BX795 or MRT67307, TBK1 was downregulated during starvation-induced autophagy, while no significant changes were detected in its levels during basal autophagy. Variability was detected in the levels of TBK1 between the biological

replicates during basal autophagy **(Figure 3.5)** that may be due to low replicate number (N=3). Therefore, further replicates need to be performed to fully confirm how TBK1 levels change during basal autophagy. Decreased TBK1 levels were also detected upon bafilomycin treatment, indicating that TBK1 may not itself be degraded via autophagy. Furthermore, this indicates that TBK1 may have different role in basal autophagy compared to starvation-induced autophagy. Activation of TBK1 involves trans-autophosphorylation, indicating that TBK1 can regulate its own activity [471]. Furthermore, it was previously suggested that autophagy can regulate the TBK1 levels during starvation [526]. Following bafilomycin treatment, when autophagosome degradation is inhibited, the overall levels of TBK1 were less upon TBK1 inhibition, suggesting that TBK1 degrades via a non-autophagic pathway upon starvation, such as by the UPS.

The proteasomal degradation of kinases by inhibition of their enzymatic activity is not unknown. Leucine-rich repeat kinase 2 (LRRK2), which is involved in Parkinson's disease pathology, undergoes proteasomal degradation following inhibition of its kinase activity [602]. TBK1 degrades upon ubiquitination via the UPS [470, 603, 604]. Therefore, TBK1 may also be degraded by the proteasome following inhibition of its kinase activity. This mechanism may be an autoregulatory pathway by which TBK1 reduces the levels of its active form, in order to regulate its function.

3.5.8 Summary

The overall results in this chapter suggest that TBK1 is involved in basal autophagy, but further experiments are required to confirm this. It has less effects on non-selective autophagy, but it is clearly involved in the formation of the omegasome. These findings are summarised diagrammatically in **Figure 3.14**. Previously, TBK1 was shown to be involved in mitophagy, xenophagy, and in the basal autophagy of specific type of cancer cells. Hence, the results obtained in this chapter imply that TBK1 has a more widespread role across several different types of autophagy than previously realised. Hence, in ALS, given that haploinsufficiency of TBK1 is implicated in pathophysiology, dysfunction of TBK1 would potentially impact on several autophagy mechanisms in neurons, via

omegasome and autophagosome formation, and autophagosome degradation. These possibilities were examined further in Chapters 4 and 5.

TBK1 phosphorylates autophagy receptors to carry out its function during autophagy. Hence, the effects of TBK1 inhibition and knock-out described in this chapter should be mostly mediated by autophagy receptors. Therefore, in the next chapter, the involvement of autophagy receptors was analysed in basal and starvation-induced autophagy in relation to TBK1.

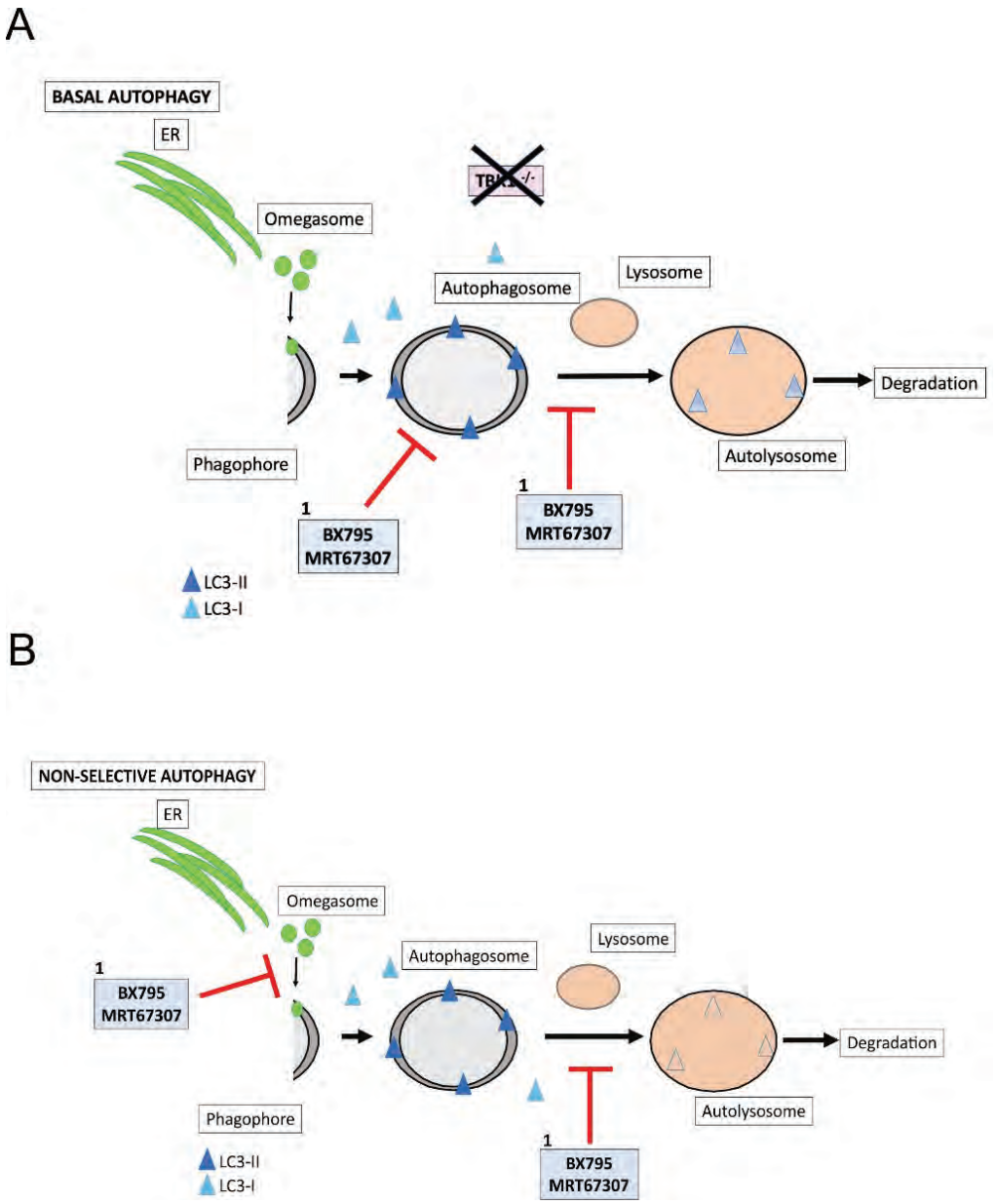


Figure 3.15. Summary of the results described in this chapter; proposed roles of TBK1 in basal and non-selective autophagy.

(A) *TBK1 is involved in basal autophagy*. The kinase activity of TBK1 may be involved in the formation of autophagosomes and their fusion with lysosomes. Knock-out of TBK1 does not affect basal autophagy. (**B)** *TBK1 is involved omegasome formation, and possibly autophagosome-lysosome fusion, during starvation-induced autophagy*. The kinase activity of TBK1 controls omegasome formation. The FC results suggested that autophagosome-fusion is mediated by TBK1, although this could not be confirmed using the other assays.

Chapter 4

Investigating the role of TBK1 in autophagy receptor regulation and ALS-linked mutations in in basal and starvation-induced autophagy

4.1 Introduction

4.1.1 Autophagy receptors in selective, basal autophagy and starvation-induced autophagy

Autophagy was long thought to be a bulk degradation system whereby the autophagosome forms around an undefined part of the cytosol, and specific cargo is not selected. However, now it is universally accepted that autophagy can be a highly selective process that can distinguish between normal and 'abnormal' cellular material to be degraded. Whilst the exact mechanism of cargo recognition remains incompletely understood, it is recognised that an ubiquitin-dependent sensor system is involved in the specific recognition of substrates [605]. Ubiquitin is recognised by autophagy receptors (also known as 'autophagy adaptors') via their ubiquitin binding domain (UBD), and they 'tether' the ubiquitinated cargo towards the nascent autophagosome for degradation [606]. Autophagy receptors have the unique capability to also bind to LC3 via their LC3-binding-domain (LIR), which is localised in the membrane of the autophagosome and phagophore. The most well-characterised autophagy receptors, that bind to both ubiquitin and LC3, are p62 [607], NBR1 [608], NDP52 [486], optineurin [132] and c-CBL [609]. Recently, a newly identified autophagy receptor, NUFIP1, was described which is involved in ribophagy, the selective degradation of ribosomes [610]. Hence autophagy receptors have important roles in selective autophagy.

A wide variety of types of selective autophagy exist in mammalian cells [390], and the list still continues to grow. Basal autophagy can be interpreted as the sum of all the selective autophagy processes occurring at any given time. Therefore, this suggests that the autophagy receptors may be involved in basal, as well as selective autophagy, however this has not yet been conclusively proven. Hence, in this Chapter it was examined whether autophagy receptors -p62, NDP52 and optineurin- are involved in basal autophagy and, if so, whether they are controlled by TBK1.

A fundamental difference between selective and non-selective autophagy is considered to be cargo recognition. Upon induction of selective autophagy, an autophagy receptor bind to the ubiquitinated cargo, which recruits the autophagic machinery, leading engulfment of the cargo. However, during non-selective autophagy, no such selectivity has been described so far. Instead, autophagosomes form upon inhibition of mTORC1,

which will in turn, induce ULK1; the initiator of autophagy [343]. In contrast, the role of ULK1 in selective autophagy is not very well understood, although it is known to relocate to mitochondria upon mitophagy [611, 612]. Nonetheless, activated ULK1 will recruit the remaining autophagy machinery, and the autophagosome forms during starvation. However, extensive, uncontrolled autophagy would be detrimental to any cell. Therefore, strict spatiotemporal control must be in place, even during starvation-induced autophagy. Degradation of autophagy regulators via polyubiquitination targets them towards the UPS for degradation during starvation, but autophagy is then returned to normal levels after the stress has been eliminated. For example, beclin1, a component of the Vps34-Beclin1 complex, undergoes degradation via Lys-11 polyubiquitination [613]. Similarly, ULK1 degradation is induced via Lys-27/ Lys-29 polyubiquitination [614]. Despite this, the stress response must only degrade non-essential elements of the cell, which raises the question of how exactly these components are determined/selected. Therefore, even during starvation-induced autophagy, there must be some selectivity towards cargo degradation and autophagy in general. Hence, in this Chapter, it was examined whether autophagy receptors mediate non-selective (starvation-induced) autophagy.

4.1.2 TBK1 phosphorylates autophagy receptors

TBK1 is involved in mitophagy [392, 456, 480] and xenophagy [487] [132], whereby TBK1 facilitates the autophagic engulfment of cargo, mitochondria and bacteria, respectively, via phosphorylation of p62 [392], NDP52 [478], Tax1 Binding Protein 1 (Tax1bp1) [478], and optineurin [132].

The phosphorylation of optineurin (S473, S513) by TBK1 enhances its binding towards polyubiquitin chains [480]. A phosphoproteomic study revealed several additional TBK1 phosphorylation sites [478] on a wide variety of autophagy receptors. TBK1 phosphorylates optineurin at nine serine residues, of which four are located in the LIR domain and four are found in the ubiquitin binding domain (UBD) [132, 478]. Furthermore, two additional threonine phosphorylation sites are located in the UBD [478]. p62 undergoes phosphorylation at ten serine residues by TBK1, one being located in the LIR, one in the UBD and one in the dimerization domain of p62 (PB1) and the rest is spread across the protein [478]. TBK1 phosphorylates five serine and two threonine residues in NDP52, where four of these sites are present in the dimerization domain, and

interestingly none are located in the LIR [478]. Tax1bp1, which supports mTOR signalling [615], is also phosphorylated by TBK1 on eight different residues (seven serine, one threonine), of which four are in the dimerization domain [478].

Together this suggests that TBK1 mediates the dimerization of autophagy receptors that is required for their activation, as well as their binding towards LC3 [596, 616, 617]. Therefore, it is a reasonable assumption that TBK1 affects the different autophagy receptors uniquely, based on the different phosphorylation by TBK1. Furthermore, if these receptors are involved in basal and starvation-induced autophagy, it is likely they are regulated by TBK1 phosphorylation.

4.1.3 The role of TBK1 in ALS

Mutations in the *TBK1* gene have been identified in ALS [17], FTD [493], glaucoma [618] and Alzheimer's disease [490]. This indicates that TBK1 may contribute to a wide variety of neurodegenerative diseases. Furthermore, TBK1 mutations are present in herpes simplex encephalitis (HSE), demonstrating that TBK1 has a role in other diseases as well as neurodegeneration [513].

To date, TBK1 E696K, which lacks optineurin binding capacity [18], has been the most well studied ALS/FTD mutant. Due to the extensive research into the role of TBK1 in mitophagy, these studies have also focused on the effect of TBK1 on mitophagy. The E696K-TBK1 mutant is not recruited to damaged mitochondria as well as WT-TBK1 [456, 478]. Furthermore, overexpression of E696K-TBK1 could not rescue the effect of TBK1 depletion on mitophagy [456, 480]. Hence these studies imply that TBK1-optineurin binding is required for mitophagy. Alternatively, misfolding of mutant TBK1 may lead to its dysfunction, however to date, no studies have demonstrated that the TBK1 mutants do misfold.

To date, more than 90 TBK1 variants have been linked to ALS, FTD or FTD/ALS [17, 18, 197, 198, 490-496, 501-503, 505, 507, 619-623]. Therefore, it is important to determine how these mutants trigger neurodegeneration and by what mechanism. Furthermore, while mutations in the *TBK1* gene account for only a small proportion of ALS/FTD cases overall, because dysfunctional autophagy is implicated in ALS and

TBK1 is thought to have important functions in autophagy, understating these mechanisms may be broadly relevant to ALS/FTD. Therefore, the previously well studied mutant, E696K, and another mutant that has not yet been examined in studies of ALS/FTD; R357Q a mutant lacking kinase activity; was examined in this chapter. Following optimisation of the techniques in chapter 3, both basal and starvation-induced autophagy were investigated.

4.2 Objectives of this chapter

Selective autophagy requires specific autophagy receptors that recognise the different types of cargo, and TBK1 is known to phosphorylate and activate p62 [392], NDP52 [478] and optineurin [132] during mitophagy and xenophagy [132, 392]. Basal autophagy can be considered to be a combination of multiple forms of selective autophagy which are most likely to be mediated via autophagy receptors, although this has been only showed with p62. In Chapter 3, some evidence was obtained that TBK1 is involved in autophagosome formation during basal autophagy, (although this could not be confirmed using every method). The results described in Chapter 3 revealed that knock-out of TBK1 influenced omegasome formation during non-selective (starvation) autophagy, and possibly autophagosome formation or fusion during non-selective autophagy.

- In this Chapter it was examined whether autophagy receptors are involved in basal and non-selective autophagy by following their expression pattern using bafilomycin A1 upon autophagy induction.
- The interaction of autophagy receptors and LC3 and TBK1 under TBK1 inhibition condition was studied using immunoblotting.
- The effect of ALS-linked TBK1 mutations on basal and starvation-induced autophagy were analysed using flow cytometer and microscopy analysis.

4.3 Materials and Methods

The following construct were used in this chapter; LC3-EGFP, LC3-EGFP-mCherry, DFCP1-EGFP, pcDNA3.1, WT-TBK1-FLAG, R357Q-TBK1-FLAG, E696K-TBK1-FLAG, G159A-TBK1-FLAG.

4.3.1 Mammalian cell culture techniques

4.3.1.1 Transfection efficiency of FLAG-TBK1

To analyse the transfection efficiency of the TBK1-FLAG constructs, HEK293T cells were transfected for 48 hr, collected in cold PBS and fixed in 4%(v/v) PFA for 10 min, then permeabilised in 0.03% saponin-PBS for 5 min and stained with APC-FLAG antibody (Biolegend) according to manufacturer's protocol. Briefly 2.5 μl of anti-FLAG-APC antibody was added to 100 μl of cell suspension and incubated for 30 min in the dark. Then cells were washed with PBS and processed with BD LSR Fortessa X-20 and analysed with FACS diva. In each analysis at least 7000 cells were screened. The baseline for TBK1 expression was determined based on cells transfected with an empty pcDNA3.1 vector stained with APC-FLAG. The percentage of cells over the threshold APC signal were taken as TBK1-FLAG expressing cells.

4.3.1.2 Analysis of TBK1 retention post-saponin treatment

To analyse the retention of TBK1-FLAG protein in the cell, HEK293T cells were transfected with TBK1-FLAG vector for 48 hr and treated with 0.03% saponin-PBS for 5 min, washed with PBS and fixed in 4% (v/v) PFA for 10 min. Then cells were stained with anti-FLAG APC antibody as described in section 4.6.1. Then cells were washed with PBS and processed with BD LSR Fortessa X-20 and analysed with FACS diva. In each analysis at least 7000 cells were screened. For TBK1 detection the same baseline was used at determined in section 4.5.1, (cells transfected with pcDNA3.1). Experimental procedures and FC analysis for 4.5.1 and 4.5.2 were carried out in parallel. Percentage of cells, fixed after saponin treatment, over the threshold APC signal were divided by the percentage of TBK1-FLAG positive cells fixed prior to permeabilization (transfection efficiency), therefore enabling determination of the relative retention of TBK1-FLAG in transfected cells only.

4.3.1.3 Analysis of mean fluorescence intensity

Mean fluorescence intensity (MFI) of TBK1-FLAG signal was analysed in TBK1-FLAG positive cells only. Subpopulation of cells were gated if the APC-FLAG signal was above the threshold of the negative control population. MF1 values were collected and analysed using FACS diva software.

4.3.1.4 Autophagy analysis of TBK1-FLAG overexpressing cells

HEK293T cells were co-transfected with TBK-FLAG and LC3-mCherry-EGFP plasmids for 44 hr then basal or starvation-induced autophagy was initiated for 4 hr. At 48 hr post-transfection cells were treated with 0.03% saponin-PBS for 5 min and fixed in 4 % (v/v) PFA for 10 min at RT in the dark, then stained with anti-FLAG-APC antibody. Stained cells processed with Fortessa BD and analysed with FACS diva. In each analysis at least 6000 cells were screened. No bleed through was detected between APC and any other channels (mCherry, EGFP) analysed or vice versa. The baseline for TBK1 expression was determined based on cells transfected with the pcDNA3.1 empty vector stained with APC-FLAG before saponin treatment (section 4.6.1). For analysis cells that showed both mCherry and TBK1-FLAG signal were gated. The ratio of $EGFP^{+}/mCherry^{+}$- $EGFP^{-}/mCherry^{+}$ was determined in this subpopulation of cells and presented in the graphs.

4.3.2 Protein analysis

For protein analyses cells were plated, transfected (LC3-EGFP) and treated (BX795/MRT67307) as described previously. Basal autophagy and starvation-induced non-selective autophagy was carried out in the last 4 hr of each experiment.

4.3.2.1 GFP-Trap immunoprecipitation

HEK293T cells was transfected with LC3-EGFP for 24 hr and treated with TBK1 inhibitor for 24 hr. Alternatively, $TBK1^{+/+}$ and $TBK1^{-/-}$ cells were transfected with LC3-EGFP for 44 hr and then basal or starvation-induced autophagy was induced. Cells were then lysed and BCA quantification was performed.

GFP-conjugated proteins were immunoprecipitated using GFP-Trap (Choromotek). Briefly, 200-400 μg of total cell lysates were diluted in 1 ml GFP-Trap buffer (10mM Tris/Cl pH 7.5, 150mMNaCl, 0.5mM EDTA, 0.5%NP-40) and incubated with 22 μl of GFP-Trap beads overnight at 4^{o}C on a rotating wheel. The next day, beads were washed 3 times in GFP-Trap buffer and proteins were eluted in Lamelli buffer (Biorad) containing NuPage reducing agent (Thermofisher) at 1x concentration at 95 ^{o}C for 10 min at. Samples were then were loaded onto Biorad SDS-polyacrylamide gels and subjected to standard immunoblotting procedures.

4.4 Results

4.4.1 Autophagy receptors do not degrade via autophagy in basal and starvation-induced autophagy

The first aim was to examine which autophagy receptors are involved in basal autophagy and non-selective autophagy with TBK1, by examining its known substrates; p62, optineurin and NDP52 [132, 392, 478]. Autophagy receptors are known to become degraded with their cargo during autophagy [624], therefore their expression levels should normally decrease during autophagy [464, 625]. If autophagic degradation is blocked, naturally or artificially with bafilomycin, the levels of the autophagy receptors should therefore show higher expression levels compared to untreated cells, if they are involved in the autophagic process being examined. Hence, firstly the expression levels of the autophagy receptors were examined in cells treated with or without bafilomycin.

Basal autophagy was followed as previous in HEK293T cells (Chapter 3, section 1.6, **Figure 3.3**) for 4 hr in serum rich media, supplemented with bafilomycin or DMSO (vehicle control). Immunoblotting of the resulting cell lysates for TBK1 and autophagy receptors (p62, NDP52, optineurin) was then performed. The expression levels of TBK1 did not change upon bafilomycin treatment using these conditions, indicating that the levels of TBK1 are not affected by inhibition of autophagosome degradation **(Figure 4.1)**. Similarly, the expression levels of p62 and NDP52 were not significantly altered in bafilomycin-treated conditions, although there was a trend towards an increase **(Figure 4.1)**. In contrast, the levels of optineurin were significantly decreased upon bafilomycin treatment, indicating that it may degrade via a different pathway such as UPS upon autophagy inhibition or potentially its translation may be decreased. Alternatively, optineurin mediates trafficking of lysosomes during autophagy in association with myosin VI [139], therefore upon inhibition of lysosome autophagosome fusion optineurin is potentially downregulated.

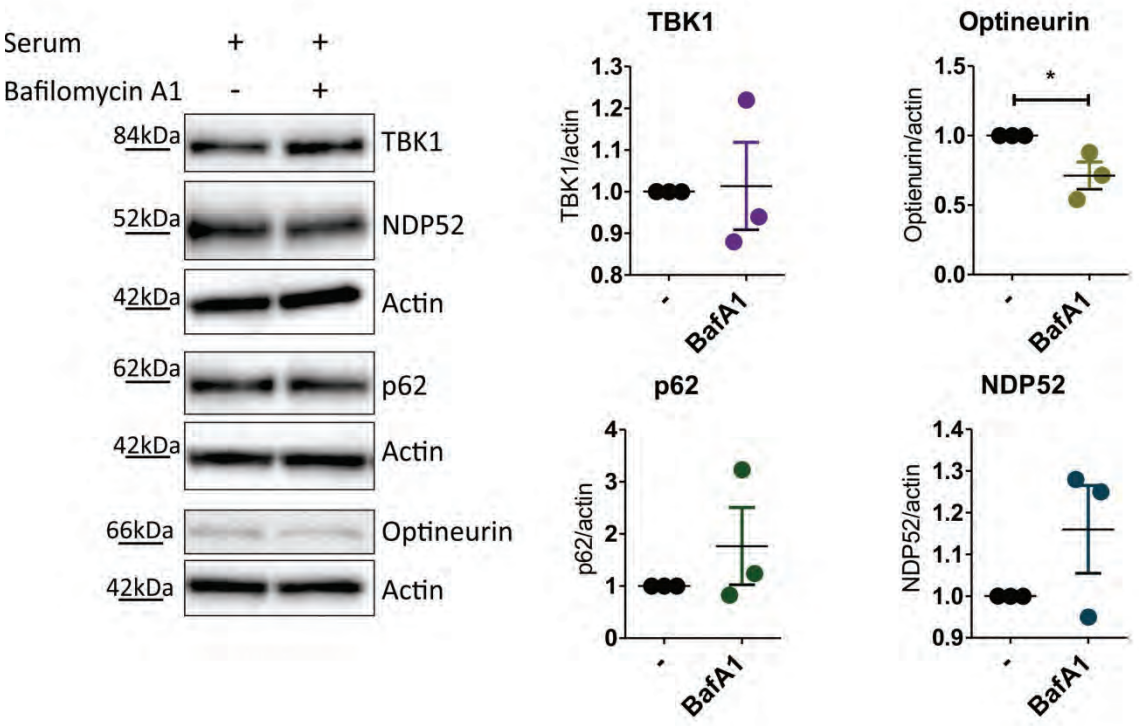


Figure 4.1 Optineurin levels decrease, but TBK1 and autophagy receptors levels do not change following bafilomycin treatment during basal autophagy. Basal autophagy in HEK293T cells was followed via immunoblotting in serum rich media, with or without 100 nM bafilomycin for 4 hr. Representative immunoblots are shown. Band intensity was quantified using ImageJ and normalised to internal loading control, actin. Relative expression levels are shown in quantification. N=3+/-SEM, unpaired t-test *<0.05. BafA1: Bafilomycin A1.

Next, it was investigated how TBK1 responds to starvation and whether the autophagy receptors are involved in starvation-induced autophagy. HEK293T cells were starved by replacing media containing serum with HBSS as previous (Chapter 3, section 4.1, **Figure 3.10**), and the expression levels of TBK1, p62, NDP52 and optineurin were examined by immunoblotting. Starved conditions were also compared to serum rich conditions (black bars in **Figure 4.2**). No statistically significant differences were detected between any of the conditions, although some trends were detected. Upon starvation, TBK1 levels showed an increased trend 1 hr after the removal of serum compared to non-starved cells, but then the levels remained relatively constant **(Figure 4.2A)**. Interestingly, when bafilomycin was used to accumulate autophagosomes, the levels of TBK1 upon starvation did not differ compared to serum rich conditions **(Figure 4.2 B)**, indicating that TBK1 does not degrade via autophagy upon starvation. In the

absence of bafilomycin, p62, NDP52 and optineurin levels were not different compared to serum rich conditions. There was a trend towards decreased levels of p62 and optineurin at 2 hr starvation compared to 1 hr, and also less optineurin was detected at 4 hr and 6 hr starvation compared to 1 hr. The levels of all three autophagy receptors showed a decreasing trend during the time course of starvation, in contrast, the autophagy receptor levels stayed constant upon bafilomycin treatment **(Figure 4.2 A/B)**. Together these results show that autophagy receptor levels do not change during starvation, indicating that they may not be involved under the conditions tested in this work.

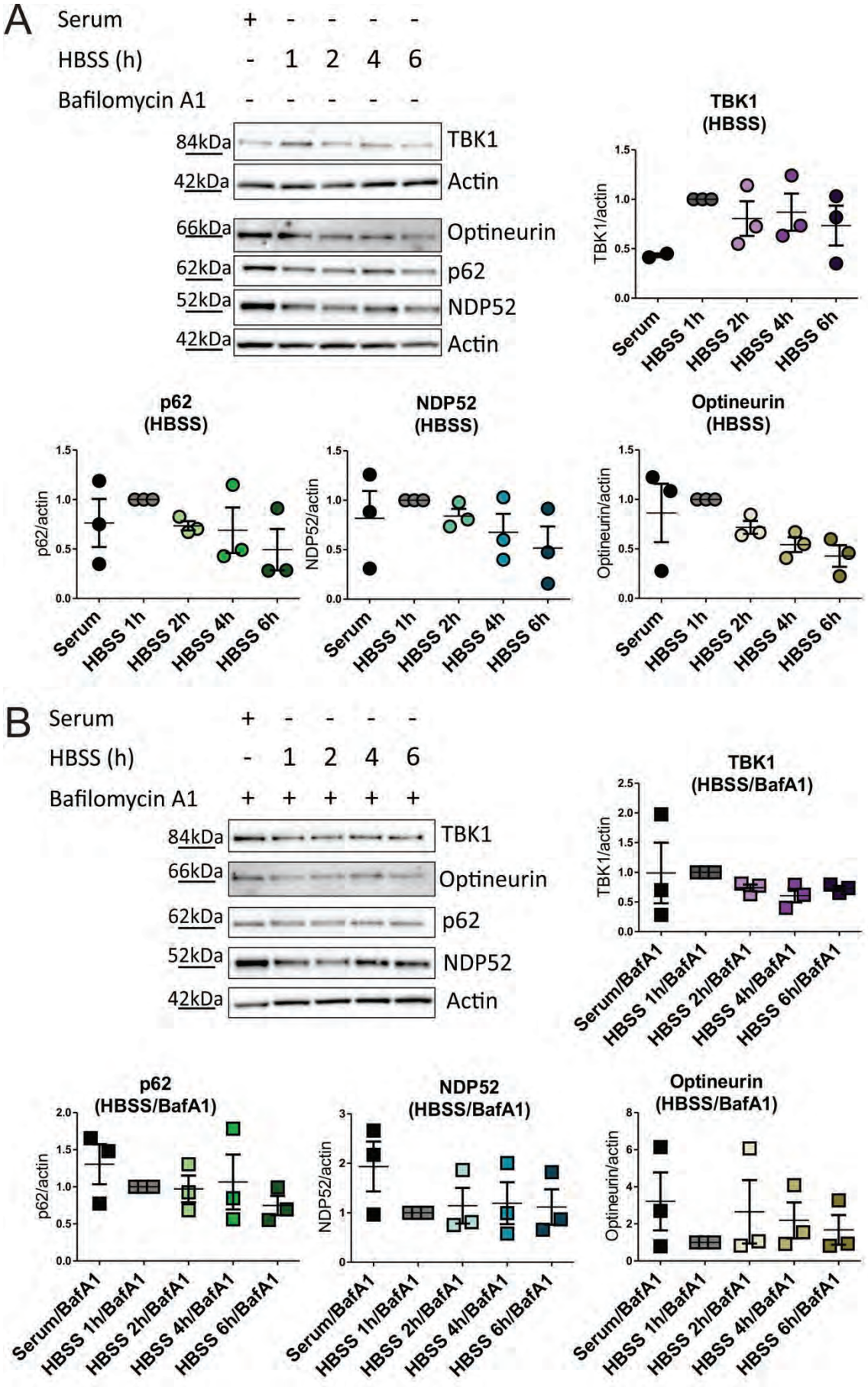

A
Serum + - - - -
HBSS (h) - 1 2 4 6
Bafilomycin A1 - - - - -
84kDa
TBK1
42kDa
Actin
66kDa
Optineurin
62kDa
p62
52kDa
NDP52
42kDa
Actin
TBK1 (HBSS)
TBK1/actin
p62 (HBSS)
p62/actin
NDP52 (HBSS)
NDP52/actin
Optineurin (HBSS)
Optineurin/actin
Serum
HBSS 1h
HBSS 2h
HBSS 4h
HBSS 6h
B
Serum + - - - -
HBSS (h) - 1 2 4 6
Bafilomycin A1 + + + + +
84kDa
TBK1
66kDa
Optineurin
62kDa
p62
52kDa
NDP52
42kDa
Actin
TBK1 (HBSS/BafA1)
TBK1/actin
p62 (HBSS/BafA1)
p62/actin
NDP52 (HBSS/BafA1)
NDP52/actin
Optineurin (HBSS/BafA1)
Optineurin/actin
Serum/BafA1
HBSS 1h/BafA1
HBSS 2h/BafA1
HBSS 4h/BafA1
HBSS 6h/BafA1

Figure 4.2. Autophagy receptors do not change upon starvation-induced autophagy. HEK293T cells were starved in HBSS, with **(B)** or without **(A)** 100 nM bafilomycin, for the indicated time. Immunoblotting of cell lysates was performed. Representative immunoblots are shown. Band intensity was quantified using ImageJ and normalised to internal loading control, actin. Relative expression levels are shown in the quantification. N=3+/-SEM, One-way ANOVA with Tukey post-hoc test. BafA1: Bafilomycin A1.

4.4.2 TBK1 inhibition increases autophagy receptor levels during basal autophagy

It was shown previously by FC (BX795) and immunoblotting (MRT67307) (see Chapter 3), that inhibition of the kinase activity of TBK1 prevents formation of the autophagosome during basal autophagy, although this could not be confirmed by the other assays. Furthermore, the autophagy receptor p62 is implicated in basal autophagy [626]. Although the results presented in **Figure 4.2** could not confirm that p62 and optineurin (and possibly NDP52) were involved in starvation-induced autophagy, a trend was apparent, implying that immunoblotting may not be sensitive enough to identify any differences in their expression upon starvation. Hence, the effect of TBK1 inhibition on expression of the autophagy receptors was examined in HEK293T cells, using BX795 and MRT67307 as described previously. Cells were then lysed and subjected to immunoblotting. The levels of p62 and NDP52 did not significantly change upon BX795 treatment in cells treated with or without bafilomycin **(Figure 4.3 A)**. Optineurin could not be quantified due to its low levels of expression. In contrast, significantly elevated levels of p62 ($p=0.03$) and NDP52 ($p=0.03$) were detected upon MRT67307 treatment in the absence of bafilomycin. Furthermore, in bafilomycin treated cells, increased NDP52 levels were detected ($p=0.04$), while an increased trend was detected for p62 levels, but this was not significant ($p=0.063$). Due to the very low optineurin expression in HEK293T cells, optineurin could not be detected in all experimental conditions. Nonetheless, even when optineurin was expressed at a detectable level by immunoblotting, in MRT67307 or H_2O treated conditions, no change was observed.

These elevated levels of p62 and NDP52 upon TBK1 inhibition with bafilomycin (MRT67307 only) may be due to abrogated autophagosome formation, consistent with the results described in Chapter 3 **(Figure 3.4/3.5)**. Alternatively, it is also possible that

TBK1 affects the synthesis or degradation of these autophagy receptors, although there is no published evidence to support this notion. These data could not be confirmed using the other TBK1 inhibitor, BX795, but they are consistent with the previous hypothesis that MRT67307 leads to a complete block in autophagosome degradation, whereas BX795 only partially blocks autophagosome degradation (Chapter 3). Nevertheless, the accumulation of autophagy receptors upon TBK1 inhibition indicates that the kinase activity of TBK1 is involved in degradation of these receptors by autophagy. Furthermore, MRT67207 treatment led to a greater differences in p62 levels compared to NDP52 levels (2.77-fold increase vs 1.74-fold increase), although in bafilomycin conditions the p62 difference was not significant.

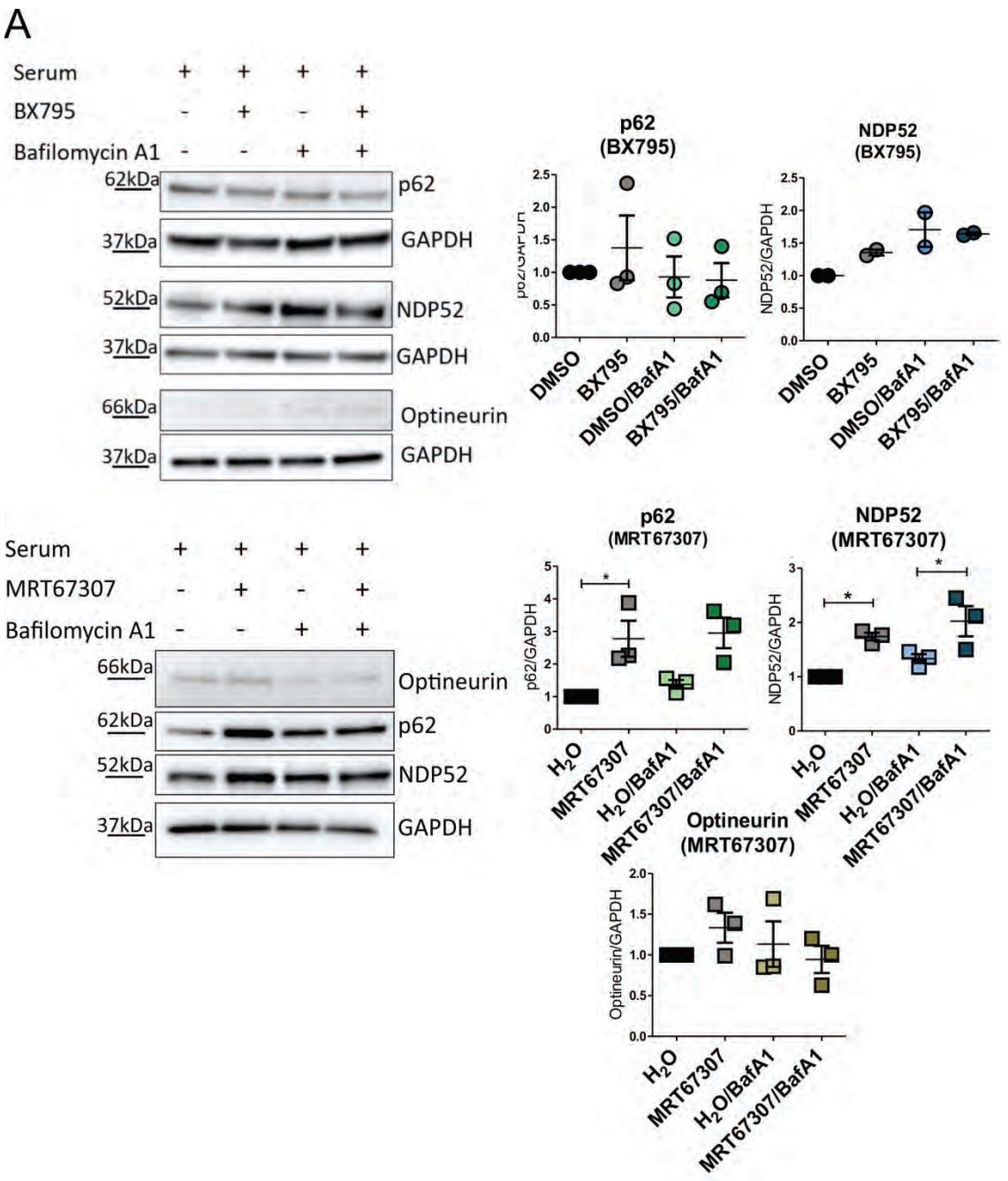


Figure 4.3. TBK1 inhibition using MRT67307 elevates p62 and NDP52 levels. HEK293T cells were treated with BX795 (1 μM) **(A)** and MRT67307 (25 nM) **(B)** or vehicle for 20 hr, and bafilomycin was added for a further 4 hr. Cell lysates were then separated on SDS-polyacrylamide gels. Immunoblotting was performed for p62, NDP52, optineurin, TBK1 and GAPDH. Representative immunoblots are shown. Band intensity was quantified using ImageJ and normalised to internal loading control, GAPDH. Relative expression levels are shown in the quantification. N=3+/-SEM, One-way ANOVA with Tukey post-hoc test. *<0.05.

4.4.3 Inhibition of TBK1's kinase activity does not prevent LC3-autophagy receptor binding during basal autophagy

Autophagy receptors bind to ubiquitinated cargo and to LC3, together forming a complex. As phosphorylation of autophagy receptors by TBK1 is crucial for the formation of this complex during mitophagy and xenophagy [132, 392], next it was evaluated whether TBK1 is required for the formation of this complex during basal autophagy. If so, this would explain the possible inhibition of autophagosome formation by TBK1 inhibition detected in Chapter 3. This analysis was only carried out using one inhibitor, BX795.

HEK293T cells were transfected with p62-EGFP, optineurin-EGFP, and LC3-EGFP constructs for 24 hr and treated with 1 μM BX795 for an additional 24 hr. EGFP-Trap was used to immunoprecipitate cell lysates expressing EGFP coupled to either p62, optineurin or LC3. Following immunoprecipitation of LC3-EGFP expressing cells using EGFP-Trap, NDP52 and p62 were detected by immunoblotting, implying that LC3 interacts with both of these receptors during basal autophagy **(Figure 4.4A)**. While p62 has been shown to be involved in basal autophagy [627], NDP52 has not been previously linked to basal autophagy. Therefore, this data implies for the first time that NDP52 takes part in basal autophagy similar to p62. Furthermore, TBK1 also immunoprecipitated with LC3 unexpectedly, because the binding between TBK1 and LC3 has not yet been described. Interestingly, significantly more p62 and NDP52 were precipitated by EGFP-Trap following TBK1 inhibition by BX795. As treatment with this inhibitor did not change the levels of p62 or NDP52 **(Figure 4.3)**, this result suggests that the kinase activity of TBK1 does not facilitate LC3/autophagy receptor binding **(Figure 4.4A)**. In contrast, it implies that the kinase activity may even inhibit the interaction between these receptors and LC3 or alternatively the inhibition of autophagosome degradation that was detected upon TBK1 inhibition prolongs the interaction between LC3 and autophagy receptors. In contrast, similar levels of TBK1 were coprecipitated with LC3 when cells were treated with BX795, indicating that the interaction between TBK1 and LC3 is independent of TBK1's kinase activity.

TBK1 was then immunoprecipitated by EGFP-Trap from cell lysates transfected with p62-EGFP, as expected, while neither NDP52, nor optineurin was detectable after

p62 pull down (data not shown). However, endogenous optineurin levels were very low in HEK293T cells **(Figure 4.3A)**, hence it may not feasible to detect optineurin after p62 pull down. Hence this result indicates that p62 does not bind to NDP52. NDP52-p62 binding has not been described previously, therefore this data provides further evidence that they do not interact with each other. Upon TBK1 inhibition, a trend towards less TBK1 precipitation by EGFP-Trap was detected, but this did not reach statistical significance ($p=0.058$). Hence further replicates are required to confirm whether the kinase activity of TBK1 is required for its interaction with p62 or not. In cells transfected with optineurin-EGFP, both p62 and TBK1, but not NDP52, were immunoprecipitated with EGFP-Trap. Furthermore, less p62 was precipitated after BX795 treatment **(Figure 4.4C)**, indicating that TBK1's kinase activity facilitates the binding between optineurin and p62. A trend towards less TBK1 was precipitated after BX795 treatment **(Figure 4.4C)**, suggested that TBK1's kinase activity is required for an interaction between optineurin and TBK1; however this was close to, but did not reach, significance ($p=0.0506$), so this would need to be further verified in the future. Immunoblotting for EGFP confirmed that p62 and optineurin were precipitated by EGFP-Trap in cells transfected with p62-EGFP or optineurin-EGFP respectively.

These results therefore imply that inhibition of TBK1's kinase activity leads to decreased binding between autophagy receptors p62 and optineurin, and possibly between p62, optineurin and TBK1, suggesting that the kinase activity of TBK1 is required. In contrast, the binding of LC3 to p62, NDP52 or TBK1, is not dependent on the kinase activity of TBK1, and this kinase activity may in fact be required to dissociate LC3 from p62 and NDP52. Hence, the binding between LC3 and these autophagy receptors is likely to be linked to the substrate binding domain of TBK1, suggesting that TBK1 may act as a scaffold to regulate LC3 and p62 or NDP52 binding. This also implies that when TBK1 is inhibited, the binding between LC3 and autophagy receptors becomes prolonged as they do not dissociate as readily, leading to abrogated degradation of the autophagosome. Overall these results imply that the kinase activity of TBK1 may be involved in the dissociation of LC3 from autophagy receptors.

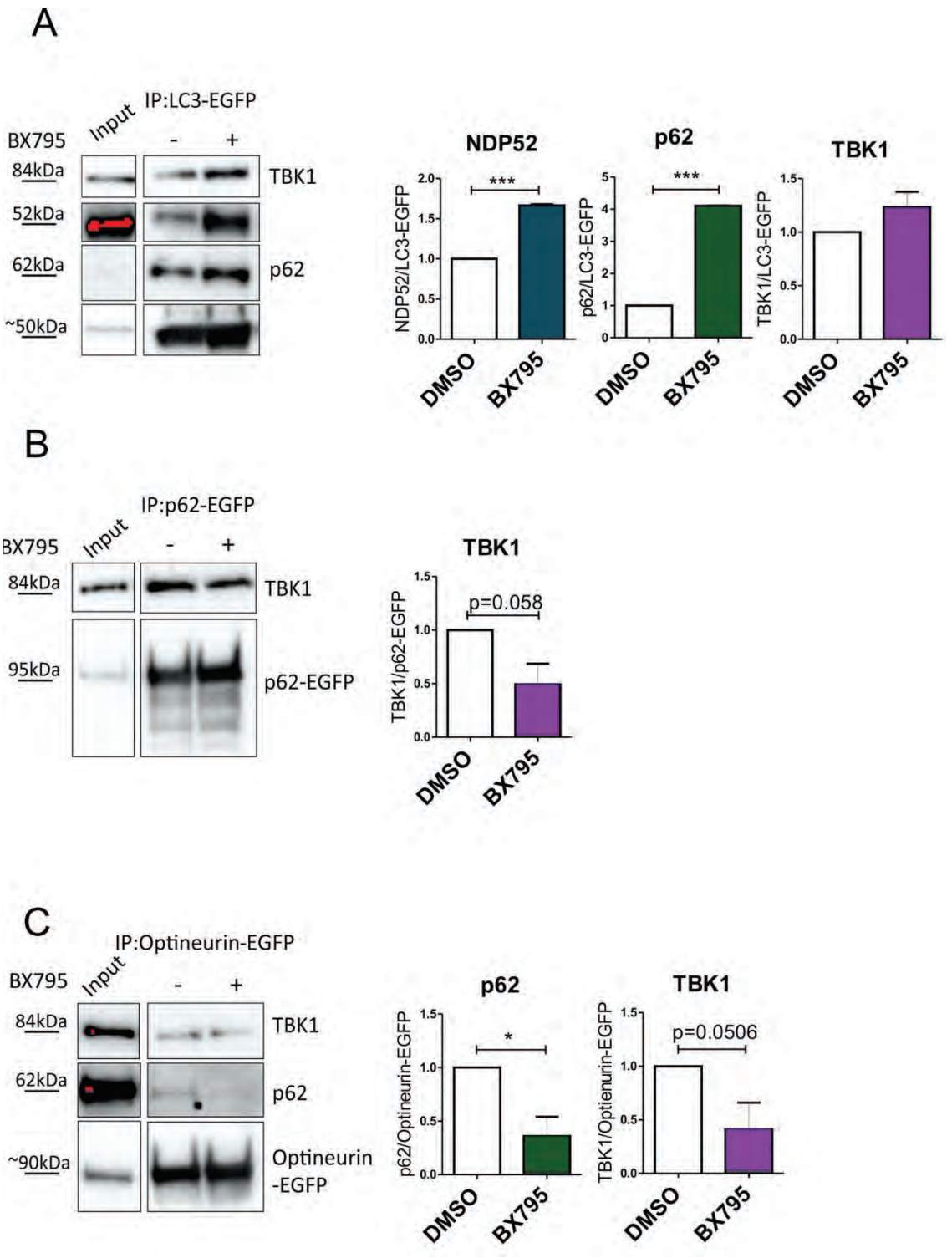


Figure 4.4. The kinase activity of TBK1 influences the interaction between autophagy receptors p62, optineurin, and TBK1. HEK293T cells were transfected with p62-EGFP, optineurin-EGFP, and LC3-EGFP and treated with BX795. Immunoprecipitation of cell lysates using EGFP-Trap was performed. Representative immunoblots are shown. Band intensity was quantified using ImageJ and normalised to

immunoprecipitated EGFP. Relative expression levels are shown in quantification. N≥2+/-SEM, unpaired t-test, *<0.05, ***<0.0005.

4.4.4 TBK1 knock-out prevents LC3-p62 binding during basal autophagy

It was proposed above that the binding between autophagy receptors p62, NDP52 and LC3 is regulated by the substrate binding site of TBK1 acting as a scaffold to bring together LC3 and autophagy receptors. Therefore, this possibility was examined further by transfecting the CRISPR/Cas9 TBK1 KO HEK293T cells (TBK1$^{-/-}$ #1, #2) with LC3-EGFP to determine how LC3 precipitates with these receptors in the absence of TBK1. Immunoprecipitation using EGFP-Trap, and immunoblotting for TBK1, optineurin, p62 and NDP52 was performed. Not surprisingly, optineurin was not detected upon EGFP-Trap immunoprecipitation, consistent with its previously observed low levels in HEK293T cells **(Figure 4.3A)**. In contrast, p62, NDP52 and TBK1 were all detected by immunoblotting after LC3 pull down in TBK1 expressing HEK293T cells **(Figure 4.5A)**. Significantly less p62 was co-immunoprecipitated with LC3-EGFP in both TBK1 knock-out clones (#1, #2), but no differences were detected in the levels of NDP52 co-immunoprecipitated in these clones. This data indicates that during basal autophagy, TBK1 is required for p62 to bind to LC3. In contrast, TBK1 is not required for NDP52's interaction with LC3, although when TBK1 is inhibited, more binding was obtained **(Figure 4.4A)**. Overall, the levels of these autophagy receptors did not change significantly in the TBK1 knock-out clones, confirming that the lower levels of p62 precipitated were not due to less expression of p62. This is in consistent with the data obtained in Chapter 3, showing that knock-out of TBK1 did not affect the formation of autophagosome during basal autophagy. However, upon bafilomycin treatment p62 levels showed a decreasing trend of expression although without reaching significance. Taken together with these immunoprecipitation results, it may be in the absence of TBK1, p62 cannot bind as well to LC3 and therefore it cannot be recruited to the autophagosome, explaining the lack of accumulation of autophagosomes upon bafilomycin.

Hence in summary these results imply that during basal autophagy, TBK1 inhibition leads to perturbation of autophagosome degradation, and possibly formation,

and that this result from an aberrant interaction between autophagy receptors (p62, NDP52) and LC3. Hence, the role of TBK1 in non-selective autophagy was examined.

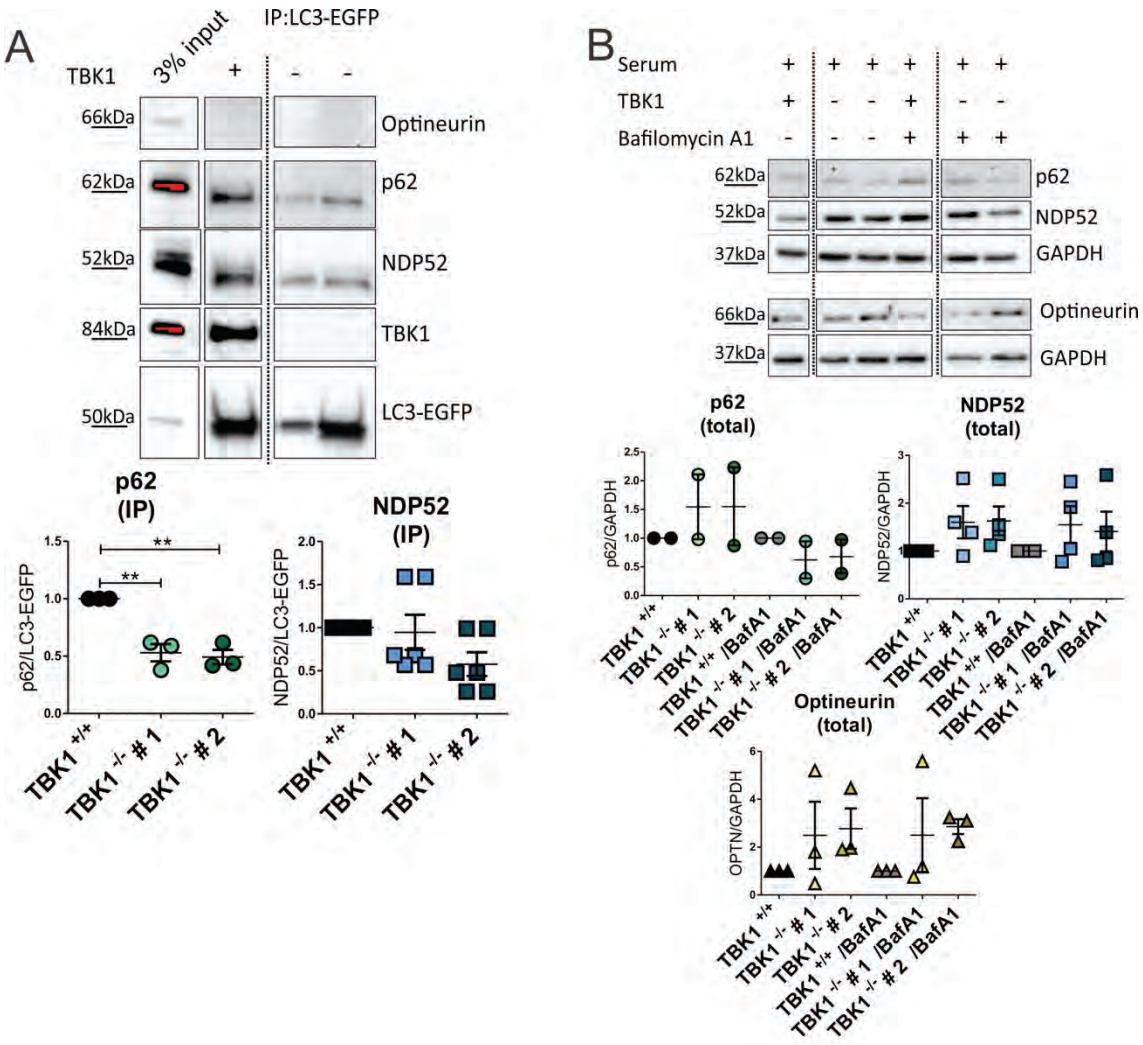


Figure 4.5. TBK1 enhances the interaction between p62 and LC3. (A) *Less precipitation between p62 and LC3 upon TBK1* knock-out. TBK1$^{+/+}$ and TBK1$^{-/-}$ (#1, #2) HEK293T cells expressing LC3-EGFP with precipitated with EGFP-Trap. Representative immunoblots are shown. Band intensity was quantified using ImageJ and normalised to immunoprecipitated LC3-EGFP. Relative expression levels are shown in the quantification. N=3+/-SEM, One-way ANOVA with Tukey post-hoc test, **<0.005. **(B)** *Expression of autophagy receptors p62, optineurin and NDP52 do not change upon TBK1 knock-out*. Basal autophagy was followed in HEK293T CRISPR/Cas9 clones TBK1$^{+/+}$ and TBK1$^{-/-}$ (#1, #2) in serum rich media supplemented with bafilomycin or DMSO as control. Immunoblotting of cell lysates for NDP52, p62, and optineurin was performed. Representative immunoblots are shown. Band intensity was quantified using

ImageJ and normalised to internal loading control, GAPDH. Relative expression levels are shown in quantification. N≥3+/-SEM. One-way ANOVA with Tukey post-hoc test. Dashed line indicates the cropping of 'control' clone.

4.4.5 TBK1 inhibition does not affect autophagy receptor levels upon starvation-induced autophagy

Next it was examined how these autophagy receptors are involved in starvation-induced autophagy when TBK1 is inhibited. Therefore, HEK293T cells were starved following TBK1 inhibition as previous. In contrast to basal autophagy, no significant differences were detected in the expression levels of NDP52, p62 and optineurin following either BX795 or MRT67307 treatment **(Figure 4.6A/B)**. Hence, these results imply that expression of the autophagy receptors examined here are not affected by the enzymatic activity of TBK1 during non-selective autophagy. Alternatively, lack of differences may have been due to the decreased TBK1 levels under inhibition as shown before (**Figure 3.12)** .

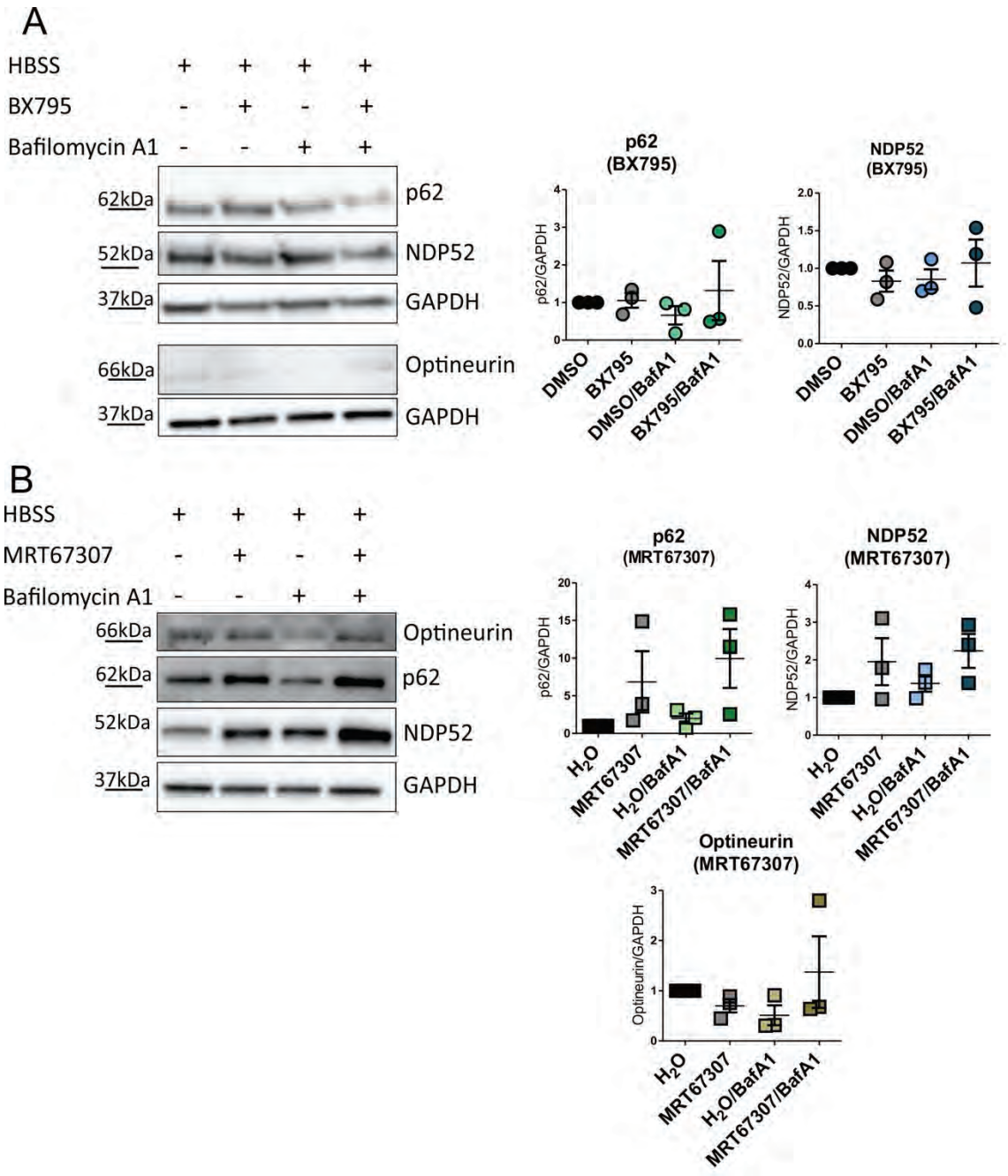


Figure 4.6. Autophagy receptors p62, optineurin and NDP52 are not affected by the kinase activity of TBK1 during non-selective autophagy. HEK293T cells were treated with BX795 (1 μM) **(A)** and MRT67307 (25 nM) **(B)** or vehicle, then starved in HBSS with or without bafilomycin. Cell lysates were separated on an SDS-polyacrylamide gel. Immunoblotting was performed for p62, NDP52, optineurin, TBK1 and GAPDH. Representative immunoblots are shown. Band intensity was quantified using ImageJ and normalised to immunoprecipitated LC3-EGFP. Relative expression levels are shown in the quantification. N=3+/-SEM, One-way ANOVA with Tukey post-hoc test.

4.4.6 TBK1 knock-out does not affect LC3 binding to autophagy receptors during starvation-induced autophagy

Next, the interaction between LC3 and the autophagy receptors was examined during starvation-induced autophagy in the CRISPR/Cas9 TBK1 KO HEK293T cells. HBSS starved (4 hr) TBK1 knock-out cells were transfected with LC3-EGFP, and LC3 was then immunoprecipitated using EGFP trap as described above, followed by immunoblotting for NDP52, p62 and optineurin. No significant differences were observed in the levels of NDP52 or p62 precipitating in the TBK1 knock-out clones compared to the parental cells **(Figure 4.7A)**. This finding indicates that during starvation-induced autophagy, knock-out of TBK1 does not affect p62 or NDP52 interaction with LC3. Immunoblotting for optineurin was also performed following immunoprecipitation using EGFP-Trap. Not surprisingly, optineurin was not detected upon EGFP-Trap immunoprecipitation, again reflecting its low expression level in HEK293T cells.

The expression levels of these autophagy receptors in response to starvation were also analysed in the TBK1 CRISPR/Cas9 clones [$TBK1^{-/-}$ (#1, #2)]. The levels of p62 did not change upon starvation in TBK1 knock-out cells compared to TBK1 expressing cells with or without bafilomycin treatment **(Figure 4.7B).** However, a trend towards a decrease was detected in p62 levels upon bafilomycin treatment, but this did not reach statistical significance. This finding implies that without TBK1, p62 does not accumulate with autophagosomes; however further experiments are required to confirm this. NDP52 and optineurin levels did not change significantly upon TBK1 knock-out

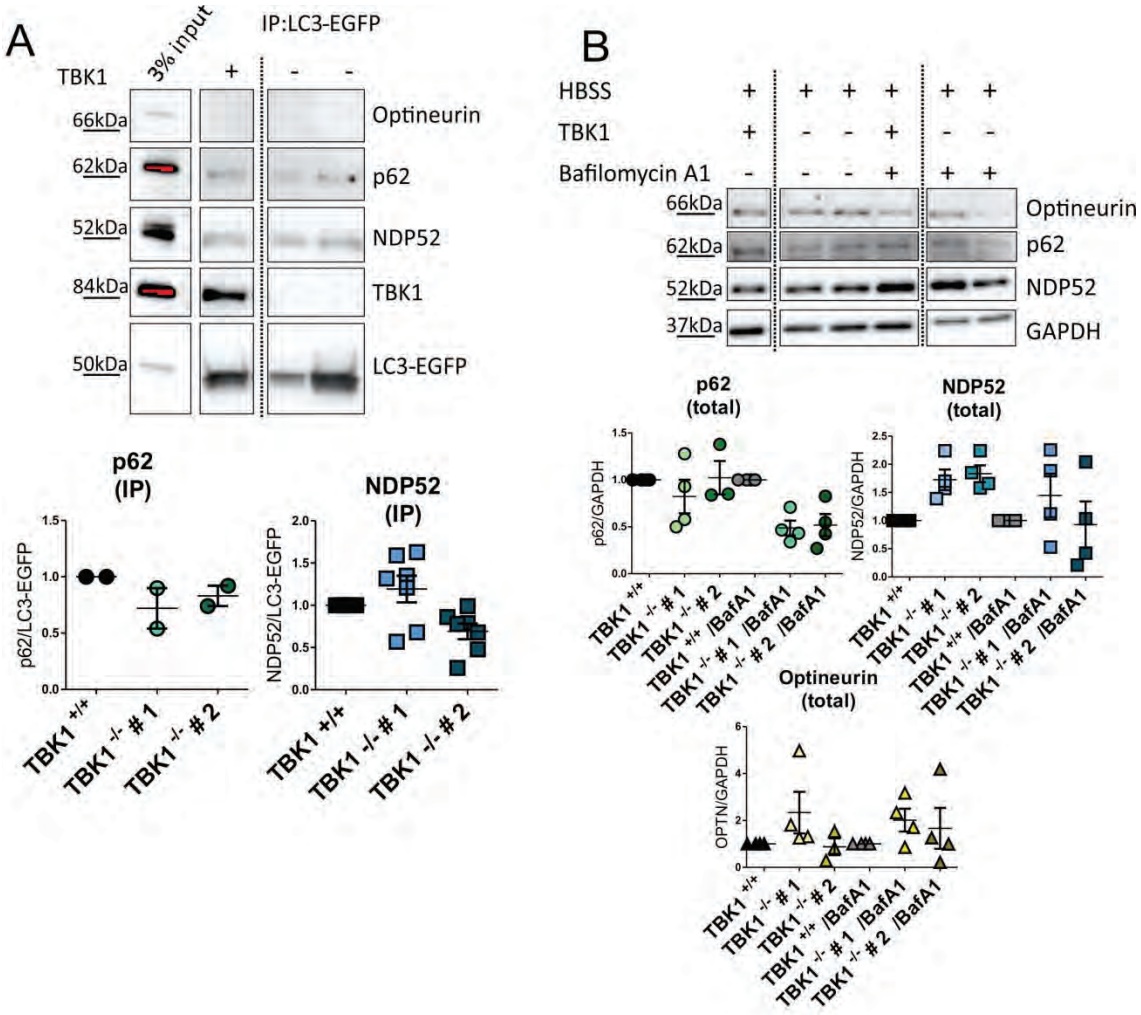


Figure 4.7. TBK1 knock-out does not affect autophagy receptor levels and interaction with LC3 during non-selective autophagy. (A) *LC3 and autophagy receptor binding is not affected by TBK1 knock-out during starvation.* TBK1$^{+/+}$ and TBK1$^{-/-}$ HEK293T cells were transfected with LC3-EGFP for 48 hr then lysed and EGFP-Trap was performed. N≥2+/-SEM, One-way ANOVA with Tukey post-hoc test. **(B)** *Expression of autophagy receptors does not change in starved HEK293T cells.* TBK1$^{+/+}$ and TBK1$^{-/-}$ HEK293T cells were starved in HBSS for 4h, then treated with 100nM bafilomycin or DMSO as a control. Then cells were lysed and immunoblotting for NDP52, p62, and optineurin was performed. N≥3+/-SEM. Dashed line indicates the cropping of 'control' clone. One-way ANOVA with Tukey post-hoc test.

4.4.7 ALS mutant TBK1 during basal and starvation-induced autophagy

Following these analyses of the role of TBK1 in both basal and non-selective (starvation-induced) autophagy, the role of the ALS-associated mutations in TBK1 was then examined. It remains unknown how the mutations in TBK1 contribute to ALS. However, in this thesis, it is hypothesised that ALS-associated TBK1 display impairments in autophagy, and that this will result in the accumulation of protein aggregates. Hence, next, it was examined how overexpression of WT and mutant TBK1 influences basal and starvation-induced autophagy in HEK293T cells. The relationship between TBK1 and the formation of protein aggregates and autophagy was examined in Chapter 5.

4.4.8 R357Q ALS-mutant TBK1 is a loss of expression mutant

To examine the pathological consequences of expression of the TBK1 mutations in ALS, a series of ALS/FTD mutants were chosen, based on the localisation of the mutation, in either the kinase domain or substrate binding domain of TBK1. This approach aimed to examine whether the phenotypes observed in ALS were due to deficient kinase activity (R357Q) or were because of the inhibition of substrate binding (E696K). The mutant R357Q is a kinase deficient form of TBK1; hence it cannot phosphorylate its protein substrates, but its substrate binding domain remains intact [18]. In contrast, the mutant E696K-TBK1 is unable to bind to optineurin, although it can bind to other autophagy receptors, and its kinase activity remains intact [18]. To differentiate between ALS-specific effects, and effects that relate to the kinase activity which may be similar in different diseases, another mutant was also included in the study. This mutant, G159A, which is associated with herpes simplex encephalitis (HSE), also displays deficient kinase activity, similar to R357Q [513]. Generation of ALS/FTD-associated mutations in TBK1 via site-directed mutagenesis was performed during my MRes studies. This is presented in Appendix I, which describes the generation and initial characterization of the ALS-TBK1 clones and represents a non-examinable part of this thesis.

Previously it has been shown that ALS mutations (R357Q, c.358+5A, L59FfsX) in TBK1 are expressed to lower levels than WT [496]. Therefore, first it was examined whether R357Q and E696K mutants show decreased expression in HEK293T cells.

TBK1 undergoes trans-autophosphorylation upon overexpression [471]. Furthermore kinase deficient TBK1 mutants that cannot auto-phosphorylate, will undergo phosphorylation if mixed with WT-TBK1 [471]. Therefore, in this study FLAG-tagged WT or mutant TBK1 were overexpressed in the CRISPR/Cas9 TBK1 knock-out cells for 48 hr (TBK1$^{-/-}$ #2). By using this strategy, possible interference of endogenous WT-TBK1 in HEK293T cells was avoided. However, when these constructs were expressed in HEK293T cells, overall expression of TBK1 was below the limit of detection by immunoblotting due to low rates of transfection (data not shown). Hence, immunoblotting was not feasible to analyse autophagy upon TBK1 overexpression. Hence all experiments were carried out using FC and microscopy analysis.

Firstly, the expression levels of the mutants compared to wildtype TBK1 were examined, using a fluorescently tagged (allophycocyanin [APC]) anti-FLAG - antibody to detect TBK1-FLAG via FC. A trend towards fewer TBK1 positive cells were detected upon R357Q-TBK1 transfection that almost reached statistical significance (p=0.051), compared to WT-TBK1 transfected cells **(Figure 4.8A)**. In contrast, the other two mutants; E696K-TBK1 and G159A-TBK1, were expressed to a similar degree as WT-TBK1. The reduced expression of R357Q-TBK1 may result from a lower transfection efficiency, so that fewer cells were transfected overall. Alternatively, R357Q-TBK1 may be expressed at lower levels in each transfected cell. In order to determine which was the case, the expression levels of TBK1-FLAG in transfected cells were analysed at the single cell level by analysing the mean fluorescent intensity (MFI) in the TBK1-FLAG expressing cell population using FC. The MFI in TBK1-FLAG positive cells was significantly lower in cells expressing R357Q compared to cells overexpressing WT-TBK1 (p=0.004) or E696K-TBK1 (p=0.02) **(Figure 4.8B)**. Consistent with the first analysis, R357Q-TBK1 possessed the lowest MFI overall, and even expressed significantly less TBK1 protein than the other ALS-mutant, E696K-TBK1 (p=0.02), whereas the expression of G159A was not different compared to WT-TBK1. In contrast, the other mutants did not show significantly lower MFI levels compared to WT-TBK1.

These findings are consistent with the previous description of lower R357Q expression compared to wildtype [496].

4.4.9 Examining the intracellular retention of TBK1-FLAG proteins

Insoluble protein aggregates are the hallmark of ALS, and TBK1 may form aggregates or be recruited into these inclusions. Previously, overexpression of the TBK1-FLAG mutants R357Q, E696K, R308Q did not lead to overt inclusion formation (MRes thesis, Appendix 1). However, in these prior studies, overexpression of TBK1-FLAG was carried out in $TBK1^{+/+}$ cells. Therefore, the presence of endogenous TBK1 may have affected the aggregation of ALS-mutant TBK1, because as mentioned above, previous studies have shown that a kinase deficient TBK1 mutant (D135N) cannot auto-phosphorylate itself. However if pre-activated WT-TBK1 is present, D135N-TBK1 will undergo phosphorylation and become active [471]. Therefore, dysfunctional TBK1 ALS mutants may reclaim their proper function if overexpressed in cell lines with endogenous TBK1, and any possible dysfunction may be masked. Therefore, it is possible that the presence of endogenous TBK1 in HEK293T cells in the previous MRes studies was a confounding factor.

Hence, the aggregation of the TBK1-FLAG WT and ALS mutants was examined in the CRISPR/Cas9 $TBK1^{-/-}$ cells, because the lack of TBK1 in these clones should ensure that no compensation by endogenous TBK1 occurs. Using the optimised FC analysis following saponin treatment, analysis of intracellular TBK1 allows determination of whether TBK1 was insoluble and retained by intracellular membranes, or soluble and freely diffusible. As previously described in Chapter 3, saponin treatment eliminates soluble cytoplasmic proteins that are not associated with intracellular membranes, such as LC3-I and GAPDH **(Figure 3.2)**. Therefore, $TBK1^{-/-}$#2 cells transfected with TBK1-FLAG constructs were analysed via FC. The percentage of cells retaining TBK1 post-saponin treatment were normalised to the percentage of TBK1 positive cells pre-saponin treatment.

In all CRISPR/Cas9 populations expressing the TBK1-FLAG constructs, a small proportion of TBK1 positive cells were detected after saponin treatment, even in those

cells expressing WT. This result indicates that WT-TBK1 is prone to become insoluble or localised to intracellular membranes **(Figure 4.8C)**. No statistical significance was detected between the different TBK1-FLAG overexpressing conditions. Overexpression of FLAG-WT or ALS/FTD TBK1 did not form any obvious cytoplasmic aggregates in TBK1$^{-/-}$ HEK293T cells analysed by microscopy **(Figure 4.10).**

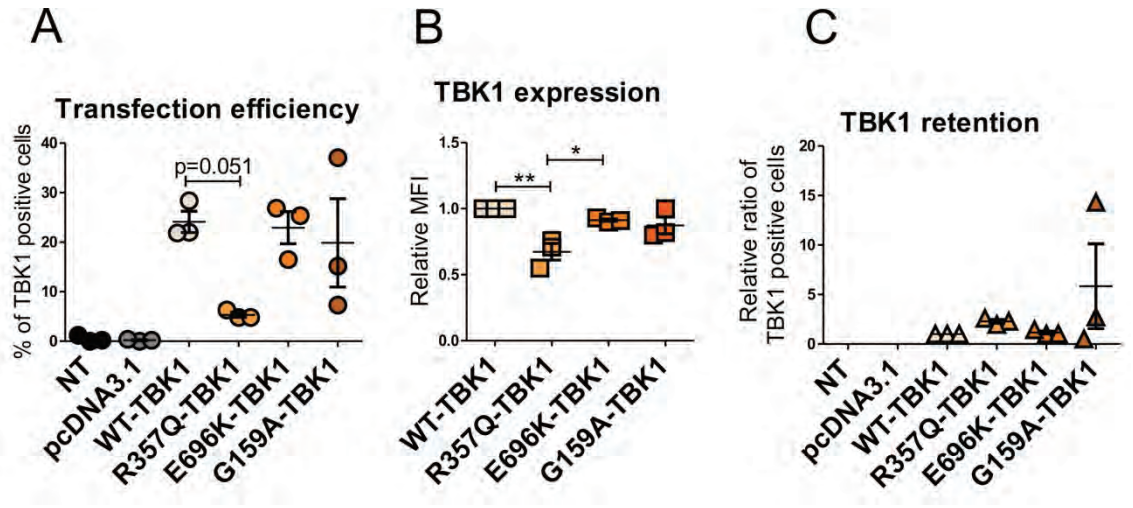


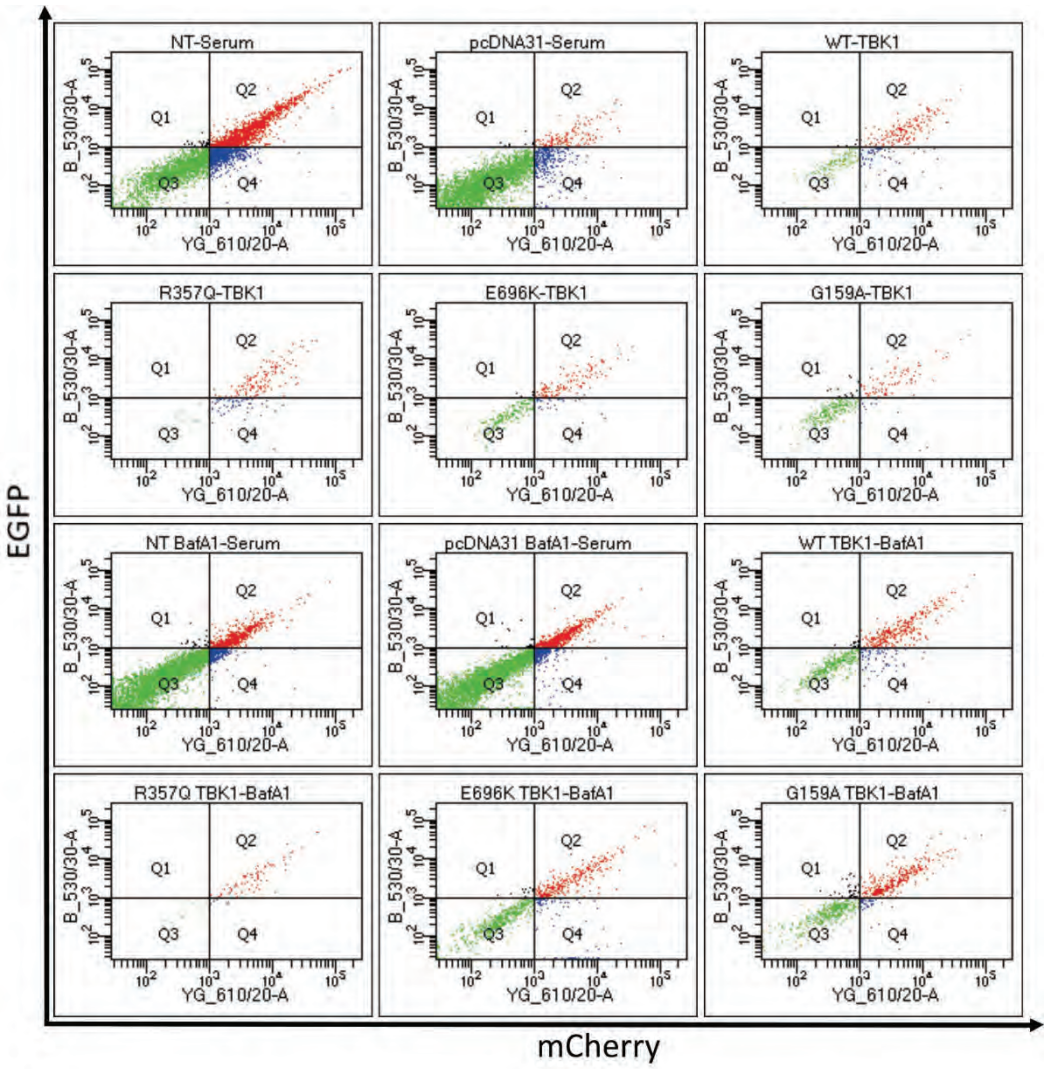
Figure 4.8. R357Q ALS-mutant TBK1 is expressed at lower levels than WT-TBK1. TBK1$^{-/-}$ #2 HEK293T cells were transfected with TBK1-FLAG constructs for 48 hr, then cells were treated with saponin, immunostained with APC-FLAG antibody, then analysed via FC. **(A)** *R357Q has a lower transfection efficiency than the other TBK1 proteins.* Percentages of TBK1 positive cells are shown in graph (pre-saponin). **(B)** *R3578Q ALS/FTD mutants express at lower levels than the other TBK1 proteins examined.* Relative comparison of mean fluorescent intensity (MFI) of TBK1 is presented. **(C)** *No significant differences in the intracellular retention of TBK1.* Percentages of TBK1 positive cells (post-saponin) were normalised to TBK1 positive cells pre-saponin. Relative comparison is shown in figure. N=3+/- SEM, One-way ANOVA with Tukey post-hoc test, *<0.05, **>0.005.

4.4.10 TBK1-FLAG overexpression impairs autophagosome degradation during basal autophagy

ALS-associated TBK1 mutations have not been investigated in relation to basal or starvation-induced autophagy previously. Hence, this was next examined here. Chapter 3 suggested that the TBK1 inhibitors perturb autophagosome-lysosome fusion and possibly autophagosome formation, during basal autophagy. Therefore, a reasonable hypothesis

was that ALS-TBK1 would inhibit autophagy. Hence, basal autophagy was analysed in HEK293T cells overexpressing WT and mutant TBK1 via FC. For the same reasons as above, the CRIPSR/Cas9 KO clones were used rather than WT HEK293T cells.

TBK1$^{-/-}$ clone #2 HEK293T cells were co-transfected with LC3-EGFP-mCherry and TBK1-FLAG constructs, and cells were analysed by FC following saponin treatment. The transfection efficiency of LC3-EGFP-mCherry was found to be higher than TBK1-FLAG, therefore not all LC3-EGFP-mCherry expressing cells were also positive for TBK1-FLAG (data not shown, pre-saponin: 39.6% vs 24%). However, on average 90% of TBK1 positive cells were transfected with LC3-EGFP-mCherry. In order to confirm that only those cells that express both LC3-EGFP-mCherry and TBK1-FLAG were analysed, the TBK1 positive subpopulation of cells were gated for analysis and only the ones that expressed LC3-EGFP-mCherry were quantitated. The low overall transfection efficiency of TBK1-FLAG shown previously **(Figure 4.8)** is also evident in these experiments by the low event numbers shown in scatter plots **(Figure 4.9)**. In non-transfected (NT) and empty vector (pcDNA3.1) transfected cells, there was no TBK1 expression as expected. Hence, all LC3-EGFP-mCherry positive cells were analysed in these populations. All cells overexpressing TBK1-FLAG displayed a significantly higher EGFP$^+$/mCherry$^+$ ratio compared to pcDNA3.1 ($p<0.0001$) (and NT- data not shown on graph, $p<0.0001$) control cells, indicating an increased number of autophagosome positive cells in these groups (**Figure 4.9**). Moreover, none of the mutant TBK1 populations showed a significant difference compared to WT-TBK1 overexpressing cells. Upon inhibition of autophagosome degradation by treatment with bafilomycin, significantly more NT ($p=0.0003$) and pcDNA3.1 ($p=0.0001$) transfected cells were EGFP$^+$/mCherry$^+$ compared to untreated cells as expected, confirming correct experimental procedures. In contrast, there was no difference in EGFP$^+$/mCherry$^+$ cells in populations expressing any of the TBK1 mutants when treated with bafilomycin. The lack of accumulation of autophagosomes in the bafilomycin treated TBK1 expressing cells suggests that overexpression of TBK1-FLAG may inhibit the fusion between the autophagosome and lysosome, which would explain why artificially inhibiting the fusion with bafilomycin has no effect. Interestingly significantly more autophagosome positive R357Q expressing cells accumulated compared to pcDNA1 transfected cells ($p=0.04$) upon bafilomycin treatment, potentially indicating that this mutant causes a more severe inhibition of autophagosome lysosome fusion than the other TBK1 proteins.


NT-Serum
pcDNA31-Serum
WT-TBK1
R357Q-TBK1
E696K-TBK1
G159A-TBK1
NT BafA1-Serum
pcDNA31 BafA1-Serum
WT TBK1-BafA1
R357Q TBK1-BafA1
E696K TBK1-BafA1
G159A TBK1-BafA1
Q1
Q2
Q3
Q4
B_530/30-A
YG_610/20-A
EGFP
mCherry

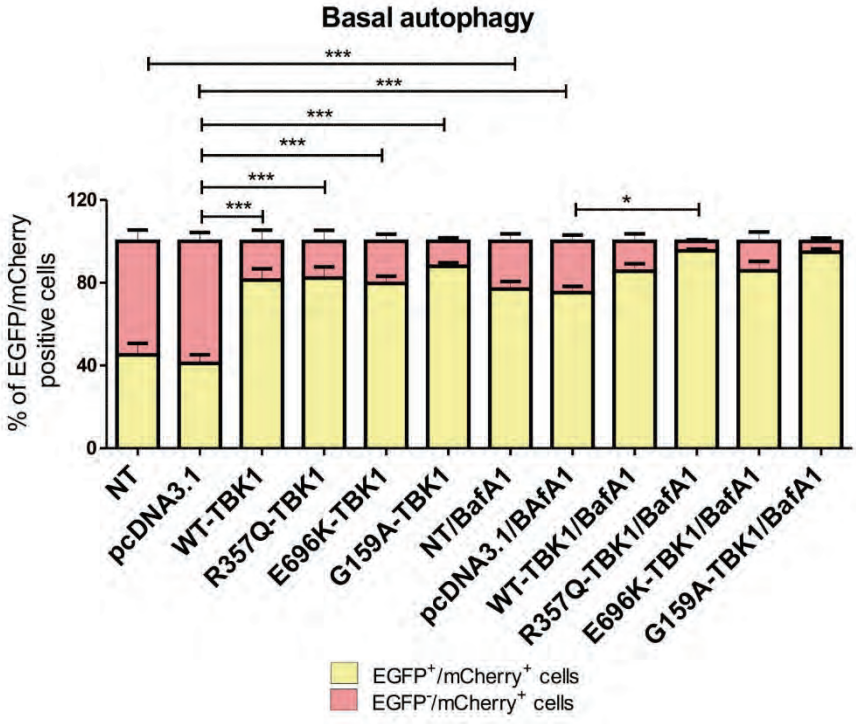
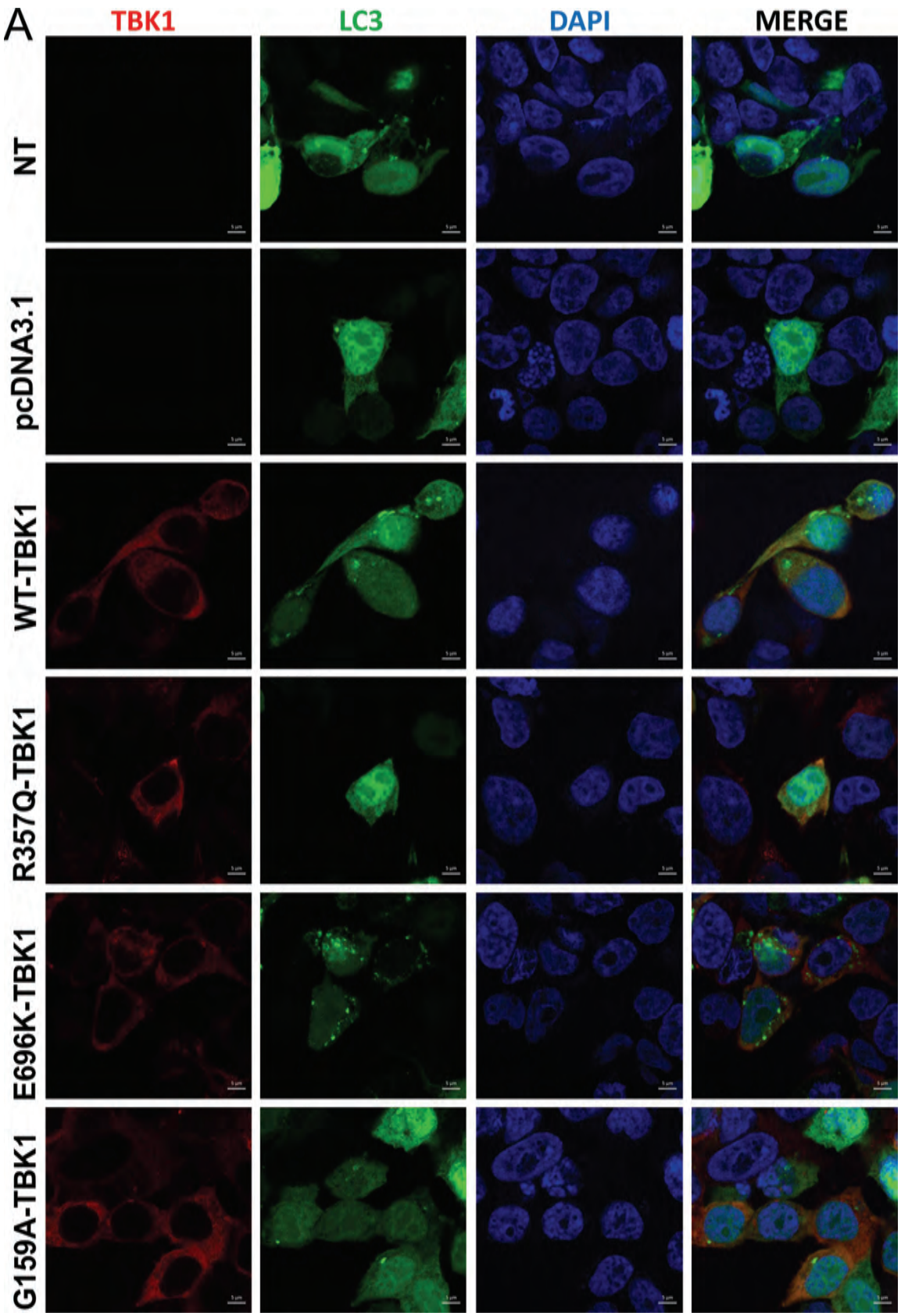
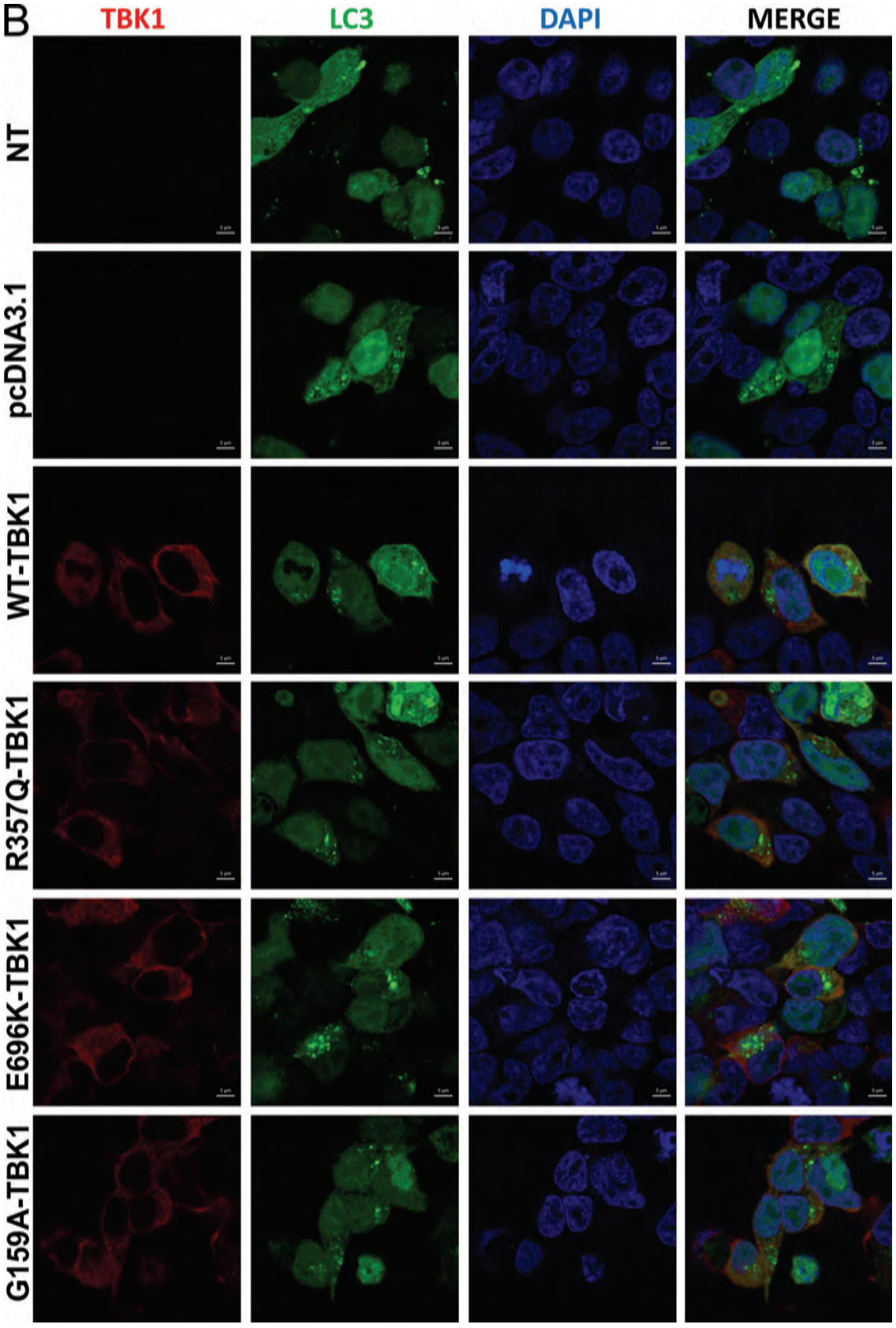

Basal autophagy
% of EGFP/mCherry positive cells
120
80
40
0
***
*
NT
pcDNA3.1
WT-TBK1
R357Q-TBK1
E696K-TBK1
G159A-TBK1
NT/BafA1
pcDNA3.1/BAfA1
WT-TBK1/BafA1
R357Q-TBK1/BafA1
E696K-TBK1/BafA1
G159A-TBK1/BafA1
EGFP+/mCherry+ cells
EGFP-/mCherry+ cells

Figure 4.9. Overexpression of TBK1-FLAG proteins leads to more autophagosomes, implying impaired fusion between the autophagosome and lysosome during basal autophagy. TBK1$^{-/-}$ #2 HEK293T cells were co-transfected with TBK1-FLAG and LC3-EGFP-mCherry constructs for 44 hr then basal autophagy was followed with or without bafilomycin for 4 hr. Cells were treated with saponin, immunostained with an APC-FLAG antibody, then analysed using FC. Representative images of flow cytometry analysis **(A)** and quantifications **(B)** are shown. Increasing EGFP signal along the y axis and increasing mCherry signal along the x axis. Q: EGFP^{+}/mCherry^{-}, Q2: EGFP^{+}/mCherry^{+}, Q3: EGFP^{-}/mCherry^{-}, Q4: EGFP^{-}/mCherry^{+}. N=3 +/- SEM, One-way ANOVA with Tukey post-hoc test, *<0.05, ***<0.0005.

As analysis of the autophagosome/autolysosome ratio upon TBK1-FLAG overexpression was analysed in post-saponin cells (to monitor insoluble/membrane bound TBK1), therefore only a unique subpopulation of cells was examined. Therefore, confocal microscopy analysis was used to examine autophagosome formation (by the formation of LC3-EGFP puncta) in TBK1 overexpressing cells to confirm the FC results. TBK1$^{-/-}$ #2 HEK293T cells were co-transfected with LC3-EGFP and pcDNA3.1, WT or mutant TBK1-FLAG constructs. Initial immunocytochemistry experiments using the anti-FLAG antibody did not provide good staining (data not shown), hence, these experiments were repeated using an anti-TBK1 antibody instead. Cells overexpressing both LC3-EGFP and TBK1-FLAG were examined individually using confocal microscopy. Overexpression of WT or mutant TBK1 did not result in inclusion formation and TBK1 showed cytoplasmic localisation **(Figure 4.10)** as detected previously (Appendix I). The number of LC3-EGFP vesicles per cell was quantified in the TBK1 overexpressing populations, but no significant differences were found between any of the groups. Furthermore, bafilomycin treatment did not significantly elevate the numbers of number of LC3-EGFP vesicles per cell. This finding provides further evidence that confocal microscope analysis is not as sensitive as FC analysis, because differences were detected for NT and pcDNA3.1 treatment **(Figure 4.10).** Despite not reaching statistical significance, some trends were noticed; WT-TBK1 and E696K-TBK1 both showed trends towards increased number of autophagosome puncta present per cell compared to pcDNA3.1 and NT cells, in contrast, overexpression G159A showed no difference compared to NT and pcDNA3.1 cells. Upon inhibition of autophagosome degradation using bafilomycin treatment, no difference was detected between control (NT,

pcDNA3.1) and TBK1-FLAG overexpressing conditions, consistent with the FC results. However, this finding could not be validated given that no difference was detected in the NT and pcDNA3.1 treated groups following bafilomycin treatment.


A
TBK1
LC3
DAPI
MERGE
NT
pcDNA3.1
WT-TBK1
R357Q-TBK1
E696K-TBK1
G159A-TBK1


B
TBK1
LC3
DAPI
MERGE
NT
pcDNA3.1
WT-TBK1
R357Q-TBK1
E696K-TBK1
G159A-TBK1

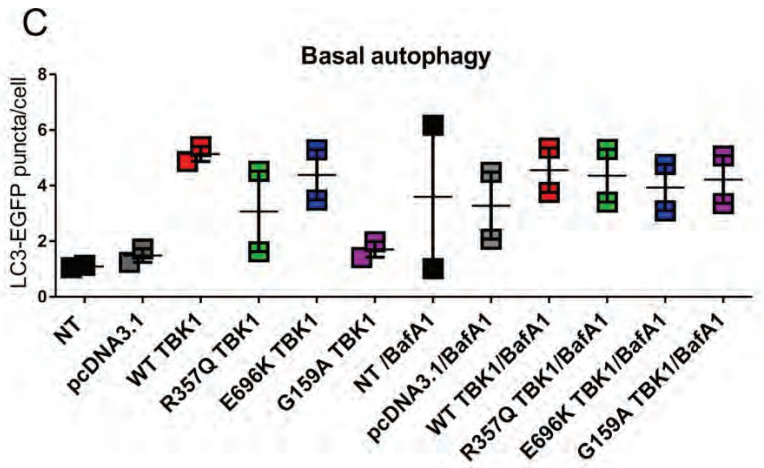
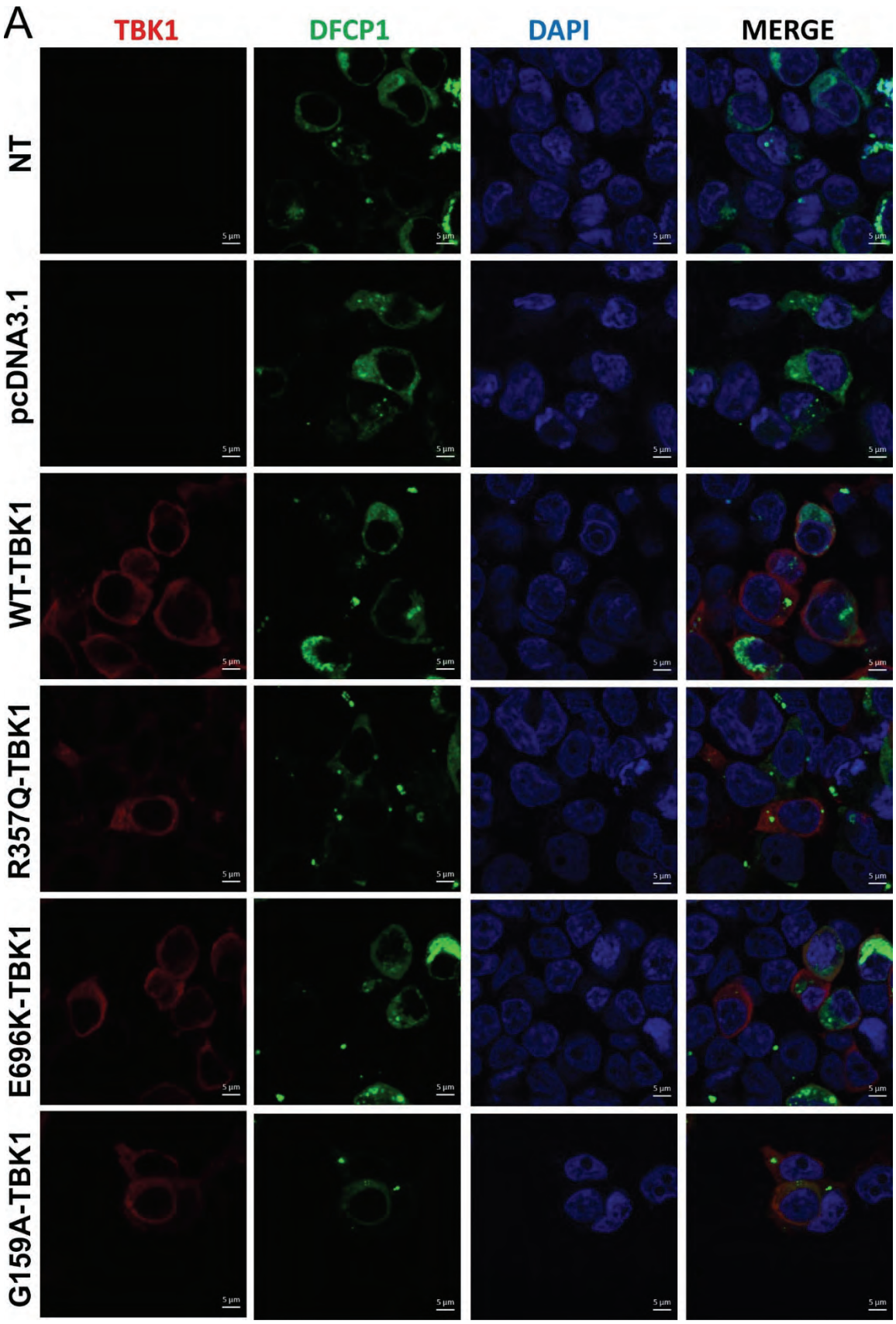


Figure 4.10. No differences in the numbers of autophagosomes in TBK1 expressing cells during basal autophagy. TBK1$^{-/-}$ #2 HEK293T cells were transfected with TBK1-FLAG and LC3-EGFP constructs for 44 hr, then basal autophagy was followed with or without bafilomycin. Cells were immunostained using an anti-TBK1 antibody and the number of LC3-EGFP puncta/cell were counted. Representative images of cells treated without **(A)** and with bafilomycin **(B)** and relative comparison of LC3-EGFP puncta numbers **(C)** are shown.

As discussed previously, omegasomes are major sources of membranes for the autophagosome in neurons [386]. Therefore, it was next examined whether overexpression of ALS-mutant TBK1 affects the formation of the omegasome. Constructs encoding DFCP1-EGFP and TBK1-FLAG were co-transfected into TBK1$^{-/-}$ #2 HEK293T cells and stained with anti-TBK1 antibody. None of the expressed TBK1-FLAG proteins significantly affected the formation of omegasome during basal autophagy **(Figure 4.11.)**.


A
TBK1
DFCP1
DAPI
MERGE
NT
pcDNA3.1
WT-TBK1
R357Q-TBK1
E696K-TBK1
G159A-TBK1
5 µm

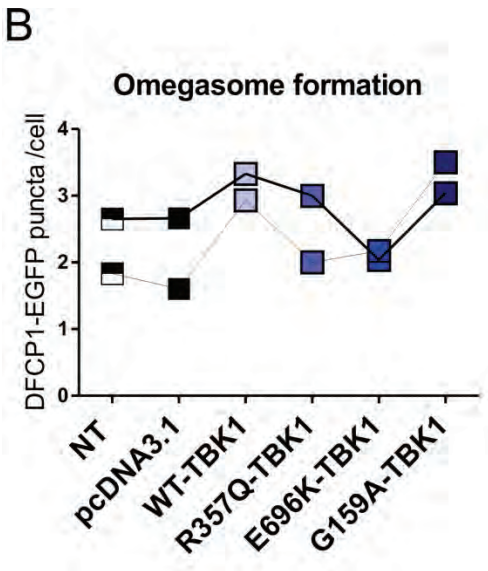


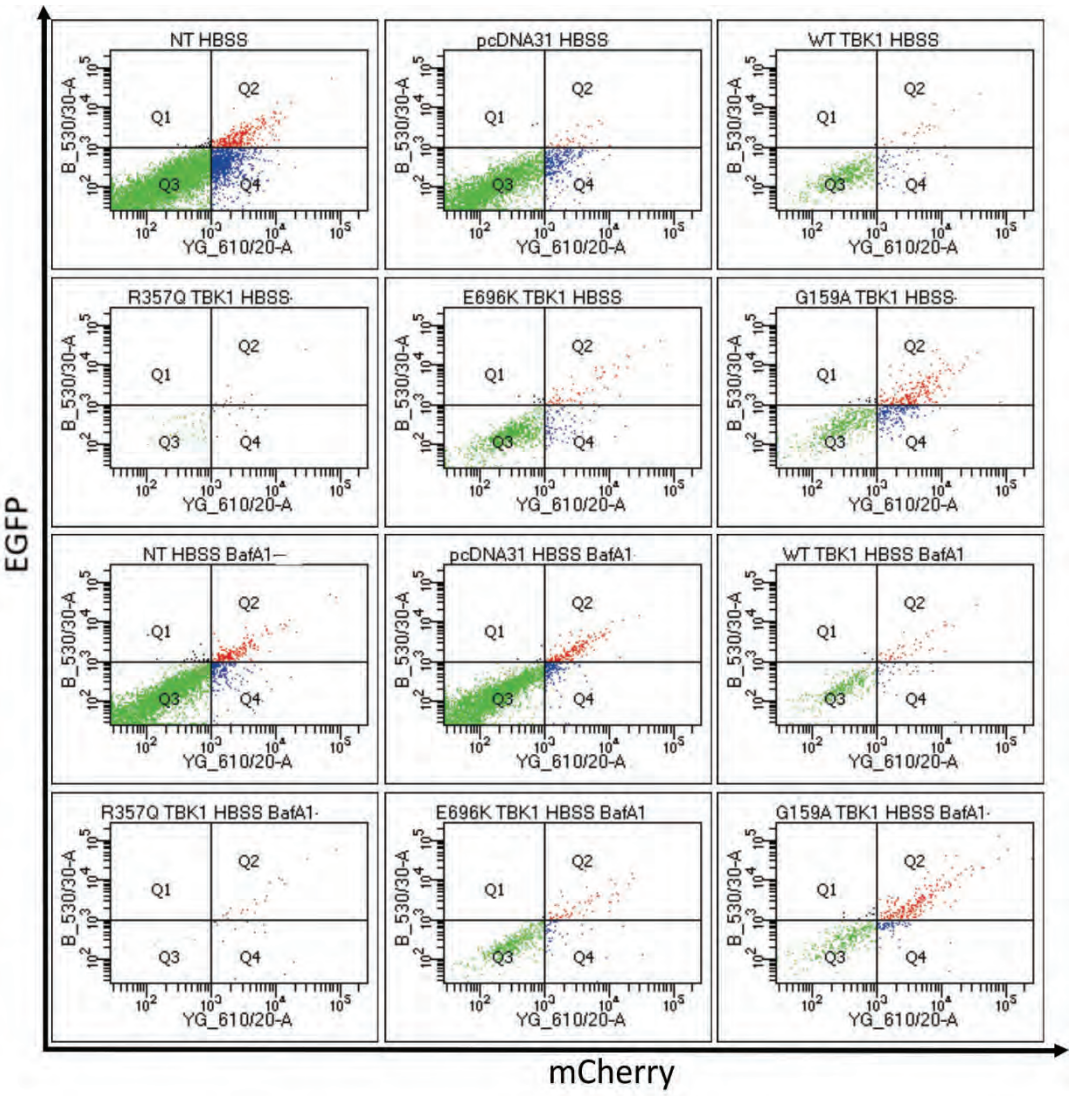
Figure 4.11. Omegasome formation is not affected by TBK1-FLAG expression during basal autophagy. TBK1$^{-/-}$ #2 HEK293T cells were transfected with TBK1-FLAG and DFCP1-EGFP constructs for 44 hr then basal autophagy was followed for 4 hr. Cells were immunostained using an anti-TBK1 antibody and the number of DFCP1-EGFP puncta/cell were counted. Representative images **(A)** and relative comparison of DFCP1-EGFP puncta numbers **(B)** are shown

4.4.11 Summary

These data indicate that the R357Q ALS/FTD mutant is expressed at a lower level than WT or the other TBK1 mutants (E696K, G159A). Therefore, this finding suggests that not all ALS/FTD mutants may cause dysfunction via haploinsufficiency as previously suggested [18] because the other ALS mutants E696K was expressed at similar levels to WT, however it should be noted that these methods of expression differ greatly. Overexpression of all TBK1-FLAG proteins led to abrogated autophagosome-lysosome fusion during basal autophagy, even WT, and R357Q may cause a potentially more severe impairment than the other mutants. This data also shows that the ALS/FTD mutants do not have different consequences compared to WT-TBK1, or the non-ALS mutant G159A.

4.4.12 Kinase deficient TBK1 mutant inhibits autophagosome degradation during starvation-induced autophagy

While it has not been conclusively determined whether neurons respond to starvation, similar to other cell types [400, 402, 425, 426, 528], the TBK1 mutations may affect other cell types relevant to ALS, including glial cells or muscle cells. Therefore, the effect of the ALS/FTD TBK1 mutations was also analysed during starvation-induced autophagy. As above, TBK1$^{-/-}$ #2 HEK293T cells were co-transfected with TBK1-FLAG and LC3-EGFP-mCherry constructs, and FC analysis was performed following 4 hr HBSS starvation. In the absence of bafilomycin, overexpression of kinase deficient TBK1 mutants, R357Q (=0.03), G159A (p=0.01), resulted in significantly more EGFP^{+}/mCherry^{+} cells compared to pcDNA3.1 controls **(Figure 4.12)**, However, similar to basal autophagy, no difference was detected between WT-TBK1 and mutant-TBK1 overexpressing cells. In the presence of bafilomycin treatment, significantly more EGFP^{+}/mCherry^{+} positive cells accumulated in pcDNA3.1 control cells (p=0.03), while no other conditions increased the proportion of EGFP^{+}/mCherry^{+} positive cells furthermore no difference was detected between WT-TBK1 or mutant-TBK1 overexpressing cells upon bafilomycin treatment. This suggests that the kinase activity of TBK1 may be involved in starvation-induced autophagy by potentially inhibiting autophagosome lysosome fusion, but further experiments are required to investigate this.


NT HBSS
pcDNA31 HBSS
WT TBK1 HBSS
R357Q TBK1 HBSS
E696K TBK1 HBSS
G159A TBK1 HBSS
NT HBSS BafA1
pcDNA31 HBSS BafA1
WT TBK1 HBSS BafA1
R357Q TBK1 HBSS BafA1
E696K TBK1 HBSS BafA1
G159A TBK1 HBSS BafA1
Q1
Q2
Q3
Q4
B_530/30-A
YG_610/20-A
EGFP
mCherry

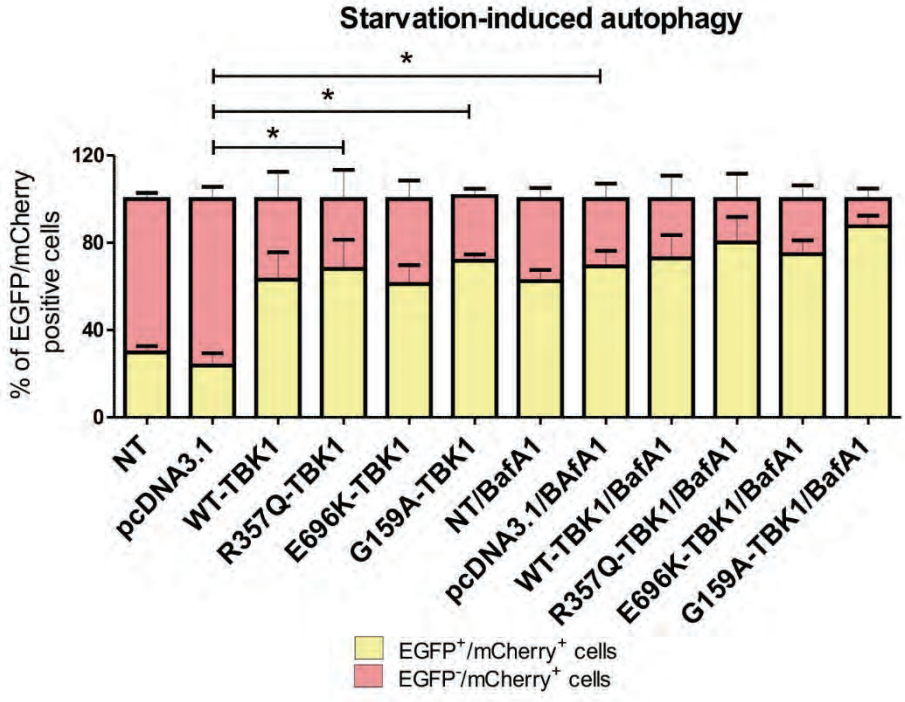
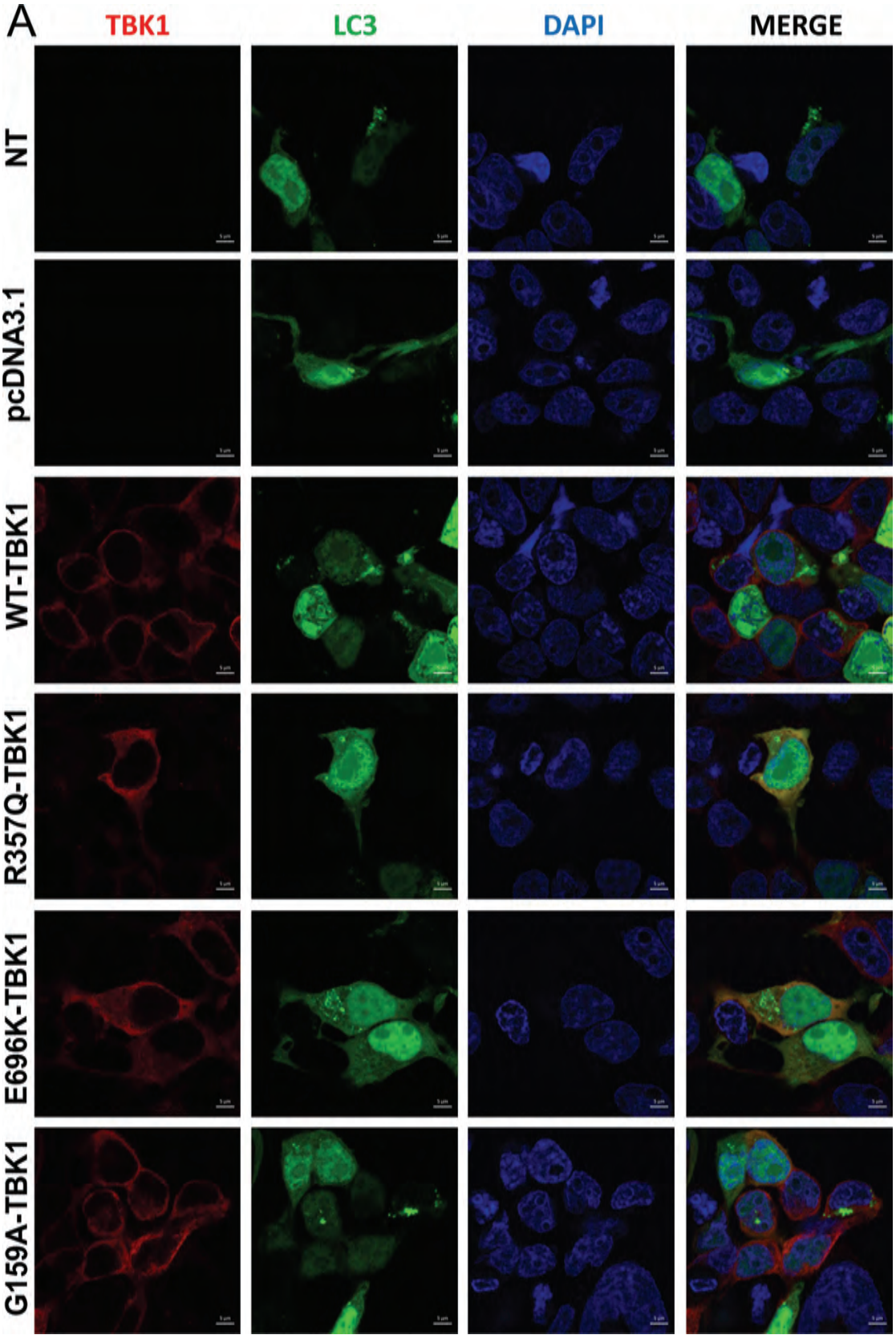
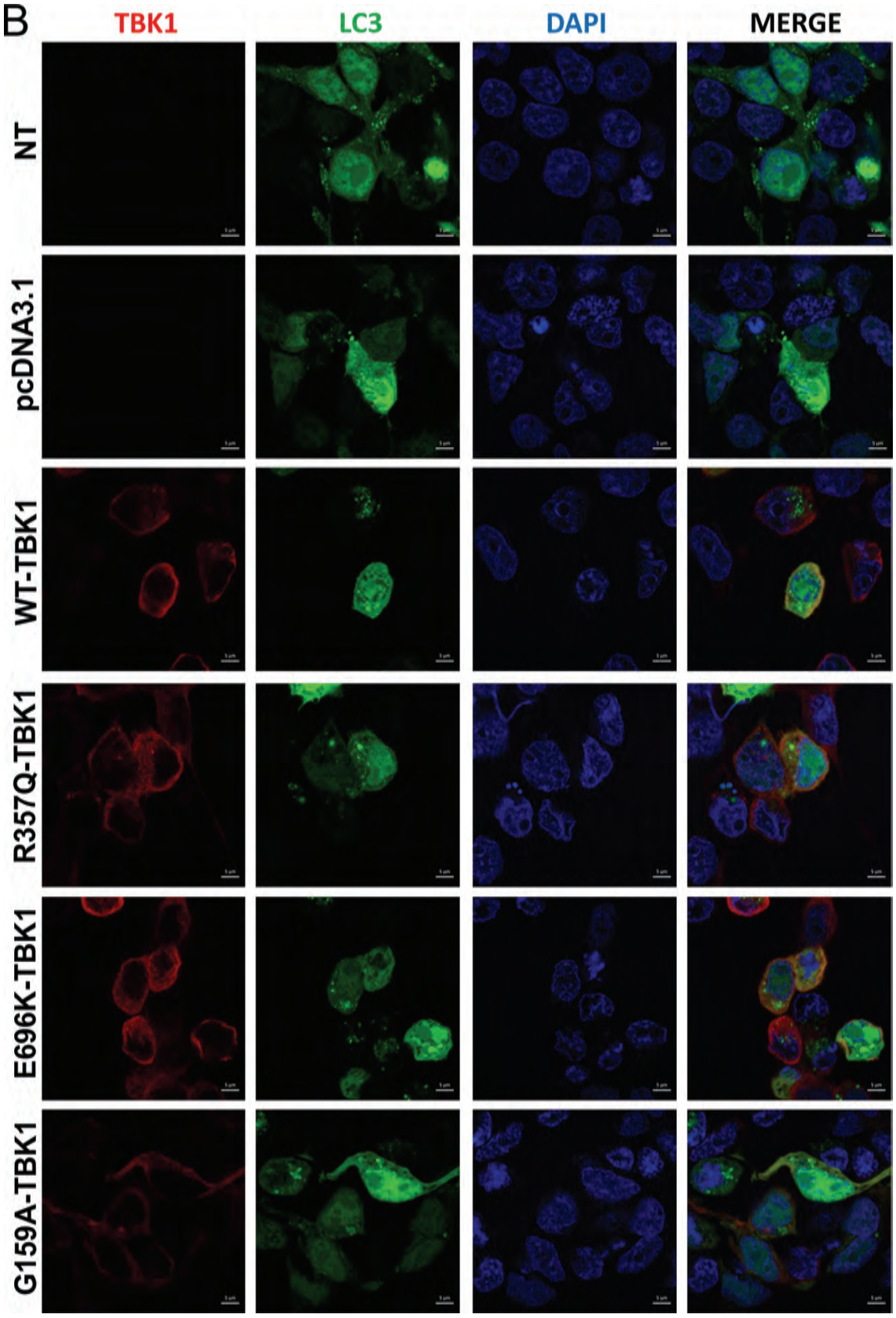

Starvation-induced autophagy
% of EGFP/mCherry positive cells
120
80
40
0
*
*
*
NT
pcDNA3.1
WT-TBK1
R357Q-TBK1
E696K-TBK1
G159A-TBK1
NT/BafA1
pcDNA3.1/BafA1
WT-TBK1/BafA1
R357Q-TBK1/BafA1
E696K-TBK1/BafA1
G159A-TBK1/BafA1
EGFP+/mCherry+ cells
EGFP-/mCherry+ cells

Figure 4.12. The TBK1 mutants do not impair autophagosome degradation during starvation-induced autophagy. TBK1$^{-/-}$ #2 HEK293T cells were co-transfected with TBK1-FLAG and LC3-EGFP-mCherry constructs for 44 hr cells, followed by starvation in HBSS for 4 hr with or without bafilomycin. Cells were treated with saponin, and immunostained with an APC-FLAG antibody, then analysed via FC. (**A)** *Representative images of FC analysis.* Increasing EGFP signal along the y axis and increasing mCherry signal along the x axis. Q1: EGFP^{+}/mCherry^{-}, Q2: EGFP^{+}/mCherry^{+}, Q3: EGFP^{-}/mCherry^{-}, Q4: EGFP^{-}/mCherry^{+}. **(B)** *Autophagosome/autolysosome ratio is shown in graph.* N=3+/- SEM, one-way ANOVA with Tukey post-hoc test, *<0.05.

Next, we aimed to confirm these results using confocal microscopy analysis. LC3-EGFP and TBK1-FLAG was overexpressed in TBK1$^{-/-}$ #2 HEK293T cells as above. The numbers of LC3-EGFP vesicles per cell were quantified in TBK1-FLAG overexpressing cells under HBSS starvation. However, no statistically significant differences was detected between the different TBK1-FLAG overexpressing condition either with or without bafilomycin **(Figure 4.13)**. Whilst this finding is consistent with the FC analysis in that the TBK1 mutants gave similar results to WT TBK1, they also further confirm that microscopy analysis is not as sensitive as the novel FC method to detect changes in autophagy.


A
TBK1
LC3
DAPI
MERGE
NT
pcDNA3.1
WT-TBK1
R357Q-TBK1
E696K-TBK1
G159A-TBK1


B
TBK1
LC3
DAPI
MERGE
NT
pcDNA3.1
WT-TBK1
R357Q-TBK1
E696K-TBK1
G159A-TBK1

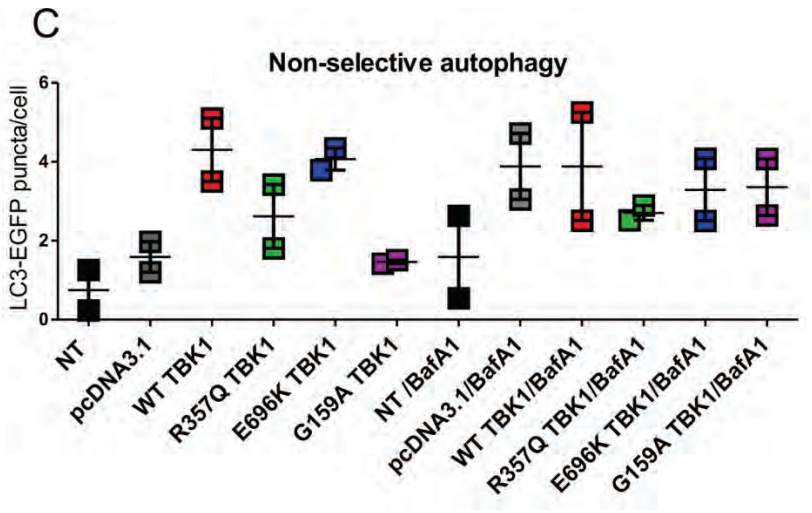
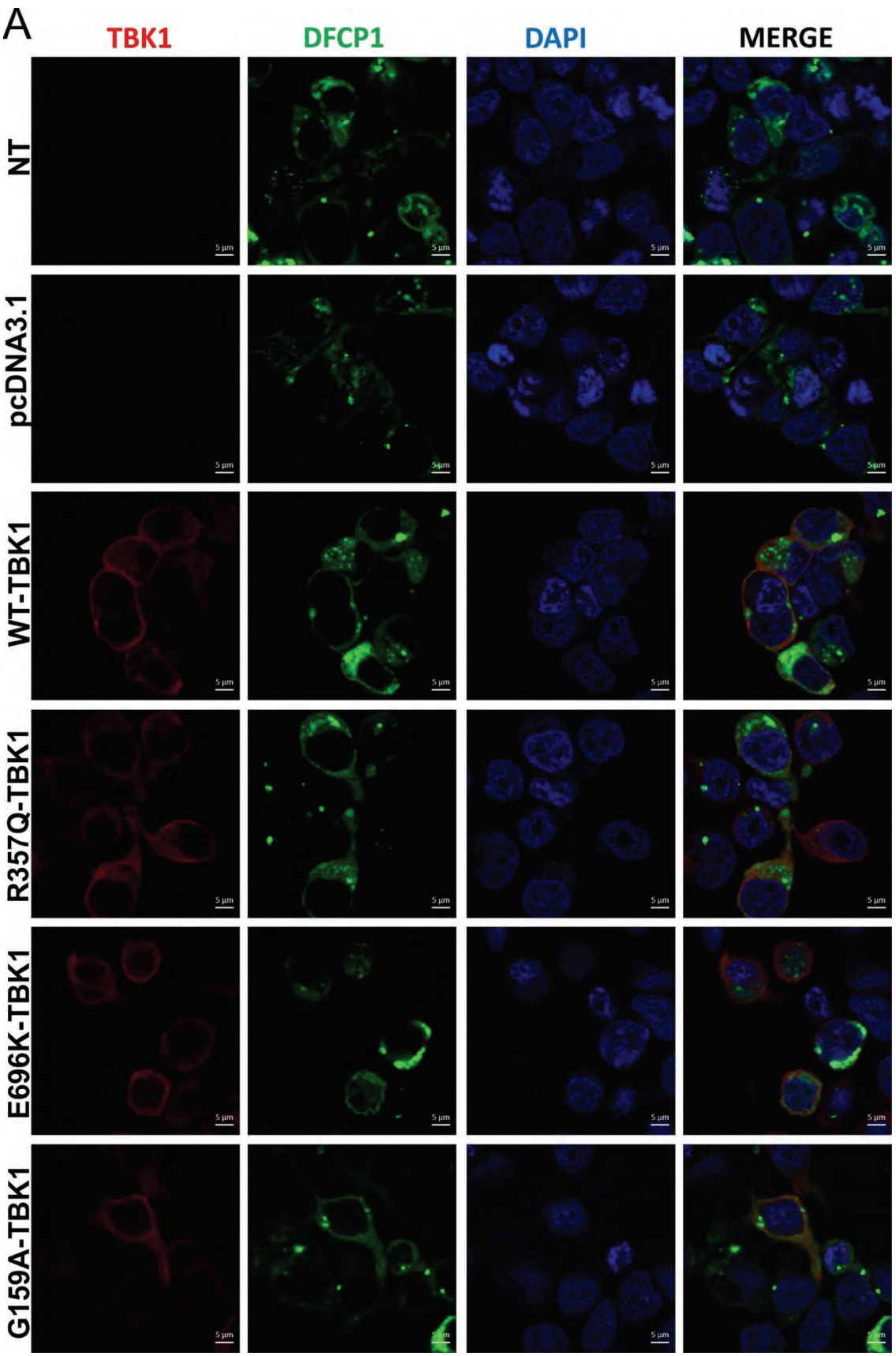


Figure 4.13. Overexpression of TBK1-FLAG does not affect autophagosome formation during starvation-induced autophagy. TBK1$^{-/-}$HEK293T cells were transfected with TBK1-FLAG and LC3-EGFP constructs for 44 hr then cells were starved for 4 hr with or without bafilomycin. Cells were fixed in 4% PFA and immunocytochemistry was performed using an anti-TBK1 antibody. LC3-EGFP puncta were quantified by confocal microscopy. Representative images of cells treated without **(A)** and with bafilomycin **(B)** and relative comparison of LC3-EGFP puncta numbers **(C)** are shown.

As it was previously shown that starvation increases omegasome formation **(Figure 3.10)**, next it was analysed whether overexpression of TBK1-FLAG proteins affects the formation of the omegasome (and consequently the phagophore) during starvation-induced autophagy. TBK1$^{-/-}$ #2 HEK293T cells were co-transfected with DFCP1-EGFP and TBK-1 constructs and starvation-induced in HBSS for 4 hr. DFCP1-EGFP positive puncta were then quantified in WT and mutant TBK1 expressing cells by confocal microscopy. Whilst overall no significant difference was detected, a decreasing trend was obvious in omegasome formation upon E696K overexpression **(Figure 4.14)**. This result implies that the interaction between TBK1 and optineurin may be required for omegasome formation during starvation-induced autophagy, although this needs to be confirmed in further studies. Furthermore, as TBK1 inhibition decreased the binding between TBK1 and optineurin **(Figure 4.4)** this may be related to impaired TBK1/optineurin binding.


A
TBK1
DFCP1
DAPI
MERGE
NT
pcDNA3.1
WT-TBK1
R357Q-TBK1
E696K-TBK1
G159A-TBK1
5 µm

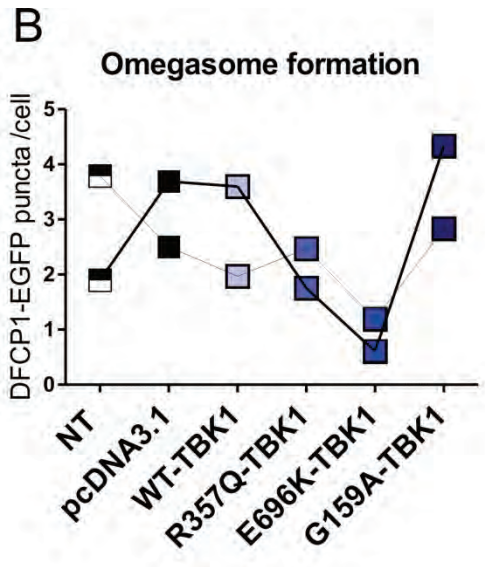


Figure 4.14. There are no differences in formation of the omegasome following overexpression of TBK1 proteins in starvation-induced autophagy. TBK1$^{-/-}$ #2 HEK293T cells were co-transfected with TBK1-FLAG and DFCP1-EGFP constructs for 44 hr, then cells were starved for 4 hr. Immunocytochemistry was performed using an anti-TBK1 antibody and the numbers of DFCP1-EGFP puncta per cells were counted. Representative images **(A)** and relative comparison of DFCP1-EGFP puncta numbers per cell **(B)** are shown.

4.4.13 Summary

These data show that during starvation, kinase deficient mutant TBK1 (R357Q, G159A) may impair autophagosome degradation, but overall this was not different to WT TBK1. Furthermore, this indicates TBK1 may be differently involved in basal and starvation-induced (non-selective) autophagy.

4.5 Discussion

Autophagy receptors have a crucial role in selective forms of autophagy, including mitophagy [392, 456, 478, 480, 481], aggrephagy [626, 628, 629] and xenophagy [132, 485, 486, 630, 631] because they tether the ubiquitinated cargo towards the forming phagophore, thus facilitating autophagosomal engulfment and degradation. While the importance of autophagy receptors is clear in selective autophagy, their role in basal autophagy and starvation-induced non-selective autophagy is still not defined. Autophagy receptors p62, NDP52 and optineurin are known to be activated by TBK1 [132, 392, 478]. Hence this suggests that the mechanism of autophagy dysfunction described in Chapter 3 may be mediated by an aberrant interaction between TBK1 and its substrates. Hence in this Chapter, to address this possibility, these autophagy receptors were examined in conditions of TBK1 inhibition and knock-out, in both basal and starvation-induced autophagy.

4.5.1 Autophagy receptors p62, NDP52 and optineurin are likely to be involved in basal autophagy and starvation-induced autophagy

Autophagy receptors are recruited with their cargo to the autophagosome, and they remain within the autophagosome throughout lysosomal degradation [390]. Therefore, quantitative analysis of their expression levels can be used to investigate their involvement in autophagy. Here, the levels of optineurin were decreased when autophagosomes were accumulated following bafilomycin treatment during basal autophagy, although the reason remains unclear (**Figure 4.1**). Optineurin itself may degrade via the proteasomal system during basal autophagy, and not via macroautophagy, although optineurin is known to localise to autophagosomes [132, 456]. The immunoblotting studies showed that p62 and NDP52 may not be recruited to autophagosomes during basal autophagy (**Figure 4.1**). However, both p62 and NDP52 immunoprecipitated with LC3, indicating they are located with the autophagosome **(Figure 4.5A)**. Co-localization between the autophagosome and NDP52, p62 or optineurin could be used to further confirm these findings. However, these data suggest that these autophagy receptors may be indeed involved in basal autophagy. Nevertheless, it must be noted that basal autophagy represents a selection of simultaneously occurring selective autophagy subtypes. Therefore, the involvement of the individual receptors in basal autophagy may be masked by the relatively low presence of individual selective

autophagy subtypes (such as mitophagy, ribophagy, reticulophagy) that require these specific autophagy receptors, potentially explaining why no significant changes were detected via immunoblotting **(Figure 4.1)**.

Starvation induces non-selective autophagy. Here it was examined whether autophagy receptors p62, NDP52 and optineurin are involved in cargo degradation. A comprehensive analysis of the role of these receptors in HEK293T cells during starvation has not been yet described. Here, p62, NDP52 and optineurin showed a decreasing trend of protein levels over time course of starvation but this was not statistically significant. In combination with the findings described in Chapter 3 it is tempting to speculate that because degradation of autophagosomes occurs during starvation, these adaptors may degrade with the autophagosomes following starvation. However, this cannot be concluded from the results obtained here. A previous proteomic study performed in human fibroblasts showed that autophagy receptors p62, NBR1, NDP52 and TAXbp1 degrade via endosomal microautophagy upon amino acid starvation in HBSS, independently of macroautophagy [581]. This occurred predominantly in the first hour of starvation and was accompanied by LC3 degradation [581]. Interestingly optineurin did not follow such degradation pattern in this study [581]. However, we cannot exclude the possibility that degradation of p62 and NDP52 results from microautophagy, because bafilomycin blocks the H+ ATPases on the lysosome that are also involved in microautophagy [581] . Therefore, degradation of proteins both by microautophagy or by macroautophagy can be inhibited by bafilomycin. While differences over the time course of starvation did not reach statistical significance, during starvation, NDP52, p62 and TBK1 immunoprecipitated with LC3 **(Figure 4.7A**). This indicates that even if their protein levels may not be detectable by immunoblotting, p26 and NDP52 are indeed involved in macroautophagy because LC3 is not involved in microautophagy at all [632]. Therefore, to confirm the involvement of these receptors in starvation-induced autophagy, co-localisation experiments between p62/NDP52 and LC3 need to be carried out in the future. The mechanisms underlying how these receptors are involved in non-selective autophagy or whether they directly function as autophagy receptors during starvation is not conclusively determined. However, this data suggest that the autophagy receptors may have a more fundamental role in non-selective autophagy than previously thought, but further experiments are necessary to confirm this.

4.5.2 TBK1 inhibition using MRT67307 elevates p62 and NDP52 levels

In Chapter 3, some data was obtained to suggest that TBK1 inhibition may lead to inhibited autophagosome-lysosome fusion, and ultimately therefore, reduced autophagosome degradation during basal autophagy. Both BX795 and MRT67307 displayed some inhibition of autophagosome-lysosome fusion in some, but not all, of the various assays examined. Consistent with these findings, increased p62 and NDP52 levels were observed upon TBK1 inhibition with MRT67307 during basal autophagy in this chapter, although only NDP52 was significant with BX795. Increased levels of autophagy receptors suggest that they cannot be degraded via autophagy. TBK1 inhibition using MRT67307 increased the accumulation of p62 during bafilomycin treatment compared to vehicle treated conditions. This may be due to the longer time frame of TBK1 inhibition (24 hr) compared to bafilomycin treatment (4 hr), whereas p62 accumulates only for 4 hr. During MRT67307 treatment, and due to the complete block in autophagosome-lysosome fusion, more p62 accumulates than in bafilomycin treated cells. Interestingly, elevated levels of p62 may further inhibit basal autophagy via a secondary mechanism, independent of TBK1. p62 directly interacts and inhibits HDAC6 [626], a histone deacetylase found in aggresomes [629]. HDAC6 interacts with the cortactin-dependent actin-remodelling machinery [626, 629, 633], leading to autophagosome-lysosome fusion via deacetylation of cortactin [626], and p62 inhibits the deacetylase activity of HDAC6 [626]. Hence, increased levels of p62 upon TBK1 inhibition may block HDAC6 and prevent autophagosome-lysosome fusion. Furthermore, HDAC6's activity is controlled via its phosphorylation status [634]. HDAC1 and HDAC2 were identified as potential substrates of TBK1 in a previous phospho-proteomic study [570]. If TBK1 phosphorylates and activates HDAC6, then in the presence of TBK1 inhibitors, less HDAC6 would be activated, and this would also further inhibit autophagosome-lysosome fusion. The possible role for HDAC6 in this process therefore could to be evaluated in the future. Cells harbouring dysfunctional TBK1 are positive for p62 aggregates [508], therefore the increased levels of p62 identified in this thesis may be due to its aggregation also, and p62 aggregation is present in ALS patients [635]. Therefore, inhibition of TBK1 may lead to aggregation and elevation of p62, contributing to neurodegeneration in ALS. The aggregation of p62 therefore needs to be evaluated in the future via microscopy analysis While it is generally accepted that autophagy receptors are degraded via the

autophagosome, and therefore their levels may mirror autophagy dysfunction, we cannot exclude the possibility that increased transcription and translation also occurred during TBK1 inhibition. Therefore, the mRNA levels of autophagy receptors p62, NDP52 and optineurin should be analysed in future studies.

4.5.3 Autophagy receptors are not affected by TBK1 inhibition during starvation-induced autophagy

In contrast to basal autophagy, during non-selective autophagy, TBK1 inhibition did not affect the levels of the autophagy receptors examined here. While it is still mostly accepted that starvation does not induce selective autophagy, a recent study showed that starvation induces ribophagy, the selective degradation of ribosomes [610]. A specific receptor, nuclear fragile X mental retardation–interacting protein 1 (NUFIP1), was identified as the ribophagy specific autophagy receptor. Upon mTORC1 inhibition, NUFIP1 translocates to ribosomes and delivers them to the autophagosome by direct binding with LC3B [610]. NUFIP1 also promotes cell survival upon starvation [610]. NUFIP1 has not been previously identified as a substrate of TBK1, and it was also shown to not undergo phosphorylation in order to translocate from cytosol to ribosome [610]. However, NUFIP1 was shown to restrict mTORC1 signalling [636], therefore implying it is involved in starvation-induced autophagy. NUFIP1 may therefore be a potential candidate substrate for TBK1, which could be analysed more in the future. Alternatively, the decreased levels of TBK1 due to inhibition that were detected in Chapter 3 **(Figure 3.12)** may explain why autophagy receptors that are implicated in non-selective autophagy (section 4.23) were not affected upon TBK1 inhibition.

4.5.4 TBK1's substrate binding domain facilitates LC3-autophagy binding

Autophagy receptors bind to LC3 via their LIR domain. Upon TBK1 inhibition, LC3-II levels increased during basal autophagy in this study (Chapter 3), in a similar fashion to p62, and NDP52 (**Figure 4.3**). This result would suggest that these autophagy receptors are recruited to the autophagosome, even in TBK1 inhibited cells. Hence immunoprecipitation of autophagy receptors with LC3 was performed, in order to examine their association under TBK1 inhibition.

TBK1 immunoprecipitated with p62, optineurin and LC3, suggesting that it interacts with all these proteins during basal autophagy. Inhibition of the kinase activity of TBK1 using BX795 resulted in less precipitation between TBK1 and adaptors p62 and optineurin, however increased precipitation was observed between these autophagy receptors and LC3. This suggests that the binding between LC3 and p62 or optineurin is not mediated by the kinase activity of TBK1, but more probably by its substrate binding domain, which is still intact when TBK1 is inhibited. Indeed, upon TBK1 knock-out, less p62 precipitated with LC3, indicating that this association is mediated by substrate binding of TBK1. However, the interactions between TBK1 and its substrates p62 or optineurin may be affected by the kinase activity of TBK1, because the binding of the TBK1 upon inhibited enzymatic activity to these proteins showed a decreased trend. Therefore, this finding implies that autophagy receptor-TBK1 interaction requires fully functional kinase active TBK1. However, reverse IP experiments with TBK1 needs to be carried out in the future to confirm these findings. Furthermore, the inclusion of negative control, involving a protein not precipitated by GFP-trap needs to be included in the

These results therefore imply that both the kinase activity and the binding domain of TBK1 are equally important for maintaining the autophagy receptor/LC3/TBK1 complex. Increased precipitation between LC3 and these adaptors may be due to inhibited autophagosome degradation, resulting in prolonged binding between LC3 and p62 or optineurin. Alternatively, the TBK1 kinase activity may be involved in the dissociation of the LC3-autophagy receptor complex, although there is current no evidence to support this mechanism. HEK293T cells were found to express low levels of optineurin, which may explain why optineurin was not detected after p62 and LC3 immunoprecipitation. Furthermore, there was apparently no interaction between NDP52 and either p62 or optineurin because no co-immunoprecipitation could be detected. This suggests that a NDP52-LC3-TBK1 complex may form separately from a p62-optineurin-LC3-TBK1 complex during basal autophagy. Furthermore, this indicates that under basal autophagy conditions, the recruitment of p62 to LC3 is mediated via TBK1. In contrast, the interaction between NDP52 and LC3 did not consistently decrease upon TBK1 knock-out indicating recruitment of NDP52 to LC3 may be independent of TBK1's substrate binding. Nonetheless, this data highlights that p62/TBK1/LC3 complex may be also important in basal autophagy, which has been previously implicated in mitophagy [392, 456, 478, 480]. This suggests less involvement for the NDP52/TBK1/LC3 complex.

Different mechanisms are in place during mitophagy compared with basal autophagy. Phosphorylation of p62 and optineurin by TBK1 is not necessary for the recruitment of these autophagy receptors to ubiquitinated mitochondria, whereas autophagosomal engulfment of mitochondria does require both p62 and optineurin phosphorylation by TBK1 [392, 456]. This indicates the binding of autophagy receptors to ubiquitinated mitochondria is independent of the kinase activity of TBK1, while their binding to LC3 requires this activity. In this Chapter, the results obtained suggest that the binding between LC3 and these autophagy receptors are mediated by the substrate binding domain of TBK1, rather than its kinase activity.

Autophagy is highly cell type dependent. Therefore, this suggests that different mechanisms are place during in different cell types and also between different subtypes of autophagy. Furthermore, the notion that fundamental differences between subtypes of autophagy is supported by the fact that TBK1 knock-out did not affect LC3-autophagy receptor binding during starvation-induced autophagy in this study. Hence TBK1 may have different roles in the different subtypes of autophagy. To confirm that TBK1 does not affect LC3-autophagy binding during starvation-induced autophagy, further immunoprecipitation studies may be carried out, including immunoprecipitation between TBK1 and autophagy receptors in upon starvation using the TBK1 inhibitors (BX795, MRT67307).

4.5.5 TBK1 mutations in Amyotrophic lateral sclerosis

A wide range of TBK1 mutations have now been identified in both ALS and FTD [17, 18, 197, 198] , and to date more than 90 variants have been described (Table 1.2) However, mutations in TBK1 are rare in ALS, and some studies have even suggested that they are a risk factor rather than being causative [637]. It remains unclear how mutations in TBK1 lead to ALS and what mechanisms are involved. Haploinsufficiency is however strongly implicated [638], and mutations in TBK1 that cause 50% or more reduction in the levels of protein expression are considered to be pathogenic [638]. RNA decay due to the presence of an early stop codon, and protein degradation due to the existence of missense variants, are amongst the reasons proposed for haploinsufficiency, and thus the underlying pathogenicity of TBK1 in ALS [638]. Furthermore, some ALS TBK1 mutants

have been directly shown to lead to haploinsufficiency. The mutation c.358+5G>A led to aberrant mRNA processing, consequently resulting in haploinsufficiency in patient derived fibroblasts, while another frameshift mutant showed abolished protein expression (p.Leu59Phefs*16) upon overexpression in human embryonic kidney cells (AD293) [496]. The findings obtained in this Chapter are also consistent with these observations. The expression levels of ALS TBK1 mutants R357Q was significantly lower than WT-TBK1 upon transfection, unlike E696K and G195A. This indicates that lower TBK1 expression is not a feature of all ALS-mutant TBK1.

TBK1-FLAG did not form insoluble protein aggregates in HEK293T cells or visible inclusions, as detected by microscopy. Furthermore, TBK1-FLAG was not detected in LC3-EGFP puncta, showing that it does not recruit to autophagosomes similar to endogenous TBK1. However, TBK1-FLAG was detected in HEK293T cells post-saponin treatment indicating that WT/R357Q/E696K/G159A TBK1 are localised to intracellular membranes, although overall no significant difference were detected between these proteins. TBK1 was previously shown to localize to the mitochondria [639] and Golgi apparatus [640] upon viral infection. However, an in-depth analysis of the normal intracellular localisation of TBK1 is currently lacking. Furthermore, there is also the possibility that ALS/FTD mutations in TBK1 may lead to increased retention in certain membrane organelles potentially underlying its pathogenicity. Therefore, further microscopy analysis involving the colocalization of WT and mutant TBK1 with specific intracellular organelles should to evaluated in the future.

4.5.6 TBK1 impairs autophagosome degradation and ALS mutants of TBK1 do not affect this

The potential pathogenicity of TBK1 mutants may be due to their dysfunctional involvement in autophagy, given that TBK1 functions in various types of autophagy. However, few studies have examined disease mechanisms in relation to ALS-associated mutant TBK1. E696K was previously shown not to relocate to damaged mitochondria during mitophagy, unlike WT TBK1, due to inhibited binding with optineurin [456]. Hence in this study, the aim was to analyse the effect of ALS-TBK1 mutants on autophagy, particularly basal autophagy, since it is known to be crucial for neuronal health [400].

Overexpression of all TBK1-FLAG resulted in inhibited autophagosome degradation during basal autophagy detected by FC compared to controls, but this was also evident with WT TBK1, implying it is a result of TBK1 overexpression, and this could not be confirmed by using confocal microscopy. However, bafilomycin's autophagosome accumulating effect could also not be detected during confocal microscopy analysis, therefore this is most likely due to the lower sensitivity of microscopy and it means that the microscopy results should be interpreted with caution. Alternatively, FC analyses the number of cells positive for autophagosomes, while confocal microscopy examined the overall number of autophagosomes. Therefore, a plausible explanation for the difference in these results is that TBK1-FLAG more strongly affects whether a cell can undergo autophagy or not, rather than how many vesicles are being produced once the autophagy is already underway. The inhibition of autophagosome degradation upon WT-TBK1 overexpression was an unexpected outcome, which may be due to increased TBK1 protein levels. Nonetheless the lack of difference between WT and mutant TBK1 suggest that pathogenicity of ALS TBK1 is most likely not mediated via impaired basal autophagy. Omegasome formation was also not affected by TBK1-FLAG during basal autophagy, consistent with the results obtained in Chapter 3 that omegasome formation is not affected by TBK inhibition in basal autophagy.

In contrast, different results were obtained during non-selective (starvation) autophagy indicating that TBK1 has distinctive roles different types of autophagy. Overexpression of kinase deficient mutants R357Q-TBK1 and G159A-TBK1 impaired autophagosome degradation compared to controls (NT/pcDNA3.1), but not WT TBK1, suggesting a potential harmful effect that is not present with WT-TBK1. Overexpression of WT-TBK1 and E696K-TBK1 did not significantly differ from control cells, indicating that they do not affect autophagosome formation or degradation during starvation-induced autophagy. Omegasome formation was also followed under starvation-induced conditions, and E696K-TBK1 overexpression appeared to decrease the formation of the omegasome during starvation. This result therefore may suggest that the TBK1-optineurin interaction may be involved in omegasome formation because E696K lacks optineurin binding [18]. However further experiments are required to confirm that this mutant perturbs omegasome formation. Interestingly, decreased omegasome formation was not associated with the formation of fewer LC3-EGFP puncta, which was expected.

Therefore, in the future the timing of the experiment should be extended to follow the effect of expression E696K-TBK1 for longer periods of time. Inhibited omegasome formation has been previously reported in ALS, because mutations in *FUS* inhibit the formation of omegasomes [324].

4.5.7 Summary

In this Chapter it was shown autophagy receptors are involved in both basal and starvation-induced autophagy, and they influence TBK1, at least during basal autophagy. Furthermore, different interactions were detected when TBK1's kinase activity was inhibited or TBK1 was knock-out . are due to abnormal interaction between TBK1 and autophagy receptors and between LC3 and autophagy receptors. In this Chapter it was analysed how ALS/FTD mutant TBK1 influences autophagy. ALS/FTD mutant TBK1 had different effect in autophagy under serum rich and starvation conditions furthermore previously showed (Chapter 3) that inhibition of TBK1 kinase activity affects basal and starvation-induced autophagy differently, therefore this data together indicats that TBK1 has different role in different types of autophagy. However, no major differences were detected between overexpression of WT TBK1 and the mutants, although differences to controls were identified, implying that overexpression of TBK1 itself may perturb autophagy.

The presence of protein aggregates in motor neurons of ALS patients is a hallmark of ALS and may be a consequence of impaired autophagy. In the 3rd and 4th Chapter it was shown how TBK1 is involved in basal and starvation-induced autophagy, therefore in the next chapter it was examined how TBK1 affects aggrephagy and the clearance of proteins such as ubiquitin via autophagy. Furthermore, aggregation of TDP-43, the major component of insoluble protein inclusion linked to ALS was also be examined.

Chapter 5

Investigating the role of TBK1 in aggrephagy and TDP-43 aggregation

5.1 Introduction

5.1.1 Protein degradation by autophagy and UPS

In mammalian cells, proteins may degrade via two pathways, either the ubiquitin proteasome system (UPS) or autophagy. The UPS is responsible for degrading 80-90% of proteins. This includes many regulated, short-lived, abnormal, denatured, or, in general, damaged proteins [641]. In contrast, autophagy primarily degrades long-live proteins, insoluble proteins and protein aggregates that are harmful for the cell. CMA uses Hsc70 (heat shock cognate protein of 70 kDa) [327] and additional co-chaperones such as BAG1, Hip, Hop, and Hsp40/DNAJB1, that bind to cytosolic targets by recognizing a specific consensus sequence (KFERQ), which is present in 30% of cellular proteins [326]. The chaperone then binds to a LAMP-2A receptor on the lysosomal membrane [328], leading to degradation.

Proteins that are destined for degradation are marked with a small, globular regulatory protein called ubiquitin (Ub). Ubiquitination is a conjugation system that requires three enzymes E1; activating enzyme, E2 conjugating enzyme, and an E3 ligase.[642]. Target proteins can by linked with a single ubiquitin (monoubiquitin) or chains of ubiquitin (polyubiquitin), attached by the assistance of an E4 ligase, which adds additional ubiquitin on the existing chain. Lysine residues at positions 6, 11, 27, 29, 33, 48, and 63 may undergo polyubiquitination [643]. However, the two most common polyubiquitination sites are K-48 and K-63.

Ubiquitin serves as a recognition signal for downstream effectors that determine the fate of the protein. Both the UPS and autophagy use ubiquitination as a target signal. In general, the UPS mainly degrades proteins labelled with K-48 poly-Ub chains only. In contrast, macroautophagic degradation of proteins usually requires K-63 poly-Ub chains attached to the target that can recruit autophagy receptors p62 and NBR1 [644, 645] [605].

The clearance of insoluble aggregate-prone proteins via macroautophagy requires the formation of aggresomes. A variety of ubiquitin ligases take part in the ubiquitination of aggregation prone proteins including; CHIP, Parkin, HRD1 and TRIM50 [646-649]. Another key protein in aggresome formation is HDAC6, which links K63-linked

polyubiquitinated aggregates to the molecular motor dynein, for transport towards the microtubule organizing centres (MTOCs) where aggresomes accumulate [200, 628, 646, 650-652]. This is followed by the interaction of autophagy receptors p62 and NBR1 that recruit the autophagic machinery [200, 628, 646, 650-652]. p62 interacts preferentially with long K63-linked chains (with more than 7 ubiquitin subunits) [71], but it can also bind short chains linked through both K48 and K63. NDP52 and optineurin has not been shown to interact with HDAC6.

5.1.2 Induction of aggrephagy by UPS inhibition

Previous studies have shown that inhibition of the UPS leads to the activation of autophagy, so that the cell can cope with the normal requirements for protein degradation [653-655]. MG132 is a peptide aldehyde that blocks the proteolytic activity of the 26S proteasome [656], therefore when added to cells it inhibits UPS-mediated protein degradation. As only these two systems can degrade proteins [216], by inhibiting the UPS, proteins are directed towards autophagy for degradation. Furthermore, insoluble proteins can only be degraded by macroautophagy [657]. It was previously shown that inhibition of the UPS by MG132 significantly increased the levels of polyubiquitinated proteins in the cell, and this was further enhanced when autophagy was inhibited via depletion of *atg6* [658]. Therefore, this result shows that following MG132 treatment, autophagy is activated and degrades polyubiquitinated proteins. Hence this phenomenon was taken advantage of in this thesis to examine aggrephagy.

5.1.3 Role of TBK1 in protein degradation

The involvement of TBK1 in protein degradation and inclusion formation has not been extensively studied. One report showed that TBK1 colocalised with $SOD1^{G93C}$ and htt-Q103 aggregates in HeLa cells, and depletion of TBK1 increased $SOD1^{G93C}$ aggregates [140]. Furthermore, overexpression of TBK1 decreased $SOD1^{G93C}$ aggregates [140]. TBK1 also co-localised with ubiquitin [140], indicating that TBK1 may have a role in ALS-linked protein aggregation. Nonetheless, heterozygous depletion of TBK1 ($TBK1^{+/-}$), mimicking haploinsufficiency, does not lead to a motor phenotype in mice [510]. However, complete TBK1 KO in mice is not feasible because these animals die between embryonic day 13.5 and 14.5, and no live births are produced [511]. These $TBK^{+/-}$ mice show no change in SOD1 and TDP-43 levels [510], indicating that

haploinsufficiency of TBK1 may not be enough to develop ALS. In contrast, in TBK1$^{+/-}$/SOD1 mice, increased p62 and GABARAPL1 accumulation was detected at early time points in disease development, possibly indicating the presence of impaired autophagy [510]. Furthermore, this may indicate that TBK1 on its own does not cause ALS, however, in the presence of other ALS-associated mutations, it may exacerbate disease progression, at least in the early disease stages. It must be mentioned that lack of sufficient TBK1 impairs microglia activation and slowed down disease progression in TBK1$^{+/-}$/SOD1 mice [510]. This suggest that the role of TBK1 in ALS may be linked to its functions in immunity.

As TBK1 mutations are features of several neurodegenerative diseases [490], all of which are associated with protein aggregation, and due to the role of TBK1 in mitophagy, xenophagy and basal autophagy (Chapter 3 and Chapter 4), it is a feasible that TBK1 is involved in the selective degradation of protein aggregates, aggrephagy. In particular, TDP-43 aggregates are the major pathological hallmark of ALS. Therefore, in the final chapter of this thesis the role of TBK1 in aggrephagy and the aggregation of TDP-43 was examined.

5.2 Objectives of this chapter

Aggrephagy is a subtype of autophagy that describes the selective degradation of protein aggregates by autophagic engulfment [628]. The presence of protein inclusions is characteristic of neurodegenerative diseases, including ALS [215]. Due to the possible involvement of TBK1 in autophagy, TBK1 may therefore have important functions in aggrephagy and therefore in the development of ALS. However, there is currently limited understanding of how TBK1 affects protein aggregation.

- In this Chapter the role of TBK1 was analysed in MG132 induced autophagy by flow cytometry and immunoblotting.
- The involvement of TBK1 in ubiquitin degradation was examined using TBK1 inhibitors and TBK1 Ko cells by following the ratio of soluble and insoluble ubiquitin as well as microscopy analysis examining ubiquitin aggregates.
- TDP-43 aggregation under TBK1 inhibition and TBK1 KO conditions were examined by immunoblotting and microscopy analysis to establish whether TBK1 is involved in inclusion formation of TDP-43.

5.3 Materials and Methods

5.3.1 Induction of aggrephagy

Aggrephagy was induced by 1 μM MG132 treatment for 24 hr. DMSO was used as vehicle control. In the last 4 hr of MG132 treatment 100 nM bafilomycin was added to inhibit autophagosome lysosome fusion.

5.3.2 Cell lysis for total ubiquitin detection

Cell were lysed in lysis buffer (50 mM Tris-HCl, 150 mM NaCl pH 7.6, 1% triton-X 100, 2%SDS, protease inhibitors (Roche), phosphatase inhibitors (Roche) and PMSF [1:500, Sigma]) for 15 min on ice, than harvested into tubes and stored at -30℃ overnight. The next day, cell lysates were centrifuged at 27.670 g for 15 min at RT and supernatant was collected. Protein lysates were subjected to BCA protein quantification and loaded onto SDS-polyacrylamide gel.

5.3.3 Fractionation of cell lysates into soluble and insoluble fractions

Cell were lysed in lysis buffer (50 mM Tris-HCl, 150 mM NaCl pH 7.6, 1% triton-X 100, protease inhibitors (Roche), phosphatase inhibitors (Roche) and PMSF [1:500, Sigma]) for 15 min on ice, than harvested into ultracentrifuge Eppendorf tubes (Beckman) and frozen overnight at -30℃. The next day, the lysates were thawed on ice and sonicated for 10x 1” bursts and ultracentrifuged (~100,000 g, 4°C, 30’) (Beckman Optima MAX-XP Ultracentrifuge). The supernatant was collected as the soluble fraction. Cell pellets were washed with lysis buffer using sonication (microtip, Sonic Ruptor, Omni International, 10x 1” bursts) and ultracentrifugation (~100,000 g, 4°C, 30’). Pellets were then lysed in lysis buffer supplemented with 2% SDS using sonication (10x 1” bursts) and ultracentrifugation (~100,000 g, 22°C ,30’). The supernatant was collected as the insoluble fraction. Protein lysates were subjected to BCA protein quantification and loaded onto SDS-polyacrylamide gels.

5.3.4 Quantification of ubiquitin

Total and fractionated ubiquitin levels were quantified using densitometry analysis using ImageJ software (v. 1.47. National Institutes of Health). For quantification,

the signal intensity was measured in the entire lane from the highest to the lowest detectable band. Lane intensity was normalised to loading control, GAPDH, and presented as relative comparison in graphs. In each experiment at least 3 biological replicates were performed.

5.3.5 Analysis of TDP-43 aggregation via immunoblotting

HEK293T cells were plated into 6-well plates for immunoblotting experiments or in 24-well plates for microscopy analysis. Cells were transfected with TDP-43 overexpressing construct (TDP- 43EGFP$^{WT/M337V}$ or TDP-43-GFP$^{WT/dNLS}$) or co-transfected with TBK1-FLAG overexpressing constructs and incubated for the indicated amount of time. Alternatively, TDP-43 transfected cells were treated with BX795 or MRT67307. Cells were fractionated as described above or fixed in 4 % PFA for microscopy analysis followed by staining as mentioned. At least 50 transfected (or co-transfected) cells were analysed.

5.3.6 Analysis of TDP-43 aggregation via microscopy analysis

Cytoplasmic mislocalisation and TDP-43 aggregation was analysed by fluorescent microscopy. Images were taken with 100x/na=1.46 objectives on a Zeiss LSM 880 inverted confocal laser-scanning microscope, equipped with a LSM-TPMT camera (Zeiss) and analyzed by Zen software (Zeiss, blue edition). Coverslip sections to image were selected blindly, based on Hoechst staining alone. Cell counting was performed blindly. Cytoplasmic mislocalisation was analyzed based on the presence of a positive GFP signal outside of nucleus. The percentage of cells with mislocalised TDP-43 was counted as follows:

(Number of cells with cytoplasmic TDP-43-GFP/Number of cells expressing TDP-GFP)x100

TDP-43 aggregates were identified as large cytoplasmic deposits with GFP florescence. The percentage of cells with TDP-43 aggregates were counted as follows:

(Number of cells with TDP-43-GFP aggregates/Number of cells expressing TDP-GFP)x100

5.3.7 Ubiquitin quantification by fluorescence microscopy

Fluorescent intensity of ubiquitin staining was analysed using ImageJ software. Cells were grown on coverslips and transfected with TBK1-FLAG constructs for 24 hr, then treated with MG132 or the respective vehicle control for 24 hr. Cells were fixed and co-stained with anti-ubiquitin (mouse) and anti-TBK1 (rabbit) antibodies. Coverslips were photographed with a Zeiss epifluorescent microscope at 40X magnification. All biological replicates and groups of cells were photographed on the same day with the same settings (exposure time, magnification, zoom). Fluorescent intensity was analysed by calculating the corrected total cell fluorescence (The Open Lab Book).

The fluorescent intensity was analysed in either TBK1-FLAG overexpressing cells only, or in all cells in control conditions (NT, pcDNA3.1). The area of measurement, area integrated intensity and mean grey value were measured for the ubiquitin signals. Background values were also calculated on each picture where no cells were present. Next corrected total cell fluorescence (CTCF) was measured according to below equation;

$$CTCF = Integrated\ density - (area\ of\ selected\ cell \times mean\ flurescence\ of\ background\ readings)$$

CTCF was then divided by the number of cells analysed to obtain the fluorescent intensity per cell. At least 100 cells were measured in each experimental condition and their average relative values were plotted.

5.4 Results

5.4.1 Optimisation of autophagy induction via inhibited ubiquitin proteasome system, to allow monitoring of aggrephagy

Autophagy was activated using MG132 to allow monitoring of protein degradation via autophagy, which in the case of aggregated, ubiquitinated proteins, are degraded by aggrephagy. First, it was established that treatment of HEK293T cells with MG132 can indeed induce autophagy and the degradation of proteins. The conditions for treating cells with MG132 were optimised by both adjusting the concentration and length of treatment; based on cell viability and capability of treatment to induce autophagy (LC3-II accumulation (data not shown). From this, 1 μM MG132 treatment for 24 hr was selected as optimised treatment conditions.

Immunoblotting was used to analyse the levels of autophagy receptors, TBK1 and LC3. The rationale for this was that because MG132 treatment inhibits the UPS, all proteins that are degraded via the UPS under basal conditions, should therefore display increased levels in lysates treated with MG132. By also treating the cells with bafilomycin, we can determine whether protein degradation is autophagy-related, or strictly due to inhibited UPS. If proteins degrade via the UPS or autophagy, their levels should increase upon inhibition of one or the other pathway. If a specific protein is degraded via both pathways, then increased accumulation of it should occur if autophagy is blocked in cells treated with bafilomycin, combined with UPS inhibition by MG132.

HEK293T cells were treated with 1 μM MG132 or DMSO as a control for 20 hr, then 100 nM bafilomycin was supplemented for additional 4 hr. Then cells were lysed and separated on SDS-polyacrylamide gels, and immunoblotting was performed. The levels of LC3-I did not increase significantly upon MG132 treatment, indicating that LC3-I does not normally degrade via the UPS **(Figure 5.1A)**. Furthermore, the LC3-I levels did not change upon bafilomycin treatment either. In contrast, the levels of LC3-II increased significantly ($p=0.02$) upon MG132 treatment, indicating the presence of increased levels of autophagosomes compared to DMSO control cells as expected.

Increased LC3-II levels may explain the lack of change in LC3-I both upon inhibition of UPS or autophagy, as it most likely converts into LC3-II. Bafilomycin further increased the levels of LC3-II in cells treated with 1 μM MG132 compared to cells without bafilomycin. Bafilomycin treatment eliminates the fusion of autophagosomes with lysosomes, therefore an increase in the presence of bafilomycin reveals the true levels of autophagosomes that degrade during this timeframe (4 hr). Unexpectedly, there was no difference in LC3-II accumulation in the presence of bafilomycin between the different DMSO and MG132 treated cells, indicating that MG132 did not enhance the formation of autophagosomes compared to vehicle treated cells. In contrast, the increase in LC3-II levels upon MG132 treatment in the absence of bafilomycin may even indicate inhibited autophagosome-lysosome fusion upon MG132 treatment, because the overall levels of autophagosomes did not vary between the different treatment conditions, but increased in the absence of the lysosomal inhibitor (schematic explanation **Figure 3.1A**, Scenario A).

The resulting increasing levels of LC3-II with MG132 in the absence of bafilomycin were accompanied by greater levels of the autophagy adaptor NDP52. Without bafilomycin, the expression levels of NDP52 increased significantly compared to DMSO treated cells **(Figure 5.1A)**. This implies that NDP52 is degraded via the UPS or NDP52 is recruited to autophagosomes. NDP52 levels increased significantly upon bafilomycin treatment in control DMSO treated cells, but not in MG132 treated cells. This result indicates that the increased NDP52 levels observed in MG132 treated cells may be due to increased levels of autophagosomes, and not inhibition of the UPS, suggesting that autophagy degrades NDP52 upon UPS inhibition. This result therefore implies NDP52 may function as an autophagy receptor in aggrephagy. Interestingly, NDP52 showed a very similar trend to LC3-II indicating that they may function together following MG1322 treatment. In contrast to NDP52, the levels of p62 did not significantly change upon MG132 treatment, although a trend towards increased levels was observed. Due to the low levels of optineurin in HEK293T cells, it was not feasible to detect optineurin during these experiments.

The expression levels of TBK1 did not change following MG132 treatment, either with or without bafilomycin treatment **(Figure 5.1A)**. This suggests that TBK1 is not

degraded by the UPS or autophagy in this time frame or its steady state levels do not change. Activation of TBK1 can be measured by its phosphorylation status [471] and treatment with 1 μM MG132 induced phosphorylation of TBK1 (S172), as determined by immunoblotting using an antibody specific for phosphorylated TBK1. Hence this result suggests that TBK1 becomes activated by inhibition of the proteasome **(Figure 5.1B)**.

Flow cytometry analysis of autophagosome formation using 1 μM MG132 treatment was then performed in cells expressing dual-tagged LC3-EGFP-mCherry. Bafilomycin treatment led to the accumulation of significantly more $EGFP^+$ cells **(Figure 5.1C)**. This result therefore confirmed ongoing autophagy degradation, therefore excluding the possibility that MG132 inhibited autophagosomes-lysosome fusion, which is one potential explanation suggested by the LC3-II immunoblots (an increase upon MG132 treatment that does not translate into an increase when bafilomycin is present). However, to conclusively determine whether MG132 induces autophagy and directed proteins towards autophagic degradation, the levels of ubiquitin were then followed.

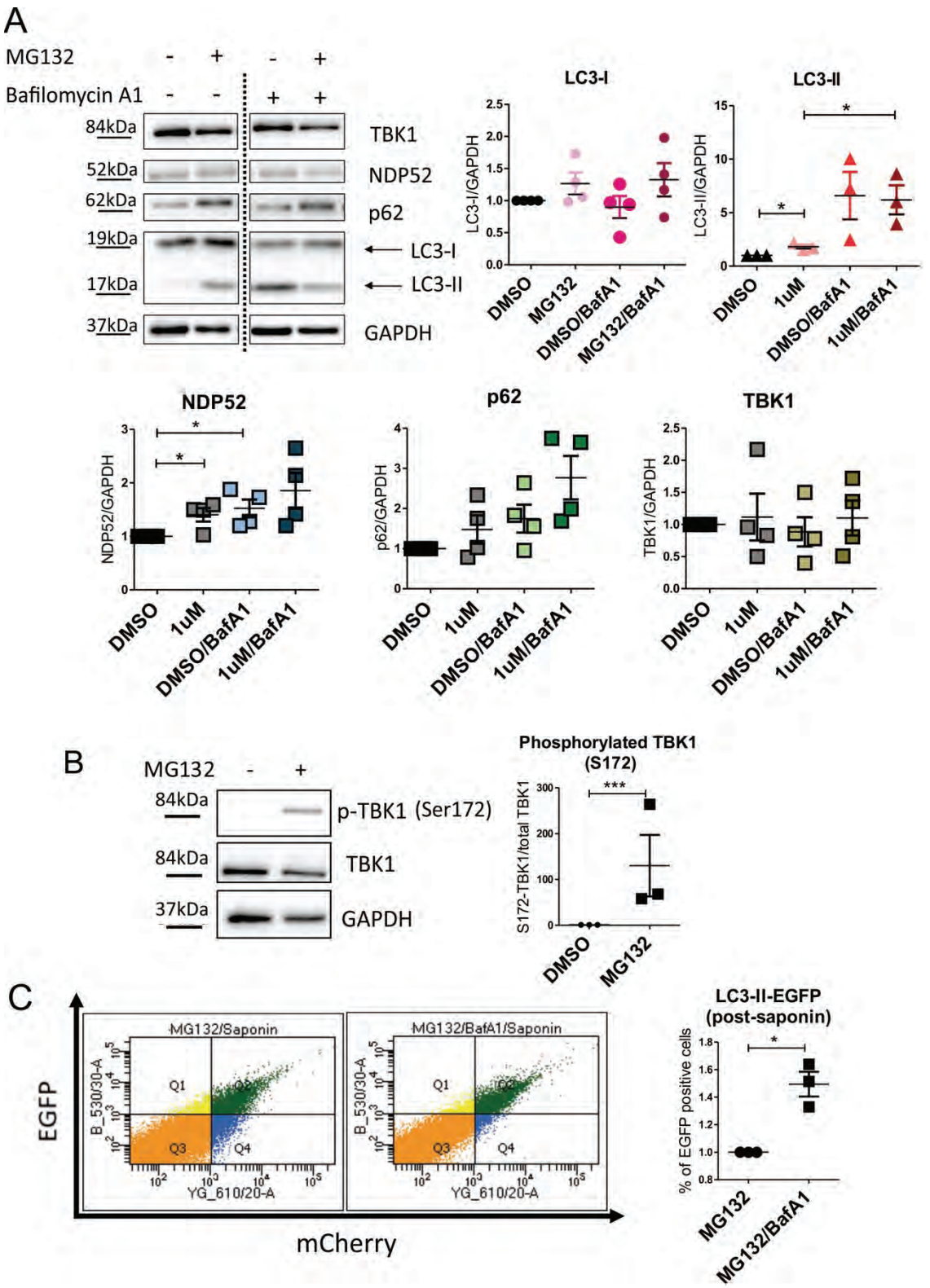
Examination of the ubiquitin levels by immunoblotting can be used to follow UPS and autophagy [658]. However, ubiquitination of proteins is a signal for degradation via both the UPS and autophagy, hence by following the presence of ubiquitin in a specific fraction, soluble (UPS) vs insoluble (autophagy), allows the assessment of the degradation of ubiquitinated cargo, and consequently aggrephagy, in a more precise manner. Soluble/insoluble fractionation has been previously used to detect insoluble form of ALS-associated genes, such as TDP-43 [659]. To show that MG132 indeed can induce aggrephagy and to establish how MG132 treatment affects the degradation of ubiquitin, lysates from MG132 treated HEK293T cells were separated into soluble and insoluble fractions using ultracentrifugation. As there are only 2 protein degradation system in a mammalian cell; UPS and autophagy, when MG132 treatment is introduced it is expected that it would direct all proteins (both soluble and insoluble) towards autophagy due to the inhibition of UPS. Furthermore, it is expected that the excess soluble ubiquitinated protein may aggregate into insoluble aggregates that can be eliminated by aggrephagy. In the presence of bafilomycin treatment that ultimately blocks the clearance of

ubiquitinated proteins via autophagy, the amount of ubiquitinated insoluble protein that is cleared out by aggrephagy accumulates and can be quantified.

Triton is a mild detergent that extracts soluble cellular proteins to generate the soluble fraction. Proteins that were not soluble in Triton were then extracted using 2% SDS to produce the insoluble fraction. The ubiquitin levels of each were then analysed by immunoblotting, and the absence of GAPDH (which should normally be soluble) in the insoluble fraction indicated that the fractionation was successful. Inhibition of the UPS by MG132 significantly increased the levels of soluble ubiquitin as expected ($p<0.0001$) **(Figure 5.1.D)**. Inhibition of autophagosome degradation via bafilomycin treatment resulted in a significant increase in the levels of soluble ubiquitin in the absence of MG132 ($p=0.03$). This represents the amount of soluble ubiquitin that is degraded by autophagy in a 4 hr period, suggesting that autophagy degrades a small portion of soluble proteins as expected, following MG132 treatment (**Figure 5.1D** soluble fraction, 1st vs 3rd column). Bafilomycin treatment however did not increase the soluble ubiquitin levels in UPS inhibited cells. This was not expected, because UPS is the major proteolytic system that degrades soluble proteins; hence it may mask the smaller effects arising from blocked autophagy.

In contrast, MG132 treatment alone did not increase insoluble ubiquitin levels (**Figure 5.1D** insoluble fraction, 1st vs 2nd column). Upon bafilomycin treatment in DMSO control cells, insoluble ubiquitin significantly accumulated as expected ($p=0.0021$) (**Figure 5.1D** insoluble fraction, 1st vs 3rd column), because autophagy is primarily responsible for the clearance of insoluble (ubiquitinated) proteins. Interestingly, bafilomycin treatment also significantly increased the levels of insoluble ubiquitin in MG1232 treated cells ($p=0.002$) (**Figure 5.1D** insoluble fraction, 2nd vs 4th column), suggesting that in the absence of a functional UPS, autophagy takes over and eliminates the insoluble ubiquitin, consistent with induction of aggrephagy. Furthermore, the activation of autophagy is so efficient that in the absence of bafilomycin, the increase in insoluble ubiquitin could not be detected as mentioned above (**Figure 5.1D** insoluble fraction, 1st vs 2nd column). This is consistent with previous evidence [658] showing that following MG132 treatment, autophagy is induced to eliminate insoluble ubiquitin. Hence, these data overall demonstrate that MG132 treatment induces degradation of

ubiquitin in HEK293T cells, although this may not be via increased autophagosome formation, as seen on the LC3-II blots. This result however indicates that proteins are targeted towards autophagy when the UPS is inhibited by MG132, and it therefore establishes the conditions to use in experiments to examine protein degradation by autophagy, which in the case of ubiquitinated aggregates, involves aggrephagy. Furthermore, these data imply that NDP52, and possibly p62, are recruited to autophagosomes when the UPS is inhibited, while TBK1 is not. Autophagy receptors (p62, NDP52) may therefore take part in cargo tethering, while TBK1 is not located to autophagosomes, as was observed previously in basal and starvation-induced autophagy.


A
MG132
Bafilomycin A1
84kDa
52kDa
62kDa
19kDa
17kDa
37kDa
TBK1
NDP52
p62
LC3-I
LC3-II
GAPDH
LC3-I
LC3-II
NDP52
p62
TBK1
DMSO
1uM
MG132
DMSO/BafA1
1uM/BafA1
MG132/BafA1
B
MG132
p-TBK1 (Ser172)
Phosphorylated TBK1 (S172)
S172-TBK1/total TBK1
C
MG132/Saponin
MG132/BafA1/Saponin
EGFP
mCherry
LC3-II-EGFP (post-saponin)
% of EGFP positive cells

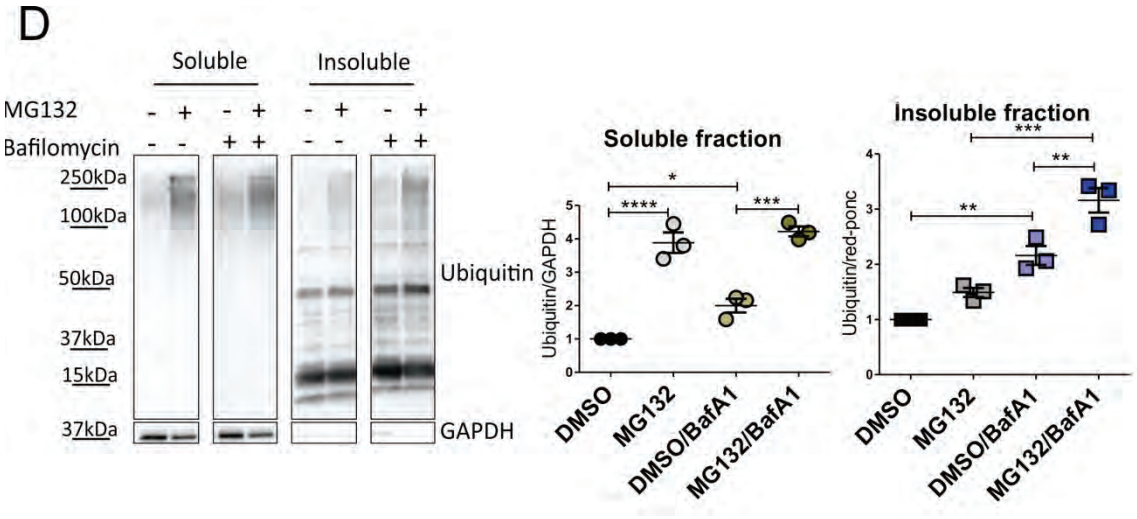


Figure 5.1. MG132 induces the degradation of insoluble ubiquitin via autophagy and not the formation of autophagosomes. (A) *Autophagosome formation is not elevated by MG132 treatment.* HEK293T cells were treated with 1 μM of MG132 for 20 hr, followed by 4 hr 100 nM bafilomycin treatment. Cells were then lysed and separated on SDS-PAGE. Representative immunoblots and quantifications are shown. N≥3+/-SEM, unpaired t-test, *<0.05, **<0.005. **(B)** *TBK1 undergoes phosphorylation upon MG132 treatment*. Representative immunoblots and quantifications are shown. N=3+/-SEM, unpaired t-test, ***<0.0005. **(C)** *Autophagosome formation is ongoing during MG132 treatment.* The percentage of $EGFP^+$ cells was analysed after saponin treatment. Representative images of FC analysis are shown. Increasing EGFP signal along the y axis and increasing mCherry signal along the x axis are shown. Q1: $EGFP^+/mCherry^-$, Q2: $EGFP^+/mCherry^+$, Q3: $EGFP^-/mCherry^-$, Q4: $EGFP^-/mCherry^+$. N=3+/-SEM, unpaired t-test, *<0.05. **(D)** *Autophagy degrades insoluble ubiquitin, consistent with aggrephagy.* Representative blots and quantifications are shown. N=3+/- SEM, one-way ANOVA with Tukey post-hoc test, *<0.05, **<0.005, ***<0.0005, ****<0.00005 (Full blot is presented in **Figure 5.15**)

5.4.2 TBK1 inhibition by MRT67307 impedes autophagosome formation following MG132 treatment

Evidence was previously provided that the kinase activity of TBK1 may be involved in autophagosome formation and degradation during basal autophagy (Chapter

3), and this may be mediated by its dysfunctional interaction with autophagy adaptors (Chapter 4). Hence, next it was examined whether TBK1 is involved in aggrephagy, MG132 was used to block the UPS and therefore direct proteins targeted for degradation towards autophagy, while simultaneously inhibiting TBK1 kinase activity using BX795, or MRT67307.

First, autophagy was analysed via flow cytometry in MG132-treated cells. Cells were transfected with LC3-EGFP-mCherry, treated with saponin and FC analysis was performed. BX795 treatment did not alter the ratio of $EGFP^+/mCherry^+$- $EGFP^-/mCherry^+$ in MG132 treated HEK293T cells **(Figure 5.2A/B)**, indicating that BX795 did not affect autophagosome-lysosome fusion. In contrast, MRT67307 treatment significantly increased the ratio of $EGFP^+/mCherry^+$ compared to H_2O control alone ($p<0.0001$) (**Figure 5.2B/C**, red square), while upon bafilomycin treatment TBK1 inhibition using MRT67307 did not alter the proportion of $EGFP^+/mCherry^+$ cells (**Figure 5.2C**, green square). This indicates that MRT67307 treatment blocked autophagosome-autolysosome fusion under conditions used to induce MG132 induced autophagy, including aggrephagy. Hence in summary, MRT67307 but not BX795 treatment, inhibited autophagosome-lysosome fusion.

To further analyse the effects of TBK1 inhibition on aggrephagy, immunoblotting was performed. The levels of LC3-I did not significantly change upon BX795 treatment with or without bafilomycin (**Figure 5.2F)**. Similarly, no changes were detected in LC3-II levels upon BX795 inhibition **(Figure 5.2G)**. MRT67307 treatment did not affect LC3-I **(Figure 5.2I)** but significantly less LC3-II accumulated upon bafilomycin treatment in MRT67307 inhibited cells compared to H_2O control cells treated with bafilomycin **(Figure 5.2J)**. This result suggests that MRT63307 treatment inhibited the formation of autophagosomes. Due to the contradictory results obtained between the two inhibitors, the role of TBK1's kinase activity in MG132 induced autophagy cannot be conclusively determined. However, as mentioned before MRT67307 is a more potent inhibitor of TBK1, therefore the elevated effects in MRT67307 treated conditions suggest that TBK1 may have role in aggrephagy.

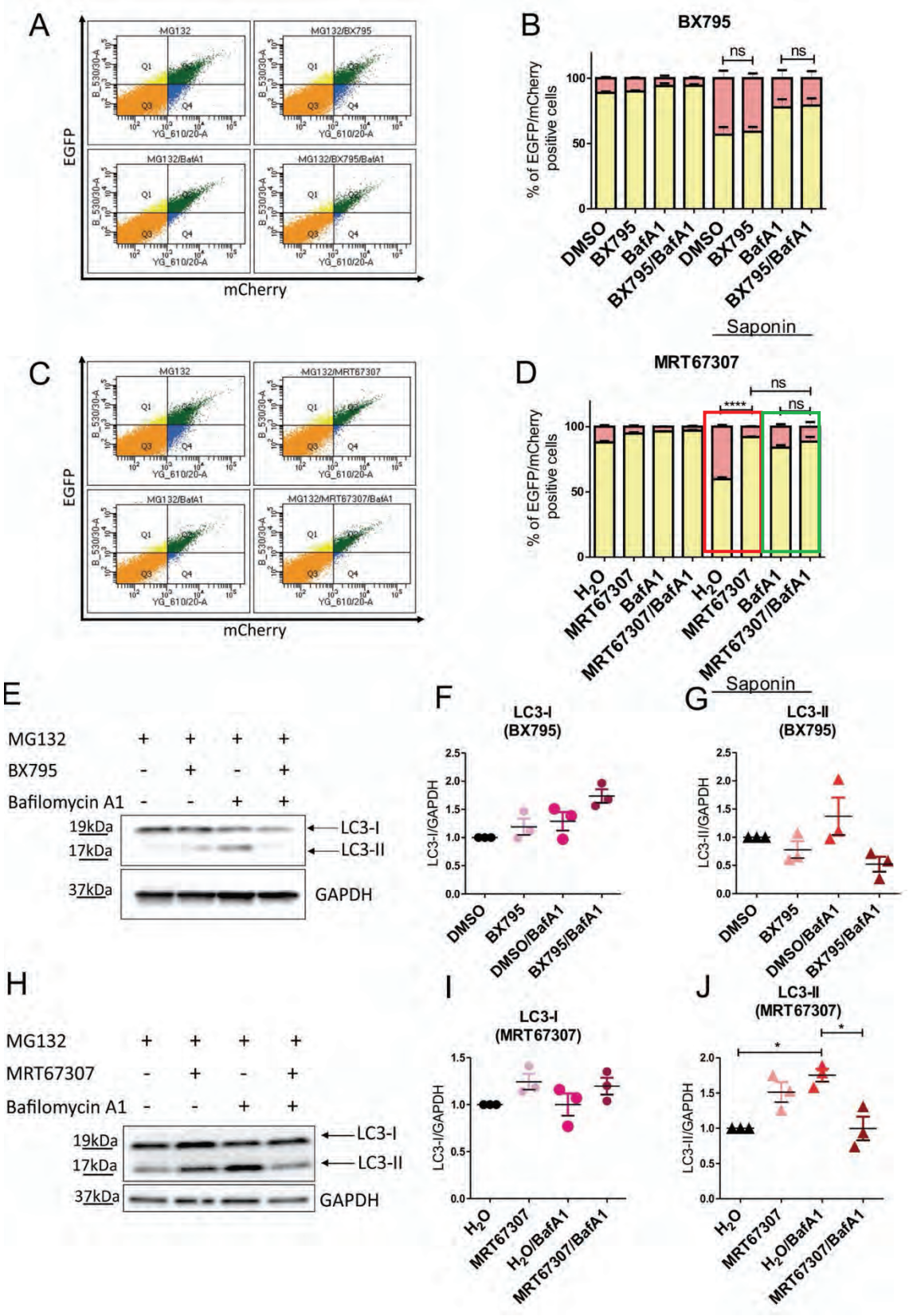


Figure 5.2. MRT67307 inhibits autophagosome formation and maturation during MG132 induced autophagy. (A-F) *MRT67307 abrogates autophagosome lysosome*

fusion. HEK293T cells were transfected with LC3-EGFP/mCherry and treated with MG132 (1 μM) in the presence or absence of BX795 (1 μM) or MRT67307 (25 nM) for 20 hr then supplemented with 100 nM bafilomycin for additional 4 hr. Representative images of FC analysis are shown **(A/C)**. Increasing EGFP signal along the y axis and increasing mCherry signal along the x axis is shown. Q1: $EGFP^+/mCherry^-$, Q2: $EGFP^+/mCherry^+$, Q3: $EGFP^-/mCherry^-$, Q4: $EGFP^-/mCherry^+$. The ratio of the $EGFP^+/mCherry^+$- $EGFP^-/mCherry^+$ cells **(B/D)** were analysed. N=3+/-SEM, one-way ANOVA with Tukey post-hoc test, ****<0.0001. **(G-L)** *MRT67307 treatment inhibits autophagosome formation.* HEK293T cells were treated with MG132 (1 μM) in the presence or absence of BX795 (1 μM) or MRT67307 (25 nM) for 20 hr then supplemented with 100 nM bafilomycin for additional 4 hr followed by immunoblotting for LC3-I, LC3-II and GAPDH. Band intensity was quantified using ImageJ and normalised to internal loading control, GAPDH. Relative expression levels are shown by quantification. N=3+/-SEM, one-way ANOVA with Tukey post-hoc test, **<0.005.

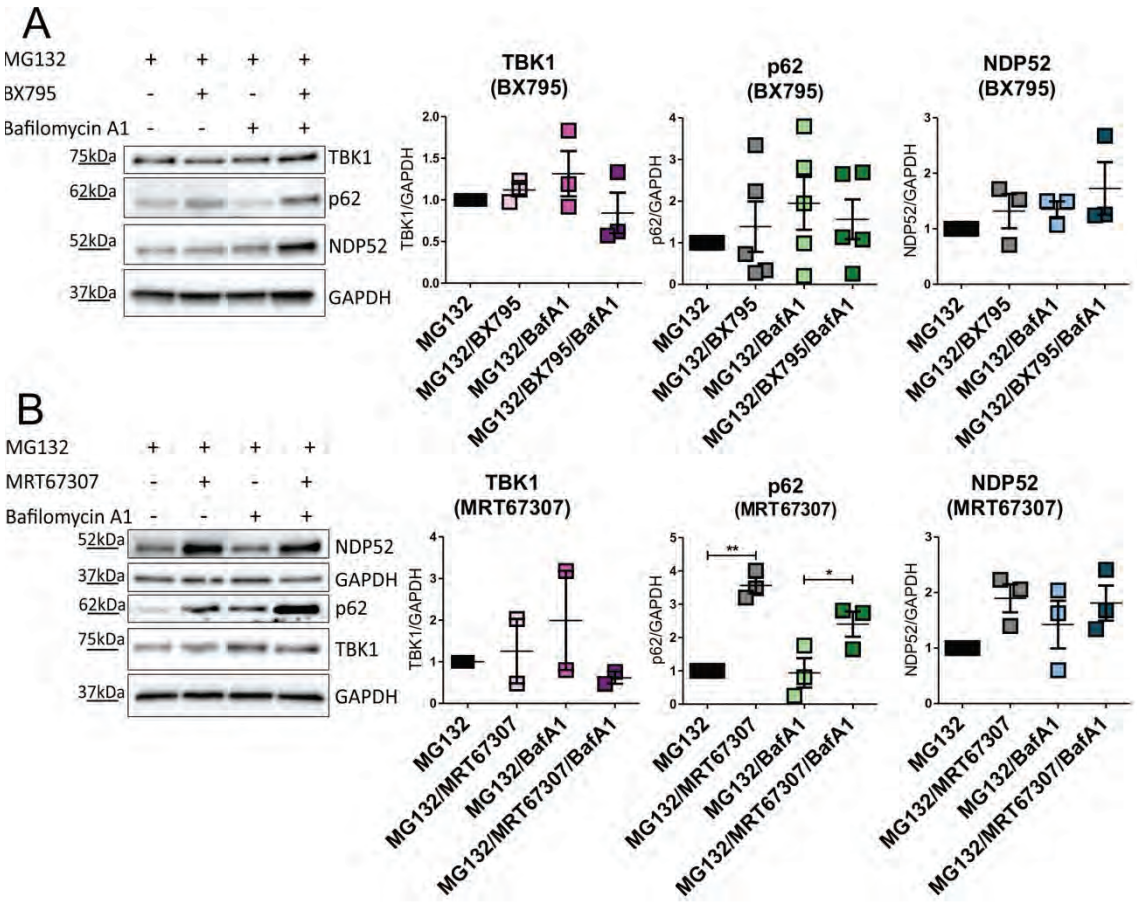
5.4.3 TBK1 inhibition by MRT67307 impairs p62 degradation upon MG132 treatment

As the Klionsky guidelines recommend that the levels of autophagy receptors should be analysed to obtain a comprehensive overview of autophagy [464], immunoblotting was performed to examine the levels of autophagy receptors and TBK1 upon MG132 treatment and TBK1 inhibition; which as described above were designed to monitor aggrephagy. Optineurin was not examined in these experiments due to its low level of expression. Interestingly, the levels of TBK1 did not change under these conditions using either BX795 or MRT67307 **(Figure 5.3A/B)**. Previously it was demonstrated that during starvation-induced autophagy (Chapter 4, **Figure 4.5**), inhibition of TBK1 led to decreased levels of its expression, which was assumed to be due to its enhanced degradation via UPS. Hence, these data imply that TBK1 is degraded by the UPS upon inhibition of its kinase activity.

BX795 treatment did not significantly affect the expression levels of NDP52 or p62. In contrast, following administration of MRT67307, the levels of p62 significantly increased (p=0.0018) **(Figure 5.3B)**. Furthermore, the levels of p62 showed an increased

trend when bafilomycin was administered (p=0.04), suggesting that p62 accumulates, possibly due to inhibition of autophagosome degradation as previously demonstrated **(Figure 5.2)**. The levels of NDP52 displayed a much more moderate change upon MRT67307 treatment and did not reach significance, indicating that p62 is more affected by TBK1 inhibition than NDP52.

These data therefore confirm that TBK1 inhibition by BX795 does not affect MG132 induced autophagy **(Figure 5.3A)**, whereas the change in expression of autophagy receptors upon MRT67307 treatment suggests perturbation of autophagosome-lysosome fusion, as shown previously **(5.3B)**. Therefore, these findings were consistent with the previous data collected via FC. However, given the conflicting findings obtained using BX795 and MRT67307, these data still cannot conclusively demonstrate that TBK1 kinase activity is involved in MG132 induced autophagy.

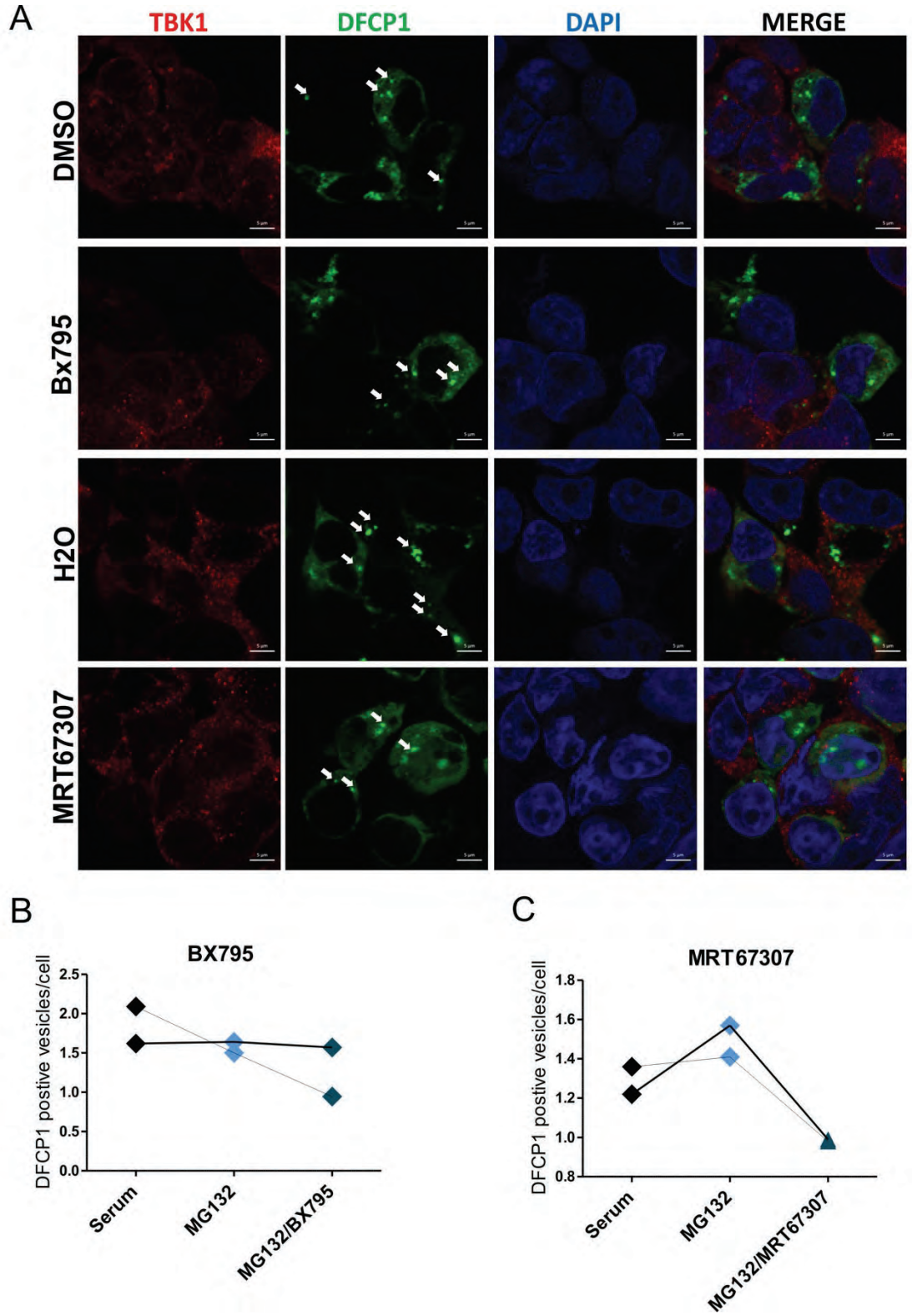


5.3. p62 accumulates following MRT67307 treatment during MG132 induced autophagy. HEK293T cells were treated with MG132 (1 μM) in the presence/absence of

BX795 (1 μM) **(A)** or MRT67307 (25 nM) **(B)** for 20 hr, then supplemented with 100 nM bafilomycin for additional 4 hr, followed by immunoblotting for TBK1, p62, NDP52 and GAPDH. Representative blots are shown. Band intensity was quantified using ImageJ and normalised to internal loading control, GAPDH. Relative expression levels are shown by quantification. N=3+/-SEM, one-way ANOVA with Tukey post-hoc test, *<0.05, **<0.005.

5.4.4 TBK1 inhibition by MRT67307 inhibits omegasome formation during MG132 induced autophagy

Next, omegasome formation was examined upon MG132 induced autophagy in cells transfected with DFCP1-EGFP and treated as above, using confocal microscopy. Omegasome formation was not induced by MG132 treatment **(5.4)**, consistent with its lack of effect on autophagosome formation **(5.1)**. Also, TBK1 did not localise to omegasomes following MG132 treatment. However, in contrast, MRT67307 treatment led to fewer omegasomes in the presence of MG132 **(5.4)**. As MRT67307 is known to be the more potent inhibitor of TBK1 [550], this finding implies that TBK1 kinase activity is involved in omegasome formation, although this must be interpreted with caution given that BX795 had no effect.



5.4. MRT67307 inhibits omegasome formation during MG132 induced autophagy. HEK293T cells expressing DFCP1-EGFP for 24 hr were treated with MG132 (1 μM) in the presence or absence of BX795 (1 μM) or MRT67307 (25 nM) followed by microscopy

analysis. DFCP1-EGFP puncta per cell were quantitated in transfected cells. Representative images and quantifications of DFCP1-EGFP puncta are shown. Scale: 5 μm.

5.4.5 Summary

These data provide some evidence that the TBK1 kinase activity is involved in aggrephagy, however, this cannot be conclusively confirmed. TBK1 inhibition by MRT67307 inhibited the formation of both the autophagosome and omegasome, and inhibited autophagosome-lysosome fusion, but these findings could not be replicated with BX795. Furthermore, as MG132 alone did not induce the formation of autophagosomes, but rather it enhanced the degradation of ubiquitin, therefore ubiquitin degradation was later analysed in regards to the involvement of TBK1 (section 5.9).

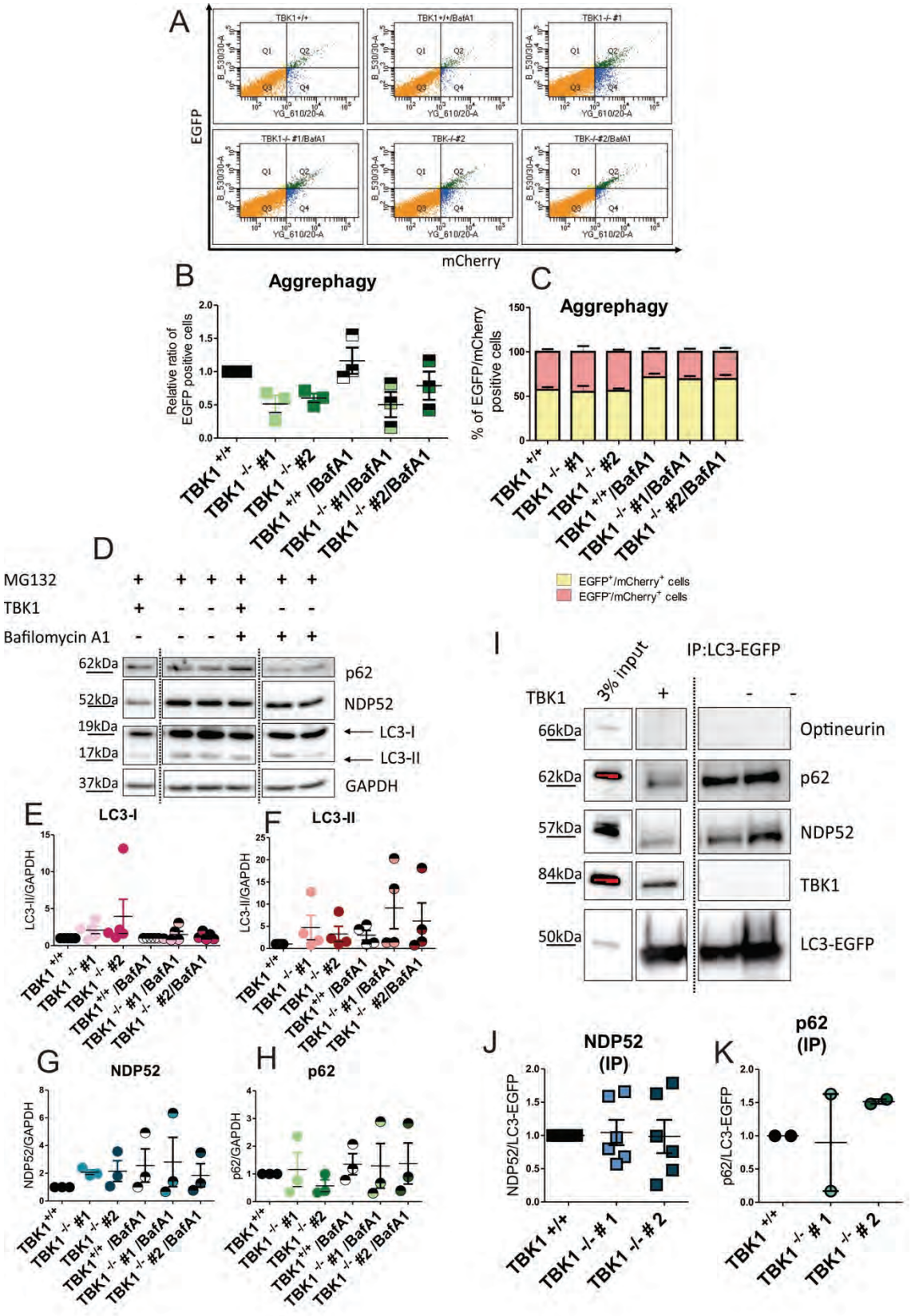
5.4.6 TBK1 knock-out does not affect autophagy upon UPS inhibition.

Previously (Chapter 3), TBK1 knock-out and TBK1 inhibition was shown to affect basal and starvation-induced autophagy differently. Hence it is also possible that knock-out of TBK1 may influence aggrephagy differently to inhibition of TBK1. Therefore, MG132 induced autophagy was induced in the previously generated CRISPR/cas9 clones and was subsequently followed by FC and immunoblotting.

Firstly, the formation of the autophagosome and its fusion with lysosome were followed via FC in cells expressing LC3-EGFP-mCherry. No differences were detected in the number of $EGFP^{+}$ cells in the CRISPR/Cas9 clones compared to TBK1 expressing cell population **(Figure 5.5B)** in the presence of MG132. Similarly, no change was detected upon bafilomycin treatment in TBK1 knock-out cells. Furthermore, the fusion of autophagosomes to autolysosomes was not significantly affected by TBK1 knock-out **(Figure 5.5C)**. Therefore, this indicates that knock-out of TBK1 does not affect MG132 induced autophagy.

Immunoblotting analysis was then performed to confirm these findings. There was no difference in the levels of LC3-II between $TBK1^{-/-}$ clones compared to $TBK1^{+/+}$ control cells in the presence of MG132 **(Figure 5.5F)**. Also, the levels of NDP52 and p62 did not show any changes in the absence of TBK1 **(Figure 5.5G/H)**. Next, the interactions between LC3 and autophagy receptors (NDP52, p62, optineurin) were analysed by immunoprecipitation using GFP trap. NDP52 and p62 immunoprecipitated with LC3 as shown previously during basal autophagy and non-selective autophagy, raising the possibility that p62 and NDP52 are involved in autophagosome formation during aggrephagy. However, there was no significant difference in the levels of NDP52 and p62 precipitated with LC3 in the CRISPR/Cas9 TBK1 knock-out clones compared to control cells **(Figure 5.5I/J/K)**.

The data presented in this section therefore suggest that knock-out n of TBK1 does not influence MG132 induced autophagy, indicative of aggrephagy, in HEK293T cells.



5.5. TBK1 knock-out does not affect MG132 induced autophagy. (A-C) *TBK1 knock-out does not affect autophagosome formation and degradation upon MG132 treatment.*

TBK1+/+ and TBK1-/-#1/#2 cells expressing LC3-EGFP-mCherry for 24 hr were treated with 1 μM MG132 for 20 hr and bafilomycin (100 nM) was administered for an additional 4 hr. Cells then were treated with saponin, fixed in 4% PFA and analysed via FC. Representative images of FC analysis are shown. Increasing EGFP signal along the y axis and increasing mCherry signal along the x axis is shown. Q1: $EGFP^{+}/mCherry^{-}$, Q2: $EGFP^{+}/mCherry^{+}$, Q3: $EGFP^{-}/mCherry^{-}$, Q4: $EGFP^{-}/mCherry^{+}$. The ratio of EGFP positive cells were analysed. N=3+/-SEM. **(D-H)** *TBK1 knock-out does not affect autophagy receptor and LC3 expression.* $TBK1^{+/+}$ and TBK1 $^{-/-}$ HEK293T cells were treated with MG132 (1 μM) for 20 hr, then supplemented with 100 nM bafilomycin for 4 hr. Cell lysates were separated on SDS-polyacrylamide gels and immunoblotting was performed. Representative blots are shown. Band intensity was quantified using ImageJ and normalised to internal loading control, GAPDH. Relative expression levels are shown by quantification. N=3+/-SEM**. (I-K)** *TBK1 knock-out does not affect LC3-autophagy receptor binding.* $TBK1^{+/+}$ and TBK1 $^{-/-}$ HEK293T cells were transfected with LC3-EGFP for 24 hr then treated with MG132 (1 μM) for 20 hr, and supplemented with 100 nM bafilomycin for additional 4 hr. Then cells were lysed and immunoprecipitation using GFP-trap was performed. Representative blots are shown. Band intensity was quantified using ImageJ and normalised to immunoprecipitated LC3-EGFP. Relative expression levels are shown by quantification. N>2+/-SEM, one-way ANOVA with Tukey post-hoc test.

5.4.7 Overexpression of TBK1 does not influence MG132 induced autophagy

The data obtained so far using the MRT67307 suggested that TBK1 may be involved in autophagosome formation and maturation following MG132 treatment to induce aggrephagy, although this finding could not be replicated with BX795. Next, overexpression of WT-TBK1 and the ALS-associated mutants were examined for their effect on MG132 induced autophagy, and hence whether dysfunctional aggrephagy was induced in TBK1-ALS.

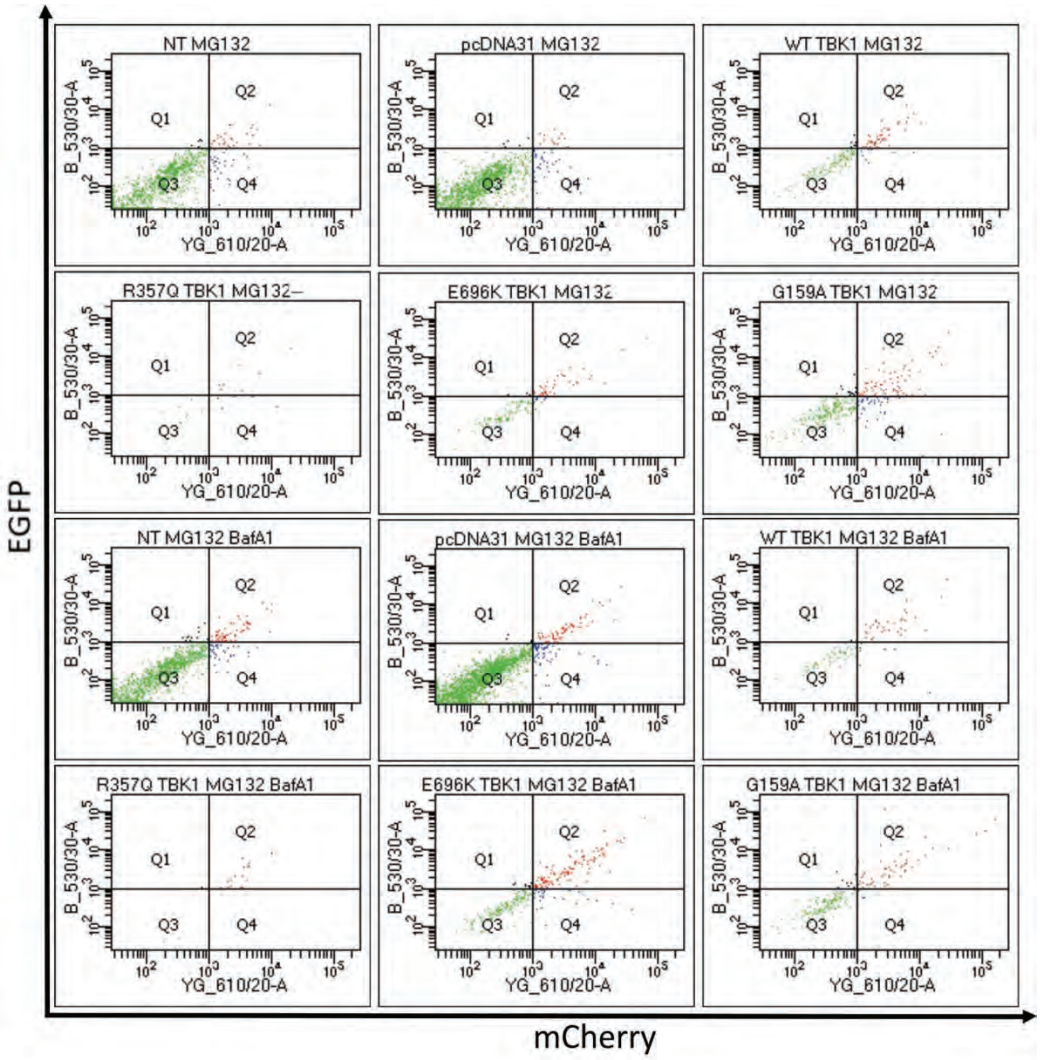
TBK1-FLAG proteins were co-expressed with LC3-EGFP-mCherry in the CRISPR/Cas9 $TBK1^{-/-}$ clone #2. The rationale for this was, as described previously, to

avoid the interference of endogenous TBK1. FC analysis was performed on cells that were positive for both TBK1 and LC3-EGFP-mCherry following treatment with saponin. However, no significant difference was detected in the ratio of $EGFP^+/mCherry^+$ cells upon overexpression of WT-TBK1 or any of the mutant-TBK1 compared to control cells (NT, pcDNA3.1) **(Figure 5.6)**, although an increasing trend was present upon TBK1-FLAG overexpression. Furthermore, the ratio of $EGFP^+/mCherry^+$ cells upon mutant TBK1 (R357Q, E696K, G159A) overexpression did not differ from WT-TBK1 expressing cells, indicating that ALS/FTD mutant TBK1 displays a similar effect as WT-TBK1. Bafilomycin treatment lead to increased proportions of autophagosome $EGFP^+/mCherry^+$ cells in pcDNA3.1 population as expected, confirming that the experiment had been performed correctly. TBK1-FLAG expressing cells did not show any significant differences compared to control cells following bafilomycin treatment. Similar to previous, the ALS/FTD mutants did not differ from WT-TBK1 expressing cells in the presence of bafilomycin. This data therefore indicates that overexpression of TBK1-FLAG did not affect MG132 induced autophagy. Furthermore, the ALS/FTD-TBK1 mutant expressing cells were no different to WT-TBK1 cells, implying that in ALS aggrephagy is not perturbed by mutant TBK1.

To further confirm the results obtained via FC, microscopy analysis was then carried out. Autophagosome formation was examined in cells expressing the LC3-EGFP overexpressing construct upon TBK1-FLAG overexpression by quantitating the numbers of LC3-EGFP vesicles. LC3-EGFP vesicles were identified in the cytoplasm as punctate structures and shown by white arrows **(Figure 5.7).** Overexpression of WT or mutant TBK1-FLAG did not affect the number of formed autophagosomes upon MG132 treatment in the presence or absence of bafilomycin. **(Figure 5.7)**. Therefore, this confirms the results obtained during FC analysis that overexpression of WT TBK1-FLAG or ALS mutants do not affect autophagosome formation and degradation during MG132 induced autophagy.

To further analyse whether ALS-mutant TBK1 may induce autophagy dysfunction via autophagosome formation, omegasome formation was analysed in cells overexpressing TBK1 conditions upon MG132 cells. There were no significant

differences in cells expressing WT-TBK1 or mutant TBK1 in omegasome formation, however a trend towards a decrease was detected in cells expressing R357Q-TBK1 **(Figure 5.8)**. Therefore, this data indicates that TBK1 is not involved in omegasome formation during MG132 induced autophagy, furthermore, ALS/FTD mutant TBK1 has a similar effect to WT-TBK1. The effect of R357Q-TBK1 on omegasome formation in MG132 cells should however be investigated in future studies.


NT MG132
pcDNA31 MG132
WT TBK1 MG132
R357Q TBK1 MG132
E696K TBK1 MG132
G159A TBK1 MG132
NT MG132 BafA1
pcDNA31 MG132 BafA1
WT TBK1 MG132 BafA1
R357Q TBK1 MG132 BafA1
E696K TBK1 MG132 BafA1
G159A TBK1 MG132 BafA1
Q1
Q2
Q3
Q4
B_530/30-A
YG_610/20-A
EGFP
mCherry

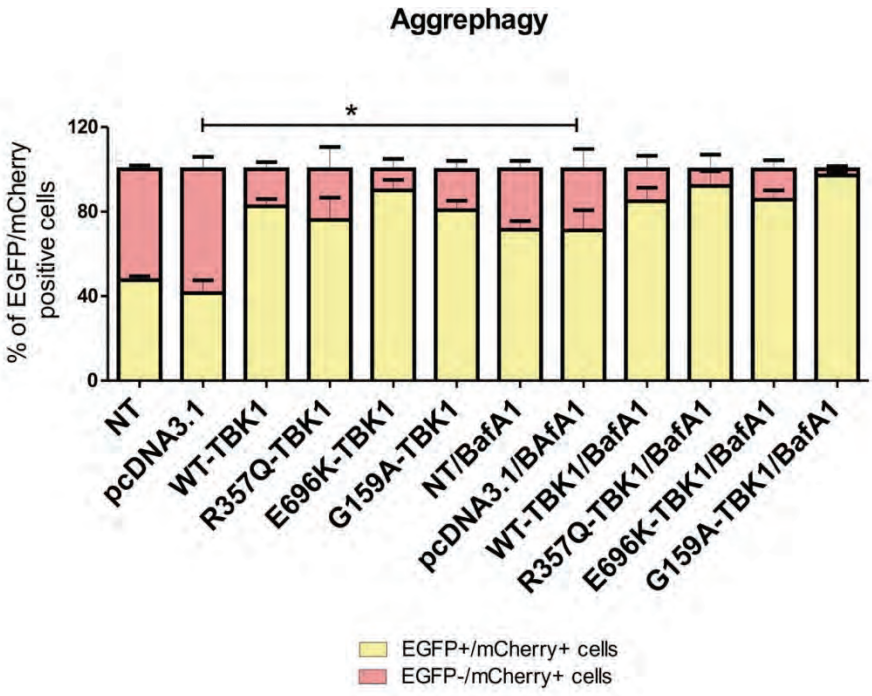
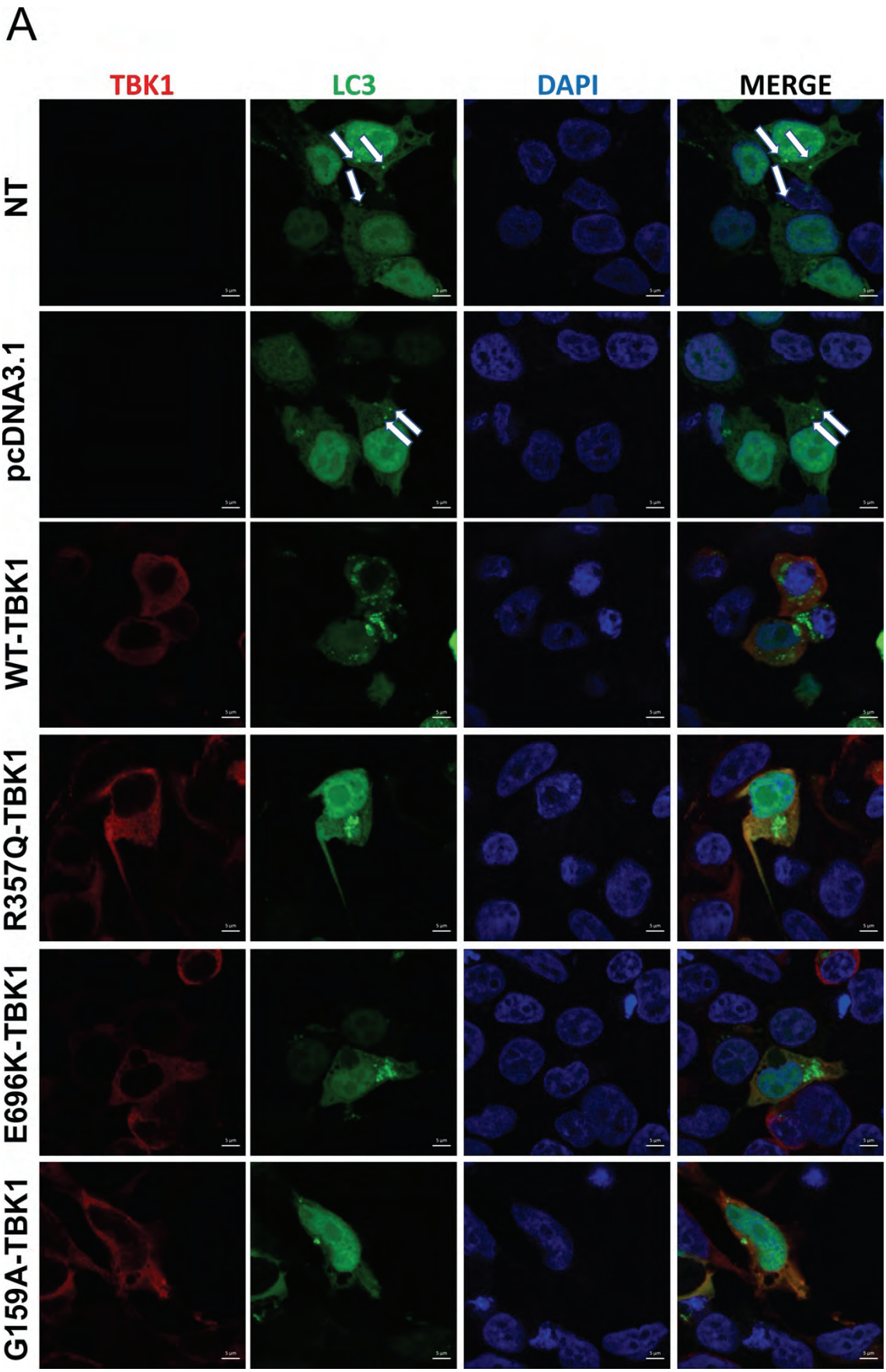
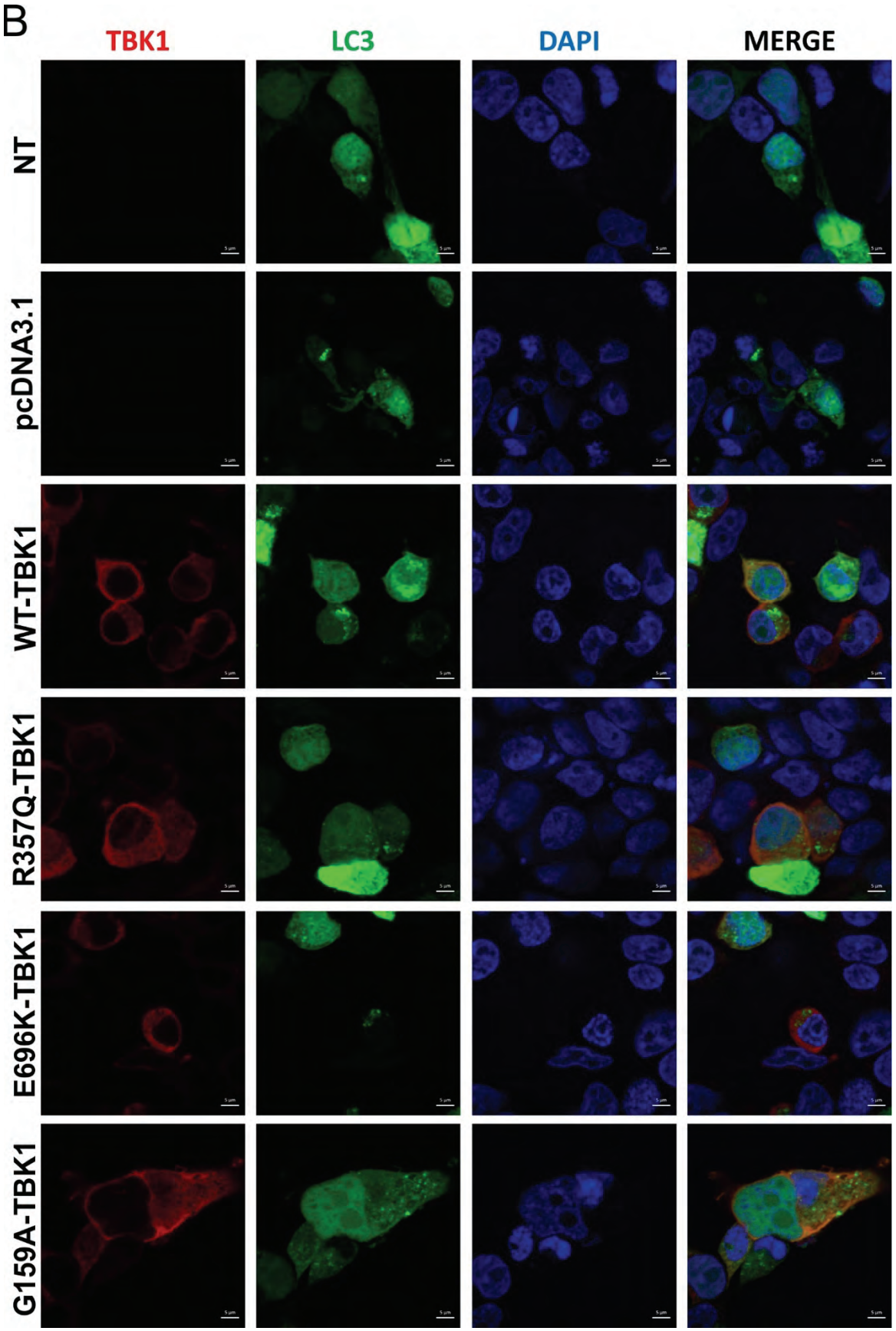

Aggrephagy
% of EGFP/mCherry positive cells
120
80
40
0
*
NT
pcDNA3.1
WT-TBK1
R357Q-TBK1
E696K-TBK1
G159A-TBK1
NT/BafA1
pcDNA3.1/BAfA1
WT-TBK1/BafA1
R357Q-TBK1/BafA1
E696K-TBK1/BafA1
G159A-TBK1/BafA1
EGFP+/mCherry+ cells
EGFP-/mCherry+ cells

Figure 5.6. TBK1-FLAG overexpression does not affect autophagosome lysosome fusion in MG132 induced autophagy. TBK1$^{-/-}$ #2 HEK293T cells co-expressing TBK1-FLAG proteins with LC3-EGFP-mCherry for 24h, were treated with MG132 (1 μM) for 24 hr, 100 nM bafilomycin for an additional 4 hr, then FC analysis was carried out. Representative images of FC analysis are shown. Increasing EGFP signal along the y axis and increasing mCherry signal along the x axis is shown. Q1: EGFP^{+}/mCherry^{-}, Q2: EGFP^{+}/mCherry^{+}, Q3: EGFP^{-}/mCherry^{-}, Q4: EGFP^{-}/mCherry^{+}. mCherry positive cells were gated and EGFP positive and negative subpopulation were graphed. N=3+/-SEM, one-way ANOVA with Tukey post-hoc test.


A
TBK1
LC3
DAPI
MERGE
NT
pcDNA3.1
WT-TBK1
R357Q-TBK1
E696K-TBK1
G159A-TBK1


B
TBK1
LC3
DAPI
MERGE
NT
pcDNA3.1
WT-TBK1
R357Q-TBK1
E696K-TBK1
G159A-TBK1

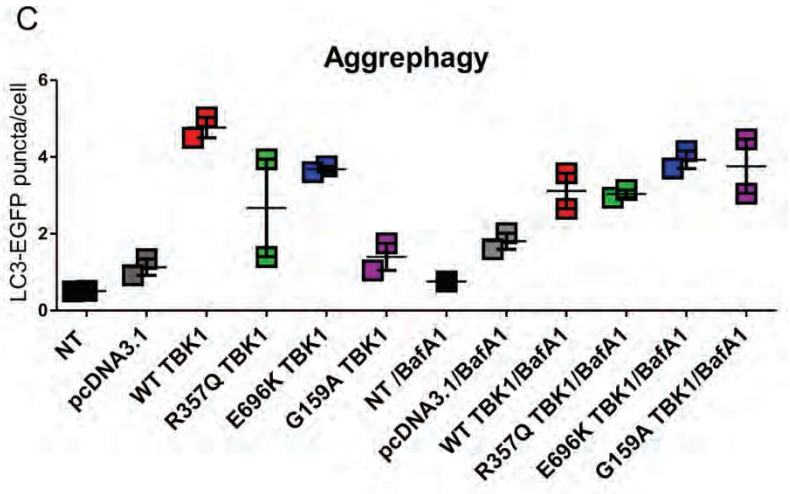
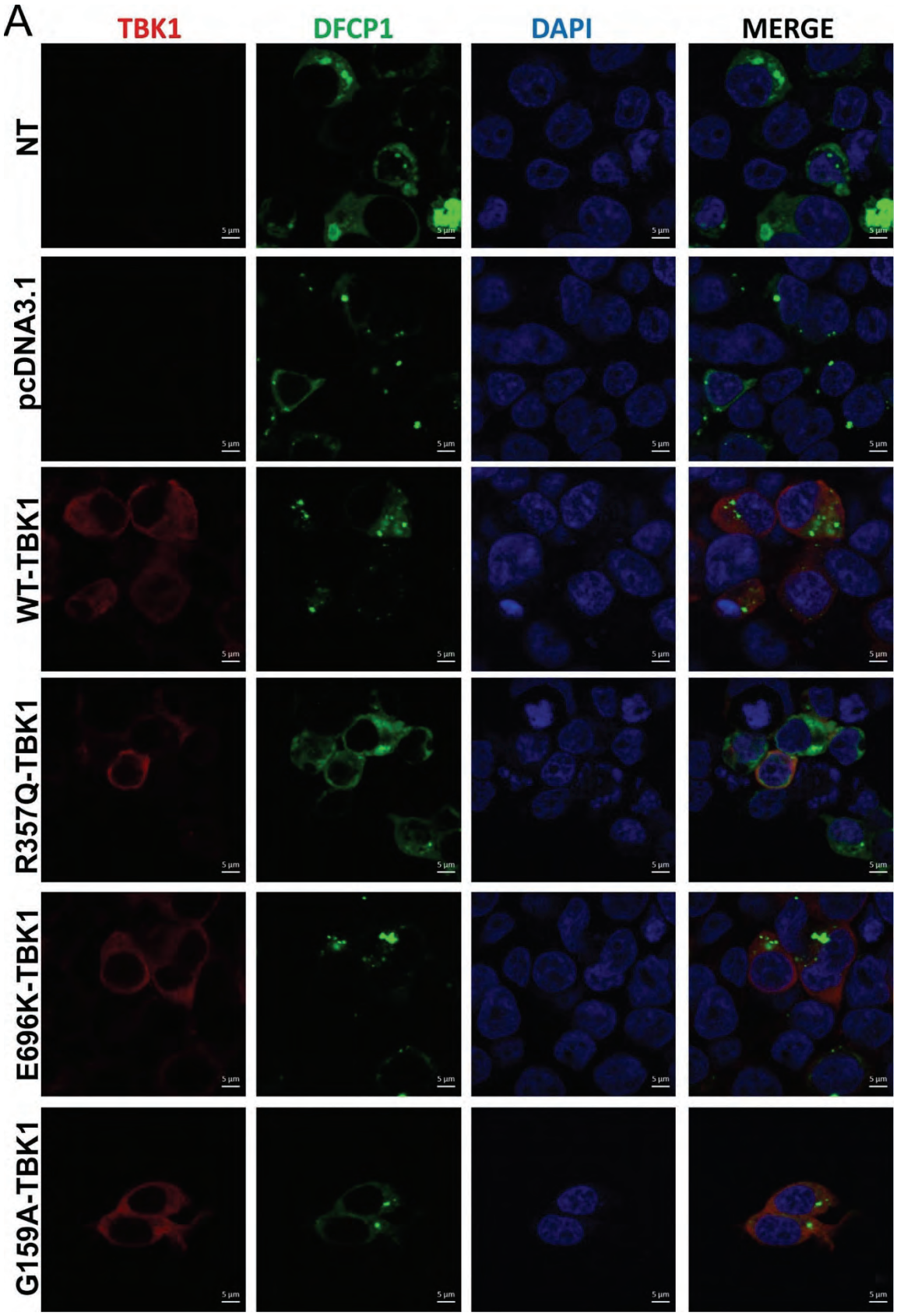


Figure 5.7. TBK1-FLAG overexpression does not affect autophagosome formation during MG132 treatment. TBK1$^{-/-}$ #2 HEK293T cells expressing TBK1-FLAG and LC3-EGFP for 24h were treated with MG132 (1 μM) for 24 hr, 100 nM bafilomycin for an additional 4 hr, then fixed and microscopy analysis was carried out. LC3-EGFP vesicles were quantitated in TBK1-FLAG overexpressing cells. Representative images and quantification of LC3-EGFP puncta/cell are shown. Scale: 5 μm.


A
TBK1
DFCP1
DAPI
MERGE
NT
pcDNA3.1
WT-TBK1
R357Q-TBK1
E696K-TBK1
G159A-TBK1
5 µm

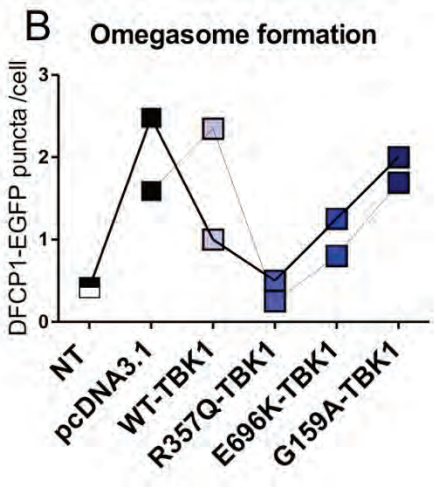


Figure 5.8. Omegasome formation is not affected by WT or mutant TBK1-FLAG overexpression in MG132 treated cells. TBK1 $^{-/-}$ #2 HEK293T cells co-expressing TBK1-FLAG proteins and DFCP1-EGFP for 24 hr, were treated with MG132 (1 μM) for 20 hr, then supplemented with 100 nM bafilomycin for an additional 4 hr. Immunocytochemistry for TBK1 was performed. DFCP1-EGFP puncta/cell were quantified in TBK1 expressing cells. Scale: 5 μm.

5.4.8 Summary

knock-out of TBK1 in CRISPR/Cas9 edited cells resulted in no difference in autophagosome formation or degradation. Furthermore, overexpression of WT or ALS-mutant TBK1 did not affect MG132 induced autophagy, as detected by two different techniques, or also on omegasome formation.

Together these findings suggest that TBK1 does not play a major role in MG132 induced autophagy. Nonetheless, it was previously shown that upon MG132 treatment, the degradation of insoluble ubiquitin was elevated showing that the clearance of ubiquitin is elevated during MG132 treatment rather than the formation of autophagosmsmes. Therefore, the effect of TBK1 inhibition and knock-out on the the degradation of ubiquitin was then examined.

5.4.9 TBK1 inhibition does not affect ubiquitin degradation

Recognition of cargo, as well as the formation and degradation of autophagosomes, is important for efficient autophagy. Analysing LC3 and the levels of autophagy receptors provides information about the formation and degradation of the autophagosome, but it does not reveal whether cargo is specifically engulfed in autophagosomes. Hence, next it was examined whether the degradation of cargo is affected by TBK1 during MG132 treatment. As the misfolded protein aggregates in ALS are ubiquitinated [660], monitoring ubiquitin can be therefore be used to assess the levels of these aggregates in the cell. Hence, ubiquitin levels were next analysed in cells treated with MG132 to induce aggrephagy.

First, ubiquitin levels were analysed by immunoblotting following inhibition of TBK1. HEK293T cells were treated with MG132 and either BX795 or MRT67307 as described previously. Firstly, the levels of total ubiquitin were examined by lysing whole cells in buffer containing 2% SDS, which solubilises all proteins. Overall, the levels of ubiquitin did not significantly change upon MG132 treatment, either in the presence or absence of TBK1 inhibitors. While a slight increase was detected in ubiquitin levels following administration of MG132, this did not reach statistical significance. Furthermore, neither BX795 nor MRT67307 treatment significantly altered ubiquitin expression **(Figure 5.9A/B)**. Furthermore 4 hr bafilomycin treatment did not increase the total levels of ubiquitin level either, suggesting that autophagy did not reduce the total cellular levels of ubiquitin. Moreover, TBK1 inhibition, using either BX795 or MRT67307, did not affect ubiquitin levels in HEK293T cells upon MG132 treatment. These data reveal that the total cellular ubiquitin levels do not change upon BX795 or MRT67307 treatment, and that induction of autophagy did not alter the ubiquitin levels.

This was initially unexpected, however the UPS and autophagy, degrade different fractions of ubiquitin [216] **(Figure 5.1)**. The UPS eliminates soluble proteins, while autophagy eliminates insoluble proteins [216]. Nonetheless, autophagy can also degrade long-lived soluble proteins. Therefore, it was hypothesised that examination of the soluble and insoluble cellular fractions separately may revealing different findings, providing a more precise overview of MG132 induced autophagy Fractionation

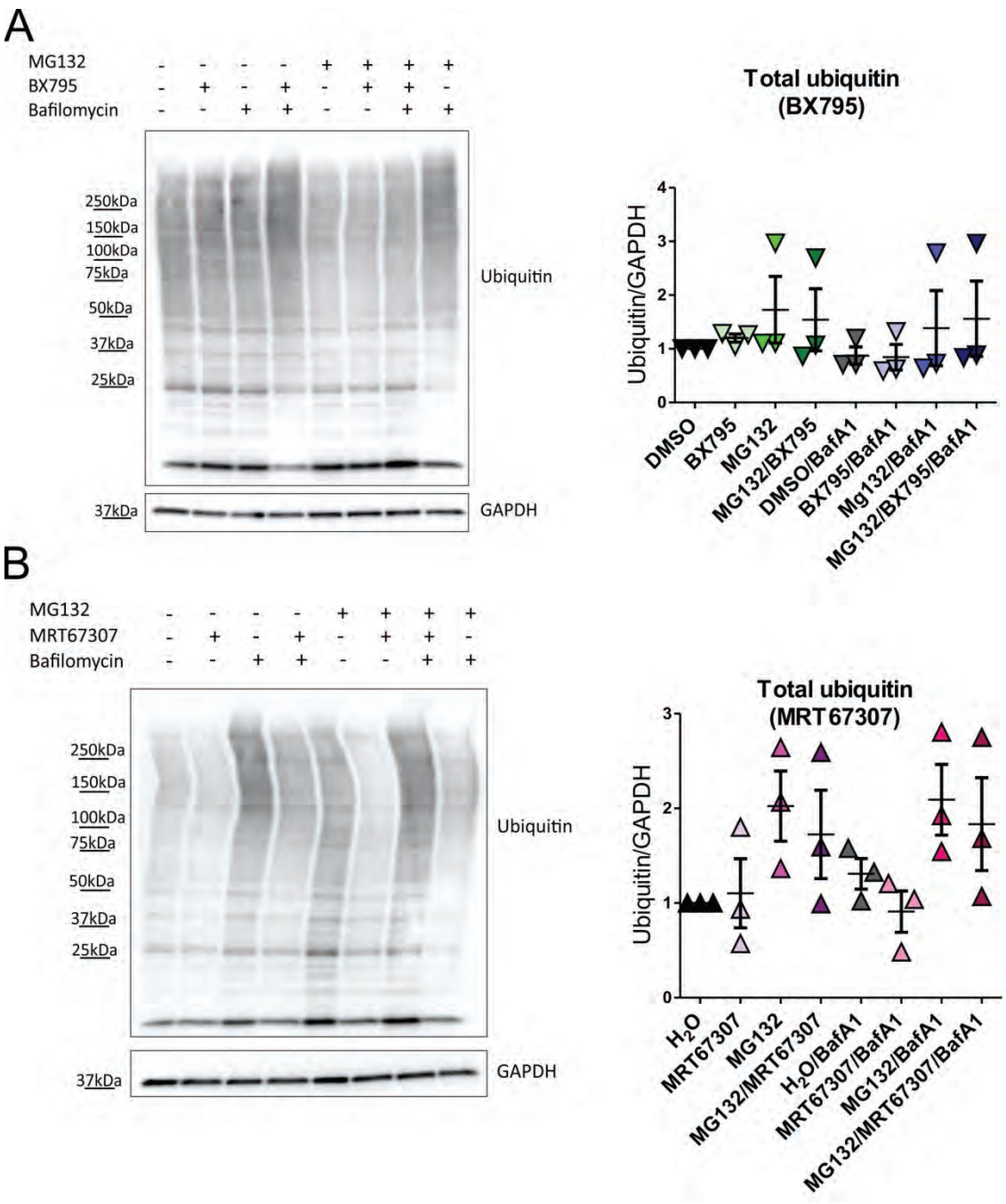
experiments were carried out using only one TBK1 inhibitor, BX795. Cells were therefore treated with BX795 with or without MG132 and bafilomycin as previous, then fractionation of cells into insoluble and soluble fractions was performed using ultracentrifugation. The cells lysates were subjected to two consecutive lysis processes in two different lysis buffers. The first buffer containing Triton extracts the soluble proteins, whereas the second buffer, containing 2% SDS, extracts the remaining insoluble proteins.

MG132 significantly increased ubiquitin levels in the soluble fraction by immunoblotting, similar to the results obtained above **(Figure 5.3./Figure 5.9C)**. However, BX795 treatment did not significantly affect the levels of soluble ubiquitin **(Figure 5.9C)**. Bafilomycin treatment increased the levels of soluble ubiquitin levels as previous, however BX795 treatment had no effect upon bafilomycin treatment, indicating that TBK1 inhibition did not affect the degradation of soluble ubiquitin. Next, the insoluble fraction was analysed by immunoblotting for ubiquitin. As described before MG132 treatment alone did not affect insoluble ubiquitin levels, however bafilomycin significantly increased the levels of insoluble ubiquitin, representing the amount of insoluble ubiquitin that is removed via autophagy.

Interestingly, administering BX795 alone did not increase the levels of insoluble ubiquitin, revealing that inhibition of TBK1 does not impair the clearance of insoluble ubiquitin. However, co-treatment with MG132 and BX795 significantly increased insoluble ubiquitin compared to both MG132 ($p=0.003$) and BX795 ($p=0.003$) only treated cells. This result implies that BX795 and MG132 treatment affects the clearance of insoluble ubiquitin and their effects may be additive.

However, in bafilomycin treated cell lysates, significantly more insoluble ubiquitin was detected when BX795 was administered compared to DMSO only ($p=0.0013$). There was also a trend towards more insoluble ubiquitin following MG132 treatment, although this did not quite reach statistical significance ($p=0.058$). However, bafilomycin treatment significantly elevated the insoluble ubiquitin levels in BX795 treated cells alone (**Figure 5.D**, 3rd vs 7th column), indicating that autophagy is actively eliminating insoluble ubiquitin, even in the TBK1 inhibited cells. Hence this result implies that inhibition of

the kinase activity of TBK1 does not impair the autophagic elimination of insoluble ubiquitin.



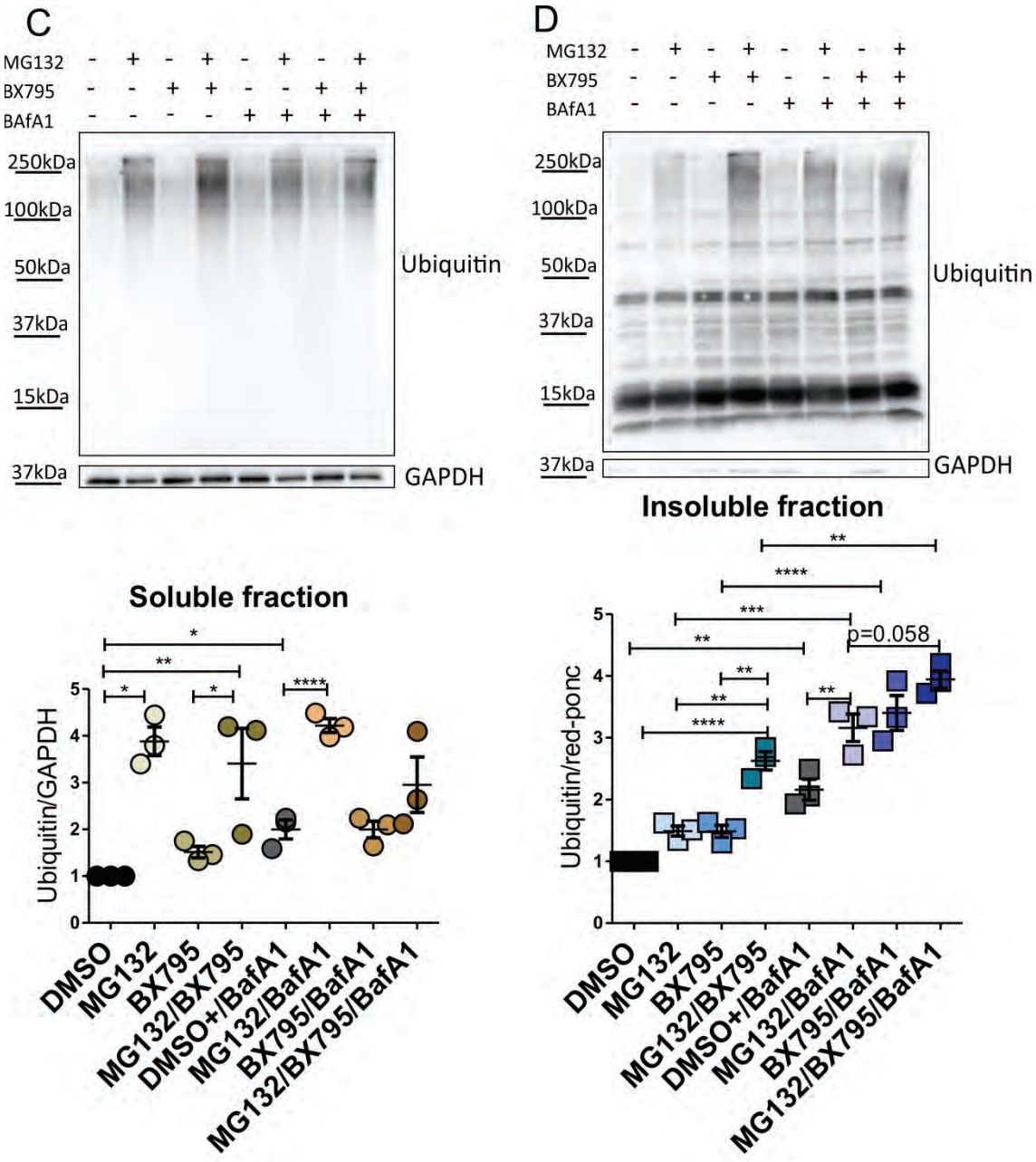


Figure 5.9. TBK1 inhibition using BX795 does not impair autophagic elimination of ubiquitin. HEK293T treated with MG132 (1 μM) and/or MRT67307 (25 nM) 20 hr and/or BX795 (1 μM), then supplemented with 100 nM bafilomycin for an additional 4 hr were immunoblotted for ubiquitin. Band intensity was quantified using ImageJ and normalised to internal loading control, GAPDH or red ponceaus staining. Relative expression levels are shown by quantification. N=3+/-SEM, one-way ANOVA with Tukey post-hoc test. *<0.05, **<0.005, ***<0.0005, ****<0.00005. **(A/B)** *TBK1 inhibition does not affect total ubiquitin levels upon MG132 treatment.* **(C-F)** *TBK1 inhibition does not affect ubiquitin degradation via autophagy.*

5.4.10 TBK1 knock-out elevates ubiquitin clearance

Next, the levels of ubiquitin were analysed in the CRISPR/Cas 9 TBK1 knock-out cells. Therefore, clones TBK1$^{-/-}$ (#1, #2) and wildtype HEK293 cells (TBK1$^{+/+}$) were treated with MG132 and fractionated into soluble and insoluble fractions. Upon MG132 treatment, significantly less soluble ubiquitin was detected using immunoblotting in both TBK1 knock-out clones **(Figure 5.10C)**. Similarly, both clones showed significantly less insoluble ubiquitin **(Figure 5.10C)**. Furthermore, upon bafilomycin treatment, more insoluble ubiquitin was detected in both TBK1 knock-out clones **(Figure 5.10D)**, while the levels of soluble ubiquitin did not change. Bafilomycin treatment inhibits the degradation of autophagosomes therefore the accumulation of ubiquitin represents the portion of ubiquitin that undergoes autophagic degradation in this time frame. In the absence of bafilomycin decreased levels of ubiquitin were detected **(Figure 5.10C),** similarly to LC3-II levels as explained in Figure 3.10 Sceanrio C, this may mean elevated degradation via autophagy or inhibited ubiquitin expression. However, upon bafilomycin treatment increased amount of ubiquitin accumulated indicating that in the absence of TBK1 the degradation of ubiquitin via autophagy were elevated and the amount of ubiquitin undergoing autophagic elimination are measured upon addition of bafilomycin. Therefore, this result suggests that in the absence of TBK1, more insoluble ubiquitin is removed via autophagy, implying that upon induction of aggrephagy, TBK1 negatively regulates the autophagic clearance of insoluble ubiquitin.

The total levels of ubiquitin were then examined in the CRISPR/Cas9 clones. Cells were treated with DMSO or MG132 for 20 hr followed by 4 hr treatment with bafilomycin, then cells were lysed in lysis buffer containing 2% SDS to extract the total ubiquitin (soluble+insoluble). In the absence of bafilomycin, no difference was detected in the total ubiquitin levels between TBK1 expressing and TBK1 knock-out cells, both in DMSO and MG132 treated cells (**Figure 5.11)**. Upon bafilomycin treatment, in the absence of MG132, there was a trend towards more total ubiquitin in the TBK1$^{-/-}$ clones compared to wildtype HEK293T cell. In contrast, in MG132 treated conditions, upon bafilomycin treatment, significantly more ubiquitin accumulated in TBK1$^{-/-}$ clone #2 compared to TBK1$^{+/+}$ cells under MG132 treatment, and there was a similar trend in the other clone, but this was not significant. This result indirectly suggests that more ubiquitin

is eliminated by autophagy in the absence of TBK1. This interesting finding therefore suggests that endogenous WT-TBK1 inhibits degradation of ubiquitin via autophagy.

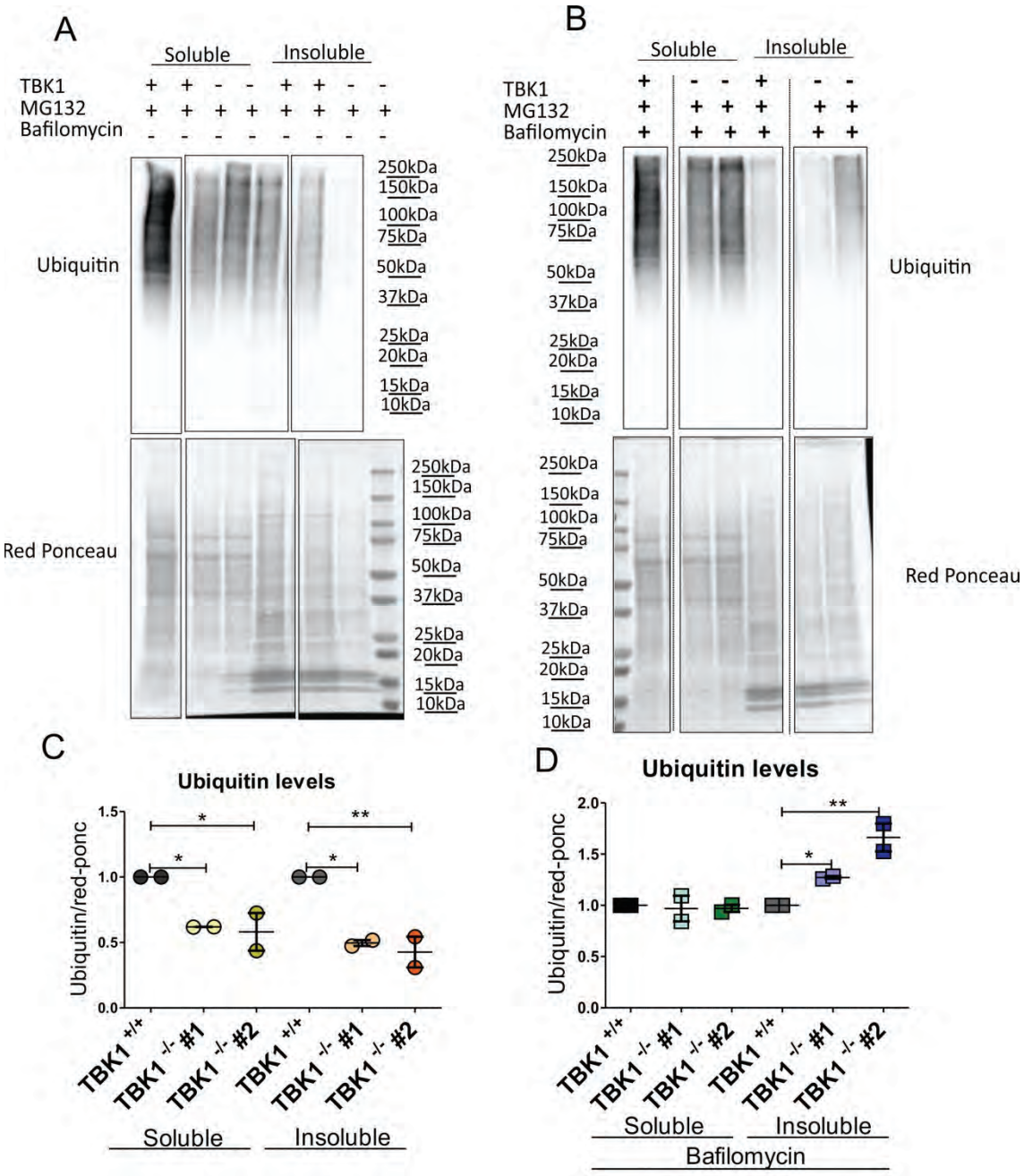


Figure 5.10. Less ubiquitin is present in CRISPR/Cas9 knock-out clones. TBK1$^{-/-}$ and TBK1$^{+/+}$ HEK293T cells were treated with MG132 (1 μM) for 20 hr, then supplemented with DMSO or 100 nM bafilomycin for an additional 4 hr. Cell lysates were fractionated into soluble and insoluble fractions using ultracentrifugation and immunoblotting using an anti-ubiquitin antibody was performed. Band intensity was quantified using ImageJ

and normalised to red ponceau staining. Representative blots are shown with **(B)** or without **(A)** bafilomycin A1 treatment. Relative expression levels are shown by quantification **(C/D).** Blots were cropped where line is to remove the 'control' clone. N=2+/-SEM, one-way ANOVA with Dunnett post-hoc test comparing to TBK1$^{+/+}$ cells, *<0.05, **<0.005.

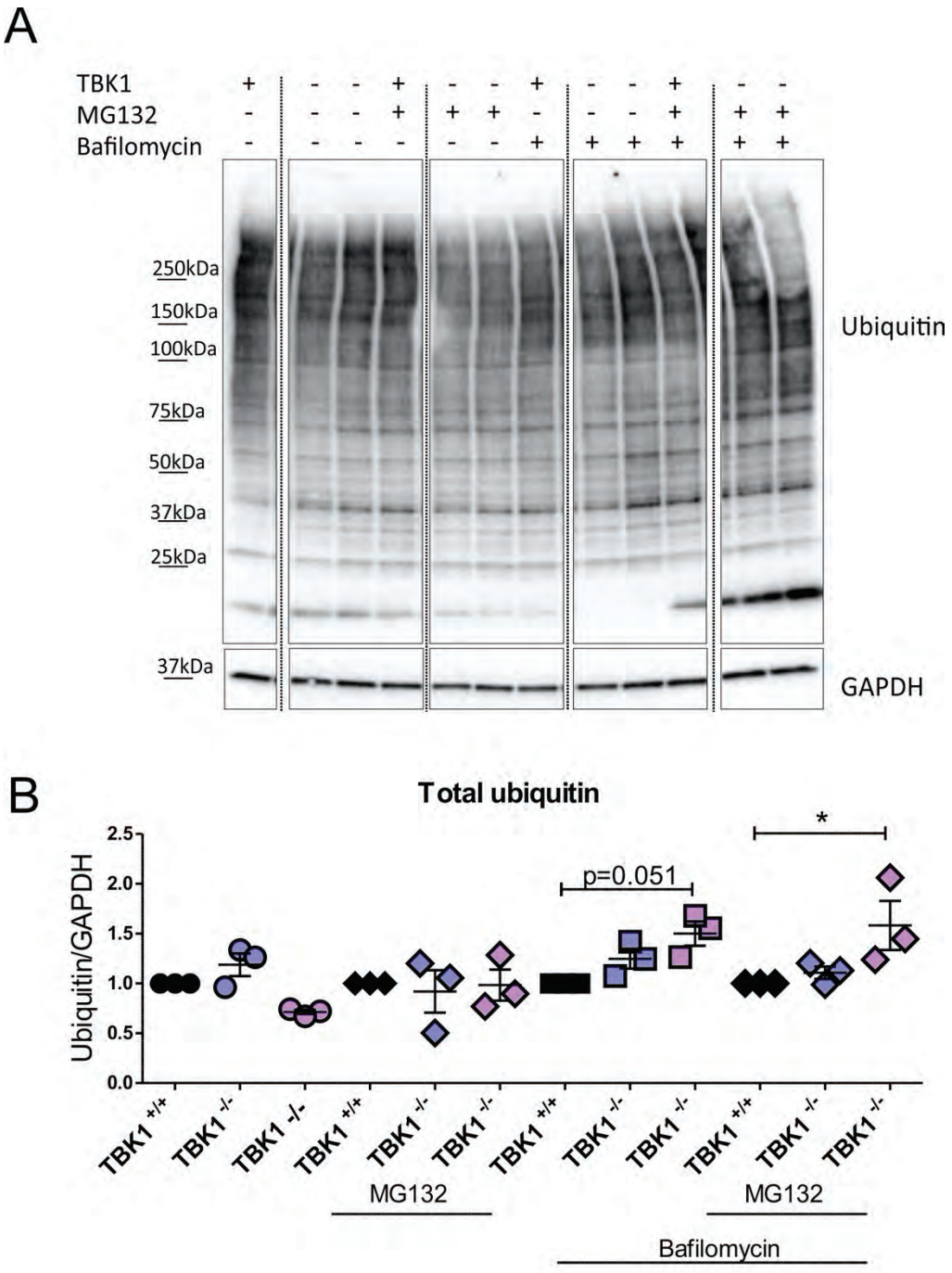


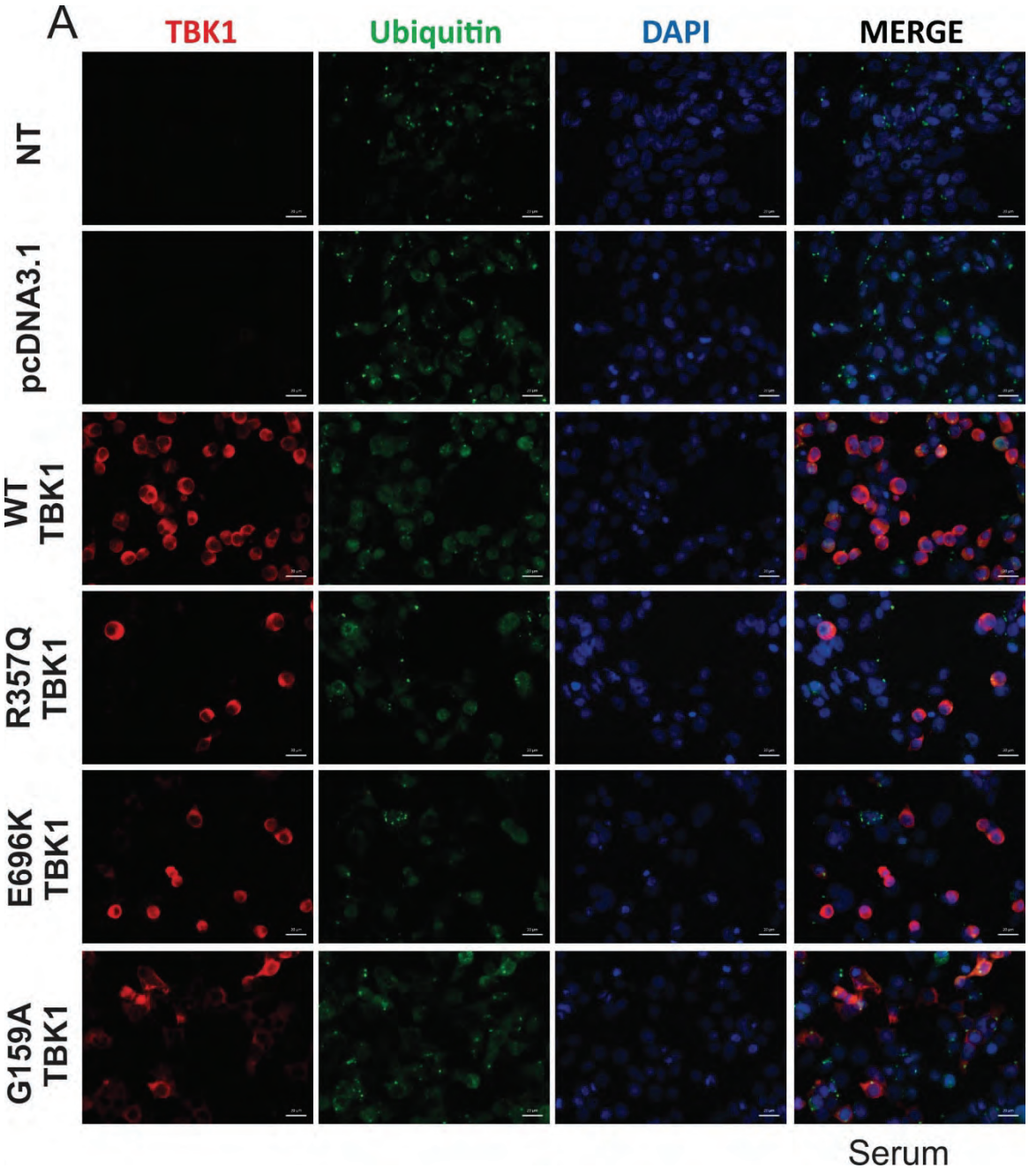
Figure 5.11. TBK1 knock-out enhances ubiquitin degradation via autophagy. TBK1$^{-/-}$ and TBK1$^{+/+}$ HEK293T cells were treated with DMSO or MG132 (1 μM) 20 hr, then supplemented with DMSO or 100 nM bafilomycin for an additional 4 hr. Immunoblotting of total cell lysates using an anti-ubiquitin antibody was performed to detect total cellular ubiquitin. Representative blot is shown **(A**). Band intensity was quantified using ImageJ and normalised to internal loading control, GAPDH. Relative expression levels are shown by quantification **(B).** N=3+/-SEM, one-way ANOVA with Dunnett post-hoc test comparing to TBK1$^{+/+}$ cells, *<0.05.

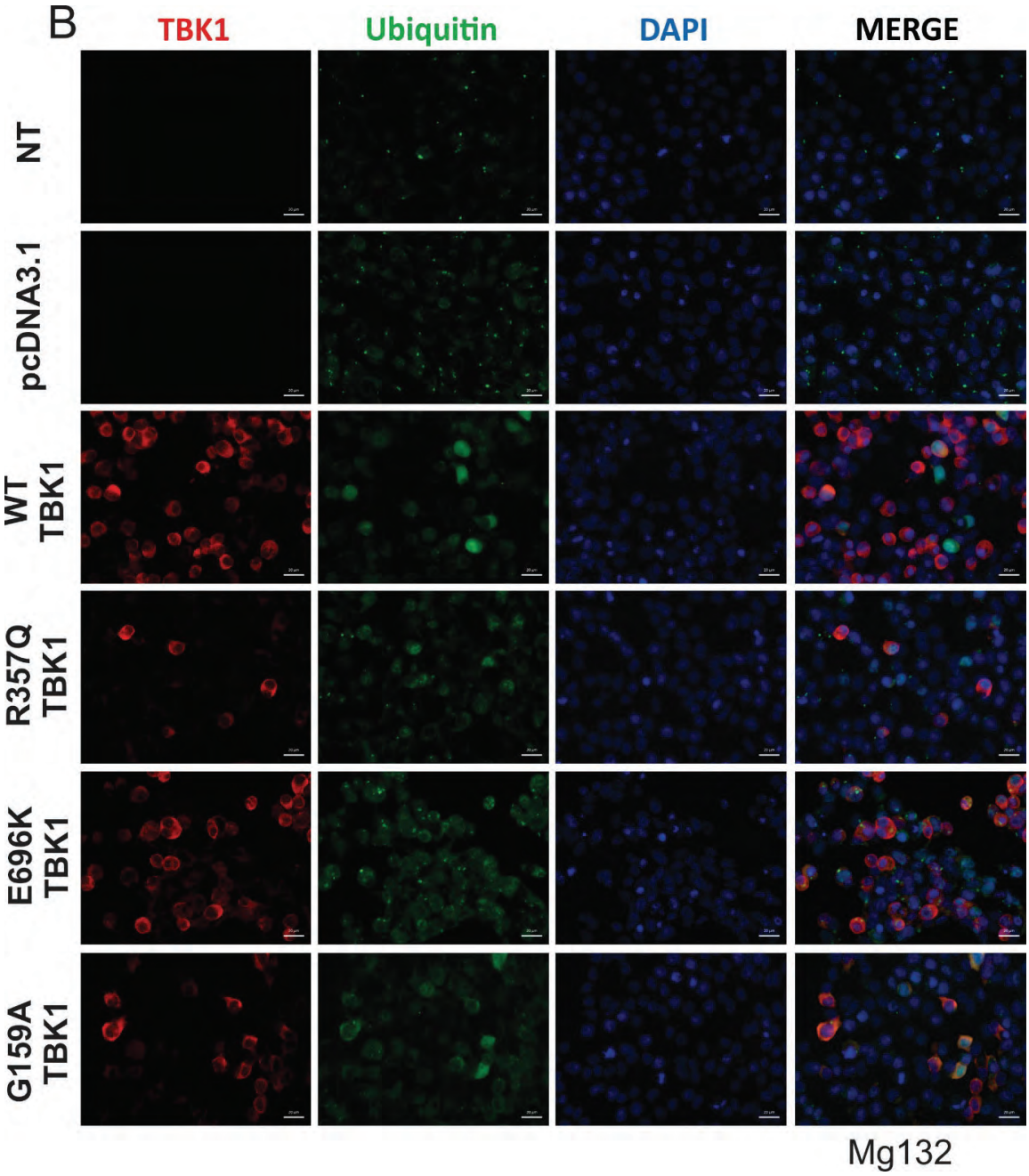
5.4.11 TBK1 overexpression elevates ubiquitin levels

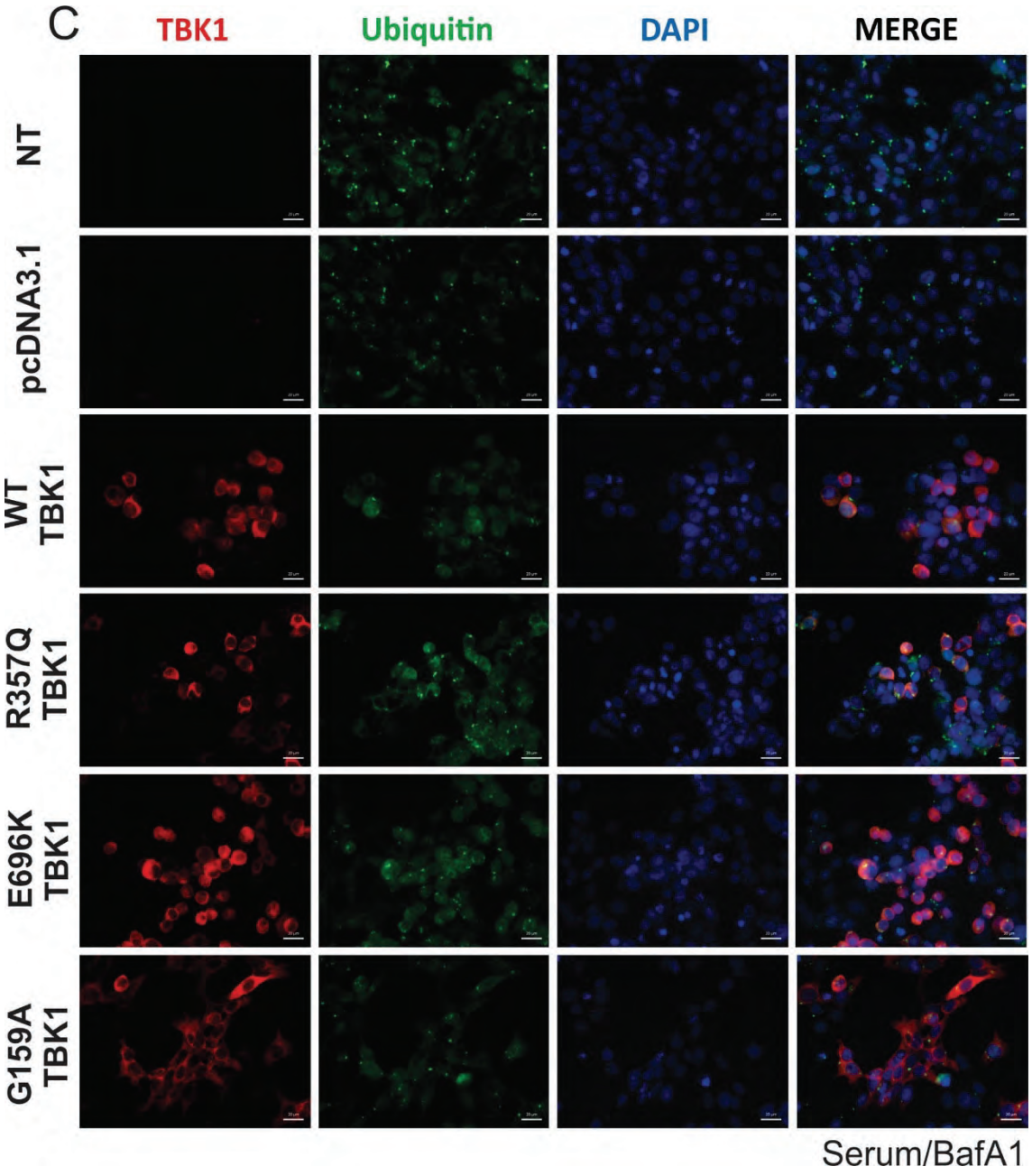
The relationship between TBK1 and ubiquitin was probed further by overexpressing WT TBK1 and ALS mutants. Due to the low transfection efficiency of the TBK1-FLAG plasmids, immunoblotting was not suitable to analyse autophagy in these experiments (data not shown). Hence, immunocytochemistry analysis was carried out. As above , the same approach was taken whereby TBK1 proteins were overexpressed in the CRISPR/Cas9 KO cells so that the results could be analysed without the background of endogenous TBK1. Hence clone TBK1$^{-/-}$ #2 HEK293T was transfected with TBK1-FLAG constructs for 24 hr, then the cells were treated with DMSO or MG132 for 20 hr, followed by an additional 4 hr treatment in the presence or absence of 100 nM bafilomycin. Immunocytochemistry using antibodies for ubiquitin and TBK1 was then performed. The overall fluorescence intensity of ubiquitin per cell was measured via ImageJ software.

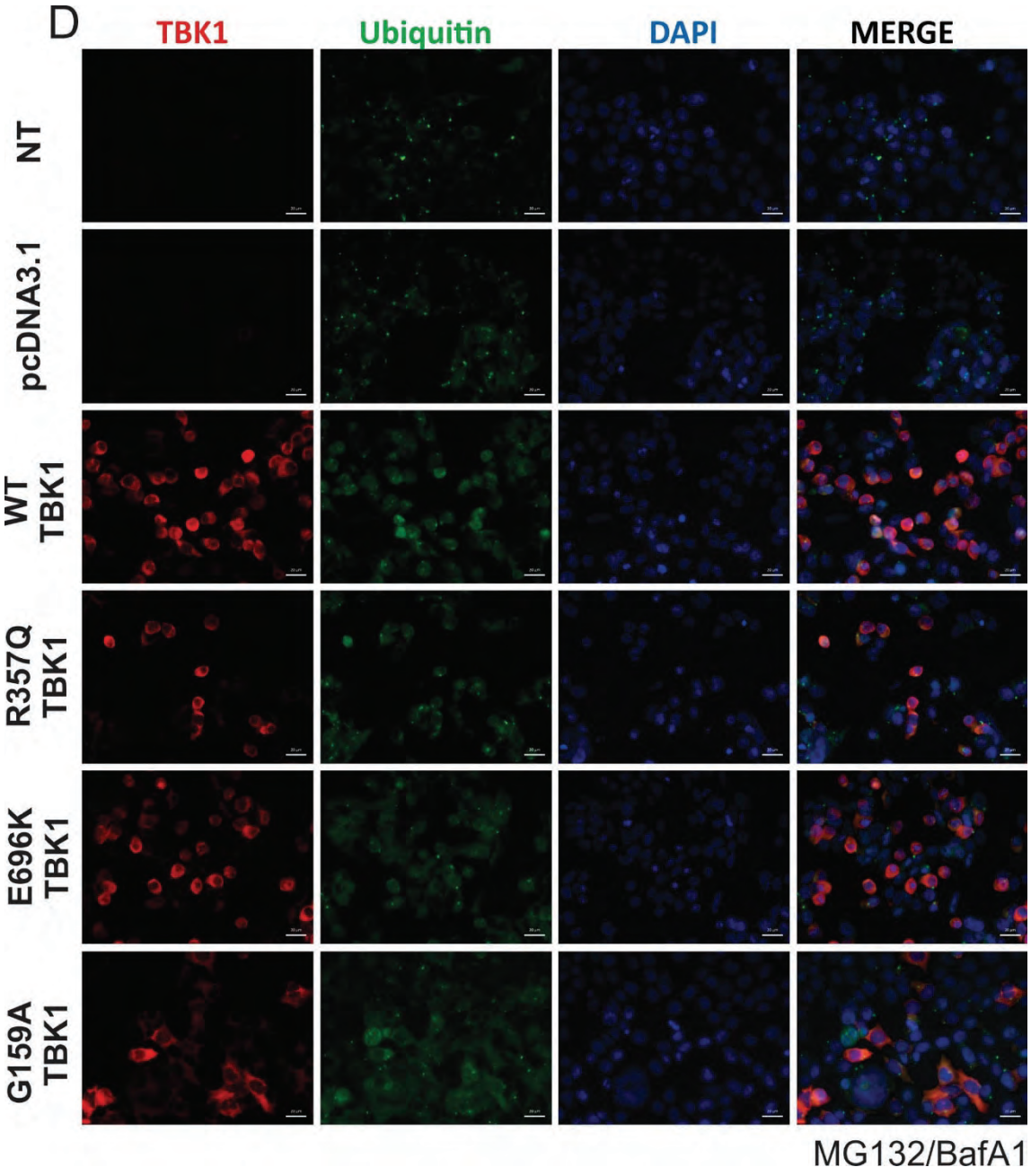
No differences in the intensities of ubiquitin were detected between the different TBK1 expressing cells and control (NT/pcDNA3.1) cells (except where stated), however a strong trend towards more ubiquitin was detected in both basal and MG132 treated conditions **(Figure 5.12)**. In basal conditions without MG132 or bafilomycin treatment, a trend towards more ubiquitin was present in cells expressing any of the TBK1-FLAG proteins compared to NT or pcDNA3.1 control cells (**Figure 5.12A**). However, upon bafilomycin treatment, no trend was detected between the control cells (NT/pcDNA3.1) and TBK1-FLAG overexpressing cells. Hence this data might indicate that overexpression of TBK1-FLAG inhibited the degradation of ubiquitin by autophagy,

even in the absence of UPS inhibition. Similarly, upon MG132 treatment, all cells overexpressing TBK1-FLAG proteins, whether WT or mutant, showed in increasing trend of more ubiquitin compared to controls (**Figure 5.12B**). Furthermore, upon MG132 and bafilomycin treatment, overexpression of TBK1-FLAG led to a trend towards elevated ubiquitin levels. These data are somewhat consistent with the previous data **(Figure 5.10)** showing that knock-out of TBK1 increases degradation of insoluble ubiquitin.


A
TBK1
Ubiquitin
DAPI
MERGE
NT
pcDNA3.1
WT TBK1
R357Q TBK1
E696K TBK1
G159A TBK1
Serum


B
TBK1
Ubiquitin
DAPI
MERGE
NT
pcDNA3.1
WT TBK1
R357Q TBK1
E696K TBK1
G159A TBK1
Mg132


C
TBK1
Ubiquitin
DAPI
MERGE
NT
pcDNA3.1
WT TBK1
R357Q TBK1
E696K TBK1
G159A TBK1
Serum/BafA1


D
TBK1
Ubiquitin
DAPI
MERGE
NT
pcDNA3.1
WT TBK1
R357Q TBK1
E696K TBK1
G159A TBK1
MG132/BafA1

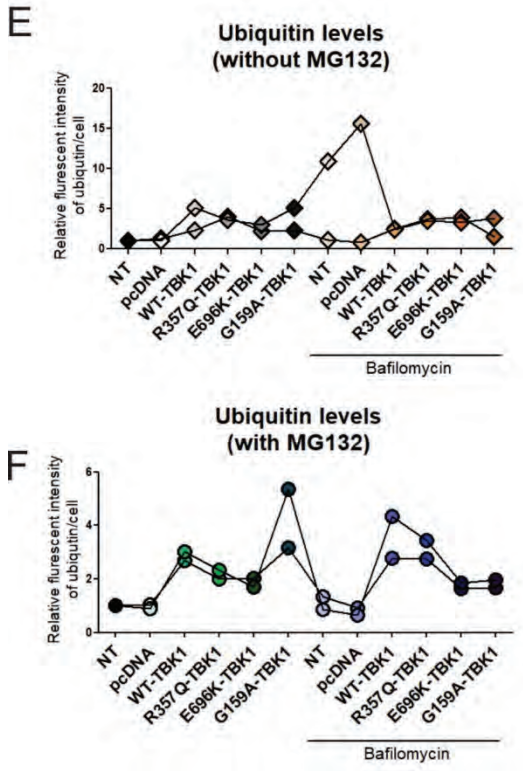


Figure 5.12. Increased fluorescent intensity of ubiquitin in G159A TBK1-FLAG overexpressing cells. Representative pictures **(A-D)** and quantification **(E/F)** are shown. TBK1$^{-/-}$ HEK293T cells were plated and transfected with TBK1-FLAG for 24 hr then treated with DMSO or MG132 (1 μM) for 20 hr, followed by with 100 nM bafilomycin for an additional 4 hr. Then cells fixed and stained for ubiquitin and TBK1. Fluorescent intensity of ubiquitin staining was analysed via ImageJ.

5.4.12 TBK1 inhibition leads to increased TDP-43 aggregation

Ubiquitinated protein inclusions are a good indicator of protein aggregation and aggrephagy. TDP-43 aggregation is the major pathological hallmark of ALS, which present in 97% of patients, including sporadic disease and most familial cases [2]. Hence examining TDP-43 aggregation is relevant to the cellular mechanisms involved in ALS. Therefore, next it was examined how TBK1 affects the aggregation of TDP-43.

First the aggregation of TDP-43 was examined in cells treated with TBK1 inhibitors and in the CRIPSR/cas9 KO cells. Firstly, the effects of BX795 on TDP-43 aggregation was analysed via immunoblotting and confocal microscopy. HEK293T cells

were transfected with TDP-43-EGFP^{WT} and an ALS mutant TDP-43^{M337V}, which is known to form aggregates in upto 50% of transfected HeLa cells [661]. Transfected cells were treated with BX795 for 24 hr starting at 4, hr post-transfection to examine how TBK1 inhibition influences the aggregation formation of TDP-43. In cells treated with BX795, there was a trend towards increased insoluble TDP-43^{WT} levels however this did not reach statistical significance **(Figure 5.13)**. However significantly more insoluble TDP-43^{M337V} was detected after 24+4 hr in BX795-treated cells. Hence these data imply that the kinase activity of TBK1 is involved in the formation of TDP-43^{M337V} aggregates, while not in TDP-43^{WT}.

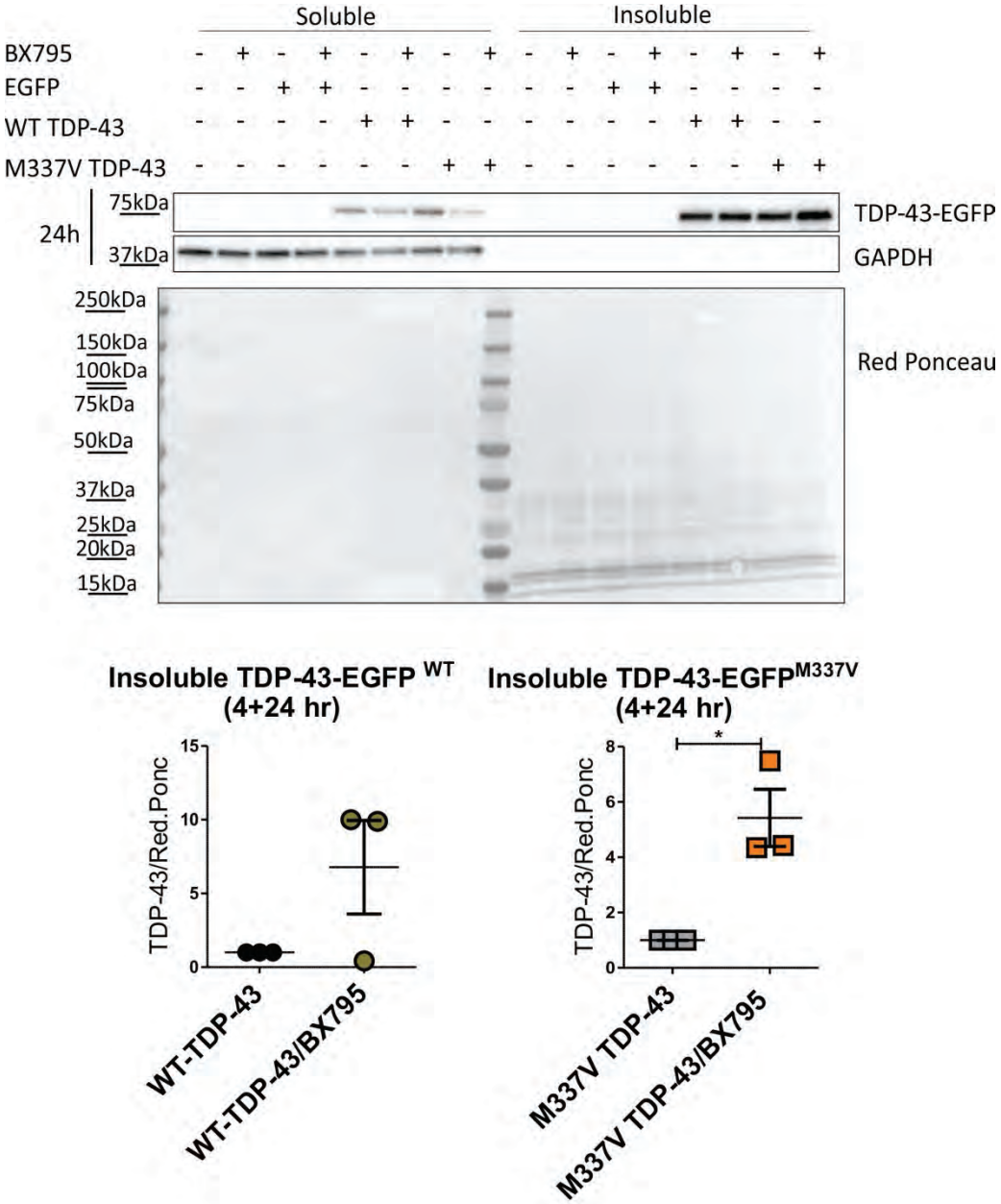


Figure 5.13. Increased levels of insoluble TDP-43^{M337V} are present in BX795 treated cells. (A) *BX795 increases insoluble TDP-43^{M337V} levels at 24 hr post transfection.* HEK293T cells were transfected with TDP-43 EGFP and treated with 1 μM BX795. Cell lysates were fractionated into soluble and insoluble fractions using triton and immunoblotting was performed. Band intensity was quantified using ImageJ and normalised to Red Ponceau. Relative expression levels are shown by quantification. N=3+/-SEM, unpaired t-test, *<0.05.

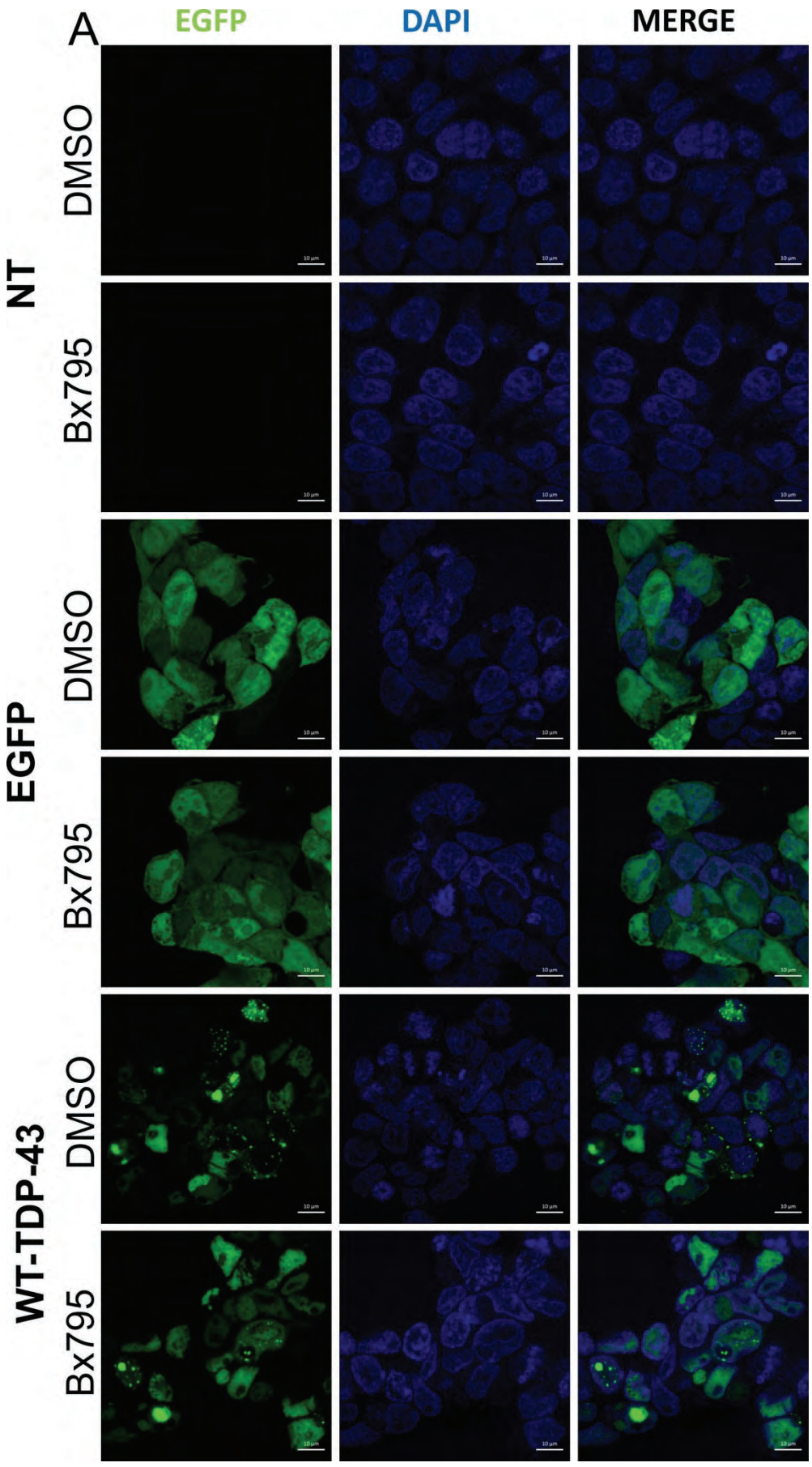
In ALS, pathological forms of TDP-43 are known to mislocalise from the nucleus to the cytoplasm, as well as form inclusions, including the mutant examined here, TDP-43^{M337V} [662]. Therefore, it is possible that TBK1 affects the cytoplasmic localisation of TDP-43. To further examine the link between TBK1 and cytoplasmic forms of TDP-43, another TDP-43 mutant was used; TDP-43 ^{dNLS}. This is an artificial mutant, but because it lacks the nuclear localisation signal (NLS) [64], TDP-43 ^{dNLS} is expressed only in the cytosol, therefore representing the pathological forms of TDP-43 typical of ALS patients.

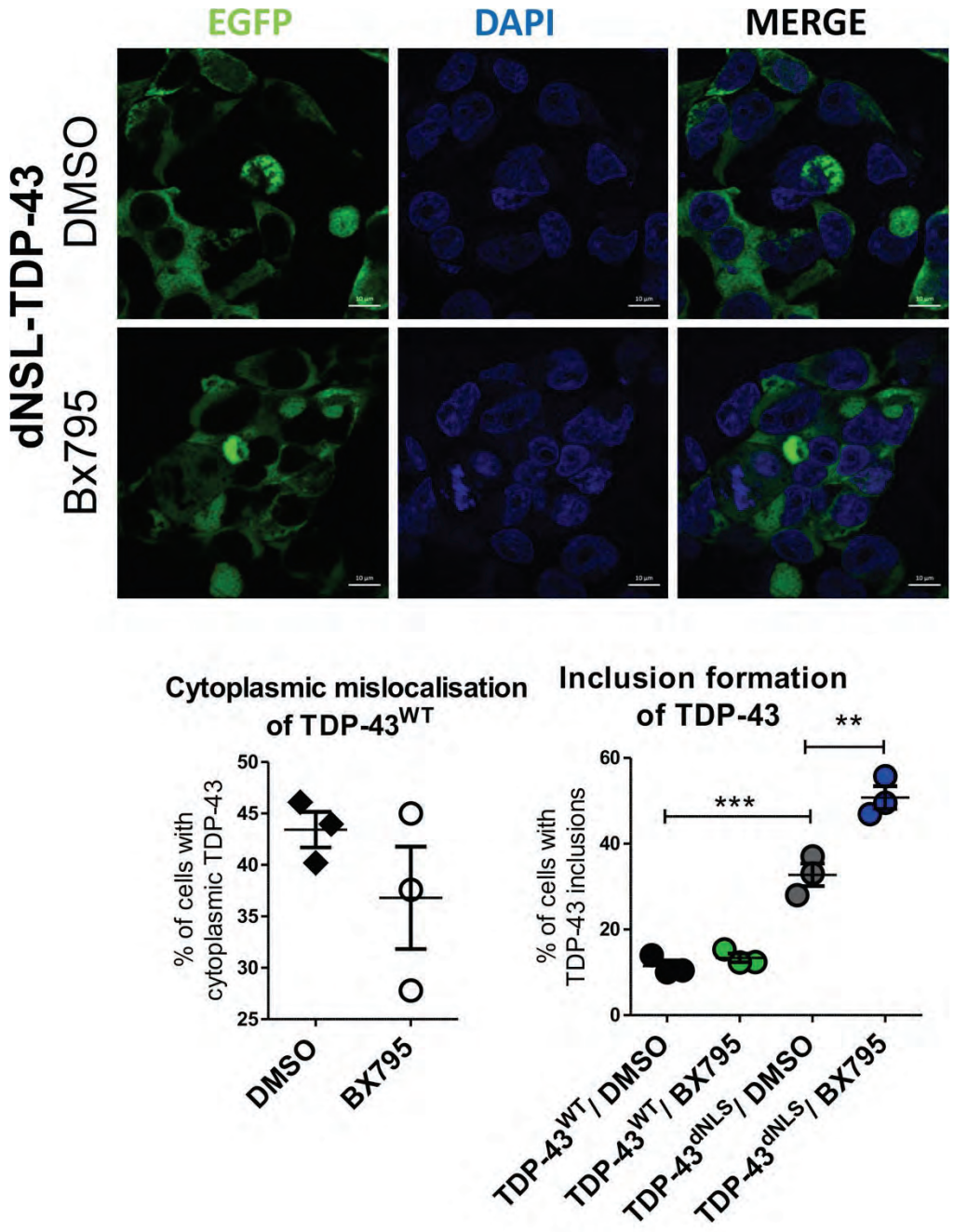
The cytoplasmic mis-localisation and aggregation of both TDP-43 ^{WT} and dNLS-TDP-43 were next analysed. Cells were transfected with WT or TDP-43-EGFP ^{dNLS} for 24 hr, then treated with BX795 or MRT67307 for 24 hr, then analysed using confocal microscopy. For cells expressing TDP-43 ^{WT}, 45% expressed cytoplasmic TDP-43, (where the EGFP signal was present outside of the nucleus) and BX795 administration did not significantly affect this proportion **(Figure 5.14A)**. Similarly, MRT67307 did not affect this proportion either (**Figure 5.14A)**. The mutant TDP-43^{dNLS} was expressed entirely in the cytosol, so it was not possible to examine mislocalisation with this mutant.

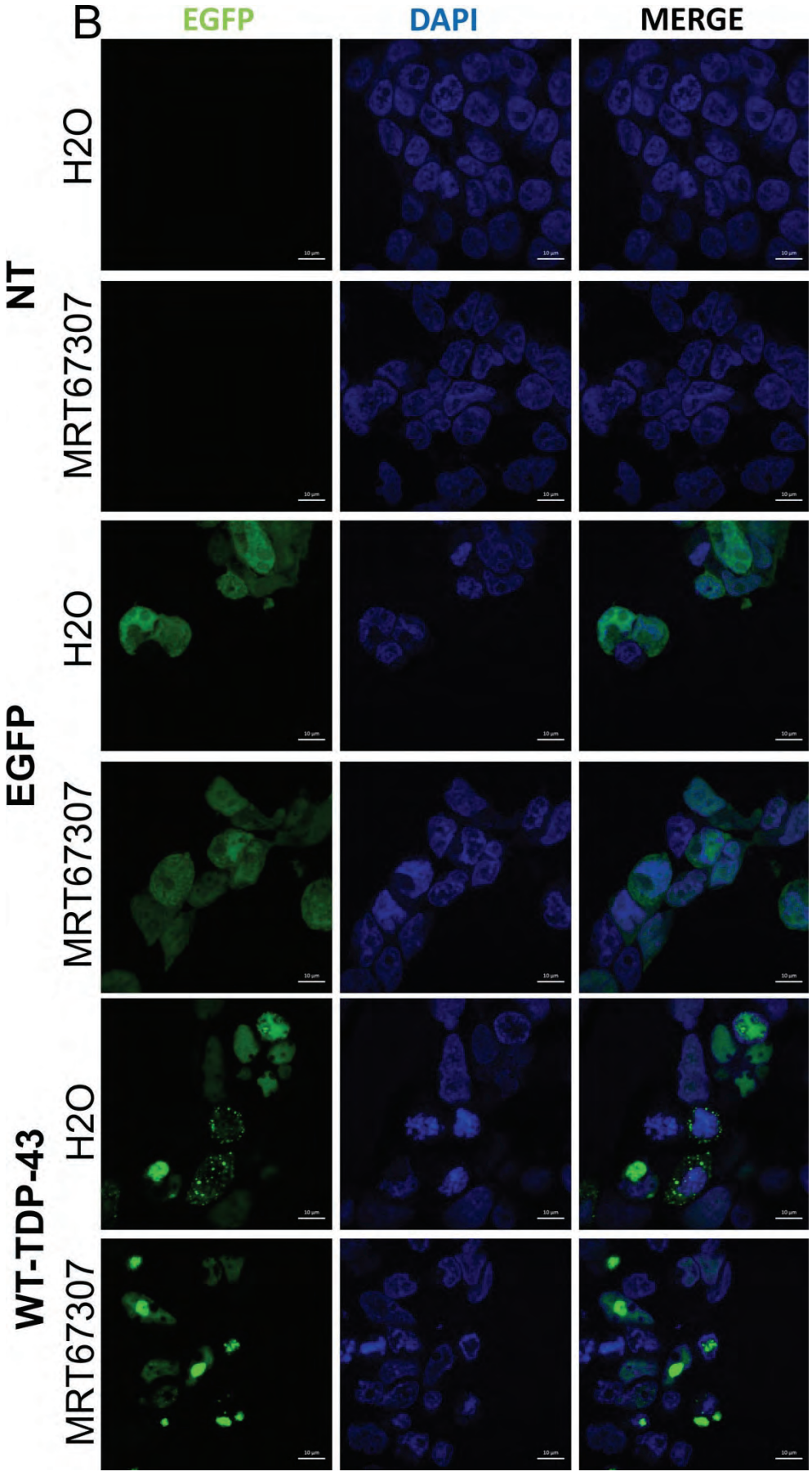
A small percentage of cells overexpressing TDP-43 ^{WT} using these constructs displayed vesicular structures that have been previously characterized elsewhere ([663]. Unpublished findings from our group (Jamali et al-PhD thesis 2020) have indicated that these vesicles colocalise with stress granule markers, HuR, therefore indicating that vesicles may be stress granules.

Approximately 15% of TDP-43-EGFP ^{WT} expressing cells contained cytoplasmic inclusions that were characterised by unshaped structures with high EGFP signal that

were very distinctive from stress granules. These inclusions localised to the cytoplasm, and cells usually only contained one inclusion. Inclusion formation of TDP-43^{WT} were not affected by BX795, similar to the results from the TDP-43 fractionation experiments. Not surprisingly, more inclusions formed in cells expressing dNLS-TDP-43 ($p=0.0003$). Approximately 33% of these cells formed inclusions in the absence of BX795, but this increased significantly following treatment ($p=0.001$). This result implies the kinase activity of TBK1 is protective against the aggregation of TDP-43 ^{dNLS}, but not against the formation of TDP-43 ^{WT} inclusions. Upon MRT67307 treatment, there was no significant difference in TDP-43^{WT} -aggregation, similar to the BX795 results. However, interestingly, and in contrast to BX795, MRT67307 treatment did not significantly alter the proportion of TDP-43 ^{dNLS} expressing cells forming inclusions. This finding therefore indicates that the observed effect of BX795 on the aggregation of TDP-43^{dNLS} was not specific to TBK1, because MRT67307 is known to be a more potent inhibitor, and it appeared to have no effect.


A
EGFP
DAPI
MERGE
NT
DMSO
Bx795
EGFP
DMSO
Bx795
WT-TDP-43
DMSO
Bx795


EGFP
DAPI
MERGE
dNSL-TDP-43
DMSO
Bx795
Cytoplasmic mislocalisation of TDP-43WT
% of cells with cytoplasmic TDP-43
50
45
40
35
30
25
DMSO
BX795
Inclusion formation of TDP-43
% of cells with TDP-43 inclusions
60
40
20
0
***
**
TDP-43WT/ DMSO
TDP-43WT/ BX795
TDP-43dNLS/ DMSO
TDP-43dNLS/ BX795


B
EGFP
DAPI
MERGE
NT
H2O
MRT67307
EGFP
H2O
MRT67307
WT-TDP-43
H2O
MRT67307

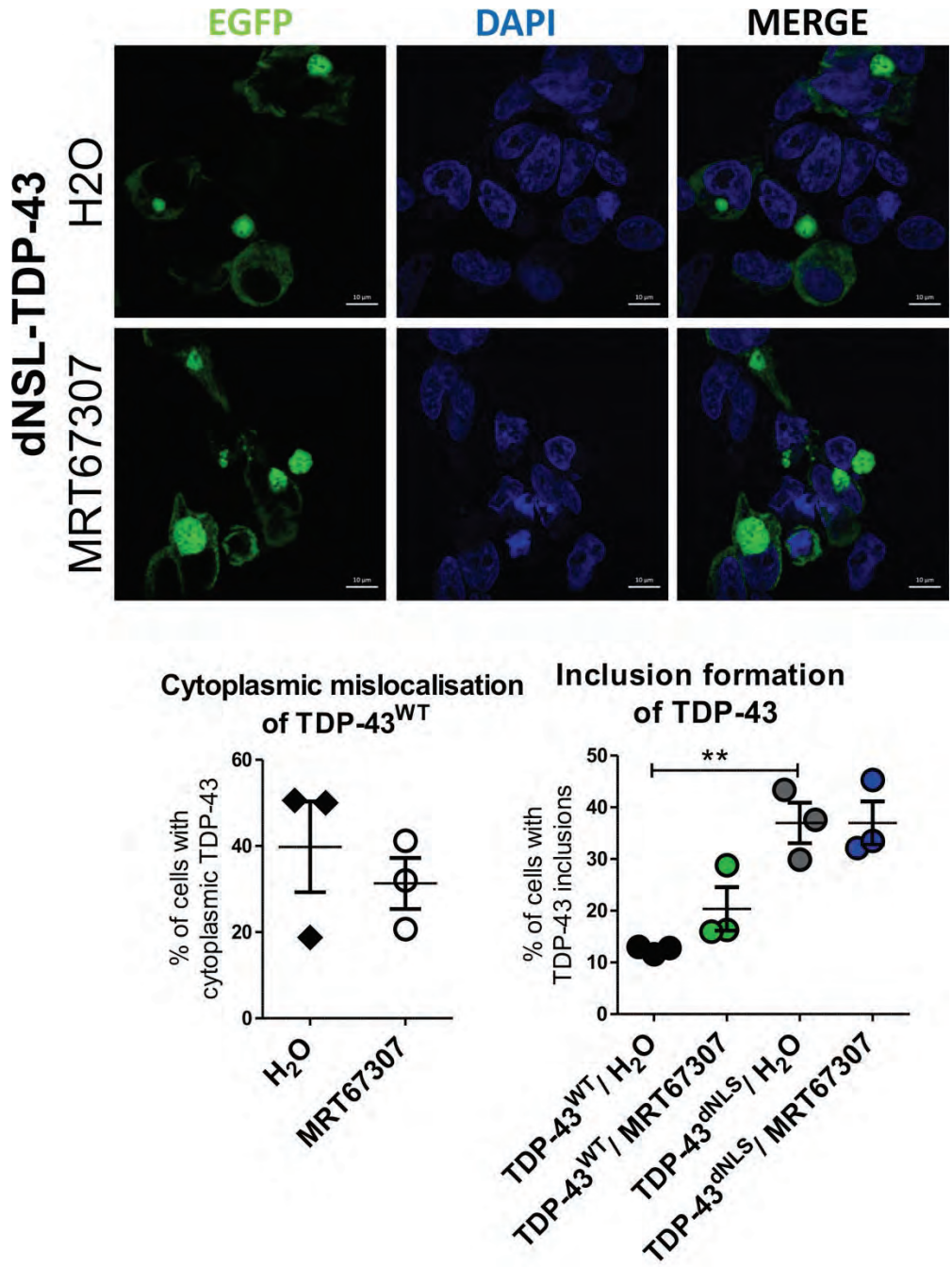


Figure 5.14 BX795 treatment induces the aggregation of TDP-43^{dNLS}. HEK293T cells were transfected with TDP-43-EGFP for 24 hr followed by treatment with BX795 or MRT6307 for 24 hr. Cells were then examined using confocal fluorescent microscopy. Representative images and quantification are shown for BX795 **(A)** and MRT67307 **(B)** treatment. N=3+/-SEM, unpaired t-test, one-way ANOVA with Tukey post-hoc test. **<0.005, ***<0.0005.

The above result indicating that MRT67307 does not affect TDP-43 aggregation was unexpected. Therefore, to further investigate how MRT67307 affects TDP-43 aggregation, soluble/insoluble fractionation was again performed.

HEK293T cells were transfected with WT and dNLS TDP-43 expressing cells were treated with MRT67307 for 24 hr. Cells were then fractionated into soluble and insoluble lysates and immunoblotting for WT and dNLS-TDP-43-EGFP was performed. A trend towards more insoluble TDP-43 was detected in MRT67307 treated cells for both TDP-43-EGFP^{WT-} and TDP-43-EGFP ^{dNLS}, however this did not reach statistical difference, consistent with the microscopy results **(Figure 5.15.)**.

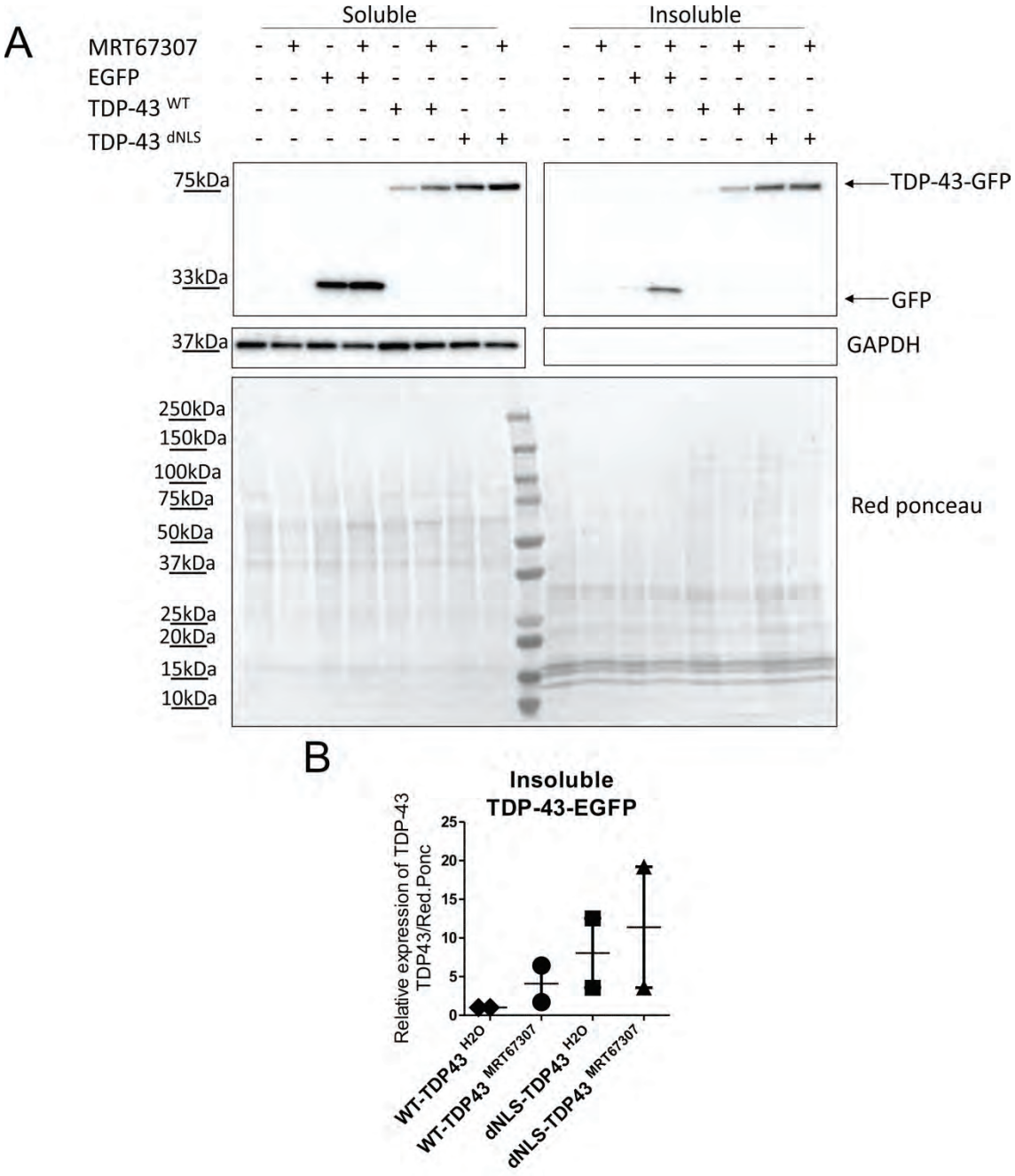


Figure 5.15. MRT67307 does not affect TDP-43 insolubility. HEK293T cells expressing WT or dNLS-TDP-43-EGFP for 24 hr were treated with MRT6307 for 24 hr. Cells were fractionated into soluble and insoluble lysates and immunoblotting for GFP was performed. Representative immunoblots **(A)** and quantifications **(B)** are shown. N=2+/-SEM

5.4.13 TBK1 knock-out n does not affect insolubility of TDP-43

To further probe how TBK1 is involved in TDP-43 aggregation, similar experiments were performed in the TBK1 CRISPR/Cas9 KO clone #2, analysing the aggregation of WT and TDP-43 aggregation ^{dNLS}. The ALS/FTD TBK1 mutants analysed above were also examined in addition to WT TBK1, to further investigate the role between TBK1 and TDP-43 in ALS. Firstly, it was examined whether knock-out of TBK1 affects the aggregation of TDP-43. Therefore TBK1$^{+/+}$ and TBK1$^{-/-}$ #1/#2 cells were transfected with TDP- 43 ^{WT} and TDP-43 ^{dNLS} for 48 hr and fractionated into soluble and insoluble fractions as above. However, the localisation of both WT **(Figure 5.16A)** and TDP-43 ^{dNLS} **(Figure 5.16B)** into the soluble and insoluble fractions was not affected significantly by the deletion of TBK1.

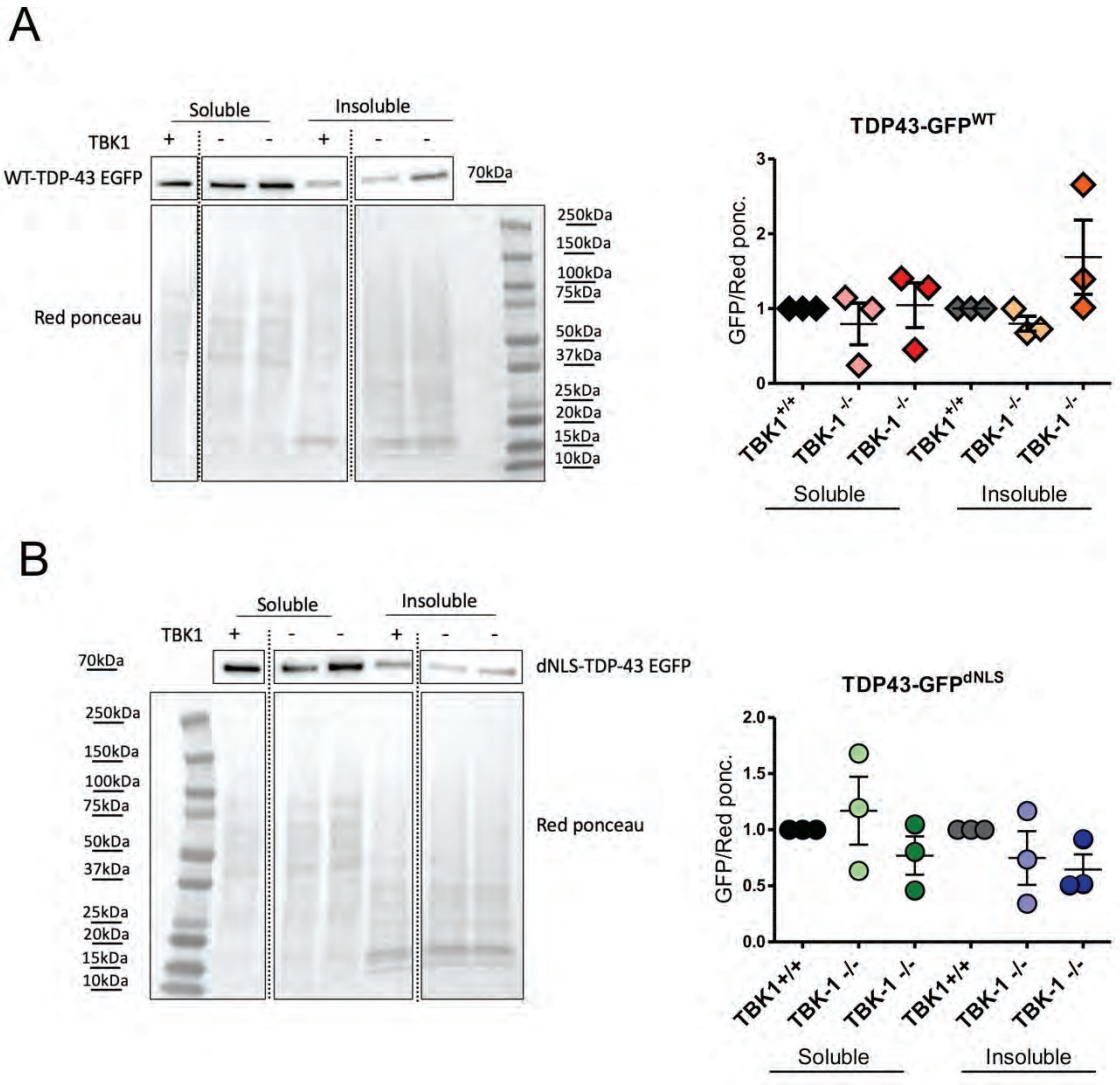


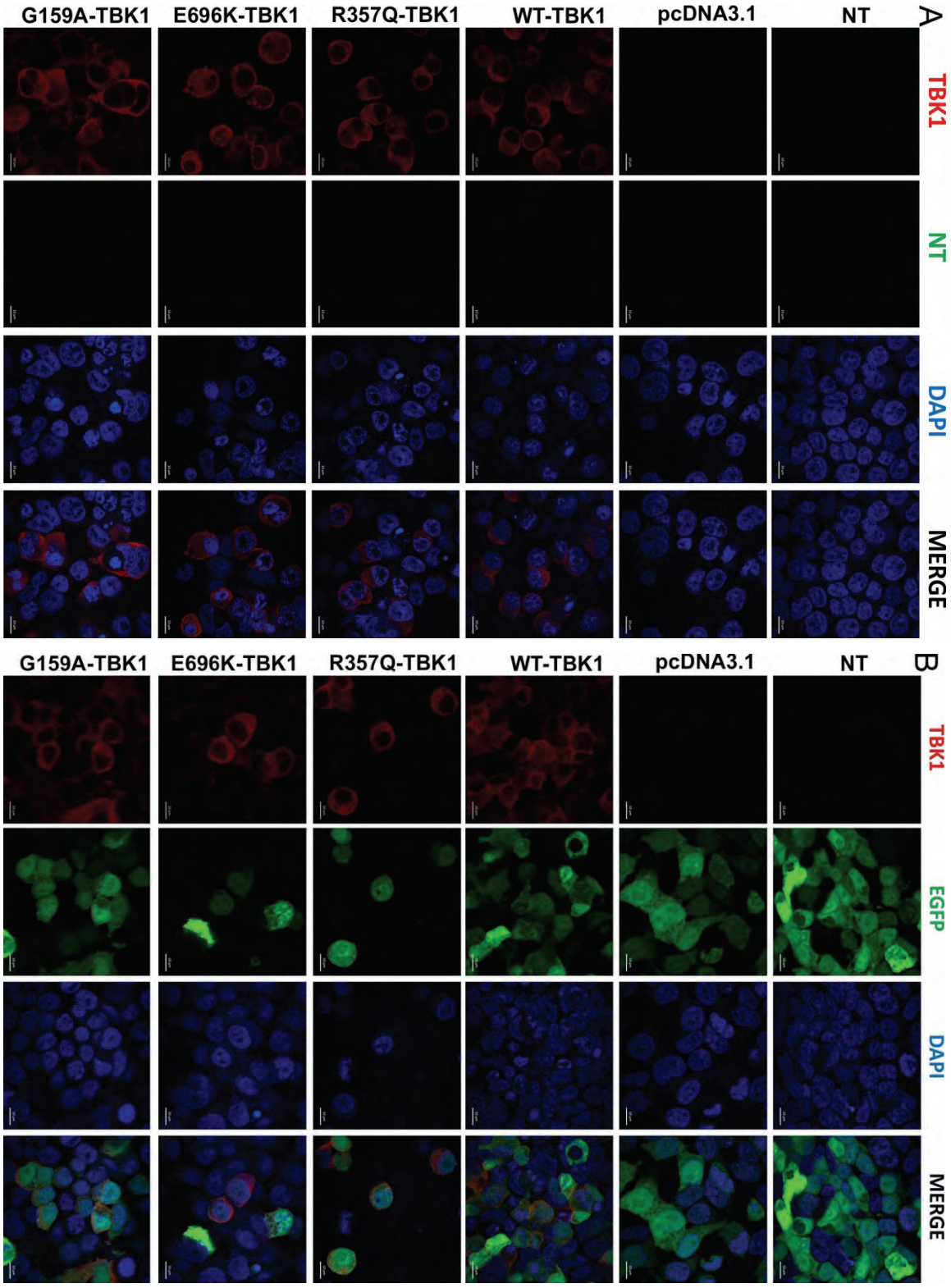
Figure 5.16. TBK1 knock-out does not affect WT and dNLS-TDP-43 insolubility. TBK1$^{+/+}$ and TBK1$^{-/-}$ (#1, #2) HEK293T cells were transfected with WT **(A)** and dNLS-TDP-43-EGFP **(B)** for 48 hr and then fractionated into soluble and insoluble fractions. Dashed lines indicate the cropping of 'control' clone.

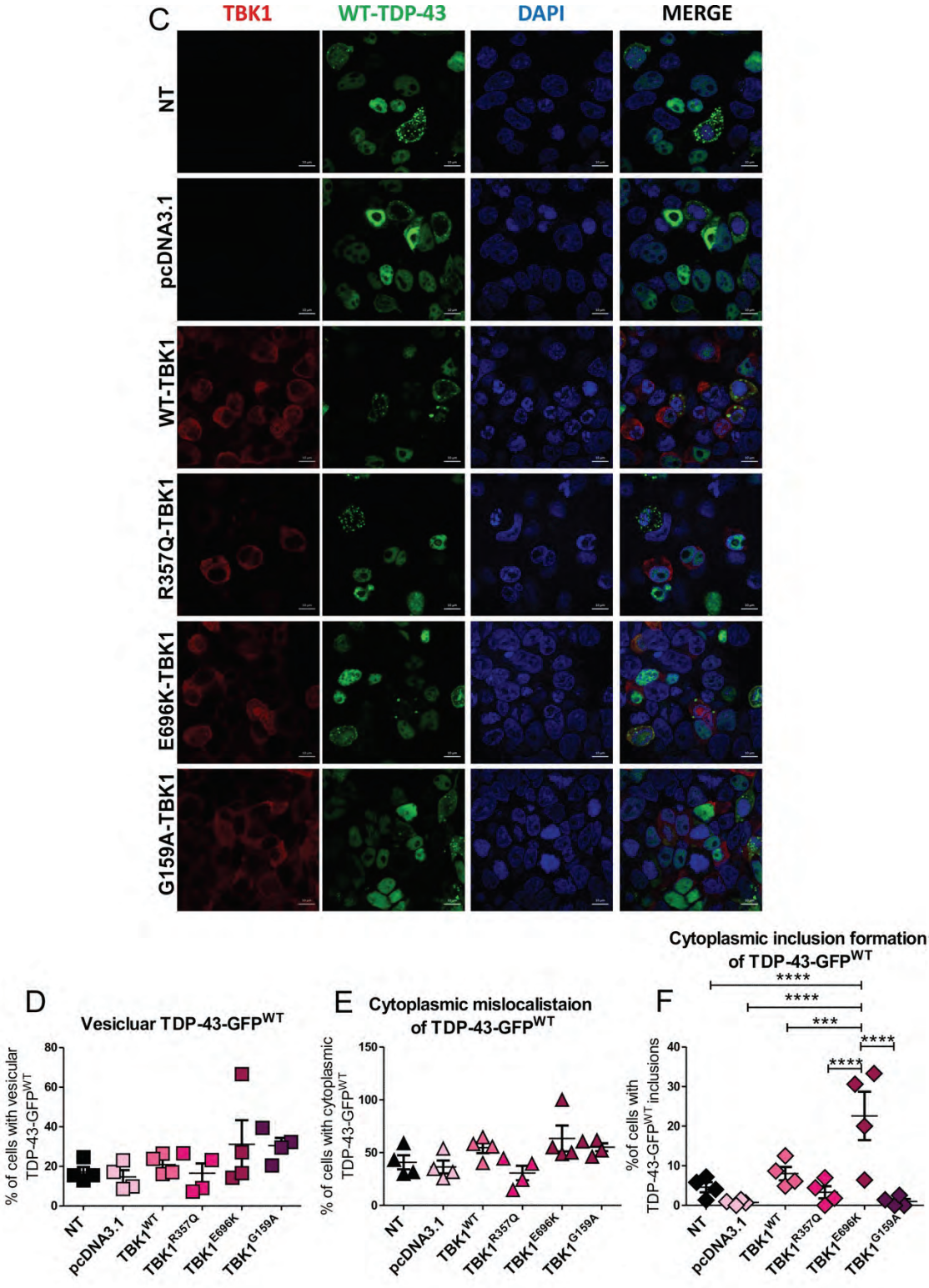
5.4.14 E696K ALS-mutant TBK1 induces the inclusion formation of TDP-43

Next, the effect of overexpression of TBK1 on TDP-43 aggregation was examined. TBK1$^{-/-}$ #2 HEK293T cells were therefore co-transfected with pLetniGFP, TDP-43-GFP ^{WT} or TDP-43-GFP ^{dNLS}, and TBK1-FLAG^{WT} or mutant constructs for 48 hr then cells were analysed via confocal fluorescent microscopy. pLenti-GFP vector expressed GFP in the cytoplasm, that was not affected by TBK1-FLAG overexpression **(Figure 5.17B)** A small percentage of cells overexpressing -TDP-43 ^{WT} displayed stress granules **(Figures 5.17 C)** as described above. Overexpression of WT or mutant TBK1-FLAG did not significantly affect the percentage of cells displaying these structures, therefore indicating that TBK1 is not involved in TDP-43 recruitment to stress granules **(Figure 5.17D)**. TDP-43 shuttles between the cytoplasm and nucleus but mainly found in the nucleus. In ALS however TDP-43 shows a cytoplasmic mislocalistaion which was therefore analysed next. Upon TDP-43^{WT} overexpression, NT and pcDNA3.1 overexpressing cells displayed cytoplasmic mislocalisation in 40.2% and 35.7% of transfected cells, respectively **(Figure 5.17C/E),** similar to the proportions detected in previous experiments **(Figure 5.14)**. This shows the basal level of what TDP-43^{WT} mislocalises. Next the cytoplasmic mislocalisation of TDP-43^{WT} was examined upon TBK1-FLAG overexpression. Overall approximately 40% of TDP-43 ^{WT} overexpressing cells displayed cytoplasmic TDP-43^{WT}, and this proportion was not affected by overexpression of WT and mutant TBK1-FLAG **(Figure 5.17C/E).** This indicates that TBK1 is not involved in the mislocalisation of TDP-43 from the nucleus to the cytoplasm.

Next, cytoplasmic inclusion formation of TDP-43^{WT} was examined. Overexpression of WT-TBK1 or most of the mutants did not significantly affect inclusion formation of TDP-43^{WT} compared to NT and pcDNA3.1 conditions (**Figure 5.17C/F)**. In

contrast, in cells expressing the optineurin binding deficient mutant TBK1^{E696K}, significantly more TDP-43 ^{WT} inclusions were obtained compared to WT-TBK1 and all other conditions (**Figure 5.17C/F)**. These data indicate that this particularly mutant promotes TDP-43 aggregation. Interestingly, different results were obtained when TDP-43^{dNLS} was expressed and its ability to aggregate was analysed. TDP-43^{dNLS} lacks the NLS therefore, TDP-43^{dNLS} solely localised to the cytoplasm [64]. TDP-43^{dNLS} forms cytoplasmic inclusion on a higher rate than TDP-43^{WT}. This time, overexpression of the mutant TBK1^{E696K} did not increase the formation of TDP-43^{dNLS} inclusions. (**Figure 5.17G/H),** and neither did any of the other TBK1-FLAG overexpressing proteins, indicating that the exptression of TBK1 does not influence the incuslion formation of TDP-43^{dNLS}.


A
G159A-TBK1
E696K-TBK1
R357Q-TBK1
WT-TBK1
pcDNA3.1
NT
TBK1
NT
DAPI
MERGE
B
G159A-TBK1
E696K-TBK1
R357Q-TBK1
WT-TBK1
pcDNA3.1
NT
TBK1
EGFP
DAPI
MERGE


C
TBK1
WT-TDP-43
DAPI
MERGE
NT
pcDNA3.1
WT-TBK1
R357Q-TBK1
E696K-TBK1
G159A-TBK1
D
Vesicluar TDP-43-GFPWT
% of cells with vesicular TDP-43-GFPWT
E
Cytoplasmic mislocalistaion of TDP-43-GFPWT
% of cells with cytoplasmic TDP-43-GFPWT
F
Cytoplasmic inclusion formation of TDP-43-GFPWT
%of cells with TDP-43-GFPWT inclusions
****
***
NT
pcDNA3.1
TBK1WT
TBK1R357Q
TBK1E696K
TBK1G159A

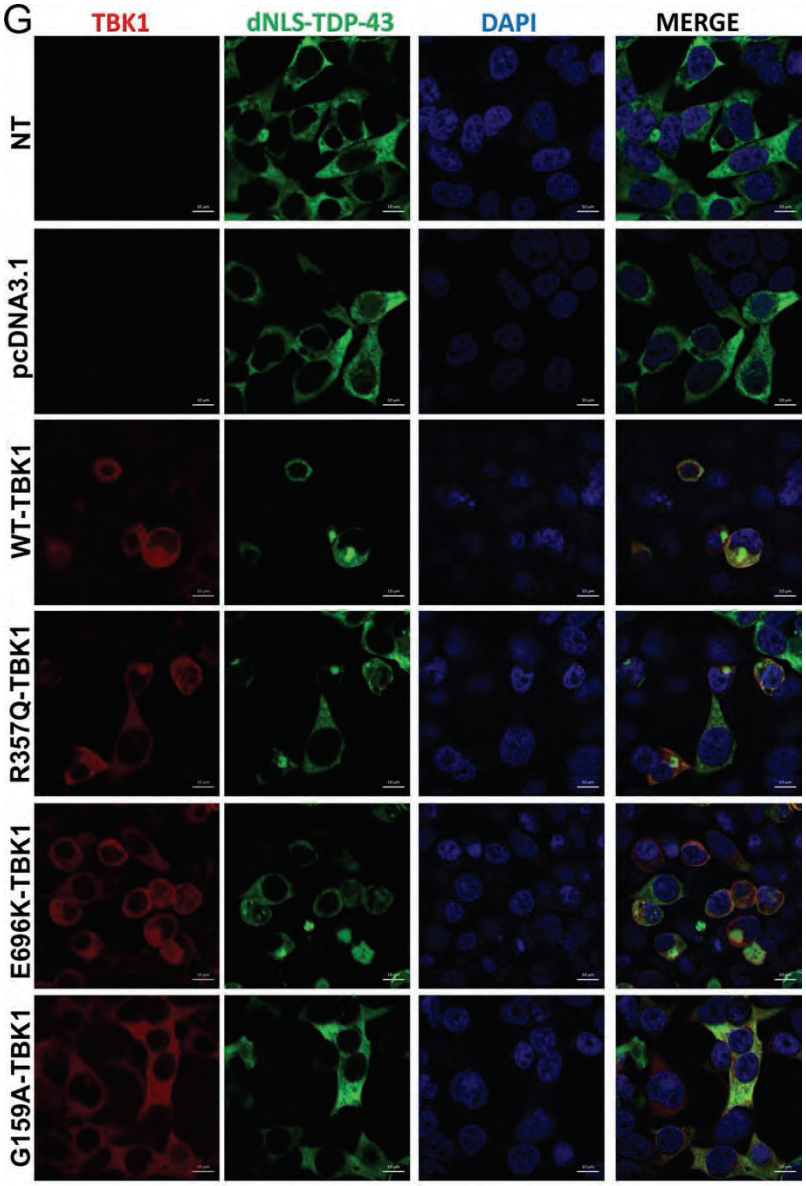

G
TBK1
dNLS-TDP-43
DAPI
MERGE
NT
pcDNA3.1
WT-TBK1
R357Q-TBK1
E696K-TBK1
G159A-TBK1
H
Cytoplasmic inclusion formation of TDP-43-GFP^dNLS
% of cells with TDP-43-GFP^dNLS inclusions
80
60
40
20
0
NT
pcDNA3.1
TBK1^WT
TBK1^R357Q
TBK1^E696K
TBK1^G159A

Figure 5.17. The E696K ALS/FTD mutant TBK1 induces WT TDP-43 aggregation. HEK293T cells were co-transfected with pLentiGFP/TDP-43-GFP^{WT}/TDP-43-GFP^{dNLS} and TBK1-FLAG vectors for 48 hr, and cytoplasmic mislocalisation and inclusion formation of TDP-43 was followed by confocal microscopy. Representative images of cells expressing TBK1-FLAG alone **(A)**, or co-transfected with pLenti-GFP empty vector **(B)**, TDP-43-EGFP^{WT} **(C)** and TDP- 43^{dNLS} **(G)** are shown. The percentage of cells displaying vesicular TDP-43, cytoplasmic mislocalisation and inclusion formation upon overexpression of TBK1-FLAG are shown in quantification **(D/E/F/H)**. N=3+/-SEM, one-way ANOVA with Tukey post-hoc test. ***<0.0005, ****<0.0001. Scale 10 μm.

5.4.15 Summary

The data presented in this chapter demonstrate that the presence and kinase activity of TBK1 are not involved in the formation of omegasomes or autophagsosmes, or autophagosome-lysosome fusion, during MG132 induced autophagy, indicative of aggrephagy.

The levels of insoluble and soluble ubiqutin were used to follow the degradtion of cargo during MG132 induced autophagy. Inhibition of TBK1's kinase activity did not affect the degradation of ubiqitin, while interestingly, knock-out of TBK1 promoted its degradation via autophagy. This result suggests that endogenous TBK1 negatively influences ubiquitin degradation.

TDP-43 inclusions are the major pathological hallmark of ALS, therefore TDP-43 aggregation was next analysed. It could not be conclusively determined whether the TBK1 kinase actvity is involved in TDP-43 aggregation because the two TBK1 inhibitors gave contradictory results. However, knock-out of TBK1 did not affect the solubility of TDP-43. Nonetheless, overexpression of E696K ALS/FTD TBK1 mutant increased inclusion formation of TDP-43 ^{WT}, but not the artifical dNLS mutant, indicating that this mutant may promote TDP-43 aggregation in ALS.

5.5 Discussion

It is already well established that compensation exists between the UPS and autophagy [664-666]. Inhibition of one process will result in activation of the other pathway to maintain intracellular homeostasis. Inhibition of the UPS pharmacologically using MG132 [664, 665] or bortezomib [666] is known to induce autophagy. Therefore, this phenomenon was taken advantage of in the studies outlined in this chapter in order to examine aggrephagy. If the UPS is inhibited, the resulting soluble and insoluble misfolded proteins that accumulate will become directed towards degradation via autophagy. Degradation of insoluble proteins via autophagy is called aggrephagy; thus monitoring insoluble proteins allows aggrephagy to be examined. MG132 was used here to inhibit the UPS, while simultaneously inducing autophagy, and the conditions were optimised. Ubiquitin immunoblotting revealed that 1 μM MG132 treatment was sufficient to induce autophagic degradation of insoluble ubiquitin. Unexpectedly, LC3 immunoblotting indicated that this did not result in increased autophagosome formation, therefore this indicates that the tethering of the insoluble ubiquitin cargo, towards the forming autophagosomes, was elevated in these cells. Both NDP52 and p62 are thought to be recruited to the autophagosome following MG132 treatment, implicating their involvement in directing the cargo, such as insoluble ubiquitin, towards autophagic degradation. Furthermore, LC3-NDP52 and LC3-p62 co-precipitation was detected in MG132 treated cells, further confirming their involvement in MG132-induced autophagy.

Several autophagy receptors have been previously linked to aggrephagy, including p62 [667-669], and NBR1 [644]. However, NDP52 has not been previously shown to be involved [670]. The most well studied receptor involved in aggrephagy is p62 [667-669], hence this receptor was examined here. The data presented in this chapter also indicates, for the first time, that NDP52 may be involved in aggrephagy. Furthermore, it also establishes that MG132 induces aggrephagy in HEK293T cells. NBR1 is however not phosphorylated by TBK1 [671], indicating that TBK1-dependent aggrephagy is also present in these cells.

Aggrephagy is still not very well characterised. Therefore, further experiments are required to confirms these findings in the future. These could involve confocal

microscopy analysis of the localisation of autophagy receptors (p62, NDP52, and potentially NBR1), possibly combined with live cell imaging to analyse the kinetics of autophagy receptor recruitment to protein aggregates during MG132 autophagy.

5.5.1 TBK1 may not regulate autophagosome formation and degradation during MG132 induced autophagy

A potential underlying mechanism by which TBK1 causes ALS is dysfunctional protein degradation. Therefore, autophagosome formation was analysed in TBK1 and UPS inhibited conditions. The two TBK1 inhibitors did not give consistent results in relation to MG132 induced autophagy. However. MRT67307 treatment led to inhibited formation of the omegasome and autophagosome, and inhibited autophagosome degradation (fusion to the lysosome). In contrast, BX795 treatment did not affect any of these processes.

The discrepancy between the results obtained using BX795 and MRT67307 suggests that the effects observed may be due to the previously reported stronger potency of MRT67307 inhibiting TBK1 [550]. Alternatively, the effects observed with MRT67307 may be due to its known ability to inhibit autophagosome formation by inhibition of ULK1 [551] rather than due to its effects on TBK1. By inhibiting ULK1, MRT67307 would inhibit the autophagic machinery and therefore this would result in decreased autophagosome formation. Nonetheless, autophagosome-lysosome fusion is not dependent on ULK1, arguing against this off-target mechanism as an explanation for the observed results. Furthermore, the concentration of MRT67307 used in this study is much lower than the IC^{50} required to inhibit ULK1 (25 nM vs 45 nM). Therefore, in order to resolve this possibility, the phosphorylation status of ULK1 needs to be analysed in the future to determine which scenario is correct. Similarly, the formation of the omegasome was unaffected in BX795 treated cells, whereas MRT67307 treatment inhibited omegasome formation. Previously the ULK1 complex has been implicated in omegasome formation [672]. Therefore, a counter argument is that tehe inhibition of omegasome formation may have been another off-target effect of MRT67307 due to its ability to inhibit the ULK1 complex. Furthermore. these IC^{50} values were established in mouse embryonic fibroblast cells [551], implying that the HEK293T cells used in this study may respond differently to this inhibitor. In contrast, knock-out of TBK1 in the CRISPR/Cas9

cells did not affect the formation and degradation of autophagosome, therefore indicating that the absence of TBK1 does not impair MG132 mediated autophagy. Furthermore, the overexpression of WT TBK1, or the ALS/FTD or HSE mutants, did not significantly affect the formation of autophagosome or the fusion of autophagosome with lysosomes. Therefore, these data suggest that TBK1 may not be involved in MG132 induced autophagy.

Very limited knowledge is currently available regarding how TBK1 affects aggrephagy and the clearance of protein aggregates. Furthermore, the few studies that do exist present conflicting findings. A recent *in-vivo* study showed that heterozygous knock-out of TBK1 leads to typical ALS pathologies in mice, manifesting in axonal degeneration, TDP-43-aggregation, neuroinflammation, neuronal loss and behavioural deficits, due to increased activity of RIPK1 [598]. Furthermore, it was shown that deletion of TBK1 prevents autophagy in motor neurons, which was identified by increased p62 levels in the cortex [509]. knock-out of TBK1 also increased the formation of mutant $SOD1^{G93C}$ aggregates, and conversely, overexpression of TBK1 inhibited the production of $SOD1^{G93C}$ aggregates. However this result was linked to these aggregates becoming more soluble, and not by activation of autophagy [140, 509]. In contrast, knock-out of TBK1 in primary motor neurons did not affect SOD1 levels [510]. Therefore, these reports show that TBK1 knock-out does not always affect protein aggregation, and even if increased aggregation is detected upon TBK1 knock-out, is not mediated by impaired autophagy. Therefore, the results obtained in this thesis are not so surprising. However, to further analyse the role of TBK1 in protein aggregation, the formation and degradation of aggregates was followed.

5.5.2 TBK1 inhibits ubiquitin degradation

MG132 induced autophagy did not induce the formation of the autophagosome in HEK293T cells, but it still led to an increased degradation of insoluble ubiquitin. Therefore, ubiquitin degradation was examined in relation to TBK1. The results indicated that inhibition of TBK1 may not influence MG132 mediated autophagosome formation or degradation and, consistent with these findings, TBK1 inhibition did not affect the degradation of soluble or insoluble ubiquitin. These data indicates that the kinase activity of TBK1 is not required for the degradation of insoluble ubiquitin.

In contrast, unexpectedly, knock-out of TBK1 elevated the degradation of insoluble ubiquitin by MG132 treatment. The total levels of ubiquitin (soluble and insoluble) did increase upon bafilomycin in both TBK1 knock-out clones, however only reached significance in one clone **(Figure 5.11)**. Therefore, this indicates that TBK1 may negatively affect the degradation of ubiquitin. This however could not be confirmed by the overexpression of TBK1.

In contrast to these findings, overexpression of TBK1 led to decreased levels of insoluble ubiquitin in NSC-34 cells in a previous study [509]. However, overexpression of TBK1 did not induce autophagy in this prior report [509], therefore the decreased levels of ubiquitin detected in the published study, cannot be explained by autophagy-mediated degradation of ubiquitin. A recent paper also demonstrated that expression of ALS-mutant TBK1 (p.Thr777rpfsX4) in motor neurons resulted in impaired aggresome degradation [508]. These cells accumulated p62 positive aggresomes and displayed decreased LC3-II levels [508] compared to WT-TBK1 motor neurons. Therefore, TBK1 may have a cell type dependent role in aggrephagy, and the possible role detected in ubiquitin degradation in this chapter may not be ALS-linked specifically.

5.5.3 TDP-43 aggregation and clearance are linked to optineurin

The pathological hallmark of ALS is the presence of phosphorylated TDP-43, which forms cytoplasmic inclusions. Therefore, examining whether TBK1 has a role in TDP-43 aggregation may show how TBK1 contributes to ALS. Inhibition of the TBK1 enzymatic activity by BX795 induced insoluble TDP-43 ^{M337V}, as detected by immunoblotting. Furthermore, TBK1 inhibition did not affect the levels of insoluble WT-TDP-43. TDP-43 is normally localised to the nucleus [35] therefore, this may suggest that TBK1 may not be able to interact with nuclear TDP-43. Microscopy analysis confirmed however that TBK1 inhibition by BX795 can lead to more inclusions formed by an artificial, non-ALS mutant TDP-43 ^{dNLS} that lacks NLS and shows cytoplasmic localisation only. In contrast, MRT67307 did not significantly alter the proportion of WT or -TDP-43^{dNLS} expressing cells forming inclusions, as detected by both microscopy and immunoblotting. Therefore, this result indicates that the observed changes on TDP-43 inclusion formation may not be because of inhibited TBK1 function. Alternatively, the experimental replicate number

may be too low to detect a significant difference upon MRT67307 treatment, especially using immunoblotting where the low transfection efficiency is another confounding factor.

Knock-out of TBK1 via CRIPSR/Cas9 editing also did not affect the insolubility of TDP-43. Similarly, knock-out of TBK1 in primary motor neurons did not affect the levels of TDP-43 [510], suggesting that loss of TBK1 may not affect TDP-43 clearance. TDP-43 is known to be cleared by autophagy, and autophagy induction prolongs the survival of human stem cell derived neurons bearing TDP-43 mutations [673]. In this thesis however, knock-out of TBK1 did not affect autophagy, therefore the lack of effect on TDP-43 is not unexpected.

TBK1 is mutated in ALS and the ALS-TBK1 mutants may promote aggregation of TDP-43. TDP-43 mislocalises from the nucleus to the cytoplasm in ALS, even if the *TARDP43* gene is not mutated. Overexpression of WT or ALS/FTD mutant TBK1 did not affect the cytoplasmic mislocalisation of TDP-43 ^{WT} in this chapter. Interestingly, however, overexpression of the E696K mutant significantly elevated the number of inclusions formed by TDP-43 ^{WT}. This mutant lacks the optineurin binding site [18], suggesting that increased formation of inclusions may be linked to optineurin binding. In contrast, the E696K mutant did not affect the formation of TDP-43^{dNLS} inclusions. Furthermore, none of the other overexpressed TBK1-FLAG proteins led to increased inclusion formation by this artificial mutant. This result would therefore indicate that optineurin may be protective against TDP-43 aggregation. However, it remains unclear why the E696K mutant had no effect on TDP-43^{dNLS} aggregation. A possible explanation is that optineurin can only interact with nuclear TDP-43. However, this is unlikely because optineurin showed co-localisation with TDP-43^{dNLS} in the cytosol of HEK293T derived cells in a previous study (QBI-293) [674]. However, it must be noted that the cells used in the previous report contained endogenous TBK1, which therefore may promote optineurin-TBK1 interaction that seems to be crucial for TDP-43 aggregation. TBK1 can bind to optineurin and that may be crucial for TDP-43 aggregation. Indeed, optineurin and TDP-43 have been shown to interact on multiple occasions. Optineurin inclusions are known to occur in TDP-43 positive ALS cases, however very rarely [675]. Furthermore, optineurin and TDP-43 frequently co-localise in cytoplasmic granules in the muscles of sporadic inclusion body myositis patients as well as in the muscles of

occulopharyngeal muscular dystrophy patients [676]. Optineurin colocalises with mutant TDP-43 (TARDBP-ND251) in Neuro2A cells [677] and optineurin regulates inclusion formation of TDP-43 in a ubiquitin binding domain dependent manner [677]. Optineurin has been previously shown to be involved in the aggregation of other proteins linked to neurodegeneration, such as mutant SOD1 and huntingtin (htt). Depletion of optineurin led to increases in both $SOD1^{G93C}$ and htt aggregates in HeLa cells [140], while overexpression of optineurin prevented htt aggregation [677]. This indicates the optineurin may have a fundamental role in protein aggregation. The pathogenicity of ALS mutant TBK1 may therefore lie in its capability to interact with optineurin.

These results described in this chapter were all obtained using overexpression of TBK1. Therefore, in the future, more physiological expression levels need to be analysed to confirm the findings obtained. Furthermore, to establish the role of TBK1 in inclusion formation, other ALS-associated aggregation prone proteins, such as FUS or SOD1, could be examined in the future. The results presented in this chapter show that TBK1 is unlikely to be involved in the formation or degradation of autophagosomse during aggrephagy. In contrast, TBK1 may negatively influence the degradation of insoluble ubiquitin via autophagy. Furthermore, ALS/FTD-TBK1 is implicated in the formation of TDP-43 inclusions. Therefore, the results described in this chapter imply a novel role for TBK1 in TDP-43 aggregation.

Chapter 6

Final discussion

Recently, TBK1 has been identified as a causative gene in ALS and FTD [17, 18]. However, it remains unclear how the mutations identified in ALS and FTD patients lead to neurodegeneration. Previous studies have suggested that haploinsufficiency may be an underlying pathogenic mechanism [18] because patient derived fibroblasts harbouring *TBK1* mutations show lower protein expression [496]. However, the molecular mechanisms leading to the lack of protein expression and motor neuron death remains undefined.

Therefore, this thesis aimed to examine how TBK1 and associated ALS/FTD mutants affect its normal involvement in different subtypes of autophagy. Due to the importance of basal autophagy in survival, maintaining homeostatsis and in the prevention of neurodegeneration [393, 400, 678], the role of TBK1 in basal autophagy was extensively analysed (Chapter 3 and Chapter 4). Insoluble protein inclusions are the pathological hallmark of ALS [2], and the accumulation of such inclusions can be caused by dysfunctional autophagy [679]. Hence in this thesis it was examined how TBK1 functions in the aggregation and removal of protein aggregates, and more precisely in those formed by TDP-43, a protein that is present in 97% of ALS cases [2] (Chapter 5). The role of TBK1 in autophagy so far has been linked to its interaction with autophagy receptors during selective autophagy. In contrast, upon nutrient deprivation, non-selective autophagy occurs where non-essential cellular components undergo autophagic degradation. Due to the lack of extensive research how the selection of non-essential cell components is being undertaken, in this thesis it was examined whether autophagy receptors and TBK1 are involved in non-selective autophagy (Chapter 3 and Chapter 4).

6.1. The difficulties involved in autophagy detection

Autophagy is a complex, multistep process that involves intricate interactions between many different proteins. Due to the complexity of this cellular process, it has been debated for some years how to accurately monitor autophagy and many publications aim to describe suitable methods [458, 460, 680-684]. Furthermore, autophagy is the only cellular pathway that has its own published guidelines (200 pages, featuring thousands of authors) that describe how to detect autophagy function and dysfunction experimentally [464]. This therefore highlights how difficult it is to accurately examine autophagy.

Despite using several different techniques in this thesis to precisely analyse autophagy, in strict accordance with the published guidelines, the results presented were contradictory and inconclusive on several occasions, further confirming the complexities in the detection of this particular pathway.

A panel of autophagy assays were selected for this study. They were designed to complement each other in order to obtain a comprehensive analysis of autophagy in the cells examined. However, each technique has its own advantages and disadvantages, and each one is more sensitive to detect a specific part of the autophagy process.

Immunoblotting of LC3 detects the conversion of LC3-I into LC3-II. This allows the quantification of phagophores and autophagosomes together and provides an overview of all phagophores/autophagosomes in the population, but it does not represent the heterogeneity in the population. Autophagy induction is dependent on which stage of the cell cycle the cells are in, especially following starvation [685]. This may explain why in certain experiments in this thesis examining starvation-induced autophagy, considerable variability was detected, not just from immunoblotting studies **(Figure 3.5)** but using other techniques as well. Immunoblotting of LC3 and/or any other autophagy markers is a quick and easy way of following autophagy.

A novel FC-saponin analysis method was established in this thesis to examine autophagy in a high throughput manner, at the single cell level. Overexpression of LC3-EGFP-mCherry allows the simultaneous examination of autophagosomes and autolysosomes, due to the quenching of the EGFP signal in the autolysosomes. The analysis of $EGFP^{+}/mCherry^{+}$ vs $EGFP^{-}/mCherry^{+}$ cells compared the cells containing autolysosomes only ($EGFP^{-}/mCherry^{+}$) or the autophagosomes that are present also ($EGFP^{+}/mCherry^{+}$). The disadvantage of this FC technique is that each cell is analysed as a whole, therefore individual vesicles (autophagosomes or autolysosomes) cannot be examined individually. However, cells are examined at a single cell level, therefore representing the heterogeneity of the cell population. It should also be mentioned that analysing autophagy via FC is not a widely used technique, only a handful of publications have previously reported using this method. However, the method established in this thesis combined previously reported techniques to design an effective, reliable and reproducible autophagy detection system.

Regardless of the novel FC analysis technique, conventional microscopy analysis and immunoblotting were also included in these studies as well for comparison. Confocal microscopy analysis allows the detection of individual LC3 autophagosome vesicles. However considerable variability was detected between replicates using confocal microscope analysis. This was seen previously during FC analysis; when only EGFP signals were examined. This summary therefore shows that even with strict experimental designs, detection of autophagy is problematic at the least.

Future perspectives: In this study saponin was used to extract soluble proteins allowing the detection of organelles bound LC3 by flow cytometry. This was confirmed by the extraction of GAPDH followed by immunoblotting. To confirm that saponin treatment does not extract insoluble proteins, future experiments should include the detection of other organelle bound insoluble protein, such as those linked to the ER membrane. In the future, to alleviate the variability between experiments, confocal microscopy analysis could include imaging of whole cells expressing LC3-EGFP-mCherry, using three-dimensional image z-stack reconstructions. Hence, autophagosomes and autophagosomes/autolysosomes could be more accurately quantified regarding their size and number. Furthermore, other autophagy markers could be examined in the analysis, including proteins indicated in the initiation of autophagy (ULK1, atg9, Beclin1) or marker of lysosome such as LAMP2a.

6.2. The role of TBK1 in autophagosome formation and degradation

TBK1 is a serine-threonine kinase [465], therefore the loss of its kinase activity may have detrimental effect on motor neurons and other cell types, due to the lack of phosphorylation of its substrates. Inhibition of TBK1's kinase activity, without interfering with its substrate binding domain, was achieved using two TBK1 inhibitors in this thesis (BX795 and MRT67307).

Treatment with the TBK1 inhibitors showed that the kinase activity of TBK1 facilitates the fusion of autophagosome with lysosomes during both basal and starvation-induced autophagy. Furthermore, the formation of autophagosomes was inhibited during

basal autophagy. In contrast, the TBK1 kinase activity did not affect autophagosome formation or degradation during MG132 induced autophagy (aggrephagy). These data indicate that TBK1 has a more widespread role in autophagy than was previously considered. However, TBK1 is not involved in every subtype of selective autophagy, but it is most likely associated with only a few such as the previously described mitophagy, and xenophagy [132, 394, 456, 478, 480, 482, 485-487, 568, 630, 631, 670]).

The data obtained in this study indicates that inhibition of TBK1 impairs autophagy and potentially leads to the accumulation of cargo/damaged organelles. Interestingly, degradation of insoluble ubiquitin, which was used to follow aggrephagy, showed that ubiquitin is not a cargo that accumulates when the TBK1 kinase activity is inhibited. This suggests that while TBK1 inhibition leads to impaired basal and starvation-induced autophagy, this may not translate into ubiquitin accumulation, implying that this is not a mechanism by which TBK1 mutations lead to ALS. This notion was confirmed upon overexpression of ALS-mutant TBK1 in this thesis. Overexpression of WT, ALS/FTD (and HSE) mutant TBK1 inhibited autophagosome-lysosome fusion during basal autophagy, implying that a gain of toxic function results when TBK1 is overexpressed. This was a somewhat unexpected result, however, it shows that the different ALS mutants do not influence basal autophagy any differently than overexpressed WT-TBK1. Hence, these mutations may not lead to ALS via impaired fusion of autophagosomes and lysosomes during basal autophagy.

In contrast, during starvation-induced autophagy, only overexpression of the kinase deficient mutant TBK1 affected autophagosome-lysosome fusion. While the results obtained from expression of the R357Q-TBK1 and G159A-TBK1 mutants were not significantly different to WT-TBK1, these data still suggest that the kinase activity of TBK1 is indeed involved in the fusion of the autophagosome with lysosomes, thus potentially impairing the cellular response to extracellular stress. Furthermore, none of the TBK1-FLAG overexpressed proteins influenced autophagosome-lysosome fusion during MG132 induced autophagy. This was consistent with the similar data obtained using the kinase inhibitors. Together this suggests that TBK1 is not involved in the formation or degradation of the autophagosome during the MG132 induced autophagy.

6.3. The role of TBK1 in omegasome formation

The membranes of the autophagosome originate in neurons from the ER. Omegasome formation has not been studied in relation to TBK1 yet, therefore in this thesis it was aimed to examine whether TBK1 affects the formation of omegasome. Inhibition of the TBK1 kinase activity inhibited omegasome formation under starvation conditions, but not under basal or MG132 induced autophagy conditions. These results imply that TBK1 is involved in the formation of the omegasome upon starvation-induced stress. Interestingly, overexpression of TBK1-FLAG proteins, either WT or any of the mutants, did not significantly affect the formation of DFCP1 vesicles, suggesting that increased levels of TBK1 do not influence omegasome formation.

Future perspectives: Future studies should include a more in-depth analysis of omegasome formation in relation to TBK1, including colocalization between DFCP1, WIPI2 and LC3.

6.4. TBK1 knock-out does not affect autophagosome formation or degradation

Knock-out of TBK1 was carried out to examine the consequences of absence of TBK1 on the different types of autophagy. Surprisingly the knock-out of TBK1 did not affect the formation or degradation of autophagosome in any of the subtypes of autophagy analysed here. In contrast, previously, knock-out of TBK1 inhibited efficient autophagosome formation around depolarized mitochondria [456], and also it inhibited autophagosome maturation during xenophagy [487]. In this thesis similar autophagy dysfunction was detected upon TBK1 inhibition. Although the previous studies did not use CRISPR/cas9 genome editing as used in this thesis. Long-term culturing of CRISPR/cas9 genome edited cells may result in the development of compensatory mechanisms in these cells, as discussed in section 3.23. In terms of TBK1, compensatory mechanisms in the CRISPR/cas9 cells used in this study is a plausible hypothesis given the important roles of TBK1 during autophagy. While TBK1 knock-out in the CRISPR/cas9 cells did not alter autophagy, during basal autophagy the binding between LC3 and p62 significantly decreased. This confirms that lack of TBK1 expression did lead to significant changes in HEK293T cells, however these changes did not translate into altered autophagy. In contrast to these findings, knock-out of TBK1 also elevated the

degradation of ubiquitin under inhibited UPS conditions (section). This suggests that TBK1 may have a negative regulatory role in ubiquitin degradation.

Future perspectives: To conclusively confirm the effects of TBK1 deletion, further experiments are required. These could include treating CRISPR/ca9 genome edited cells 72 hr after transfection and perform immunoblotting only on TBK1 knock-out cells using a Cell Sorter, so that TBK1 knock-out cells can be analysed shortly after knock out, therefore eliminating long-term in-vitro culturing and possibly compensatory mechanisms. Sorted cells could be used for immunoblotting experiments or placed back to culture and analyse them following transfection with different LC3 constructs.

6.5. TBK1 is involved in TDP-43 aggregation

TDP-43 aggregates are present in 97% of all ALS patients, even if the *TARDBP* gene is not mutated [2]. Therefore, it was examined whether TBK1 is involved in the formation of TDP-43 aggregates. Inhibition of TBK1 kinase activity did not conclusively prove that TBK1 regulates TDP-43 aggregation or clearance. In contrast, expression of the ALS/FTD mutant E696K-TBK1, which lacks the capacity to bind towards optineurin, led to elevated formation of TDP-43 aggregates. TDP-43 aggregates are known to be degraded by autophagy whereas soluble TDP-43 is degraded via the UPS [686]. Therefore, a possible explanation for increased TDP-43 inclusion formation in the presence of E696K-TBK1 would be that the E696K mutant inhibits autophagic degradation of TDP-43. Similarly, overexpression of E696K led to inhibited autophagosome degradation during basal autophagy, which represents similar conditions as TDP-43 transfected cells, which are kept in serum rich media for the entire experiment. This raises the question of why the other ALS mutants or WT-TBK1 did not induce TDP-43 aggregation, when they still inhibited autophagsosme degradation upon overexpression. The most plausible explanation is that the optineurin binding capacity of TBK1 may be a very important factor in TDP-43 aggregation. Previously, optineurin was shown to mediate the aggrephagy of both $SOD1^{G93C}$ and htt^{Q103} [140].

Future directions: In the future it should be examined whether ALS-TBK1 mutant proteins affect the formation of other aggregation prone proteins, including mutant FUS,

mutant SOD1, or even the C9orf72 DPRs, or whether the TBK1 mutant affects TDP-43 only.

6.6. Involvement of autophagy receptors in basal, starvation and MG132 induced autophagy

Autophagy receptors tether cargo towards the forming phagophore and provide the link between the autophagosome membrane protein, LC3, and the degrading cargo [390]. Autophagy receptors, such as optineurin, p62 or NDP52 are known to be involved in selective autophagy, including mitophagy, xenophagy and aggrephagy. Furthermore, the majority of their functions in this regard are mediated by TBK [392, 394, 456, 478, 480-482, 485-487, 628, 630, 631, 670, 687]. In this thesis, it was examined how these autophagy receptors take part in basal and non-selective autophagy.

NDP52 and p62 immunoprecipitated with LC3 during all the types of autophagy examined in this thesis; basal autophagy, starvation-induced autophagy and MG132 induced autophagy, indicating their involvement in cargo tethering. In the absence of TBK1, the LC3 and p62 interaction weakened during basal autophagy, suggesting that TBK1 actively takes part in p62-mediated cargo tethering during basal autophagy. Interestingly, the kinase activity of TBK1 facilitates the interaction between the two autophagy receptors, p62 and optineurin, during basal autophagy. In contrast, TBK1 knock-out did not affect the interaction between autophagy receptors and LC3 during starvation-induced and MG132 induced autophagy, indicating that TBK1 does not take part in cargo tethering in these two types of autophagy. This was not surprising because TBK1 was also not involved in the formation of autophagosome during these two types of autophagy, confirming that TBK1 is not involved in these processes.

Future perspectives: To further confirm that TBK1 does not influence the autophagy receptors and LC3 interactions during starvation and MG132 induced autophagy upon TBK1 inhibitions, further immunoprecipitation experiments could be performed. Immunoprecipitation of TBK1 upon inhibition should be performed to confirm the binding between TBK1, LC3 and autophagy receptors during different types of autophagy.

It should also be noted that experiments in this thesis were carried out using HEK293T cells, derived from human kidney, are cancerous. Therefore, further experiments using neuronal cell lines, or preferably neurons or neuron derived IPSCs, are needed to confirm the finding presented in this study. Furthermore, the use of an in-vivo disease model would also be worthwhile in the future to validate the results described in this thesis.

6.7. Major finding of this thesis

In summary, here it was showed the first time that; **(Figure 6.1)**

- The TBK1 kinase activity may be involved in regulating autophagosome and lysosome fusion in starvation-induced autophagy, but it is not involved in MG132 induced autophagy, representing aggrephagy.
- The TBK1 kinase activity facilitates interactions between the different autophagy receptors and TBK1 enhances the p62 and LC3 interaction.
- The TBK1 kinase activity may facilitate omegasome formation during starvation-induced autophagy, but not during basal or MG132 induced autophagy.
- Overexpression of ALS/FTD TBK1 mutants (R357Q, E696K) do not affect basal, starvation or MG132 induced autophagy compared to WT-TBK1.
- Inhibition of TBK1 does not affect degradation of ubiquitin or the formation of TDP-43 aggregates.
- Knock-out of TBK1 elevates ubiquitin degradation via autophagy.
- ALS/FTD mutant TBK1^{E696K} induces the formation of TDP-43^{WT} aggregation but not the artificial cytoplasmic mutant TDP-43 ^{dNLS}.

Furthermore, it was also demonstrated in contrast to previous studies that;

- Knock-out of TBK1 does not affect autophagosome formation or degradation in HEK293T cells during basal, starvation or MG132 induced autophagy.

Therefore, the data demonstrated in this thesis propose new roles for TBK1 in basal and starvation-induced autophagy in the formation of the omegasome. They also show that specific mutations in *TBK1* in ALS enhance the aggregation of TDP-43^{WT}.

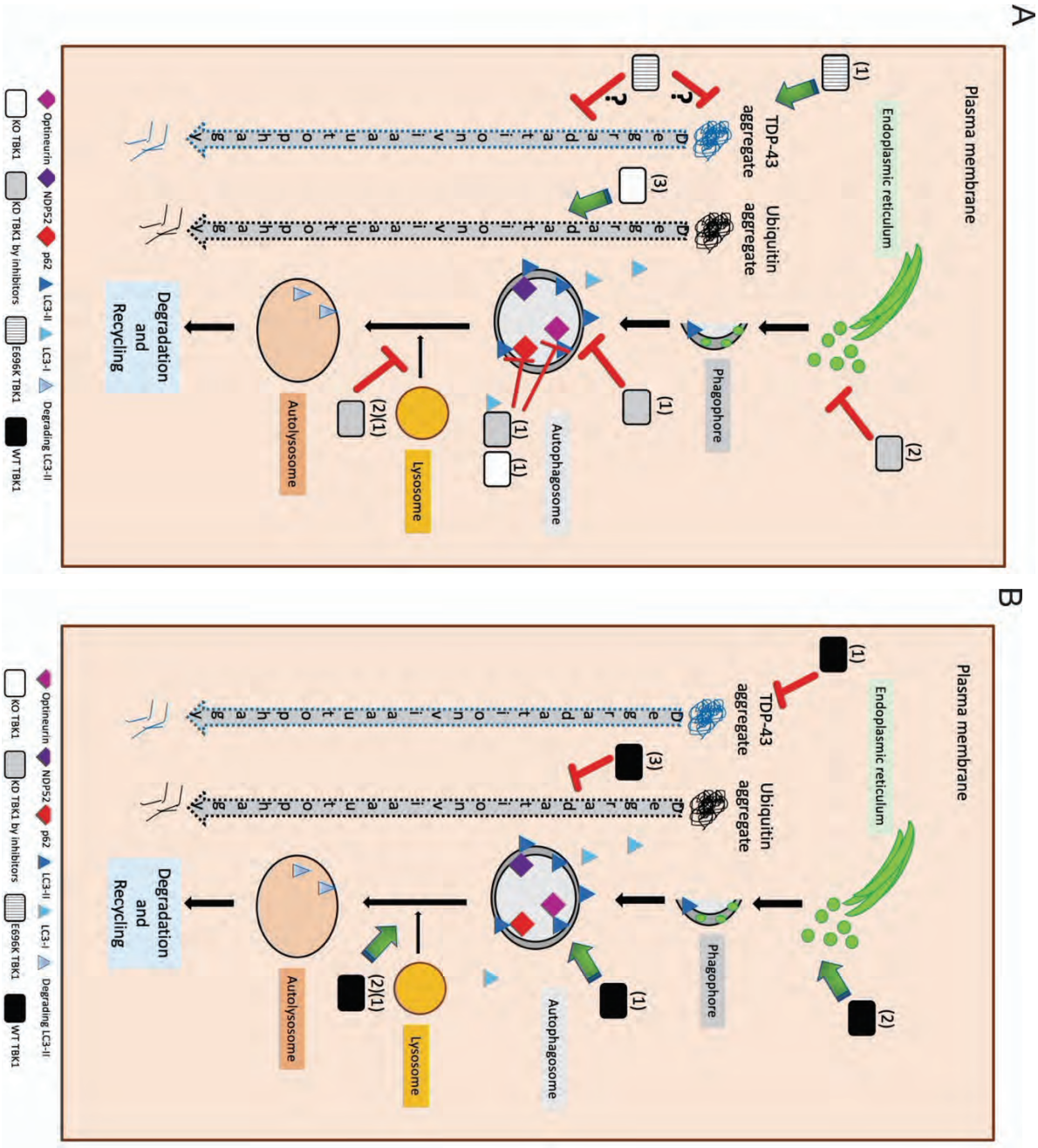


Figure 6.1. Schematic overview of results obtained in this thesis and proposed role of TBK1 in autophagy. (A) Kinase deficient TBK1 blocks the degradation of the autophagosome during basal and starvation-induced autophagy, and the formation of the omegasome, during starvation-induced autophagy. TBK1 inhibition decreased the binding between the autophagy receptors and induced the binding between LC3 and p62 or optineurin. Knock-out of TBK1 decreased the biding between LC3 and autophagy receptor, p62. Knock-out of TBK1 enhances autophagic degradation of ubiquitin. ALS/FTD mutant TBK1, E696K, induces TDP-43 inclusion formation. **(B)** TBK1 facilitates the fusion of the autophagosome with the lysosome and mediates the binding between autophagy receptors and LC3 during basal autophagy, therefore facilitating

autophagic degradation. TBK1 inhibits the autophagic clearance of ubiquitin. Mutations in the optineurin binding domain of TBK1 in ALS promote TDP-43 aggregation, potentially underlying its pathogenicity in ALS. (1): basal autophagy, (2): starvation-induced autophagy; (3); aggrephagy.

6.8. Limitations of the study

The experiments described in this thesis were carried out with the strictest rigor. However, the data obtained may be limited due to the experimental systems used in this study.

Firstly, the data obtained in this study were all obtained using *in-vitro* cell culture models using HEK293T, human embryonic kidney cells, which had been previously immortalized by transduction with sheared adenovirus 5 DNA [516]. While the HEK293T cell line is widely used in molecular biology studies, it obviously bears few neuron-like characteristics. It does however express neurofilament subunits, which are typically found in neurons [688]. Therefore, the results obtained in this thesis should be confirmed ideally using in-vivo models or alternatively using primary neuron cultures, such as human primary cortical or motor neurons expressing TBK1 proteins, or IPSC-derived motor neurons.

Secondly, another possible limitation of the study may be in the culturing of cells. HEK293T cells were cultured in Dulbecco's modified Eagle's medium (DMEM) supplemented with 10 % fetal bovine serum. DMEM contains 4.5g/L D-glucose, which represents diabetic levels of glucose supplementation, although these are standard conditions used for *in vitro* cell culture. Studies have shown that high glucose inhibits autophagy [689-691], therefore more physiological glucose levels during culturing may enhance differences seen upon TBK1 dysfunction.

Thirdly, TBK1's kinase activity was examined using compounds that were developed as specific TBK1 inhibitors. However, inhibitors often have off-target effects. Strict experimental designs and inhibitor concentrations were used to minimise off-target effects in this study, however in the future, some of the known alternative targets of these inhibitors could be examined in the assays used in this thesis.

Lastly, the consequences of ALS/FTD mutant TBK1 proteins on autophagy were evaluated by overexpression, which are higher than physiological/endogenous protein levels. As it was observed in this thesis, overexpression of even WT TBK1 resulted in unexpected inhibitory effects in basal and starvation-induced autophagy. Analysis of endogenous levels of these TBK1 proteins could be analysed in the future by introducing site specific mutations in the genome of cells using CRISPR/cas9 editing or potentially using patient derived IPSCs.

6.9. Future perspectives

As well as the future studies already discussed above, it would be worthwhile to examine the role of TBK1 in neuroinflammation in the future. Neuroinflammation refers to an inflammatory response of the central nervous system. It is accepted that non-cell autonomous responses mediated by microglia and astrocytes are one of the underlying mechanisms for ALS (section 1.2.8). Furthermore, previous studies have shown that TBK1 is involved microglial activation in the transgenic SOD1G93A mouse model of ALS [510], and TBK1 inhibits RIPK1 [598] which mediates axonal degradation via neuroinflammation [692]. Neuroinflammation was shown to induce autophagy flux blockage and caused neural excitotoxicity during stress induced hypertension in rats [693]. In contrast autophagy induction in microglia, promotes microglia polarization toward M2 (anti-inflammatory) phenotype inflammation resolution [694]. Therefore ALS-TBK1 may lead to detrimental neuroinflammatory response via influencing autophagy of microglia that may explain its causative role in ALS.

Chapter 7

Supplementary data

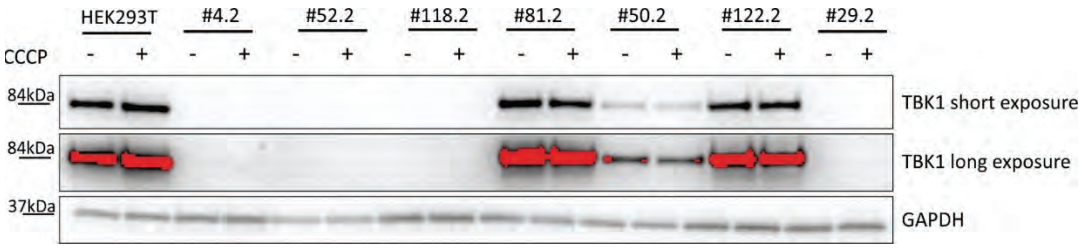


Figure S1. Levels of TBK1 in CRISPR/Cas9 knock-out cells.

CRIPSR/Cas9 edited HEK293T cells were incubated overnight and treated with 30uM of carbonyl cyanide m-chlorophenylhydrazone (CCCP-Sigma) for 30min, lysed and immunoblotting for TBK1 was performed. *Lack of TBK1 expression is evident on the oversaturated blot (middle blot).* Every second lane represents HEK293T cells treated with CCCP to depolarise the mitochondria.

Appendix I

Appendix I describes the generation of the mutant TBK1 FLAG overexpressing constructs used in this thesis. The data presented here was part of Master of Research (MRes) thesis titled "Cellular Pathogenic Mechanisms Linked to TBK1 and Optineurin in Amyotrophic Lateral Sclerosis" submitted by the author to Macquarie University in 2016. Therefore, the data presented in Appendix I are not examinable, however, they are included for easier understanding of the data presented in this PhD thesis. All data was extracted from MRes thesis, however, the figures were prepared to fit into the style of this thesis.

Single point mutations were introduced into WT-TBK1 using pcDNA3.1-FLAG-WT-TBK1 plasmid as a template (a kind gift of Jean-Laurent Casanova -The Rockefeller University, New York). Site directed mutagenesis was performed using a Q5® Site-Directed Mutagenesis Kit (New England Biolabs), following the manufacturer's instructions. Primers were designed to introduce nucleotide substitutions using NEBaseChanger (http://nebasechanger.neb.com/) into the WT-TBK1 sequence using NCBI database (NCBI Reference Sequence: NM_013254.3). Mutagenesis primers were used to create the following mutations; R357Q mutations FP: 5'-ctacgaagggcaacgcttagtct-3', RP: 5'-ataagttcttgatttgaagaaataattttgg-3'. E696K mutation FP: 5'-attaaaggaaaagatggaagggg-3', RP: 5'-ttcttcataccaagagtcatttc-3'. The successful incorporation of these mutations was confirmed by sequencing **(Figure A1.A)**. Immunoblotting using anti-human-TBK1 antibodies confirmed overexpression of R357Q -TBK1 and E696K-TBK1 **(Figure A1.B)**. Other mutations are also represented on this blot that were not used in this thesis (R308Q, E643X, D50A). Detection of phosphorylated TBK1 indicates that R357Q has significant lower levels of autoactivation, confirming its kinase deficiency.

TBK1-FLAG overexpression was also detected by confocal imaging and all overexpressed TBK1 proteins formed a cytoplasmic diffuse pattern when examined by microscopy. None of the TBK1 mutants formed visible inclusions upon overexpression **(Figure A2**).

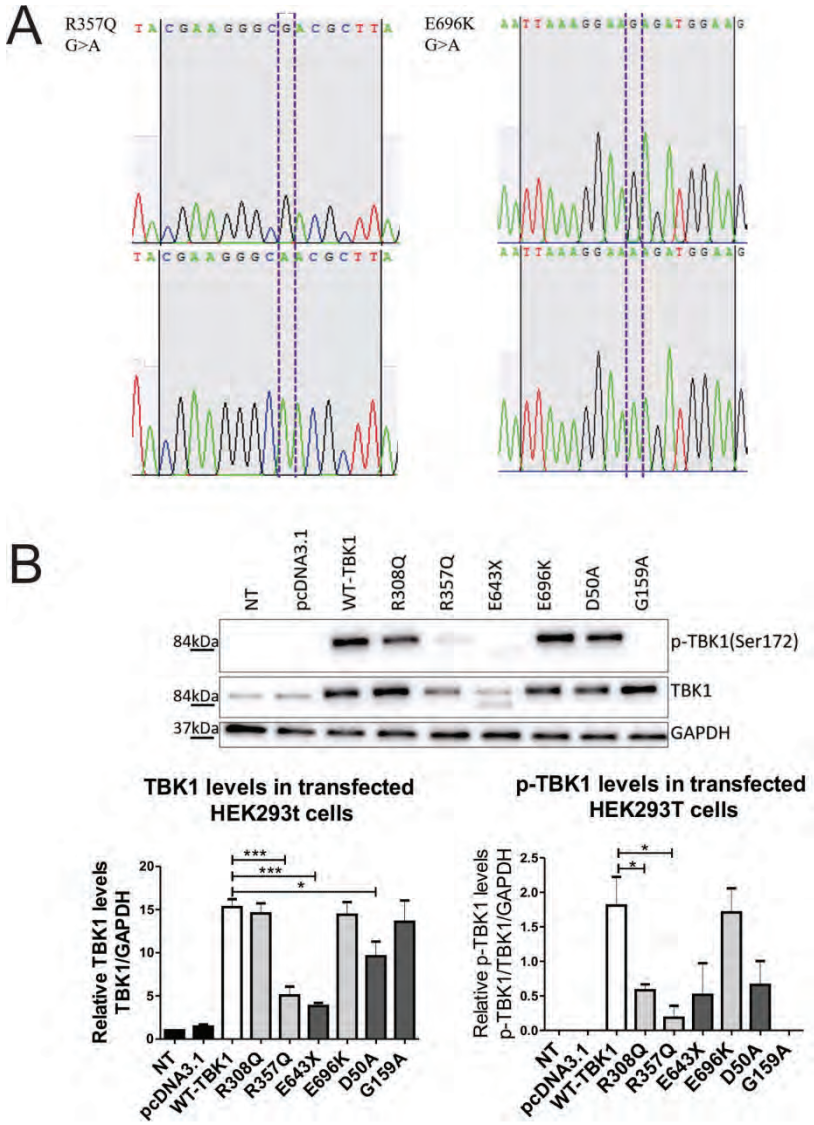


Figure A1: Generation and overexpression of TBK1-FLAG in HEK293T cells

(A) *Sequencing of the generated R357Q, E696K and mutant constructs.* Mutagenesis was successful in each case, as indicated by the presence of the altered nucleotides at the appropriate position in the TBK1 sequence, as indicated by the black arrows. **(B)** *Total and p-TBK1(Ser172) detection in WT and mutant TBK1 overexpressing HEK293 cells*. Total TBK1 and p-TBK1 detection by immunoblotting in TBK1 transfected HEK293 cells. Blot was stripped and reprobed for GAPDH as a loading control. Quantitative comparison of total endogenous, WT and mutant TBK1 levels in HEK293 cells using ImageJ. N=4, Quantitative comparison of endogenous, WT and mutant p-TBK1 levels in HEK293 cells using ImageJ. N=3, Mean +/- SEM is presented on the graphs. ***P>0.0005, *P>0.05(Unpaired Student-t-test) NT; non-transfected, WT; wildtype.

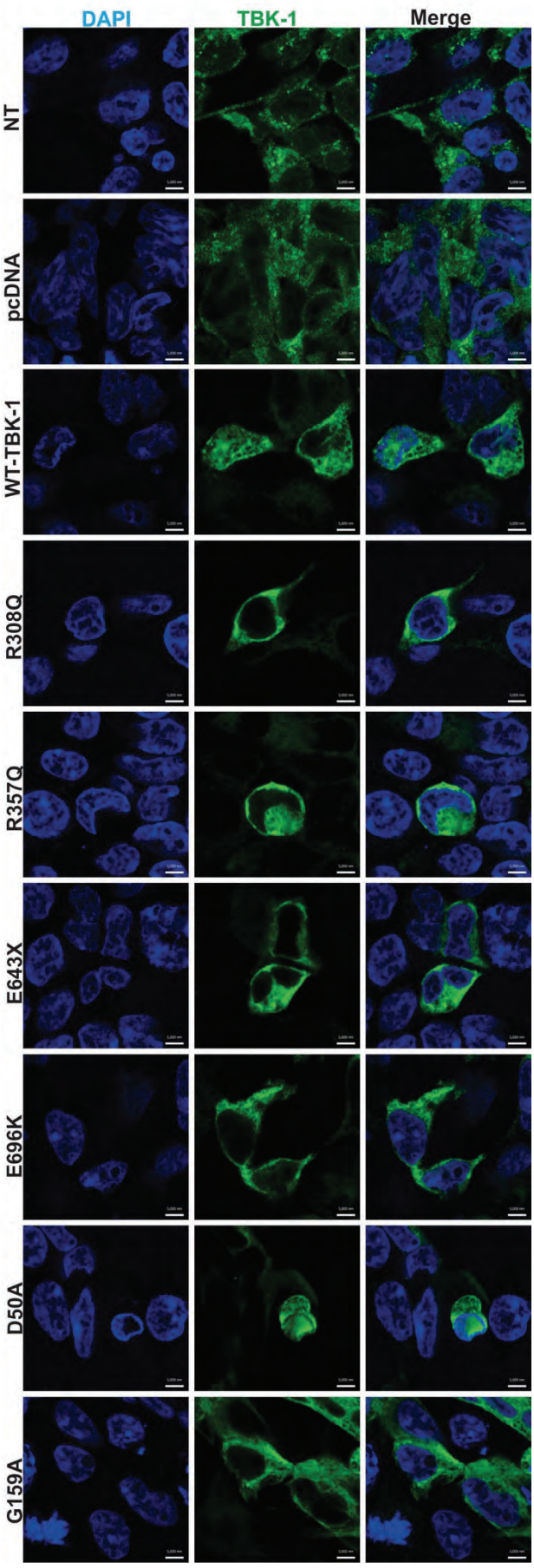

DAPI
TBK-1
Merge
NT
pcDNA
WT-TBK-1
R308Q
R357Q
E643X
E696K
D50A
G159A

Figure A2: Detection of overexpressed TBK1 via immunocytochemistry and confocal fluorescent microscopy in HEK293T cells. Endogenous TBK1 is expressed in a punctuate pattern in NT and pcDNA3.1 conditions, consistent with previous observations. Every cell examined displayed TBK1 staining. In contrast, overexpressed TBK1 was expressed in a diffuse cytoplasmic, non-punctuate pattern, in both WT and mutant TBK1 transfected cells. The microscope settings (gain function) were adjusted to only detect exogenous TBK1, hence there is an apparent lack of signal in several cells. Scale bar: 5μm.

Appendix II

Appendix II shows STR analysis, performed by the Garvan Institute, of the CRISPR/Cas9 edited HEK293T cells. STR results are labelled with #, where #1 corresponds to clone 118.2, #2-clone 52.2, #3- clone 122.2, #4-HEK293T.

CELL-LINE IDENTIFICATION SERVICE REPORT FORM		
Title: CELL-LINE IDENTIFICATION SERVICE REPORT FORM	Document No	30.A
	Version:	3
	Effective Date:	15th August 2015

GARVAN INSTITUTE

NATA

Accredited for compliance with ISO/IEC 17025. The results of the tests, calibrations and/or measurements included in this document are traceable to Australian/national standards

Certificate of Analysis

Authorisation

Authorised by:	Pavel Bitter
Date:	26/04/2018
Reviewed by:	Eve Radunz
Date:	25/04/2018

Sender

Name:	Audrey Ragagnin
Address:	Macquarie Univeristy Dept of Biomedical Sciences 2 Technology Place, NSW, 2109, Macquarie University
Email:	'audrey.ragagnin@mq.edu.au'

Cell Line Sample

Sample Name:	#1 (Reka 17/04/2018)
Garvan Sample ID:	704
Submission Date:	16/04/2018

Testing Performed

Identification of human cell lines is performed by analysis of microsatellite profiles. A set of 18 selected and established loci of tetra- and pentanucleotide repeats is amplified via PCR with the extracted DNA of the cell-line cells. The results are compared to other holdings of the same cell line. Microsatellite profiles can vary with the passage number due to intrinsic genetic instability; some markers show addition or loss of alleles. Therefore samples from the same cell-line can produce similar but slightly different profiles. Cell-line IDs are considered to be a match if their profiles are more than 80% identical.

The results included here relate only to the sample tested. This test report shall not be reproduced except in full, without full written approval of the testing laboratory. This test is for research use only and is not appropriate for human clinical or diagnostic samples.

Analysis Performed

Three databases: ATCC, DSMZ and Garvan internal database are referred to for performing the final STR profile analysis. Nine out of the 18 available loci/markers are compared to these databases (D5S818, D13S317, D7S820, D16S539, VWA, TH01, AM, TPOX, CSF1PO). The match is based on the number of shared alleles between the sample being tested and the reference cell line from the database. This is then expressed as a percentage or an evaluation value. Only the highest percentage match (can be more than one) will be reported. In case, no matches were found in these available databases, following three scenarios may apply:

1. Client will be requested for the cell line vendor information
2. Client will be requested for the DNA profile of cell line being tested and then matched to this available information
3. For DNA profiles that are proprietary or cannot be shared, only the STR profile generated at GMG will be sent for the client to match and compare.

Garvan Molecular Genetics

STR Profile - Sample

Sample Name	#1 (Reka 17/04/2018)
Source	Cells
Garvan ID	704
D5S818	8,10
D13S317	11,12,13,15
D7S820	10,11
D16S539	9,13
vWA	16,19,20
TH01	7,9.3
Amel	X
TPOX	11
CSF1PO	11,12
D8S1179	11,12,14
D21S11	28,29,30.2
D3S1358	14,15,16,17
D2S1338	19
D19S433	17,18
D18S51	17
FGA	23,24
Penta E	7,13,15
Penta D	9,10

Reference/Repository Sample

Sample Name	293T
Source	ATCC-ACS-4500; 100% match with ATCC HEK 293T/17(sample slightly overloaded hence some run artefacts)
Garvan ID	005
D5S818	8,9
D13S317	12,14
D7S820	11
D16S539	13,9
vWA	16,19
TH01	7,9.3
Amel	X
TPOX	11
CSF1PO	11,12
D8S1179	12,14
D21S11	28,30.2
D3S1358	15,17
D2S1338	19
D19S433	12.1,18
D18S51	17,18
FGA	23
Penta E	15,7
Penta D	10,9

Comments

The sample is 87% identical to HEK 293T/17. 87% similarity is considered related according to the ASN-0002 Standard. Cell lines with >80 % match are considered to be related; derived from a common ancestry. Cell lines with between a 55 % to 80 % match require further profiling for authentication of relatedness. In saying cell line samples have a common ancestry, these samples may come from the same cell line; from two separate cell lines that were derived from the same donor; one cell line may be derived from the other; or one cell line may be misidentified or cross-contaminated.Cell lines with >80 % match are considered to be related; derived from a common ancestry. Cell lines with between a 55 % to 80 % match require further profiling for authentication of relatedness. In saying cell line samples have a common ancestry, these samples may come from the same cell line; from two separate cell lines that were derived from the same donor; one cell line may be derived from the other; or one cell line may be misidentified or cross-contaminated.

Garvan Molecular Genetics
L8, 384 Victoria Street
Darlinghurst, 2010, NSW
Ph: (02) 92958384
http://www.garvan.org.au
mailto:gmg@garvan.org.au

Document Version Details		
	Name/Date	**Title**
Originally Created by	Pavel Bitter	Molecular Genetics Facility Manager
Date created	15.08.2014	
Current version	3	
Date reviewed	21.08.2015	
Reviewed by	Hiren Sheth	Services Coordinator
Authorized by	Deborah Kelly	Quality Manager
Date authorized	15.08.2014	
Issued Date	15.08.2014	

CELL-LINE IDENTIFICATION SERVICE REPORT FORM		
Title: CELL-LINE IDENTIFICATION SERVICE REPORT FORM	Document No	30.A
	Version:	3
	Effective Date:	15th August 2015

GARVAN INSTITUTE

NATA

Accredited for compliance with ISO/IEC 17025
The results of the tests, calibrations and/or measurements included in this document are traceable to Australian/national standards

Certificate of Analysis

Authorisation

Authorised by:	Pavel Bitter
Date:	26/04/2018
Reviewed by:	Eve Radunz
Date:	25/04/2018

Sender

Name:	Audrey Ragagnin
Address:	Macquarie Univeristy Dept of Biomedical Sciences 2 Technology Place, NSW, 2109, Macquarie University
Email:	'audrey.ragagnin@mq.edu.au'

Cell Line Sample

Sample Name:	#2 (Reka 17/04/2018)
Garvan Sample ID:	705
Submission Date:	16/04/2018

Testing Performed

Identification of human cell lines is performed by analysis of microsatellite profiles. A set of 18 selected and established loci of tetra- and pentanucleotide repeats is amplified via PCR with the extracted DNA of the cell-line cells. The results are compared to other holdings of the same cell line. Microsatellite profiles can vary with the passage number due to intrinsic genetic instability; some markers show addition or loss of alleles. Therefore samples from the same cell-line can produce similar but slightly different profiles. Cell-line IDs are considered to be a match if their profiles are more than 80% identical.

The results included here relate only to the sample tested. This test report shall not be reproduced except in full, without full written approval of the testing laboratory. This test is for research use only and is not appropriate for human clinical or diagnostic samples.

Analysis Performed

Three databases: ATCC, DSMZ and Garvan internal database are referred to for performing the final STR profile analysis. Nine out of the 18 available loci/markers are compared to these databases (D5S818, D13S317, D7S820, D16S539, VWA, TH01, AM, TPOX, CSF1PO). The match is based on the number of shared alleles between the sample being tested and the reference cell line from the database. This is then expressed as a percentage or an evaluation value. Only the highest percentage match (can be more than one) will be reported. In case, no matches were found in these available databases, following three scenarios may apply:

1. Client will be requested for the cell line vendor information
2. Client will be requested for the DNA profile of cell line being tested and then matched to this available information
3. For DNA profiles that are proprietary or cannot be shared, only the STR profile generated at GMG will be sent for the client to match and compare.

Garvan Molecular Genetics

STR Profile - Sample

Sample Name	#2 (Reka 17/04/2018)
Source	Cells
Garvan ID	705
D5S818	8,9
D13S317	11,12,13
D7S820	10,11
D16S539	9,13
vWA	16,19
TH01	7,9.3
Amel	X
TPOX	11
CSF1PO	11,12
D8S1179	11,12,15
D21S11	28,29,30.2
D3S1358	14,16,17
D2S1338	19
D19S433	16,17,18
D18S51	17
FGA	23,24
Penta E	7,13,15
Penta D	9,10

Reference/Repository Sample

Sample Name	293T
Source	ATCC-ACS-4500; 100% match with ATCC HEK 293T/17(sample slightly overloaded hence some run artefacts)
Garvan ID	005
D5S818	8,9
D13S317	12,14
D7S820	11
D16S539	13,9
vWA	16,19
TH01	7,9.3
Amel	X
TPOX	11
CSF1PO	11,12
D8S1179	12,14
D21S11	28,30.2
D3S1358	15,17
D2S1338	19
D19S433	12.1,18
D18S51	17,18
FGA	23
Penta E	15,7
Penta D	10,9

Comments

The sample is 84% identical to HEK 293T/17. 84% similarity is considered related according to the ASN-0002 Standard. Cell lines with >80 % match are considered to be related; derived from a common ancestry. Cell lines with between a 55 % to 80 % match require further profiling for authentication of relatedness. In saying cell line samples have a common ancestry, these samples may come from the same cell line; from two separate cell lines that were derived from the same donor; one cell line may be derived from the other; or one cell line may be misidentified or cross-contaminated.Cell lines with >80 % match are considered to be related; derived from a common ancestry. Cell lines with between a 55 % to 80 % match require further profiling for authentication of relatedness. In saying cell line samples have a common ancestry, these samples may come from the same cell line; from two separate cell lines that were derived from the same donor; one cell line may be derived from the other; or one cell line may be misidentified or cross-contaminated.

Appendix II

Garvan Molecular Genetics
L8, 384 Victoria Street
Darlinghurst, 2010, NSW
Ph: (02) 92958384
http://www.garvan.org.au
mailto:gmg@garvan.org.au

Document Version Details		
	Name/Date	**Title**
Originally Created by	Pavel Bitter	Molecular Genetics Facility Manager
Date created	15.08.2014	
Current version	3	
Date reviewed	21.08.2015	
Reviewed by	Hiren Sheth	Services Coordinator
Authorized by	Deborah Kelly	Quality Manager
Date authorized	15.08.2014	
Issued Date	15.08.2014	

CELL-LINE IDENTIFICATION SERVICE REPORT FORM		
Title: CELL-LINE IDENTIFICATION SERVICE REPORT FORM	Document No	30.A
	Version:	3
	Effective Date:	15th August 2015

GARVAN INSTITUTE

NATA

Accredited for compliance with ISO/IEC 17025. The results of the tests, calibrations and/or measurements included in this document are traceable to Australian/national standards.

Certificate of Analysis

Authorisation

Authorised by:	Pavel Bitter
Date:	26/04/2018
Reviewed by:	Eve Radunz
Date:	25/04/2018

Sender

Name:	Audrey Ragagnin
Address:	Macquarie Univeristy Dept of Biomedical Sciences 2 Technology Place, NSW, 2109, Macquarie University
Email:	'audrey.ragagnin@mq.edu.au'

Cell Line Sample

Sample Name:	#3 (Reka 17/04/2018)
Garvan Sample ID:	706
Submission Date:	16/04/2018

Testing Performed

Identification of human cell lines is performed by analysis of microsatellite profiles. A set of 18 selected and established loci of tetra- and pentanucleotide repeats is amplified via PCR with the extracted DNA of the cell-line cells. The results are compared to other holdings of the same cell line. Microsatellite profiles can vary with the passage number due to intrinsic genetic instability; some markers show addition or loss of alleles. Therefore samples from the same cell-line can produce similar but slightly different profiles. Cell-line IDs are considered to be a match if their profiles are more than 80% identical.

The results included here relate only to the sample tested. This test report shall not be reproduced except in full, without full written approval of the testing laboratory. This test is for research use only and is not appropriate for human clinical or diagnostic samples.

Analysis Performed

Three databases: ATCC, DSMZ and Garvan internal database are referred to for performing the final STR profile analysis. Nine out of the 18 available loci/markers are compared to these databases (D5S818, D13S317, D7S820, D16S539, VWA, TH01, AM, TPOX, CSF1PO). The match is based on the number of shared alleles between the sample being tested and the reference cell line from the database. This is then expressed as a percentage or an evaluation value. Only the highest percentage match (can be more than one) will be reported. In case, no matches were found in these available databases, following three scenarios may apply:

1. Client will be requested for the cell line vendor information
2. Client will be requested for the DNA profile of cell line being tested and then matched to this available information
3. For DNA profiles that are proprietary or cannot be shared, only the STR profile generated at GMG will be sent for the client to match and compare.

Garvan Molecular Genetics

STR Profile - Sample

Sample Name	#3 (Reka 17/04/2018)
Source	Cells
Garvan ID	706
D5S818	8,9
D13S317	11,12,13,15
D7S820	10,11
D16S539	9,13
vWA	16,19,20
TH01	7,9.3
Amel	X
TPOX	11
CSF1PO	11,12
D8S1179	11,14
D21S11	28,29,30.2
D3S1358	14,16,17
D2S1338	19
D19S433	17,18
D18S51	17
FGA	23,24
Penta E	7,15
Penta D	9,9.4

Reference/Repository Sample

Sample Name	293T
Source	ATCC-ACS-4500; 100% match with ATCC HEK 293T/17(sample slightly overloaded hence some run artefacts)
Garvan ID	005
D5S818	8,9
D13S317	12,14
D7S820	11
D16S539	13,9
vWA	16,19
TH01	7,9.3
Amel	X
TPOX	11
CSF1PO	11,12
D8S1179	12,14
D21S11	28,30.2
D3S1358	15,17
D2S1338	19
D19S433	12.1,18
D18S51	17,18
FGA	23
Penta E	15,7
Penta D	10,9

Comments

The sample is 81% identical to HEK 293T/17. 81% similarity is considered related according to the ASN-0002 Standard. Cell lines with >80 % match are considered to be related; derived from a common ancestry. Cell lines with between a 55 % to 80 % match require further profiling for authentication of relatedness. In saying cell line samples have a common ancestry, these samples may come from the same cell line; from two separate cell lines that were derived from the same donor; one cell line may be derived from the other; or one cell line may be misidentified or cross-contaminated.Cell lines with >80 % match are considered to be related; derived from a common ancestry. Cell lines with between a 55 % to 80 % match require further profiling for authentication of relatedness. In saying cell line samples have a common ancestry, these samples may come from the same cell line; from two separate cell lines that were derived from the same donor; one cell line may be derived from the other; or one cell line may be misidentified or cross-contaminated.

Garvan Molecular Genetics
L8, 384 Victoria Street
Darlinghurst, 2010, NSW
Ph: (02) 92958384
http://www.garvan.org.au
mailto:gmg@garvan.org.au

Document Version Details		
	Name/Date	**Title**
Originally Created by	Pavel Bitter	Molecular Genetics Facility Manager
Date created	15.08.2014	
Current version	3	
Date reviewed	21.08.2015	
Reviewed by	Hiren Sheth	Services Coordinator
Authorized by	Deborah Kelly	Quality Manager
Date authorized	15.08.2014	
Issued Date	15.08.2014	

CELL-LINE IDENTIFICATION SERVICE REPORT FORM		
Title: CELL-LINE IDENTIFICATION SERVICE REPORT FORM	Document No	30.A
	Version:	3
	Effective Date:	15th August 2015

GARVAN INSTITUTE

NATA

Accredited for compliance with ISO/IEC 17025
The results of the tests, calibrations and/or measurements included in this document are traceable to Australian/national standards

Certificate of Analysis

Authorisation

Authorised by:	Pavel Bitter
Date:	26/04/2018
Reviewed by:	Eve Radunz
Date:	25/04/2018

Sender

Name:	Audrey Ragagnin
Address:	Macquarie Univeristy Dept of Biomedical Sciences 2 Technology Place, NSW, 2109, Macquarie University
Email:	'audrey.ragagnin@mq.edu.au'

Cell Line Sample

Sample Name:	#4 (Reka 17/04/2018)
Garvan Sample ID:	707
Submission Date:	16/04/2018

Testing Performed

Identification of human cell lines is performed by analysis of microsatellite profiles. A set of 18 selected and established loci of tetra- and pentanucleotide repeats is amplified via PCR with the extracted DNA of the cell-line cells. The results are compared to other holdings of the same cell line. Microsatellite profiles can vary with the passage number due to intrinsic genetic instability; some markers show addition or loss of alleles. Therefore samples from the same cell-line can produce similar but slightly different profiles. Cell-line IDs are considered to be a match if their profiles are more than 80% identical.

The results included here relate only to the sample tested. This test report shall not be reproduced except in full, without full written approval of the testing laboratory. This test is for research use only and is not appropriate for human clinical or diagnostic samples.

Analysis Performed

Three databases: ATCC, DSMZ and Garvan internal database are referred to for performing the final STR profile analysis. Nine out of the 18 available loci/markers are compared to these databases (D5S818, D13S317, D7S820, D16S539, VWA, TH01, AM, TPOX, CSF1PO). The match is based on the number of shared alleles between the sample being tested and the reference cell line from the database. This is then expressed as a percentage or an evaluation value. Only the highest percentage match (can be more than one) will be reported. In case, no matches were found in these available databases, following three scenarios may apply:

1. Client will be requested for the cell line vendor information
2. Client will be requested for the DNA profile of cell line being tested and then matched to this available information
3. For DNA profiles that are proprietary or cannot be shared, only the STR profile generated at GMG will be sent for the client to match and compare.

Garvan Molecular Genetics

STR Profile - Sample

Sample Name	#4 (Reka 17/04/2018)
Source	Cells
Garvan ID	707
D5S818	8,9
D13S317	11,12,13,14
D7S820	10,11
D16S539	9,13
vWA	16,19,20,22
TH01	7,9.3
Amel	X
TPOX	11
CSF1PO	11,12
D8S1179	11,12,14
D21S11	28,29,30.2
D3S1358	14,16,17
D2S1338	19
D19S433	17,18
D18S51	17
FGA	23,24
Penta E	7,15
Penta D	9,10

Reference/Repository Sample

Sample Name	293T
Source	ATCC-ACS-4500; 100% match with ATCC HEK 293T/17(sample slightly overloaded hence some run artefacts)
Garvan ID	005
D5S818	8,9
D13S317	12,14
D7S820	11
D16S539	13,9
vWA	16,19
TH01	7,9.3
Amel	X
TPOX	11
CSF1PO	11,12
D8S1179	12,14
D21S11	28,30.2
D3S1358	15,17
D2S1338	19
D19S433	12.1,18
D18S51	17,18
FGA	23
Penta E	15,7
Penta D	10,9

Comments

The sample is 90% identical to HEK 293T/17. 90% similarity is considered related according to the ASN-0002 Standard. Cell lines with >80 % match are considered to be related; derived from a common ancestry. Cell lines with between a 55 % to 80 % match require further profiling for authentication of relatedness. In saying cell line samples have a common ancestry, these samples may come from the same cell line; from two separate cell lines that were derived from the same donor; one cell line may be derived from the other; or one cell line may be misidentified or cross-contaminated.Cell lines with >80 % match are considered to be related; derived from a common ancestry. Cell lines with between a 55 % to 80 % match require further profiling for authentication of relatedness. In saying cell line samples have a common ancestry, these samples may come from the same cell line; from two separate cell lines that were derived from the same donor; one cell line may be derived from the other; or one cell line may be misidentified or cross-contaminated.

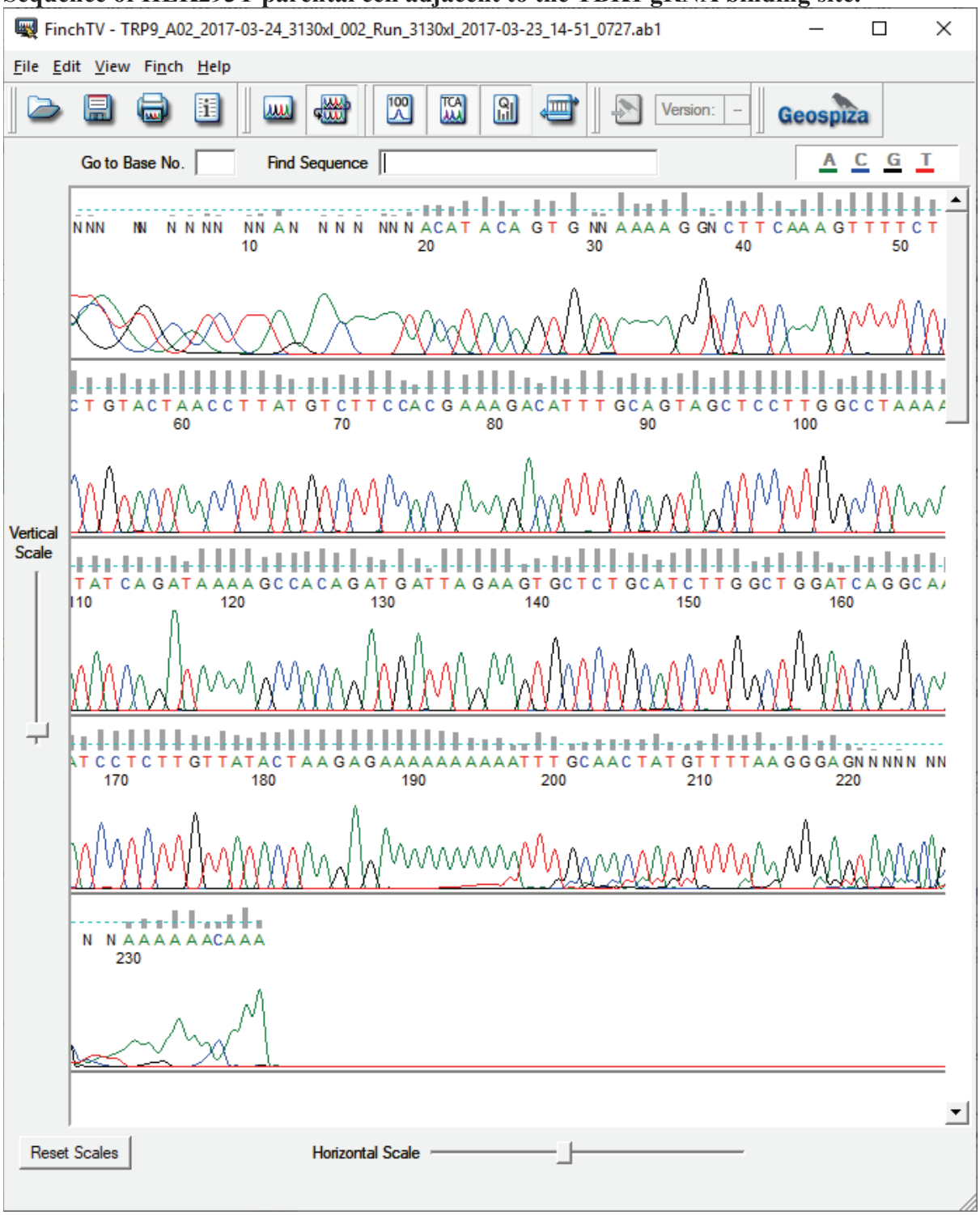
Appendix II

Garvan Molecular Genetics
L8, 384 Victoria Street
Darlinghurst, 2010, NSW
Ph: (02) 92958384
http://www.garvan.org.au
mailto:gmg@garvan.org.au

Document Version Details		
	Name/Date	**Title**
Originally Created by	Pavel Bitter	Molecular Genetics Facility Manager
Date created	15.08.2014	
Current version	3	
Date reviewed	21.08.2015	
Reviewed by	Hiren Sheth	Services Coordinator
Authorized by	Deborah Kelly	Quality Manager
Date authorized	15.08.2014	
Issued Date	15.08.2014	

Appendix III

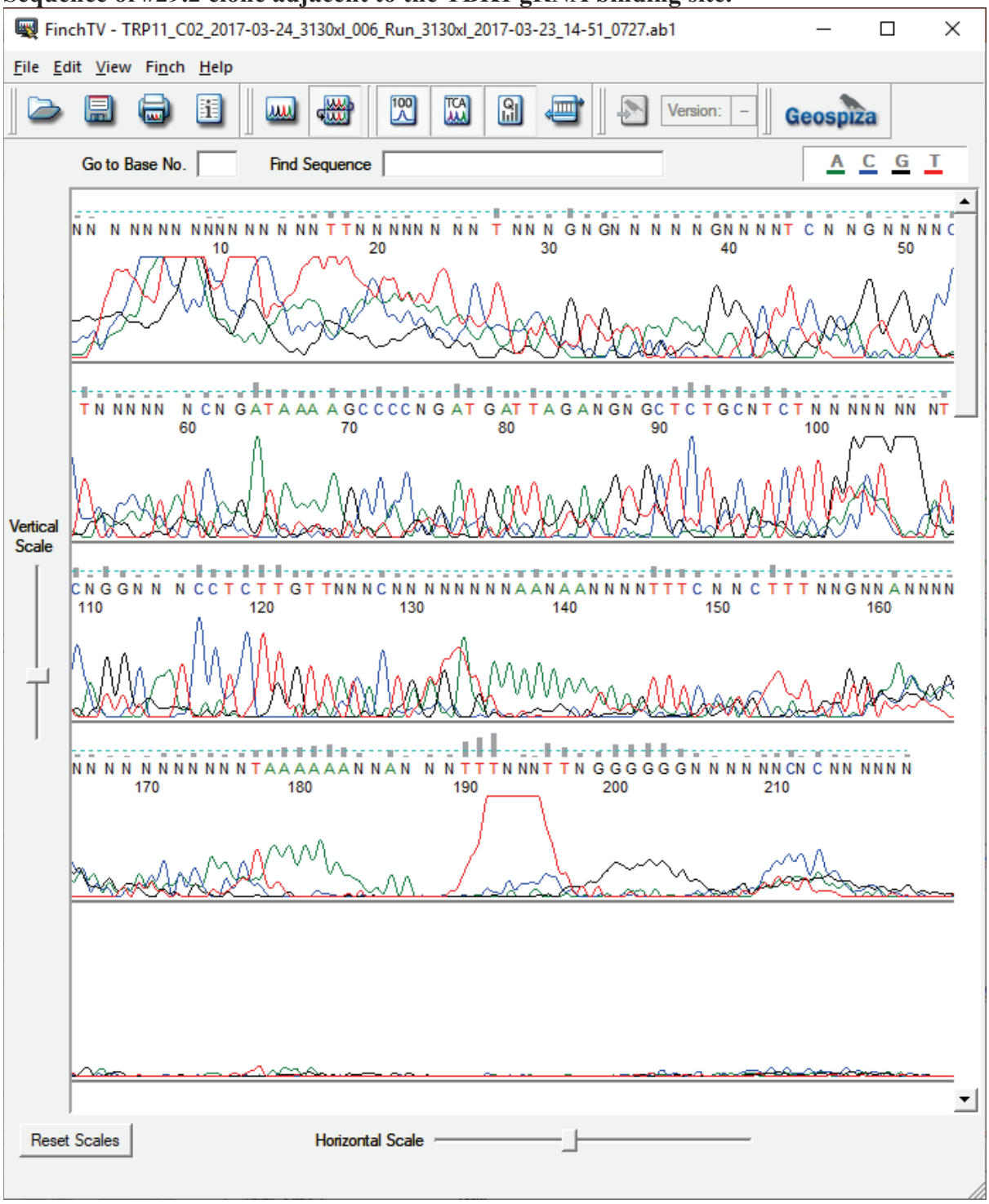
Sequence of HEK293T parental cell adjacent to the TBK1 gRNA binding site.



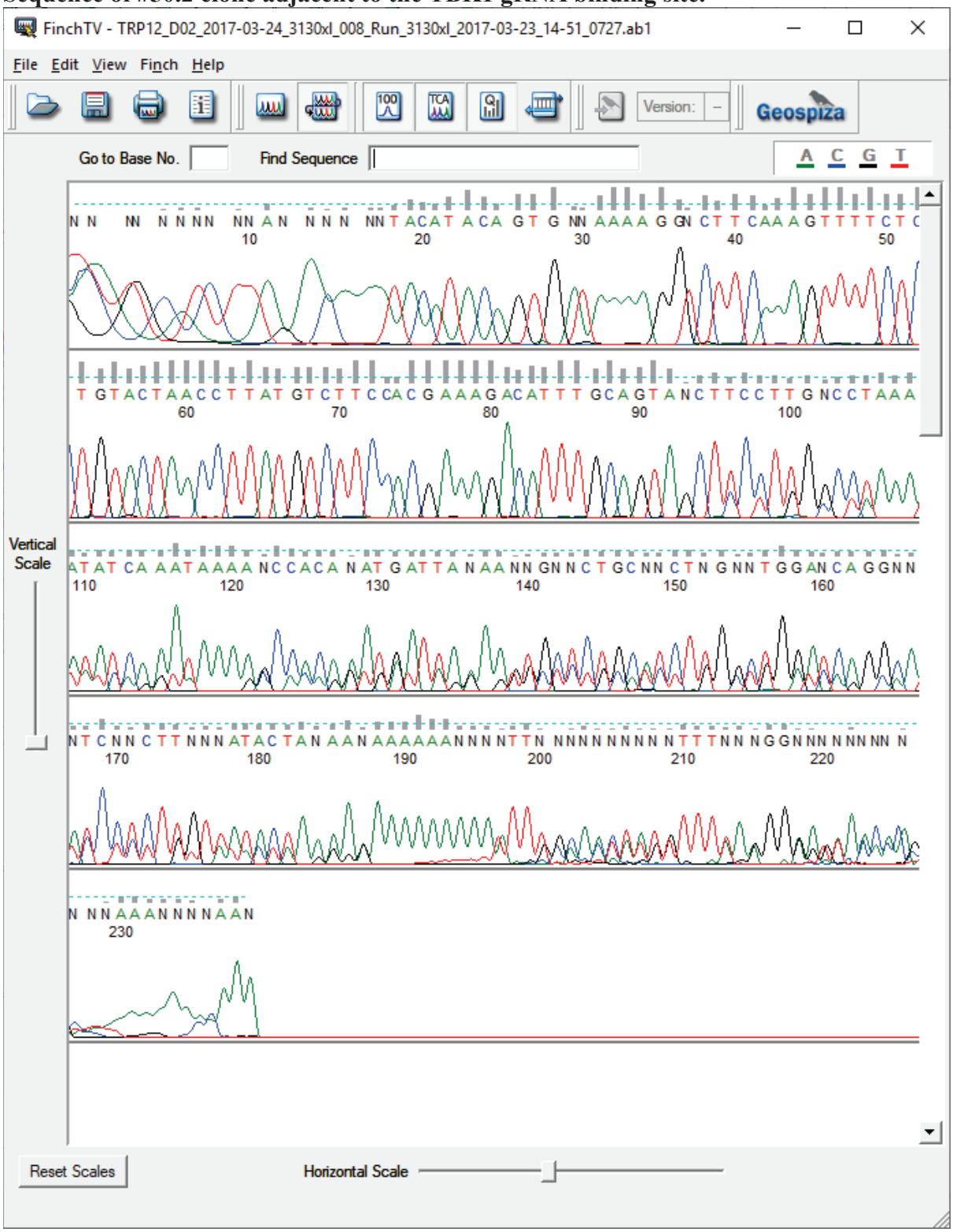
Sequence of #4.2 clone adjacent to the TBK1 gRNA binding site.



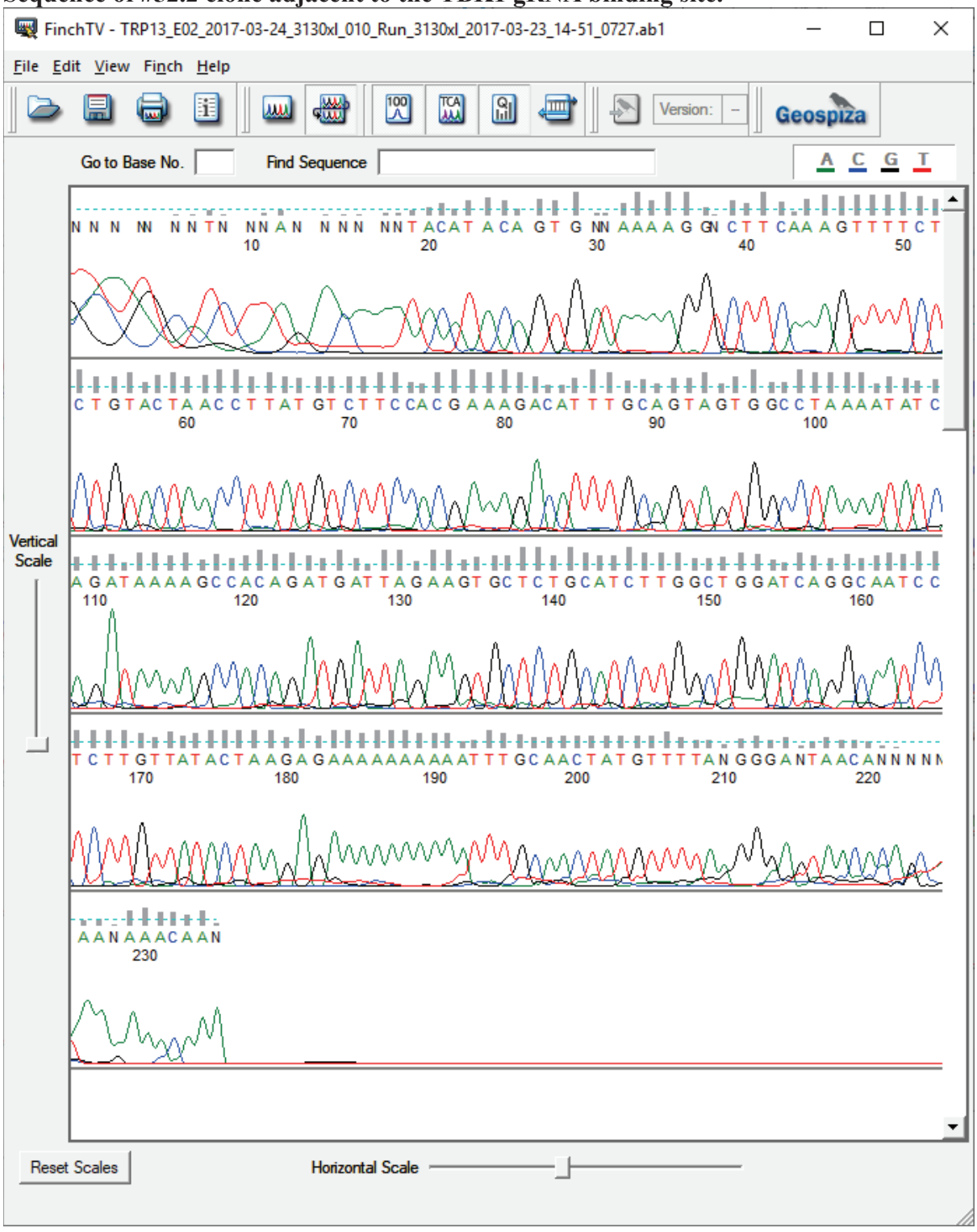
Sequence of #29.2 clone adjacent to the TBK1 gRNA binding site.



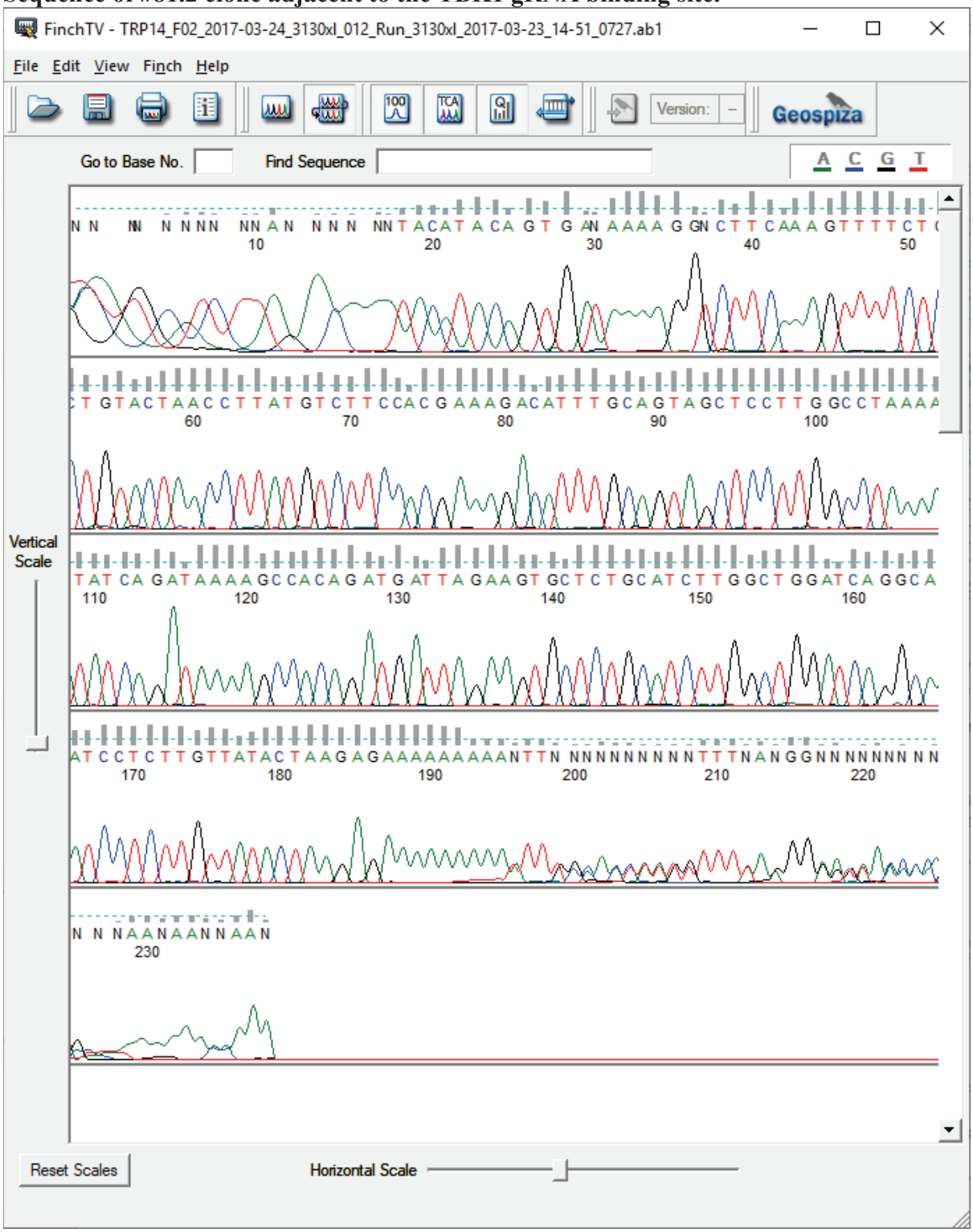
Sequence of #50.2 clone adjacent to the TBK1 gRNA binding site.



Sequence of #52.2 clone adjacent to the TBK1 gRNA binding site.



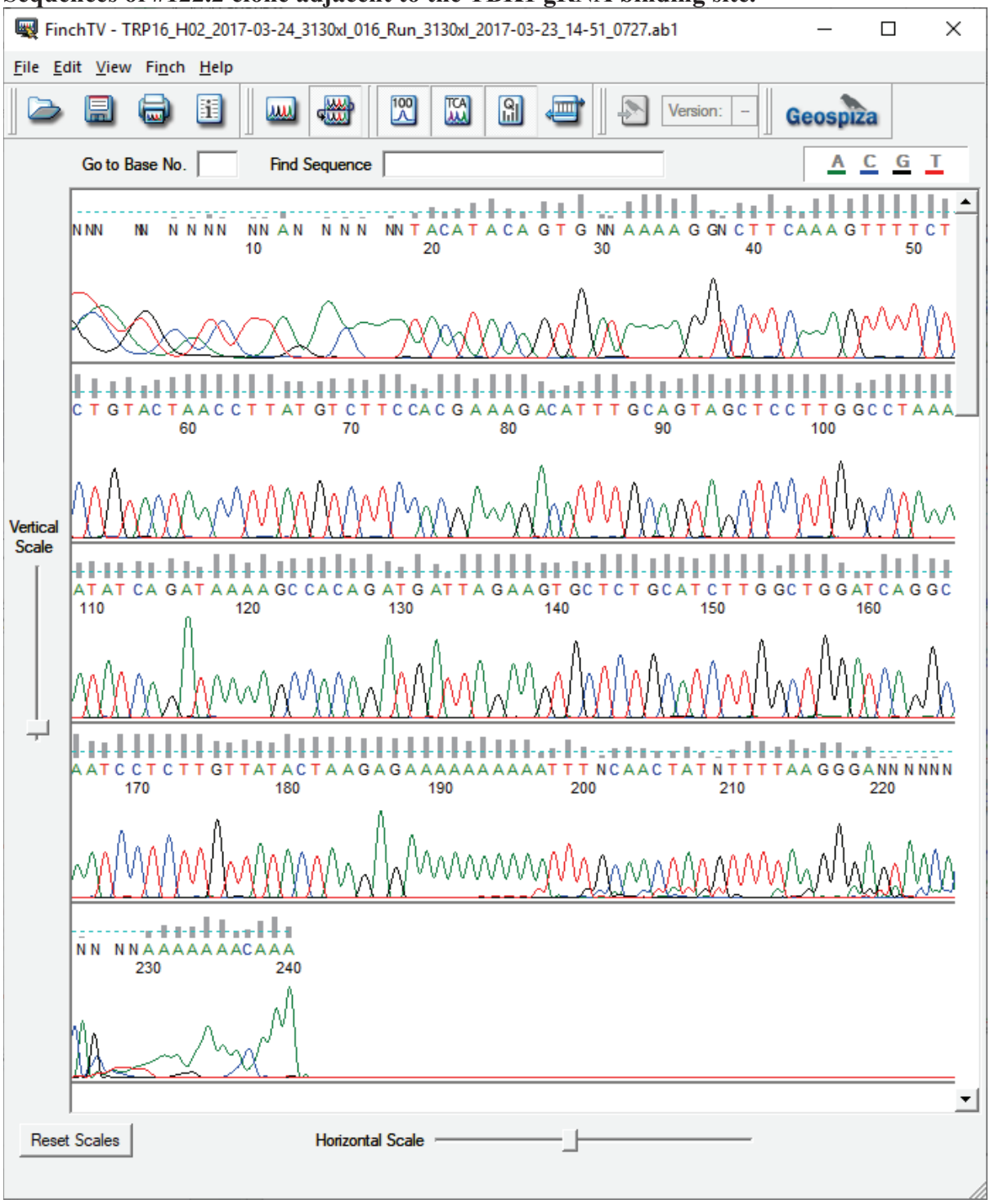
Sequence of #81.2 clone adjacent to the TBK1 gRNA binding site.



Sequence of #118.2 clone adjacent to the TBK1 gRNA binding site.



Sequences of #122.2 clone adjacent to the TBK1 gRNA binding site.



References

1. Logroscino, G. and M. Piccininni, *Amyotrophic Lateral Sclerosis Descriptive Epidemiology: The Origin of Geographic Difference.* Neuroepidemiology, 2019. **52**(1-2): p. 93-103.
2. Ling, S.C., M. Polymenidou, and D.W. Cleveland, *Converging mechanisms in ALS and FTD: disrupted RNA and protein homeostasis.* Neuron, 2013. **79**(3): p. 416-38.
3. Grad, L.I., et al., *Clinical Spectrum of Amyotrophic Lateral Sclerosis (ALS).* Cold Spring Harb Perspect Med, 2017. **7**(8).
4. Tartaglia, M.C., et al., *Differentiation Between Primary Lateral Sclerosis and Amyotrophic Lateral Sclerosis: Examination of Symptoms and Signs at Disease Onset and During Follow-up.* JAMA Neurology, 2007. **64**(2): p. 232-236.
5. Agarwal, S., et al., *Primary lateral sclerosis and the amyotrophic lateral sclerosis-frontotemporal dementia spectrum.* J Neurol, 2018. **265**(8): p. 1819-1828.
6. Kihira, T., et al., *Involvement of Onuf's nucleus in amyotrophic lateral sclerosis.* J Neurol Sci, 1997. **147**(1): p. 81-8.
7. Kanouchi, T., T. Ohkubo, and T. Yokota, *Can regional spreading of amyotrophic lateral sclerosis motor symptoms be explained by prion-like propagation?* Journal of Neurology, Neurosurgery & Psychiatry, 2012. **83**(7): p. 739.
8. Turner, M.R., et al., *Pattern of spread and prognosis in lower limb-onset ALS.* Amyotrophic lateral sclerosis : official publication of the World Federation of Neurology Research Group on Motor Neuron Diseases, 2010. **11**(4): p. 369-373.
9. McDermott, C.J. and P.J. Shaw, *Diagnosis and management of motor neurone disease.* BMJ (Clinical research ed.), 2008. **336**(7645): p. 658-662.
10. Swinnen, B. and W. Robberecht, *The phenotypic variability of amyotrophic lateral sclerosis.* Nat Rev Neurol, 2014. **10**(11): p. 661-70.
11. Chio, A., et al., *Phenotypic heterogeneity of amyotrophic lateral sclerosis: a population based study.* J Neurol Neurosurg Psychiatry, 2011. **82**(7): p. 740-6.
12. Brooks, B.R., et al., *El Escorial revisited: revised criteria for the diagnosis of amyotrophic lateral sclerosis.* Amyotrophic Lateral Sclerosis and Other Motor Neuron Disorders, 2000. **1**(5): p. 293-299.
13. Brooks, B.R., *El Escorial World Federation of Neurology criteria for the diagnosis of amyotrophic lateral sclerosis. Subcommittee on Motor Neuron Diseases/Amyotrophic Lateral Sclerosis of the World Federation of Neurology Research Group on Neuromuscular Diseases and the El Escorial "Clinical limits of amyotrophic lateral sclerosis" workshop contributors.* J Neurol Sci, 1994. **124 Suppl**: p. 96-107.
14. Costa, J., M. Swash, and M. de Carvalho, *Awaji Criteria for the Diagnosis of Amyotrophic Lateral Sclerosis: A Systematic ReviewAwaji Criteria for Amyotrophic Lateral Sclerosis.* JAMA Neurology, 2012. **69**(11): p. 1410-1416.
15. Chiò, A., et al., *Global epidemiology of amyotrophic lateral sclerosis: a systematic review of the published literature.* Neuroepidemiology, 2013. **41**(2): p. 118-130.

16. Renton, A.E., A. Chio, and B.J. Traynor, *State of play in amyotrophic lateral sclerosis genetics.* Nat Neurosci, 2014. **17**(1): p. 17-23.
17. Cirulli, E.T., et al., *Exome sequencing in amyotrophic lateral sclerosis identifies risk genes and pathways.* Science, 2015. **347**(6229): p. 1436-41.
18. Freischmidt, A., et al., *Haploinsufficiency of TBK1 causes familial ALS and fronto-temporal dementia.* Nat Neurosci, 2015. **18**(5): p. 631-6.
19. Greenway, M.J., et al., *ANG mutations segregate with familial and'sporadic'amyotrophic lateral sclerosis.* Nature genetics, 2006. **38**(4): p. 411-413.
20. Bannwarth, S., et al., *A mitochondrial origin for frontotemporal dementia and amyotrophic lateral sclerosis through CHCHD10 involvement.* Brain, 2014. **137**(Pt 8): p. 2329-45.
21. Nishimura, A.L., et al., *A mutation in the vesicle-trafficking protein VAPB causes late-onset spinal muscular atrophy and amyotrophic lateral sclerosis.* Am J Hum Genet, 2004. **75**(5): p. 822-31.
22. Johnson, J.O., et al., *Exome Sequencing Reveals VCP Mutations as a Cause of Familial ALS.* Neuron, 2010. **68**(5): p. 857-864.
23. Johnson, J.O., et al., *Mutations in the Matrin 3 gene cause familial amyotrophic lateral sclerosis.* Nat Neurosci, 2014. **17**(5): p. 664-666.
24. Williams, K.L., et al., *CCNF mutations in amyotrophic lateral sclerosis and frontotemporal dementia.* Nat Commun, 2016. **7**: p. 11253.
25. Maruyama, H., et al., *Mutations of optineurin in amyotrophic lateral sclerosis.* Nature, 2010. **465**(7295): p. 223-226.
26. Fecto, F., et al., *SQSTM1 mutations in familial and sporadic amyotrophic lateral sclerosis.* Archives of neurology, 2011. **68**(11): p. 1440-1446.
27. Deng, H.X., et al., *Mutations in UBQLN2 cause dominant X-linked juvenile and adult-onset ALS and ALS/dementia.* Nature, 2011. **477**(7363): p. 211-5.
28. Munch, C., et al., *Point mutations of the p150 subunit of dynactin (DCTN1) gene in ALS.* Neurology, 2004. **63**(4): p. 724-6.
29. Cohen, T.J., V.M. Lee, and J.Q. Trojanowski, *TDP-43 functions and pathogenic mechanisms implicated in TDP-43 proteinopathies.* Trends Mol Med, 2011. **17**(11): p. 659-67.
30. Lukavsky, P.J., et al., *Molecular basis of UG-rich RNA recognition by the human splicing factor TDP-43.* Nat Struct Mol Biol, 2013. **20**(12): p. 1443-9.
31. Jiang, L.-L., et al., *Two mutations G335D and Q343R within the amyloidogenic core region of TDP-43 influence its aggregation and inclusion formation.* Scientific Reports, 2016. **6**: p. 23928.
32. Mompean, M., et al., *The TDP-43 N-terminal domain structure at high resolution.* Febs j, 2016. **283**(7): p. 1242-60.
33. Kuo, P.H., et al., *The crystal structure of TDP-43 RRM1-DNA complex reveals the specific recognition for UG- and TG-rich nucleic acids.* Nucleic Acids Res, 2014. **42**(7): p. 4712-22.
34. Qin, H., et al., *TDP-43 N terminus encodes a novel ubiquitin-like fold and its unfolded form in equilibrium that can be shifted by binding to ssDNA.* Proc Natl Acad Sci U S A, 2014. **111**(52): p. 18619-24.

35. Winton, M.J., et al., *Disturbance of nuclear and cytoplasmic TAR DNA-binding protein (TDP-43) induces disease-like redistribution, sequestration, and aggregate formation.* Journal of Biological Chemistry, 2008. **283**(19): p. 13302-13309.
36. Ayala, Y.M., et al., *Structural determinants of the cellular localization and shuttling of TDP-43.* Journal of cell science, 2008. **121**(22): p. 3778-3785.
37. Buratti, E. and F.E. Baralle, *Characterization and functional implications of the RNA binding properties of nuclear factor TDP-43, a novel splicing regulator of CFTR exon 9.* J Biol Chem, 2001. **276**(39): p. 36337-43.
38. Ou, S.H., et al., *Cloning and characterization of a novel cellular protein, TDP-43, that binds to human immunodeficiency virus type 1 TAR DNA sequence motifs.* J Virol, 1995. **69**(6): p. 3584-96.
39. Coyne, A.N., B.L. Zaepfel, and D.C. Zarnescu, *Failure to Deliver and Translate-New Insights into RNA Dysregulation in ALS.* Front Cell Neurosci, 2017. **11**: p. 243.
40. Polymenidou, M., et al., *Long pre-mRNA depletion and RNA missplicing contribute to neuronal vulnerability from loss of TDP-43.* Nat Neurosci, 2011. **14**(4): p. 459-68.
41. Tollervey, J.R., et al., *Characterizing the RNA targets and position-dependent splicing regulation by TDP-43.* Nat Neurosci, 2011. **14**(4): p. 452-8.
42. Xiao, S., et al., *RNA targets of TDP-43 identified by UV-CLIP are deregulated in ALS.* Mol Cell Neurosci, 2011. **47**(3): p. 167-80.
43. Hill, S.J., et al., *Two familial ALS proteins function in prevention/repair of transcription-associated DNA damage.* Proc Natl Acad Sci U S A, 2016. **113**(48): p. E7701-e7709.
44. Mitra, J., et al., *Motor neuron disease-associated loss of nuclear TDP-43 is linked to DNA double-strand break repair defects.* Proc Natl Acad Sci U S A, 2019.
45. Mitra, J., et al., *Motor neuron disease-associated loss of nuclear TDP-43 is linked to DNA double-strand break repair defects.* Proc Natl Acad Sci U S A, 2019. **116**(10): p. 4696-4705.
46. Arai, T., et al., *TDP-43 is a component of ubiquitin-positive tau-negative inclusions in frontotemporal lobar degeneration and amyotrophic lateral sclerosis.* Biochem Biophys Res Commun, 2006. **351**(3): p. 602-11.
47. Neumann, M., et al., *Ubiquitinated TDP-43 in frontotemporal lobar degeneration and amyotrophic lateral sclerosis.* Science, 2006. **314**(5796): p. 130-133.
48. Neumann, M., et al., *TDP-43-positive white matter pathology in frontotemporal lobar degeneration with ubiquitin-positive inclusions.* J Neuropathol Exp Neurol, 2007. **66**(3): p. 177-83.
49. Hasegawa, M., et al., *Phosphorylated TDP-43 in frontotemporal lobar degeneration and amyotrophic lateral sclerosis.* Annals of neurology, 2008. **64**(1): p. 60-70.
50. Igaz, L.M., et al., *Enrichment of C-terminal fragments in TAR DNA-binding protein-43 cytoplasmic inclusions in brain but not in spinal cord of frontotemporal lobar degeneration and amyotrophic lateral sclerosis.* Am J Pathol, 2008. **173**(1): p. 182-94.

51. Inukai, Y., et al., *Abnormal phosphorylation of Ser409/410 of TDP-43 in FTLD-U and ALS.* FEBS Letters, 2008. **582**(19): p. 2899-2904.
52. Tan, R.H., et al., *ALS/FTLD: experimental models and reality.* Acta Neuropathol, 2017. **133**(2): p. 177-196.
53. Zou, Z.Y., et al., *Genetic epidemiology of amyotrophic lateral sclerosis: a systematic review and meta-analysis.* J Neurol Neurosurg Psychiatry, 2017. **88**(7): p. 540-549.
54. Johnson, B.S., et al., *TDP-43 is intrinsically aggregation-prone, and amyotrophic lateral sclerosis-linked mutations accelerate aggregation and increase toxicity.* J Biol Chem, 2009. **284**(30): p. 20329-39.
55. Igaz, L.M., et al., *Dysregulation of the ALS-associated gene TDP-43 leads to neuronal death and degeneration in mice.* The Journal of clinical investigation, 2011. **121**(2): p. 726.
56. Vanden Broeck, L., et al., *Functional complementation in Drosophila to predict the pathogenicity of TARDBP variants: evidence for a loss-of-function mechanism.* Neurobiol Aging, 2015. **36**(2): p. 1121-9.
57. Ederle, H. and D. Dormann, *TDP-43 and FUS en route from the nucleus to the cytoplasm.* FEBS Lett, 2017. **591**(11): p. 1489-1507.
58. Berning, B.A. and A.K. Walker, *The Pathobiology of TDP-43 C-Terminal Fragments in ALS and FTLD.* Frontiers in neuroscience, 2019. **13**: p. 335-335.
59. Walker, A.K., et al., *ALS-associated TDP-43 induces endoplasmic reticulum stress, which drives cytoplasmic TDP-43 accumulation and stress granule formation.* PLoS One, 2013. **8**(11): p. e81170.
60. Liu-Yesucevitz, L., et al., *Tar DNA binding protein-43 (TDP-43) associates with stress granules: analysis of cultured cells and pathological brain tissue.* PLoS One, 2010. **5**(10): p. e13250.
61. McDonald, K.K., et al., *TAR DNA-binding protein 43 (TDP-43) regulates stress granule dynamics via differential regulation of G3BP and TIA-1.* Hum Mol Genet, 2011. **20**(7): p. 1400-10.
62. Dewey, C.M., et al., *TDP-43 is directed to stress granules by sorbitol, a novel physiological osmotic and oxidative stressor.* Mol Cell Biol, 2011. **31**(5): p. 1098-108.
63. Protter, D.S.W. and R. Parker, *Principles and Properties of Stress Granules.* Trends in Cell Biology, 2016. **26**(9): p. 668-679.
64. Walker, A.K., et al., *Functional recovery in new mouse models of ALS/FTLD after clearance of pathological cytoplasmic TDP-43.* Acta Neuropathol, 2015. **130**(5): p. 643-60.
65. Arnold, E.S., et al., *ALS-linked TDP-43 mutations produce aberrant RNA splicing and adult-onset motor neuron disease without aggregation or loss of nuclear TDP-43.* Proceedings of the National Academy of Sciences, 2013. **110**(8): p. E736-E745.
66. Iguchi, Y., et al., *Loss of TDP-43 causes age-dependent progressive motor neuron degeneration.* Brain, 2013: p. awt029.

67. DeJesus-Hernandez, M., et al., *Expanded GGGGCC hexanucleotide repeat in noncoding region of C9ORF72 causes chromosome 9p-linked FTD and ALS.* Neuron, 2011. **72**(2): p. 245-256.
68. Renton, A.E., et al., *A hexanucleotide repeat expansion in C9ORF72 is the cause of chromosome 9p21-linked ALS-FTD.* Neuron, 2011. **72**(2): p. 257-68.
69. Rutherford, N.J., et al., *Length of normal alleles of C9ORF72 GGGGCC repeat do not influence disease phenotype.* Neurobiol Aging, 2012. **33**(12): p. 2950.e5-7.
70. Harms, M.B., et al., *Lack of C9ORF72 coding mutations supports a gain of function for repeat expansions in amyotrophic lateral sclerosis.* Neurobiol Aging, 2013. **34**(9): p. 2234.e13-9.
71. van der Zee, J., et al., *A pan-European study of the C9orf72 repeat associated with FTLD: geographic prevalence, genomic instability, and intermediate repeats.* Hum Mutat, 2013. **34**(2): p. 363-73.
72. Beck, J., et al., *Large C9orf72 hexanucleotide repeat expansions are seen in multiple neurodegenerative syndromes and are more frequent than expected in the UK population.* American journal of human genetics, 2013. **92**(3): p. 345-353.
73. van Blitterswijk, M., et al., *Association between repeat sizes and clinical and pathological characteristics in carriers of C9ORF72 repeat expansions (Xpansize-72): a cross-sectional cohort study.* Lancet Neurol, 2013. **12**(10): p. 978-88.
74. Mizielinska, S., et al., *C9orf72 frontotemporal lobar degeneration is characterised by frequent neuronal sense and antisense RNA foci.* Acta Neuropathol, 2013. **126**(6): p. 845-57.
75. Donnelly, C.J., et al., *RNA toxicity from the ALS/FTD C9ORF72 expansion is mitigated by antisense intervention.* Neuron, 2013. **80**(2): p. 415-28.
76. Lagier-Tourenne, C., et al., *Targeted degradation of sense and antisense C9orf72 RNA foci as therapy for ALS and frontotemporal degeneration.* Proc Natl Acad Sci U S A, 2013. **110**(47): p. E4530-9.
77. Zu, T., et al., *RAN proteins and RNA foci from antisense transcripts in C9ORF72 ALS and frontotemporal dementia.* Proc Natl Acad Sci U S A, 2013. **110**(51): p. E4968-77.
78. Gendron, T.F., et al., *Antisense transcripts of the expanded C9ORF72 hexanucleotide repeat form nuclear RNA foci and undergo repeat-associated non-ATG translation in c9FTD/ALS.* Acta neuropathologica, 2013. **126**(6): p. 829-844.
79. Gendron, T.F., et al., *Antisense transcripts of the expanded C9ORF72 hexanucleotide repeat form nuclear RNA foci and undergo repeat-associated non-ATG translation in c9FTD/ALS.* Acta Neuropathol, 2013. **126**(6): p. 829-44.
80. Mori, K., et al., *The C9orf72 GGGGCC repeat is translated into aggregating dipeptide-repeat proteins in FTLD/ALS.* Science, 2013. **339**(6125): p. 1335-8.
81. Ash, P.E., et al., *Unconventional translation of C9ORF72 GGGGCC expansion generates insoluble polypeptides specific to c9FTD/ALS.* Neuron, 2013. **77**(4): p. 639-46.
82. Mori, K., et al., *Bidirectional transcripts of the expanded C9orf72 hexanucleotide repeat are translated into aggregating dipeptide repeat proteins.* Acta Neuropathol, 2013. **126**(6): p. 881-93.

83. Waite, A.J., et al., *Reduced C9orf72 protein levels in frontal cortex of amyotrophic lateral sclerosis and frontotemporal degeneration brain with the C9ORF72 hexanucleotide repeat expansion.* Neurobiology of aging, 2014. **35**(7): p. 1779.e5-1779.e13.
84. Ciura, S., et al., *Loss of function of C9orf72 causes motor deficits in a zebrafish model of amyotrophic lateral sclerosis.* Ann Neurol, 2013. **74**(2): p. 180-7.
85. Elden, A.C., et al., *Ataxin-2 intermediate-length polyglutamine expansions are associated with increased risk for ALS.* Nature, 2010. **466**(7310): p. 1069-75.
86. Haeusler, A.R., et al., *C9orf72 nucleotide repeat structures initiate molecular cascades of disease.* Nature, 2014. **507**(7491): p. 195-200.
87. Su, Z., et al., *Discovery of a biomarker and lead small molecules to target r(GGGGCC)-associated defects in c9FTD/ALS.* Neuron, 2014. **83**(5): p. 1043-50.
88. Konopka, A. and J.D. Atkin, *The Emerging Role of DNA Damage in the Pathogenesis of the C9orf72 Repeat Expansion in Amyotrophic Lateral Sclerosis.* Int J Mol Sci, 2018. **19**(10).
89. Wen, X., et al., *Antisense proline-arginine RAN dipeptides linked to C9ORF72-ALS/FTD form toxic nuclear aggregates that initiate in vitro and in vivo neuronal death.* Neuron, 2014. **84**(6): p. 1213-25.
90. Swinnen, B., et al., *A zebrafish model for C9orf72 ALS reveals RNA toxicity as a pathogenic mechanism.* Acta Neuropathol, 2018. **135**(3): p. 427-443.
91. Balendra, R. and A.M. Isaacs, *C9orf72-mediated ALS and FTD: multiple pathways to disease.* Nature reviews. Neurology, 2018. **14**(9): p. 544-558.
92. Gendron, T.F., et al., *Cerebellar c9RAN proteins associate with clinical and neuropathological characteristics of C9ORF72 repeat expansion carriers.* Acta neuropathologica, 2015. **130**(4): p. 559-573.
93. Mackenzie, I.R., et al., *Dipeptide repeat protein pathology in C9ORF72 mutation cases: clinico-pathological correlations.* Acta Neuropathol, 2013. **126**(6): p. 859-79.
94. Mizielinska, S., et al., *C9orf72 repeat expansions cause neurodegeneration in Drosophila through arginine-rich proteins.* Science, 2014. **345**(6201): p. 1192-1194.
95. Tran, H., et al., *Differential Toxicity of Nuclear RNA Foci versus Dipeptide Repeat Proteins in a Drosophila Model of C9ORF72 FTD/ALS.* Neuron, 2015. **87**(6): p. 1207-1214.
96. Shao, Q., et al., *C9orf72 deficiency promotes motor deficits of a C9ALS/FTD mouse model in a dose-dependent manner.* Acta Neuropathologica Communications, 2019. **7**(1): p. 32.
97. Farg, M.A., et al., *The DNA damage response (DDR) is induced by the C9orf72 repeat expansion in amyotrophic lateral sclerosis.* Hum Mol Genet, 2017. **26**(15): p. 2882-2896.
98. Lanson, N.A., Jr. and U.B. Pandey, *FUS-related proteinopathies: lessons from animal models.* Brain Res, 2012. **1462**: p. 44-60.
99. Guerrero, E.N., et al., *TDP-43/FUS in motor neuron disease: Complexity and challenges.* Progress in Neurobiology, 2016. **145-146**: p. 78-97.

100. Crozat, A., et al., *Fusion of CHOP to a novel RNA-binding protein in human myxoid liposarcoma.* Nature, 1993. **363**(6430): p. 640-4.
101. Lagier-Tourenne, C., M. Polymenidou, and D.W. Cleveland, *TDP-43 and FUS/TLS: emerging roles in RNA processing and neurodegeneration.* Human molecular genetics, 2010. **19**(R1): p. R46-R64.
102. Tan, A.Y., et al., *TLS/FUS (translocated in liposarcoma/fused in sarcoma) regulates target gene transcription via single-stranded DNA response elements.* Proceedings of the National Academy of Sciences, 2012. **109**(16): p. 6030.
103. Tan, A.Y. and J.L. Manley, *TLS Inhibits RNA Polymerase III Transcription.* Molecular and Cellular Biology, 2010. **30**(1): p. 186.
104. Hallier, M., et al., *The Transcription Factor Spi-1/PU.1 Interacts with the Potential Splicing Factor TLS.* Journal of Biological Chemistry, 1998. **273**(9): p. 4838-4842.
105. Uranishi, H., et al., *Involvement of the Pro-oncoprotein TLS (Translocated in Liposarcoma) in Nuclear Factor-κB p65-mediated Transcription as a Coactivator.* Journal of Biological Chemistry, 2001. **276**(16): p. 13395-13401.
106. Li, X., M. Decker, and J.J. Westendorf, *TEThered to Runx: Novel binding partners for runx factors.* Blood Cells, Molecules, and Diseases, 2010. **45**(1): p. 82-85.
107. Bertolotti, A., et al., *hTAF(II)68, a novel RNA/ssDNA-binding protein with homology to the pro-oncoproteins TLS/FUS and EWS is associated with both TFIID and RNA polymerase II.* The EMBO Journal, 1996. **15**(18): p. 5022-5031.
108. Belzil, V.V., et al., *Mutations in FUS cause FALS and SALS in French and French Canadian populations.* Neurology, 2009. **73**(15): p. 1176-9.
109. Neumann, M., et al., *Abundant FUS-immunoreactive pathology in neuronal intermediate filament inclusion disease.* Acta Neuropathol, 2009. **118**(5): p. 605-16.
110. Doi, H., et al., *The RNA-binding protein FUS/TLS is a common aggregate-interacting protein in polyglutamine diseases.* Neuroscience Research, 2010. **66**(1): p. 131-133.
111. Woulfe, J., D.A. Gray, and I.R. Mackenzie, *FUS-immunoreactive intranuclear inclusions in neurodegenerative disease.* Brain Pathol, 2010. **20**(3): p. 589-97.
112. Orozco, D., et al., *Loss of fused in sarcoma (FUS) promotes pathological Tau splicing.* EMBO reports, 2012. **13**(8): p. 759.
113. Qiu, H., et al., *ALS-associated mutation FUS-R521C causes DNA damage and RNA splicing defects.* J Clin Invest, 2014. **124**(3): p. 981-99.
114. Huang, C., et al., *FUS transgenic rats develop the phenotypes of amyotrophic lateral sclerosis and frontotemporal lobar degeneration.* PLoS Genet, 2011. **7**(3): p. e1002011.
115. Qiu, H., et al., *ALS-associated mutation FUS-R521C causes DNA damage and RNA splicing defects.* The Journal of clinical investigation, 2014. **124**(3): p. 981-999.
116. Funikov, S.Y., et al., *FUS(1-359) transgenic mice as a model of ALS: pathophysiological and molecular aspects of the proteinopathy.* Neurogenetics, 2018. **19**(3): p. 189-204.
117. Rosen, D.R., et al., *Mutations in Cu/Zn superoxide dismutase gene are associated with familial amyotrophic lateral sclerosis.* Nature, 1993. **362**(6415): p. 59-62.

118. Tafuri, F., et al., *SOD1 misplacing and mitochondrial dysfunction in amyotrophic lateral sclerosis pathogenesis.* Frontiers in cellular neuroscience, 2015. **9**: p. 336-336.
119. Okado-Matsumoto, A. and I. Fridovich, *Subcellular distribution of superoxide dismutases (SOD) in rat liver: Cu,Zn-SOD in mitochondria.* J Biol Chem, 2001. **276**(42): p. 38388-93.
120. Sturtz, L.A., et al., *A fraction of yeast Cu,Zn-superoxide dismutase and its metallochaperone, CCS, localize to the intermembrane space of mitochondria. A physiological role for SOD1 in guarding against mitochondrial oxidative damage.* J Biol Chem, 2001. **276**(41): p. 38084-9.
121. Wang, J., G. Xu, and D.R. Borchelt, *Mapping superoxide dismutase 1 domains of non-native interaction: roles of intra- and intermolecular disulfide bonding in aggregation.* Journal of Neurochemistry, 2006. **96**(5): p. 1277-1288.
122. Pardo, C.A., et al., *Superoxide dismutase is an abundant component in cell bodies, dendrites, and axons of motor neurons and in a subset of other neurons.* Proceedings of the National Academy of Sciences, 1995. **92**(4): p. 954.
123. Canosa, A., et al., *A novel p.Ser108LeufsTer15 SOD1 mutation leading to the formation of a premature stop codon in an apparently sporadic ALS patient: insights into the underlying pathomechanisms.* Neurobiol Aging, 2018. **72**: p. 189.e11-189.e17.
124. Philips, T. and J.D. Rothstein, *Rodent Models of Amyotrophic Lateral Sclerosis.* Current protocols in pharmacology, 2015. **69**: p. 5.67.1-5.67.21.
125. Gurney, M.E., et al., *Motor neuron degeneration in mice that express a human Cu,Zn superoxide dismutase mutation.* Science, 1994. **264**(5166): p. 1772-5.
126. Gurney, M.E., *The use of transgenic mouse models of amyotrophic lateral sclerosis in preclinical drug studies.* Journal of the Neurological Sciences, 1997. **152**: p. s67-s73.
127. Alexander, G.M., et al., *Effect of transgene copy number on survival in the G93A SOD1 transgenic mouse model of ALS.* Brain Res Mol Brain Res, 2004. **130**(1-2): p. 7-15.
128. Wong, P.C., et al., *An adverse property of a familial ALS-linked SOD1 mutation causes motor neuron disease characterized by vacuolar degeneration of mitochondria.* Neuron, 1995. **14**(6): p. 1105-16.
129. Bruijn, L.I., et al., *ALS-linked SOD1 mutant G85R mediates damage to astrocytes and promotes rapidly progressive disease with SOD1-containing inclusions.* Neuron, 1997. **18**(2): p. 327-38.
130. Ripps, M.E., et al., *Transgenic mice expressing an altered murine superoxide dismutase gene provide an animal model of amyotrophic lateral sclerosis.* Proc Natl Acad Sci U S A, 1995. **92**(3): p. 689-93.
131. Ying, H. and B.Y. Yue, *Cellular and molecular biology of optineurin.* Int Rev Cell Mol Biol, 2012. **294**: p. 223-58.
132. Wild, P., et al., *Phosphorylation of the autophagy receptor optineurin restricts Salmonella growth.* Science, 2011. **333**(6039): p. 228-33.
133. Hattula, K. and J. Peranen, *FIP-2, a coiled-coil protein, links Huntingtin to Rab8 and modulates cellular morphogenesis.* Curr Biol, 2000. **10**(24): p. 1603-6.

134. Schwamborn, K., et al., *Phorbol esters and cytokines regulate the expression of the NEMO-related protein, a molecule involved in a NF-kappa B-independent pathway.* J Biol Chem, 2000. **275**(30): p. 22780-9.
135. Li, Y., J. Kang, and M.S. Horwitz, *Interaction of an adenovirus E3 14.7-kilodalton protein with a novel tumor necrosis factor alpha-inducible cellular protein containing leucine zipper domains.* Mol Cell Biol, 1998. **18**(3): p. 1601-10.
136. Stroissnigg, H., et al., *FIP-2, an IkappaB-kinase-gamma-related protein, is associated with the Golgi apparatus and translocates to the marginal band during chicken erythroblast differentiation.* Exp Cell Res, 2002. **278**(2): p. 133-45.
137. Toth, R.P. and J.D. Atkin, *Dysfunction of Optineurin in Amyotrophic Lateral Sclerosis and Glaucoma.* Front Immunol, 2018. **9**: p. 1017.
138. Fifita, J.A., et al., *A novel amyotrophic lateral sclerosis mutation in OPTN induces ER stress and Golgi fragmentation in vitro.* Amyotroph Lateral Scler Frontotemporal Degener, 2017. **18**(1-2): p. 126-133.
139. Sundaramoorthy, V., et al., *Defects in optineurin- and myosin VI-mediated cellular trafficking in amyotrophic lateral sclerosis.* Hum Mol Genet, 2015. **24**(13): p. 3830-46.
140. Korac, J., et al., *Ubiquitin-independent function of optineurin in autophagic clearance of protein aggregates.* J Cell Sci, 2013. **126**(Pt 2): p. 580-92.
141. Genin, E.C., et al., *CHCHD10 mutations promote loss of mitochondrial cristae junctions with impaired mitochondrial genome maintenance and inhibition of apoptosis.* EMBO molecular medicine, 2016. **8**(1): p. 58-72.
142. Nguyen, H.P., C. Van Broeckhoven, and J. van der Zee, *ALS Genes in the Genomic Era and their Implications for FTD.* Trends Genet, 2018. **34**(6): p. 404-423.
143. Salton, M., et al., *Matrin 3 Binds and Stabilizes mRNA.* PLOS ONE, 2011. **6**(8): p. e23882.
144. Coelho, M.B., et al., *Nuclear matrix protein Matrin3 regulates alternative splicing and forms overlapping regulatory networks with PTB.* Embo j, 2015. **34**(5): p. 653-68.
145. Boehringer, A., et al., *ALS Associated Mutations in Matrin 3 Alter Protein-Protein Interactions and Impede mRNA Nuclear Export.* Sci Rep, 2017. **7**(1): p. 14529.
146. D'Angiolella, V., M. Esencay, and M. Pagano, *A cyclin without cyclin-dependent kinases: cyclin F controls genome stability through ubiquitin-mediated proteolysis.* Trends Cell Biol, 2013. **23**(3): p. 135-40.
147. Bai, C., et al., *SKP1 connects cell cycle regulators to the ubiquitin proteolysis machinery through a novel motif, the F-box.* Cell, 1996. **86**(2): p. 263-74.
148. Lee, A., et al., *Pathogenic mutation in the ALS/FTD gene, CCNF, causes elevated Lys48-linked ubiquitylation and defective autophagy.* Cell Mol Life Sci, 2018. **75**(2): p. 335-354.
149. Kakizuka, A., *Roles of VCP in human neurodegenerative disorders.* Biochemical Society Transactions, 2008. **36**(1): p. 105.
150. Wang, T., et al., *Pathogenic Mutations in the Valosin-containing Protein/p97(VCP) N-domain Inhibit the SUMOylation of VCP and Lead to Impaired Stress Response.* J Biol Chem, 2016. **291**(27): p. 14373-84.

151. Corrado, L., et al., *Variations in the coding and regulatory sequences of the angiogenin (ANG) gene are not associated to ALS (amyotrophic lateral sclerosis) in the Italian population.* J Neurol Sci, 2007. **258**(1-2): p. 123-7.
152. Millecamps, S., et al., *SOD1, ANG, VAPB, TARDBP, and FUS mutations in familial amyotrophic lateral sclerosis: genotype-phenotype correlations.* J Med Genet, 2010. **47**(8): p. 554-60.
153. Luigetti, M., et al., *SOD1 G93D sporadic amyotrophic lateral sclerosis (SALS) patient with rapid progression and concomitant novel ANG variant.* Neurobiol Aging, 2011. **32**(10): p. 1924.e15-8.
154. Padhi, A.K., et al., *Mechanisms of loss of functions of human angiogenin variants implicated in amyotrophic lateral sclerosis.* PLoS One, 2012. **7**(2): p. e32479.
155. Daoud, H. and G.A. Rouleau, *A role for ubiquilin 2 mutations in neurodegeneration.* Nat Rev Neurol, 2011. **7**(11): p. 599-600.
156. Holzbaur, E.L. and M.K. Tokito, *Localization of the DCTN1 gene encoding p150Glued to human chromosome 2p13 by fluorescence in situ hybridization.* Genomics, 1996. **31**(3): p. 398-9.
157. Ticozzi, N., et al., *Mutational analysis reveals the FUS homolog TAF15 as a candidate gene for familial amyotrophic lateral sclerosis.* Am J Med Genet B Neuropsychiatr Genet, 2011. **156b**(3): p. 285-90.
158. Wu, C.H., et al., *Mutations in the profilin 1 gene cause familial amyotrophic lateral sclerosis.* Nature, 2012. **488**(7412): p. 499-503.
159. Kim, H.J., et al., *Mutations in prion-like domains in hnRNPA2B1 and hnRNPA1 cause multisystem proteinopathy and ALS.* Nature, 2013. **495**(7442): p. 467-73.
160. Smith, B.N., et al., *Exome-wide rare variant analysis identifies TUBA4A mutations associated with familial ALS.* Neuron, 2014. **84**(2): p. 324-31.
161. van Rheenen, W., et al., *Genome-wide association analyses identify new risk variants and the genetic architecture of amyotrophic lateral sclerosis.* Nat Genet, 2016. **48**(9): p. 1043-8.
162. Fang, X., et al., *The NEK1 interactor, C21ORF2, is required for efficient DNA damage repair.* Acta Biochim Biophys Sin (Shanghai), 2015. **47**(10): p. 834-41.
163. Figlewicz, D.A., et al., *Polymorphism in the multi-phosphorylation domain of the human neurofilament heavy-subunit-encoding gene.* Gene, 1993. **132**(2): p. 297-300.
164. Jaiswal, M.K., *Riluzole and edaravone: A tale of two amyotrophic lateral sclerosis drugs.* Med Res Rev, 2019. **39**(2): p. 733-748.
165. Miller, R.G., et al., *Riluzole for amyotrophic lateral sclerosis (ALS)/motor neuron disease (MND).* Cochrane Database Syst Rev, 2002(2): p. Cd001447.
166. Bensimon, G., L. Lacomblez, and V. Meininger, *A controlled trial of riluzole in amyotrophic lateral sclerosis. ALS/Riluzole Study Group.* N Engl J Med, 1994. **330**(9): p. 585-91.
167. Lacomblez, L., et al., *Dose-ranging study of riluzole in amyotrophic lateral sclerosis. Amyotrophic Lateral Sclerosis/Riluzole Study Group II.* Lancet, 1996. **347**(9013): p. 1425-31.

168. Fang, T., et al., *Stage at which riluzole treatment prolongs survival in patients with amyotrophic lateral sclerosis: a retrospective analysis of data from a dose-ranging study.* The Lancet Neurology, 2018. **17**(5): p. 416-422.
169. Zhou, Y. and N.C. Danbolt, *Glutamate as a neurotransmitter in the healthy brain.* Journal of neural transmission (Vienna, Austria : 1996), 2014. **121**(8): p. 799-817.
170. Jaiswal, M.K., *Riluzole But Not Melatonin Ameliorates Acute Motor Neuron Degeneration and Moderately Inhibits SOD1-Mediated Excitotoxicity Induced Disrupted Mitochondrial Ca(2+) Signaling in Amyotrophic Lateral Sclerosis.* Front Cell Neurosci, 2016. **10**: p. 295.
171. Jaiswal, M.K., et al., *Impairment of mitochondrial calcium handling in a mtSOD1 cell culture model of motoneuron disease.* BMC Neurosci, 2009. **10**: p. 64.
172. Jaiswal, M.K., *Calcium, mitochondria, and the pathogenesis of ALS: the good, the bad, and the ugly.* Frontiers in cellular neuroscience, 2013. **7**: p. 199-199.
173. *Safety and efficacy of edaravone in well defined patients with amyotrophic lateral sclerosis: a randomised, double-blind, placebo-controlled trial.* Lancet Neurol, 2017. **16**(7): p. 505-512.
174. Sawada, H., *Clinical efficacy of edaravone for the treatment of amyotrophic lateral sclerosis.* Expert Opin Pharmacother, 2017. **18**(7): p. 735-738.
175. Perez-Gonzalez, A. and A. Galano, *OH radical scavenging activity of Edaravone: mechanism and kinetics.* J Phys Chem B, 2011. **115**(5): p. 1306-14.
176. Jami, M.-S., et al., *Edaravone leads to proteome changes indicative of neuronal cell protection in response to oxidative stress.* Neurochemistry international, 2015. **90**: p. 134-141.
177. Rowland, L.P., *Primary lateral sclerosis: disease, syndrome, both or neither?* Journal of the Neurological Sciences, 1999. **170**(1): p. 1-4.
178. Singer, M.A., et al., *Primary lateral sclerosis: clinical and laboratory features in 25 patients.* J Clin Neuromuscul Dis, 2005. **7**(1): p. 1-9.
179. Le Forestier, N., et al., *Does primary lateral sclerosis exist? A study of 20 patients and a review of the literature.* Brain, 2001. **124**(Pt 10): p. 1989-99.
180. Pringle, C.E., et al., *Primary lateral sclerosis. Clinical features, neuropathology and diagnostic criteria.* Brain, 1992. **115 (Pt 2)**: p. 495-520.
181. Statland, J.M., et al., *Primary Lateral Sclerosis.* Neurol Clin, 2015. **33**(4): p. 749-60.
182. Floeter, M.K. and R. Mills, *Progression in primary lateral sclerosis: a prospective analysis.* Amyotrophic lateral sclerosis : official publication of the World Federation of Neurology Research Group on Motor Neuron Diseases, 2009. **10**(5-6): p. 339-346.
183. Ince, P.G., et al., *Corticospinal tract degeneration in the progressive muscular atrophy variant of ALS.* Neurology, 2003. **60**(8): p. 1252-1258.
184. Liewluck, T. and D.S. Saperstein, *Progressive Muscular Atrophy.* Neurologic Clinics, 2015. **33**(4): p. 761-773.
185. Rascovsky, K., et al., *Sensitivity of revised diagnostic criteria for the behavioural variant of frontotemporal dementia.* Brain, 2011. **134**(9): p. 2456-2477.
186. Gorno-Tempini, M.L., et al., *Classification of primary progressive aphasia and its variants.* Neurology, 2011. **76**(11): p. 1006.

187. Coyle-Gilchrist, I.T.S., et al., *Prevalence, characteristics, and survival of frontotemporal lobar degeneration syndromes.* Neurology, 2016. **86**(18): p. 1736.
188. Wood, E.M., et al., *Development and Validation of Pedigree Classification Criteria for Frontotemporal Lobar DegenerationFrontotemporal Lobar DegenerationFrontotemporal Lobar Degeneration.* JAMA Neurology, 2013. **70**(11): p. 1411-1417.
189. Hutton, M., et al., *Association of missense and 5'-splice-site mutations in tau with the inherited dementia FTDP-17.* Nature, 1998. **393**(6686): p. 702-5.
190. Baker, M., et al., *Mutations in progranulin cause tau-negative frontotemporal dementia linked to chromosome 17.* Nature, 2006. **442**(7105): p. 916-9.
191. Cruts, M., et al., *Null mutations in progranulin cause ubiquitin-positive frontotemporal dementia linked to chromosome 17q21.* Nature, 2006. **442**(7105): p. 920-4.
192. Gijselinck, I., et al., *A C9orf72 promoter repeat expansion in a Flanders-Belgian cohort with disorders of the frontotemporal lobar degeneration-amyotrophic lateral sclerosis spectrum: a gene identification study.* Lancet Neurol, 2012. **11**(1): p. 54-65.
193. Broustal, O., et al., *FUS mutations in frontotemporal lobar degeneration with amyotrophic lateral sclerosis.* J Alzheimers Dis, 2010. **22**(3): p. 765-9.
194. Gellera, C., et al., *Ubiquilin 2 mutations in Italian patients with amyotrophic lateral sclerosis and frontotemporal dementia.* Journal of Neurology, Neurosurgery & Psychiatry, 2013. **84**(2): p. 183.
195. Wong, T.H., et al., *Three VCP Mutations in Patients with Frontotemporal Dementia.* J Alzheimers Dis, 2018. **65**(4): p. 1139-1146.
196. Le Ber, I., et al., *SQSTM1 Mutations in French Patients With Frontotemporal Dementia or Frontotemporal Dementia With Amyotrophic Lateral SclerosisSQSTM1 Mutations in Patients With FTD or FTD-ALSSQSTM1 Mutations in Patients With FTD or FTD-ALS.* JAMA Neurology, 2013. **70**(11): p. 1403-1410.
197. Pottier, C., et al., *Whole-genome sequencing reveals important role for TBK1 and OPTN mutations in frontotemporal lobar degeneration without motor neuron disease.* Acta Neuropathol, 2015. **130**(1): p. 77-92.
198. Le Ber, I., et al., *TBK1 mutation frequencies in French frontotemporal dementia and amyotrophic lateral sclerosis cohorts.* Neurobiol Aging, 2015. **36**(11): p. 3116.e5-3116.e8.
199. Morgan, S. and R.W. Orrell, *Pathogenesis of amyotrophic lateral sclerosis.* British Medical Bulletin, 2016. **119**(1): p. 87-98.
200. Kopito, R.R., *Aggresomes, inclusion bodies and protein aggregation.* Trends in Cell Biology, 2000. **10**(12): p. 524-530.
201. Forsberg, K., et al., *Glial nuclear aggregates of superoxide dismutase-1 are regularly present in patients with amyotrophic lateral sclerosis.* Acta Neuropathologica, 2011. **121**(5): p. 623-634.
202. Groen, E.J.N., et al., *FUS Mutations in Familial Amyotrophic Lateral Sclerosis in the NetherlandsFUS Mutations in FALS.* JAMA Neurology, 2010. **67**(2): p. 224-230.

203. Hewitt, C., et al., *Novel FUS/TLS Mutations and Pathology in Familial and Sporadic Amyotrophic Lateral SclerosisFamilial/Sporadic Amyotrophic Lateral Sclerosis.* JAMA Neurology, 2010. **67**(4): p. 455-461.
204. Osawa, T., et al., *Optineurin in neurodegenerative diseases.* Neuropathology, 2011. **31**(6): p. 569-74.
205. Johnston, J.A., et al., *Formation of high molecular weight complexes of mutant Cu, Zn-superoxide dismutase in a mouse model for familial amyotrophic lateral sclerosis.* Proc Natl Acad Sci U S A, 2000. **97**(23): p. 12571-6.
206. Münch, C., J. O'Brien, and A. Bertolotti, *Prion-like propagation of mutant superoxide dismutase-1 misfolding in neuronal cells.* Proceedings of the National Academy of Sciences, 2011. **108**(9): p. 3548.
207. Chattopadhyay, M., et al., *Initiation and elongation in fibrillation of ALS-linked superoxide dismutase.* Proc Natl Acad Sci U S A, 2008. **105**(48): p. 18663-8.
208. Münch, C. and A. Bertolotti, *Self-propagation and transmission of misfolded mutant SOD1: prion or prion-like phenomenon?* Cell Cycle, 2011. **10**(11): p. 1711.
209. Kumar, V., et al., *Protein aggregation and neurodegenerative diseases: From theory to therapy.* European Journal of Medicinal Chemistry, 2016. **124**: p. 1105-1120.
210. Lin, W.-L. and D.W. Dickson, *Ultrastructural localization of TDP-43 in filamentous neuronal inclusions in various neurodegenerative diseases.* Acta neuropathologica, 2008. **116**(2): p. 205-213.
211. Robinson, J.L., et al., *TDP-43 skeins show properties of amyloid in a subset of ALS cases.* Acta neuropathologica, 2013. **125**(1): p. 121-131.
212. Okamoto, K., Y. Mizuno, and Y. Fujita, *Bunina bodies in amyotrophic lateral sclerosis.* Neuropathology, 2008. **28**(2): p. 109-115.
213. Mackenzie, I.R., et al., *Pathological TDP-43 distinguishes sporadic amyotrophic lateral sclerosis from amyotrophic lateral sclerosis with SOD1 mutations.* Annals of neurology, 2007. **61**(5): p. 427-434.
214. Tan, C.-F., et al., *TDP-43 immunoreactivity in neuronal inclusions in familial amyotrophic lateral sclerosis with or without SOD1 gene mutation.* Acta neuropathologica, 2007. **113**(5): p. 535-542.
215. Blokhuis, A.M., et al., *Protein aggregation in amyotrophic lateral sclerosis.* Acta Neuropathol, 2013. **125**(6): p. 777-94.
216. Lilienbaum, A., *Relationship between the proteasomal system and autophagy.* International journal of biochemistry and molecular biology, 2013. **4**(1): p. 1-26.
217. Bertolotti, A., et al., *hTAF(II)68, a novel RNA/ssDNA-binding protein with homology to the pro-oncoproteins TLS/FUS and EWS is associated with both TFIID and RNA polymerase II.* Embo j, 1996. **15**(18): p. 5022-31.
218. Ibrahim, F., et al., *Identification of in vivo, conserved, TAF15 RNA binding sites reveals the impact of TAF15 on the neuronal transcriptome.* Cell Rep, 2013. **3**(2): p. 301-8.
219. Izhar, L., et al., *A Systematic Analysis of Factors Localized to Damaged Chromatin Reveals PARP-Dependent Recruitment of Transcription Factors.* Cell Rep, 2015. **11**(9): p. 1486-500.

220. Jobert, L., et al., *Human U1 snRNA forms a new chromatin-associated snRNP with TAF15.* EMBO Rep, 2009. **10**(5): p. 494-500.
221. Ankarcrona, M., et al., *Glutamate-induced neuronal death: a succession of necrosis or apoptosis depending on mitochondrial function.* Neuron, 1995. **15**(4): p. 961-73.
222. Fray, A.E., et al., *The expression of the glial glutamate transporter protein EAAT2 in motor neuron disease: an immunohistochemical study.* Eur J Neurosci, 1998. **10**(8): p. 2481-9.
223. Rothstein, J.D., et al., *Selective loss of glial glutamate transporter GLT-1 in amyotrophic lateral sclerosis.* Ann Neurol, 1995. **38**(1): p. 73-84.
224. Sasaki, S., T. Komori, and M. Iwata, *Excitatory amino acid transporter 1 and 2 immunoreactivity in the spinal cord in amyotrophic lateral sclerosis.* Acta Neuropathol, 2000. **100**(2): p. 138-44.
225. Boehmer, C., et al., *Post-translational regulation of EAAT2 function by co-expressed ubiquitin ligase Nedd4-2 is impacted by SGK kinases.* J Neurochem, 2006. **97**(4): p. 911-21.
226. van Landeghem, F.K., et al., *Decreased expression of glutamate transporters in astrocytes after human traumatic brain injury.* J Neurotrauma, 2006. **23**(10): p. 1518-28.
227. Howland, D.S., et al., *Focal loss of the glutamate transporter EAAT2 in a transgenic rat model of SOD1 mutant-mediated amyotrophic lateral sclerosis (ALS).* Proc Natl Acad Sci U S A, 2002. **99**(3): p. 1604-9.
228. Guo, H., et al., *Increased expression of the glial glutamate transporter EAAT2 modulates excitotoxicity and delays the onset but not the outcome of ALS in mice.* Human Molecular Genetics, 2003. **12**(19): p. 2519-2532.
229. Milanese, M., et al., *Abnormal exocytotic release of glutamate in a mouse model of amyotrophic lateral sclerosis.* J Neurochem, 2011. **116**(6): p. 1028-42.
230. Meyer, T., et al., *The RNA of the glutamate transporter EAAT2 is variably spliced in amyotrophic lateral sclerosis and normal individuals.* J Neurol Sci, 1999. **170**(1): p. 45-50.
231. Wuolikainen, A., et al., *Disease-Related Changes in the Cerebrospinal Fluid Metabolome in Amyotrophic Lateral Sclerosis Detected by GC/TOFMS.* PLOS ONE, 2011. **6**(4): p. e17947.
232. Vargas, M.R. and J.A. Johnson, *Astrogliosis in amyotrophic lateral sclerosis: role and therapeutic potential of astrocytes.* Neurotherapeutics, 2010. **7**(4): p. 471-81.
233. Geloso, M.C., et al., *The Dual Role of Microglia in ALS: Mechanisms and Therapeutic Approaches.* Frontiers in aging neuroscience, 2017. **9**: p. 242-242.
234. Murray, P.J. and T.A. Wynn, *Protective and pathogenic functions of macrophage subsets.* Nat Rev Immunol, 2011. **11**(11): p. 723-37.
235. Ullian, E.M., K.S. Christopherson, and B.A. Barres, *Role for glia in synaptogenesis.* Glia, 2004. **47**(3): p. 209-16.
236. Volterra, A. and J. Meldolesi, *Astrocytes, from brain glue to communication elements: the revolution continues.* Nat Rev Neurosci, 2005. **6**(8): p. 626-40.

237. Sloan, S.A. and B.A. Barres, *Mechanisms of astrocyte development and their contributions to neurodevelopmental disorders.* Curr Opin Neurobiol, 2014. **27**: p. 75-81.
238. Yamanaka, K., et al., *Astrocytes as determinants of disease progression in inherited amyotrophic lateral sclerosis.* Nat Neurosci, 2008. **11**(3): p. 251-3.
239. Wang, L., D.H. Gutmann, and R.P. Roos, *Astrocyte loss of mutant SOD1 delays ALS disease onset and progression in G85R transgenic mice.* Hum Mol Genet, 2011. **20**(2): p. 286-93.
240. Boillee, S., C. Vande Velde, and D.W. Cleveland, *ALS: a disease of motor neurons and their nonneuronal neighbors.* Neuron, 2006. **52**(1): p. 39-59.
241. Wang, L., et al., *The effect of mutant SOD1 dismutase activity on non-cell autonomous degeneration in familial amyotrophic lateral sclerosis.* Neurobiol Dis, 2009. **35**(2): p. 234-40.
242. Liddelow, S.A., et al., *Neurotoxic reactive astrocytes are induced by activated microglia.* Nature, 2017. **541**(7638): p. 481-487.
243. Clarke, L.E., et al., *Normal aging induces A1-like astrocyte reactivity.* Proc Natl Acad Sci U S A, 2018. **115**(8): p. E1896-e1905.
244. Miller, S.J., *Astrocyte Heterogeneity in the Adult Central Nervous System.* Frontiers in Cellular Neuroscience, 2018. **12**(401).
245. Mackenzie, I.R., et al., *Pathological heterogeneity in amyotrophic lateral sclerosis with FUS mutations: two distinct patterns correlating with disease severity and mutation.* Acta Neuropathol, 2011. **122**(1): p. 87-98.
246. Niebroj-Dobosz, I., et al., *Myelin composition of spinal cord in a model of amyotrophic lateral sclerosis (ALS) in SOD1G93A transgenic rats.* Folia Neuropathol, 2007. **45**(4): p. 236-41.
247. Kang, S.H., et al., *Degeneration and impaired regeneration of gray matter oligodendrocytes in amyotrophic lateral sclerosis.* Nat Neurosci, 2013. **16**(5): p. 571-9.
248. Lino, M.M., C. Schneider, and P. Caroni, *Accumulation of SOD1 mutants in postnatal motoneurons does not cause motoneuron pathology or motoneuron disease.* J Neurosci, 2002. **22**(12): p. 4825-32.
249. Pramatarova, A., et al., *Neuron-specific expression of mutant superoxide dismutase 1 in transgenic mice does not lead to motor impairment.* J Neurosci, 2001. **21**(10): p. 3369-74.
250. Clement, A.M., et al., *Wild-type nonneuronal cells extend survival of SOD1 mutant motor neurons in ALS mice.* Science, 2003. **302**(5642): p. 113-7.
251. Yamanaka, K., et al., *Astrocytes as determinants of disease progression in inherited amyotrophic lateral sclerosis.* Nature neuroscience, 2008. **11**(3): p. 251-253.
252. Basso, M., et al., *Mutant Copper-Zinc Superoxide Dismutase (SOD1) Induces Protein Secretion Pathway Alterations and Exosome Release in Astrocytes: IMPLICATIONS FOR DISEASE SPREADING AND MOTOR NEURON PATHOLOGY IN AMYOTROPHIC LATERAL SCLEROSIS.* Journal of Biological Chemistry, 2013. **288**(22): p. 15699-15711.

253. Haidet-Phillips, A.M., et al., *Astrocytes from familial and sporadic ALS patients are toxic to motor neurons.* Nature biotechnology, 2011. **29**(9): p. 824-828.
254. Meyer, K., et al., *Direct conversion of patient fibroblasts demonstrates non-cell autonomous toxicity of astrocytes to motor neurons in familial and sporadic ALS.* Proceedings of the National Academy of Sciences, 2014. **111**(2): p. 829.
255. Nagai, M., et al., *Astrocytes expressing ALS-linked mutated SOD1 release factors selectively toxic to motor neurons.* Nature Neuroscience, 2007. **10**: p. 615.
256. Di Giorgio, F.P., et al., *Human embryonic stem cell-derived motor neurons are sensitive to the toxic effect of glial cells carrying an ALS-causing mutation.* Cell Stem Cell, 2008. **3**(6): p. 637-48.
257. Beers, D.R., et al., *Wild-type microglia extend survival in PU.1 knockout mice with familial amyotrophic lateral sclerosis.* Proc Natl Acad Sci U S A, 2006. **103**(43): p. 16021-6.
258. Turner, M.R., et al., *Evidence of widespread cerebral microglial activation in amyotrophic lateral sclerosis: an [11C](R)-PK11195 positron emission tomography study.* Neurobiol Dis, 2004. **15**(3): p. 601-9.
259. Baas, P.W., et al., *Polarity orientation of microtubules in hippocampal neurons: uniformity in the axon and nonuniformity in the dendrite.* Proc Natl Acad Sci U S A, 1988. **85**(21): p. 8335-9.
260. Hirokawa, N., *Kinesin and dynein superfamily proteins and the mechanism of organelle transport.* Science, 1998. **279**(5350): p. 519-26.
261. Qiu, W., et al., *Dynein achieves processive motion using both stochastic and coordinated stepping.* Nat Struct Mol Biol, 2012. **19**(2): p. 193-200.
262. DeWitt, M.A., et al., *Cytoplasmic Dynein Moves Through Uncoordinated Stepping of the AAA+ Ring Domains.* Science, 2012. **335**(6065): p. 221.
263. Brenner, D., et al., *Hot-spot KIF5A mutations cause familial ALS.* Brain, 2018. **141**(3): p. 688-697.
264. Hirano, A., et al., *Fine structural study of neurofibrillary changes in a family with amyotrophic lateral sclerosis.* J Neuropathol Exp Neurol, 1984. **43**(5): p. 471-80.
265. Hirano, A., et al., *Fine structural observations of neurofilamentous changes in amyotrophic lateral sclerosis.* J Neuropathol Exp Neurol, 1984. **43**(5): p. 461-70.
266. Che, D.L., P.D. Chowdary, and B. Cui, *A close look at axonal transport: Cargos slow down when crossing stationary organelles.* Neuroscience letters, 2016. **610**: p. 110-116.
267. Kieran, D., et al., *A mutation in dynein rescues axonal transport defects and extends the life span of ALS mice.* J Cell Biol, 2005. **169**(4): p. 561-7.
268. Bilsland, L.G., et al., *Deficits in axonal transport precede ALS symptoms in vivo.* Proc Natl Acad Sci U S A, 2010. **107**(47): p. 20523-8.
269. Magrane, J., et al., *Abnormal mitochondrial transport and morphology are common pathological denominators in SOD1 and TDP43 ALS mouse models.* Hum Mol Genet, 2014. **23**(6): p. 1413-24.
270. Vande Velde, C., et al., *Misfolded SOD1 associated with motor neuron mitochondria alters mitochondrial shape and distribution prior to clinical onset.* PLoS One, 2011. **6**(7): p. e22031.

271. Morotz, G.M., et al., *Amyotrophic lateral sclerosis-associated mutant VAPBP56S perturbs calcium homeostasis to disrupt axonal transport of mitochondria.* Hum Mol Genet, 2012. **21**(9): p. 1979-88.
272. Wang, W., et al., *The ALS disease-associated mutant TDP-43 impairs mitochondrial dynamics and function in motor neurons.* Hum Mol Genet, 2013. **22**(23): p. 4706-19.
273. Maday, S., K.E. Wallace, and E.L. Holzbaur, *Autophagosomes initiate distally and mature during transport toward the cell soma in primary neurons.* J Cell Biol, 2012. **196**(4): p. 407-17.
274. Aoki, Y., et al., *C9orf72 and RAB7L1 regulate vesicle trafficking in amyotrophic lateral sclerosis and frontotemporal dementia.* Brain, 2017. **140**(4): p. 887-897.
275. Stenmark, H., *Rab GTPases as coordinators of vesicle traffic.* Nat Rev Mol Cell Biol, 2009. **10**(8): p. 513-25.
276. Hadano, S., et al., *Mice deficient in the Rab5 guanine nucleotide exchange factor ALS2/alsin exhibit age-dependent neurological deficits and altered endosome trafficking.* Hum Mol Genet, 2006. **15**(2): p. 233-50.
277. Lai, C., et al., *Amyotrophic lateral sclerosis 2-deficiency leads to neuronal degeneration in amyotrophic lateral sclerosis through altered AMPA receptor trafficking.* J Neurosci, 2006. **26**(45): p. 11798-806.
278. Schwenk, B.M., et al., *TDP-43 loss of function inhibits endosomal trafficking and alters trophic signaling in neurons.* The EMBO journal, 2016. **35**(21): p. 2350-2370.
279. Soo, K., et al., *Rab1-dependent ER–Golgi transport dysfunction is a common pathogenic mechanism in SOD1, TDP-43 and FUS-associated ALS.* Acta Neuropathologica, 2015: p. 1-19.
280. Fujita, Y., et al., *Fragmentation of the Golgi apparatus of the anterior horn cells in patients with familial amyotrophic lateral sclerosis with SOD1 mutations and posterior column involvement.* J Neurol Sci, 2000. **174**(2): p. 137-40.
281. Oyanagi, K., et al., *Spinal anterior horn cells in sporadic amyotrophic lateral sclerosis show ribosomal detachment from, and cisternal distention of the rough endoplasmic reticulum.* Neuropathol Appl Neurobiol, 2008. **34**(6): p. 650-8.
282. Sasaki, S., *Endoplasmic reticulum stress in motor neurons of the spinal cord in sporadic amyotrophic lateral sclerosis.* J Neuropathol Exp Neurol, 2010. **69**(4): p. 346-55.
283. Atkin, J.D., et al., *Endoplasmic reticulum stress and induction of the unfolded protein response in human sporadic amyotrophic lateral sclerosis.* Neurobiology of disease, 2008. **30**(3): p. 400-407.
284. Sundaramoorthy, V., et al., *Extracellular wildtype and mutant SOD1 induces ER-Golgi pathology characteristic of amyotrophic lateral sclerosis in neuronal cells.* Cell Mol Life Sci, 2013. **70**(21): p. 4181-95.
285. Farg, M.A., et al., *Mutant FUS induces endoplasmic reticulum stress in amyotrophic lateral sclerosis and interacts with protein disulfide-isomerase.* Neurobiol Aging, 2012. **33**(12): p. 2855-68.

286. Halloran, M., et al., *Amyotrophic lateral sclerosis-linked UBQLN2 mutants inhibit endoplasmic reticulum to Golgi transport, leading to Golgi fragmentation and ER stress.* Cell Mol Life Sci, 2019.
287. Dafinca, R., et al., *C9orf72 Hexanucleotide Expansions Are Associated with Altered Endoplasmic Reticulum Calcium Homeostasis and Stress Granule Formation in Induced Pluripotent Stem Cell-Derived Neurons from Patients with Amyotrophic Lateral Sclerosis and Frontotemporal Dementia.* STEM CELLS, 2016. **34**(8): p. 2063-2078.
288. Saxena, S., E. Cabuy, and P. Caroni, *A role for motoneuron subtype-selective ER stress in disease manifestations of FALS mice.* Nat Neurosci, 2009. **12**(5): p. 627-36.
289. Madabhushi, R., L. Pan, and L.H. Tsai, *DNA damage and its links to neurodegeneration.* Neuron, 2014. **83**(2): p. 266-282.
290. Rulten, S.L. and G.J. Grundy, *Non-homologous end joining: Common interaction sites and exchange of multiple factors in the DNA repair process.* Bioessays, 2017. **39**(3).
291. Walker, C., et al., *C9orf72 expansion disrupts ATM-mediated chromosomal break repair.* Nature Neuroscience, 2017. **20**: p. 1225.
292. Sama, R.R.K., C.L. Ward, and D.A. Bosco, *Functions of FUS/TLS From DNA Repair to Stress Response: Implications for ALS.* ASN Neuro, 2014. **6**(4): p. 1759091414544472.
293. Wang, W.-Y., et al., *Interaction of FUS and HDAC1 regulates DNA damage response and repair in neurons.* Nature neuroscience, 2013. **16**(10): p. 1383-1391.
294. Carroll, J., et al., *Expression of a pathogenic mutation of SOD1 sensitizes aprataxin-deficient cells and mice to oxidative stress and triggers hallmarks of premature ageing.* Human molecular genetics, 2015. **24**(3): p. 828-840.
295. Penndorf, D., et al., *DNA strand breaks and TDP-43 mislocation are absent in the murine hSOD1G93A model of amyotrophic lateral sclerosis in vivo and in vitro.* PloS one, 2017. **12**(8): p. e0183684-e0183684.
296. Carrì, M.T., et al., *Neurodegeneration in amyotrophic lateral sclerosis: the role of oxidative stress and altered homeostasis of metals.* Brain Research Bulletin, 2003. **61**(4): p. 365-374.
297. Shaw, P.J., et al., *Oxidative damage to protein in sporadic motor neuron disease spinal cord.* Ann Neurol, 1995. **38**(4): p. 691-5.
298. Beal, M.F., et al., *Increased 3-nitrotyrosine in both sporadic and familial amyotrophic lateral sclerosis.* Ann Neurol, 1997. **42**(4): p. 644-54.
299. Ferrante, R.J., et al., *Evidence of Increased Oxidative Damage in Both Sporadic and Familial Amyotrophic Lateral Sclerosis.* Journal of Neurochemistry, 1997. **69**(5): p. 2064-2074.
300. Bogdanov, M., et al., *Increased oxidative damage to DNA in ALS patients.* Free Radical Biology and Medicine, 2000. **29**(7): p. 652-658.
301. Shibata, N., et al., *Morphological evidence for lipid peroxidation and protein glycoxidation in spinal cords from sporadic amyotrophic lateral sclerosis patients.* Brain Research, 2001. **917**(1): p. 97-104.

302. Andrus, P.K., et al., *Protein oxidative damage in a transgenic mouse model of familial amyotrophic lateral sclerosis.* J Neurochem, 1998. **71**(5): p. 2041-8.
303. Bogdanov, M.B., et al., *Elevated "Hydroxyl Radical" Generation In Vivo in an Animal Model of Amyotrophic Lateral Sclerosis.* Journal of Neurochemistry, 1998. **71**(3): p. 1321-1324.
304. Hall, E.D., et al., *Relationship of oxygen radical-induced lipid peroxidative damage to disease onset and progression in a transgenic model of familial ALS.* Journal of Neuroscience Research, 1998. **53**(1): p. 66-77.
305. Tsang, C.K., et al., *Superoxide dismutase 1 acts as a nuclear transcription factor to regulate oxidative stress resistance.* Nat Commun, 2014. **5**: p. 3446.
306. Gohil, V.M. and M.L. Greenberg, *Mitochondrial membrane biogenesis: phospholipids and proteins go hand in hand.* The Journal of cell biology, 2009. **184**(4): p. 469-472.
307. Vandecasteele, G., G. Szabadkai, and R. Rizzuto, *Mitochondrial calcium homeostasis: mechanisms and molecules.* IUBMB Life, 2001. **52**(3-5): p. 213-9.
308. Wang, C. and R.J. Youle, *The role of mitochondria in apoptosis*.* Annual review of genetics, 2009. **43**: p. 95-118.
309. Bélanger, M., I. Allaman, and Pierre J. Magistretti, *Brain Energy Metabolism: Focus on Astrocyte-Neuron Metabolic Cooperation.* Cell Metabolism, 2011. **14**(6): p. 724-738.
310. Atsumi, T., *The ultrastructure of intramuscular nerves in amyotrophic lateral sclerosis.* Acta Neuropathologica, 1981. **55**(3): p. 193-198.
311. Sasaki, S. and M. Iwata, *Mitochondrial alterations in the spinal cord of patients with sporadic amyotrophic lateral sclerosis.* Journal of Neuropathology and Experimental Neurology, 2007. **66**(1): p. 10-16.
312. Allen, S.P., et al., *Superoxide dismutase 1 mutation in a cellular model of amyotrophic lateral sclerosis shifts energy generation from oxidative phosphorylation to glycolysis.* Neurobiology of Aging, 2014. **35**(6): p. 1499-1509.
313. Smith, R.G., et al., *Presence of 4-hydroxynonenal in cerebrospinal fluid of patients with sporadic amyotrophic lateral sclerosis.* Annals of Neurology, 1998. **44**(4): p. 696-699.
314. Simpson, E.P., et al., *Increased lipid peroxidation in sera of ALS patients: A potential biomarker of disease burden.* Neurology, 2004. **62**(10): p. 1758-1765.
315. Shaw, P.J., et al., *Oxidative damage to protein in sporadic motor neuron disease spinal cord.* Annals of Neurology, 1995. **38**(4): p. 691-695.
316. Pasinelli, P., et al., *Amyotrophic lateral sclerosis-associated SOD1 mutant proteins bind and aggregate with Bcl-2 in spinal cord mitochondria.* Neuron, 2004. **43**(1): p. 19-30.
317. Hong, K., et al., *Full-length TDP-43 and its C-terminal fragments activate mitophagy in NSC34 cell line.* Neuroscience Letters, 2012. **530**(2): p. 144-149.
318. Magrané, J., et al., *Abnormal mitochondrial transport and morphology are common pathological denominators in SOD1 and TDP43 ALS mouse models.* Human Molecular Genetics, 2014. **23**(6): p. 1413-1424.

319. Wang, W., et al., *The ALS disease-associated mutant TDP-43 impairs mitochondrial dynamics and function in motor neurons.* Human Molecular Genetics, 2013. **22**(23): p. 4706-4719.
320. Higgins, C.M., C. Jung, and Z. Xu, *ALS-associated mutant SOD1G93A causes mitochondrial vacuolation by expansion of the intermembrane space and by involvement of SOD1 aggregation and peroxisomes.* BMC Neurosci, 2003. **4**: p. 16.
321. De vos, K.J., et al., *Familial amyotrophic lateral sclerosis-linked SOD1 mutants perturb fast axonal transport to reduce axonal mitochondria content.* Human Molecular Genetics, 2007. **16**(22): p. 2720-2728.
322. Tradewell, M.L., et al., *Arginine methylation by prmt1 regulates nuclear-cytoplasmic localization and toxicity of FUS/TLS harbouring ALS-linked mutations.* Human Molecular Genetics, 2012. **21**(1): p. 136-149.
323. Xia, Q., et al., *TDP-43 loss of function increases TFEB activity and blocks autophagosome-lysosome fusion.* The EMBO journal, 2016. **35**(2): p. 121-142.
324. Soo, K.Y., et al., *ALS-associated mutant FUS inhibits macroautophagy which is restored by overexpression of Rab1.* Cell death discovery, 2015. **1**: p. 15030-15030.
325. Sullivan, P.M., et al., *The ALS/FTLD associated protein C9orf72 associates with SMCR8 and WDR41 to regulate the autophagy-lysosome pathway.* Acta Neuropathol Commun, 2016. **4**(1): p. 51.
326. Dice, J.F., *Peptide sequences that target cytosolic proteins for lysosomal proteolysis.* Trends Biochem Sci, 1990. **15**(8): p. 305-9.
327. Chiang, H.L., et al., *A role for a 70-kilodalton heat shock protein in lysosomal degradation of intracellular proteins.* Science, 1989. **246**(4928): p. 382-5.
328. Cuervo, A.M. and J.F. Dice, *A receptor for the selective uptake and degradation of proteins by lysosomes.* Science, 1996. **273**(5274): p. 501-3.
329. Salvador, N., et al., *Import of a cytosolic protein into lysosomes by chaperone-mediated autophagy depends on its folding state.* J Biol Chem, 2000. **275**(35): p. 27447-56.
330. Marzella, L., J. Ahlberg, and H. Glaumann, *Autophagy, heterophagy, microautophagy and crinophagy as the means for intracellular degradation.* Virchows Arch B Cell Pathol Incl Mol Pathol, 1981. **36**(2-3): p. 219-34.
331. Mijaljica, D., M. Prescott, and R.J. Devenish, *Microautophagy in mammalian cells: revisiting a 40-year-old conundrum.* Autophagy, 2011. **7**(7): p. 673-82.
332. Tekirdag, K. and A.M. Cuervo, *Chaperone-mediated autophagy and endosomal microautophagy: Joint by a chaperone.* J Biol Chem, 2018. **293**(15): p. 5414-5424.
333. Sahu, R., et al., *Microautophagy of cytosolic proteins by late endosomes.* Dev Cell, 2011. **20**(1): p. 131-9.
334. Uytterhoeven, V., et al., *Hsc70-4 Deforms Membranes to Promote Synaptic Protein Turnover by Endosomal Microautophagy.* Neuron, 2015. **88**(4): p. 735-748.
335. Mukherjee, A., et al., *Selective endosomal microautophagy is starvation-inducible in Drosophila.* Autophagy, 2016. **12**(11): p. 1984-1999.

336. Olsvik, H.L., et al., *Endosomal microautophagy is an integrated part of the autophagic response to amino acid starvation.* Autophagy, 2019. **15**(1): p. 182-183.
337. Feng, Y., et al., *The machinery of macroautophagy.* Cell Research, 2013. **24**: p. 24.
338. Reggiori, F. and C. Ungermann, *Autophagosome Maturation and Fusion.* Journal of Molecular Biology, 2017. **429**(4): p. 486-496.
339. Suzuki, K. and Y. Ohsumi, *Current knowledge of the pre-autophagosomal structure (PAS).* FEBS Lett, 2010. **584**(7): p. 1280-6.
340. Takeshige, K., et al., *Autophagy in yeast demonstrated with proteinase-deficient mutants and conditions for its induction.* J Cell Biol, 1992. **119**(2): p. 301-11.
341. Tsukada, M. and Y. Ohsumi, *Isolation and characterization of autophagy-defective mutants of Saccharomyces cerevisiae.* FEBS Lett, 1993. **333**(1-2): p. 169-74.
342. Matsuura, A., et al., *Apg1p, a novel protein kinase required for the autophagic process in Saccharomyces cerevisiae.* Gene, 1997. **192**(2): p. 245-50.
343. Mizushima, N., *The role of the Atg1/ULK1 complex in autophagy regulation.* Curr Opin Cell Biol, 2010. **22**(2): p. 132-9.
344. Ganley, I.G., et al., *ULK1.ATG13.FIP200 complex mediates mTOR signaling and is essential for autophagy.* J Biol Chem, 2009. **284**(18): p. 12297-305.
345. Russell, R.C., et al., *ULK1 induces autophagy by phosphorylating Beclin-1 and activating VPS34 lipid kinase.* Nature cell biology, 2013. **15**(7): p. 741-750.
346. Di Bartolomeo, S., et al., *The dynamic interaction of AMBRA1 with the dynein motor complex regulates mammalian autophagy.* The Journal of cell biology, 2010. **191**(1): p. 155-168.
347. Hurley, J.H. and L.N. Young, *Mechanisms of Autophagy Initiation.* Annual review of biochemistry, 2017. **86**: p. 225-244.
348. Carlsson, S.R. and A. Simonsen, *Membrane dynamics in autophagosome biogenesis.* Journal of Cell Science, 2015. **128**(2): p. 193.
349. Proikas-Cezanne, T., et al., *WIPI proteins: essential PtdIns3P effectors at the nascent autophagosome.* Journal of Cell Science, 2015. **128**(2): p. 207.
350. Reggiori, F., et al., *The Atg1-Atg13 complex regulates Atg9 and Atg23 retrieval transport from the pre-autophagosomal structure.* Dev Cell, 2004. **6**(1): p. 79-90.
351. He, C., et al., *Recruitment of Atg9 to the preautophagosomal structure by Atg11 is essential for selective autophagy in budding yeast.* The Journal of Cell Biology, 2006. **175**(6): p. 925.
352. Young, A.R.J., et al., *Starvation and ULK1-dependent cycling of mammalian Atg9 between the TGN and endosomes.* Journal of Cell Science, 2006. **119**(18): p. 3888.
353. Nakatogawa, H., *Two ubiquitin-like conjugation systems that mediate membrane formation during autophagy.* Essays Biochem, 2013. **55**: p. 39-50.
354. Mizushima, N., et al., *A protein conjugation system essential for autophagy.* Nature, 1998. **395**(6700): p. 395-8.
355. Shintani, T., et al., *Apg10p, a novel protein-conjugating enzyme essential for autophagy in yeast.* Embo j, 1999. **18**(19): p. 5234-41.

356. Mizushima, N., T. Noda, and Y. Ohsumi, *Apg16p is required for the function of the Apg12p-Apg5p conjugate in the yeast autophagy pathway.* Embo j, 1999. **18**(14): p. 3888-96.
357. Kuma, A., et al., *Formation of the approximately 350-kDa Apg12-Apg5.Apg16 multimeric complex, mediated by Apg16 oligomerization, is essential for autophagy in yeast.* J Biol Chem, 2002. **277**(21): p. 18619-25.
358. Hanada, T., et al., *The Atg12-Atg5 conjugate has a novel E3-like activity for protein lipidation in autophagy.* J Biol Chem, 2007. **282**(52): p. 37298-302.
359. Tanida, I., et al., *Apg7p/Cvt2p: A novel protein-activating enzyme essential for autophagy.* Mol Biol Cell, 1999. **10**(5): p. 1367-79.
360. Kim, J., et al., *Apg7p/Cvt2p is required for the cytoplasm-to-vacuole targeting, macroautophagy, and peroxisome degradation pathways.* Mol Biol Cell, 1999. **10**(5): p. 1337-51.
361. Schlumpberger, M., et al., *AUT1, a gene essential for autophagocytosis in the yeast Saccharomyces cerevisiae.* J Bacteriol, 1997. **179**(4): p. 1068-76.
362. Ichimura, Y., et al., *A ubiquitin-like system mediates protein lipidation.* Nature, 2000. **408**(6811): p. 488-92.
363. Kirisako, T., et al., *Formation process of autophagosome is traced with Apg8/Aut7p in yeast.* J Cell Biol, 1999. **147**(2): p. 435-46.
364. Nakatogawa, H., Y. Ichimura, and Y. Ohsumi, *Atg8, a ubiquitin-like protein required for autophagosome formation, mediates membrane tethering and hemifusion.* Cell, 2007. **130**(1): p. 165-78.
365. Chernomordik, L.V. and M.M. Kozlov, *Membrane hemifusion: crossing a chasm in two leaps.* Cell, 2005. **123**(3): p. 375-82.
366. Xie, Z., U. Nair, and D.J. Klionsky, *Atg8 controls phagophore expansion during autophagosome formation.* Mol Biol Cell, 2008. **19**(8): p. 3290-8.
367. Fujita, N., et al., *An Atg4B Mutant Hampers the Lipidation of LC3 Paralogues and Causes Defects in Autophagosome Closure.* Molecular Biology of the Cell, 2008. **19**(11): p. 4651-4659.
368. Nair, U., et al., *A role for Atg8-PE deconjugation in autophagosome biogenesis.* Autophagy, 2012. **8**(5): p. 780-93.
369. Huotari, J. and A. Helenius, *Endosome maturation.* The EMBO journal, 2011. **30**(17): p. 3481-3500.
370. Kimura, S., T. Noda, and T. Yoshimori, *Dynein-dependent movement of autophagosomes mediates efficient encounters with lysosomes.* Cell Struct Funct, 2008. **33**(1): p. 109-22.
371. Korolchuk, V.I., et al., *Lysosomal positioning coordinates cellular nutrient responses.* Nat Cell Biol, 2011. **13**(4): p. 453-60.
372. Jordens, I., et al., *The Rab7 effector protein RILP controls lysosomal transport by inducing the recruitment of dynein-dynactin motors.* Curr Biol, 2001. **11**(21): p. 1680-5.
373. Nakamura, S. and T. Yoshimori, *New insights into autophagosome–lysosome fusion.* Journal of Cell Science, 2017. **130**(7): p. 1209.
374. Nguyen, T.N., et al., *Atg8 family LC3/GABARAP proteins are crucial for autophagosome–lysosome fusion but not autophagosome formation during*

PINK1/Parkin mitophagy and starvation. The Journal of Cell Biology, 2016. **215**(6): p. 857.
375. Maruyama, Y., et al., *LC3B is indispensable for selective autophagy of p62 but not basal autophagy.* Biochem Biophys Res Commun, 2014. **446**(1): p. 309-15.
376. Kabeya, Y., et al., *LC3, GABARAP and GATE16 localize to autophagosomal membrane depending on form-II formation.* J Cell Sci, 2004. **117**(Pt 13): p. 2805-12.
377. Weidberg, H., et al., *LC3 and GATE-16/GABARAP subfamilies are both essential yet act differently in autophagosome biogenesis.* Embo j, 2010. **29**(11): p. 1792-802.
378. Takayama, K., A. Matsuura, and E. Itakura, *Dissection of ubiquitinated protein degradation by basal autophagy.* FEBS Lett, 2017. **591**(9): p. 1199-1211.
379. Yla-Anttila, P., et al., *3D tomography reveals connections between the phagophore and endoplasmic reticulum.* Autophagy, 2009. **5**(8): p. 1180-5.
380. Fujita, N., et al., *An Atg4B mutant hampers the lipidation of LC3 paralogues and causes defects in autophagosome closure.* Mol Biol Cell, 2008. **19**(11): p. 4651-9.
381. Axe, E.L., et al., *Autophagosome formation from membrane compartments enriched in phosphatidylinositol 3-phosphate and dynamically connected to the endoplasmic reticulum.* J Cell Biol, 2008. **182**(4): p. 685-701.
382. Hailey, D.W., et al., *Mitochondria supply membranes for autophagosome biogenesis during starvation.* Cell, 2010. **141**(4): p. 656-67.
383. Ravikumar, B., et al., *Plasma membrane contributes to the formation of pre-autophagosomal structures.* Nat Cell Biol, 2010. **12**(8): p. 747-57.
384. Geng, J., et al., *Post-Golgi Sec proteins are required for autophagy in Saccharomyces cerevisiae.* Mol Biol Cell, 2010. **21**(13): p. 2257-69.
385. Hamasaki, M., et al., *Autophagosomes form at ER-mitochondria contact sites.* Nature, 2013. **495**(7441): p. 389-93.
386. Maday, S. and E.L.F. Holzbaur, *Autophagosome biogenesis in primary neurons follows an ordered and spatially regulated pathway.* Developmental cell, 2014. **30**(1): p. 71-85.
387. van Leeuwen, W., F. van der Krift, and C. Rabouille, *Modulation of the secretory pathway by amino-acid starvation.* The Journal of Cell Biology, 2018. **217**(7): p. 2261.
388. Jeong, Y.T., et al., *The ULK1-FBXW5-SEC23B nexus controls autophagy.* Elife, 2018. **7**.
389. Cui, Y., et al., *A COPII subunit acts with an autophagy receptor to target endoplasmic reticulum for degradation.* Science, 2019. **365**(6448): p. 53.
390. Zaffagnini, G. and S. Martens, *Mechanisms of Selective Autophagy.* Journal of molecular biology, 2016. **428**(9 Pt A): p. 1714-1724.
391. Anding, A.L. and E.H. Baehrecke, *Cleaning House: Selective Autophagy of Organelles.* Dev Cell, 2017. **41**(1): p. 10-22.
392. Matsumoto, G., et al., *TBK1 controls autophagosomal engulfment of polyubiquitinated mitochondria through p62/SQSTM1 phosphorylation.* Hum Mol Genet, 2015. **24**(15): p. 4429-42.

393. Komatsu, M., et al., *Impairment of starvation-induced and constitutive autophagy in Atg7-deficient mice.* The Journal of cell biology, 2005. **169**(3): p. 425-434.
394. Wong, Y.C. and E.L. Holzbaur, *Optineurin is an autophagy receptor for damaged mitochondria in parkin-mediated mitophagy that is disrupted by an ALS-linked mutation.* Proc Natl Acad Sci U S A, 2014. **111**(42): p. E4439-48.
395. Zhang, T. and S. Ghaemmaghami, *Global analysis of cellular protein flux quantifies the selectivity of basal autophagy.* Autophagy, 2016. **12**(8): p. 1411-2.
396. Clark, S.G., et al., *Basal autophagy is required for promoting dendritic terminal branching in Drosophila sensory neurons.* PLOS ONE, 2018. **13**(11): p. e0206743.
397. Bourouis, M., et al., *Control of basal autophagy rate by vacuolar peduncle.* PLoS One, 2019. **14**(2): p. e0209759.
398. Into, T., et al., *Basal autophagy prevents autoactivation or enhancement of inflammatory signals by targeting monomeric MyD88.* Scientific reports, 2017. **7**(1): p. 1009-1009.
399. Seino, J., et al., *Basal autophagy is required for the efficient catabolism of sialyloligosaccharides.* J Biol Chem, 2013. **288**(37): p. 26898-907.
400. Kuma, A., et al., *The role of autophagy during the early neonatal starvation period.* Nature, 2004. **432**(7020): p. 1032-6.
401. Hara, T., et al., *Suppression of basal autophagy in neural cells causes neurodegenerative disease in mice.* Nature, 2006. **441**(7095): p. 885-9.
402. Mizushima, N., et al., *In vivo analysis of autophagy in response to nutrient starvation using transgenic mice expressing a fluorescent autophagosome marker.* Molecular biology of the cell, 2004. **15**(3): p. 1101-1111.
403. Heitman, J., N.R. Movva, and M.N. Hall, *Targets for cell cycle arrest by the immunosuppressant rapamycin in yeast.* Science, 1991. **253**(5022): p. 905-9.
404. Rabanal-Ruiz, Y., Elsje G. Otten, and Viktor I. Korolchuk, *mTORC1 as the main gateway to autophagy.* Essays In Biochemistry, 2017. **61**(6): p. 565.
405. Laplante, M. and D.M. Sabatini, *mTOR signaling at a glance.* Journal of Cell Science, 2009. **122**(20): p. 3589.
406. Aylett, C.H., et al., *Architecture of human mTOR complex 1.* Science, 2016. **351**(6268): p. 48-52.
407. Zhang, Y., et al., *Rheb is a direct target of the tuberous sclerosis tumour suppressor proteins.* Nat Cell Biol, 2003. **5**(6): p. 578-81.
408. Tee, A.R., et al., *Tuberous sclerosis complex gene products, Tuberin and Hamartin, control mTOR signaling by acting as a GTPase-activating protein complex toward Rheb.* Curr Biol, 2003. **13**(15): p. 1259-68.
409. Tee, A.R., et al., *Tuberous sclerosis complex-1 and -2 gene products function together to inhibit mammalian target of rapamycin (mTOR)-mediated downstream signaling.* Proc Natl Acad Sci U S A, 2002. **99**(21): p. 13571-6.
410. Gao, X., et al., *Tsc tumour suppressor proteins antagonize amino-acid-TOR signalling.* Nat Cell Biol, 2002. **4**(9): p. 699-704.
411. Huang, J. and B.D. Manning, *The TSC1-TSC2 complex: a molecular switchboard controlling cell growth.* Biochem J, 2008. **412**(2): p. 179-90.

412. Gwinn, D.M. and R.J. Shaw, *3 - AMPK Control of mTOR Signaling and Growth*, in *The Enzymes*, F. Tamanoi and M.N. Hall, Editors. 2010, Academic Press. p. 49-75.
413. Noda, T. and Y. Ohsumi, *Tor, a phosphatidylinositol kinase homologue, controls autophagy in yeast.* J Biol Chem, 1998. **273**(7): p. 3963-6.
414. Saxton, R.A. and D.M. Sabatini, *mTOR Signaling in Growth, Metabolism, and Disease.* Cell, 2017. **168**(6): p. 960-976.
415. Hentges, K.E., et al., *FRAP/mTOR is required for proliferation and patterning during embryonic development in the mouse.* Proc Natl Acad Sci U S A, 2001. **98**(24): p. 13796-801.
416. Cloëtta, D., et al., *Inactivation of mTORC1 in the developing brain causes microcephaly and affects gliogenesis.* The Journal of neuroscience : the official journal of the Society for Neuroscience, 2013. **33**(18): p. 7799-7810.
417. Kassai, H., et al., *Selective activation of mTORC1 signaling recapitulates microcephaly, tuberous sclerosis, and neurodegenerative diseases.* Cell Rep, 2014. **7**(5): p. 1626-1639.
418. Kwon, C.H., et al., *Pten regulates neuronal arborization and social interaction in mice.* Neuron, 2006. **50**(3): p. 377-88.
419. Nie, D., et al., *Tsc2-Rheb signaling regulates EphA-mediated axon guidance.* Nat Neurosci, 2010. **13**(2): p. 163-72.
420. Beaumont, V., et al., *Phosphorylation and local presynaptic protein synthesis in calcium- and calcineurin-dependent induction of crayfish long-term facilitation.* Neuron, 2001. **32**(3): p. 489-501.
421. Fujikake, N., M. Shin, and S. Shimizu, *Association Between Autophagy and Neurodegenerative Diseases.* Frontiers in neuroscience, 2018. **12**: p. 255-255.
422. Son, J.H., et al., *Neuronal autophagy and neurodegenerative diseases.* Experimental & molecular medicine, 2012. **44**(2): p. 89-98.
423. Benito-Cuesta, I., et al., *Assessment of Autophagy in Neurons and Brain Tissue.* Cells, 2017. **6**(3): p. 25.
424. Maday, S. and E.L.F. Holzbaur, *Compartment-Specific Regulation of Autophagy in Primary Neurons.* The Journal of Neuroscience, 2016. **36**(22): p. 5933.
425. Young, J.E., R.A. Martinez, and A.R. La Spada, *Nutrient deprivation induces neuronal autophagy and implicates reduced insulin signaling in neuroprotective autophagy activation.* The Journal of biological chemistry, 2009. **284**(4): p. 2363-2373.
426. Mohamed, N.-V., et al., *Starvation and inhibition of lysosomal function increased tau secretion by primary cortical neurons.* Scientific reports, 2014. **4**: p. 5715-5715.
427. Sasaki, S., *Autophagy in spinal cord motor neurons in sporadic amyotrophic lateral sclerosis.* Journal of Neuropathology & Experimental Neurology, 2011. **70**(5): p. 349-359.
428. Almeida, S., et al., *Modeling key pathological features of frontotemporal dementia with C9ORF72 repeat expansion in iPSC-derived human neurons.* Acta Neuropathol, 2013. **126**(3): p. 385-99.

429. Webster, C.P., et al., *The C9orf72 protein interacts with Rab1a and the ULK1 complex to regulate initiation of autophagy.* The EMBO journal, 2016. **35**(15): p. 1656-1676.
430. Wei, Y., *Autophagic induction of amyotrophic lateral sclerosis-linked Cu/Zn superoxide dismutase 1 G93A mutant in NSC34 cells.* Neural Regen Res, 2014. **9**(1): p. 16-24.
431. Tian, F., et al., *In vivo optical imaging of motor neuron autophagy in a mouse model of amyotrophic lateral sclerosis.* Autophagy, 2011. **7**(9): p. 985-992.
432. Zhang, F., et al., *Interaction between Familial Amyotrophic Lateral Sclerosis (ALS)-linked SOD1 Mutants and the Dynein Complex.* Journal of Biological Chemistry, 2007. **282**(22): p. 16691-16699.
433. Feng, H.L., et al., *Combined lithium and valproate treatment delays disease onset, reduces neurological deficits and prolongs survival in an amyotrophic lateral sclerosis mouse model.* Neuroscience, 2008. **155**(3): p. 567-572.
434. Fornai, F., et al., *Lithium delays progression of amyotrophic lateral sclerosis.* Proceedings of the National Academy of Sciences, 2008. **105**(6): p. 2052.
435. Watanabe, S., et al., *Intracerebroventricular administration of Cystatin C ameliorates disease in SOD1-linked amyotrophic lateral sclerosis mice.* Journal of Neurochemistry, 2018. **145**(1): p. 80-89.
436. Castillo, K., et al., *Trehalose delays the progression of amyotrophic lateral sclerosis by enhancing autophagy in motoneurons.* Autophagy, 2013. **9**(9): p. 1308-1320.
437. Zhang, X., et al., *MTOR-independent, autophagic enhancer trehalose prolongs motor neuron survival and ameliorates the autophagic flux defect in a mouse model of amyotrophic lateral sclerosis.* Autophagy, 2014. **10**(4): p. 588-602.
438. Mancuso, R., et al., *Resveratrol Improves Motoneuron Function and Extends Survival in SOD1G93A ALS Mice.* Neurotherapeutics, 2014. **11**(2): p. 419-432.
439. Zhang, X., et al., *Rapamycin treatment augments motor neuron degeneration in SOD1G93A mouse model of amyotrophic lateral sclerosis.* Autophagy, 2011. **7**(4): p. 412-425.
440. Pizzasegola, C., et al., *Treatment with lithium carbonate does not improve disease progression in two different strains of SOD1 mutant mice.* Amyotrophic Lateral Sclerosis, 2009. **10**(4): p. 221-228.
441. Perera, N.D., et al., *Rilmenidine promotes MTOR-independent autophagy in the mutant SOD1 mouse model of amyotrophic lateral sclerosis without slowing disease progression.* Autophagy, 2018. **14**(3): p. 534-551.
442. Stoica, R., et al., *ER–mitochondria associations are regulated by the VAPB–PTPIP51 interaction and are disrupted by ALS/FTD-associated TDP-43.* Nature Communications, 2014. **5**: p. 3996.
443. Gomez-Suaga, P., et al., *The ER-Mitochondria Tethering Complex VAPB-PTPIP51 Regulates Autophagy.* Current Biology, 2017. **27**(3): p. 371-385.
444. Bose, J.K., C.-C. Huang, and C.K.J. Shen, *Regulation of Autophagy by Neuropathological Protein TDP-43.* Journal of Biological Chemistry, 2011. **286**(52): p. 44441-44448.

445. Komatsu, M., et al., *Homeostatic levels of p62 control cytoplasmic inclusion body formation in autophagy-deficient mice.* Cell, 2007. **131**(6): p. 1149-63.
446. Gal, J., et al., *Sequestosome 1/p62 links familial ALS mutant SOD1 to LC3 via an ubiquitin-independent mechanism.* Journal of Neurochemistry, 2009. **111**(4): p. 1062-1073.
447. Tresse, E., et al., *VCP/p97 is essential for maturation of ubiquitin-containing autophagosomes and this function is impaired by mutations that cause IBMPFD.* Autophagy, 2010. **6**(2): p. 217-227.
448. Ju, J.S., et al., *Valosin-containing protein (VCP) is required for autophagy and is disrupted in VCP disease.* J Cell Biol, 2009. **187**(6): p. 875-88.
449. Yeo, B.K., et al., *Valosin-containing protein is a key mediator between autophagic cell death and apoptosis in adult hippocampal neural stem cells following insulin withdrawal.* Molecular Brain, 2016. **9**(1): p. 31.
450. Gómez-Suaga, P., et al., *The VAPB-PTPIP51 endoplasmic reticulum-mitochondria tethering proteins are present in neuronal synapses and regulate synaptic activity.* Acta Neuropathologica Communications, 2019. **7**(1): p. 35.
451. Zhao, Y.G., et al., *The ER Contact Proteins VAPA/B Interact with Multiple Autophagy Proteins to Modulate Autophagosome Biogenesis.* Curr Biol, 2018. **28**(8): p. 1234-1245.e4.
452. Levine, T.P., et al., *The product of C9orf72, a gene strongly implicated in neurodegeneration, is structurally related to DENN Rab-GEFs.* Bioinformatics, 2013. **29**(4): p. 499-503.
453. Zhang, D., et al., *Discovery of Novel DENN Proteins: Implications for the Evolution of Eukaryotic Intracellular Membrane Structures and Human Disease.* Front Genet, 2012. **3**: p. 283.
454. Farg, M.A., et al., *C9ORF72, implicated in amytrophic lateral sclerosis and frontotemporal dementia, regulates endosomal trafficking.* Hum Mol Genet, 2014. **23**(13): p. 3579-95.
455. Ao, X., L. Zou, and Y. Wu, *Regulation of autophagy by the Rab GTPase network.* Cell Death Differ, 2014. **21**(3): p. 348-58.
456. Moore, A.S. and E.L. Holzbaur, *Dynamic recruitment and activation of ALS-associated TBK1 with its target optineurin are required for efficient mitophagy.* Proc Natl Acad Sci U S A, 2016. **113**(24): p. E3349-58.
457. Mizushima, N. and T. Yoshimori, *How to Interpret LC3 Immunoblotting.* Autophagy, 2007. **3**(6): p. 542-545.
458. Yoshii, S.R. and N. Mizushima, *Monitoring and Measuring Autophagy.* International journal of molecular sciences, 2017. **18**(9): p. 1865.
459. Mizushima, N., T. Yoshimori, and B. Levine, *Methods in mammalian autophagy research.* Cell, 2010. **140**(3): p. 313-326.
460. Zhang, Z., R. Singh, and M. Aschner, *Methods for the Detection of Autophagy in Mammalian Cells.* Current protocols in toxicology, 2016. **69**: p. 20.12.1-20.12.26.
461. Orhon, I. and F. Reggiori, *Assays to Monitor Autophagy Progression in Cell Cultures.* Cells, 2017. **6**(3): p. 20.
462. Mishra, P., V. Ammanathan, and R. Manjithaya, *Chemical Biology Strategies to Study Autophagy.* Frontiers in Cell and Developmental Biology, 2018. **6**: p. 160.

463. Marx, V., *Autophagy: eat thyself, sustain thyself.* Nat Methods, 2015. **12**(12): p. 1121-5.
464. Klionsky, D.J., et al., *Guidelines for the use and interpretation of assays for monitoring autophagy (3rd edition).* Autophagy, 2016. **12**(1): p. 1-222.
465. Pomerantz, J.L. and D. Baltimore, *NF-kappaB activation by a signaling complex containing TRAF2, TANK and TBK1, a novel IKK-related kinase.* The EMBO Journal, 1999. **18**(23): p. 6694-6704.
466. Larabi, A., et al., *Crystal structure and mechanism of activation of TANK-binding kinase 1.* Cell Rep, 2013. **3**(3): p. 734-46.
467. Li, J., et al., *Crystal structure of the ubiquitin-like domain of human TBK1.* Protein Cell, 2012. **3**(5): p. 383-91.
468. Fitzgerald, K.A., et al., *IKKepsilon and TBK1 are essential components of the IRF3 signaling pathway.* Nat Immunol, 2003. **4**(5): p. 491-6.
469. Saul, V.V., et al., *SUMO modification of TBK1 at the adaptor-binding C-terminal coiled-coil domain contributes to its antiviral activity.* Biochim Biophys Acta, 2015. **1853**(1): p. 136-43.
470. Cui, J., et al., *NLRP4 negatively regulates type I interferon signaling by targeting the kinase TBK1 for degradation via the ubiquitin ligase DTX4.* Nat Immunol, 2012. **13**(4): p. 387-95.
471. Ma, X., et al., *Molecular basis of Tank-binding kinase 1 activation by transautophosphorylation.* Proceedings of the National Academy of Sciences, 2012. **109**(24): p. 9378-9383.
472. Clark, K., et al., *Use of the pharmacological inhibitor BX795 to study the regulation and physiological roles of TBK1 and IkappaB kinase epsilon: a distinct upstream kinase mediates Ser-172 phosphorylation and activation.* J Biol Chem, 2009. **284**(21): p. 14136-46.
473. Wilkinson, K.A. and J.M. Henley, *Mechanisms, regulation and consequences of protein SUMOylation.* The Biochemical journal, 2010. **428**(2): p. 133-145.
474. Tu, D., et al., *Structure and ubiquitination-dependent activation of TANK-binding kinase 1.* Cell Rep, 2013. **3**(3): p. 747-58.
475. Ikeda, F., et al., *Involvement of the ubiquitin-like domain of TBK1/IKK-i kinases in regulation of IFN-inducible genes.* The EMBO journal, 2007. **26**(14): p. 3451-3462.
476. Bingol, B. and M. Sheng, *Mechanisms of mitophagy: PINK1, Parkin, USP30 and beyond.* Free Radical Biology and Medicine, 2016. **100**: p. 210-222.
477. Cookson, M.R., *Parkinsonism due to mutations in PINK1, parkin, and DJ-1 and oxidative stress and mitochondrial pathways.* Cold Spring Harbor perspectives in medicine, 2012. **2**(9): p. a009415-a009415.
478. Richter, B., et al., *Phosphorylation of OPTN by TBK1 enhances its binding to Ub chains and promotes selective autophagy of damaged mitochondria.* Proc Natl Acad Sci U S A, 2016. **113**(15): p. 4039-44.
479. Vargas, J.N.S., et al., *Spatiotemporal Control of ULK1 Activation by NDP52 and TBK1 during Selective Autophagy.* Molecular Cell, 2019. **74**(2): p. 347-362.e6.
480. Heo, J.M., et al., *The PINK1-PARKIN Mitochondrial Ubiquitylation Pathway Drives a Program of OPTN/NDP52 Recruitment and TBK1 Activation to Promote Mitophagy.* Mol Cell, 2015. **60**(1): p. 7-20.

481. Lazarou, M., et al., *The ubiquitin kinase PINK1 recruits autophagy receptors to induce mitophagy.* Nature, 2015. **524**(7565): p. 309-314.
482. Heo, J.M., et al., *RAB7A phosphorylation by TBK1 promotes mitophagy via the PINK-PARKIN pathway.* Sci Adv, 2018. **4**(11): p. eaav0443.
483. Minowa-Nozawa, A., et al., *Rab35 GTPase recruits NDP52 to autophagy targets.* The EMBO journal, 2017. **36**(18): p. 2790-2807.
484. Bauckman, K.A., N. Owusu-Boaitey, and I.U. Mysorekar, *Selective autophagy: xenophagy.* Methods (San Diego, Calif.), 2015. **75**: p. 120-127.
485. Thurston, T.L., et al., *Recruitment of TBK1 to cytosol-invading Salmonella induces WIPI2-dependent antibacterial autophagy.* The EMBO journal, 2016. **35**(16): p. 1779-1792.
486. Thurston, T.L., et al., *The TBK1 adaptor and autophagy receptor NDP52 restricts the proliferation of ubiquitin-coated bacteria.* Nat Immunol, 2009. **10**(11): p. 1215-21.
487. Pilli, M., et al., *TBK-1 promotes autophagy-mediated antimicrobial defense by controlling autophagosome maturation.* Immunity, 2012. **37**(2): p. 223-34.
488. Tumbarello, D.A., et al., *Autophagy receptors link myosin VI to autophagosomes to mediate Tom1-dependent autophagosome maturation and fusion with the lysosome.* Nat Cell Biol, 2012. **14**(10): p. 1024-35.
489. Sato, M., et al., *The autophagy receptor ALLO-1 and the IKKE-1 kinase control clearance of paternal mitochondria in Caenorhabditis elegans.* Nat Cell Biol, 2018. **20**(1): p. 81-91.
490. Verheijen, J., et al., *Common and rare TBK1 variants in early-onset Alzheimer disease in a European cohort.* Neurobiol Aging, 2018. **62**: p. 245.e1-245.e7.
491. van der Zee, J., et al., *TBK1 Mutation Spectrum in an Extended European Patient Cohort with Frontotemporal Dementia and Amyotrophic Lateral Sclerosis.* Human mutation, 2017. **38**(3): p. 297-309.
492. Muller, K., et al., *Comprehensive analysis of the mutation spectrum in 301 German ALS families.* J Neurol Neurosurg Psychiatry, 2018. **89**(8): p. 817-827.
493. Gijselinck, I., et al., *Loss of TBK1 is a frequent cause of frontotemporal dementia in a Belgian cohort.* Neurology, 2015. **85**(24): p. 2116-25.
494. de Majo, M., et al., *ALS-associated missense and nonsense TBK1 mutations can both cause loss of kinase function.* Neurobiol Aging, 2018. **71**: p. 266.e1-266.e10.
495. Wilke, C., et al., *Beyond ALS and FTD: the phenotypic spectrum of TBK1 mutations includes PSP-like and cerebellar phenotypes.* Neurobiol Aging, 2018. **62**: p. 244.e9-244.e13.
496. Pozzi, L., et al., *TBK1 mutations in Italian patients with amyotrophic lateral sclerosis: genetic and functional characterisation.* J Neurol Neurosurg Psychiatry, 2017. **88**(10): p. 869-875.
497. Lattante, S., et al., *Coexistence of variants in TBK1 and in other ALS-related genes elucidates an oligogenic model of pathogenesis in sporadic ALS.* Neurobiol Aging, 2019.
498. Williams, K.L., et al., *Novel TBK1 truncating mutation in a familial amyotrophic lateral sclerosis patient of Chinese origin.* Neurobiol Aging, 2015. **36**(12): p. 3334.e1-3334.e5.

499. Caroppo, P., et al., *Semantic and nonfluent aphasic variants, secondarily associated with amyotrophic lateral sclerosis, are predominant frontotemporal lobar degeneration phenotypes in TBK1 carriers.* Alzheimers Dement (Amst), 2015. **1**(4): p. 481-6.
500. Kim, Y.E., et al., *Genetic and functional analysis of TBK1 variants in Korean patients with sporadic amyotrophic lateral sclerosis.* Neurobiol Aging, 2017. **50**: p. 170.e1-170.e6.
501. Shu, S., et al., *Screening of the TBK1 gene in familial and sporadic amyotrophic lateral sclerosis patients of Chinese origin.* Amyotroph Lateral Scler Frontotemporal Degener, 2016. **17**(7-8): p. 605-607.
502. Tsai, P.C., et al., *Mutational analysis of TBK1 in Taiwanese patients with amyotrophic lateral sclerosis.* Neurobiol Aging, 2016. **40**: p. 191.e11-191.e16.
503. Borghero, G., et al., *TBK1 is associated with ALS and ALS-FTD in Sardinian patients.* Neurobiol Aging, 2016. **43**: p. 180.e1-5.
504. Tohnai, G., et al., *Frequency and characteristics of the TBK1 gene variants in Japanese patients with sporadic amyotrophic lateral sclerosis.* Neurobiol Aging, 2018. **64**: p. 158.e15-158.e19.
505. Jiao, B., et al., *Rare TBK1 variants in patients with frontotemporal dementia and amyotrophic lateral sclerosis in a Chinese cohort.* Transl Neurodegener, 2018. **7**: p. 31.
506. McCombe, P.A., et al., *Patient with ALS with a novel TBK1 mutation, widespread brain involvement, behaviour changes and metabolic dysfunction.* J Neurol Neurosurg Psychiatry, 2019. **90**(8): p. 952-954.
507. Piaceri, I., et al., *Association of the New Variant Tyr424Asp at TBK1 Gene with Amyotrophic Lateral Sclerosis and Cognitive Decline.* J Alzheimers Dis, 2018. **61**(1): p. 41-46.
508. Catanese, A., et al., *Retinoic acid worsens ATG10-dependent autophagy impairment in TBK1-mutant hiPSC-derived motoneurons through SQSTM1/p62 accumulation.* Autophagy, 2019: p. 1-19.
509. Duan, W., et al., *Deletion of Tbk1 disrupts autophagy and reproduces behavioral and locomotor symptoms of FTD-ALS in mice.* Aging (Albany NY), 2019. **11**(8): p. 2457-2476.
510. Brenner, D., et al., *Heterozygous Tbk1 loss has opposing effects in early and late stages of ALS in mice.* J Exp Med, 2019. **216**(2): p. 267-278.
511. Bonnard, M., et al., *Deficiency of T2K leads to apoptotic liver degeneration and impaired NF-kappaB-dependent gene transcription.* Embo j, 2000. **19**(18): p. 4976-85.
512. N'Diaye, E.N., et al., *PLIC proteins or ubiquilins regulate autophagy-dependent cell survival during nutrient starvation.* EMBO Rep, 2009. **10**(2): p. 173-9.
513. Herman, M., et al., *Heterozygous TBK1 mutations impair TLR3 immunity and underlie herpes simplex encephalitis of childhood.* J Exp Med, 2012. **209**(9): p. 1567-82.
514. Ren, H., et al., *DJ-1, a cancer and Parkinson's disease associated protein, regulates autophagy through JNK pathway in cancer cells.* Cancer Letters, 2010. **297**(1): p. 101-108.

515. Nagabhushana, A., et al., *Regulation of endocytic trafficking of transferrin receptor by optineurin and its impairment by a glaucoma-associated mutant.* BMC Cell Biol, 2010. **11**: p. 4.
516. Graham, F.L., et al., *Characteristics of a human cell line transformed by DNA from human adenovirus type 5.* J Gen Virol, 1977. **36**(1): p. 59-74.
517. Schweers, R.L., et al., *NIX is required for programmed mitochondrial clearance during reticulocyte maturation.* Proc Natl Acad Sci U S A, 2007. **104**(49): p. 19500-5.
518. Degenhardt, K., et al., *Autophagy promotes tumor cell survival and restricts necrosis, inflammation, and tumorigenesis.* Cancer Cell, 2006. **10**(1): p. 51-64.
519. Guo, J.Y., et al., *Activated Ras requires autophagy to maintain oxidative metabolism and tumorigenesis.* Genes Dev, 2011. **25**(5): p. 460-70.
520. Lock, R., et al., *Autophagy facilitates glycolysis during Ras-mediated oncogenic transformation.* Mol Biol Cell, 2011. **22**(2): p. 165-78.
521. Yang, S., et al., *Pancreatic cancers require autophagy for tumor growth.* Genes Dev, 2011. **25**(7): p. 717-29.
522. Guo, J.Y., B. Xia, and E. White, *Autophagy-mediated tumor promotion.* Cell, 2013. **155**(6): p. 1216-9.
523. Nyfeler, B. and C.H. Eng, *Revisiting autophagy addiction of tumor cells.* Autophagy, 2016. **12**(7): p. 1206-1207.
524. Barbie, D.A., et al., *Systematic RNA interference reveals that oncogenic KRAS-driven cancers require TBK1.* Nature, 2009. **462**: p. 108.
525. Newman, A.C., et al., *TBK1 Kinase Addiction in Lung Cancer Cells Is Mediated via Autophagy of Tax1bp1/Ndp52 and Non-Canonical NF-κB Signalling.* PLOS ONE, 2012. **7**(11): p. e50672.
526. Yang, S., et al., *Autophagy Inhibition Dysregulates TBK1 Signaling and Promotes Pancreatic Inflammation.* Cancer Immunol Res, 2016. **4**(6): p. 520-30.
527. Liang, C., et al., *Beclin1-binding UVRAG targets the class C Vps complex to coordinate autophagosome maturation and endocytic trafficking.* Nat Cell Biol, 2008. **10**(7): p. 776-87.
528. Yue, Z., et al., *The cellular pathways of neuronal autophagy and their implication in neurodegenerative diseases.* Biochimica et Biophysica Acta (BBA) - Molecular Cell Research, 2009. **1793**(9): p. 1496-1507.
529. Klionsky, D.J., et al., *Guidelines for the use and interpretation of assays for monitoring autophagy.* Autophagy, 2012. **8**(4): p. 445-544.
530. Klionsky, D.J., et al., *Guidelines for the use and interpretation of assays for monitoring autophagy in higher eukaryotes.* Autophagy, 2008. **4**(2): p. 151-75.
531. Yoshimori, T., *How to Interpret LC3 Immunoblotting AU - Mizushima, Noboru.* Autophagy, 2007. **3**(6): p. 542-545.
532. Mauvezin, C. and T.P. Neufeld, *Bafilomycin A1 disrupts autophagic flux by inhibiting both V-ATPase-dependent acidification and Ca-P60A/SERCA-dependent autophagosome-lysosome fusion.* Autophagy, 2015. **11**(8): p. 1437-8.
533. Kneen, M., et al., *Green Fluorescent Protein as a Noninvasive Intracellular pH Indicator.* Biophysical Journal, 1998. **74**(3): p. 1591-1599.

534. Hundeshagen, P., et al., *Concurrent detection of autolysosome formation and lysosomal degradation by flow cytometry in a high-content screen for inducers of autophagy.* BMC Biol, 2011. **9**: p. 38.
535. Maulucci, G., et al., *Quantitative analysis of autophagic flux by confocal pH-imaging of autophagic intermediates.* Autophagy, 2015. **11**(10): p. 1905-1916.
536. Farkas, T. and M. Jaattela, *Renilla Luciferase-LC3 Based Reporter Assay for Measuring Autophagic Flux.* Methods Enzymol, 2017. **588**: p. 1-13.
537. Shvets, E., E. Fass, and Z. Elazar, *Utilizing flow cytometry to monitor autophagy in living mammalian cells.* Autophagy, 2008. **4**(5): p. 621-628.
538. Degtyarev, M., M. Reichelt, and K. Lin, *Novel quantitative autophagy analysis by organelle flow cytometry after cell sonication.* PLoS One, 2014. **9**(1): p. e87707.
539. Zappavigna, S., et al., *Measurement of Autophagy by Flow Cytometry*, in *Adult Stem Cells: Methods and Protocols*, P. Di Nardo, S. Dhingra, and D.K. Singla, Editors. 2017, Springer New York: New York, NY. p. 209-216.
540. Larsen, K.B., et al., *A reporter cell system to monitor autophagy based on p62/SQSTM1.* Autophagy, 2010. **6**(6): p. 784-93.
541. Warnes, G., *Flow cytometric assays for the study of autophagy.* Methods, 2015. **82**: p. 21-28.
542. Clement, J.F., S. Meloche, and M.J. Servant, *The IKK-related kinases: from innate immunity to oncogenesis.* Cell Res, 2008. **18**(9): p. 889-99.
543. Wang, T., et al., *Discovery of azabenzimidazole derivatives as potent, selective inhibitors of TBK1/IKKepsilon kinases.* Bioorg Med Chem Lett, 2012. **22**(5): p. 2063-9.
544. Richters, A., et al., *Identification and further development of potent TBK1 inhibitors.* ACS Chem Biol, 2015. **10**(1): p. 289-98.
545. Li, J., et al., *Selective TBK1/IKKi dual inhibitors with anticancer potency.* International journal of cancer, 2014. **134**(8): p. 1972-1980.
546. Goncalves, A., et al., *Functional dissection of the TBK1 molecular network.* PLoS One, 2011. **6**(9): p. e23971.
547. Yu, T., et al., *TBK1 inhibitors: a review of patent literature (2011 - 2014).* Expert Opin Ther Pat, 2015. **25**(12): p. 1385-96.
548. Feldman, R.I., et al., *Novel small molecule inhibitors of 3-phosphoinositide-dependent kinase-1.* J Biol Chem, 2005. **280**(20): p. 19867-74.
549. Bain, J., et al., *The selectivity of protein kinase inhibitors: a further update.* Biochem J, 2007. **408**(3): p. 297-315.
550. Clark, K., et al., *Novel cross-talk within the IKK family controls innate immunity.* Biochem. J, 2011. **434**: p. 93-104.
551. Petherick, K.J., et al., *Pharmacological inhibition of ULK1 kinase blocks mammalian target of rapamycin (mTOR)-dependent autophagy.* J Biol Chem, 2015. **290**(18): p. 11376-83.
552. Jansen, R., et al., *Identification of genes that are associated with DNA repeats in prokaryotes.* Mol Microbiol, 2002. **43**(6): p. 1565-75.
553. Mojica, F.J., et al., *Biological significance of a family of regularly spaced repeats in the genomes of Archaea, Bacteria and mitochondria.* Mol Microbiol, 2000. **36**(1): p. 244-6.

554. Mojica, F.J., et al., *Intervening sequences of regularly spaced prokaryotic repeats derive from foreign genetic elements.* J Mol Evol, 2005. **60**(2): p. 174-82.
555. Barrangou, R., et al., *CRISPR provides acquired resistance against viruses in prokaryotes.* Science, 2007. **315**(5819): p. 1709-12.
556. Makarova, K.S., et al., *A putative RNA-interference-based immune system in prokaryotes: computational analysis of the predicted enzymatic machinery, functional analogies with eukaryotic RNAi, and hypothetical mechanisms of action.* Biol Direct, 2006. **1**: p. 7.
557. Carte, J., et al., *Cas6 is an endoribonuclease that generates guide RNAs for invader defense in prokaryotes.* Genes Dev, 2008. **22**(24): p. 3489-96.
558. Brouns, S.J., et al., *Small CRISPR RNAs guide antiviral defense in prokaryotes.* Science, 2008. **321**(5891): p. 960-4.
559. Hale, C.R., et al., *RNA-guided RNA cleavage by a CRISPR RNA-Cas protein complex.* Cell, 2009. **139**(5): p. 945-56.
560. Makarova, K.S., et al., *Evolution and classification of the CRISPR-Cas systems.* Nat Rev Microbiol, 2011. **9**(6): p. 467-77.
561. Jore, M.M., et al., *Structural basis for CRISPR RNA-guided DNA recognition by Cascade.* Nature Structural &Amp; Molecular Biology, 2011. **18**: p. 529.
562. Jinek, M., et al., *A programmable dual-RNA-guided DNA endonuclease in adaptive bacterial immunity.* Science, 2012. **337**(6096): p. 816-21.
563. Mali, P., et al., *RNA-guided human genome engineering via Cas9.* Science, 2013. **339**(6121): p. 823-6.
564. Doudna, J.A. and E. Charpentier, *Genome editing. The new frontier of genome engineering with CRISPR-Cas9.* Science, 2014. **346**(6213): p. 1258096.
565. Sharma, S., *Age-related nonhomologous end joining activity in rat neurons.* Brain Res Bull, 2007. **73**(1-3): p. 48-54.
566. Rodgers, K. and M. McVey, *Error-Prone Repair of DNA Double-Strand Breaks.* J Cell Physiol, 2016. **231**(1): p. 15-24.
567. Aird, E.J., et al., *Increasing Cas9-mediated homology-directed repair efficiency through covalent tethering of DNA repair template.* Communications Biology, 2018. **1**(1): p. 54.
568. Vargas, J.N.S., et al., *Spatiotemporal Control of ULK1 Activation by NDP52 and TBK1 during Selective Autophagy.* Molecular Cell, 2019.
569. Cooper, J.M., et al., *TBK1 Provides Context-Selective Support of the Activated AKT/mTOR Pathway in Lung Cancer.* Cancer Research, 2017. **77**(18): p. 5077.
570. Kim, J.Y., et al., *Dissection of TBK1 signaling via phosphoproteomics in lung cancer cells.* Proc Natl Acad Sci U S A, 2013. **110**(30): p. 12414-9.
571. Liu, W., et al., *Inhibition of TBK1 attenuates radiation-induced epithelial-mesenchymal transition of A549 human lung cancer cells via activation of GSK-3beta and repression of ZEB1.* Lab Invest, 2014. **94**(4): p. 362-70.
572. Eng, K.E., et al., *A novel quantitative flow cytometry-based assay for autophagy.* Autophagy, 2010. **6**(5): p. 634-41.
573. Köchl, R., et al., *Microtubules Facilitate Autophagosome Formation and Fusion of Autophagosomes with Endosomes.* Traffic, 2006. **7**(2): p. 129-145.

574. Seeman, P., D. Cheng, and G.H. Iles, *Structure of membrane holes in osmotic and saponin hemolysis.* J Cell Biol, 1973. **56**(2): p. 519-27.
575. Jamur, M.C. and C. Oliver, *Permeabilization of Cell Membranes*, in *Immunocytochemical Methods and Protocols*, C. Oliver and M.C. Jamur, Editors. 2010, Humana Press: Totowa, NJ. p. 63-66.
576. Musiwaro, P., et al., *Characteristics and requirements of basal autophagy in HEK 293 cells.* Autophagy, 2013. **9**(9): p. 1407-17.
577. Hasan, M., et al., *Chronic innate immune activation of TBK1 suppresses mTORC1 activity and dysregulates cellular metabolism.* Proc Natl Acad Sci U S A, 2017. **114**(4): p. 746-751.
578. Nanao, T., et al., *Cellular localization and tissue distribution of endogenous DFCP1 protein.* Biomed Res, 2015. **36**(2): p. 121-33.
579. Zhang, X.-H., et al., *Off-target Effects in CRISPR/Cas9-mediated Genome Engineering.* Molecular Therapy - Nucleic Acids, 2015. **4**: p. e264.
580. Kim, J.K., et al., *TBK1 regulates prostate cancer dormancy through mTOR inhibition.* Neoplasia (New York, N.Y.), 2013. **15**(9): p. 1064-1074.
581. Mejlvang, J., et al., *Starvation induces rapid degradation of selective autophagy receptors by endosomal microautophagy.* J Cell Biol, 2018. **217**(10): p. 3640-3655.
582. Ponpuak, M., et al., *Delivery of cytosolic components by autophagic adaptor protein p62 endows autophagosomes with unique antimicrobial properties.* Immunity, 2010. **32**(3): p. 329-41.
583. He, Y., et al., *p38 MAPK inhibits autophagy and promotes microglial inflammatory responses by phosphorylating ULK1.* The Journal of Cell Biology, 2018. **217**(1): p. 315.
584. Joo, Joung H., et al., *Hsp90-Cdc37 Chaperone Complex Regulates Ulk1- and Atg13-Mediated Mitophagy.* Molecular Cell, 2011. **43**(4): p. 572-585.
585. Cheng, Y., et al., *CRISPR/Cas9-Mediated Chicken TBK1 Gene Knockout and Its Essential Role in STING-Mediated IFN-beta Induction in Chicken Cells.* Front Immunol, 2018. **9**: p. 3010.
586. Tsai, S.Q., et al., *GUIDE-seq enables genome-wide profiling of off-target cleavage by CRISPR-Cas nucleases.* Nat Biotechnol, 2015. **33**(2): p. 187-197.
587. Akcakaya, P., et al., *In vivo CRISPR editing with no detectable genome-wide off-target mutations.* Nature, 2018. **561**(7723): p. 416-419.
588. Fu, Y., et al., *Improving CRISPR-Cas nuclease specificity using truncated guide RNAs.* Nat Biotechnol, 2014. **32**(3): p. 279-284.
589. Hsu, P.D., et al., *DNA targeting specificity of RNA-guided Cas9 nucleases.* Nat Biotechnol, 2013. **31**(9): p. 827-32.
590. Pattanayak, V., et al., *High-throughput profiling of off-target DNA cleavage reveals RNA-programmed Cas9 nuclease specificity.* Nat Biotechnol, 2013. **31**(9): p. 839-43.
591. Fu, Y., et al., *High-frequency off-target mutagenesis induced by CRISPR-Cas nucleases in human cells.* Nat Biotechnol, 2013. **31**(9): p. 822-6.
592. Kuscu, C., et al., *Genome-wide analysis reveals characteristics of off-target sites bound by the Cas9 endonuclease.* Nat Biotechnol, 2014. **32**(7): p. 677-83.

593. Ran, F.A., et al., *Double nicking by RNA-guided CRISPR Cas9 for enhanced genome editing specificity.* Cell, 2013. **154**(6): p. 1380-9.
594. Cullot, G., et al., *CRISPR-Cas9 genome editing induces megabase-scale chromosomal truncations.* Nat Commun, 2019. **10**(1): p. 1136.
595. Ha, S., et al., *Phosphorylation of p62 by AMP-activated protein kinase mediates autophagic cell death in adult hippocampal neural stem cells.* Journal of Biological Chemistry, 2017. **292**(33): p. 13795-13808.
596. Lim, J., et al., *Proteotoxic Stress Induces Phosphorylation of p62/SQSTM1 by ULK1 to Regulate Selective Autophagic Clearance of Protein Aggregates.* PLOS Genetics, 2015. **11**(2): p. e1004987.
597. Settembre, C., et al., *TFEB links autophagy to lysosomal biogenesis.* Science, 2011. **332**(6036): p. 1429-33.
598. Xu, D., et al., *TBK1 Suppresses RIPK1-Driven Apoptosis and Inflammation during Development and in Aging.* Cell, 2018. **174**(6): p. 1477-1491.e19.
599. Polson, H.E.J., et al., *Mammalian Atg18 (WIPI2) localizes to omegasome-anchored phagophores and positively regulates LC3 lipidation.* Autophagy, 2010. **6**(4): p. 506-522.
600. Polson, H.E., et al., *Mammalian Atg18 (WIPI2) localizes to omegasome-anchored phagophores and positively regulates LC3 lipidation.* Autophagy, 2010. **6**(4): p. 506-22.
601. Bodur, C., et al., *The IKK-related kinase TBK1 activates mTORC1 directly in response to growth factors and innate immune agonists.* Embo j, 2018. **37**(1): p. 19-38.
602. Lobbestael, E., et al., *Pharmacological LRRK2 kinase inhibition induces LRRK2 protein destabilization and proteasomal degradation.* Scientific reports, 2016. **6**: p. 33897-33897.
603. Zurek, B., et al., *TRIM27 negatively regulates NOD2 by ubiquitination and proteasomal degradation.* PLoS One, 2012. **7**(7): p. e41255.
604. Zheng, Q., et al., *Siglec1 suppresses antiviral innate immune response by inducing TBK1 degradation via the ubiquitin ligase TRIM27.* Cell Res, 2015. **25**(10): p. 1121-36.
605. Grumati, P. and I. Dikic, *Ubiquitin signaling and autophagy.* Journal of Biological Chemistry, 2018. **293**(15): p. 5404-5413.
606. Weidberg, H., E. Shvets, and Z. Elazar, *Biogenesis and cargo selectivity of autophagosomes.* Annu Rev Biochem, 2011. **80**: p. 125-56.
607. Bjørkøy, G., et al., *p62/SQSTM1 forms protein aggregates degraded by autophagy and has a protective effect on huntingtin-induced cell death.* The Journal of Cell Biology, 2005. **171**(4): p. 603.
608. Kirkin, V., et al., *A role for NBR1 in autophagosomal degradation of ubiquitinated substrates.* Mol Cell, 2009. **33**(4): p. 505-16.
609. Sandilands, E., et al., *Autophagic targeting of Src promotes cancer cell survival following reduced FAK signalling.* Nat Cell Biol, 2011. **14**(1): p. 51-60.
610. Wyant, G.A., et al., *NUFIP1 is a ribosome receptor for starvation-induced ribophagy.* Science, 2018. **360**(6390): p. 751.

611. Egan, D.F., et al., *Phosphorylation of ULK1 (hATG1) by AMP-activated protein kinase connects energy sensing to mitophagy.* Science, 2011. **331**(6016): p. 456-61.
612. Liu, L., et al., *Mitochondrial outer-membrane protein FUNDC1 mediates hypoxia-induced mitophagy in mammalian cells.* Nat Cell Biol, 2012. **14**(2): p. 177-85.
613. Platta, H.W., et al., *Nedd4-dependent lysine-11-linked polyubiquitination of the tumour suppressor Beclin 1.* Biochem J, 2012. **441**(1): p. 399-406.
614. Nazio, F., et al., *Fine-tuning of ULK1 mRNA and protein levels is required for autophagy oscillation.* J Cell Biol, 2016. **215**(6): p. 841-856.
615. Whang, M.I., et al., *The Ubiquitin Binding Protein TAX1BP1 Mediates Autophagosome Induction and the Metabolic Transition of Activated T Cells.* Immunity, 2017. **46**(3): p. 405-420.
616. Matsumoto, G., et al., *Serine 403 phosphorylation of p62/SQSTM1 regulates selective autophagic clearance of ubiquitinated proteins.* Mol Cell, 2011. **44**(2): p. 279-89.
617. Long, J., et al., *Dimerisation of the UBA domain of p62 inhibits ubiquitin binding and regulates NF-kappaB signalling.* J Mol Biol, 2010. **396**(1): p. 178-94.
618. Kawase, K., et al., *Confirmation of TBK1 duplication in normal tension glaucoma.* Exp Eye Res, 2012. **96**(1): p. 178-80.
619. Williams, K.L., et al., *Novel TBK1 truncating mutation in a familial amyotrophic lateral sclerosis patient of Chinese origin.* Neurobiol Aging, 2015.
620. Pottier, C., et al., *Genome-wide analyses as part of the international FTLD-TDP whole-genome sequencing consortium reveals novel disease risk factors and increases support for immune dysfunction in FTLD.* Acta Neuropathol, 2019.
621. Yu, H., et al., *Association of the TBK1 mutation p.Ile334Thr with frontotemporal dementia and literature review.* Mol Genet Genomic Med, 2019.
622. Pottier, C., et al., *Genome-wide analyses as part of the international FTLD-TDP whole-genome sequencing consortium reveals novel disease risk factors and increases support for immune dysfunction in FTLD.* Acta Neuropathol, 2019. **137**(6): p. 879-899.
623. Yu, H., et al., *Association of the TBK1 mutation p.Ile334Thr with frontotemporal dementia and literature review.* Molecular genetics & genomic medicine, 2019. **7**(3): p. e547-e547.
624. Bjorkoy, G., et al., *Monitoring autophagic degradation of p62/SQSTM1.* Methods Enzymol, 2009. **452**: p. 181-97.
625. Cui, J., et al., *Age-related changes in the function of autophagy in rat kidneys.* Age (Dordr), 2012. **34**(2): p. 329-39.
626. Yan, J., et al., *SQSTM1/p62 Interacts with HDAC6 and Regulates Deacetylase Activity.* PLOS ONE, 2013. **8**(9): p. e76016.
627. Pankiv, S., et al., *p62/SQSTM1 binds directly to Atg8/LC3 to facilitate degradation of ubiquitinated protein aggregates by autophagy.* J Biol Chem, 2007. **282**(33): p. 24131-45.
628. Lamark, T. and T. Johansen, *Aggrephagy: selective disposal of protein aggregates by macroautophagy.* International journal of cell biology, 2012. **2012**.

629. Lee, J.Y., et al., *HDAC6 controls autophagosome maturation essential for ubiquitin-selective quality-control autophagy.* Embo j, 2010. **29**(5): p. 969-80.
630. Ravenhill, B.J., et al., *The Cargo Receptor NDP52 Initiates Selective Autophagy by Recruiting the ULK Complex to Cytosol-Invading Bacteria.* Mol Cell, 2019.
631. Ravenhill, B.J., et al., *The Cargo Receptor NDP52 Initiates Selective Autophagy by Recruiting the ULK Complex to Cytosol-Invading Bacteria.* Mol Cell, 2019. **74**(2): p. 320-329.e6.
632. Li, W.W., J. Li, and J.K. Bao, *Microautophagy: lesser-known self-eating.* Cell Mol Life Sci, 2012. **69**(7): p. 1125-36.
633. Zhang, X., et al., *HDAC6 Modulates Cell Motility by Altering the Acetylation Level of Cortactin.* Molecular Cell, 2007. **27**(2): p. 197-213.
634. Watabe, M. and T. Nakaki, *Protein kinase CK2 regulates the formation and clearance of aggresomes in response to stress.* J Cell Sci, 2011. **124**(Pt 9): p. 1519-32.
635. Gal, J., et al., *p62 accumulates and enhances aggregate formation in model systems of familial amyotrophic lateral sclerosis.* J Biol Chem, 2007. **282**(15): p. 11068-77.
636. Layman, A.A.K., et al., *Ndfip1 restricts mTORC1 signalling and glycolysis in regulatory T cells to prevent autoinflammatory disease.* Nature Communications, 2017. **8**: p. 15677.
637. Cui, R., et al., *Association between TBK1 mutations and risk of amyotrophic lateral sclerosis/frontotemporal dementia spectrum: a meta-analysis.* Neurol Sci, 2018. **39**(5): p. 811-820.
638. Freischmidt, A., et al., *Association of Mutations in TBK1 With Sporadic and Familial Amyotrophic Lateral Sclerosis and Frontotemporal Dementia.* JAMA Neurol, 2017. **74**(1): p. 110-113.
639. Suzuki, T., et al., *Cell type-specific subcellular localization of phospho-TBK1 in response to cytoplasmic viral DNA.* PLoS One, 2013. **8**(12): p. e83639.
640. Pourcelot, M., et al., *The Golgi apparatus acts as a platform for TBK1 activation after viral RNA sensing.* BMC Biology, 2016. **14**(1): p. 69.
641. Rock, K.L., et al., *Inhibitors of the proteasome block the degradation of most cell proteins and the generation of peptides presented on MHC class I molecules.* Cell, 1994. **78**(5): p. 761-71.
642. Hershko, A. and A. Ciechanover, *The ubiquitin system.* Annu Rev Biochem, 1998. **67**: p. 425-79.
643. Swatek, K.N. and D. Komander, *Ubiquitin modifications.* Cell Research, 2016. **26**: p. 399.
644. Kirkin, V., et al., *A Role for NBR1 in Autophagosomal Degradation of Ubiquitinated Substrates.* Molecular Cell, 2009. **33**(4): p. 505-516.
645. Zatloukal, K., et al., *p62 Is a Common Component of Cytoplasmic Inclusions in Protein Aggregation Diseases.* The American Journal of Pathology, 2002. **160**(1): p. 255-263.
646. Olzmann, J.A., et al., *Parkin-mediated K63-linked polyubiquitination targets misfolded DJ-1 to aggresomes via binding to HDAC6.* J Cell Biol, 2007. **178**(6): p. 1025-38.

647. Mishra, A., et al., *The ubiquitin ligase E6-AP is induced and recruited to aggresomes in response to proteasome inhibition and may be involved in the ubiquitination of Hsp70-bound misfolded proteins.* J Biol Chem, 2009. **284**(16): p. 10537-45.
648. Zhang, X. and S.B. Qian, *Chaperone-mediated hierarchical control in targeting misfolded proteins to aggresomes.* Mol Biol Cell, 2011. **22**(18): p. 3277-88.
649. Mao, J., et al., *A critical role of Hrd1 in the regulation of optineurin degradation and aggresome formation.* Hum Mol Genet, 2017. **26**(10): p. 1877-1889.
650. Matthias, P., M. Yoshida, and S. Khochbin, *HDAC6 a new cellular stress surveillance factor.* Cell Cycle, 2008. **7**(1): p. 7-10.
651. Johnston, J.A., C.L. Ward, and R.R. Kopito, *Aggresomes: A Cellular Response to Misfolded Proteins.* The Journal of Cell Biology, 1998. **143**(7): p. 1883.
652. Ichimura, Y., et al., *Structural basis for sorting mechanism of p62 in selective autophagy.* J Biol Chem, 2008. **283**(33): p. 22847-57.
653. Ge, P.-f., et al., *Inhibition of autophagy induced by proteasome inhibition increases cell death in human SHG-44 glioma cells.* Acta Pharmacologica Sinica, 2009. **30**: p. 1046.
654. Bao, W., et al., *Induction of autophagy by the MG132 proteasome inhibitor is associated with endoplasmic reticulum stress in MCF7 cells.* Mol Med Rep, 2016. **13**(1): p. 796-804.
655. Harhouri, K., et al., *MG132-induced progerin clearance is mediated by autophagy activation and splicing regulation.* EMBO Mol Med, 2017. **9**(9): p. 1294-1313.
656. Lee, D.H. and A.L. Goldberg, *Proteasome inhibitors: valuable new tools for cell biologists.* Trends Cell Biol, 1998. **8**(10): p. 397-403.
657. Wang, D.-w., et al., *The different roles of selective autophagic protein degradation in mammalian cells.* Oncotarget, 2015. **6**(35): p. 37098-37116.
658. Ding, W.-X., et al., *Linking of Autophagy to Ubiquitin-Proteasome System Is Important for the Regulation of Endoplasmic Reticulum Stress and Cell Viability.* The American Journal of Pathology, 2007. **171**(2): p. 513-524.
659. Walker, A.K., et al., *An insoluble frontotemporal lobar degeneration-associated TDP-43 C-terminal fragment causes neurodegeneration and hippocampus pathology in transgenic mice.* Human molecular genetics, 2015. **24**(25): p. 7241-7254.
660. Stieber, A., J.O. Gonatas, and N.K. Gonatas, *Aggregation of ubiquitin and a mutant ALS-linked SOD1 protein correlate with disease progression and fragmentation of the Golgi apparatus.* Journal of the Neurological Sciences, 2000. **173**(1): p. 53-62.
661. Jiang, L.-L., et al., *Two mutations G335D and Q343R within the amyloidogenic core region of TDP-43 influence its aggregation and inclusion formation.* Scientific reports, 2016. **6**: p. 23928-23928.
662. Wobst, H.J., et al., *Cytoplasmic Relocalization of TAR DNA-Binding Protein 43 Is Not Sufficient to Reproduce Cellular Pathologies Associated with ALS In vitro.* Frontiers in molecular neuroscience, 2017. **10**: p. 46-46.

663. Walker, A.K., et al., *ALS-associated TDP-43 induces endoplasmic reticulum stress, which drives cytoplasmic TDP-43 accumulation and stress granule formation.* PloS one, 2013. **8**(11): p. e81170-e81170.
664. Wu, W.K., et al., *Induction of autophagy by proteasome inhibitor is associated with proliferative arrest in colon cancer cells.* Biochem Biophys Res Commun, 2008. **374**(2): p. 258-63.
665. Fan, T., et al., *Proteasome inhibition promotes autophagy and protects from endoplasmic reticulum stress in rat alveolar macrophages exposed to hypoxia-reoxygenation injury.* J Cell Physiol, 2018. **233**(10): p. 6748-6758.
666. Selimovic, D., et al., *Bortezomib/proteasome inhibitor triggers both apoptosis and autophagy-dependent pathways in melanoma cells.* Cell Signal, 2013. **25**(1): p. 308-18.
667. Janssen, A.F.J., et al., *Probing aggrephagy using chemically-induced protein aggregates.* Nature Communications, 2018. **9**(1): p. 4245.
668. Liu, X., et al., *The BEACH-containing protein WDR81 coordinates p62 and LC3C to promote aggrephagy.* J Cell Biol, 2017. **216**(5): p. 1301-1320.
669. Zaffagnini, G., et al., *p62 filaments capture and present ubiquitinated cargos for autophagy.* The EMBO journal, 2018. **37**(5): p. e98308.
670. Lopez-Montero, N., et al., *Intracellular Salmonella induces aggrephagy of host endomembranes in persistent infections.* Autophagy, 2016. **12**(10): p. 1886-1901.
671. Nicot, A.-S., et al., *Phosphorylation of NBR1 by GSK3 modulates protein aggregation.* Autophagy, 2014. **10**(6): p. 1036-1053.
672. Karanasios, E., et al., *Dynamic association of the ULK1 complex with omegasomes during autophagy induction.* Journal of Cell Science, 2013. **126**(22): p. 5224.
673. Barmada, S.J., et al., *Autophagy induction enhances TDP43 turnover and survival in neuronal ALS models.* Nature Chemical Biology, 2014. **10**: p. 677.
674. Wang, P., et al., *Acetylation-induced TDP-43 pathology is suppressed by an HSF1-dependent chaperone program.* Nature Communications, 2017. **8**(1): p. 82.
675. Hortobagyi, T., et al., *Optineurin inclusions occur in a minority of TDP-43 positive ALS and FTLD-TDP cases and are rarely observed in other neurodegenerative disorders.* Acta Neuropathol, 2011. **121**(4): p. 519-27.
676. Yamashita, S., et al., *Optineurin is potentially associated with TDP-43 and involved in the pathogenesis of inclusion body myositis.* Neuropathol Appl Neurobiol, 2013. **39**(4): p. 406-16.
677. Shen, W.C., et al., *Mutations in the ubiquitin-binding domain of OPTN/optineurin interfere with autophagy-mediated degradation of misfolded proteins by a dominant-negative mechanism.* Autophagy, 2015. **11**(4): p. 685-700.
678. Hara, T., et al., *Suppression of basal autophagy in neural cells causes neurodegenerative disease in mice.* Nature, 2006. **441**(7095): p. 885-889.
679. Ramesh, N. and U.B. Pandey, *Autophagy Dysregulation in ALS: When Protein Aggregates Get Out of Hand.* Frontiers in molecular neuroscience, 2017. **10**: p. 263-263.
680. Puleston, D., et al., *Techniques for the Detection of Autophagy in Primary Mammalian Cells.* Cold Spring Harbor Protocols, 2015. **2015**(9): p. pdb.top070391.

681. Chen, Y., M.B. Azad, and S.B. Gibson, *Methods for detecting autophagy and determining autophagy-induced cell deathThis review is one of a selection of papers published in a Special Issue on Oxidative Stress in Health and Disease.* Canadian Journal of Physiology and Pharmacology, 2010. **88**(3): p. 285-295.
682. Phadwal, K., et al., *A novel method for autophagy detection in primary cells.* Autophagy, 2012. **8**(4): p. 677-689.
683. Martinet, W., et al., *Detection of autophagy in tissue by standard immunohistochemistry: possibilities and limitations.* Autophagy, 2006. **2**(1): p. 55-7.
684. Singh, B. and S. Bhaskar, *Methods for Detection of Autophagy in Mammalian Cells*, in *Stem Cells and Aging : Methods and Protocols*, K. Turksen, Editor. 2019, Springer New York: New York, NY. p. 245-258.
685. Tasdemir, E., et al., *Cell cycle-dependent induction of autophagy, mitophagy and reticulophagy.* Cell Cycle, 2007. **6**(18): p. 2263-7.
686. Scotter, E.L., et al., *Differential roles of the ubiquitin proteasome system and autophagy in the clearance of soluble and aggregated TDP-43 species.* Journal of Cell Science, 2014. **127**(6): p. 1263.
687. Lamark, T. and T. Johansen, *Aggrephagy: Selective Disposal of Protein Aggregates by Macroautophagy.* International Journal of Cell Biology, 2012. **2012**: p. 736905.
688. Shaw, G., et al., *Preferential transformation of human neuronal cells by human adenoviruses and the origin of HEK 293 cells.* Faseb j, 2002. **16**(8): p. 869-71.
689. Maruyama, R., et al., *Morphological and biochemical characterization of basal and starvation-induced autophagy in isolated adult rat cardiomyocytes.* Am J Physiol Heart Circ Physiol, 2008. **295**(4): p. H1599-607.
690. Williams, T., et al., *Basal autophagy induction without AMP-activated protein kinase under low glucose conditions.* Autophagy, 2009. **5**(8): p. 1155-65.
691. Hariharan, N., et al., *Deacetylation of FoxO by Sirt1 Plays an Essential Role in Mediating Starvation-Induced Autophagy in Cardiac Myocytes.* Circ Res, 2010. **107**(12): p. 1470-82.
692. Ito, Y., et al., *RIPK1 mediates axonal degeneration by promoting inflammation and necroptosis in ALS.* Science, 2016. **353**(6299): p. 603-8.
693. Du, D., et al., *Neuroinflammation contributes to autophagy flux blockage in the neurons of rostral ventrolateral medulla in stress-induced hypertension rats.* Journal of Neuroinflammation, 2017. **14**(1): p. 169.
694. Jin, M.-M., et al., *A Critical Role of Autophagy in Regulating Microglia Polarization in Neurodegeneration.* Frontiers in aging neuroscience, 2018. **10**: p. 378-378.